Springer Handbook of Acoustics



Rossing
Editor

Springer

Amazon EX1014 Page 1

Springer Handbook of Acoustics

Amazon EX1014 Page 2

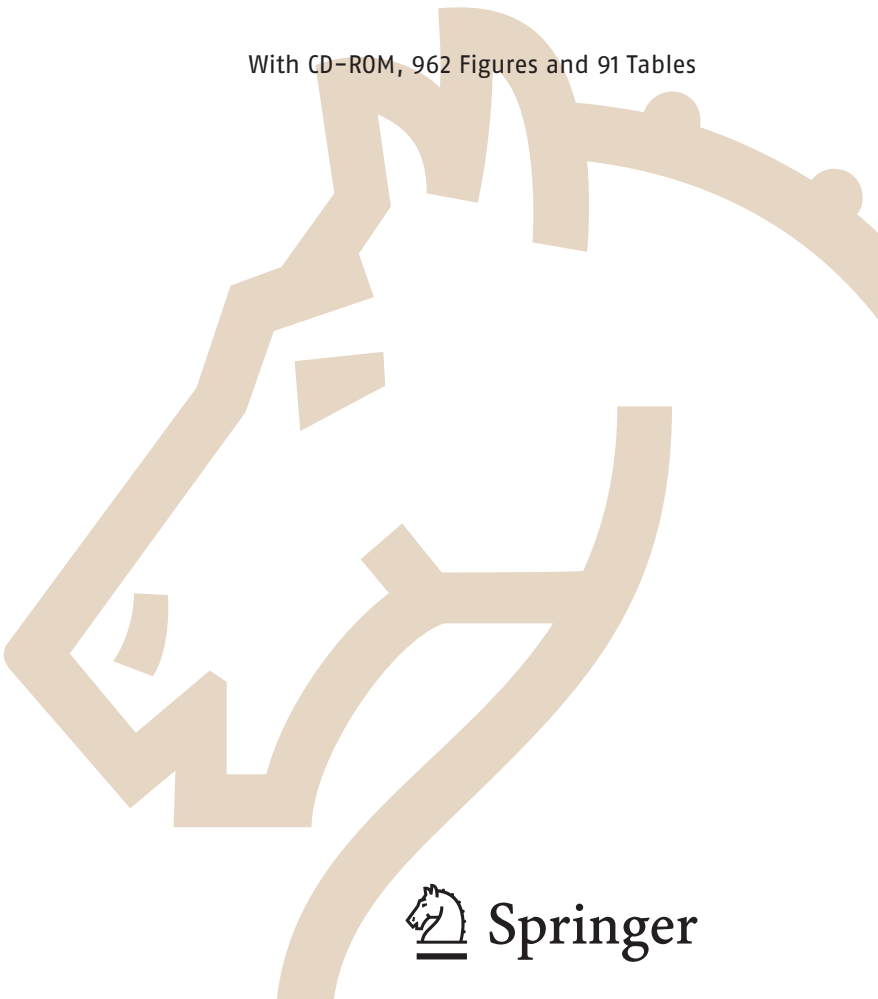
Springer Handbooks provide a concise compilation of approved key information on methods of research, general principles, and functional relationships in physical sciences and engineering. The world's leading experts in the fields of physics and engineering will be assigned by one or several renowned editors to write the chapters comprising each volume. The content is selected by these experts from Springer sources (books, journals, online content) and other systematic and approved recent publications of physical and technical information.

The volumes are designed to be useful as readable desk reference books to give a fast and comprehensive overview and easy retrieval of essential reliable key information, including tables, graphs, and bibliographies. References to extensive sources are provided.

Springer Handbook of Acoustics

Thomas D. Rossing (Ed.)

With CD-ROM, 962 Figures and 91 Tables



Springer

Amazon EX1014 Page 4

Editor:

Thomas D. Rossing
Stanford University
Center for Computer Research in Music and Acoustics
Stanford, CA 94305, USA

Editorial Board:

Manfred R. Schroeder, University of Göttingen, Germany
William M. Hartmann, Michigan State University, USA
Neville H. Fletcher, Australian National University, Australia
Floyd Dunn, University of Illinois, USA
D. Murray Campbell, The University of Edinburgh, UK

Library of Congress Control Number: 2006927050

ISBN: 978-0-387-30446-5 e-ISBN: 0-387-30425-0
Printed on acid free paper

© 2007, Springer Science+Business Media, LLC New York
All rights reserved. This work may not be translated or copied in whole or in part without the written permission of the publisher (Springer Science+Business Media, LLC New York, 233 Spring Street, New York, NY 10013, USA), except for brief excerpts in connection with reviews or scholarly analysis. Use in connection with any form of information storage and retrieval, electronic adaptation, computer software, or by similar or dissimilar methodology now known or hereafter developed is forbidden. The use in this publication of trade names, trademarks, service marks, and similar terms, even if they are not identified as such, is not to be taken as an expression of opinion as to whether or not they are subject to proprietary rights.

The use of designations, trademarks, etc. in this publication does not imply, even in the absence of a specific statement, that such names are exempt from the relevant protective laws and regulations and therefore free for general use.

Product liability: The publisher cannot guarantee the accuracy of any information about dosage and application contained in this book. In every individual case the user must check such information by consulting the relevant literature.

Production and typesetting: LE-TeX GbR, Leipzig
Handbook Manager: Dr. W. Skolaut, Heidelberg
Typography and layout: schreiberVIS, Seeheim
Illustrations:
schreiberVIS, Seeheim & Hippmann GbR, Schwarzenbruck
Cover design: eStudio Calamar Steinen, Barcelona
Cover production: WMXDesign GmbH, Heidelberg
Printing and binding: Stürtz AG, Würzburg

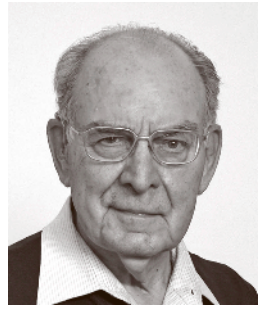
SPIN 11309031 100/3100/YL 5 4 3 2 1 0

Foreword

The present handbook covers a very wide field. Its 28 chapters range from the history of acoustics to sound propagation in the atmosphere; from nonlinear and underwater acoustics to thermoacoustics and concert hall acoustics. Also covered are musical acoustics, including computer and electronic music; speech and singing; animal (including whales) communication as well as bioacoustics in general, psychoacoustics and medical acoustics. In addition, there are chapters on structural acoustics, vibration and noise, including optical methods for their measurement; microphones, their calibration, and microphone and hydrophone arrays; acoustic holography; model analysis and much else needed by the professional engineer and scientist.

Among the authors we find many illustrious names: Yoichi Ando, Mack Breazeale, Babrina Dunmire, Neville Fletcher, Anders Gade, William Hartmann, William Kuperman, Werner Lauterborn, George Maling, Brian Moore, Allan Pierce, Thomas Rossing, Johan Sundberg, Eric Young, and many more. They hail from countries around the world: Australia, Canada, Denmark, France, Germany, Japan, Korea, Sweden, the United Kingdom, and the USA. There is no doubt that this handbook will fill many needs, nay be irreplaceable in the art of exercising today's many interdisciplinary tasks devolving on acoustics. No reader could wish for a wider and more expert coverage. I wish the present tome the wide acceptance and success it surely deserves.

Göttingen, March 2007 Manfred R. Schroeder



Prof. Dr. M. R. Schroeder
University Professor
Speach and Acoustics Laboratory
University of Göttingen,
Germany

Amazon EX1014 Page 6

Preface



Prof. em. T. D. Rossing
Northern Illinois University
Presently visiting Professor
of Music at Stanford University

"A handbook," according to the dictionary, "is a book capable of being conveniently carried as a ready reference." Springer has created the Springer Handbook series on important scientific and technical subjects, and we feel fortunate that they have included acoustics in this category.

Acoustics, the science of sound, is a rather broad subject to be covered in a single handbook. It embodies many different academic disciplines, such as physics, mechanical and electrical engineering, mathematics, speech and hearing sciences, music, and architecture. There are many technical areas in acoustics; the Acoustical Society of America, for example, includes 14 technical committees representing different areas of acoustics. It is impossible to cover all of these areas in a single handbook. We have tried to include as many as possible of the "hot" topics in this interdisciplinary field, including basic science and technological applications. We apologize to the reader whose favorite topics are not included.

We have grouped the 28 chapters in the book into eight parts: Propagation of Sound; Physical and Nonlinear Acoustics; Architectural Acoustics; Hearing and Signal Processing; Music, Speech, and Electroacoustics; Biological and Medical Acoustics; Structural Acoustics and Noise; and Engineering Acoustics. The chapters are of varying length. They also reflect the individual writing styles of the various authors, all of whom are authorities in their fields. Although an attempt was made to keep the mathematical level of the chapters as even as possible, readers will note that some chapters are more mathematical than others; this is unavoidable and in fact lends some degree of richness to the book.

We are indebted to many persons, especially Werner Skolaut, the manager of the Springer Handbooks, and to the editorial board, consisting of Neville Fletcher, Floyd Dunn, William Hartmann, and Murray Campbell, and for their advice. Each chapter was reviewed by two authoritative reviewers, and we are grateful to them for their services. But most of all we thank the authors, all of whom are busy people but devoted much time to carefully preparing their chapters.

Stanford, April 2007 Thomas D. Rossing

Amazon EX1014 Page 7

List of Authors

Iskander Akhatov
North Dakota State University
Center for Nanoscale Science and Engineering,
Department of Mechanical Engineering
111 Dolve Hall
Fargo, ND 58105-5285, USA
e-mail: *iskander.akhatov@ndsu.edu*

Yoichi Ando
3917-680 Takachiho
899-6603 Makizono, Kirishima, Japan
e-mail: *andoy@cameo.plala.or.jp*

Keith Attenborough
The University of Hull
Department of Engineering
Cottingham Road
Hull, HU6 7RX, UK
e-mail: *k.attenborough@hull.ac.uk*

Whitlow W. L. Au
Hawaii Institute of Marine Biology
P.O. Box 1106
Kailua, HI 96734, USA
e-mail: *wau@hawaii.edu*

Kirk W. Beach
University of Washington
Department of Surgery
Seattle, WA 98195, USA
e-mail: *kwbeach@u.washington.edu*

Mack A. Breazeale
University of Mississippi
National Center for Physical Acoustics
027 NCPA Bldg.
University, MS 38677, USA
e-mail: *breazeal@olemiss.edu*

Antoine Chaigne
Unité de Mécanique (UME)
Ecole Nationale Supérieure de Techniques
Avancées (ENSTA)
Chemin de la Hunière
91761 Palaiseau, France
e-mail: *antoine.chaigne@ensta.fr*

Perry R. Cook
Princeton University
Department of Computer Science
35 Olden Street
Princeton, NJ 08540, USA
e-mail: *prc@cs.princeton.edu*

James Cowan
Resource Systems Group Inc.
White River Junction, VT 85001, USA
e-mail: *jcowan@rsginc.com*

Mark F. Davis
Dolby Laboratories
100 Potrero Ave,
San Francisco, CA 94103, USA
e-mail: *mfd@dolby.com*

Barbrina Dunmire
University of Washington
Applied Physics Laboratory
1013 NE 40th Str.
Seattle, WA 98105, USA
e-mail: *mrbean@u.washington.edu*

Neville H. Fletcher
Australian National University
Research School of Physical Sciences and
Engineering
Canberra, ACT 0200, Australia
e-mail: *neville.fletcher@anu.edu.au*

Anders Christian Gade
Technical University of Denmark
Acoustic Technology, Oersted.DTU
Building 352
2800 Lyngby, Denmark
e-mail: *acg@oersted.dtu.dk*,
anders.gade@get2net.dk

Colin Gough
University of Birmingham
School of Physics and Astronomy
Birmingham, B15 2TT, UK
e-mail: *c.gough@bham.ac.uk*

Amazon EX1014 Page 8

William M. Hartmann
Michigan State University
1226 BPS Building
East Lansing, MI 48824, USA
e-mail: *hartmann@pa.msu.edu*

Finn Jacobsen
Ørsted DTU, Technical University of Denmark
Acoustic Technology
Ørsteds Plads, Building 352
2800 Lyngby, Denmark
e-mail: *fja@oersted.dtu.dk*

Yang-Hann Kim
Korea Advanced Institute of Science
and Technology (KAIST)
Department of Mechanical Engineering
Center for Noise and Vibration Control (NOVIC)
Acoustics and Vibration Laboratory
373-1 Kusong-dong, Yusong-gu
Daejeon, 305-701, Korea
e-mail: *yanghannkim@kaist.ac.kr*

William A. Kuperman
University of California at San Diego
Scripps Institution of Oceanography
9500 Gilman Drive
La Jolla, CA 92093-0701, USA
e-mail: *wkuperman@ucsd.edu*

Thomas Kurz
Universität Göttingen
Friedrich-Hund-Platz 1
37077 Göttingen, Germany
e-mail: *t.kurz@dpi.physik.uni-goettingen.de*

Marc O. Lammers
Hawaii Institute of Marine Biology
P.O. Box 1106
Kailua, HI 96734, USA
e-mail: *lammers@hawaii.edu*

Werner Lauterborn
Universität Göttingen
Drittes Physikalisches Institut
Friedrich-Hund-Platz 1
37077 Göttingen, Germany
e-mail:
w.lauterborn@dpi.physik.uni-goettingen.de

Björn Lindblom
Stockholm University
Department of Linguistics
10691 Stockholm, Sweden
e-mail: *lindblom@ling.su.se*,
blindblom@mail.utexas.edu

George C. Maling, Jr.
Institute of Noise Control Engineering of the USA
60 High Head Road
Harpswell, ME 04079, USA
e-mail: *maling@alum.mit.edu*

Michael McPherson
The University of Mississippi
Department of Physics and Astronomy
123 Lewis Hall
P. O. Box 1848
University, MS 38677, USA
e-mail: *mcph@phy.olemiss.edu*

Nils-Erik Molin
Luleå University of Technology
Experimental Mechanics
SE-971 87 Luleå, Sweden
e-mail: *nem@ltu.se*

Brian C. J. Moore
University of Cambridge
Department of Experimental Psychology
Downing Street
Cambridge, CB2 3EB, UK
e-mail: *bcjm@cam.ac.uk*

Alan D. Pierce
Boston University
College of Engineering
Boston, MA , USA
e-mail: *adp@bu.edu*

Thomas D. Rossing
Stanford University
Center for Computer Research in Music and
Acoustics (CCRMA)
Department of Music
Stanford, CA 94305, USA
e-mail: *rossing@ccrma.stanford.edu*

Amazon EX1014 Page 9

Philippe Roux
Université Joseph Fourier
Laboratoire de Geophysique Interne et Tectonophysique
38041 Grenoble, France
e-mail: *philippe.roux@obs.ujf-grenoble.fr*

Johan Sundberg
KTH–Royal Institute of Technology
Department of Speech, Music, and Hearing
SE-10044 Stockholm, Sweden
e-mail: *pjohan@speech.kth.se*

Gregory W. Swift
Los Alamos National Laboratory
Condensed Matter and Thermal Physics Group
Los Alamos, NM 87545, USA
e-mail: *swift@lanl.gov*

George S. K. Wong
Institute for National Measurement Standards (INMS)
National Research Council Canada (NRC)
1200 Montreal Road
Ottawa, ON K1A 0R6, Canada
e-mail: *George.Wong@nrc-cnrc.gc.ca*

Eric D. Young
Johns Hopkins University
Baltimore, MD 21205, USA
e-mail: *eyoung@jhu.edu*

Amazon EX1014 Page 10

Contents

List of Abbreviations XXI

1 **Introduction to Acoustics**
Thomas D. Rossing 1
1.1 Acoustics: The Science of Sound 1
1.2 Sounds We Hear 1
1.3 Sounds We Cannot Hear: Ultrasound and Infrasound 2
1.4 Sounds We Would Rather Not Hear: Environmental Noise Control 2
1.5 Aesthetic Sound: Music 3
1.6 Sound of the Human Voice: Speech and Singing 3
1.7 How We Hear: Physiological and Psychological Acoustics 4
1.8 Architectural Acoustics 4
1.9 Harnessing Sound: Physical and Engineering Acoustics 5
1.10 Medical Acoustics 5
1.11 Sounds of the Sea 6
References 6

Part A Propagation of Sound

2 **A Brief History of Acoustics**
Thomas D. Rossing 9
2.1 Acoustics in Ancient Times 9
2.2 Early Experiments on Vibrating Strings, Membranes and Plates 10
2.3 Speed of Sound in Air 10
2.4 Speed of Sound in Liquids and Solids 11
2.5 Determining Frequency 11
2.6 Acoustics in the 19th Century 12
2.7 The 20th Century 15
2.8 Conclusion 23
References 23

3 **Basic Linear Acoustics**
Alan D. Pierce 25
3.1 Introduction 27
3.2 Equations of Continuum Mechanics 28
3.3 Equations of Linear Acoustics 35
3.4 Variational Formulations 40
3.5 Waves of Constant Frequency 45
3.6 Plane Waves 47

Amazon EX1014 Page 11

3.7 Attenuation of Sound 49
3.8 Acoustic Intensity and Power 58
3.9 Impedance 60
3.10 Reflection and Transmission 61
3.11 Spherical Waves 65
3.12 Cylindrical Waves 75
3.13 Simple Sources of Sound 82
3.14 Integral Equations in Acoustics 87
3.15 Waveguides, Ducts, and Resonators 89
3.16 Ray Acoustics 94
3.17 Diffraction 98
3.18 Parabolic Equation Methods 107
References 108

4 **Sound Propagation in the Atmosphere**
Keith Attenborough 113
4.1 A Short History of Outdoor Acoustics 113
4.2 Applications of Outdoor Acoustics 114
4.3 Spreading Losses 115
4.4 Atmospheric Absorption 116
4.5 Diffraction and Barriers 116
4.6 Ground Effects 120
4.7 Attenuation Through Trees and Foliage 129
4.8 Wind and Temperature Gradient Effects on Outdoor Sound 131
4.9 Concluding Remarks 142
References 143

5 **Underwater Acoustics**
William A. Kuperman, Philippe Roux 149
5.1 Ocean Acoustic Environment 151
5.2 Physical Mechanisms 155
5.3 SONAR and the SONAR Equation 165
5.4 Sound Propagation Models 167
5.5 Quantitative Description of Propagation 177
5.6 SONAR Array Processing 179
5.7 Active SONAR Processing 185
5.8 Acoustics and Marine Animals 195
5.A Appendix: Units 201
References 201

Part B Physical and Nonlinear Acoustics

6 **Physical Acoustics**
Mack A. Breazeale, Michael McPherson 207
6.1 Theoretical Overview 209
6.2 Applications of Physical Acoustics 219

6.3 Apparatus 226
6.4 Surface Acoustic Waves 231
6.5 Nonlinear Acoustics 234
References 237

7 **Thermoacoustics**
Gregory W. Swift 239
7.1 History 239
7.2 Shared Concepts 240
7.3 Engines 244
7.4 Dissipation 249
7.5 Refrigeration 250
7.6 Mixture Separation 253
References 254

8 **Nonlinear Acoustics in Fluids**
Werner Lauterborn, Thomas Kurz, Iskander Akhatov 257
8.1 Origin of Nonlinearity 258
8.2 Equation of State 259
8.3 The Nonlinearity Parameter *B/A* 260
8.4 The Coefficient of Nonlinearity β 262
8.5 Simple Nonlinear Waves 263
8.6 Lossless Finite-Amplitude Acoustic Waves 264
8.7 Thermoviscous Finite-Amplitude Acoustic Waves 268
8.8 Shock Waves 271
8.9 Interaction of Nonlinear Waves 273
8.10 Bubbly Liquids 275
8.11 Sonoluminescence 286
8.12 Acoustic Chaos 289
References 293

Part C Architectural Acoustics

9 **Acoustics in Halls for Speech and Music**
Anders Christian Gade 301
9.1 Room Acoustic Concepts 302
9.2 Subjective Room Acoustics 303
9.3 Subjective and Objective Room Acoustic Parameters 306
9.4 Measurement of Objective Parameters 314
9.5 Prediction of Room Acoustic Parameters 316
9.6 Geometric Design Considerations 323
9.7 Room Acoustic Design of Auditoria for Specific Purposes 334
9.8 Sound Systems for Auditoria 346
References 349

10 **Concert Hall Acoustics Based on Subjective Preference Theory**
Yoichi Ando 351
10.1 Theory of Subjective Preference for the Sound Field 353
10.2 Design Studies 361
10.3 Individual Preferences of a Listener and a Performer 370
10.4 Acoustical Measurements of the Sound Fields in Rooms 377
References 384

11 **Building Acoustics**
James Cowan 387
11.1 Room Acoustics 387
11.2 General Noise Reduction Methods 400
11.3 Noise Ratings for Steady Background Sound Levels 403
11.4 Noise Sources in Buildings 405
11.5 Noise Control Methods for Building Systems 407
11.6 Acoustical Privacy in Buildings 419
11.7 Relevant Standards 424
References 425

Part D Hearing and Signal Processing

12 **Physiological Acoustics**
Eric D. Young 429
12.1 The External and Middle Ear 429
12.2 Cochlea 434
12.3 Auditory Nerve and Central Nervous System 449
12.4 Summary 452
References 453

13 **Psychoacoustics**
Brian C. J. Moore 459
13.1 Absolute Thresholds 460
13.2 Frequency Selectivity and Masking 461
13.3 Loudness 468
13.4 Temporal Processing in the Auditory System 473
13.5 Pitch Perception 477
13.6 Timbre Perception 483
13.7 The Localization of Sounds 484
13.8 Auditory Scene Analysis 485
13.9 Further Reading and Supplementary Materials 494
References 495

14 **Acoustic Signal Processing**
William M. Hartmann 503
14.1 Definitions 504
14.2 Fourier Series 505

Amazon EX1014 Page 14

14.3 Fourier Transform 507
14.4 Power, Energy, and Power Spectrum 510
14.5 Statistics 511
14.6 Hilbert Transform and the Envelope 514
14.7 Filters 515
14.8 The Cepstrum 517
14.9 Noise 518
14.10 Sampled data 520
14.11 Discrete Fourier Transform 522
14.12 The *z*-Transform 524
14.13 Maximum Length Sequences 526
14.14 Information Theory 528
References 530

Part E Music, Speech, Electroacoustics

15 **Musical Acoustics**
Colin Gough 533
15.1 Vibrational Modes of Instruments 535
15.2 Stringed Instruments 554
15.3 Wind Instruments 601
15.4 Percussion Instruments 641
References 661

16 **The Human Voice in Speech and Singing**
Björn Lindblom, Johan Sundberg 669
16.1 Breathing 669
16.2 The Glottal Sound Source 676
16.3 The Vocal Tract Filter 682
16.4 Articulatory Processes, Vowels and Consonants 687
16.5 The Syllable 695
16.6 Rhythm and Timing 699
16.7 Prosody and Speech Dynamics 701
16.8 Control of Sound in Speech and Singing 703
16.9 The Expressive Power of the Human Voice 706
References 706

17 **Computer Music**
Perry R. Cook 713
17.1 Computer Audio Basics 714
17.2 Pulse Code Modulation Synthesis 717
17.3 Additive (Fourier, Sinusoidal) Synthesis 719
17.4 Modal (Damped Sinusoidal) Synthesis 722
17.5 Subtractive (Source-Filter) Synthesis 724
17.6 Frequency Modulation (FM) Synthesis 727
17.7 FOFs, Wavelets, and Grains 728

Amazon EX1014 Page 15

17.8 Physical Modeling (The Wave Equation) 730
17.9 Music Description and Control 735
17.10 Composition 737
17.11 Controllers and Performance Systems 737
17.12 Music Understanding and Modeling by Computer 738
17.13 Conclusions, and the Future 740
References 740

18 **Audio and Electroacoustics**
Mark F. Davis 743
18.1 Historical Review 744
18.2 The Psychoacoustics of Audio and Electroacoustics 747
18.3 Audio Specifications 751
18.4 Audio Components 757
18.5 Digital Audio 768
18.6 Complete Audio Systems 775
18.7 Appraisal and Speculation 778
References 778

Part F Biological and Medical Acoustics

19 **Animal Bioacoustics**
Neville H. Fletcher 785
19.1 Optimized Communication 785
19.2 Hearing and Sound Production 787
19.3 Vibrational Communication 788
19.4 Insects 788
19.5 Land Vertebrates 790
19.6 Birds 795
19.7 Bats 796
19.8 Aquatic Animals 797
19.9 Generalities 799
19.10 Quantitative System Analysis 799
References 802

20 **Cetacean Acoustics**
Whitlow W. L. Au, Marc O. Lammers 805
20.1 Hearing in Cetaceans 806
20.2 Echolocation Signals 813
20.3 Odontocete Acoustic Communication 821
20.4 Acoustic Signals of Mysticetes 827
20.5 Discussion 830
References 831

21 **Medical Acoustics**
Kirk W. Beach, Barbrina Dunmire 839
21.1 Introduction to Medical Acoustics 841

Amazon EX1014 Page 16

21.2 Medical Diagnosis; Physical Examination 842
21.3 Basic Physics of Ultrasound Propagation in Tissue 848
21.4 Methods of Medical Ultrasound Examination 857
21.5 Medical Contrast Agents 882
21.6 Ultrasound Hyperthermia in Physical Therapy 889
21.7 High-Intensity Focused Ultrasound (HIFU) in Surgery 890
21.8 Lithotripsy of Kidney Stones 891
21.9 Thrombolysis 892
21.10 Lower-Frequency Therapies 892
21.11 Ultrasound Safety 892
References 895

Part G Structural Acoustics and Noise

22 Structural Acoustics and Vibrations

Antoine Chaigne 901
22.1 Dynamics of the Linear Single-Degree-of-Freedom (1-DOF) Oscillator 903
22.2 Discrete Systems 907
22.3 Strings and Membranes 913
22.4 Bars, Plates and Shells 920
22.5 Structural–Acoustic Coupling 926
22.6 Damping 940
22.7 Nonlinear Vibrations 947
22.8 Conclusion. Advanced Topics 957
References 958

23 Noise

George C. Maling, Jr. 961
23.1 Instruments for Noise Measurements 965
23.2 Noise Sources 970
23.3 Propagation Paths 991
23.4 Noise and the Receiver 999
23.5 Regulations and Policy for Noise Control 1006
23.6 Other Information Resources 1010
References 1010

Part H Engineering Acoustics

24 Microphones and Their Calibration

George S. K. Wong 1021
24.1 Historic References on Condenser Microphones and Calibration 1024
24.2 Theory 1024
24.3 Reciprocity Pressure Calibration 1026
24.4 Corrections 1029

Amazon EX1014 Page 17

24.5 Free-Field Microphone Calibration 1039
24.6 Comparison Methods for Microphone Calibration 1039
24.7 Frequency Response Measurement with Electrostatic Actuators 1043
24.8 Overall View on Microphone Calibration 1043
24.A Acoustic Transfer Impedance Evaluation 1045
24.B Physical Properties of Air 1045
References 1048

25 **Sound Intensity**
Finn Jacobsen 1053
25.1 Conservation of Sound Energy 1054
25.2 Active and Reactive Sound Fields 1055
25.3 Measurement of Sound Intensity 1058
25.4 Applications of Sound Intensity 1068
References 1072

26 **Acoustic Holography**
Yang-Hann Kim 1077
26.1 The Methodology of Acoustic Source Identification 1077
26.2 Acoustic Holography: Measurement, Prediction and Analysis 1079
26.3 Summary 1092
26.A Mathematical Derivations of Three Acoustic Holography Methods and Their Discrete Forms 1092
References 1095

27 **Optical Methods for Acoustics and Vibration Measurements**
Nils-Erik Molin 1101
27.1 Introduction 1101
27.2 Measurement Principles and Some Applications 1105
27.3 Summary 1122
References 1123

28 **Modal Analysis**
Thomas D. Rossing 1127
28.1 Modes of Vibration 1127
28.2 Experimental Modal Testing 1128
28.3 Mathematical Modal Analysis 1133
28.4 Sound-Field Analysis 1136
28.5 Holographic Modal Analysis 1137
References 1138

Acknowledgements 1139
About the Authors 1141
Detailed Contents 1147
Subject Index 1167

Amazon EX1014 Page 18

List of Abbreviations

A

ABR	auditory brainstem responses
AC	articulation class
ACF	autocorrelation function
ADC	analog-to-digital converter
ADCP	acoustic Doppler current profiler
ADP	ammonium dihydrogen phosphate
AM	amplitude modulated
AMD	air moving device
AN	auditory nerve
ANSI	American National Standards Institute
AR	assisted resonance
ASW	apparent source width
AUV	automated underwater vehicle

B

BB	bite block
BEM	boundary-element method
BER	bit error rate
BF	best frequency
BR	bass ratio

C

CAATI	computed angle-of-arrival transient imaging
CAC	ceiling attenuation class
CCD	charge-coupled device
CDF	cumulative distribution function
CMU	concrete masonry unit
CN	cochlear nucleus
CND	cumulative normal distribution
CSDM	cross-spectral-density matrix

D

DAC	digital-to-analog converter
DL	difference limen
DOF	degree of freedom
DRS	directed reflection sequence
DSL	deep scattering layer
DSP	digital speckle photography
DSP	digital signal processing
DSPI	digital speckle-pattern interferometry

E

EARP	equal-amplitude random-phase
EDT	early decay time
EDV	end diastolic velocity
EEG	electroencephalography
EOF	empirical orthogonal function
EOH	electro-optic holography
ERB	equivalent rectangular bandwidth
ESPI	electronic speckle-pattern interferometry

F

FCC	Federal Communications Commission
FEA	finite-element analysis
FEM	finite-element method
FERC	Federal Energy Regulatory Commission
FFP	fast field program
FFT	fast Fourier transform
FIR	finite impulse response
FM	frequency modulated
FMDL	frequency modulation detection limen
FOM	figure of merit
FRF	frequency response function
FSK	frequency shift keying

G

GA	genetic algorithm

H

HVAC	heating, ventilating and air conditioning

I

IACC	interaural cross-correlation coefficient
IACF	interaural cross-correlation function
IAD	interaural amplitude difference
ICAO	International Civil Aircraft Organization
IF	intermediate frequency
IFFT	inverse fast Fourier transform
IHC	inner hair cells
IIR	infinite impulse response
IM	intermodulation
IRF	impulse response function
ISI	intersymbol interference
ITD	interaural time difference
ITDG	initial time delay gap

J

JND	just noticeable difference

Amazon EX1014 Page 19

K

KDP	potassium dihydrogen phosphate

L

LDA	laser Doppler anemometry
LDV	laser Doppler vibrometry
LEF	lateral energy fraction
LEV	listener envelopment
LL	listening level
LOC	lateral olivocochlear system
LP	long-play vinyl record
LTAS	long-term-average spectra

M

MAA	minimum audible angle
MAF	minimum audible field
MAP	minimum audible pressure
MCR	multichannel reverberation
MDOF	multiple degree of freedom
MEG	magnetoencephalogram
MEMS	microelectromechanical system
MFDR	maximum flow declination rate
MFP	matched field processing
MIMO	multiple-input multiple-output
MLM	maximum-likelihood method
MLS	maximum length sequence
MOC	medial olivocochlear system
MRA	main response axis
MRI	magnetic resonance imaging
MTF	modulation transfer function
MTS	multichannel television sound
MV	minimum variance

N

NDT	nondestructive testing
NMI	National Metrology Institute
NRC	noise reduction coefficient

O

OAE	otoacoustic emission
ODS	operating deflexion shape
OHC	outer hair cells
OITC	outdoor–indoor transmission class
OR	or operation
OSHA	Occupational Safety and Health Administration

P

PC	phase conjugation
PCM	pulse code modulation
PD	probability of detection
PDF	probability density function
PE	parabolic equation
PFA	probability of false alarm
PIV	particle image velocimetry
PL	propagation loss
PLIF	planar laser-induced fluorescent
PM	phase modulation
PMF	probability mass function
PS	phase stepping
PS	peak systolic
PSD	power spectral density
PSK	phase shift keying
PTC	psychophysical tuning curve
PVDF	polyvinylidene fluoride
PZT	lead zirconate titanate

Q

QAM	quadrature amplitude modulation

R

RASTI	rapid speech transmission index
REL	resting expiratory level
RF	radio frequency
RIAA	Recording Industry Association of America
RMS	root-mean-square
ROC	receiving operating characteristic
RUS	resonant ultrasound spectroscopy

S

s.c.	supporting cells
S/N	signal-to-noise
SAA	sound absorption average
SAC	spatial audio coding
SAW	surface acoustic wave
SBSL	single-bubble sonoluminescence
SDOF	single degree of freedom
SE	signal excess
SEA	statistical energy analysis
SG	spiral ganglion
SI	speckle interferometry
SIL	speech interference level
SIL	sound intensity level
SISO	single-input single-output
SL	sensation level
SM	scala media
SNR	signal-to-noise ratio
SOC	superior olivary complex
SP	speckle photography
SPL	sound pressure level
SR	spontaneous discharge rate
ST	scala tympani

Amazon EX1014 Page 20

STC	sound transmission class
STI	speech transmission index
SV	scala vestibuli
SVR	slow vertex response

T

TDAC	time-domain alias cancellation
TDGF	time-domain Green's function
THD	total harmonic distortion
TL	transmission loss
TLC	total lung capacity
TMTF	temporal modulation transfer function
TNM	traffic noise model
TR	treble ratio
TR	time reversal
TTS	temporary threshold shift
TVG	time-varied gain

U

UMM	unit modal mass

V

VBR	variable bitrate
VC	vital capacity

W

WS	working standard

X

XOR	exclusive or

1. Introduction to Acoustics

This brief introduction may help to persuade the reader that acoustics covers a wide range of interesting topics. It is impossible to cover all these topics in a single handbook, but we have attempted to include a sampling of hot topics that represent current acoustical research, both fundamental and applied.

Acoustics is the science of sound. It deals with the production of sound, the propagation of sound from the source to the receiver, and the detection and perception of sound. The word *sound* is often used to describe two different things: an auditory sensation in the ear, and the disturbance in a medium that can cause this sensation. By making this distinction, the age-old question "If a tree falls in a forest and no one is there to hear it, does it make a sound?" can be answered.

1.1 Acoustics: The Science of Sound 1
1.2 Sounds We Hear 1
1.3 Sounds We Cannot Hear: Ultrasound and Infrasound 2
1.4 Sounds We Would Rather Not Hear: Environmental Noise Control 2
1.5 Aesthetic Sound: Music 3
1.6 Sound of the Human Voice: Speech and Singing 3
1.7 How We Hear: Physiological and Psychological Acoustics 4
1.8 Architectural Acoustics 4
1.9 Harnessing Sound: Physical and Engineering Acoustics 5
1.10 Medical Acoustics 5
1.11 Sounds of the Sea 6
References 6

1.1 Acoustics: The Science of Sound

Acoustics has become a broad interdisciplinary field encompassing the academic disciplines of physics, engineering, psychology, speech, audiology, music, architecture, physiology, neuroscience, and others. Among the branches of acoustics are architectural acoustics, physical acoustics, musical acoustics, psychoacoustics, electroacoustics, noise control, shock and vibration, underwater acoustics, speech, physiological acoustics, etc.

Sound can be produced by a number of different processes, which include the following.

Vibrating bodies: when a drumhead or a noisy machine vibrates, it displaces air and causes the local air pressure to fluctuate.

Changing airflow: when we speak or sing, our vocal folds open and close to let through puffs of air. In a siren, holes on a rapidly rotating plate alternately pass and block air, resulting in a loud sound.

Time-dependent heat sources: an electrical spark produces a crackle; an explosion produces a bang due to the expansion of air caused by rapid heating. Thunder results from rapid heating by a bolt of lightning.

Supersonic flow: shock waves result when a supersonic airplane or a speeding bullet forces air to flow faster than the speed of sound.

1.2 Sounds We Hear

The range of sound intensity and the range of frequency to which the human auditory system responds is quite remarkable. The intensity ratio between the sounds that bring pain to our ears and the weakest sounds we can hear is more than 10^{12}. The frequency ratio between the highest and lowest frequencies we

Amazon EX1014 Page 22

can hear is nearly 10^3, or more than nine octaves (each octave representing a doubling of frequency). Human vision is also quite remarkable, but the frequency range does not begin to compare to that of human hearing. The frequency range of vision is a little less than one octave (about $4\times10^{14}-7\times10^{14}$ Hz). Within this one octave range we can identify more than 7 million colors. Given that the frequency range of the ear is nine times greater, one can imagine how many sound *colors* might be possible.

Humans and other animals use sound to communicate, and so it is not surprising that human hearing is most sensitive over the frequency range covered by human speech. This is no doubt a logical outcome of natural selection. This same match is found throughout much of the animal kingdom. Simple observations show that small animals generally use high frequencies for communication while large animals use low frequencies. In Chap. 19, it is shown that song frequency f scales with animal mass M roughly as $f \propto M^{-1/3}$.

The least amount of sound energy we can hear is of the order of 10^{-20} J (cf. sensitivity of the eye: about one quantum of light in the middle of the visible spectrum $\approx 4\times10^{-19}$ J). The upper limit of the sound pressure that can be generated is set approximately by atmospheric pressure. Such an ultimate sound wave would have a sound pressure level of about 191 dB. In practice, of course, nonlinear effects set in well below this level and limit the maximum pressure. A large-amplitude sound wave will change waveform and finally break into a shock, approaching a sawtooth waveform. Nonlinear effects are discussed in Chap. 8.

1.3 Sounds We Cannot Hear: Ultrasound and Infrasound

Sound waves below the frequency of human hearing are called *infrasound*, while sound waves with frequency above the range of human hearing are called *ultrasound*. These sounds have many interesting properties, and are being widely studied. Ultrasound is very important in medical and industrial imaging. It also forms the basis of a growing number of medical procedures, both diagnostic and therapeutic (see Chap. 21). Ultrasound has many applications in scientific research, especially in the study of solids and fluids (see Chap. 6).

Frequencies as high as 500 MHz have been generated, with a wavelength of about 0.6 μm in air. This is on the order of the wavelength of light and within an order of magnitude of the mean free path of air molecules. A gas ceases to behave like a continuum when the wavelength of sound becomes of the order of the mean free path, and this sets an upper limit on the frequency of sound that can propagate. In solids the assumption of continuum extends down to the intermolecular spacing of approximately 0.1 nm, with a limiting frequency of about 10^{12} Hz. The ultimate limit is actually reached when the wavelength is twice the spacing of the unit cell of a crystal, where the propagation of multiply scattered sound resembles the diffusion of heat [1.1].

Natural phenomena are prodigious generators of infrasound. When Krakatoa exploded, windows were shattered hundreds of miles away by the infrasonic wave. The ringing of both the Earth and the atmosphere continued for hours. The sudden shock wave of an explosion propels a complex infrasonic signal far beyond the shattered perimeter. Earthquakes generate intense infrasonic waves. The faster moving P (primary) waves arrive at distant locations tens of seconds before the destructive S (secondary) waves. (The P waves carry information; the S waves carry energy.) Certain animals and fish can sense these infrasonic precursors and react with fear and anxiety.

A growing amount of astronomical evidence indicates that primordial sound waves at exceedingly low frequency propagated in the universe during its first 380 000 years while it was a plasma of charged particles and thus opaque to electromagnetic radiation. Sound is therefore older than light.

1.4 Sounds We Would Rather Not Hear: Environmental Noise Control

Noise has been receiving increasing recognition as one of our critical environmental pollution problems. Like air and water pollution, noise pollution increases with population density; in our urban areas, it is a serious threat to our quality of life. Noise-induced hearing loss is a major health problem for millions of people employed in noisy environments. Besides actual hearing loss, humans are affected in many other ways by high levels of noise. Interference with speech, interruption of sleep, and other physiological and psychological effects

of noise have been the subject of considerable study. Noise control is discussed in Chap. 23. The propagation of sound in air in Chap. 4, and building acoustics is the subject of Chap. 11.

Fortunately for the environment, even the noisiest machines convert only a small part of their total energy into sound. A jet aircraft, for example, may produce a kilowatt of acoustic power, but this is less than 0.02% of its mechanical output. Automobiles emit approximately 0.001% of their power as sound. Nevertheless, the shear number of machines operating in our society makes it crucial that we minimize their sound output and take measures to prevent the sound from propagating throughout our environment. Although reducing the emitted noise is best done at the source, it is possible, to some extent, to block the transmission of this noise from the source to the receiver. Reduction of classroom noise, which impedes learning in so many schools, is receiving increased attention from government officials as well as from acousticians [1.2].

1.5 Aesthetic Sound: Music

Music may be defined as an art form using sequences and clusters of sounds. Music is carried to the listener by sound waves. The science of musical sound is often called musical acoustics and is discussed in Chap. 15.

Musical acoustics deals with the production of sound by musical instruments, the transmission of music from the performer to the listener, and the perception and cognition of sound by the listener. Understanding the production of sound by musical instruments requires understanding how they vibrate and how they radiate sound. Transmission of sound from the performer to the listener involves a study of concert hall acoustics (covered in Chaps. 9 and 10) and the recording and reproduction of musical sound (covered in Chap. 15). Perception of musical sound is based on psychoacoustics, which is discussed in Chap. 13.

Electronic musical instruments have become increasingly important in contemporary music. Computers have made possible artificial musical intelligence, the synthesis of new musical sounds and the accurate and flexible re-creation of traditional musical sounds by artificial means. Not only do computers talk and sing and play music, they listen to us doing the same, and our interactions with computers are becoming more like our interactions with each other. Electronic and computer music is discussed in Chap. 17.

1.6 Sound of the Human Voice: Speech and Singing

It is difficult to overstate the importance of the human voice. Of all the members of the animal kingdom, we alone have the power of articulate speech. Speech is our chief means of communication. In addition, the human voice is our oldest musical instrument. Speech and singing, the closely related functions of the human voice, are discussed in a unified way in Chap. 16.

In the simplest model of speech production, the vocal folds act as the source and the vocal tract as a filter of the source sound. According to this model, the spectrum envelope of speech sound can be thought of as the product of two components:

Speech sound = source spectrum × filter function.

The nearly triangular waveform of the air flow from the glottis has a spectrum of harmonics that diminish in amplitude roughly as $1/n^2$ (i. e., at a rate of $-12\,\mathrm{dB/octave}$). The formants or resonances of the vocal tract create the various vowel sounds. The vocal tract can be shaped by movements of the tongue, the lips, and the soft palate to tune the formants and articulate the various speech sounds.

Sung vowels are fundamentally the same as spoken vowels, although singers do make vowel modifications in order to improve the musical tone, especially in their high range. In order to produce tones over a wide range of pitch, singers use muscular action in the larynx, which leads to different registers.

Much research has been directed at computer recognition and synthesis of speech. Goals of such research include voice-controlled word processors, voice control of computers and other machines, data entry by voice, etc.In general it is more difficult for a computer to understand language than to speak it.

1.7 How We Hear: Physiological and Psychological Acoustics

The human auditory system is complex in structure and remarkable in function. Not only does it respond to a wide range of stimuli, but it precisely identifies the pitch, timbre, and direction of a sound. Some of the hearing function is done in the organ we call the ear; some of it is done in the central nervous system as well.

Physiological acoustics, which is discussed in Chap. 12, focuses its attention mainly on the peripheral auditory system, especially the cochlea. The dynamic behavior of the cochlea is a subject of great interest. It is now known that the maximum response along the basilar membrane of the cochlea has a sharper peak in a living ear than in a dead one.

Resting on the basilar membrane is the delicate and complex organ of Corti, which contains several rows of hair cells to which are attached auditory nerve fibers. The inner hair cells are mainly responsible for transmitting signals to the auditory nerve fibers, while the more-numerous outer hair cells act as biological amplifiers. It is estimated that the outer hair cells add about 40 dB of amplification to very weak signals, so that hearing sensitivity decreases by a considerable amount when these delicate cells are destroyed by overexposure to noise.

Our knowledge of the cochlea has now progressed to a point where it is possible to construct and implant electronic devices in the cochlea that stimulate the auditory nerve. A cochlear implant is an electronic device that restores partial hearing in many deaf people [1.3]. It is surgically implanted in the inner ear and activated by a device worn outside the ear. An implant has four basic parts: a microphone, a speech processor and transmitter, a receiver inside the ear, and electrodes that transmit impulses to the auditory nerve and thence to the brain.

Psychoacoustics (psychological acoustics), the subject of Chap. 13, deals with the relationships between the physical characteristics of sounds and their perceptual attributes, such as loudness, pitch, and timbre.

The threshold of hearing depends upon frequency, the lowest being around 3–4 kHz, where the ear canal has a resonance, and rising considerably at low frequency. Temporal resolution, such as the ability to detect brief gaps between stimuli or to detect modulation of a sound, is a subject of considerable interest, as is the ability to localize the sound source. Sound localization depends upon detecting differences in arrival time and differences in intensity at our two ears, as well as spectral cues that help us to localize a source in the median plane.

Most sound that reaches our ears comes from several different sources. The extent to which we can perceive each source separately is sometimes called segregation. One important cue for perceptual separation of nearly simultaneous sounds is onset and offset disparity. Another is spectrum change with time. When we listen to rapid sequence of sounds, they may be grouped together (fusion) or they may be perceived as different streams (fission). It is difficult to judge the temporal order of sounds that are perceived in different streams.

1.8 Architectural Acoustics

To many lay people, an acoustician is a person who designs concert halls. That is an important part of architectural acoustics, to be sure, but this field incorporates much more. Architectural acousticians seek to understand and to optimize the sound environment in rooms and buildings of all types, including those used for work, residential living, education, and leisure. In fact, some of the earliest attempts to optimize sound transmission were practised in the design of ancient amphitheaters, and the acoustical design of outdoor spaces for concerts and drama still challenge architects.

In a room, most of the sound waves that reach the listener's ear have been reflected by one or more surfaces of the room or by objects in the room. In a typical room, sound waves undergo dozens of reflections before they become inaudible. It is not surprising, therefore, that the acoustical properties of rooms play an important role in determining the nature of the sound heard by a listener. Minimizing extraneous noise is an important part of the acoustical design of rooms and buildings of all kinds. Chapter 9 presents the principles of room acoustics and applies them to performance and assembly halls, including theaters and lecture halls, opera halls, concert halls, worship halls, and auditoria.

The subject of concert hall acoustics is almost certain to provoke a lively discussion by both performers and serious listeners. Musicians recognize the importance of the concert hall in communication between performer and listener. Opinions of new halls tend to polarize toward extremes of very good or very bad. In considering concert and opera halls, it is important to seek a common language for musicians and acousticians

in order to understand how objective measurements relate to subjective qualities [1.4, 5]. Chapter 10 discusses subjective preference theory and how it relates to concert hall design.

Two acoustical concerns in buildings are providing the occupants with privacy and with a quiet environment, which means dealing with noise sources within the building as well as noise transmitted from outside. The most common noise sources in buildings, other than the inhabitants, are related to heating, ventilating, and air conditioning (HVAC) systems, plumbing systems, and electrical systems. Quieting can best be done at the source, but transmission of noise throughout the building must also be prevented. The most common external noise sources that affect buildings are those associated with transportation, such as motor vehicles, trains, and airplanes. There is no substitute for massive walls, although doors and windows must receive attention as well. Building acoustics is discussed in Chap. 11.

1.9 Harnessing Sound: Physical and Engineering Acoustics

It is sometimes said that physicists study nature, engineers attempt to improve it. Physical acoustics and engineering acoustics are two very important areas of acoustics. Physical acousticians investigate a wide range of scientific phenomena, including the propagation of sound in solids, liquids, and gases, and the way sound interacts with the media through which it propagates. The study of ultrasound and infrasound are especially interesting. Physical acoustics is discussed in Chap. 6.

Acoustic techniques have been widely used to study the structural and thermodynamic properties of materials at very low temperatures. Studying the propagation of ultrasound in metals, dielectric crystals, amorphous solids, and magnetic materials has yielded valuable information about their elastic, structural and other properties. Especially interesting has been the propagation of sound in superfluid helium. Second sound, an unusual type of temperature wave, was discovered in 1944, and since that time so-called third sound, fourth sound, and fifth sound have been described [1.6].

Nonlinear effects in sound are an important part of physical acoustics. Nonlinear effects of interest include waveform distortion, shock-wave formation, interactions of sound with sound, acoustic streaming, cavitation, and acoustic levitation. Nonlinearity leads to distortion of the sinusoidal waveform of a sound wave so that it becomes nearly triangular as the shock wave forms. On the other hand, local disturbances, called *solitons*, retain their shape over large distances.

The study of the interaction of sound and light, called acoustooptics, is an interesting field in physical acoustics that has led to several practical devices. In an acoustooptic modulator, for example, sound waves form a sort of moving optical diffraction grating that diffracts and modulates a laser beam.

Sonoluminescence is the name given to a process by which intense sound waves can generate light. The light is emitted by bubbles in a liquid excited by sound. The observed spectra of emitted light seem to indicate temperatures hotter than the surface of the sun. Some experimental evidence indicates that nuclear fusion may take place in bubbles in deuterated acetone irradiated with intense ultrasound.

Topics of interest in engineering acoustics cover a wide range and include: transducers and arrays, underwater acoustic systems, acoustical instrumentation, audio engineering, acoustical holography and acoustical imaging, ultrasound, and infrasound. Several of these topics are covered in Chaps. 5, 18, 24, 25, 26, 27, and 28. Much effort has been directed into engineering increasingly small transducers to produce and detect sound. Microphones are being fabricated on silicon chips as parts of integrated circuits.

The interaction of sound and heat, called thermoacoustics, is an interesting field that applies principles of physical acoustics to engineering systems. The thermoacoustic effect is the conversion of sound energy to heat or visa versa. In thermoacoustic processes, acoustic power can pump heat from a region of low temperature to a region of higher temperature. This can be used to construct heat engines or refrigerators with no moving parts. Thermoacoustics is discussed in Chap. 7.

1.10 Medical Acoustics

Two uses of sound that physicians have employed for many years are *auscultation*, listening to the body with a stethoscope, and *percussion*, sound generation by the striking the chest or abdomen to assess transmission or

resonance. The most exciting new developments in medical acoustics, however, involve the use of ultrasound, both diagnostic imaging and therapeutic applications.

There has been a steady improvement in the quality of diagnostic ultrasound imaging. Two important commercial developments have been the advent of real-time three-dimensional (3-D) imaging and the development of hand-held scanners. Surgeons can now carry out procedures without requiring optical access. Although measurements on isolated tissue samples show that acoustic attenuation and backscatter correlate with pathology, implementing algorithms to obtain this information on a clinical scanner is challenging at the present time.

The therapeutic use of ultrasound has blossomed in recent years. Shock-wave lithotripsy is the predominant surgical operation for the treatment of kidney stones. Shock waves also appear to be effective at helping heal broken bones. High-intensity focused ultrasound is used to heat tissue selectivity so that cells can be destroyed in a local region. Ultrasonic devices appear to hold promise for treating glaucoma, fighting cancer, and controlling internal bleeding. Advanced therapies, such as puncturing holes in the heart, promoting localized drug delivery, and even carrying out brain surgery through an intact skull appear to be feasible with ultrasound [1.7].

Other applications of medical ultrasound are included in Chap. 21.

1.11 Sounds of the Sea

Oceans cover more than 70% of the Earth's surface. Sound waves are widely used to explore the oceans, because they travel much better in sea water than light waves. Likewise, sound waves are used, by humans and dolphins alike, to communicate under water, because they travel much better than radio waves. Acoustical oceanography has many military, as well as commercial applications. Much of our understanding of underwater sound propagation is a result of research conducted during and following World War II. Underwater acoustics is discussed in Chap. 5.

The speed of sound in water, which is about 1500 m/s, increases with increasing static pressure by about 1 part per million per kilopascal, or about 1% per 1000 m of depth, assuming temperature remains constant. The variation with temperature is an increase of about 2% per °C temperature rise. Refraction of sound, due to these changes in speed, along with reflection at the surface and the bottom, lead to waveguides at various ocean depths. During World War II, a *deep channel* was discovered in which sound waves could travel distances in excess of 3000 km. This phenomenon gave rise to the deep channel or sound fixing and ranging (SOFAR) channel, which could be used to locate, by acoustic means, airmen downed at sea.

One of the most important applications of underwater acoustics is sound navigation and ranging (SONAR). The purpose of most sonar systems is to detect and localize a target, such as submarines, mines, fish, or surface ships. Other SONARs are designed to measure some quantity, such as the ocean depth or the speed of ocean currents.

An interesting phenomenon called cavitation occurs when sound waves of high intensity propagate through water. When the rarefaction tension phase of the sound wave is great enough, the medium ruptures and cavitation bubbles appear. Cavitation bubbles can be produced by the tips of high-speed propellers. Bubbles affect the speed of sound as well as its attenuation [1.7, 8].

References

1.1 U. Ingard: Acoustics. In: *Handbook of Physics*, 2nd edn., ed. by E.U. Condon, H. Odishaw (McGraw-Hill, New York 1967)

1.2 B. Seep, R. Glosemeyer, E. Hulce, M. Linn, P. Aytar, R. Coffeen: *Classroom Acoustics* (Acoustical Society of America, Melville 2000, 2003)

1.3 M.F. Dorman, B.S. Wilson: The design and function of cochlear implants, Am. Scientist **19**, 436–445 (2004)

1.4 L.L. Beranek: *Music, Acoustics and Architecture* (Wiley, New York 1962)

1.5 L. Beranek: *Concert Halls and Opera Houses*, 2nd edn. (Springer, Berlin, Heidelberg, New York 2004)

1.6 G. Williams: Low-temperature acoustics. In: *McGraw-Hill Encyclopedia of Physics*, 2nd edn., ed. by S. Parker (McGraw-Hill, New York 1993)

1.7 R.O. Cleveland: Biomedical ultrasound/bioresponse to vibration. In: *ASA at 75*, ed. by H.E. Bass, W.J. Cavanaugh (Acoustical Society of America, Melville 2004)

1.8 H. Medwin, C.S. Clay: *Fundamentals of Acoustical Oceanography* (Academic, Boston 1998)

Amazon EX1014 Page 27

Part A Propagation

Part A Propagation of Sound

2 A Brief History of Acoustics
Thomas D. Rossing, Stanford, USA

3 Basic Linear Acoustics
Alan D. Pierce, Boston, USA

4 Sound Propagation in the Atmosphere
Keith Attenborough, Hull, UK

5 Underwater Acoustics
William A. Kuperman, La Jolla, USA
Philippe Roux, Grenoble, France

2. A Brief History of Acoustics

Although there are certainly some good historical treatments of acoustics in the literature, it still seems appropriate to begin a handbook of acoustics with a brief history of the subject. We begin by mentioning some important experiments that took place before the 19th century. Acoustics in the 19th century is characterized by describing the work of seven outstanding acousticians: Tyndall, von Helmholtz, Rayleigh, Stokes, Bell, Edison, and Koenig. Of course this sampling omits the mention of many other outstanding investigators.

To represent acoustics during the 20th century, we have selected eight areas of acoustics, again not trying to be all-inclusive. We select the eight areas represented by the first eight technical areas in the Acoustical Society of America. These are architectural acoustics, physical acoustics, engineering acoustics, structural acoustics, underwater acoustics, physiological and psychological acoustics, speech, and musical acoustics. We apologize to readers whose main interest is in another area of acoustics. It is, after all, a broad interdisciplinary field.

2.1 Acoustics in Ancient Times 9
2.2 Early Experiments on Vibrating Strings, Membranes and Plates 10
2.3 Speed of Sound in Air 10
2.4 Speed of Sound in Liquids and Solids 11
2.5 Determining Frequency 11
2.6 Acoustics in the 19th Century 12
2.6.1 Tyndall 12
2.6.2 Helmholtz 12
2.6.3 Rayleigh 13
2.6.4 George Stokes 13
2.6.5 Alexander Graham Bell 14
2.6.6 Thomas Edison 14
2.6.7 Rudolph Koenig 14
2.7 The 20th Century 15
2.7.1 Architectural Acoustics 15
2.7.2 Physical Acoustics 16
2.7.3 Engineering Acoustics 18
2.7.4 Structural Acoustics 19
2.7.5 Underwater Acoustics 19
2.7.6 Physiological and Psychological Acoustics 20
2.7.7 Speech 21
2.7.8 Musical Acoustics 21
2.8 Conclusion 23
References 23

2.1 Acoustics in Ancient Times

Acoustics is the science of sound. Although sound waves are nearly as old as the universe, the scientific study of sound is generally considered to have its origin in ancient Greece. The word acoustics is derived from the Greek word *akouein*, to hear, although Sauveur appears to have been the first person to apply the term acoustics to the science of sound in 1701 [2.1].

Pythagoras, who established mathematics in Greek culture during the sixth century BC, studied vibrating strings and musical sounds. He apparently discovered that dividing the length of a vibrating string into simple ratios produced consonant musical intervals. According to legend, he also observed how the pitch of the string changed with tension and the tones generated by striking musical glasses, but these are probably just legends [2.2].

Although the Greeks were certainly aware of the importance of good acoustical design in their many fine theaters, the Roman architect Vitruvius was the first to write about it in his monumental *De Architectura*, which includes a remarkable understanding and analysis of theater acoustics: "We must choose a site in which the voice may fall smoothly, and not be returned by reflection so as to convey an indistinct meaning to the ear."

Amazon EX1014 Page 29

2.2 Early Experiments on Vibrating Strings, Membranes and Plates

Much of early acoustical investigations were closely tied to musical acoustics. Galileo reviewed the relationship of the pitch of a string to its vibrating length, and he related the number of vibrations per unit time to pitch. Joseph Sauveur made more-thorough studies of frequency in relation to pitch. The English mathematician Brook Taylor provided a dynamical solution for the frequency of a vibrating string based on the assumed curve for the shape of the string when vibrating in its fundamental mode. Daniel Bernoulli set up a partial differential equation for the vibrating string and obtained solutions which d'Alembert interpreted as waves traveling in both directions along the string [2.3].

The first solution of the problem of vibrating membranes was apparently the work of S. D. Poisson, and the circular membrane was handled by R. F. A. Clebsch. Vibrating plates are somewhat more complex than vibrating membranes. In 1787 *E. F. F. Chladni* described his method of using sand sprinkled on vibrating plates to show nodal lines [2.4]. He observed that the addition of one nodal circle raised the frequency of a circular plate by about the same amount as adding two nodal diameters, a relationship that Lord Rayleigh called Chladni's law. Sophie Germain wrote a fourth-order equation to describe plate vibrations, and thus won a prize provided by the French emperor Napoleon, although Kirchhoff later gave a more accurate treatment of the boundary conditions. *Rayleigh*, of course, treated both membranes and plates in his celebrated book *Theory of Sound* [2.5].

Chladni generated his vibration patterns by "strewing sand" on the plate, which then collected along the nodal lines. Later he noticed that fine shavings from the hair of his violin bow did not follow the sand to the nodes, but instead collected at the antinodes. *Savart* noted the same behavior for fine lycopodium powder [2.6]. Michael *Faraday* explained this as being due to acoustic streaming [2.7]. Mary *Waller* published several papers and a book on Chladni patterns, in which she noted that particle diameter should exceed 100 μm in order to collect at the nodes [2.8]. Chladni figures of some of the many vibrational modes of a circular plate are shown in Fig. 2.1.

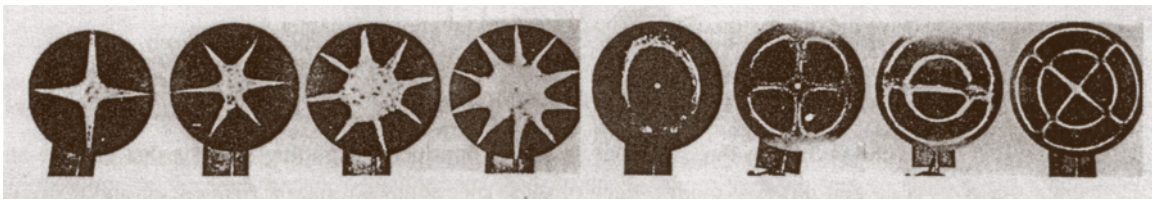


Fig. 2.1 Chladni patterns on a circular plate. The first four have two, three, four, and five nodal lines but no nodal circles; the second four have one or two nodal circles

2.3 Speed of Sound in Air

From earliest times, there was agreement that sound is propagated from one place to another by some activity of the air. Aristotle understood that there is actual motion of air, and apparently deduced that air is compressed. The Jesuit priest Athanasius Kircher was one of the first to observe the sound in a vacuum chamber, and since he could hear the bell he concluded that air was not necessary for the propagation of sound. Robert Boyle, however, repeated the experiment with a much improved pump and noted the much-observed decrease in sound intensity as the air is pumped out. We now know that sound propagates quite well in rarified air, and that the decrease in intensity at low pressure is mainly due to the impedance mismatch between the source and the medium as well as the impedance mismatch at the walls of the container.

As early as 1635, Gassendi measured the speed of sound using firearms and assuming that the light of the flash is transmitted instantaneously. His value came out to be 478 m/s. Gassendi noted that the speed of sound did not depend on the pitch of the sound, contrary to the view of Aristotle, who had taught that high notes are transmitted faster than low notes. In a more careful experiment, Mersenne determined the speed of sound to be 450 m/s [2.9]. In 1650, G. A. Borelli and V. Viviani of the Accademia del Cimento of Florence obtained a value

of 350 m/s for the speed of sound [2.10]. Another Italian, G. L. Bianconi, showed that the speed of sound in air increases with temperature [2.11].

The first attempt to calculate the speed of sound through air was apparently made by Sir Isaac Newton. He assumed that, when a pulse is propagated through a fluid, the particles of the fluid move in simple harmonic motion, and that if this is true for one particle, it must be true for all adjacent ones. The result is that the speed of sound is equal to the square root of the ratio of the atmospheric pressure to the density of the air. This leads to values that are considerably less than those measured by Newton (at Trinity College in Cambridge) and others.

In 1816, Pierre Simon Laplace suggested that in Newton's and Lagrange's calculations an error had been made in using for the volume elasticity of the air the pressure itself, which is equivalent to assuming the elastic motions of the air particles take place at constant temperature. In view of the rapidity of the motions, it seemed more reasonable to assume that the compressions and rarefactions follow the adiabatic law. The adiabatic elasticity is greater than the isothermal elasticity by a factor γ, which is the ratio of the specific heat at constant pressure to that at constant volume. The speed of sound should thus be given by $c = (\gamma p/\rho)^{1/2}$, where p is the pressure and ρ is the density. This gives much better agreement with experimental values [2.3].

2.4 Speed of Sound in Liquids and Solids

The first serious attempt to measure the speed of sound in liquid was probably that of the Swiss physicist Daniel Colladon, who in 1826 conducted studies in Lake Geneva. In 1825, the Academy of Sciences in Paris had announced as the prize competition for 1826 the measurement of the compressibility of the principal liquids. Colladon measured the static compressibility of several liquids, and he decided to check the accuracy of his measurements by measuring the speed of sound, which depends on the compressibility. The compressibility of water computed from the speed of sound turned out to be very close to the statically measured values [2.12]. Oh yes, he won the prize from the Academy.

In 1808, the French physicist *J. B. Biot* measured the speed of sound in a 1000 m long iron water pipe in Paris by direct timing of the sound travel [2.13]. He compared the arrival times of the sound through the metal and through the air and determined that the speed is much greater in the metal. Chladni had earlier studied the speed of sound in solids by noting the pitch emanating from a struck solid bar, just as we do today. He deduced that the speed of sound in tin is about 7.5 times greater than in air, while in copper it was about 12 times greater. Biot's values for the speed in metals agreed well with Chladni's.

2.5 Determining Frequency

Much of the early research on sound was tied to musical sound. Vibrating strings, membranes, plates, and air columns were the bases of various musical instruments. Music emphasized the importance of ratios for the different tones. A string could be divided into halves or thirds or fourths to give harmonious pitches. It was also known that pitch is related to frequency. Marin Mersenne (1588–1648) was apparently the first to determine the frequency corresponding to a given pitch. By working with a long rope, he was able determine the frequency of a standing wave on the length, mass, and tension of the rope. He then used a short wire under tension and from his rope formula he was able to compute the frequency of oscillation [2.14]. The relationship between pitch and frequency was later improved by Joseph Sauveur, who counted beats between two low-pitched organ pipes differing in pitch by a semitone. Sauveur deduced that "the relation between sounds of low and high pitch is exemplified in the ratio of the numbers of vibrations which they both make in the same time." [2.1]. He recognized that two sounds differing a musical fifth have frequencies in the ratio of 3:2. We have already commented that Sauveur was the first to apply the term *acoustics* to the science of sound. "I have come then to the opinion that there is a science superior to music, and I call it *acoustics*; it has for its object sound in general, whereas music has for its objects sounds agreeable to the ear." [2.1]

Amazon EX1014 Page 31

Tuning forks were widely used for determining pitch by the 19th century. Johann Scheibler (1777–1837) developed a tuning-fork *tonometer* which consisted of some 56 tuning forks. One was adjusted to the pitch of A above middle C, and another was adjusted by ear to be one octave lower. The others were then adjusted to differ successively by four vibrations per second above the lower A. Thus, he divided the octave into 55 intervals, each of about four vibrations per second. He then measured the number of beats in each interval, the sum total of such beats giving him the absolute frequency. He determined the frequency of the lower A to be 220 vibrations per second and the upper A to be 440 vibrations per second [2.15].

Felix Savart (1791–1841) used a rapidly rotating toothed wheel with 600 teeth to produce sounds of high frequency. He estimated the upper frequency threshold of hearing to be 24 000 vibrations per second. Charles Wheatstone (1802–1875) pioneered the use of rapidly rotating mirrors to study periodic events. This technique was later used by Rudolph Koenig and others to study speech sounds.

2.6 Acoustics in the 19th Century

Acoustics really blossomed in the 19th century. It is impossible to describe but a fraction of the significant work in acoustics during this century. We will try to provide a skeleton, at least, by mentioning the work of a few scientists. Especially noteworthy is the work of Tyndall, von Helmholtz, and Rayleigh, so we begin with them.

2.6.1 Tyndall

John Tyndall was born in County Carlow, Ireland in 1820. His parents were unable to finance any advanced education. After working at various jobs, he traveled to Marburg, Germany where he obtained a doctorate. He was appointed Professor of Natural Philosophy at the Royal Institution in London, where he displayed his skills in popular lecturing. In 1872 he made a lecture tour in the United States, which was a great success. His first lectures were on heat, and in 1863 these lectures were published under the title *Heat as a Mode of Motion*.

In 1867 he published his book *On Sound* with seven chapters. Later he added chapters on the transmission of sound through the atmosphere and on combinations of musical tones. In two chapters on vibrations of rods, plates, and bells, he notes that longitudinal vibrations produced by rubbing a rod lengthwise with a cloth or leather treated with rosin excited vibrations of higher frequency than the transverse vibrations. He discusses the determination of the waveform of musical sounds. By shining an intense beam of light on a mirror attached to a tuning fork and then to a slowly rotating mirror, as Lissajous had done, he spread out the waveform of the oscillations.

Tyndall is well remembered for his work on the effect of fog on transmission of sound through the atmosphere. He had succeeded Faraday as scientific advisor to the Elder Brethren of Trinity House, which supervised lighthouses and pilots in England. When fog obscures the lights of lighthouses, ships depend on whistles, bells, sirens, and even gunfire for navigation warnings. In 1873 Tyndall began a systematic study of sound propagation over water in various weather conditions in the straits of Dover. He noted great inconsistencies in the propagation.

2.6.2 Helmholtz

Hermann von Helmholtz was educated in medicine. He had wanted to study physics, but his father could not afford to support him, and the Prussian government offered financial support for students of medicine who would sign up for an extended period of service with the military. He was assigned a post in Potsdam, where he was able to set up his own laboratory in physics and physiology. The brilliance of his work led to cancelation of his remaining years of army duty and to his appointment as Professor of Physiology at Königsberg. He gave up the practice of medicine and wrote papers on physiology, color perception, and electricity. His first important paper in acoustics appears to have been his *On Combination Tones*, published in 1856 [2.16].

His book *On Sensations of Tone* (1862) combines his knowledge of both physiology and physics and music as well. He worked with little more than a stringed instrument, tuning forks, his siren, and his famous resonators to show that pitch is due to the fundamental frequency but the quality of a musical sound is due to the presence of upper partials. He showed how the ear can separate out the various components of a complex tone. He concluded that the quality of a tone depends solely on the

Amazon EX1014 Page 32

number and relative strength of its partial tone and not on their relative phase.

In order to study vibrations of violin stings and speech sounds, von Helmholtz invented a vibration microscope, which displayed Lissajous patterns of vibration. One lens of the microscope is attached to the prong of a tuning fork, so a fixed spot appears to move up and down. A spot of luminous paint is then applied to the string, and a bow is drawn horizontally across the vertical string. The point on the horizontally vibrating violin string forms a Lissajous pattern as it moves. By viewing patterns for a bowed violin string, von Helmholtz was able to determine the actual motion of the string, and such motion is still referred to as Helmholtz motion.

Much of Helmholtz's book is devoted to discussion of hearing. Using a double siren, he studied difference tones and combination tones. He determined that beyond about 30 beats per second, the listener no longer hears individual beats but the tone becomes jarring or rough. He postulated that individual nerve fibers acted as vibrating strings, each resonating at a different frequency. Noting that skilled musicians "can distinguish with certainty a difference in pitch arising from half a vibration in a second in the doubly accented octave", he concluded that some 1000 different pitches might be distinguished in the octave between 50 and 100 cycles per second, and since there are 4500 nerve fibers in the cochlea, this represented about one fiber for each two cents of musical interval. He admitted, however "that we cannot precisely ascertain what parts of the ear actually vibrate sympathetically with individual tones."

2.6.3 Rayleigh

Rayleigh was a giant. He contributed to so many areas of physics, and his contributions to acoustics were monumental. His book *Theory of Sound* still has an honored place on the desk of every acoustician (alongside von Helmholtz's book, perhaps). In addition to his book, he published some 128 papers on acoustics. He anticipated so many interesting things. I have sometimes made the statement that every time I have a good idea about sound Rayleigh steals it and puts it into his book.

John William Strutt, who was to become the third Baron Rayleigh, was born at the family estate in Terling England in 1842. (Milk from the Rayleigh estate has supplied many families in London to this day.) He enrolled at Eton, but illness caused him to drop out, and he completed his schooling at a small academy in Torquay before entering Trinity College, Cambridge. His ill health may have been a blessing for the rest of the world. After nearly dying of rheumatic fever, he took a long cruise up the Nile river, during which he concentrated on writing his *Science of Sound*.

Soon after he returned to England, his father died and he became the third Baron Rayleigh and inherited title to the estate at Terling, where he set up a laboratory. When James Clerk Maxwell died in 1879, Rayleigh was offered the position as Cavendish Professor of Physics at Cambridge. He accepted it, in large measure because there was an agricultural depression at the time and his farm tenants were having difficulties in making rent payments [2.15].

Rayleigh's book and his papers cover such a wide range of topics in acoustics that it would be impractical to attempt to describe them here. His brilliant use of mathematics set the standard for subsequent writings on acoustics. The first volume of his book develops the theory of vibrations and its applications to strings, bars, membranes, and plates, while the second volume begins with aerial vibrations and the propagation of waves in fluids.

Rayleigh combined experimental work with theory in a very skillful way. Needing a way to determine the intensity of a sound source, he noted that a light disk suspended in a beam of sound tended to line up with its plane perpendicular to the direction of the fluid motion. The torque on the disk is proportional to the sound intensity. By suspending a light mirror in a sound field, the sound intensity could be determined by means of a sensitive optical lever. The arrangement, known as a Rayleigh disk, is still used to measure sound intensity.

Another acoustical phenomenon that bears his name is the propagation of Rayleigh waves on the plane surface of an elastic solid. Rayleigh waves are observed on both large and small scales. Most of the shaking felt from an earthquake is due to Rayleigh waves, which can be much larger than the seismic waves. Surface acoustic wave (SAW) filters and sensors make use of Rayleigh waves.

2.6.4 George Stokes

George Gabriel Stokes was born in County Sligo, Ireland in 1819. His father was a Protestant minister, and all of his brothers became priests. He was educated at Bristol College and Pembroke College, Cambridge. In 1841 he graduated as senior wrangler (the top First Class degree) in the mathematical tripos and he was the first Smith's prize man. He was awarded a Fellowship at Pembroke College and later appointed Lucasian professor of mathematics at Cambridge. The position paid rather poorly,

however, so he accepted an additional position as professor of physics at the Government School of Mines in London.

William Hopkins, his Cambridge tutor, advised him to undertake research into hydrodynamics, and in 1842 he published a paper *On the steady motion of incompressible fluids.* In 1845 he published his classic paper *On the theories of the internal friction of fluids in motion*, which presents a three-dimensional equation of motion of a viscous fluid that has come to be known as the Stokes–Navier equation. Although he discovered that Navier, Poisson, and Saint-Venant had also considered the problem, he felt that his results were obtained with sufficiently different assumptions to justify publication. The Stokes–Navier equation of motion of a viscous, compressible fluid is still the starting point for much of the theory of sound propagation in fluids.

2.6.5 Alexander Graham Bell

Alexander Graham Bell was born in Edinburgh, Scotland in 1847. He taught music and elocution in Scotland before moving to Canada with his parents in 1868, and in 1871 he moved to Boston as a teacher of the deaf. In his spare time he worked on the *harmonic telegraph*, a device that would allow two or more electrical signals to be transmitted on the same wire. Throughout his life, Bell had been interested in the education of deaf people, which interest lead him to invent the microphone and, in 1876, his *electrical speech machine*, which we now call a telephone. He was encouraged to work steadily on this invention by Joseph Henry, secretary of the Smithsonian Institution and a highly respected physicist and inventor.

Bell's telephone was a great financial, as well as technical success. Bell set up a laboratory on his estate near Braddock, Nova Scotia and continued to improve the telephone as well as to work on other inventions. The magnetic transmitter was replaced by Thomas Edison's carbon microphone, the rights to which he obtained as a result of mergers and patent lawsuits [2.15].

2.6.6 Thomas Edison

The same year that Bell was born in Scotland (1847), Thomas A. Edison, the great inventor, was born in Milan, Ohio. At the age of 14 he published his own small newspaper, probably the first newspaper to be sold on trains. Also aged 14 he contracted scarlet fever which destroyed most of his hearing. His first invention was an improved stock-ticker for which he was paid $40 000. Shortly after setting up a laboratory in Menlo Park, New Jersey, he invented (in 1877) the first phonograph. This was followed (in 1879) by the incandescent electric light bulb and a few years later by the Vitascope, which led to the first silent motion pictures. Other inventions included the dictaphone, mimeograph and storage battery.

The first published article on the phonograph appeared in *Scientific American* in 1877 after Edition visited the New York offices of the journal and demonstrated his machine. Later he demonstrated his machine in Washington for President Hayes, members of Congress and other notables. Many others made improvements to Edison's talking machine, but the credit still goes to Edison for first showing that the human voice could be recorded for posterity.

In its founding year (1929), the Acoustical Society of America (ASA) made Thomas Edison an honorary fellow, an honor which was not again bestowed during the 20 years that followed.

2.6.7 Rudolph Koenig

Rudolph Koenig was born in Koenigsberg (now Kaliningrad), Russia in 1832 and attended the university there at a time when von Helmholtz was a Professor of Physiology there. A few years after taking his degree, Koenig moved to Paris where he studied violin making under Villaume. He started his own business making acoustical apparatus, which he did with great care and talent. He devoted more than 40 years to making the best acoustical equipment of his day, many items of which are still in working order in museums and acoustics laboratories. Koenig, who never married, lived in the small front room of his Paris apartment, which was also his office and stock room, while the building and testing of instruments was done in the back rooms by Koenig and a few assistants. We will attempt to describe but a few of his acoustical instruments, but they have been well documented by *Greenslade* [2.17], *Beyer* [2.18], and others. The two largest collections of Koenig apparatus in North America are at the Smithsonian Institution and the University of Toronto.

Koenig made tuning forks of all sizes. A large 64 Hz fork formed the basis for a tuning-fork clock. A set of forks covering a range of frequencies in small steps was called a *tonometer* by Johann Scheibler. For his own use, Koenig made a tonometer consisting of 154 forks ranging in frequency from 16 to 21 845 Hz. Many tuning forks were mounted on hollow wooden resonators. He made both cylindrical and spherical Helmholtz resonators of all sizes.

Amazon EX1014 Page 34

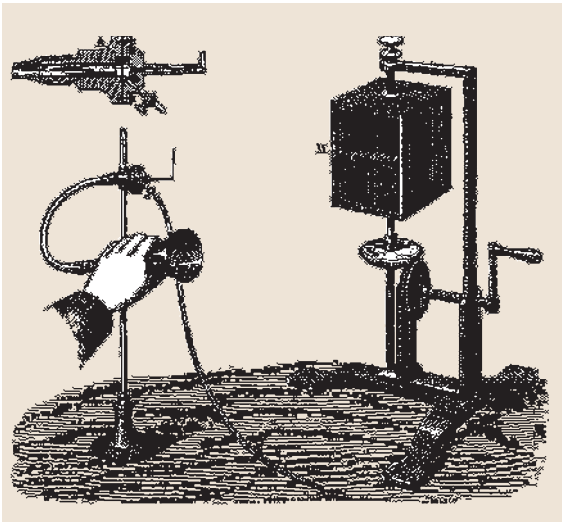


Fig. 2.2 Koenig's manometric flame apparatus. The image of the oscillating flame is seen in the rotating mirror (after [2.17])

To his contemporaries, Koenig was probably best known for his invention (1862) of the manometric flame apparatus, shown in Fig. 2.2, which allowed the visualization of acoustic signals. The manometric capsule is divided into two parts by a thin flexible membrane. Sounds waves are collected by a funnel, pass down the rubber tube, and cause the membrane to vibrate. Vibrations of the membrane cause a periodic change in the supply of gas to the burner, so the flame oscillates up and down at the frequency of the sound. The oscillating flame is viewed in the rotating mirror.

Koenig made apparatus for both the Fourier analysis and the synthesis of sound. At the 1876 exhibition, the instrument was used to show eight harmonics of a sung vowel. The Fourier analyzer included eight Helmholtz resonators, tuned to eight harmonics, which fed eight manometric flames. The coefficients of the various sinusoidal terms related to the heights of the eight flame images. The Helmholtz resonators could be tuned to different frequencies. The Fourier synthesizer had 10 electromagnetically-driven tuning forks and 10 Helmholtz resonators. A hole in each resonator could be opened or closed by means of keys [2.17].

2.7 The 20th Century

The history of acoustics in the 20th century could be presented in several ways. In his definitive history, *Beyer* [2.15] devotes one chapter to each quarter century, perhaps the most sensible way to organize the subject. One could divide the century at the year 1929, the year the Acoustical Society of America was founded. One of the events in connection with the 75th anniversary of this society was the publication of a snapshot history of the Society written by representatives from the 15 technical committees and edited by Henry *Bass* and William *Cavanaugh* [2.19]. Since we make no pretense of covering all areas of acoustics nor of reporting all acoustical developments in the 20th century, we will merely select a few significant areas of acoustics and try to discuss briefly some significant developments in these. For want of other criteria, we have selected the nine areas of acoustics that correspond to the first eight technical committees in the Acoustical Society of America.

2.7.1 Architectural Acoustics

Wallace Clement Sabine (1868–1919) is generally considered to be the father of architectural acoustics. He was the first to make quantitative measurements on the acoustics of rooms. His discovery that the product of total absorption and the duration of residual sound is a constant still forms the basis of sound control in rooms. His pioneering work was not done entirely by choice, however. As a 27-year old professor at Harvard University, he was assigned by the President to determine corrective measures for the lecture room at Harvard's Fogg Art Museum. As he begins his famous paper on reverberation [2.20] "The following investigation was not undertaken at first by choice but devolved on the writer in 1895 through instructions from the Corporation of Harvard University to propose changes for remedying the acoustical difficulties in the lecture-room of the Fogg Art Museum, a building that had just been completed."

Sabine determined the reverberation time in the Fogg lecture room by using an organ pipe and a chronograph. He found the reverberation time in the empty room to be 5.62 seconds. Then he started adding seat cushions from the Sanders Theater and measuring the resulting reverberation times. He developed an empirical formula $T = 0.164\,\mathrm{V/A}$, where T is reverberation time, V is volume (in cubic feet) and A is the average absorption



Fig. 2.3 Interior of Symphony Hall in Boston whose acoustical design by Wallace Clement Sabine set a standard for concert halls

coefficient times the total area (in square feet) of the walls, ceiling and floor. This formula is still called the Sabine reverberation formula.

Following his success with the Fogg lecture room, Sabine was asked to come up with acoustical specifications for the New Boston Music Hall, now known as Symphony Hall, which would ensure hearing superb music from every seat. Sabine answered with a shoebox shape for the building to keep out street noise. Then, using his mathematical formula for reverberation time, Sabine carefully adjusted the spacing between the rows of seats, the slant of the walls, the shape of the stage, and materials used in the walls to produce the exquisite sound heard today at Symphony Hall (see Fig. 2.3).

Vern Knudsen (1893–1974), physicist at University of California Los Angeles (UCLA) and third president of the Acoustical Society of America, was one of many persons who contributed to architectural acoustics in the first half of the 20th century. His collaboration with Hans Kneser of Germany led to an understanding of molecular relaxation phenomena in gases and liquids. In 1932 he published a book on *Architectural Acoustics* [2.21], and in 1950, a book *Architectural Designing in Acoustics* with *Cyril Harris* [2.22], which summarized most of what was known about the subject by the middle of the century.

In the mid 1940s Richard Bolt, a physicist at the Massachusetts Institute of Technology (MIT), was asked by the United Nations (UN) to design the acoustics for one of the UN's new buildings. Realizing the work that was ahead of him, he asked Leo Beranek to join him. At the same time they hired another MIT professor, Robert Newman, to help with the work with the United Nations; together they formed the firm of Bolt, Beranek, and Newman (BBN), which was to become one of the foremost architectural consulting firms in the world. This firm has provided acoustical consultation for a number of notable concert halls, including Avery Fisher Hall in New York, the Koussevitzky Music Shed at Tanglewood, Davies Symphony Hall in San Francisco, Roy Thompson Hall in Toronto, and the Center for the Performing Arts in Tokyo [2.23]. They are also well known for their efforts in pioneering the Arpanet, forerunner of the Internet.

Recipients of the Wallace Clement Sabine award for accomplishments in architectural acoustics, include Vern Knudsen, Floyd Watson, Leo Beranek, Erwin Meyer, Hale Sabine, Lothar Cremer, Cyril Harris, Thomas Northwood, Richard Waterhouse, Harold Marshall, Russell Johnson, and Alfred Warnock. The work of each of these distinguished acousticians could be a chapter in the history of acoustics but space does not allow it.

2.7.2 Physical Acoustics

Although all of acoustics, the science of sound, incorporates the laws of physics, we usually think of physical acoustics as being concerned with fundamental acoustic wave propagation phenomena, including transmission, reflection, refraction, interference, diffraction, scattering, absorption, dispersion of sound and the use of acoustics to study physical properties of matter and to produce changes in these properties. The foundations for physical acoustics were laid by such 19th century giants as von Helmholtz, Rayleigh, Tyndall, Stokes, Kirchhoff, and others.

Ultrasonic waves, sound waves with frequencies above the range of human hearing, have attracted the attention of many physicists and engineers in the 20th century. An early source of ultrasound was the Galton whistle, used by Francis Galton to study the upper threshold of hearing in animals. More powerful sources of ultrasound followed the discovery of the piezoelectric effect in crystals by Jacques and Pierre Curie. They found that applying an electric field to the plates of certain natural crystals such as quartz produced changes in thickness. Later in the century, highly efficient ceramic piezoelectric transducers were used to produce high-intensity ultrasound in solids, liquids, and gases.

Amazon EX1014 Page 36

Probably the most important use of ultrasound nowadays is in ultrasonic imaging, in medicine (sonograms) as well as in the ocean (sonar). Ultrasonic waves are used in many medical diagnostic procedures. They are directed toward a patient's body and reflected when they reach boundaries between tissues of different densities. These reflected waves are detected and displayed on a monitor. Ultrasound can also be used to detect malignancies and hemorrhaging in various organs. It is also used to monitor real-time movement of heart valves and large blood vessels. Air, bone, and other calcified tissues absorb most of the ultrasound beam; therefore this technique cannot be used to examine the bones or the lungs.

The father of sonar (sound navigation and ranging) was Paul Langevin, who used active echo ranging sonar at about 45 kHz to detect mines during World War I. Sonar is used to explore the ocean and study marine life in addition to its many military applications [2.24]. New types of sonar include synthetic aperture sonar for high-resolution imaging using a moving hydrophone array and computed angle-of-arrival transient imaging (CAATI).

Infrasonic waves, which have frequencies below the range of human hearing, have been less frequently studied than ultrasonic waves. Natural phenomena are prodigious generators of infrasound. When the volcano Krakatoa exploded, windows were shattered hundreds of miles away by the infrasonic wave. The *ringing* of both earth and atmosphere continued for hours. It is believed that infrasound actually formed the upper pitch of this natural volcanic explosion, tones unmeasurably deep forming the actual central harmonic of the event. Infrasound from large meteoroids that enter our atmosphere have very large amplitudes, even great enough to break glass windows [2.25]. Ultralow-pitch earthquake sounds are keenly felt by animals and sensitive humans. Quakes occur in distinct stages. Long before the final breaking release of built-up earth tensions, there are numerous and succinct precursory shocks. Deep shocks produce strong infrasonic impulses up to the surface, the result of massive heaving ground strata. Certain animals (fish) can actually hear infrasonic precursors.

Aeroacoustics, a branch of physical acoustics, is the study of sound generated by (or in) flowing fluids. The mechanism for sound or noise generation may be due to turbulence in flows, resonant effects in cavities or waveguides, vibration of boundaries of structures etc. A flow may alter the propagation of sound and boundaries can lead to scattering; both features play a significant part in altering the noise received at a particular observation point. A notable pioneer in aeroacoustics was Sir James Lighthill (1924–1998), whose analyses of the sounds generated in a fluid by turbulence have had appreciable importance in the study of nonlinear acoustics. He identified quadrupole sound sources in the inhomogeneities of turbulence as a major source of the noise from jet aircraft engines, for example [2.26].

There are several sources of nonlinearity when sound propagates through gases, liquids, or solids. At least since the time of Stokes, it has been known that in fluids compressions propagate slightly faster than rarefactions, which leads to distortion of the wave front and even to the formation of shock waves. Richard Fay (1891–1964) noted that the waveform takes on the shape of a sawtooth. In 1935 Eugene Fubini–Ghiron demonstrated that the pressure amplitude in a nondissipative fluid is proportional to an infinite series in the harmonics of the original signal [2.15]. Several books treat nonlinear sound propagation, including those by *Beyer* [2.27] and by *Hamilton* and *Blackstock* [2.28].

Measurements of sound propagation in liquid helium have led to our basic understanding of cryogenics and also to several surprises. The attenuation of sound shows a sharp peak near the so-called lambda point at which helium takes on superfluid properties. This behavior was explained by Lev Landau (1908–1968) and others. Second sound, the propagation of waves consisting of periodic oscillations of temperature and entropy, was discovered in 1944 by V. O. Peshkov. Third sound, a surface wave of the superfluid component was reported in 1958, whereas fourth sound was discovered in 1962 by K. A. Shapiro and Isadore Rudnick. Fifth sound, a thermal wave, has also been reported, as has *zero* sound [2.15].

While there a number of ways in which light can interact with sound, the term *optoacoustics* typically refers to sound produced by high-intensity light from a laser. The optoacoustic (or photoacoustic) effect is characterized by the generation of sound through interaction of electromagnetic radiation with matter. Absorption of single laser pulses in a sample can effectively generate optoacoustic waves through the thermoelastic effect. After absorption of a short pulse the heated region thermally expands, creating a mechanical disturbance that propagates into the surrounding medium as a sound wave. The waves are recorded at the surface of the sample with broadband ultrasound transducers

Sonoluminescence uses sound to produce light. Sonoluminescence, the emission of light by bubbles in a liquid excited by sound, was discovered by H. Frenzel and H. Schultes in 1934, but was not considered very

Amazon EX1014 Page 37

interesting at the time. A major breakthrough occurred when Felipe Gaitan and his colleagues were able to produce single-bubble sonoluminescence, in which a single bubble, trapped in a standing acoustic wave, emits light with each pulsation [2.29].

The wavelength of the emitted light is very short, with the spectrum extending well into the ultraviolet. The observed spectrum of emitted light seems to indicate a temperature in the bubble of at least 10 000 °C, and possibly a temperature in excess of one million degrees C. Such a high temperature makes the study of sonoluminescence especially interesting for the possibility that it might be a means to achieve thermonuclear fusion. If the bubble is hot enough, and the pressures in it high enough, fusion reactions like those that occur in the Sun could be produced within these tiny bubbles.

When sound travels in small channels, oscillating heat also flows to and from the channel walls, leading to a rich variety of *thermoacoustic* effects. In 1980, Nicholas *Rott* developed the mathematics describing acoustic oscillations in a gas in a channel with an axial temperature gradient, a problem investigated by Rayleigh and Kirchhoff without much success [2.30]. Applying Rott's mathematics, *Hofler*, et al. invented a standing-wave thermoacoustic refrigerator in which the coupled oscillations of gas motion, temperature, and heat transfer in the sound wave are phased so that heat is absorbed at low temperature and waste heat is rejected at higher temperature [2.31].

Recipients of the ASA silver medal in physical acoustics since it was first awarded in 1975 have included Isadore Rudnick, Martin Greenspan, Herbert McSkimin, David Blackstock, Mack Breazeale, Allan Pierce, Julian Maynard, Robert Apfel, Gregory Swift, and Philip Marston.

2.7.3 Engineering Acoustics

It is virtually impossible to amplify sound waves. Electrical signals, on the other hand, are relatively easy to amplify. Thus a practical system for amplifying sound includes input and output *transducers*, together with the electronic amplifier. Transducers have occupied a central role in engineering acoustics during the 20th century.

The transducers in a sound amplifying system are microphones and loudspeakers. The first microphones were Bell's magnetic transmitter and the loosely packed carbon microphones of Edison and Berliner. A great step forward in 1917 was the invention of the condenser microphone by Edward Wente (1889–1972). In 1962, James West and Gerhard Sessler invented the foil electret or electret condenser microphone, which has become the most ubiquitous microphone in use. It can be found in everything from telephones to children's toys to medical devices. Nearly 90% of the approximately one billion microphones manufactured annually are electret designs.

Ernst W. Siemens was the first to describe the *dynamic* or moving-coil loudspeaker, with a circular coil of wire in a magnetic field and supported so that it could move axially. John Stroh first described the conical paper diaphragm that terminated at the rim of the speaker in a section that was flat except for corrugations. In 1925, Chester W. Rice and Edward W. Kellogg at General Electric established the basic principle of the direct-radiator loudspeaker with a small coil-driven mass-controlled diaphragm in a baffle with a broad mid-frequency range of uniform response. In 1926, Radio Corporation of America (RCA) used this design in the *Radiola* line of alternating current (AC)-powered radios. In 1943 James Lansing introduced the Altec-Lansing 604 duplex radiator which combined an efficient 15 inch woofer with a high-frequency compression driver and horn [2.32].

In 1946, Paul Klipsch introduced the Klipschorn, a corner-folded horn that made use of the room boundaries themselves to achieve efficient radiation at low frequency. In the early 1940s, the Jensen company popularized the vented box or bass reflex loudspeaker enclosure. In 1951, specific loudspeaker driver parameters and appropriate enclosure alignments were described by Neville Thiele and later refined by Richard Small. Thiele–Small parameters are now routinely published by loudspeaker manufacturers and used by professionals and amateurs alike to design vented enclosures [2.33].

The Audio Engineering Society was formed in 1948, the same year the microgroove 33 1/3 rpm long-play vinyl record (LP) was introduced by Columbia Records. The founding of this new society had the unfortunate effect of distancing engineers primarily interested in audio from the rest of the acoustics engineering community.

Natural piezoelectric crystals were used to generate sound waves for underwater signaling and for ultrasonic research. In 1917 Paul Langevin obtained a large crystal of natural quartz from which $10 \times 10 \times 1.6$ cm slices could be cut. He constructed a transmitter that sent out a beam powerful enough to kill fish in its near field [2.15]. After World Wart II, materials, such as potassium dihydrogen phosphate (KDP), ammonium dihydrogen phosphate (ADP) and barium titanate replaced natural quartz in transducers. There are several

Amazon EX1014 Page 38

piezoelectric ceramic compositions in common use today: barium titanate, lead zirconate titanate (PZT) and modified iterations such as lead lanthanum zirconate titanate (PLZT), lead metaniobate and lead magnesium niobate (PMN, including electrostrictive formulations). The PZT compositions are the most widely used in applications involving light shutters, micro-positioning devices, speakers and medical array transducers

Recipients of the ASA silver medal in engineering acoustics have included Harry Olson, Hugh Knowles, Benjamin Bauer, Per Bruel, Vincent Salmon, Albert Bodine, Joshua Greenspon, Alan Powell, James West, Richard Lyon, and Ilene Busch-Vishniac. Interdisciplinary medals have gone to Victor Anderson, Steven Garrett, and Gerhard Sessler.

2.7.4 Structural Acoustics

The vibrations of solid structures was discussed at some length by Rayleigh, Love, Timoshenko, Clebsch, Airey, Lamb, and others during the 19th and early 20th centuries. Nonlinear vibrations were considered by G. Duffing in 1918. R. N. Arnold and G. B. Warburton solved the complete boundary-value problem of the free vibration of a finite cylindrical shell. Significant advances have been made in our understanding of the radiation, scattering, and response of fluid-loaded elastic plates by G. Maidanik, E. Kerwin, M. Junger, and D. Feit.

Statistical energy analysis (SEA), championed by Richard Lyon and Gideon Maidanik, had its beginnings in the early 1960s. In the 1980s, Christian Soize developed the fuzzy structure theory to predict the mid-frequency dynamic response of a master structure coupled with a large number of complex secondary subsystems. The structural and geometric details of the latter are not well defined and therefore labeled as *fuzzy*.

A number of good books have been written on the vibrations of simple and complex structures. Especially noteworthy, in my opinion, are books by *Cremer* et al. [2.34], *Junger* and *Feit* [2.35], *Leissa* [2.36], [2.37], and *Skudrzyk* [2.38]. Statistical energy analysis is described by *Lyon* [2.39]. Near-field acoustic holography, developed by Jay Maynard and Earl Williams, use pressure measurements in the near field of a vibrating object to determine its source distribution on the vibrating surface [2.40]. A near-field acoustic hologram of a rectangular plate driven at a point is shown in Fig. 2.4.

The ASA has awarded its Trent–Crede medal, which recognizes accomplishment in shock and vibration, to Carl Vigness, Raymond Mindlin, Elias Klein, J. P. Den Hartog, Stephen Crandall, John Snowdon, Eric Ungar, Miguel Junger, Gideon Maidanik, Preston Smith, David Feit, and Sabih Hayek.

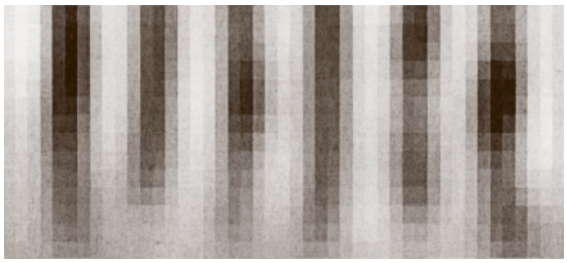


Fig. 2.4 Near-field hologram of pressure near a rectangular plate driven at 1858 Hz at a point (courtesy of Earl Williams)

2.7.5 Underwater Acoustics

The science of underwater technology in the 20th century is based on the remarkable tools of transduction that the 19th century gave us. It was partly motivated by the two world wars and the cold war and the threats raised by submarines and underwater mines. Two nonmilitary commercial fields that have been important driving forces in underwater acoustics are geophysical prospecting and fishing. The extraction of oil from the seafloor now supplies 25% of our total supply [2.41].

Essential to understanding underwater sound propagation is detailed knowledge about the speed of sound in the sea. In 1924, *Heck* and *Service* published tables on the dependence of sound speed on temperature, salinity, and pressure [2.42]. Summer conditions, with strong solar heating and a warm atmosphere, give rise to sound speeds that are higher near the surface and decrease with depth, while winter conditions, with cooling of the surface, reverses the temperature gradient. Thus, sound waves will bend downward under summer conditions and upward in the winter.

Submarine detection can be either passive (listening to the sounds made by the submarine) or active (transmiting a signal and listen for the echo). Well into the 1950s, both the United States and United Kingdom chose active high-frequency systems since passive systems at that time were limited by the ship's radiated noise and the self noise of the arrays. During World War II, underwater acoustics research results were secret, but at the end of the war, the National Defense Research Council (NDRC) published the results. The Sub-Surface Warfare Division alone produced 22 volumes [2.41]. Later the NDRC was disbanded and projects were trans-

Amazon EX1014 Page 39

ferred to the Navy (some reports have been published by IEEE).

The absorption in seawater was found to be much higher than predicted by classical theory. O. B. Wilson and R. W. Leonard concluded that this was due to the relaxation frequency of magnesium sulfate, which is present in low concentration in the sea [2.43]. Ernest Yeager and Fred Fisher found that boric acid in small concentrations exhibits a relaxation frequency near 1 kHz. In 1950 the papers of Tolstoy and Clay discussed propagation in shallow water. At the Scripps Institution of Oceanography Fred Fisher and Vernon Simmons made resonance measurements of seawater in a 200 l glass sphere over a wide range of frequencies and temperature, confirming the earlier results and improving the empirical absorption equation [2.41].

Ambient noise in the sea is due to a variety of causes, such as ships, marine mammals, snapping shrimp, and dynamic processes in the sea itself. Early measurements of ambient noise, made under Vern Knudsen, came to be known as the Knudsen curves. Wittenborn made measurements with two hydrophones, one in the sound channel and the other below it. A comparison of the noise levels showed about a 20 dB difference over the low-frequency band but little difference at high frequency. It has been suggested that a source of low-frequency noise is the collective oscillation of bubble clouds.

The ASA pioneers medal in underwater acoustics has been awarded to Harvey Hayes, Albert Wood, Warren Horton, Frederick Hunt, Harold Saxton, Carl Eckart, Claude Horton, Arthur Williams, Fred Spiess, Robert Urick, Ivan Tolstoy, Homer Bucker, William Kuperman, Darrell Jackson, and Frederick Tappert.

2.7.6 Physiological and Psychological Acoustics

Physiological acoustics deals with the peripheral auditory system, including the cochlear mechanism, stimulus encoding in the auditory nerve, and models of auditory discrimination.

This field of acoustics probably owes more to Georg von Békésy (1899–1972) than any other person. Born in Budapest, he worked for the Hungarian Telephone Co., the University of Budapest, the Karolinska Institute in Stockholm, Harvard University, and the University of Hawaii. In 1962 he was awarded the Nobel prize in physiology and medicine for his research on the ear. He determined the static and dynamic properties of the basilar membrane, and he built a mechanical model of the cochlea. He was probably the first person to observe eddy currents in the fluid of the cochlea. Josef Zwislocki (1922–) reasoned that the existence of such fluid motions would inevitably lead to nonlinearities, although Helmholtz had pretty much assumed that the inner ear was a linear system [2.44].

In 1971 William Rhode succeeded in making measurements on a live cochlea for the first time. Using the Mössbauer effect to measure the velocity of the basilar membrane, he made a significant discovery. The frequency tuning was far sharper than that reported for dead cochleae. Moreover, the response was highly nonlinear, with the gain increasing by orders of magnitude at low sound levels. There is an active amplifier in the cochlea that boosts faint sounds, leading to a strongly compressive response of the basilar membrane. The work of Peter Dallos, Bill Brownell, and others identified the outer hair cells as the cochlear amplifiers [2.45].

It is possible, by inserting a tiny electrode into the auditory nerve, to pick up the electrical signals traveling in a single fiber of the auditory nerve from the cochlea to the brain. Each auditory nerve fiber responds over a certain range of frequency and pressure. Nelson Kiang and others have determined that tuning curves of each fiber show a maximum in sensitivity. Within several hours after death, the basilar membrane response decreases, the frequency of maximum response shifts down, and the response curve broadens.

Psychological acoustics or *psychoacoustics* deals with subjective attributes of sound, such as loudness, pitch, and timbre and how they relate to physically measurable quantities such as the sound level, frequency, and spectrum of the stimulus.

At the Bell Telephone laboratories, Harvey Fletcher, first president of the Acoustical Society of America, and W. A. Munson determined contours of equal loudness by having listeners compare a large number of tones to pure tones of 1000 Hz. These contours of equal loudness came to be labeled by an appropriate number of *phon*s. S. S. Stevens is responsible for the loudness scale of *sone*s and for ways to calculate the loudness in *sone*s. His proposal to express pitch in *mels* did not become as widely adopted, however, probably because musicians and others prefer to express pitch in terms of the musical scale.

The threshold for detecting pure tones is mostly determined by the sound transmission through the outer and middle ear; to a first approximation the inner ear (the cochlea) is equally sensitive to all frequencies, except the very highest and lowest. In 1951, J. C. R. *Licklider* (1915–1990), who is well known for his work on developing the Internet, put the results of several hearing

surveys together [2.46]. Masking of one tone by another was discussed in a classic paper by *Wegel* and *Lane* who showed that low-frequency tones can mask higher-frequency tones better than the reverse [2.47].

Two major theories of pitch perception gradually developed on the basis of experiments in many laboratories. They are usually referred to as the place (or frequency) theory and the periodicity (or time) theory. By observing wavelike motions of the basilar membrane caused by sound stimulation, Békésy provided support for the place theory. In the late 1930s, however, J. F. Schouten and his colleagues performed pitch-shift experiments that provided support for the periodicity theory of pitch. Modern theories of pitch perception often combine elements of both of these [2.48].

Recipients of the ASA von Békésy medal have been Jozef Zwislocki, Peter Dallos, and Murray Sachs, while the silver medal in psychological and physiological acoustics has been awarded to Lloyd Jeffress, Ernest Wever, Eberhard Zwicker, David Green, Nathaniel Durlach, Neal Viemeister, and Brian Moore.

2.7.7 Speech

The production, transmission, and perception of speech have always played an important role in acoustics. Harvey Fletcher published his book *Speech and Hearing* in 1929, the same year as the first meeting of the Acoustical Society of America. The first issue of the *Journal of the Acoustical Society of America* included papers on speech by G. Oscar Russell, Vern Knudsen, Norman French and Walter Koenig, Jr.

In 1939, Homer Dudley invented the vocoder, a system in which speech was analyzed into component parts consisting of the pitch fundamental frequency of the voice, the noise, and the intensities of the speech in a series of band-pass filters. This machine, which was demonstrated at New York World's Fair, could speak simple phrases.

An instrument that is particularly useful for speech analysis is the *sound spectrograph*, originally developed at the Bell Telephone laboratories around 1945. This instrument records a sound-level frequency–time plot for a brief sample of speech on which the sound level is represent by the degree of blackness in a two-dimensional time–frequency graph, as shown in Fig. 2.5. Digital versions of the sound spectrograph are used these days, but the display format is similar to the original machine.

Phonetic aspects of speech research blossomed at the Bell Telephone laboratories and elsewhere in the 1950s. Gordon Peterson and his colleagues produced several studies of vowels. Gunnar Fant published a complete survey of the field in *Acoustic Theory of Speech Production* [2.49]. The pattern playback, developed at Haskins Laboratories, dominated early research using synthetic speech in the United States. James Flanagan (1925–) demonstrated the significance of the use of our understanding of fluid dynamics in analyzing the behavior of the glottis. Kenneth Stevens and Arthur House noted that the bursts of air from the glottis had a triangular waveform that led to a rich spectrum of harmonics.

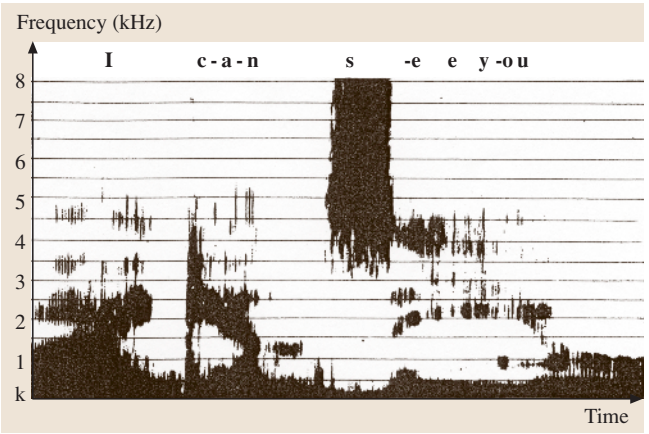


Fig. 2.5 Speech spectrogram of a simple sentence ("I can see you") recorded on a sound spectrograph

Speech synthesis and automatic recognition of speech have been important topics in speech research. Dennis Klatt (1938–1988) developed a system for synthesizing speech, and shortly before his death he gave the first completely intelligible synthesized speech paper presented to the ASA [2.50]. *Fry* and *Denes* constructed a system in which speech was fed into an acoustic recognizer that compares "the changing spectrum of the speech wave with certain reference patterns and indicates the occurrence of the phoneme whose reference pattern best matches that of the incoming wave" [2.51].

Recipients of the ASA silver medal in speech communication have included Franklin Cooper, Gunnar Fant, Kenneth Stevens, Dennis Klatt, Arthur House, Peter Ladefoged, and Patricia Kuhl.

2.7.8 Musical Acoustics

Musical acoustics deals with the production of musical sound, its transmission to the listener, and its perception. Thus this interdisciplinary field overlaps architectural

Amazon EX1014 Page 41

acoustics, engineering acoustics, and psychoacoustics. The study of the singing voice also overlaps the study of speech. In recent years, the scientific study of musical performance has also been included in musical acoustics.

Because the transmission and perception of sound have already been discussed, we will concentrate on the production of musical sound by musical instruments, including the human voice. It is convenient to classify musical instruments into families in accordance with the way they produce sound: string, wind, percussion, and electronic.

Bowed string instruments were probably the first to attract the attention of scientific researchers. The modern violin was developed largely in Italy in the 16th century by Gaspara da Salo and the Amati family. In the 18th century, Antonio Stradivari, a pupil of Nicolo Amati, and Guiseppi Guarneri created instruments with great brilliance that have set the standard for violin makers since that time. Outstanding contributions to our understanding of violin acoustics have been made by Felix Savart, Hermann von Helmholtz, Lord Rayleigh, C. V. Raman, Frederick Saunders, and Lothar Cremer, all of whom also distinguished themselves in fields other than violin acoustics. In more recent times, the work of Professor Saunders has been continued by members of the Catgut Acoustical Society, led by Carleen Hutchins. This work has made good use of modern tools such as computers, holographic interferometers, and fast Fourier transform (FFT) analyzers. One noteworthy product of modern violin research has been the development of an octet of scaled violins, covering the full range of musical performance.

The piano, invented by Bartolomeo Cristofori in 1709, is one of the most versatile of all musical instruments. One of the foremost piano researcher of our time is Harold Conklin. After he retired from the Baldwin Piano Co, he published a series of three papers in *JASA* (J. Acoustical Society of America) that could serve as a textbook for piano researchers [2.52]. Gabriel Weinreich explained the behavior of coupled piano strings and the aftersound which results from this coupling. Others who have contributed substantially to our understanding of piano acoustics are Anders Askenfelt, Eric Jansson, Juergen Meyer, Klaus Wogram, Ingolf Bork, Donald Hall, Isao Nakamura, Hideo Suzuki, and Nicholas Giordano. Many other string instruments have been studied scientifically, but space does not allow a discussion of their history here.

Pioneers in the study of wind instruments included Arthur Benade (1925–1987), John Backus (1911–1988), and John Coltman (1915–). Backus, a research physicist, studied both brass and woodwind instruments, especially the nonlinear flow control properties of woodwind reeds. He improved the capillary method for measuring input impedance of air columns, and he developed synthetic reeds for woodwind instruments. Benade's extensive work led to greater understanding of mode conversion in flared horns, a model of woodwind instrument bores based on the acoustics of a lattice of tone holes, characterization of wind instruments in terms of cutoff frequencies, and radiation from brass and woodwind instruments. His two books *Horns, Strings and Harmony* and *Fundamentals of Musical Acoustics* have both been reprinted by Dover Books. Coltman, a physicist and executive at the Westinghouse Electric Corporation, devoted much of his spare time to the study of the musical, historical, and acoustical aspects of the flute and organ pipes. He collected more than 200 instruments of the flute family, which he used in his studies. More recently, flutes, organ pipes, and other wind instruments have been studied by Neville Fletcher and his colleagues in Australia.

The human voice is our oldest musical instrument, and its acoustics has been extensively studied by Johan Sundberg and colleagues in Stockholm. A unified discussion of speech and the singing voice appears in this handbook.

The acoustics of percussion instruments from many different countries have been studied by Thomas *Rossing* and his students, and many of them are described in his book *Science of Percussion Instruments* [2.53] as well as in his published papers.

Electronic music technology was made possible with the invention of the vacuum tube early in the 20th century. In 1919 Leon Theremin invented the aetherophone (later called the Theremin), an instrument whose vacuum-tube oscillators can be controlled by the proximity of the player's hands to two antennae. In 1928, Maurice Martenot built the Ondes Martenot. In 1935 Laurens Hammond used magnetic tone-wheel generators as the basis for his electromechanical organ, which became a very popular instrument. Analog music synthesizers became popular around the middle of the 20th century. In the mid 1960s, Robert Moog and Donald Buchla built successful voltage-controlled music synthesizers which gave way to a revolution in the way composers could easily synthesize new sounds. Gradually, however, analog music synthesizers gave way to digital techniques making use of digital computers. Although many people contributed to the development of computer music, Max Mathews is often called the fa-

ther of computer music, since he developed the MUSIC I program that begat many successful music synthesis programs and blossomed into a rich resource for musical expression [2.54].

The ASA has awarded its silver medal in musical acoustics to Carleen Hutchins, Arthur Benade, John Backus, Max Mathews, Thomas Rossing, Neville Fletcher, and Johan Sundberg.

2.8 Conclusion

This brief summary of acoustics history has only scratched the surface. Many fine books on the subject appear in the list of references, and readers are urged to explore the subject further. The science of sound is a fascinating subject that draws from many different disciplines.

References

2.1 R.B. Lindsay: *Acoustics: Historical and Philosophical Development* (Dowden, Hutchinson & Ross, Stroudsburg, PA 1973) p. 88, Translation of Sauveur's paper

2.2 F.V. Hunt: *Origins in Acoustics* (Acoustical Society of America, Woodbury, NY 1992)

2.3 R.B. Lindsay: The story of acoustics, J. Acoust. Soc. Am. **39**, 629–644 (1966)

2.4 E.F.F. Chladni: *Entdeckungen über die Theorie des Klanges* (Breitkopf und Härtel, Leipzig 1787)

2.5 Lord Rayleigh J.W. Strutt: *The Theory of Sound*, Vol. 1, 2nd edn. (Macmillan, London 1894), reprinted by Dover, 1945

2.6 M. Savart: Recherches sur les vibrations normales, Ann. Chim. **36**, 187–208 (1827)

2.7 M. Faraday: On a peculiar class of acoustical figures; and on certain forms assumed by groups of particles upon vibrating elastic surfaces, Philos. Trans. R. Soc. **121**, 299–318 (1831)

2.8 M.D. Waller: *Chladni Figures: A Study in Symmetry* (Bell, London 1961)

2.9 L.M.A. Lenihan: Mersenne and Gassendi. An early chapter in the history of shound, Acustica **2**, 96–99 (1951)

2.10 D.C. Miller: *Anecdotal History of the Science of Sound* (Macmillan, New York 1935) p. 20

2.11 L.M.A. Lenihan: The velocity of sound in air, Acustica **2**, 205–212 (1952)

2.12 J.-D. Colladon, J.K.F. Sturm: Mémoire sur la compression des liquides et la vitresse du son dans l'eau, Ann. Chim. Phys. **36**, 113 (1827)

2.13 J.B. Biot: Ann. Chim. Phys. **13**, 5 (1808)

2.14 M. Mersenne: *Harmonie Universelle* (Crmoisy, Paris 1636), Translated into English by J. Hawkins, 1853

2.15 R.T. Beyer: *Sounds of Our Times* (Springer, New York 1999)

2.16 H. von Helmholtz: On sensations of tone, Ann. Phys. Chem **99**, 497–540 (1856)

2.17 T.B. Greenslade jr: The Acoustical Apparatus of Rudolph Koenig, The Phys. Teacher **30**, 518–524 (1992)

2.18 R.T. Beyer: Rudolph Koenig, 1832–1902, ECHOES **9**(1), 6 (1999)

2.19 H.E. Bass, W.J. Cavanaugh (Eds.): *ASA at 75* (Acoustical Society of America, Melville 2004)

2.20 W.C. Sabine: *Reverberation* (The American Architect, 1900), Reprinted in Collected Papers on Acoustics by Wallace Clement Sabine, Dover, New York, 1964

2.21 V.O. Knudsen: *Architectural Acoustics* (Wiley, New York 1932)

2.22 V.O. Knudsen, C. Harris: *Acoustical Designing in Architecture* (Wiley, New York 1950), Revised edition published in 1978 by the Acoustical Society of America

2.23 L. Beranek: *Concert and Opera Halls, How They Sound* (Acoustical Society of America, Woodbury 1996)

2.24 C.M. McKinney: The early history of high frequency, short range, high resolution, active sonar, ECHOES **12**(2), 4–7 (2002)

2.25 D.O. ReVelle: Gobal infrasonic monitoring of large meteoroids, ECHOES **11**(1), 5 (2001)

2.26 J. Lighthill: *Waves in Fluids* (Cambridge Univ. Press, Cambridge 1978)

2.27 R. Beyer: *Nonlinear Acoustics* (US Dept. of the Navy, Providence 1974), Revised and reissued by ASA, NY 1997

2.28 M.F. Hamilton, D.T. Blackstock (Eds.): *Nonlinear Acoustics* (Academic, San Diego 1998)

2.29 D.F. Gaitan, L.A. Crum, C.C. Church, R.A. Roy: Sonoluminescence and bubble dynamics for a single, stable, cavitation bubble, J. Acoust. Soc. Am. **91**, 3166–3183 (1992)

2.30 N. Rott: Thermoacoustics, Adv. Appl. Mech. **20**, 135–175 (1980)

2.31 T. Hofler, J.C. Wheatley, G. W. Swift, and A. Migliori: Acoustic cooling engine:, 1988 US Patent No. 4,722,201.

2.32 G.L. Augspurger: Theory, ingenuity, and wishful wizardry in loudspeaker design–A half-century of progress?, J. Acoust. Soc. Am. **77**, 1303–1308 (1985)

2.33 A.N. Thiele: Loudspeakers in vented boxes, Proc. IRE Aust. **22**, 487–505 (1961), Reprinted in J. Aud. Eng. Soc. 19, 352–392, 471–483 (1971)

2.34 L. Cremer, M. Heckl, E.E. Ungar: *Structure Borne Sound: Structural Vibrations and Sound Radiation at Audio Frequencies*, 2nd edn. (Springer, New York 1990)

2.35 M.C. Junger, D. Feit: *Sound, Structures, and Their Interaction*, 2nd edn. (MIT Press, 1986)

2.36 A.W. Leissa: *Vibrations of Plates* (Acoustical Society of America, Melville, NY 1993)

2.37 A.W. Leissa: *Vibrations of Shells* (Acoustical Society of America, Melville, NY 1993)

2.38 E. Skudrzyk: *Simple and Complex Vibratory Systems* (Univ. Pennsylvania Press, Philadelphia 1968)

2.39 R.H. Lyon: *Statistical Energy Analysis of Dynamical System, Theory and Applicationss* (MIT Press, Cambridge 1975)

2.40 E.G. Williams: *Fourier Acoustics: Sound Radiation and Nearfield Acoustic Holography* (Academic, San Diego 1999)

2.41 R.R. Goodman: A brief history of underwater acoustics. In: *ASA at 75*, ed. by H.E. Bass, W.J. Cavanaugh (Acoustical Society of America, Melville 2004)

2.42 N.H. Heck, J.H. Service: *Velocity of Sound in Seawater* (SUSC&GS Special Publication 108, 1924)

2.43 O.B. Wilson, R.W. Leonard: Measurements of sound absorption in aqueous salt solutions by a resonator method, J. Acoust. Soc. Am. **26**, 223 (1954)

2.44 H. von Helmholtz: *Die Lehre von den Tonempfindungen* (Longmans, New York 1862), Translated by Alexander Ellis as *On the Sensations of Tone* and reprinted by Dover, 1954

2.45 M.B. Sachs: The History of Physiological Acoustics. In: *ASA at 75*, ed. by H.E. Bass, W.J. Cavanaugh (Acoustical Society of America, Melville 2004)

2.46 J.C.R. Licklider: Basic correlates of the auditory stimulus. In: *Handbook of Experimental Psychology*, ed. by S.S. Stevens (J. Wiley, New York 1951)

2.47 R.L. Wegel, C.E. Lane: The auditory masking of one pure tone by another and its probable relation to the dynamics of the inner ear, Phys. Rev. **23**, 266–285 (1924)

2.48 B.C.J. Moore: Frequency analysis and pitch perception. In: *Human Psychophysics*, ed. by W.A. Yost, A.N. Popper, R.R. Fay (Springer, New York 1993)

2.49 G. Fant: *Acoustical Thoery of Speech Production* (Mouton, The Hague 1960)

2.50 P. Ladefoged: The study of speech communication in the acoustical society of america. In: *ASA at 75*, ed. by H.E. Bass, W.J. Cavanaugh (Acoustical Society of America, Melville 2004)

2.51 D.B. Fry, P. Denes: Mechanical speech recognition. In: *Communication Theory*, ed. by W. Jackson. (Butterworth, London 1953)

2.52 H.A. Conklin Jr: Design and tone in the mechanoacoustic piano, Parts I, II, and III, J. Acoust. Soc. Am. **99**, 3286–3296 (1996), **100**, 695–708 (1996), and **100**, 1286–1298 (1996)

2.53 T.D. Rossing: *The Science of Percussion Instruments* (World Scientific, Singapore 2000)

2.54 T.D. Rossing, F.R. Moore, P.A. Wheeler: *Science of Sound*, 3rd edn. (Addison-Wesley, San Francisco 2002),

Amazon EX1014 Page 44

3. Basic Linear Acoustics

This chapter deals with the physical and mathematical aspects of sound when the disturbances are, in some sense, small. Acoustics is usually concerned with small-amplitude phenomena, and consequently a linear description is usually applicable. Disturbances are governed by the properties of the medium in which they occur, and the governing equations are the equations of continuum mechanics, which apply equally to gases, liquids, and solids. These include the mass, momentum, and energy equations, as well as thermodynamic principles. The viscosity and thermal conduction enter into the versions of these equations that apply to fluids. Fluids of typical great interest are air and sea water, and consequently this chapter includes a summary of their relevant acoustic properties. The foundation is also laid for the consideration of acoustic waves in elastic solids, suspensions, bubbly liquids, and porous media.

This is a long chapter, and a great number of what one might term classical acoustics topics are included, especially topics that one might encounter in an introductory course in acoustics: the wave theory of sound, the wave equation, reflection of sound, transmission from one media to another, propagation through ducts, radiation from various types of sources, and the diffraction of sound.

3.1 **Introduction** 27

3.2 **Equations of Continuum Mechanics** 28
- 3.2.1 Mass, Momentum, and Energy Equations 28
- 3.2.2 Newtonian Fluids and the Shear Viscosity 30
- 3.2.3 Equilibrium Thermodynamics 30
- 3.2.4 Bulk Viscosity and Thermal Conductivity 30
- 3.2.5 Navier–Stokes–Fourier Equations 31
- 3.2.6 Thermodynamic Coefficients 31
- 3.2.7 Ideal Compressible Fluids 32
- 3.2.8 Suspensions and Bubbly Liquids . 32
- 3.2.9 Elastic Solids 33

3.3 **Equations of Linear Acoustics** 35
- 3.3.1 The Linearization Process 35
- 3.3.2 Linearized Equations for an Ideal Fluid 36
- 3.3.3 The Wave Equation 36
- 3.3.4 Wave Equations for Isotropic Elastic Solids 36
- 3.3.5 Linearized Equations for a Viscous Fluid 37
- 3.3.6 Acoustic, Entropy, and Vorticity Modes 37
- 3.3.7 Boundary Conditions at Interfaces 39

3.4 **Variational Formulations** 40
- 3.4.1 Hamilton's Principle 40
- 3.4.2 Biot's Formulation for Porous Media 42
- 3.4.3 Disturbance Modes in a Biot Medium 43

3.5 **Waves of Constant Frequency** 45
- 3.5.1 Spectral Density 45
- 3.5.2 Fourier Transforms 45
- 3.5.3 Complex Number Representation 46
- 3.5.4 Time Averages of Products 47

3.6 **Plane Waves** 47
- 3.6.1 Plane Waves in Fluids 47
- 3.6.2 Plane Waves in Solids 48

3.7 **Attenuation of Sound** 49
- 3.7.1 Classical Absorption 49
- 3.7.2 Relaxation Processes 50
- 3.7.3 Continuously Distributed Relaxations 52
- 3.7.4 Kramers–Krönig Relations 52
- 3.7.5 Attenuation of Sound in Air 55
- 3.7.6 Attenuation of Sound in Sea Water 57

3.8 **Acoustic Intensity and Power** 58
- 3.8.1 Energy Conservation Interpretation 58
- 3.8.2 Acoustic Energy Density and Intensity 58
- 3.8.3 Acoustic Power 59
- 3.8.4 Rate of Energy Dissipation 59
- 3.8.5 Energy Corollary for Elastic Waves 60

Amazon EX1014 Page 45

3.9 **Impedance** 60
3.9.1 Mechanical Impedance 60
3.9.2 Specific Acoustic Impedance 60
3.9.3 Characteristic Impedance 60
3.9.4 Radiation Impedance 61
3.9.5 Acoustic Impedance 61

3.10 **Reflection and Transmission** 61
3.10.1 Reflection at a Plane Surface 61
3.10.2 Reflection at an Interface 62
3.10.3 Theory of the Impedance Tube 62
3.10.4 Transmission through Walls and Slabs 63
3.10.5 Transmission through Limp Plates 64
3.10.6 Transmission through Porous Blankets 64
3.10.7 Transmission through Elastic Plates 64

3.11 **Spherical Waves** 65
3.11.1 Spherically Symmetric Outgoing Waves 65
3.11.2 Radially Oscillating Sphere 66
3.11.3 Transversely Oscillating Sphere 67
3.11.4 Axially Symmetric Solutions 68
3.11.5 Scattering by a Rigid Sphere 73

3.12 **Cylindrical Waves** 75
3.12.1 Cylindrically Symmetric Outgoing Waves 75
3.12.2 Bessel and Hankel Functions 77
3.12.3 Radially Oscillating Cylinder 81
3.12.4 Transversely Oscillating Cylinder .. 81

3.13 **Simple Sources of Sound** 82
3.13.1 Volume Sources 82
3.13.2 Small Piston in a Rigid Baffle 82
3.13.3 Multiple and Distributed Sources. 82
3.13.4 Piston of Finite Size in a Rigid Baffle 83
3.13.5 Thermoacoustic Sources 84
3.13.6 Green's Functions 85
3.13.7 Multipole Series 85
3.13.8 Acoustically Compact Sources 86
3.13.9 Spherical Harmonics 86

3.14 **Integral Equations in Acoustics** 87
3.14.1 The Helmholtz–Kirchhoff Integral 87
3.14.2 Integral Equations for Surface Fields 88

3.15 **Waveguides, Ducts, and Resonators** 89
3.15.1 Guided Modes in a Duct 89
3.15.2 Cylindrical Ducts 90
3.15.3 Low-Frequency Model for Ducts .. 90
3.15.4 Sound Attenuation in Ducts 91
3.15.5 Mufflers and Acoustic Filters 92
3.15.6 Non-Reflecting Dissipative Mufflers 93
3.15.7 Expansion Chamber Muffler 93
3.15.8 Helmholtz Resonators 93

3.16 **Ray Acoustics** 94
3.16.1 Wavefront Propagation 94
3.16.2 Reflected and Diffracted Rays 95
3.16.3 Inhomogeneous Moving Media ... 96
3.16.4 The Eikonal Approximation 96
3.16.5 Rectilinear Propagation of Amplitudes 97

3.17 **Diffraction** 98
3.17.1 Posing of the Diffraction Problem 98
3.17.2 Rays and Spatial Regions 98
3.17.3 Residual Diffracted Wave 99
3.17.4 Solution for Diffracted Waves 102
3.17.5 Impulse Solution 102
3.17.6 Constant-Frequency Diffraction .. 103
3.17.7 Uniform Asymptotic Solution 103
3.17.8 Special Functions for Diffraction .. 104
3.17.9 Plane Wave Diffraction 105
3.17.10 Small-Angle Diffraction 106
3.17.11 Thin-Screen Diffraction 107

3.18 **Parabolic Equation Methods** 107

References 108

Part A | 3

List of symbols

B_V	bulk modulus at constant entropy
c	speed of sound
c_p	specific heat at constant pressure
c_v	specific heat at constant volume
D/Dt	convective time derivative
$\mathfrak{D}$	rate of energy dissipation per unit volume
$\boldsymbol{e}_i$	unit vector in the direction of increasing x_i
f	frequency, cycles per second
$\boldsymbol{f}$	force per unit volume
f_1, f_2	volume fractions
$\boldsymbol{g}$	acceleration associated with gravity
h	absolute humidity, fraction of molecules that are water
$H(\omega)$	transfer function
$\boldsymbol{I}$	acoustic intensity (energy flux)
k	wavenumber
$\mathfrak{L}$	Lagrangian density

Amazon EX1014 Page 46

M	average molecular weight
$\boldsymbol{n}$	unit vector normal to a surface
p	pressure
$\hat{p}(\omega)$	Fourier transform of $p(t)$, complex amplitude
$\boldsymbol{q}$	heat flux vector
Q	quality factor
R_0	universal gas constant
Re	real part
s	entropy per unit mass
S	surface, surface area
$\boldsymbol{t}$	traction vector, force per unit area
T	absolute temperature
$\mathfrak{T}$	kinetic energy per unit volume
u	internal energy per unit mass
$\boldsymbol{u}$	locally averaged displacement field of solid matter
$\boldsymbol{U}$	locally averaged displacement field of fluid matter
$\mathfrak{U}$	strain energy per unit volume
$\boldsymbol{v}$	fluid velocity
V	volume
w	acoustic energy density
α	attenuation coefficient
β	coefficient of thermal expansion
γ	specific heat ratio
δ_{ij}	Kronecker delta
$\delta(t)$	delta function
∂	partial differentiation operator
ϵ	expansion parameter
ϵ_{ij}	component of the strain tensor
ζ	location of pole in the complex plane
η	loss factor
θ_{I}	angle of incidence
κ	coefficient of thermal conduction
λ	wavelength
λ_{L}	Lamè constant for a solid
μ	(shear) viscosity
μ_{B}	bulk viscosity
μ_{L}	Lamè constant for a solid
ν	Poisson's ratio
ξ	internal variable in irreversible thermodynamics
ξ_j	component of the displacement field
π	ratio of circle circumference to diameter
ρ	density, mass per unit volume
σ_{ij}	component of the stress tensor
τ_{B}	characteristic time in the Biot model
τ_ν	relaxation time associated with ν-th process
ϕ	phase constant
Φ	scalar potential
$\chi(x)$	nominal phase change in propagation distance x
$\boldsymbol{\Psi}$	vector potential
ω	angular frequency, radians per second

3.1 Introduction

Small-amplitude phenomena can be described to a good approximation in terms of linear algebraic and linear differential equations. Because acoustic phenomenon are typically of small amplitude, the analysis that accompanies most applications of acoustics consequently draws upon a linearized theory, briefly referred to as linear acoustics.

One reason why one chooses to view acoustics as a linear phenomenon, unless there are strong indications of the importance of nonlinear behavior, is the intrinsic conceptual simplicity brought about by the principle of superposition, which can be loosely described by the relation

$$\mathfrak{L}(af_1 + bf_2) = a\mathfrak{L}(f_1) + b\mathfrak{L}(f_2)\,, \tag{3.1}$$

where f_1 and f_2 are two *causes* and $\mathfrak{L}(f)$ is the set of possible mathematical or computational steps that predicts the *effect* of the cause f, such steps being describable so that they are the same for any such cause. The quantities a and b are arbitrary numbers. Doubling a cause doubles the effect, and the effect of a sum of two causes is the sum of the effects of each of the separate causes.

Thus, for example, a complicated sound field caused by several sources can be regarded as a sum of fields, each of which is caused by an individual source. Moreover, if there is assurance that the governing equations have time-independent coefficients, then the concept of frequency has great utility. Waves of each frequency propagate independently, so one can analyze the generation and propagation of each frequency separately, and then combine the results.

Nevertheless, linear acoustics should always be regarded as an approximation, and the understanding of nonlinear aspects of acoustics is of increasing importance in modern applications. Consequently, part of

Amazon EX1014 Page 47

the task of the present chapter is to explain in what sense linear acoustics is an approximation. An extensive discussion of the extent to which the linearization approximation is valid is not attempted, but a discussion is given of the manner in which the linear equations result from nonlinear equations that are regarded as more nearly exact.

The historical origins [3.1] of linear acoustics reach back to antiquity, to *Pythagoras* and *Aristotle* [3.2], both of whom are associated with ancient Greece, and also to persons associated with other ancient civilizations. The mathematical theory began with Mersenne, Galileo, and Newton, and developed into its more familiar form during the time of *Euler* and *Lagrange* [3.3]. Prominent contributors during the 19-th century include Poisson, Laplace, Cauchy, Green, Stokes, Helmholtz, Kirchhoff, and Rayleigh. The latter's book [3.4], *The Theory of Sound*, is still widely read and quoted today.

3.2 Equations of Continuum Mechanics

Sound can propagate through liquids, gases, and solids. It can also propagate through composite media such as suspensions, mixtures, and porous media. In any portion of a medium that is of uniform composition, the general equations that are assumed to apply are those that are associated with the theory of continuum mechanics.

3.2.1 Mass, Momentum, and Energy Equations

The primary equations governing sound are those that account for the conservation of mass and energy, and for changes in momentum. These may be written in the form of either partial differential equations or integral equations. The former is the customary starting point for the derivation of approximate equations for linear acoustics. Extensive discussions of the equations of continuum mechanics can be found in texts by *Thompson* [3.5], *Fung* [3.6], *Shapiro* [3.7], *Batchelor* [3.8], *Truesdell* [3.9]), and *Landau* and *Lifshitz* [3.10], and in the encyclopedia article by *Truesdell* and *Toupin* [3.11].

The conservation of mass is described by the partial differential equation,

$$\frac{\partial \rho}{\partial t} + \nabla\cdot(\rho \boldsymbol{v}) = 0\,, \tag{3.2}$$

where ρ is the (possibly position- and time-dependent) mass density (mass per unit volume of the material), and $\boldsymbol{v}$ is the local and instantaneous particle velocity, defined so that $\rho\boldsymbol{v}\cdot\boldsymbol{n}$ is the net mass flowing per unit time per unit area across an arbitrary stationary surface within the material whose local unit outward normal vector is $\boldsymbol{n}$.

The generalization of Newton's second law to a continuum is described by Cauchy's equation of motion, which is written in Cartesian coordinates as

$$\rho\frac{\mathrm{D}\boldsymbol{v}}{\mathrm{D}t} = \sum_{ij} \boldsymbol{e}_i \frac{\partial \sigma_{ij}}{\partial x_j} + \boldsymbol{g}\rho\,. \tag{3.3}$$

Here the Eulerian description is used, with each field variable regarded as a function of actual spatial position coordinates and time. (The alternate description is the Lagrangian description, where the field variables are regarded as functions of the coordinates that the material being described would have in some reference configuration.) The σ_{ij} are the Cartesian components of the stress tensor. The quantities $\boldsymbol{e}_i$ are the unit vectors in a Cartesian coordinate system. These stress tensor components are such that

$$\boldsymbol{t} = \sum_{i,j} \boldsymbol{e}_i \sigma_{ij} n_j \tag{3.4}$$

is the traction vector, the *surface* force per unit area on any given surface with local unit outward normal $\boldsymbol{n}$.

The second term on the right of (3.3) is a body-force term associated with gravity, with $\boldsymbol{g}$ representing the vector acceleration due to gravity. In some instances, it may be appropriate (as in the case of analyses of transduction) to include body-force terms associated with external electromagnetic fields, but such are excluded from consideration in the present chapter.

The time derivative operator on the left side of (3.3) is Stokes' total time derivative operator [3.12],

$$\frac{\mathrm{D}}{\mathrm{D}t} = \frac{\partial}{\partial t} + \boldsymbol{v}\cdot\nabla\,, \tag{3.5}$$

with the two terms corresponding to: (i) the time derivative as would be seen by an observer at rest, and (ii) the convective time derivative. This total time derivative applied to the particle velocity field yields the particle acceleration field, so the right side of (3.3) is the apparent force per unit volume on an element of the continuum.

The stress tensor's Cartesian component σ_{ij} is, in accordance with (3.4), the i-th component of the surface force per unit area on a segment of the (internal and hypothetical) surface of a small element of the continuum, when the unit outward normal to the surface is in

Amazon EX1014 Page 48

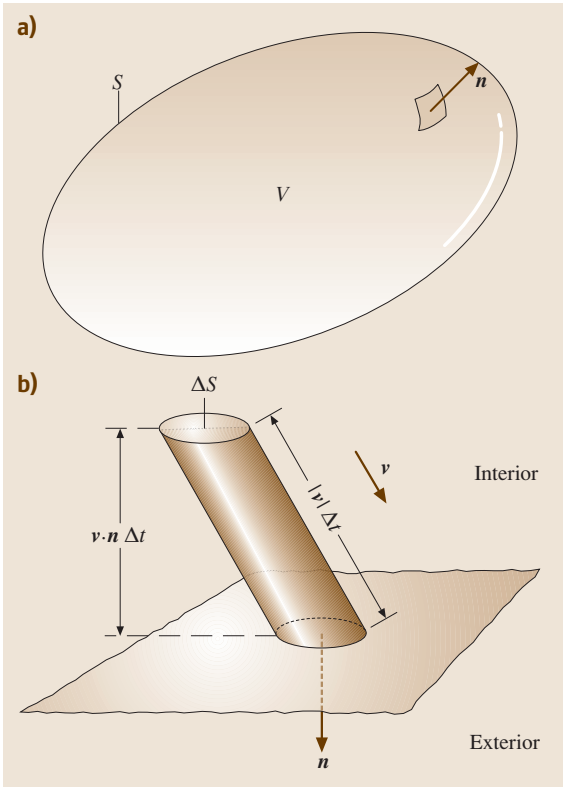


Fig. 3.1 Sketches supporting the identification of $\rho \boldsymbol{v}\cdot\boldsymbol{n}$ as mass flowing per unit area and per unit time through a surface whose unit outward normal is $\boldsymbol{n}$. All the matter in the slanted cylinder's volume flows through the area ΔS in time Δt

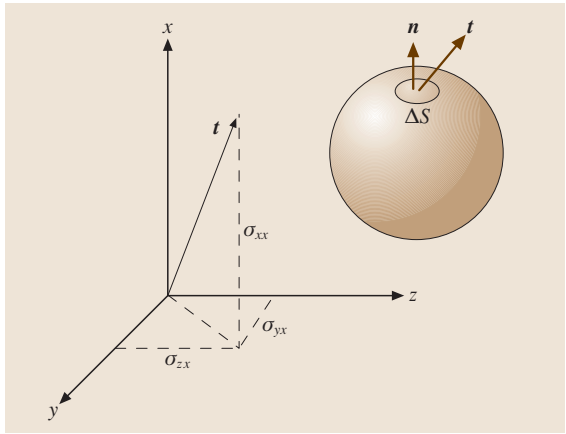


Fig. 3.2 Traction vector on a surface whose unit normal $\boldsymbol{n}$ is in the $+x$-direction

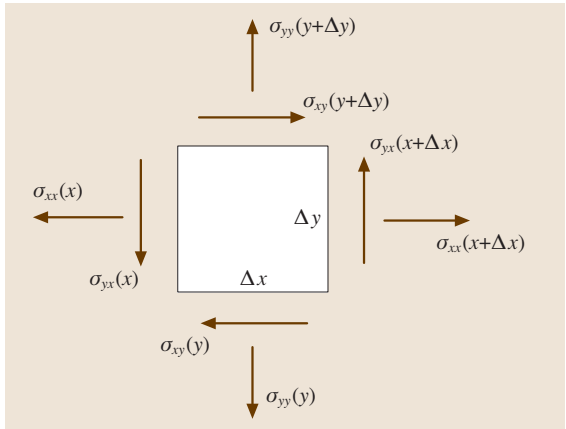


Fig. 3.3 Two-dimensional sketch supporting the identification of the force per unit volume associated with stress in terms of partial derivatives of the stress components

the j-th direction. This surface force is caused by interactions with the neighboring particles just outside the surface or by the transfer of momentum due to diffusion of molecules across the surface.

The stress-force term on the right side of (3.3) results from the surface-force definition of the stress components and from a version of the divergence theorem, so that the stress-related force per unit volume is

$$\boldsymbol{f}_{\text{stress}} \to \frac{1}{V}\int_S \boldsymbol{t}(\boldsymbol{n})\,\mathrm{d}S \to \frac{1}{V}\int_S \sum_{ij} \boldsymbol{e}_i \sigma_{ij} n_j\,\mathrm{d}S$$
$$\to \frac{1}{V}\int_V \sum_{ij} \boldsymbol{e}_i \frac{\partial \sigma_{ij}}{\partial x_j}\,\mathrm{d}V \to \sum_{ij} \boldsymbol{e}_i \frac{\partial \sigma_{ij}}{\partial x_j}\,. \quad (3.6)$$

Here V is an arbitrary but small volume enclosing the point of interest, and S is the surface enclosing that volume; the quantity $\boldsymbol{n}$ is the unit outward normal vector to the surface.

Considerations of the net torque that such surface forces would exert on a small element, and the requirement that the angular acceleration of the element be finite in the limit of very small element dimensions, leads to the conclusion,

$$\sigma_{ij} = \sigma_{ji}\,, \quad (3.7)$$

so the stress tensor is symmetric.

The equations described above are supplemented by an energy conservation relation,

$$\rho \frac{\mathrm{D}}{\mathrm{D}t}\left(\tfrac{1}{2}v^2 + u\right) = \sum_{ij} \frac{\partial}{\partial x_j}\left(\sigma_{ij} v_i\right) + \rho \boldsymbol{g}\cdot\boldsymbol{v} - \nabla\cdot\boldsymbol{q}\,, \quad (3.8)$$

Amazon EX1014 Page 49

which involves the internal energy u per unit mass and the heat flux vector $\boldsymbol{q}$. The latter has the interpretation that its dot product with any unit normal vector represents the heat energy flowing per unit time and per unit area across any internal surface with the corresponding unit normal. An alternate version,

$$\rho \frac{\mathrm{D}u}{\mathrm{D}t} = \sum_{ij} \sigma_{ij} \frac{\partial v_i}{\partial x_j} - \nabla \cdot \boldsymbol{q} \,, \tag{3.9}$$

of the energy equation results when the vector dot product of $\boldsymbol{v}$ with (3.3) is subtracted from (3.8). [In carrying through the derivation, one recognizes that $\boldsymbol{v} \cdot (\rho \mathrm{D}\boldsymbol{v}/\mathrm{D}t)$ is $(1/2)\rho \mathrm{D}v^2/\mathrm{D}t$.]

3.2.2 Newtonian Fluids and the Shear Viscosity

The above equations apply to both fluids and solids. Additional equations needed to complete the set must take into account the properties of the material that make up the continuum. Air and water, for example, are fluids, and their viscous behavior corresponds to that for newtonian fluids, so that the stress tensor is given by

$$\sigma_{ij} = \sigma_\mathrm{n} \delta_{ij} + \mu \phi_{ij} \,, \tag{3.10}$$

which involves the rate-of-shear tensor,

$$\phi_{ij} = \frac{\partial v_i}{\partial x_j} + \frac{\partial v_j}{\partial x_i} - \frac{2}{3} \nabla \cdot \boldsymbol{v} \delta_{ij} \,, \tag{3.11}$$

which is defined so that the sum of its diagonal elements is zero. The quantity σ_n that appears in (3.10) is the average normal stress component, and μ is the shear viscosity, while δ_{ij} is the Kronecker delta, equal to unity if the two indices are equal and otherwise equal to zero.

3.2.3 Equilibrium Thermodynamics

Further specification of the equations governing sound requires some assumptions concerning the extent to which equilibrium or near-equilibrium thermodynamics applies to acoustic disturbances. In the simplest idealization, which neglects relaxation processes, one assumes that the thermodynamic variables describing the perturbations are related just as for quasi-equilibrium processes, so one can use an equation of state of the form

$$s = s(u, \rho^{-1}) \,, \tag{3.12}$$

which has the corresponding differential relation [3.13],

$$T \,\mathrm{d}s = \mathrm{d}u + p \,\mathrm{d}\rho^{-1} \,, \tag{3.13}$$

in accordance with the second law of thermodynamics. Here s is the entropy per unit mass, T is the absolute temperature, and p is the absolute pressure. The reciprocal of the density, which appears in the above relations, is recognized as the specific volume. (Here the adjective specific means per unit mass.)

For the case of an ideal gas with temperature-independent specific heats, which is a common idealization for air, the function in (3.12) is given by

$$s = \frac{R_0}{M} \ln \left(u^{1/(\gamma-1)} \rho^{-1} \right) + s_0 \,. \tag{3.14}$$

Here s_0 is independent of u and ρ^{-1}, while M is the average molecular weight (average molecular mass in atomic mass units), and R_0 is the universal gas constant (equal to Boltzmann's constant divided by the mass in an atomic mass unit), equal to 8314 J/kgK. The quantity γ is the specific heat ratio, equal to approximately 7/5 for diatomic gases, to 5/3 for monatomic gases, and to 9/7 for polyatomic gases whose molecules are not collinear. For air (which is primarily a mixture of diatomic oxygen, diatomic nitrogen, with approximately 1% monatomic argon), γ is 1.4 and M is 29.0. (The expression given here for entropy neglects the contribution of internal vibrations of diatomic molecules, which cause the specific heats and γ to depend slightly on temperature. When one seeks to explain the absorption of sound in air, a nonequilibrium entropy [3.14] is used which depends on the fractions of O_2 and N_2 molecules that are in their first excited vibrational states, in addition to the quantities u and ρ^{-1}.)

For other substances, a knowledge of the first and second derivatives of s, evaluated at some representative thermodynamic state, is sufficient for most linear acoustics applications.

3.2.4 Bulk Viscosity and Thermal Conductivity

The average normal stress must equal the negative of the thermodynamic pressure that enters into (3.13), when the fluid is in equilibrium. Consideration of the requirement that the equations be the same regardless of the choice of directions of the coordinate axes, plus the assumption of a newtonian fluid, lead to the relation [3.12],

$$\sigma_\mathrm{n} = -p + \mu_\mathrm{B} \nabla \cdot \boldsymbol{v} \,, \tag{3.15}$$

which involves the bulk viscosity μ_B. Also, the Fourier model for heat conduction [3.15] requires that the heat flux vector $\boldsymbol{q}$ be proportional to the gradient of the

Amazon EX1014 Page 50

temperature,

$$\boldsymbol{q} = -\kappa \nabla T \,, \tag{3.16}$$

where κ is the coefficient of thermal conduction.

Transport Properties of Air

Regarding the values of the viscosities and the thermal conductivity that enter into the above expressions, the values for air are approximated [3.16–18] by

$$\mu_S = \mu_0 \left(\frac{T}{T_0}\right)^{3/2} \frac{T_0 + T_S}{T + T_S} \,, \tag{3.17}$$

$$\mu_B = 0.6 \mu_S \,, \tag{3.18}$$

$$\kappa = \kappa_0 \left(\frac{T}{T_0}\right)^{3/2} \frac{T_0 + T_A \, e^{-T_B/T_0}}{T + T_A \, e^{-T_B/T}} \,. \tag{3.19}$$

Here T_S is 110.4 K, T_A is 245.4 K, T_B is 27.6 K, T_0 is 300 K, μ_0 is 1.846×10^{-5} kg/(ms), and κ_0 is 2.624×10^{-2} W/(mK).

Transport Properties of Water

The corresponding values of the viscosities and the thermal conductivity of water depend only on temperature and are given by [3.19, 20]

$$\mu_S = 1.002 \times 10^{-3} \, e^{-0.0248 \Delta T} \,, \tag{3.20}$$

$$\mu_B = 3 \mu_S \,, \tag{3.21}$$

$$\kappa = 0.597 + 0.0017 \Delta T - 7.5 \times 10^{-6} (\Delta T)^2 \,. \tag{3.22}$$

The quantities that appear in these equations are understood to be in MKS units, and ΔT is the temperature relative to 283.16 K (10 °C).

3.2.5 Navier–Stokes–Fourier Equations

The assumptions represented by (3.12, 13, 15), and (3.16) cause the governing continuum mechanics equations for a fluid to reduce to

$$\frac{\partial \rho}{\partial t} + \nabla \cdot (\rho \boldsymbol{v}) = 0 \,, \tag{3.23}$$

$$\rho \frac{\mathrm{D}\boldsymbol{v}}{\mathrm{D}t} = -\nabla p + \nabla \left(\mu_B \nabla \cdot \boldsymbol{v}\right) + \sum_{ij} \boldsymbol{e}_i \frac{\partial}{\partial x_j} (\mu \phi_{ij}) + \boldsymbol{g} \rho \,, \tag{3.24}$$

$$\rho T \frac{\mathrm{D}s}{\mathrm{D}t} = \tfrac{1}{2} \mu \sum_{ij} \phi_{ij}^2 + \mu_B \left(\nabla \cdot \boldsymbol{v}\right)^2 + \nabla \cdot (\kappa \nabla T) \,, \tag{3.25}$$

which are known as the Navier–Stokes–Fourier equations for compressible flow.

3.2.6 Thermodynamic Coefficients

An implication of the existence of an equation of state of the form of (3.12) is that any thermodynamic variable can be regarded as a function of any other two (independent) thermodynamic variables. The pressure p, for example, can be regarded as a function of ρ and T, or of s and ρ. In the expression of differential relations, such as that which gives $\mathrm{d}p$ as a linear combination of $\mathrm{d}s$ and $\mathrm{d}\rho$, it is helpful to express the coefficients in terms of a relatively small number of commonly tabulated quantities. A standard set of such includes:

1. the square of the sound speed,

$$c^2 = \left(\frac{\partial p}{\partial \rho}\right)_s \,, \tag{3.26}$$

2. the bulk modulus at constant entropy,

$$B_V = \rho c^2 = \rho \left(\frac{\partial p}{\partial \rho}\right)_s \,, \tag{3.27}$$

3. the specific heat at constant pressure,

$$c_p = T \left(\frac{\partial s}{\partial T}\right)_p \,, \tag{3.28}$$

4. the specific heat at constant volume,

$$c_v = T \left(\frac{\partial s}{\partial T}\right)_\rho \,, \tag{3.29}$$

5. the coefficient of thermal expansion,

$$\beta = \rho \left(\frac{\partial (1/\rho)}{\partial T}\right)_p \,. \tag{3.30}$$

(The subscripts on the partial derivatives indicate the independent thermodynamic quantity that is kept fixed during the differentiation.) The subscript V on B_V is included here to remind one that the modulus is associated with changes in volume. For a fixed mass of fluid the decrease in volume per unit volume per unit increase in pressure is the bulk compressibility, and the reciprocal of this is the bulk modulus.

The coefficients that are given here are related by the thermodynamic identity,

$$\gamma - 1 = T \beta^2 c^2 / c_p \,, \tag{3.31}$$

where γ is the specific heat ratio,

$$\gamma = \frac{c_p}{c_v} \,. \tag{3.32}$$

Amazon EX1014 Page 51

In terms of the thermodynamic coefficients defined above, the differential relations of principal interest in acoustics are

$$\mathrm{d}\rho = \frac{1}{c^2}\mathrm{d}p - \left(\frac{\rho\beta T}{c_\mathrm{p}}\right)\mathrm{d}s\,, \tag{3.33}$$

$$\mathrm{d}T = \left(\frac{T\beta}{\rho c_\mathrm{p}}\right)\mathrm{d}p + \left(\frac{T}{c_\mathrm{p}}\right)\mathrm{d}s\,. \tag{3.34}$$

Thermodynamic Coefficients for an Ideal Gas

For an ideal gas, which is the common idealization for air, it follows from (3.12) and (3.13) (with the abbreviation R for R_0/M) that the thermodynamic coefficients are given by

$$c^2 = \gamma RT = \frac{\gamma p}{\rho}\,, \tag{3.35}$$

$$c_\mathrm{p} = \frac{\gamma R}{\gamma - 1}\,, \tag{3.36}$$

$$c_\mathrm{v} = \frac{R}{\gamma - 1}\,, \tag{3.37}$$

$$\beta = \frac{1}{T}\,. \tag{3.38}$$

For air, R is 287 J/kgK and γ is 1.4, so c_p and c_v are 1005 J/kgK and 718 J/kgK. A temperature of 293.16 K and a pressure of 10^5 Pa yield a sound speed of 343 m/s and a density ρ of 1.19 kg/m^3.

Thermodynamic Properties of Water

For pure water [3.21], the sound speed is approximately given in MKS units by

$$c = 1447 + 4.0\Delta T + 1.6\times 10^{-6} p\,. \tag{3.39}$$

Here c is in meters per second, ΔT is temperature relative to 283.16 K (10 °C), and p is absolute pressure in pascals. The pressure and temperature dependence of the density [3.19] is approximately given by

$$\rho \approx 999.7 + 0.048\times 10^{-5} p - 0.088\Delta T - 0.007(\Delta T)^2\,. \tag{3.40}$$

The coefficient of thermal expansion is given by

$$\beta \approx (8.8 + 0.022\times 10^{-5} p + 1.4\Delta T)\times 10^{-5}\,, \tag{3.41}$$

and the coefficient of specific heat at constant pressure is approximately given by

$$c_\mathrm{p} \approx 4192 - 0.40\times 10^{-5} p - 1.6\Delta T\,. \tag{3.42}$$

The specific heat ratio is very close to unity, the deviation being described by

$$\frac{\gamma - 1}{\gamma} \approx 0.0011\left(1 + \frac{\Delta T}{6} + 0.0024\times 10^{-5} p\right)^2\,. \tag{3.43}$$

The values for sea water are somewhat different, because of the presence of dissolved salts. An approximate expression for the speed of sound in sea water [3.22] is given by

$$c \approx 1490 + 3.6\Delta T + 1.6\times 10^{-6} p + 1.3\Delta S\,. \tag{3.44}$$

Here ΔS is the deviation of the salinity in parts per thousand from a nominal value of 35.

3.2.7 Ideal Compressible Fluids

If viscosity and thermal conductivity are neglected at the outset, then the Navier–Stokes equation (3.24) reduces to

$$\rho\frac{\mathrm{D}\boldsymbol{v}}{\mathrm{D}t} = -\nabla p + \boldsymbol{g}\rho\,, \tag{3.45}$$

which is known as the Euler equation. The energy equation (3.25) reduces to the isentropic flow condition

$$\frac{\mathrm{D}s}{\mathrm{D}t} = 0\,. \tag{3.46}$$

Moreover, the latter in conjunction with the differential equation of state (3.33) yields

$$\frac{\mathrm{D}p}{\mathrm{D}t} = c^2\frac{\mathrm{D}\rho}{\mathrm{D}t}\,. \tag{3.47}$$

The latter combines with the conservation of mass relation (3.2) to yield

$$\frac{\mathrm{D}p}{\mathrm{D}t} + \rho c^2\nabla\cdot\boldsymbol{v} = 0\,, \tag{3.48}$$

where ρc^2 is recognized as the bulk modulus B_V.

In many applications of acoustics, it is these equations that are used as a starting point.

3.2.8 Suspensions and Bubbly Liquids

Approximate equations of the same general form as those for an ideal fluid result for fluids that have small particles of a different material suspended in them. Let the fluid itself have ambient density ρ_1 and let the material of the suspended particles have ambient density ρ_2.

The fractions of the overall volume that are occupied by the two materials are denoted by f_1 and f_2, so that $f_1 + f_2 = 1$. Thus, a volume V contains a mass

$$M = \rho_1 f_1 V + \rho_2 f_2 V\,. \tag{3.49}$$

Amazon EX1014 Page 52

The equivalent density M/V is consequently

$$\rho_{\mathrm{eq}} = \rho_1 f_1 + \rho_2 f_2 \,. \tag{3.50}$$

The equivalent bulk modulus is deduced by considering the decrease $-\Delta V$ of such a volume due to an increment Δp of pressure with the assumption that the pressure is uniform throughout the volume, so that

$$-\Delta V = V_1 \frac{\Delta p}{B_{\mathrm{V},1}} + V_2 \frac{\Delta p}{B_{\mathrm{V},2}} \,, \tag{3.51}$$

where $V_1 = f_1 V$ and $V_2 = f_2 V$ are the volumes occupied by the two materials. The equivalent bulk modulus consequently satisfies the relation

$$\frac{1}{B_{\mathrm{V,eq}}} = \frac{f_1}{B_{\mathrm{V},1}} + \frac{f_2}{B_{\mathrm{V},2}} \,. \tag{3.52}$$

The bulk modulus for any material is the density times the sound speed squared, so the effective sound speed for the mixture satisfies the relation

$$\frac{1}{\rho_{\mathrm{eq}} c_{\mathrm{eq}}^2} = \frac{f_1}{\rho_1 c_1^2} + \frac{f_2}{\rho_2 c_2^2} \,, \tag{3.53}$$

whereby

$$\frac{1}{c_{\mathrm{eq}}^2} = \left(\frac{f_1}{\rho_1 c_1^2} + \frac{f_2}{\rho_2 c_2^2} \right) (\rho_1 f_1 + \rho_2 f_2) \,. \tag{3.54}$$

The latter relation, rewritten in an equivalent form, is sometimes referred to as *Wood's* equation [3.23], and can be traced back to a paper by *Mallock* [3.24].

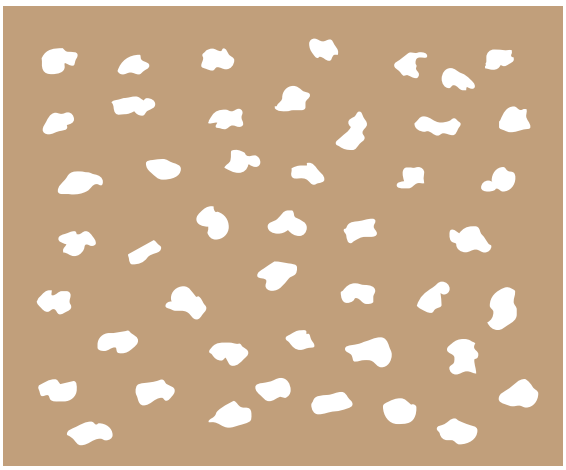


Fig. 3.4 Sketch of a fluid with embedded particles suspended within it

3.2.9 Elastic Solids

For analyses of acoustic wave propagation in solids (including crystals), the idealization of a linear elastic solid [3.6, 25–28] is often used. The solid particle displacements are regarded as sufficiently small that convective time derivatives can be neglected, so the Cauchy equation, given previously by (3.3), reduces, with the omission of the invariably negligible gravity term, to an equation, whose i-th Cartesian component is

$$\rho \frac{\partial^2 \xi_i}{\partial t^2} = \sum_{j=1}^{3} \frac{\partial \sigma_{ij}}{\partial x_j} \,. \tag{3.55}$$

Here ρ is the density; $\xi_i(\boldsymbol{x}, t)$ is the i-th Cartesian component of the displacement of the particle nominally at $\boldsymbol{x}$. This displacement is measured relative to the particle's ambient position. Also, the ambient stress is presumed sufficiently small or slowly varying with position that it is sufficient to take the stress components that appear in Cauchy's equation as being those associated with the disturbance. These should vanish when there is no strain associated with the disturbance.

The stress tensor components σ_{ij} are ordinarily taken to be linearly dependent on the (linear) strain components,

$$\epsilon_{ij} = \frac{1}{2} \left(\frac{\partial \xi_i}{\partial x_j} + \frac{\partial \xi_j}{\partial x_i} \right) \,, \tag{3.56}$$

so that

$$\sigma_{ij} = \sum_{kl} K_{ijkl} \epsilon_{kl} \,. \tag{3.57}$$

The number of required distinct elastic coefficients is limited for various reasons. One is that the stress tensor is symmetric and another is that the strain tensor is symmetric. Also, if the quasistatic work required to achieve a given state of deformation is independent of the detailed history of the deformation, then there must be a strain-energy density function $\mathfrak{U}$ that, in the limit of small deformations, is a bilinear function of the strains. There are only six different strain components and the number of their distinct products is $6+5+4+3+2+1 = 21$, and such is the maximum number of coefficients that one might need. Any intrinsic symmetry, such as exists in various types of crystals, will reduce this number further [3.29].

Strain Energy

The increment of work done during a deformation by stress components on a small element of a solid that is

Amazon EX1014 Page 53

initially a small box (Δx by Δy by Δz) is

$$\delta[\text{Work}] = \sum_i \sigma_{ii} \left(\frac{\partial}{\partial x_i} \delta\xi_i \right) \Delta x \Delta y \Delta z + \sum_{i \neq j} \sigma_{ij} \left(\frac{\partial}{\partial x_j} \delta\xi_i \right) \Delta x \Delta y \Delta z \,, \quad (3.58)$$

where here σ_{ij} is interpreted as the i-th component of the force per unit area on a surface whose outward normal is in the direction of increasing x_j. With use of the symmetry of the stress tensor and of the definition of the strain tensor components, one obtains the incremental strain energy per unit volume as

$$\delta\mathfrak{U} = \sum_{ij} \sigma_{ij} \delta\epsilon_{ij} \,. \quad (3.59)$$

If the reference state, where $\mathfrak{U} = 0$, is taken as that in which the strain is zero, and given that each stress component is a linear combination of the strain components, then the above integrates to

$$\mathfrak{U} = \sum_{ij} \frac{1}{2} \sigma_{ij} \epsilon_{ij} \,. \quad (3.60)$$

Here the stresses are understood to be given in terms of the strains by an appropriate stress–strain relation of the general form of (3.57).

Because of the symmetry of both the stress tensor and the strain tensor, the internal energy $\mathfrak{U}$ per unit can be regarded as a function of only the six distinct strain components: ϵ_{xx}, ϵ_{yy}, ϵ_{zz}, ϵ_{xy}, ϵ_{yz}, and ϵ_{xz}. Consequently, with such an understanding, it follows from the differential relation (3.59) that

$$\frac{\partial\mathfrak{U}}{\partial\epsilon_{xx}} = \sigma_{xx} \,; \qquad \frac{\partial\mathfrak{U}}{\partial\epsilon_{xy}} = 2\sigma_{xy} \,, \quad (3.61)$$

with analogous relations for derivatives with respect to the other distinct strain components.

Isotropic Solids

If the properties of the solid are such that they are independent of the orientation of the axes of the Cartesian coordinate system, then the solid is said to be isotropic. This idealization is usually regarded as good if the solid is made up of a random assemblage of many small grains. The tiny grains are possibly crystalline with directional properties, but the orientation of the grains is random, so that an element composed of a large number of grains has no directional orientation. For such an isotropic solid the number of different coefficients in the stress–strain relation (3.57) is only two, and the relation can be taken in the general form

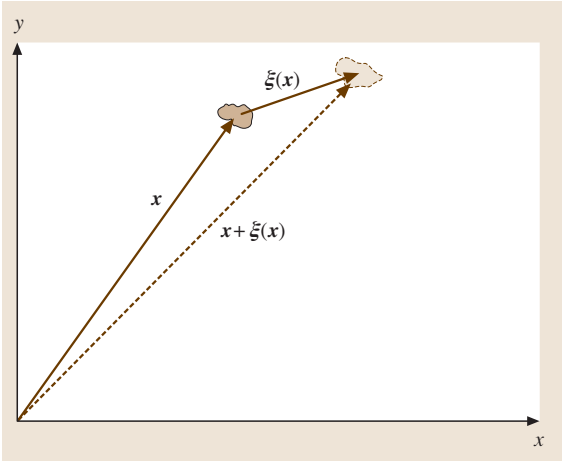


Fig. 3.5 Displacement field vector $\boldsymbol{\xi}$ in a solid. A material point normally at $\boldsymbol{x}$ is displaced to $\boldsymbol{x} + \boldsymbol{\xi}(\boldsymbol{x})$

$$\sigma_{ij} = 2\mu_L \epsilon_{ij} + \lambda_L \delta_{ij} \sum_{k=1}^{3} \epsilon_{kk} \,. \quad (3.62)$$

This involves two material constants, termed the Lamè constants, and here denoted by λ_L and μ_L (the latter being the same as the shear modulus G).

Equivalently, one can express the strain components in terms of the stress components by the inverse of the above set of relations. The generic form is sometimes written

$$\epsilon_{ij} = \frac{1+\nu}{E} \sigma_{ij} - \frac{\nu}{E} \sum_k \sigma_{kk} \delta_{ij} \,, \quad (3.63)$$

where E is the elastic modulus and ν is Poisson's ratio. The relation of these two constants to the Lamè constants is such that

$$\lambda_L = \frac{\nu E}{(1+\nu)(1-2\nu)} \,, \quad (3.64)$$

$$\mu_L = G = \frac{E}{2(1+\nu)} \,. \quad (3.65)$$

In undergraduate texts on the mechanics of materials, the relations (3.63) are often written out separately for the diagonal and off-diagonal strain elements, so

Amazon EX1014 Page 54

Table 3.1 Representative numbers for the elastic properties of various materials. (A comprehensive data set, giving values appropriate to specific details concerning the circumstances and the nature of the specimens, can be found at the web site for MatWeb, Material Property Data)

Material	E(Pa)	ν	λ_L(Pa)	μ_L(Pa)	ρ(kg/m^3)
Aluminum	7.0×10^{10}	0.33	5.1×10^{10}	2.6×10^{10}	2.8×10^{3}
Brass	10.5×10^{10}	0.34	8.3×10^{10}	3.9×10^{10}	8.4×10^{3}
Copper	12.0×10^{10}	0.34	9.5×10^{10}	4.5×10^{10}	8.9×10^{3}
Iron	12.0×10^{10}	0.25	4.8×10^{10}	4.8×10^{10}	7.2×10^{3}
Lead	1.4×10^{10}	0.43	3.2×10^{10}	0.5×10^{10}	11.3×10^{3}
Steel	20.0×10^{10}	0.28	9.9×10^{10}	7.8×10^{10}	7.8×10^{3}
Titanium	11.0×10^{10}	0.34	8.7×10^{10}	4.1×10^{10}	4.5×10^{3}

that,

$$\epsilon_{xx} = \frac{1}{E}[\sigma_{xx} - \nu(\sigma_{yy} + \sigma_{zz})] \,, \tag{3.66}$$

$$\gamma_{xy} = 2\epsilon_{xy} = \frac{1}{G}\sigma_{xy} \,, \tag{3.67}$$

with analogous relations for the other strain components. The nomenclature γ_{xy} is used for what is often termed the shear strain, this being twice as large as that shear strain that is defined as a component of a strain tensor.

The strain energy density $\mathfrak{U}$ of an isotropic solid results from (3.60) and (3.62), the result being

$$\mathfrak{U} = \mu_L \sum_{ij} \epsilon_{ij}^2 + \frac{1}{2}\lambda_L \left(\sum_k \epsilon_{kk}\right)^2 \,. \tag{3.68}$$

In the idealized and simplified model of acoustic propagation in solids, the conservation of mass and energy is not explicitly invoked. The density that appears on the right side of (3.55) is regarded as time independent, and as that appropriate for the undisturbed state of the solid.

3.3 Equations of Linear Acoustics

The equations that one ordinarily deals with in acoustics are linear in the field amplitudes, where the fields of interest are quantities that depend on position and time. The basic governing equations are partial differential equations.

3.3.1 The Linearization Process

Sound results from a time-varying perturbation of the dynamic and thermodynamic variables that describe the medium. For sound in fluids (liquids and gases), the quantities appropriate to the ambient medium (i. e., the medium in the absence of a disturbance) are customarily represented [3.30] by the subscript 0, and the perturbations are represented by a prime on the corresponding symbol. Thus one expresses the total pressure as

$$p = p_0 + p' \,, \tag{3.69}$$

with corresponding expressions for fluctuations in specific entropy, fluid velocity, and density. The linear equations that govern acoustical disturbances are then determined by the first-order terms in the expansion of the governing nonlinear equations in the primed variables. The zeroth-order terms cancel out completely because the ambient variables should themselves correspond to a valid state of motion of the medium. Thus, for example, the linearized version of the conservation of mass relation in (3.2) is

$$\frac{\partial \rho'}{\partial t} + \nabla\cdot(\boldsymbol{v}_0\rho' + \boldsymbol{v}'\rho_0) = 0 \,. \tag{3.70}$$

The possible forms of the linear equations differ in complexity according to what is assumed about the medium's ambient state and according to what dissipative terms are included in the original governing equations. In the establishment of a rationale for using simplified models, it is helpful to think in terms of the order of magnitudes and characteristic scales of the coefficients in more nearly comprehensive models. If the

Amazon EX1014 Page 55

spatial region of interest has bounding dimensions that are smaller than any scale length over which the ambient variables vary by a respectable fraction, then it may be appropriate to idealize the coefficients in the governing equations as if the ambient medium were spatially uniform or homogeneous. Similarly, if the characteristic wave periods or propagation times are much less than characteristic time scales for the ambient medium, then it may be appropriate to idealize the coefficients as being time independent. Examination of orders of magnitudes of terms suggests that the ambient velocity may be neglected if it is much less than the sound speed c. The first-order perturbation to the gravitational force term can ordinarily be neglected [3.31] if the previously stated conditions are met and if the quantity g/c is sufficiently smaller than any characteristic frequency of the disturbance. Analogous inferences can be made about the thermal conductivity and viscosity. However, the latter may be important [3.32] in the interaction of acoustic waves in fluids with adjacent solid bodies.

A discussion of the restrictions on using linear equations and of neglecting second- and higher-order terms in the primed variables is outside the scope of the present chapter, but it should be noted that one regards p' as small [3.30] if it is substantially less than $\rho_0 c^2$, and $|\boldsymbol{v}'|$ as small if it is much less than c, where c is the sound speed defined via (3.26). It is not necessary that p' be much less than p_0, and it is certainly not necessary that $|\boldsymbol{v}'|$ be less than $|\boldsymbol{v}_0|$.

3.3.2 Linearized Equations for an Ideal Fluid

The customary equations for linear acoustics neglect dissipation processes and consequently can be derived from the equations for flow of a compressible ideal fluid, given in (3.45) through (3.48). If one neglects gravity at the outset, and assumes the ambient fluid velocity is zero, then the ambient pressure is constant. In such a case, (3.48) leads after linearization to

$$\frac{\partial p}{\partial t} + \rho c^2 \nabla \cdot \boldsymbol{v} = 0 \,, \tag{3.71}$$

and the Euler equation (3.45) leads to

$$\rho \frac{\partial \boldsymbol{v}}{\partial t} = -\nabla p \,. \tag{3.72}$$

Here a common notational convention is used to delete primes and subscripts. The density ρ here is understood to be the ambient density ρ_0, while p and $\boldsymbol{v}$ are understood to be the acoustically induced perturbations to the pressure and fluid velocity.

These two coupled equations for p and $\boldsymbol{v}$ remain applicable when the ambient density and sound speed vary with position.

3.3.3 The Wave Equation

A single partial differential equation for the acoustic part of the pressure results when one takes the time derivative of (3.71) and then uses (3.72) to reexpress the time derivative of the fluid velocity in terms of pressure. The resulting equation, as derived by Bergmann [3.31] for the case when the density varies with position, is

$$\nabla \cdot \left(\frac{1}{\rho} \nabla p \right) - \frac{1}{\rho c^2} \frac{\partial^2 p}{\partial t^2} = 0 \,. \tag{3.73}$$

If the ambient density is independent of position, then this reduces to

$$\nabla^2 p - \frac{1}{c^2} \frac{\partial^2 p}{\partial t^2} = 0 \,, \tag{3.74}$$

which dates back to Euler and which is what is ordinarily termed the wave equation of linear acoustics. Often this is written as

$$\Box^2 p = 0 \,, \tag{3.75}$$

in terms of the d'Alembertian operator defined by

$$\Box^2 = \nabla^2 - c^{-2} \partial^2 / \partial t^2 \,. \tag{3.76}$$

3.3.4 Wave Equations for Isotropic Elastic Solids

When the ambient density and the Lamé constants are independent of position, the Cauchy equation and the stress–strain relations described by (3.55, 56), and (3.62) can be combined to the single vector equation,

$$\frac{\partial^2 \boldsymbol{\xi}}{\partial t^2} = \left(c_1^2 - c_2^2 \right) \nabla (\nabla \cdot \boldsymbol{\xi}) + c_2^2 \nabla^2 \boldsymbol{\xi} \,, \tag{3.77}$$

which is equivalently written as

$$\frac{\partial^2 \boldsymbol{\xi}}{\partial t^2} = c_1^2 \nabla (\nabla \cdot \boldsymbol{\xi}) - c_2^2 \nabla \times (\nabla \times \boldsymbol{\xi}) \,. \tag{3.78}$$

Here the quantities c_1 and c_2 are defined by

$$c_1^2 = \frac{\lambda_L + 2\mu_L}{\rho} \,, \tag{3.79}$$

$$c_2^2 = \frac{\mu_L}{\rho} \,. \tag{3.80}$$

Because any vector field may be decomposed into a sum of two fields, one with zero curl and the other with zero divergence, one can set the displacement vector $\boldsymbol{\xi}$ to

$$\boldsymbol{\xi} = \nabla\Phi + \nabla\times\boldsymbol{\Psi} \tag{3.81}$$

in terms of a scalar and a vector potential. This expression will satisfy (3.77) identically, provided the two potentials separately satisfy

$$\nabla^2\Phi - \frac{1}{c_1^2}\frac{\partial^2\Phi}{\partial t^2} = 0\,, \tag{3.82}$$

$$\nabla^2\boldsymbol{\Psi} - \frac{1}{c_2^2}\frac{\partial^2\boldsymbol{\Psi}}{\partial t^2} = 0\,. \tag{3.83}$$

Both of these equations are of the form of the simple wave equation of (3.74). The first corresponds to longitudinal wave propagation, and the second corresponds to shear wave propagation. The quantities c_1 and c_2 are referred to as the dilatational and shear wave speeds, respectively.

If the displacement field is irrotational, so that the curl of the displacement vector is zero (as is so for sound in fluids), then each component of the displacement field satisfies (3.82). If the displacement field is solenoidal, so that its divergence is zero, then each component of the displacement satisfies (3.83).

3.3.5 Linearized Equations for a Viscous Fluid

For the restricted but relatively widely applicable case when the Navier–Stokes–Fourier equations are presumed to hold and the characteristic scales of the ambient medium and the disturbance are such that the ambient flow is negligible, and the coefficients are idealizable as constants, the linear equations have the form appropriate for a disturbance in a homogeneous, time-independent, non-moving medium, these equations being

$$\frac{\partial\rho'}{\partial t} + \rho_0\nabla\cdot\boldsymbol{v}' = 0\,, \tag{3.84}$$

$$\rho_0\frac{\partial\boldsymbol{v}'}{\partial t} = -\nabla p' + \left(\frac{1}{3}\mu + \mu_\mathrm{B}\right)\nabla\left(\nabla\cdot\boldsymbol{v}'\right) + \mu\nabla^2\boldsymbol{v}'\,, \tag{3.85}$$

$$\rho_0 T_0\frac{\partial s'}{\partial t} = \kappa\nabla^2 T'\,, \tag{3.86}$$

$$\rho' = \frac{1}{c^2}p' - \left(\frac{\rho\beta T}{c_\mathrm{p}}\right)_0 s'\,, \tag{3.87}$$

$$T' = \left(\frac{T\beta}{\rho c_\mathrm{p}}\right)_0 p' + \left(\frac{T}{c_\mathrm{p}}\right)_0 s'\,. \tag{3.88}$$

The primes on the perturbation field variables are needed here to distinguish them from the corresponding ambient quantities.

3.3.6 Acoustic, Entropy, and Vorticity Modes

In general, any solution of the linearized equations for a fluid with viscosity and thermal conductivity can be regarded [3.30, 32–34] as a sum of three basic types of solutions. The common terminology for these is: (i) the acoustic mode, (ii) the entropy mode, and (iii) the vorticity mode. Thus, with appropriate subscripts denoting the various fundamental mode types, one writes the fluid velocity perturbation in the form,

$$\boldsymbol{v}' = \boldsymbol{v}_\mathrm{ac} + \boldsymbol{v}_\mathrm{ent} + \boldsymbol{v}_\mathrm{vor}\,, \tag{3.89}$$

with similar decompositions for the other field variables. The decomposition is intended to be such that, for waves of constant frequency, each field variable's contribution from any given mode satisfies a partial differential equation that is second order [rather than of some higher order as might be derived from (3.84)–(3.88)] in the spatial derivatives. That such a decomposition is possible follows from a theorem [3.35, 36] that any solution of a partial differential equation of, for example, the form,

$$\left(\nabla^2+\lambda_1\right)\left(\nabla^2+\lambda_2\right)\left(\nabla^2+\lambda_3\right)\psi = 0\,, \tag{3.90}$$

can be written as a sum,

$$\psi = \psi_1 + \psi_2 + \psi_3\,, \tag{3.91}$$

where the individual terms each satisfy second-order differential equations of the form,

$$\left(\nabla^2+\lambda_i\right)\psi_i = 0\,. \tag{3.92}$$

This decomposition is possible providing no two of the λ_i are equal. [In regard to (3.90), one should note that each of the three operator factors is a second-order differential operator, so the overall equation is a sixth-order partial differential equation. One significance of the theorem is that one has replaced the seemingly formidable problem of solving a sixth-order partial differential equation by that of solving three second-order partial differential equations.]

Amazon EX1014 Page 57

Linear acoustics is primarily concerned with solutions of the equations that govern the acoustic mode, while conduction heat transfer is primarily concerned with solutions of the equations that govern the entropy mode. However, the simultaneous consideration of all three solutions is often necessary when one seeks to satisfy boundary conditions at solid surfaces. The decomposition becomes relatively simple when the characteristic angular frequency is sufficiently small that

$$\omega \ll \frac{\rho c^2}{(4/3)\mu + \mu_B} , \tag{3.93}$$

$$\omega \ll \frac{\rho c^2 c_p}{\kappa} . \tag{3.94}$$

These conditions are invariably well met in all applications of interest. For air the right sides of the two inequalities correspond to frequencies of the order of 10^9 Hz, while for water they correspond to frequencies of the order of 10^{12} Hz. If the inequalities are not satisfied, it is also possible that the Navier–Stokes–Fourier model is not appropriate, since the latter presumes that the variations are sufficiently slow that the medium can be regarded as being in quasi-thermodynamic equilibrium.

The acoustic mode and the entropy mode are both characterized by the vorticity (curl of the fluid velocity) being identically zero. (This characterization is consistent with the theorem that any vector field can be decomposed into a sum of a field with zero divergence and a field with zero curl.) In the limit of zero viscosity and zero thermal conductivity [which is a limit consistent with (3.93) and (3.94)], the acoustic mode is characterized by zero entropy perturbations, while the entropy mode is a time-independent entropy perturbation, with zero pressure perturbation. These identifications allow the approximate equations governing the various modes to be developed in the limit for which the inequalities are valid. In carrying out the development, it is convenient to use an expansion parameter defined by,

$$\epsilon = \frac{\omega\mu}{\rho_0 c^2} , \tag{3.95}$$

where ω is a characteristic angular frequency, or equivalently, the reciprocal of a characteristic time for the perturbation. In the ordering, ϵ is regarded as small, μ_B/μ and $\kappa/\mu c_p$ are regarded as of order unity, and all time derivative operators are regarded as of order ω.

Acoustic Mode

To zeroth order in ϵ, the acoustic mode is what results when the thermal conductivity and the viscosities are identically zero and the entropy perturbation is also zero. In such a case, the relations (3.71) and (3.72) are valid and one obtains the wave equation of (3.74). All of the field variables in the acoustic mode satisfy this wave equation to zeroth order in ϵ. This is so because the governing equations have constant coefficients.

When one wishes to take into account the corrections that result to first order in ϵ, the entropy perturbation is no longer regarded as identically zero, but its magnitude can be deduced by replacing the T' that appears in (3.86) by only the first term in the sum of (3.88), the substitution being represented by

$$T_{ac} = \frac{T_0 \beta}{\rho_0 c_p} p_{ac} . \tag{3.96}$$

To the same order of approximation one may use the zeroth-order wave equation (3.74) to express the right side of (3.86) in terms of a second-order time derivative of the acoustic-mode pressure. The resulting equation can then be integrated once in time with the constant of integration set to zero because the acoustic mode's entropy perturbation must vanish when the corresponding pressure perturbation is identically zero. Thus one obtains the acoustic-mode entropy as

$$s_{ac} \approx \frac{\kappa\beta}{\rho_0^2 c^2 c_p} \frac{\partial p_{ac}}{\partial t} , \tag{3.97}$$

correct to first order in ϵ.

This expression for the entropy perturbation is substituted into (3.87) and the resulting expression for ρ_{ac} is substituted into the conservation of mass relation, represented by (3.84), so that one obtains

$$\frac{\partial p_{ac}}{\partial t} - \frac{(\gamma-1)\kappa}{\rho_0 c^2 c_p} \frac{\partial^2 p_{ac}}{\partial t^2} + \rho_0 c^2 \nabla \cdot \boldsymbol{v}_{ac} = 0 . \tag{3.98}$$

The vorticity in the acoustic mode is zero,

$$\nabla \times \boldsymbol{v}_{ac} = 0 , \tag{3.99}$$

so the momentum balance equation (3.85) simplifies to one where the right side is a gradient. Then with an appropriate substitution for the divergence of the fluid velocity from (3.84), one finds that the momentum balance equation to first order in ϵ takes the form

$$\rho_0 \frac{\partial \boldsymbol{v}_{ac}}{\partial t} = -\nabla \left\{ p_{ac} + \frac{1}{\rho_0 c^2} [(4/3)\mu + \mu_B] \frac{\partial p_{ac}}{\partial t} \right\} . \tag{3.100}$$

Amazon EX1014 Page 58

The latter and (3.84), in a manner similar to that in which the wave equation of (3.73) is derived, yield the dissipative wave equation represented by

$$\nabla^2 p_{\rm ac} - \frac{1}{c^2}\frac{\partial^2 p_{\rm ac}}{\partial t^2} + \frac{2\delta_{\rm cl}}{c^4}\frac{\partial^3 p_{\rm ac}}{\partial t^3} = 0\,. \tag{3.101}$$

The quantity $\delta_{\rm cl}$, defined by

$$\delta_{\rm cl} = \frac{1}{2\rho_0}\left[(4/3)\mu + \mu_{\rm B} + (\gamma-1)(\kappa/c_{\rm p})\right]\,, \tag{3.102}$$

is a constant that characterizes the classical dissipation in the acoustic mode.

Entropy Mode

For the entropy mode, the pressure perturbation vanishes to zeroth order in ϵ, while the entropy perturbation does not. Thus for this mode, (3.87) and (3.88) approximate in zeroth order to

$$\rho_{\rm ent} = -\left(\frac{\rho\beta T}{c_{\rm p}}\right)_0 s_{\rm ent}\,, \tag{3.103}$$

$$T_{\rm ent} = \left(\frac{T}{c_{\rm p}}\right)_0 s_{\rm ent}\,. \tag{3.104}$$

The latter when substituted into the energy equation (3.86) yields the diffusion equation of conduction heat transfer,

$$\frac{\partial s_{\rm ent}}{\partial t} = \frac{\kappa}{\rho_0 c_{\rm p}}\nabla^2 s_{\rm ent}\,. \tag{3.105}$$

All of the entropy-mode field variables, including $T_{\rm ent}$, satisfy this diffusion equation to lowest order in ϵ.

The mass conservation equation, with an analogous substitution from (3.103) and another substitution from (3.88), integrates to

$$\boldsymbol{v}_{\rm ent} = \frac{\beta T_0 \kappa}{\rho_0 c_{\rm p}^2}\nabla s_{\rm ent}\,, \tag{3.106}$$

so there is a weak fluid flow caused by entropy or temperature gradients in the entropy mode. The substitution of this expression for the fluid velocity into the linearized Navier–Stokes equation (3.85) subsequently yields a lowest-order expression for the entropy-mode contribution to the pressure perturbation, this being

$$p_{\rm ent} = \frac{\beta T_0}{c_{\rm p}}[(4/3)\mu + \mu_{\rm B} - (\kappa/c_{\rm p})]\frac{\partial s_{\rm ent}}{\partial t}\,. \tag{3.107}$$

Vorticity Mode

For the vorticity mode, the divergence of the fluid velocity is identically zero,

$$\nabla\cdot\boldsymbol{v}_{\rm vor} = 0\,. \tag{3.108}$$

The mass conservation equation (3.84) and the thermodynamic relations, (3.87) and (3.88), consequently require that all of the thermodynamic field quantities with subscript 'vor' are zero. The Navier–Stokes equation (3.85) accordingly requires that each component of the fluid velocity associated with this mode satisfy the vorticity diffusion equation

$$\rho_0\frac{\partial \boldsymbol{v}_{\rm vor}}{\partial t} = \mu\nabla^2\boldsymbol{v}_{\rm vor}\,. \tag{3.109}$$

3.3.7 Boundary Conditions at Interfaces

For the model of a fluid without viscosity or thermal conduction, such as is governed by (3.71)–(3.75), the appropriate boundary conditions at an interface are that the normal component of the fluid velocity be continuous and that the pressure be continuous;

$$\boldsymbol{v}_1\cdot\boldsymbol{n}_{12} = \boldsymbol{v}_2\cdot\boldsymbol{n}_{12}\,; \qquad p_1 = p_2\,. \tag{3.110}$$

At a rigid nonmoving surface, the normal component must consequently vanish,

$$\boldsymbol{v}\cdot\boldsymbol{n} = 0\,, \tag{3.111}$$

but no restrictions are placed on the tangential component of the velocity. The model also places no requirements on the value of the temperature at a solid surface.

When viscosity is taken into account, no matter how small it may be, the model demands additional boundary conditions. An additional condition invariably imposed is that the tangential components of the velocity also be continuous, the rationale [3.37] being that a fluid should not slip any more freely with respect to an interface than it does with itself; this lack of slip is invariably observed [3.38] when the motion is examined sufficiently close to an interface. Similarly, when thermal conduction is taken into account, the rational interpretation of the model requires that the temperature be continuous at an interface. Newton's third law requires that the shear stresses exerted across an interface be continuous, and the conservation of energy requires that the normal component of the heat flux be continuous.

Amazon EX1014 Page 59

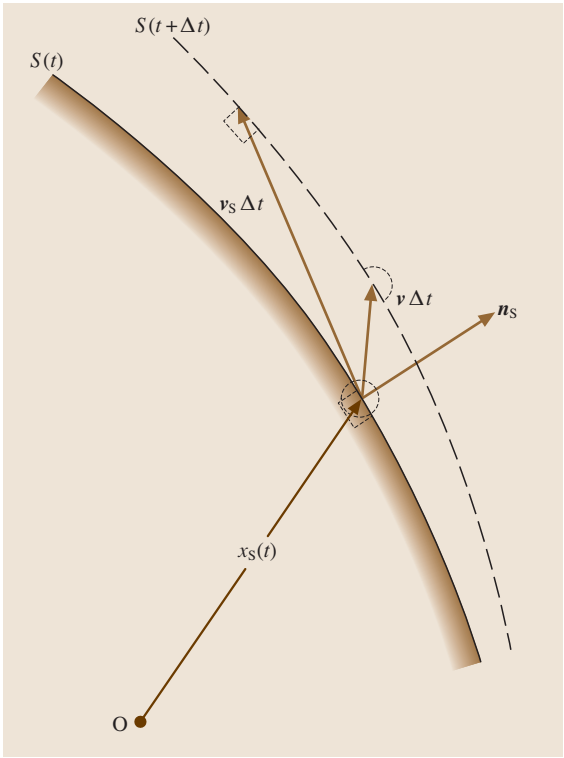


Fig. 3.6 Graphical proof that the normal component of fluid velocity should be continuous at any interface. The interface surface is denoted by $S(t)$, and $\boldsymbol{x}_S(t)$ is the location of any material particle on either side of the interface, but located just at the interface. Both it and the particle on the other side of the interface that neighbors it at time t will continue to stay on the interface, although they may be displaced tangentially

The apparent paradox, that tiny but nonzero values of the viscosity and thermal conductivity should drastically alter the basic nature of the boundary conditions at an interface, is resolved by acoustic boundary-layer theory. Under normal circumstances, disturbances associated with sound are almost entirely in the acoustic mode except in oscillating acoustic boundary layers near interfaces. In these boundary layers, a portion of the disturbance is in the entropy and vorticity modes. These modes make insignificant contributions to the total perturbation pressure and normal velocity component, but have temperature and tangential velocity components, respectively, that are comparable to those of the acoustic mode. The boundary and continuity conditions can be satisfied by the sum of the three mode fields, but not by the acoustic mode field alone. However, the entropy and vorticity mode fields typically die out rapidly with distance from an interface. The characteristic decay lengths [3.30] when the disturbance has an angular frequency ω are

$$\ell_{\text{vor}} = \left(\frac{2\mu}{\omega\rho}\right)^{1/2}, \tag{3.112}$$

$$\ell_{\text{ent}} = \left(\frac{2\kappa}{\omega\rho c_p}\right)^{1/2}. \tag{3.113}$$

Given that the parameter ϵ in (3.95) is much less than unity, these lengths are much shorter than a characteristic wavelength. If they are, in addition, much shorter than the dimensions of the space to which the acoustic field is confined, then the acoustic boundary layer has a minor effect on the acoustic field outside the boundary layer. However, because dissipation of energy can occur within such boundary layers, the existence of a boundary layer can have a long-term accumulative effect. This can be manifested by the larger attenuation of sound waves propagating in pipes [3.39] and in the finite Q (quality factors) of resonators.

3.4 Variational Formulations

Occasionally, the starting point for acoustical analysis is not a set of partial differential equations, such as those described in the previous section, but instead a variational principle. The attraction of such an alternate approach is that it is a convenient departure point for making approximations. The most fundamental of the variational principles is the version of Hamilton's principle [3.40, 41] that applies to a continuum.

3.4.1 Hamilton's Principle

The standard version is that where the displacement field $\boldsymbol{\xi}(\boldsymbol{x}, t)$ is taken as the field variable. The medium is

Amazon EX1014 Page 60

assumed to have no ambient motion, and viscosity and thermal conduction are ignored.

At any given instant and near any given point there is a kinetic energy density taken as

$$\mathfrak{T} = \frac{1}{2}\rho \sum_i \left(\frac{\partial \xi_i}{\partial t}\right)^2 . \tag{3.114}$$

This is the kinetic energy per unit volume; the quantity ρ is understood to be the ambient density, this being an appropriate approximation given that the principle should be consistent with a linear formulation.

The second density of interest is the strain energy density, $\mathfrak{U}$, which is presumed to be a bilinear function of the displacement field components and of their spatial derivatives. For an isotropic linear elastic solid, this is given by (3.68), which can be equivalently written, making use of the definition of the strain components, as

$$\mathfrak{U} = \frac{1}{4}\mu_{\mathrm{L}} \sum_{ij} \left(\frac{\partial \xi_i}{\partial x_j} + \frac{\partial \xi_j}{\partial x_i}\right)^2 + \frac{1}{2}\lambda_{\mathrm{L}} \left(\nabla \cdot \boldsymbol{\xi}\right)^2 . \tag{3.115}$$

For the case of a compressible fluid, the stress tensor is given by

$$\sigma_{ij} = -p\delta_{ij} = \rho c^2 \nabla \cdot \boldsymbol{\xi} \delta_{ij} . \tag{3.116}$$

Here p is the pressure associated with the disturbance, and the second version follows from the time integration of (3.71). The general expression (3.60) consequently yields

$$\mathfrak{U} = \frac{1}{2}\rho c^2 \left(\nabla \cdot \boldsymbol{\xi}\right)^2 \tag{3.117}$$

for the strain energy density in a fluid.

There are other examples that can be considered for which there are different expressions for the strain energy density.

Given the kinetic and strain energy densities, one constructs a Lagrangian density,

$$\mathfrak{L} = \mathfrak{T} - \mathfrak{U} . \tag{3.118}$$

Hamilton's principle then takes the form

$$\delta \iiiint \mathfrak{L} \, \mathrm{d}x \, \mathrm{d}y \, \mathrm{d}z \, \mathrm{d}t = 0 . \tag{3.119}$$

Here the integration is over an arbitrary volume and arbitrary time interval. The symbol δ implies a variation from the exact solution of the problem of interest. In such a variation, the local and instantaneous value $\boldsymbol{\xi}(\boldsymbol{x}, t)$ is considered to deviate by an infinitesimal amount $\delta\boldsymbol{\xi}(\boldsymbol{x}, t)$.

The variation of the Lagrangian is calculated in the same manner as one determines differentials using the chain rule of differentiation. One subsequently uses the fact that a variation of a derivative is the derivative of a variation. One then integrates by parts, whenever necessary, so that one eventually obtains, an equation of the form

$$\iiiint \sum_i [\text{expression}]_i \delta\xi_i \, \mathrm{d}x \, \mathrm{d}y \, \mathrm{d}z \, \mathrm{d}t + [\text{boundary terms}] = 0 . \tag{3.120}$$

Here the boundary terms result from the integrations by parts, and they involve values of the variations at the boundaries (integration limits) of the fourfold integration domain. If one takes the variations to be zero at these boundaries, but otherwise arbitrary within the domain, one concludes that the coefficient expressions of the $\delta\xi_i$ within the integrand must be identically zero when the displacement field is the correct solution. Consequently, one infers that the displacement field components must satisfy

$$[\text{expression}]_i = 0 . \tag{3.121}$$

The detailed derivation yields the above with the form

$$\frac{\partial \mathfrak{L}}{\partial \xi_i} - \frac{\partial}{\partial t}\left(\frac{\partial \mathfrak{L}}{\partial(\partial \xi_i/\partial t)}\right) - \sum_j \frac{\partial}{\partial x_j}\left(\frac{\partial \mathfrak{L}}{\partial(\partial \xi_i/\partial x_j)}\right) + \sum_{jk} \frac{\partial^2}{\partial x_j \partial x_k}\left(\frac{\partial \mathfrak{L}}{\partial(\partial^2 \xi_i/\partial x_j \partial x_k)}\right) - \ldots = 0 . \tag{3.122}$$

This, along with its counterparts for the other displacement components, is sometimes referred to as the Lagrange–Euler equation(s). The terms that are required correspond to those spatial derivatives on which the strain energy density $\mathfrak{U}$ depends.

For the case of an isotropic solid, the Lagrange–Euler equations correspond to those of (3.77), which is equivalently written, given that the Lamé coefficients are independent of position, as

$$\rho \frac{\partial^2 \boldsymbol{\xi}}{\partial t^2} = \rho\left(c_1^2 - c_2^2\right)\nabla\left(\nabla \cdot \boldsymbol{\xi}\right) + \rho c_2^2 \nabla^2 \boldsymbol{\xi} . \tag{3.123}$$

For a fluid, the analogous result is

$$\rho \frac{\partial^2 \boldsymbol{\xi}}{\partial t^2} = \nabla(\rho c^2 \nabla \cdot \boldsymbol{\xi}) . \tag{3.124}$$

Amazon EX1014 Page 61

The more familiar Bergmann version (3.73) of the wave equation results from this if one divides both sides by ρ, then takes the divergence, and subsequently sets

$$p = -\rho c^2 \nabla \cdot \boldsymbol{\xi} \,. \tag{3.125}$$

Here the variational principle automatically yields a wave equation that is suitable for inhomogeneous media, where ρ and c vary with position.

3.4.2 Biot's Formulation for Porous Media

A commonly used model for waves in porous media follows from a formulation developed by *Biot* [3.42], with a version of Hamilton's principle used in the formulation. The medium consists of a solid matrix that is connected, so that it can resist shear stresses, and within which are small pores filled with a compressible fluid.

Two displacement fields are envisioned, one associated with the local average displacement $\boldsymbol{U}$ of the fluid matter, the other associated with the average displacement $\boldsymbol{u}$ of the solid matter. The average here is understood to be an average over scales large compared to representative pore sizes or grain sizes, but yet small compared to whatever lengths are of dominant interest. Because nonlinear effects are believed minor, the kinetic and strain energies per unit volume, again averaged over such length scales, are taken to be quadratic in the displacement fields and their derivatives. The overall medium is presumed to be isotropic, so the two energy densities must be unchanged under coordinate rotations. These innocuous assumptions lead to the general expressions

$$\mathfrak{T} = \frac{1}{2}\rho_{11}\frac{\partial \boldsymbol{u}}{\partial t}\cdot\frac{\partial \boldsymbol{u}}{\partial t} + \rho_{12}\frac{\partial \boldsymbol{U}}{\partial t}\cdot\frac{\partial \boldsymbol{u}}{\partial t} + \frac{1}{2}\rho_{22}\frac{\partial \boldsymbol{U}}{\partial t}\cdot\frac{\partial \boldsymbol{U}}{\partial t} \,, \tag{3.126}$$

$$\mathfrak{U} = \frac{1}{4}N\sum_{ij}\left(\frac{\partial u_i}{\partial x_j} + \frac{\partial u_j}{\partial x_i}\right)^2 + \frac{1}{2}A\,(\nabla\cdot\boldsymbol{u})^2 + Q\,(\nabla\cdot\boldsymbol{u})\,(\nabla\cdot\boldsymbol{U}) + \frac{1}{2}R\,(\nabla\cdot\boldsymbol{U})^2 \,. \tag{3.127}$$

where there are seven, possibly position-dependent, constants. The above form assumes that there is no potential energy associated with shear deformation in the fluid and that there is no potential energy associated with the relative displacements of the solid and the fluid. The quantities $\boldsymbol{U}$ and $\boldsymbol{u}$ here, which are displacements, should not be confused with velocities, although these symbols are used for velocities in much of the literature. They are used here for displacements, because they were used as such by Biot in his original paper.

Because the two energy densities must be nonnegative, the constants that appear here are constrained so that

$$\rho_{11} \geq 0 \,; \quad \rho_{22} \geq 0 \,; \quad \rho_{11}\rho_{22} - \rho_{12}^2 \geq 0 \,, \tag{3.128}$$

$$N \geq 0 \,; \quad A + 2N \geq 0 \,; \quad R \geq 0 \,; \quad (A+2N)R - Q^2 \geq 0 \,. \tag{3.129}$$

The coupling constants, ρ_{12} and Q, can in principle be either positive or negative, but their magnitudes are constrained by the equations above.

It is presumed that this idealization for the energy densities will apply best at low frequencies, and one can conceive of a possible low-frequency disturbance where the solid and the fluid move locally together, with the locking being caused by the viscosity in the fluid and by the boundary condition that displacements at interfaces must be continuous. In such circumstances the considerations that lead to the composite density of (3.50) should apply, so one should have

$$\rho_{11} + 2\rho_{12} + \rho_{22} = \rho_{\mathrm{eq}} = f_s\rho_s + f_{\mathrm{f}}\rho_{\mathrm{f}} \,. \tag{3.130}$$

Here f_s and f_{f} are the volume fractions of the material that are solid and fluid, respectively. The latter is referred to as the porosity.

In general, the various constants have to be inferred from experiment, and it is difficult to deduce them from first principles. An extensive discussion of these constants with some representative values can be found in the monograph by *Stoll* [3.43].

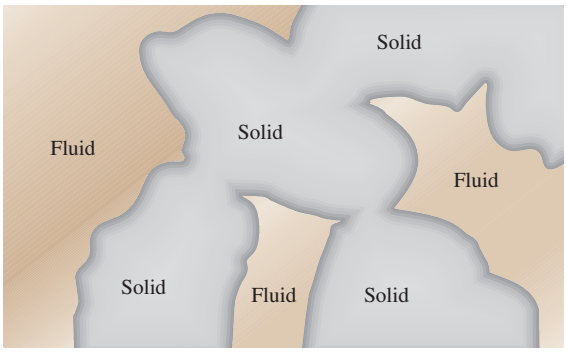


Fig. 3.7 Sketch of a portion of a porous medium in which a compressible fluid fills the pores within a solid matrix. Grains that touch each other are in welded contact, insofar as small-amplitude disturbances are concerned

Amazon EX1014 Page 62

Because the friction associated with the motion of the fluid with respect to the solid matrix is inherently nonconservative (i. e., energy is lost), the original version (3.119) of Hamilton's principle does not apply. The applicable extension includes a term that represents the time integral of the virtual work done by nonconservative forces during a variation. If such nonconservative forces are taken to be distributed over the volume, with the forces per unit volume on the fluid denoted by $\mathfrak{F}$ and those on the solid denoted by $\mathfrak{f}$, then the modified version of Hamilton's principle is

$$\iiiint (\delta\mathfrak{L} + \mathfrak{F}\cdot\delta\boldsymbol{U} + \mathfrak{f}\cdot\delta\boldsymbol{u})\ \mathrm{d}x\ \mathrm{d}y\ \mathrm{d}z\ \mathrm{d}t = 0. \tag{3.131}$$

Moreover, one infers that

$$\mathfrak{F} = -\mathfrak{f}\,, \tag{3.132}$$

since the virtual work associated with friction between the solid matrix and the fluid must vanish if the two are moved together.

The Lagrange–Euler equations that result from the above variational principle are

$$\frac{\partial}{\partial t}\left(\frac{\partial\mathfrak{L}}{\partial\,(\partial U_i/\partial t)}\right) + \sum_j \frac{\partial}{\partial x_j}\left(\frac{\partial\mathfrak{L}}{\partial\left(\partial U_i/\partial x_j\right)}\right) = \mathfrak{F}_i\,, \tag{3.133}$$

$$\frac{\partial}{\partial t}\left(\frac{\partial\mathfrak{L}}{\partial\,(\partial u_i/\partial t)}\right) + \sum_j \frac{\partial}{\partial x_j}\left(\frac{\partial\mathfrak{L}}{\partial\left(\partial u_i/\partial x_j\right)}\right) = \mathfrak{f}_i\,. \tag{3.134}$$

Biot, in his original exposition, took the internal distributed forces to be proportional to the relative velocities, reminiscent of dashpots, so that

$$\mathfrak{F}_i = -\mathfrak{f}_i = -b\left(\frac{\partial U_i}{\partial t} - \frac{\partial u_i}{\partial t}\right)\,. \tag{3.135}$$

Here the quantity b can be regarded as the apparent dashpot constant per unit volume. This form is such that the derived equations, in the limit of vanishingly small frequencies, are consistent with Darcy's law [3.44] for steady fluid flow through a porous medium.

The equations that result from this formulation, when written out explicitly, are

$$\begin{aligned}&\frac{\partial^2}{\partial t^2}\left(\rho_{11}\boldsymbol{u} + \rho_{12}\boldsymbol{U}\right) - \nabla(A'\nabla\cdot\boldsymbol{u} + Q\nabla\cdot\boldsymbol{U})\\ &+ \nabla\times[N\,(\nabla\times\boldsymbol{u})] = b\frac{\partial}{\partial t}\,(\boldsymbol{U} - \boldsymbol{u})\ ,\end{aligned} \tag{3.136}$$

$$\begin{aligned}&\frac{\partial^2}{\partial t^2}\,(\rho_{12}\boldsymbol{u} + \rho_{22}\boldsymbol{U}) - \nabla\,(Q\nabla\cdot\boldsymbol{u} + R\nabla\cdot\boldsymbol{U})\\ &= -b\frac{\partial}{\partial t}\,(\boldsymbol{U} - \boldsymbol{u})\ ,\end{aligned} \tag{3.137}$$

with the abbreviation $A' = A + 2N$. Here, and in what follows, it is assumed that the various material constants are independent of position, although some of the derived equations may be valid to a good approximation even when this is not the case.

3.4.3 Disturbance Modes in a Biot Medium

Disturbances that satisfy the equations derived in the previous section can be represented as a superposition of three basic modal disturbances. These are here denoted as the acoustic mode, the Darcy mode, and the shear mode, and one writes

$$\boldsymbol{u} = \boldsymbol{u}_{\mathrm{ac}} + \boldsymbol{u}_{\mathrm{D}} + \boldsymbol{u}_{\mathrm{sh}}\,, \tag{3.138}$$

$$\boldsymbol{U} = \boldsymbol{U}_{\mathrm{ac}} + \boldsymbol{U}_{\mathrm{D}} + \boldsymbol{U}_{\mathrm{sh}}\,. \tag{3.139}$$

At low frequencies, the motion in the acoustic mode and in the shear mode is nearly such that the fluid and solid displacements are the same,

$$\boldsymbol{U}_{\mathrm{ac}} \approx \boldsymbol{u}_{\mathrm{ac}}\,; \qquad \boldsymbol{U}_{\mathrm{sh}} \approx \boldsymbol{u}_{\mathrm{sh}}\,. \tag{3.140}$$

The lowest-order (in frequency divided by the dashpot parameter b) approximation results from taking the sum of (3.136) and (3.137) and then setting $\boldsymbol{u} = \boldsymbol{U}$, yielding

$$\rho_{\mathrm{eq}}\frac{\partial^2}{\partial t^2}\boldsymbol{U} - \nabla(B_{\mathrm{V,B}}\nabla\cdot\boldsymbol{U}) + \nabla\times[G_{\mathrm{B}}\,(\nabla\times\boldsymbol{U})] = 0\,, \tag{3.141}$$

with the abbreviations

$$\rho_{\mathrm{eq}} = \rho_{11} + 2\rho_{12} + \rho_{22}\,, \tag{3.142}$$

$$B_{\mathrm{V,B}} = A + 2N + 2Q + R\,, \tag{3.143}$$

$$G_{\mathrm{B}} = N\,, \tag{3.144}$$

for the apparent density, bulk modulus, and shear modulus of the Biot medium. The same equation results for the solid displacement field $\boldsymbol{u}$ in this approximation.

Acoustic Mode

For the acoustic mode, the curl of each displacement field is zero, so

$$\rho_{\mathrm{eq}}\frac{\partial^2}{\partial t^2}\boldsymbol{U} - \nabla\left(B_{\mathrm{V,B}}\nabla\cdot\boldsymbol{U}\right) = 0\,. \tag{3.145}$$

One can identify an apparent pressure disturbance associated with this mode, so that

$$p_{\mathrm{ac}} \approx -B_{\mathrm{V,B}}\nabla\cdot\boldsymbol{U}\,, \tag{3.146}$$

Amazon EX1014 Page 63

and this will satisfy the wave equation

$$\nabla^2 p_{\rm ac} - \frac{1}{c_{\rm ac}^2}\frac{\partial^2 p_{\rm ac}}{\partial t^2} = 0\,, \tag{3.147}$$

where

$$c_{\rm ac}^2 = \frac{B_{\rm V,B}}{\rho_{\rm eq}} \tag{3.148}$$

is the square of the apparent sound speed for disturbances carried by the acoustic mode.

The equations just derived can be improved by an iteration procedure to take into account that the dashpot constant has a finite (rather than an infinite) value. To the next order of approximation, one obtains

$$\nabla^2 \boldsymbol{U}_{\rm ac} - \frac{1}{c_{\rm ac}^2}\frac{\partial^2}{\partial t^2}\boldsymbol{U}_{\rm ac} = -\frac{\tau_{\rm B}}{c_{\rm ac}^2}\frac{\partial^3}{\partial t^3}\boldsymbol{U}_{\rm ac}\,. \tag{3.149}$$

This wave equation with an added (dissipative) term holds for each component of $\boldsymbol{U}_{\rm ac}$ and of $\boldsymbol{u}_{\rm ac}$, as well as for the pressure $p_{\rm ac}$. The time constant $\tau_{\rm B}$ which appears here is given by

$$\tau_{\rm B} = \frac{D^2}{bB_{\rm V,B}^2\rho_{\rm eq}}\,, \tag{3.150}$$

where

$$\begin{aligned} D = {} & (\rho_{11}+\rho_{12})(R+Q) \\ & -(\rho_{22}+\rho_{12})(A+2N+Q) \end{aligned} \tag{3.151}$$

is a parameter that characterizes the mismatch between the material properties of the fluid and the solid. The appearance of the dissipative term in the wave equation is associated with the imperfect locking of the two displacement fields, so that

$$\boldsymbol{U}_{\rm ac} - \mathrm{u}_{\rm ac} \approx \frac{D}{bB_{\rm V,B}}\frac{\partial \boldsymbol{u}_{\rm ac}}{\partial t}\,. \tag{3.152}$$

One should note that (3.149) is of the same general mathematical form as the dissipative wave equation (3.101).

Shear mode

For the shear mode, the divergence of each displacement field is zero, so (3.141) reduces to

$$\rho_{\rm eq}\frac{\partial^2}{\partial t^2}\boldsymbol{U} + \nabla\times[G_{\rm B}\,(\nabla\times\boldsymbol{U})] = 0\,, \tag{3.153}$$

where this holds to lowest order for both $\boldsymbol{U}_{\rm sh}$ and $\boldsymbol{u}_{\rm sh}$, these being equal in this approximation. A mathematical identity for the curl of a curl reduces this to

$$\nabla^2 \boldsymbol{u}_{\rm sh} - \frac{1}{c_{\rm sh}^2}\frac{\partial^2 \boldsymbol{u}_{\rm sh}}{\partial t^2} = 0\,, \tag{3.154}$$

where

$$c_{\rm sh}^2 = \frac{G_{\rm B}}{\rho_{\rm eq}}\,. \tag{3.155}$$

An iteration process that takes into account that the two displacement fields are not exactly the same yields

$$\boldsymbol{u}_{\rm sh} - \mathrm{U}_{\rm sh} \approx \frac{\rho_{22}+\rho_{12}}{b}\frac{\partial \mathrm{U}_{\rm sh}}{\partial t}\,, \tag{3.156}$$

with the result that the wave equation above is replaced by a dissipative wave equation

$$\nabla^2 \boldsymbol{u}_{\rm sh} - \frac{1}{c_{\rm sh}^2}\frac{\partial^2 \boldsymbol{u}_{\rm sh}}{\partial t^2} = -\frac{(\rho_{22}+\rho_{12})^2}{G_{\rm B}b}\frac{\partial^3 \boldsymbol{u}_{\rm sh}}{\partial t^3}\,. \tag{3.157}$$

Darcy Mode

For the Darcy mode, the curl of both displacement fields is zero,

$$\nabla\times\boldsymbol{U}_{\rm D} = 0\,; \qquad \nabla\times\boldsymbol{u}_{\rm D} = 0\,. \tag{3.158}$$

The inertia term in both (3.136) and (3.137) is negligible to a lowest approximation, and the compatibility of the two equations requires

$$(A'+Q)\boldsymbol{u}_{\rm D} = -(R+Q)\boldsymbol{U}_{\rm D}\,, \tag{3.159}$$

so that the fluid and the solid move in opposite directions.

Given the above observation and the neglect of the inertia terms, either of (3.136) and (3.137) reduces to the diffusion equation

$$\nabla^2 \boldsymbol{U}_{\rm D} = \kappa_{\rm D}\frac{\partial \boldsymbol{U}_{\rm D}}{\partial t}\,, \tag{3.160}$$

with the same equation also being satisfied by $\boldsymbol{u}_{\rm D}$. Here

$$\kappa_{\rm D} = \frac{bB_{\rm V,B}}{A'R - Q^2} \tag{3.161}$$

is a constant whose reciprocal characterizes the tendency of the medium to allow diffusion of fluid through the solid matrix. This is independent of any of the inertial densities, and it is always positive.

Amazon EX1014 Page 64

3.5 Waves of Constant Frequency

One of the principal terms used in describing sound is that of frequency. Although certainly not all acoustic disturbances are purely sinusoidal oscillations of a quantity (such as pressure or displacement) that oscillates with constant frequency about a mean value, it is usually possible to characterize (at least to an order of magnitude) any such disturbance by one or a limited number of representative frequencies, these being the reciprocals of the characteristic time scales. Such a description is highly useful, because it gives one some insight into what detailed physical effects are relevant and of what instrumentation is applicable. The simplest sort of acoustic signal would be one where a quantity such as the fluctuating part p of the pressure is oscillating with time t as

$$p = A\cos(\omega t - \phi)\,. \tag{3.162}$$

Here the amplitude A and phase constant ϕ are independent of t (but possibly dependent on position). The quantity ω is called the angular frequency and has the units of radians divided by time (for example, rad/s or simply s^{-1}, when the unit of time is the second). The number f of repetitions per unit time is what one normally refers to as the frequency (without a modifier), such that $\omega = 2\pi f$. The value of f in hertz (abbreviated to Hz) is the frequency in cycles (repetitions) per second. The period $T = 1/f$ is the time interval between repetitions.

The human ear responds [3.45] almost exclusively to frequencies between roughly 20 Hz and 20 kHz. Consequently, sounds composed of frequencies below 20 Hz are said to be infrasonic; those composed of frequencies above 20 kHz are said to be ultrasonic. The scope of acoustics, given its general definition as a physical phenomenon, is not limited to audible frequencies.

3.5.1 Spectral Density

The term frequency spectrum is often used in relation to sound. Often the use is somewhat loose, but there are circumstances for which the terminology can be made precise. If the fluctuating physical quantity p associated with the acoustic disturbance is a sum of sinusoidal disturbances, the n-th being $p_n = A_n\cos(2\pi f_n t - \phi_n)$ and having frequency f_n, no two frequencies being the same, then the set of mean squared amplitudes can be taken as a description of the spectrum of the signal. Also, if the sound is made up of many different frequencies, then one can use the time-averaged sum of the p_n^2 that correspond to those frequencies within a given specified frequency band as a measure of the strength of the signal within that frequency band. This sum divided by the width of the frequency band often approaches a quasi-limit as the bandwidth becomes small, but with the number of included terms still being moderately large, and with this quasi-limit being a definite smooth function of the center frequency of the band. This quasi-limit is called the spectral density p_f^2 of the signal . Although an idealized quantity, it can often be repetitively measured to relatively high accuracy; instrumentation for the measurement of spectral densities or of integrals of spectral densities over specified (such as octaves) frequency bands is widely available commercially.

The utility of the spectral density concept rests on the principle of superposition and on a version of Parseval's theorem, which states that, when the signal is a sum of discrete frequency components, then if averages are taken over a sufficiently long time interval,

$$(p^2)_{\mathrm{av}} = \sum_n \left(p_n^2\right)_{\mathrm{av}}\,. \tag{3.163}$$

Consequently, in the quasi-limit corresponding to the spectral density description, one has the mean squared pressure expressed as an integral over spectral density,

$$(p^2)_{\mathrm{av}} = \int_0^\infty p_f^2(f)\,\mathrm{d}f\,. \tag{3.164}$$

The spectral density at a given frequency times a narrow bandwidth centered at that frequency is interpreted as the contribution to the mean squared acoustic pressure from that frequency band.

If the signal is a linear response to a source (or excitation) characterized by some time variation $s(t)$ with spectral density $s_f^2(f)$, then the spectral density of the response is

$$p_f^2(f) = |H_{ps}(2\pi f)|^2 s_f^2(f)\,, \tag{3.165}$$

where the proportionality factor $|H_{ps}(2\pi f)|^2$ is the square of the absolute magnitude of a transfer function that is independent of the excitation, but which does depend on frequency. For any given frequency, this transfer function can be determined from the response to a known sinusoidal excitation with the same frequency. Thus the analysis for constant-frequency excitation is fundamental, even when the situation of interest may involve broadband excitation.

Amazon EX1014 Page 65

3.5.2 Fourier Transforms

Analogous arguments can be made for transient excitation and transient signals, where time-dependent quantities are represented by integrals over Fourier transforms, so that

$$p(t) = \int_{-\infty}^{\infty} \hat{p}(\omega)\, \mathrm{e}^{-\mathrm{i}\omega t}\, \mathrm{d}\omega \,, \tag{3.166}$$

with

$$\hat{p}(\omega) = \frac{1}{2\pi} \int_{-\infty}^{\infty} p(t)\, \mathrm{e}^{\mathrm{i}\omega t}\, \mathrm{d}t \,. \tag{3.167}$$

Here $\hat{p}(\omega)$ is termed the Fourier transform of $p(t)$, and $p(t)$ is conversely termed the inverse Fourier transform of $\hat{p}(\omega)$. Definitions of the Fourier transform vary in the acoustics literature. What is used here is what is commonly used for analyses of wave propagation problems. Whatever definition is used must be accompanied by a definition of the inverse Fourier transform, so that the inverse Fourier transform produces the original function. In all such cases, given that $p(t)$ and ω are real, one has

$$\hat{p}(-\omega) = \hat{p}(\omega)^* \,, \tag{3.168}$$

where the asterisk denotes the complex conjugate. Thus, the magnitude of the Fourier transform need only be known for positive frequencies. The phase changes sign when one changes the sign of the frequency.

Parseval's theorem for Fourier transforms is

$$\int_{-\infty}^{\infty} p^2(t)\, \mathrm{d}t = 4\pi \int_{0}^{\infty} |\hat{p}(\omega)|^2\, \mathrm{d}\omega \,, \tag{3.169}$$

so that $4\pi |\hat{p}(\omega)|^2\, \Delta\omega$ can be regarded as to the contribution to the time integral of $p^2(t)$ from a narrow band of (positive) frequencies of width $\Delta\omega$.

3.5.3 Complex Number Representation

Insofar as the governing equations are linear with coefficients independent of time, disturbances that vary sinusoidally with time can propagate without change of frequency. Such sinusoidally varying disturbances of constant frequency have the same repetition period (the reciprocal of the frequency) at every point, but the phase will in general vary from point to point.

When one considers a disturbance of fixed frequency or one frequency component of a multifrequency disturbance, it is convenient to use a complex number representation, such that each field amplitude is written [3.4, 46]

$$p = \mathrm{Re}(\hat{p}\, \mathrm{e}^{-\mathrm{i}\omega t}) \,. \tag{3.170}$$

Here $\hat{p}$ is called the complex amplitude of the acoustic pressure and in general varies with position. (The use of the $\mathrm{e}^{-\mathrm{i}\omega t}$ time dependence is traditional among acoustics professionals who are primarily concerned with the wave aspects of acoustics. In the vibrations literature, one often finds instead a postulated $\mathrm{e}^{\mathrm{j}\omega t}$ time dependence. The use of j as the square root of -1 instead of i is a carryover from the analysis of oscillations in electrical circuits, where i is reserved for electrical current.)

If one inserts expressions such as (3.170) into a homogeneous linear ordinary or partial differential equation with real time-independent coefficients, the result can always be written in the form

$$\mathrm{Re}\left(\Phi\, \mathrm{e}^{-\mathrm{i}\omega t}\right) = 0 \,, \tag{3.171}$$

where the quantity Φ is an expression depending on the complex amplitudes and their spatial derivatives, but not depending on time. The requirement that (3.171) should hold for all values of time consequently can be satisfied if and only if

$$\Phi = 0 \,. \tag{3.172}$$

Moreover, the form of the expression Φ can be readily obtained from the original equation with a simple prescription: replace all field variables by their complex amplitudes and replace all time derivatives using the substitution

$$\frac{\partial}{\partial t} \to -\mathrm{i}\omega \,. \tag{3.173}$$

Thus, for example, the linear acoustic equations given by (3.71) and (3.72) reduce to

$$-\mathrm{i}\omega\hat{p} + \rho c^2 \nabla \cdot \hat{\boldsymbol{v}} = 0 \,, \tag{3.174}$$

$$-\mathrm{i}\omega\rho\hat{\boldsymbol{v}} = -\nabla\hat{p} \,. \tag{3.175}$$

The wave equation in (3.74) reduces (with $k = \omega/c$ denoting the wavenumber) to

$$\nabla^2\hat{p} + k^2\hat{p} = 0 \,, \tag{3.176}$$

which is the Helmholtz equation [3.47] for the complex pressure amplitude.

Amazon EX1014 Page 66

3.5.4 Time Averages of Products

When dealing with waves of constant frequency, one often makes use of averages over a wave period of the product of two quantities that oscillate with the same frequency. Let

$$p = \mathrm{Re}\left(\hat{p}\,\mathrm{e}^{-\mathrm{i}\omega t}\right)\ ; \qquad v = \mathrm{Re}\left(\hat{v}\,\mathrm{e}^{-\mathrm{i}\omega t}\right) \tag{3.177}$$

be two such quantities. Then the time average of their product is

$$[p(t)v(t)]_{\mathrm{av}} = |\hat{p}||\hat{v}|[\cos(\omega t - \phi_p)\cos(\omega t - \phi_v)]_{\mathrm{av}}, \tag{3.178}$$

where ϕ_p and ϕ_v are the phases of $\hat{p}$ and $\hat{v}$.

The trigonometric identity

$$\cos(A)\cos(B) = \frac{1}{2}\left[\cos(A+B) + \cos(A-B)\right]\ , \tag{3.179}$$

with appropriate identifications for A and B, yields a term which averages out to zero and a term which is independent of time. Thus one has

$$[p(t)v(t)]_{\mathrm{av}} = \frac{1}{2}|\hat{p}||\hat{v}|\cos(\phi_p - \phi_v)\ , \tag{3.180}$$

or, equivalently

$$[p(t)v(t)]_{\mathrm{av}} = \frac{1}{2}|\hat{p}||\hat{v}|\mathrm{Re}(\mathrm{e}^{\mathrm{i}(\phi_p - \phi_v)})\ , \tag{3.181}$$

which in turn can be written

$$[p(t)v(t)]_{\mathrm{av}} = \frac{1}{2}\mathrm{Re}(\hat{p}\hat{v}^*)\ . \tag{3.182}$$

The asterisk here denotes the complex conjugate. Because the real part of a complex conjugate is the same as the real part of the original complex number, it is immaterial whether one takes the complex conjugate of $\hat{p}$ or $\hat{v}$, but one takes the complex conjugate of only one.

3.6 Plane Waves

A solution of the wave equation that plays a central role in many acoustical concepts is that of a plane traveling wave.

3.6.1 Plane Waves in Fluids

The mathematical representation of a plane wave is such that all acoustic field quantities vary with time and with one Cartesian coordinate. That coordinate is taken here as x; consequently, all the acoustic quantities are independent of y and z. The Laplacian reduces to a second partial derivative with respect to x and the d'Alembertian can be expressed as the product of two first-order operators, so that the wave equation takes the form

$$\left(\frac{\partial}{\partial x} - \frac{1}{c}\frac{\partial}{\partial t}\right)\left(\frac{\partial}{\partial x} + \frac{1}{c}\frac{\partial}{\partial t}\right)p = 0\ . \tag{3.183}$$

The solution of this equation is a sum of two expressions, each of which is such that operation by one or the other of the two factors in (3.183) yields zero. Such a solution is represented by

$$p(x,t) = f(x-ct) + g(x+ct)\ , \tag{3.184}$$

where f and g are two arbitrary functions. The argument combination $x-ct$ of the first term is such that the function f with that argument represents a plane wave traveling forward in the $+x$-direction at a velocity c. The second term in (3.184) similarly represents a plane wave traveling backwards in the $-x$-direction, also at a velocity c. For a traveling plane wave, not only the shape, but also the amplitude is conserved during propagation. A typical situation for which wave propagation can be adequately described by traveling plane waves is that of low-frequency sound propagation in a duct. Diverging or converging (focused) waves can often be approximately regarded as planar within regions of restricted extent.

The fluid velocity that corresponds to the plane wave solution above has y and z components that are identically zero, but the x-component, in accordance with (3.71) and (3.72), is

$$v_x = \frac{1}{\rho c}f(x-ct) - \frac{1}{\rho c}g(x+ct)\ . \tag{3.185}$$

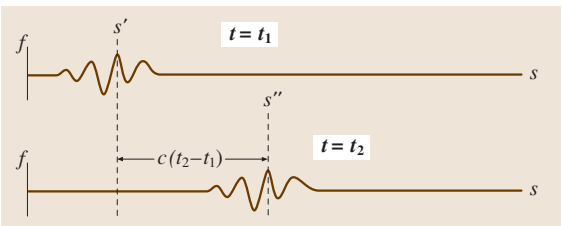


Fig. 3.8 Waveform propagating in the $+s$-direction with constant speed c. Shown are plots of the function $f(s-ct)$ versus s at two successive values of the time t

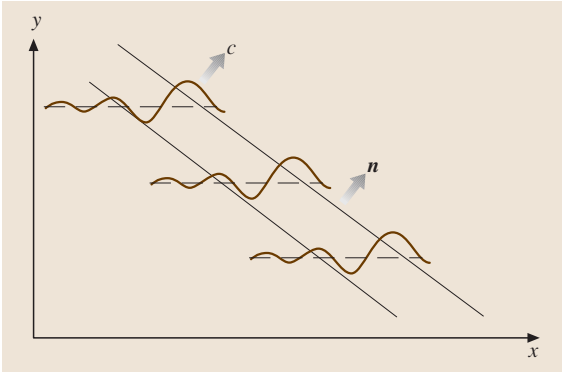


Fig. 3.9 Plane wave propagating in the direction of the unit vector $\boldsymbol{n}$

The general rule that emerges from this is that, for a plane wave propagating in the direction corresponding to unit vector $\boldsymbol{n}$, the acoustic part of the pressure is

$$p = f(\boldsymbol{n}\cdot\boldsymbol{x} - ct) \tag{3.186}$$

for some generic function f of the indicated argument, while the acoustically induced fluid velocity is

$$\boldsymbol{v} = \frac{\boldsymbol{n}}{\rho c}\, p\,. \tag{3.187}$$

Because the fluid velocity is in the same direction as that of the wave propagation, such waves are said to be longitudinal. (Electromagnetic plane waves in free space, in contrast, are transverse. Both the electric field vector and the magnetic field vector are perpendicular to the direction of propagation.)

For a plane wave traveling along the $+x$-axis at a velocity c, the form of (3.186) implies that one can represent a constant-frequency acoustic pressure disturbance by the expression

$$p = |P|\cos\left[k(x-ct)+\phi_0\right] = \mathrm{Re}\left(P\,\mathrm{e}^{\mathrm{i}k(x-ct)}\right), \tag{3.188}$$

with the angular frequency identified as

$$\omega = ck\,. \tag{3.189}$$

Alternately, if the complex amplitude representation of (3.170) is used, one writes the complex amplitude of the acoustic pressure as

$$\hat{p} = P\,\mathrm{e}^{\mathrm{i}kx}\,, \tag{3.190}$$

where P is a complex number related to the constants that appear in (3.188) as

$$P = |P|\,\mathrm{e}^{\mathrm{i}\phi_0}\,. \tag{3.191}$$

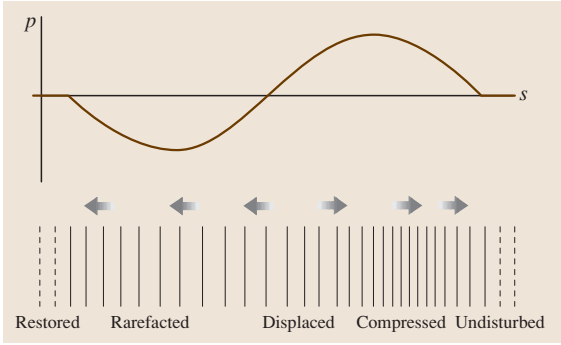


Fig. 3.10 Fluid velocity and pressure in a one-cycle sinusoidal pulse propagating in the $+x$-direction

Here $|P|$ is the amplitude of the disturbance, ϕ_0 is a phase constant, and k is a constant termed the wavenumber. The wavelength λ is the increment in propagation distance x required to change the argument of the cosine by 2π radians, so

$$k = \frac{2\pi}{\lambda}\,. \tag{3.192}$$

Also, the increment in t required to change the argument by 2π is the period T, which is the reciprocal of the frequency f, so one has

$$\lambda = \frac{c}{f}\,. \tag{3.193}$$

3.6.2 Plane Waves in Solids

Plane acoustic waves in isotropic elastic solids [3.26] have properties similar to those of waves in fluids. Dilatational (or longitudinal) plane waves are such that the curl of the displacement field vanishes, so the displacement vector must be parallel to the direction of propagation. (Dilation means expansion and is the antonym of compression. Dilatational plane waves could equally well be termed compressional plane waves. Seismologists refer to dilational waves as P-waves, where the letter P stands for primary. They refer to shear waves as S-waves, where the letter S stands for secondary.) A comparison of (3.82) with the wave equation (3.74) indicates that such a wave must propagate with a speed c_1 determined by (3.79). Thus, a wave propagating in the $+x$-direction has no y and z components of displacement, and has an x-component described by

$$\xi_x = F(x - c_1 t)\,, \tag{3.194}$$

where F is an arbitrary function. The stress components can be deduced from (3.56, 57, 79, 80). These equations,

as well as symmetry considerations, require for a dilatational wave propagating in the x-direction, that the off-diagonal elements of the stress tensor vanish. The diagonal elements are given by

$$\sigma_{xx} = \rho c_1^2 F'(x - c_1 t) \,, \tag{3.195}$$

$$\sigma_{yy} = \sigma_{zz} = \rho\left(c_1^2 - 2c_2^2\right) F'(x - c_1 t) \,. \tag{3.196}$$

Here the primes denote derivatives with respect to the total argument.

The divergence of the displacement field in a shear wave is zero, so a plane shear wave must cause a displacement perpendicular to the direction of propagation. Shear waves are therefore transverse waves. Equation (3.83), when considered in a manner similar to that described above for the wave equation for waves in fluids, leads to the conclusion that plane shear waves must propagate with a speed c_2. A plane shear wave polarized in the y-direction and propagating in the x-direction will have only a y-component of displacement, given by

$$\xi_y = F(x - c_2 t) \,. \tag{3.197}$$

The only nonzero stress components are the shear stresses

$$\sigma_{yx} = \rho c_2^2 F'(x - c_2 t) = \sigma_{xy} \,. \tag{3.198}$$

3.7 Attenuation of Sound

Plane waves of constant frequency propagating through bulk materials have amplitudes that typically decrease exponentially with increasing propagation distance, such that the magnitude of the complex pressure amplitude varies as

$$|\hat{p}(x)| = |\hat{p}(0)|\, \mathrm{e}^{-\alpha x} \,. \tag{3.199}$$

The quantity α is the plane wave attenuation coefficient and has units of nepers per meter (Np/m); it is an intrinsic frequency-dependent property of the material. This exponential decrease of amplitude is called attenuation or absorption of sound and is associated with the transfer of acoustic energy to the internal energy of the material. (If $|\hat{p}|^2$ decreases to a tenth of its original value, it is said to have decreased by 10 decibels (dB), so an attenuation constant of α nepers per meter is equivalent to an attenuation constant of $[20/(\ln 10)]\alpha$ decibels per meter, or 8.6859α decibels per meter.)

3.7.1 Classical Absorption

The attenuation of sound due to the classical processes of viscous energy absorption and thermal conduction is derivable [3.33] from the dissipative wave equation (3.101) given previously for the acoustics mode. Dissipative processes enter into this equation through a parameter δ_{cl}, which is defined by (3.102). To determine the attenuation of waves governed by such a dissipative wave equation, one sets the perturbation pressure equal to

$$p_{\mathrm{ac}} = P\, \mathrm{e}^{-\mathrm{i}\omega t}\, \mathrm{e}^{\mathrm{i}kx} \,, \tag{3.200}$$

where P is independent of position and k is a complex number. Such a substitution, with reasoning such as that which leads from (3.171) to (3.172), yields an algebraic equation that can be nontrivially (amplitude not identically zero) satisfied only if k satisfies the relation

$$k^2 = \frac{\omega^2}{c^2} + \mathrm{i}\frac{2\delta_{\mathrm{cl}}\omega^3}{c^3} \,. \tag{3.201}$$

The root that corresponds to waves propagating in the $+x$-direction is that which evolves to (3.189) in the limit of no absorption, and for which the real part of k is positive. Thus to first order in δ_{cl}, one has the complex wavenumber

$$k = \frac{\omega}{c} + \mathrm{i}\frac{\delta_{\mathrm{cl}}\omega^2}{c^3} \,. \tag{3.202}$$

The attenuation coefficient is the imaginary part of this, in accordance with (3.199), so

$$\alpha_{\mathrm{cl}} = \frac{\delta_{\mathrm{cl}}\omega^2}{c^3} \,. \tag{3.203}$$

This is termed the classical attenuation coefficient for acoustic waves in fluids and is designated by the subscript 'cl'. The distinguishing characteristic of this classical attenuation coefficient is its quadratic increase with increasing frequency.

The same type of frequency dependence is obeyed by the acoustic and shear wave modes for the Biot model of porous media in the limit of low frequencies. From (3.149) one derives

$$\alpha_{\mathrm{ac}} = \frac{\tau_{\mathrm{B}}}{2c_{\mathrm{ac}}}\omega^2 \,, \tag{3.204}$$

Amazon EX1014 Page 69

and, from (3.157), one derives

$$\alpha_{\mathrm{sh}} = \frac{c_{\mathrm{sh}}(\rho_{22}+\rho_{12})^2}{2G_{\mathrm{B}}b}\omega^2 \,. \tag{3.205}$$

3.7.2 Relaxation Processes

For many substances, including air, sea water, biological tissues, marine sediments, and rocks, the variation of the absorption coefficient with frequency is not quadratic [3.48–50], and the classical model is insufficient to predict the magnitude of the absorption coefficient. The substitution of a different value of the bulk viscosity is insufficient to remove the discrepancy, because this would still yield the quadratic frequency dependence. The successful theory to account for such discrepancies in air and sea water and other fluids is in terms of relaxation processes. The physical nature of the relaxation processes vary from fluid to fluid, but a general theory in terms of irreversible thermodynamics [3.51–53] yields appropriate equations.

The equation of state for the instantaneous (rather than equilibrium) entropy is written as

$$s = s(u, \rho^{-1}, \xi) \,, \tag{3.206}$$

where ξ represents one or more internal variables. The differential relation of (3.13) is replaced by

$$T\,\mathrm{d}s = \mathrm{d}u + p\,\mathrm{d}\rho^{-1} + \sum_\nu A_\nu\,\mathrm{d}\xi_\nu \,, \tag{3.207}$$

where the affinities A_ν are defined by this equation. These vanish when the fluid is in equilibrium with a given specified internal energy and density. The pressure p here is the same as enters into the expression (3.15) for the average normal stress, and the T is the same as enters into the Fourier law (3.16) of heat conduction. The mass conservation law (3.2) and the Navier–Stokes equation (3.24) remain unchanged, but the energy equation, expressed in (3.25) in terms of entropy, is replaced by the entropy balance equation

$$\rho\frac{\mathrm{D}s}{\mathrm{D}t} + \nabla\cdot\frac{\boldsymbol{q}}{T} = \sigma_s \,. \tag{3.208}$$

Here the quantity σ_s, which indicates the rate of irreversible entropy production per unit volume, is given by

$$T\sigma_s = \mu_{\mathrm{B}}(\nabla\cdot\boldsymbol{v})^2 + \tfrac{1}{2}\mu\sum_{ij}\phi_{ij}^2 + \frac{\kappa}{T}(\nabla T)^2 + \rho\sum_\nu A_\nu\frac{\mathrm{D}\xi_\nu}{\mathrm{D}t} \,. \tag{3.209}$$

One needs in addition relations that specify how the internal variables ξ_ν relax to their equilibrium values. The simplest assumption, and one which is substantiated for air and sea water, is that these relax independently according to the rule [3.54]

$$\frac{\mathrm{D}\xi_\nu}{\mathrm{D}t} = -\frac{1}{\tau_\nu}\left(\xi_\nu - \xi_{\nu,\mathrm{eq}}\right) \,. \tag{3.210}$$

The relaxation times τ_ν that appear here are positive and independent of the internal variables.

When the linearization process is applied to the nonlinear equations for the model just described of a fluid with internal relaxation, one obtains the set of equations

$$\frac{\partial\rho'}{\partial t} + \rho_0\nabla\cdot\boldsymbol{v}' = 0 \,, \tag{3.211}$$

$$\rho_0\frac{\partial\boldsymbol{v}'}{\partial t} = -\nabla p' + (1/3\mu + \mu_{\mathrm{B}}) \times\nabla(\nabla\cdot\boldsymbol{v}') + \mu\nabla^2\boldsymbol{v}' \,, \tag{3.212}$$

$$\rho_0 T_0\frac{\partial s'}{\partial t} = \kappa\nabla^2 T' \,, \tag{3.213}$$

$$\rho' = \frac{1}{c^2}p' - \left(\frac{\rho\beta T}{c_{\mathrm{p}}}\right)_0 s' + \sum_\nu\left(\xi_\nu' - \xi_{\nu,\mathrm{eq}}'\right)a_\nu \,, \tag{3.214}$$

$$T' = \left(\frac{T\beta}{\rho c_{\mathrm{p}}}\right)_0 p' + \left(\frac{T}{c_{\mathrm{p}}}\right)_0 s' + \sum_\nu\left(\xi_\nu' - \xi_{\nu,\mathrm{eq}}'\right)b_\nu \,, \tag{3.215}$$

$$\frac{\partial\xi_\nu'}{\partial t} = -\frac{1}{\tau_\nu}\left(\xi_\nu' - \xi_{\nu,\mathrm{eq}}'\right) \,, \tag{3.216}$$

$$\xi_{\nu,\mathrm{eq}}' = m_\nu s' + n_\nu p' \,. \tag{3.217}$$

Here a_ν, b_ν, m_ν, and n_ν are constants whose values depend on the ambient equilibrium state.

For absorption of sound, the interest is in the acoustic mode, and so approximations corresponding to those discussed in the context of (3.93) through (3.101) can also be made here. The quantities a_ν and b_ν are treated as small, so that one obtains, to first order in ϵ and in these quantities, a wave equation of the form

$$\nabla^2 p_{\mathrm{ac}} - \frac{1}{c^2}\frac{\partial^2}{\partial t^2}\left(p_{\mathrm{ac}} - \frac{2\delta_{\mathrm{cl}}}{c^2}\frac{\partial p_{\mathrm{ac}}}{\partial t} - 2\sum_\nu\frac{(\Delta c)_\nu}{c}\tau_\nu\frac{\partial p_\nu}{\partial t}\right) = 0 \,. \tag{3.218}$$

Amazon EX1014 Page 70

The auxiliary internal variables that enter here satisfy the supplemental relaxation equations

$$\frac{\partial p_\nu}{\partial t} = -\frac{1}{\tau_\nu}\,(p_\nu - p_{\mathrm{ac}})\ . \tag{3.219}$$

Here the notation is such that the p_ν are given in terms of previously introduced quantities by

$$p_\nu = \xi'_\nu / n_\nu\ . \tag{3.220}$$

The sound speed increments that appear in (3.218) represent the combinations

$$(\Delta c)_\nu = 1/2 a_\nu n_\nu c^2\ . \tag{3.221}$$

Equations (3.218) and (3.219) are independent of the explicit physical interpretation of the relaxation processes. Insofar as acoustic propagation is concerned, any relaxation process is characterized by two parameters, the relaxation time τ_ν and the sound speed increment $(\Delta c)_\nu$. The various parameters that enter into the irreversible thermodynamics formulation of (3.214) through (3.216) affect the propagation of sound only as they enter into the values of the relaxation times and of the sound speed increments. The replacement of internal variables by quantities p_ν with the units of pressure implies no assumption as to the precise nature of the relaxation process. [An alternate formulation for a parallel class of relaxation processes concerns structural relaxation [3.55]. The substance can locally have more than one state, each of which has a different compressibility. The internal variables are associated with the deviations of the probabilities of the system being in each of the states from the probabilities that would exist were the system in quasistatic equilibrium. The equations that result are mathematically the same as (3.218) and (3.219).]

The attenuation of plane waves governed by (3.218) and (3.219) is determined when one inserts substitutions of the form of (3.200) for p_{ac} and the p_ν. The relaxation equations yield the relations

$$\hat{p}_\nu = \frac{1}{1 - \mathrm{i}\omega\tau_\nu}\,\hat{p}_{\mathrm{ac}}\ . \tag{3.222}$$

These, when inserted into the complex amplitude version of (3.218), yield the dispersion relation

$$k^2 = \frac{\omega^2}{c^2}\left(1 + \mathrm{i}\frac{2\omega\delta_{\mathrm{cl}}}{c^2} + \sum_\nu \frac{2(\Delta c)_\nu}{c}\,\frac{\mathrm{i}\omega\tau_\nu}{1 - \mathrm{i}\omega\tau_\nu}\right)\ . \tag{3.223}$$

To first order in the small parameters, δ_{cl} and $(\Delta c)_\nu$, this yields the complex wavenumber

$$k = \frac{\omega}{c}\left(1 + \mathrm{i}\frac{\omega\delta_{\mathrm{cl}}}{c^2} + \sum_\nu \frac{(\Delta c)_\nu}{c}\,\frac{\mathrm{i}\omega\tau_\nu}{1 - \mathrm{i}\omega\tau_\nu}\right)\ , \tag{3.224}$$

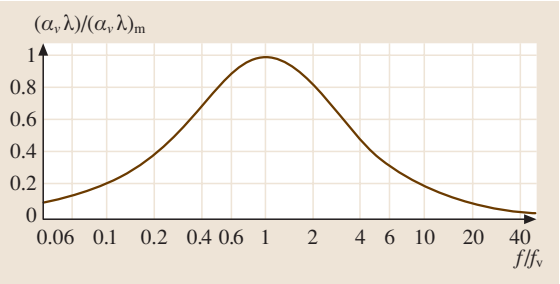


Fig. 3.11 Attenuation per wavelength (in terms of characteristic parameters) for propagation in a medium with a single relaxation process. Here the wavelength λ is $2\pi c/\omega$, and the ratio f/f_ν of frequency to relaxation frequency is $\omega\tau_\nu$. The curve as constructed is independent of c and $(\Delta c)_\nu$

which corresponds to waves propagating in the $+x$-direction. The attenuation coefficient, determined by the imaginary part of (3.224), can be written

$$\alpha = \alpha_{\mathrm{cl}} + \sum_\nu \alpha_\nu\ . \tag{3.225}$$

The first term is the classical attenuation determined by (3.203). The remaining terms correspond to the incremental attenuations produced by the separate relaxation processes, these being

$$\alpha_\nu = \frac{(\Delta c)_\nu}{c^2}\,\frac{\omega^2\tau_\nu}{1 + (\omega\tau_\nu)^2}\ . \tag{3.226}$$

Any such term increases quadratically with frequency at low frequencies, as would be the case for classical absorption (with an increased bulk viscosity), but it approaches a constant value at high frequencies.

The labeling of the quantities $(\Delta c)_\nu$ as sound speed increments follows from an examination of the real part of the complex wavenumber, given by

$$k_{\mathrm{R}} = \frac{\omega}{c}\left(1 - \sum_\nu \frac{(\Delta c)_\nu}{c}\,\frac{(\omega\tau_\nu)^2}{1 + (\omega\tau_\nu)^2}\right)\ . \tag{3.227}$$

The ratio, of ω to k_{R}, is identified as the phase velocity v_{ph} of the wave. In the limit of low frequencies, the phase velocity predicted by (3.227) is the quantity c, which is the sound speed for a quasi-equilibrium process. In the limit of high frequencies, however, to first order in the $(\Delta c)_\nu$, the phase velocity approaches the limit

$$v_{\mathrm{ph}} \to c + \sum_\nu (\Delta c)_\nu\ . \tag{3.228}$$

Consequently, each $(\Delta c)_\nu$ corresponds to the net increase in phase velocity of the sound wave that occurs

Amazon EX1014 Page 71

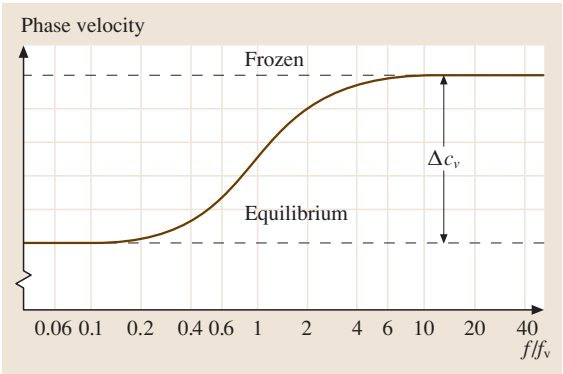


Fig. 3.12 Change in phase velocity as a function of frequency for propagation in a medium with a single relaxation process. The asymptote at zero frequency is the equilibrium sound speed c, and that in the limit of infinite frequency is the frozen sound speed $c + \Delta c_v$

when the frequency is increased from a value small compared to the relaxation frequency to one large compared to the relaxation frequency. Here the term relaxation frequency is used to denote the reciprocal of the product of 2π with the relaxation time.

3.7.3 Continuously Distributed Relaxations

It is sometimes argued that, for heterogeneous media such as biological tissue and rocks, the attenuation is due to a statistical distribution of relaxation times, so that the sum in (3.224) should be replaced by an integral, yielding

$$k = \frac{\omega}{c}\left(1 + \mathrm{i}\frac{\omega\delta_{\mathrm{cl}}}{c^2} + \frac{1}{c}\int_0^\infty \frac{\mathrm{d}(\Delta c)}{\mathrm{d}\tau}\frac{\mathrm{i}\omega\tau}{1-\mathrm{i}\omega\tau}\,\mathrm{d}\tau\right), \tag{3.229}$$

and so that the attenuation constant due to the relaxation processes becomes

$$\sum_\nu \alpha_\nu \to \frac{1}{c^2}\int_0^\infty \frac{\mathrm{d}(\Delta c)}{\mathrm{d}\tau}\frac{\omega^2\tau}{1+(\omega\tau)^2}\,\mathrm{d}\tau\,. \tag{3.230}$$

Here, the quantity

$$\frac{\mathrm{d}(\Delta c)}{\mathrm{d}\tau}\Delta\tau \tag{3.231}$$

is interpreted as the additional increment in phase velocity at high frequencies due to all the relaxation processes whose relaxation times are in the interval $\Delta\tau$.

Such a continuous distribution of relaxation processes is intrinsically capable of explaining a variety of experimentally observed frequency dependencies of $\alpha(\omega)$. A simple example is that where

$$\frac{\mathrm{d}(\Delta c)}{\mathrm{d}\tau} = \frac{K}{\tau^q}\,, \tag{3.232}$$

with K being a constant independent of τ, and with q being a specified exponent, with $0 < q < 2$. In such a case the integral in (3.230) becomes

$$\frac{1}{c^2}\int_0^\infty \frac{\mathrm{d}(\Delta c)}{\mathrm{d}\tau}\frac{\omega^2\tau}{1+(\omega\tau)^2}\,\mathrm{d}\tau = \frac{K}{c^2}\omega^q\int_0^\infty \frac{u^{1-q}}{1+u^2}\,\mathrm{d}u \tag{3.233}$$

giving a power-law dependence on ω that varies as ω^q. Although the hypothesis of (3.232) is probably unrealistic over all ranges of relaxation time τ, its being nearly satisfied over an extensive range of such times could yield predictions that would explain a power-law dependence. (The integral that appears here is just a numerical constant, which is finite provided $0 < q < 2$. The integral emerges when one changes the integration variable from τ to $u = \omega\tau$.)

The corresponding increment in the reciprocal $1/v_{\mathrm{ph}} = k_{\mathrm{R}}/\omega$ of the phase velocity v_{ph} is

$$\Delta\left(\frac{1}{v_{\mathrm{ph}}}\right) = -\frac{1}{c^2}\int_0^\infty \frac{\mathrm{d}(\Delta c)}{\mathrm{d}\tau}\frac{\omega^2\tau^2}{1+(\omega\tau)^2}\,\mathrm{d}\tau\,. \tag{3.234}$$

Insertion of (3.232) into this yields

$$\Delta\left(\frac{1}{v_{\mathrm{ph}}}\right) = -\frac{K}{c^2}\omega^{q-1}\int_0^\infty \frac{u^{2-q}}{1+u^2}\,\mathrm{d}u\,, \tag{3.235}$$

which varies with ω as ω^{q-1}. In this case, however, the integral exists only if $1 < q < 3$, so the overall analysis has credibility only if $1 < q < 2$.

3.7.4 Kramers–Krönig Relations

In attempts to explain or predict the frequency dependence of attenuation and phase velocity in materials, some help is found from the principle of causality [3.56]. Suppose one has a plane wave traveling in the $+x$-direction and that, at $x = 0$, the acoustic pressure is a transient given by

$$p(0,t) = \int_{-\infty}^\infty \hat{p}(\omega)\mathrm{e}^{-\mathrm{i}\omega t}\,\mathrm{d}\omega = 2\mathrm{Re}\int_0^\infty \hat{p}(\omega)\mathrm{e}^{-\mathrm{i}\omega t}\,\mathrm{d}\omega. \tag{3.236}$$

Amazon EX1014 Page 72

Then the transient at a distant positive value of x is given by

$$p(x,t) = 2\mathrm{Re}\int_0^\infty \hat{p}(\omega)\,\mathrm{e}^{-\mathrm{i}\omega t}\,\mathrm{e}^{\mathrm{i}kx}\,\mathrm{d}\omega\,, \tag{3.237}$$

where $k = k(\omega)$ is the complex wavenumber, the imaginary part of which is the attenuation coefficient.

The causality argument is now made that, if $p(0,t)$ vanishes at all times before some time t_0 in the past, then so should $p(x,t)$. One defines $k(\omega)$ for negative values of frequency so that

$$k(-\omega) = -k^*(\omega)\,. \tag{3.238}$$

This requires that the real and imaginary parts of the complex wavenumber be such that

$$k_\mathrm{R}(-\omega) = -k_\mathrm{R}(\omega)\,; \qquad k_\mathrm{I}(-\omega) = k_\mathrm{I}(\omega)\,, \tag{3.239}$$

so that the real part is odd, and the imaginary part is even in ω. This extension to negative frequencies allows one to write (3.237) in the form

$$p(x,t) = \int_{-\infty}^\infty \hat{p}(\omega)\,\mathrm{e}^{-\mathrm{i}\omega t}\,\mathrm{e}^{\mathrm{i}kx}\,\mathrm{d}\omega\,. \tag{3.240}$$

The theory of complex variables assures one that this integral will indeed vanish for sufficiently early times if: (i) one can regard the integrand as being defined for complex values of ω, and (ii) one can regard the integrand as having certain general properties in the upper half of the complex ω plane. In particular, it must be analytic (no poles, no branch cuts, no points where a power series does not exist) in this upper half of the comp;ex plane. Another condition is that, when t has a sufficiently negative value, the integrand goes to zero as $|\omega| \to \infty$ in the upper half-plane. The possibility of the latter can be tested with the question of whether

$$\mathrm{Re}\,[-\mathrm{i}\omega t + \mathrm{i}kx)] \to -\infty \qquad \text{as} \quad \omega \to \mathrm{i}\infty\,, \tag{3.241}$$

with $t < 0$ and $x > 0$. In any event, for all these conditions to be met, the complex wavenumber $k(\omega)$, considered as a complex function of the complex variable ω, has to be analytic in the upper half-plane. One cannot say at the outset, without having a well-defined causal mathematical model, just how it behaves at infinity, but various experimental data suggests it approaches a polynomial with a leading exponent of not more than two. Also, analysis on specific cases suggests it is always such that k/ω is analytic and, moreover, finite at $\omega = 0$.

Contour Integral Identity

Given these general properties of the complex wavenumber, one considers the contour integral

$$I_\mathrm{A}(\zeta_1,\zeta_2,\zeta_3,\zeta_4) = \oint \frac{k/\omega}{(\omega-\zeta_1)(\omega-\zeta_2)(\omega-\zeta_3)(\omega-\zeta_4)}\,\mathrm{d}\omega\,, \tag{3.242}$$

where the contour is closed, the integration proceeds in the counterclockwise sense, the contour is entirely in the upper half plane, and where the contour encloses the four poles at ζ_1, ζ_2, etc., all of which are in the upper half-plane.

(The number of poles that one includes is somewhat arbitrary, and four is a judicious compromise for the present chapter. The original [3.57,58] analysis directed toward acoustical applications included only two, but this led to divergent integrals when the result was applied to certain experimental laws that had been extrapolated to high frequencies. The more poles one includes, the less dependent is the prediction on details of extrapolations to frequencies outside the range of experimental data.)

The integral can be deformed to one which proceeds along the real axis from $-\infty$ to ∞ and which is then completed by a semicircle of infinite radius that encloses the upper half-plane. Because of the supposed behavior of k at ∞ in the upper half-plane, the latter integral is zero and one has

$$I_\mathrm{A}(\zeta_1,\zeta_2,\zeta_3,\zeta_4) = \int_{-\infty}^\infty \frac{k/\omega}{(\omega-\zeta_1)(\omega-\zeta_2)(\omega-\zeta_3)(\omega-\zeta_4)}\,\mathrm{d}\omega\,. \tag{3.243}$$

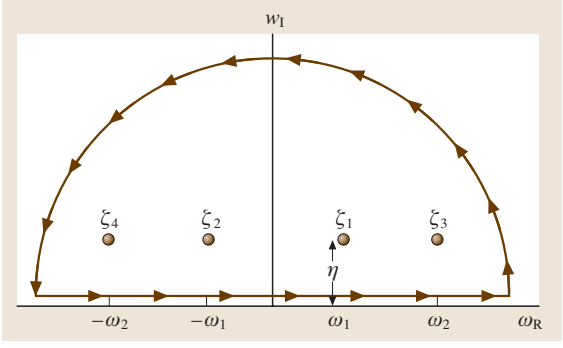


Fig. 3.13 Contour integral in the complex frequency plane used in the derivation of one version of the Kramers–Krönig relations

Amazon EX1014 Page 73

Furthermore, the residue theorem yields

$$I_A(\zeta_1,\zeta_2,\zeta_3,\zeta_4) = \frac{2\pi i(k/\omega)_1}{(\zeta_1-\zeta_2)(\zeta_1-\zeta_3)(\zeta_1-\zeta_4)} + \frac{2\pi i(k/\omega)_2}{(\zeta_2-\zeta_1)(\zeta_2-\zeta_3)(\zeta_2-\zeta_4)} + \frac{2\pi i(k/\omega)_3}{(\zeta_3-\zeta_1)(\zeta_3-\zeta_2)(\zeta_3-\zeta_4)} + \frac{2\pi i(k/\omega)_4}{(\zeta_4-\zeta_1)(\zeta_4-\zeta_2)(\zeta_4-\zeta_3)}\,, \quad (3.244)$$

where $(k/\omega)_1$ is k/ω evaluated at $\omega=\zeta_1$, etc.

To take advantage of the symmetry properties (3.239), one sets

$$\zeta_1=\omega_1+i\eta\,, \qquad \zeta_3=-\omega_1+i\eta\,;$$
$$\zeta_2=\omega_2+i\eta\,; \qquad \zeta_4=-\omega_2+i\eta\,, \quad (3.245)$$

so that the poles occur in pairs, symmetric about the imaginary axis. One next lets the small positive parameter η go to zero, and recognizes that

$$\lim_{\epsilon\to 0}\lim_{\eta\to 0}\int_{\omega_1-\epsilon}^{\omega_1+\epsilon}\frac{f(\omega)}{\omega-\omega_1-i\eta}\,d\omega=\pi i f(\omega_1)\,. \quad (3.246)$$

Thus in this limit, the integral (3.243) becomes represented as a principal value plus a set of four *narrow gap* terms that that are recognized as one half of the right side of (3.244). The resulting mathematical identity is

$$\Pr\int_{-\infty}^{\infty}\frac{k/\omega}{(\omega^2-\omega_1^2)(\omega^2-\omega_2^2)}\,d\omega=\frac{i\pi}{\omega_1^2-\omega_2^2}\times\left(\frac{k(\omega_1)+k(-\omega_1)}{2\omega_1^2}-\frac{k(\omega_2)+k(-\omega_2)}{2\omega_2^2}\right). \quad (3.247)$$

Real Part Within the Integrand

When one uses the symmetry properties (3.239), the above reduces to

$$2\Pr\int_0^{\infty}\frac{k_R(\omega)}{\omega(\omega^2-\omega_1^2)(\omega^2-\omega_2^2)}\,d\omega=-\frac{\pi}{\omega_1^2-\omega_2^2}\left(\frac{k_I(\omega_1)}{\omega_1^2}-\frac{k_I(\omega_2)}{\omega_2^2}\right). \quad (3.248)$$

The significant thing about this result and the key to its potential usefulness is that the left side involves only the real part of $k(\omega)$ and the right side only the imaginary. Thus if one knew the real part completely and knew the imaginary part for only one frequency, one could find the imaginary part for any other frequency with the relation

$$\frac{k_I(\omega)}{\omega^2}=\frac{k_I(\omega_1)}{\omega_1^2}+\frac{2(\omega_1^2-\omega^2)}{\pi}\times\Pr\int_0^{\infty}\frac{k_R(\omega')}{\omega'(\omega'^2-\omega_1^2)(\omega'^2-\omega^2)}\,d\omega'\,. \quad (3.249)$$

Here the notation is slightly altered: ω' is the dummy variable of integration, ω_1 is the value of the angular frequency at which one presumably already knows k_I, and ω is that angular frequency for which the value is predicted by the right side. Relations such as this which allow predictions of one part of $k(\omega)$ from another part are known as Kramers–Krönig relations.

Other Kramers–Krönig relations can be obtained from (3.247) with a suitable replacement for k/ω in the integrand and/or taking limits with ω_1 or ω_2 approaching either 0 or ∞. One can also add or subtract simple functions to the integrand where the resulting extra integrals are known. For example, if one sets k/ω to unity in (3.247) one obtains the identity

$$\Pr\int_0^{\infty}\frac{d\omega'}{(\omega'^2-\omega_1^2)(\omega'^2-\omega^2)}=0\,. \quad (3.250)$$

Thus, (3.249) can be equivalently written

$$\frac{k_I(\omega)}{\omega^2}=\frac{k_I(\omega_1)}{\omega_1^2}+\frac{2(\omega_1^2-\omega^2)}{\pi}\times\Pr\int_0^{\infty}\frac{[k_R(\omega')/\omega']-[k_R(\omega')/\omega']_0}{(\omega'^2-\omega_1^2)(\omega'^2-\omega^2)}\,d\omega'\,, \quad (3.251)$$

where the subscript 0 indicates that the quantity is evaluated in the limit of zero frequency. A further step is to take the limit as $\omega_1\to 0$, so that one obtains

$$\frac{k_I(\omega)}{\omega^2}=\left[\frac{k_I(\omega)}{\omega^2}\right]_0-\frac{2\omega^2}{\pi}\times\Pr\int_0^{\infty}\frac{[k_R(\omega')/\omega']-[k_R(\omega')/\omega']_0}{\omega'^2(\omega'^2-\omega^2)}\,d\omega'\,. \quad (3.252)$$

The numerator in the integrand is recognized as the difference in the reciprocals of the phase velocities, at $\omega=\omega'$ and at $\omega=0$. The validity of the equality requires the integrand to be sufficiently well behaved near

$\omega' = 0$, and this is consistent with k_R being odd in ω and representable locally as a power series. Validity also requires that k_I/ω^2 be finite at $\omega = 0$, which is consistent with the relaxation models mentioned in the section below. The existence of the integral also places a restriction on the asymptotic dependence of k_R as $\omega \to \infty$.

A possible consequence of the last relation is that

$$\lim_{\omega\to\infty}\left(\frac{k_I(\omega)}{\omega^2}\right) = \left(\frac{k_I(\omega)}{\omega^2}\right)_0 + \frac{2}{\pi}\int_0^\infty \frac{[k_R(\omega')/\omega'] - [k_R(\omega')/\omega']_0}{\omega'^2}\,d\omega' \,. \quad (3.253)$$

The validity of this requires that the integral exists, which is so if the phase velocity approaches a constant at high frequency. An implication is that the attenuation must approach a constant multiplied by ω^2 at high frequency, where the constant is smaller than that at low frequency if the phase velocity at high frequency is higher than that at low frequency.

Imaginary Part Within the Integrand

Analogous results, only with the integration over the imaginary part of k, result when k/ω is replaced by k in (3.247). Doing so yields

$$2\,\mathrm{Pr}\int_0^\infty \frac{k_I(\omega)}{(\omega^2-\omega_1^2)(\omega^2-\omega_2^2)}\,d\omega = \frac{\pi}{\omega_1^2-\omega_2^2}\left(\frac{k_R(\omega_1)}{\omega_1} - \frac{k_R(\omega_2)}{\omega_2}\right) , \quad (3.254)$$

which in turn yields

$$\frac{k_R(\omega)}{\omega} = \frac{k_R(\omega_1)}{\omega_1} - \frac{2(\omega_1^2-\omega^2)}{\pi} \times \mathrm{Pr}\int_0^\infty \frac{k_I(\omega')}{(\omega'^2-\omega_1^2)(\omega'^2-\omega^2)}\,d\omega' \,. \quad (3.255)$$

Then, taking of the limit $\omega_1 \to 0$, one obtains

$$\frac{k_R(\omega)}{\omega} = \left(\frac{k_R(\omega)}{\omega}\right)_0 + \frac{2\omega^2}{\pi}\,\mathrm{Pr}\int_0^\infty \frac{k_I(\omega')}{\omega'^2(\omega'^2-\omega^2)}\,d\omega' . \quad (3.256)$$

This latter expression requires that k_I/ω^2 be integrable near $\omega = 0$.

Attenuation Proportional to Frequency

Some experimental data for various materials suggest that, for those materials, k_I is directly proportional to ω over a wide range of frequencies. The relation (3.256) is inapplicable if one seeks the corresponding expression for phase velocity. Instead, one uses (3.255), treating ω_1 as a parameter. If one inserts

$$k_I(\omega) = K\omega \quad (3.257)$$

into (3.255), the resulting integral can be performed analytically, with the result

$$\frac{k_R(\omega)}{\omega} = \frac{k_R(\omega_1)}{\omega_1} - \frac{2}{\pi}K\ln\left(\frac{\omega}{\omega_1}\right) . \quad (3.258)$$

(The simplest procedure for deriving this is to replace the infinite upper limit by a large finite number and then separate the integrand using the method of partial fractions. After evaluation of the individual terms, one takes the limit as the upper limit goes to infinity, and discovers appropriate cancelations.) The properties of the logarithm are such that the above indicates that the quantity

$$\frac{k_R(\omega)}{\omega} + \frac{2}{\pi}K\ln(\omega) = \text{constant} \quad (3.259)$$

is independent of ω. This deduction is independent of the choice of ω_1, but the analysis does not tell one what the constant should be. A concise restating of the result is that there is some positive number ω_0, such that

$$\frac{k_R(\omega)}{\omega} = \frac{2}{\pi}K\ln\left(\frac{\omega_0}{\omega}\right) . \quad (3.260)$$

The result is presumably valid at best only over the range of frequencies for which (3.257) is valid. Since negative phase velocities are unlikely, it must also be such that the parameter ω_0 is above this range. This approximate result also predicts a zero phase velocity in the limit of zero frequency, and this is also likely to be unrealistic. But there may nevertheless be some range of frequencies for which both (3.257) and (3.260) would give a good fit to experimental data.

3.7.5 Attenuation of Sound in Air

In air, the relaxation processes that affect sound attenuation are those associated with the (quantized) internal vibrations of the diatomic molecules O_2 and N_2. The ratio of the numbers of molecules in the ground and

Amazon EX1014 Page 75

first excited vibrational states is a function of temperature when the gas is in thermodynamic equilibrium, but during an acoustic disturbance the redistribution of molecules to what is appropriate to the concurrent gas temperature is not instantaneous. The knowledge that the relaxation processes are vibrational relaxation processes and that only the ground and first excited states are appreciably involved allows the sound speed increments to be determined from first principles. One need only determine the difference in sound speeds resulting from the two assumptions: (i) that the distribution of vibrational energy is frozen, and (ii) that the vibrational energy is always distributed as for a gas in total thermodynamic equilibrium. The resulting sound speed increments [3.14] are

$$\frac{(\Delta c)_\nu}{c} = \frac{(\gamma-1)^2}{2\gamma}\frac{n_\nu}{n}\left(\frac{T_\nu^*}{T}\right)^2 \mathrm{e}^{-T_\nu^*/T}\,, \tag{3.261}$$

where n is the total number of molecules per unit volume and n_ν is the number of molecules of the type corresponding to the designation parameter ν. The quantity T is the absolute temperature, and T_ν^* is a characteristic temperature, equal to the energy jump ΔE between the two vibrational states divided by Boltzmann's constant. The value of T_1^* (corresponding to O_2 relaxation) is 2239 K, and the value of T_2^* (corresponding to N_2 relaxation) is 3352 K. For air the fraction n_1/n of molecules that are O_2 is 0.21, while the fraction n_2/n of molecules that are N_2 is 0.78. At a representative temperature of 20 °C, the calculated value of $(\Delta c)_1$ is 0.11 m/s, while that for $(\Delta c)_2$ is 0.023 m/s.

Because relaxation in a gas is caused by two-body collisions, the relaxation times at a given absolute temperature must vary inversely with the absolute pressure. The relatively small (and highly variable) number of water-vapor molecules in the air has a significant effect on the relaxation times because collisions of diatomic molecules with H_2O molecules are much more likely to cause a transition between one internal vibrational quantum state and another. Semi-empirical expressions for the two relaxation times for air are given [3.59, 60] by

$$\frac{p_{\mathrm{ref}}}{p}\frac{1}{2\pi\tau_1} = 24 + 4.04\times10^6 h\left(\frac{0.02+100h}{0.391+100h}\right)\,, \tag{3.262}$$

$$\frac{p_{\mathrm{ref}}}{p}\frac{1}{2\pi\tau_2} = \left(\frac{T_{\mathrm{ref}}}{T}\right)^{1/2}(9+2.8\times10^4 h\,\mathrm{e}^{-F}) \tag{3.263}$$

$$F = 4.17\left[\left(\frac{T_{\mathrm{ref}}}{T}\right)^{1/3} - 1\right]\,. \tag{3.264}$$

The subscript 1 corresponds to O_2 relaxation, and the subscript 2 corresponds to N_2 relaxation. The quantity h here is the fraction of the air molecules that are H_2O molecules; the reference temperature is 293.16 K; and the reference pressure is 10^5 Pa. The value of h can be determined from the commonly reported relative humidity (RH, expressed as a percentage) and the vapor pressure of water at the local temperature according to the defining relation

$$h = 10^{-2}(\mathrm{RH})\frac{p_{\mathrm{vp}}(T)}{p}\,. \tag{3.265}$$

However, as indicated in (3.262) and (3.263), the physics of the relaxation process depends on the absolute humidity and has no direct involvement with the value of the vapor pressure of water. A table of the vapor pressure of water may be found in various references; some representative values in pascals are 872, 1228, 1705, 2338,

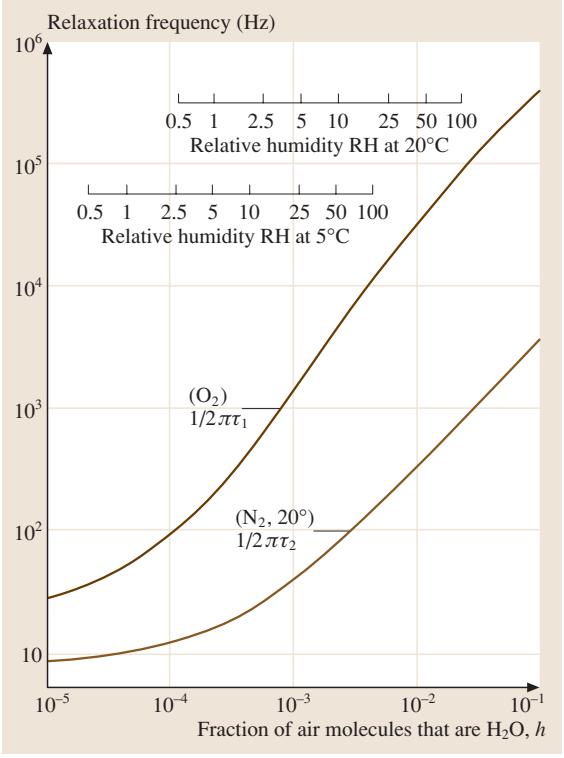


Fig. 3.14 Relaxation frequencies of air as a function of absolute humidity. The pressure is 1.0 atmosphere

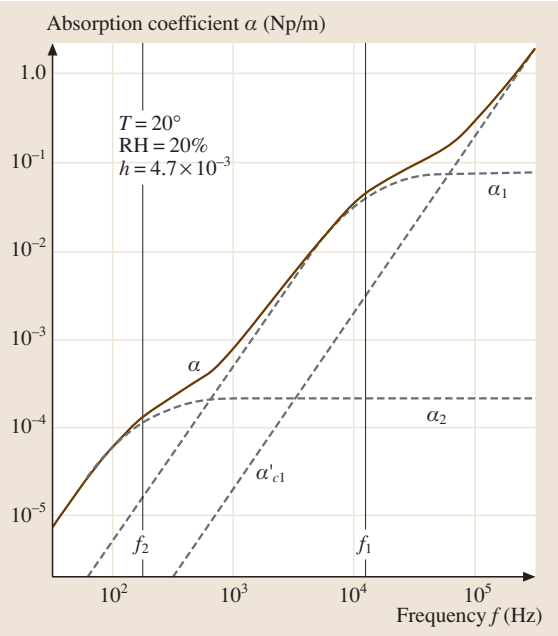


Fig. 3.15 Attenuation of sound in air as a function of frequency (log–log plot). The slopes of the initial portions of the dashed lines correspond to a quadratic dependence on frequency

4243, and 7376 Pa at temperatures of 5, 10, 15, 20, 30, and 40°C, respectively.

Because of the two relaxation frequencies, the frequency dependence of the attenuation coefficient for sound in air has three distinct regions. At very low frequencies, where the frequency is much lower than that associated with molecular nitrogen, the attenuation associated with vibrational relaxation of nitrogen molecules dominates. The dependence is nearly quadratic in frequency, with an apparent bulk viscosity that is associated with the nitrogen relaxation. In an intermediate region, where the frequency is substantially larger than that associated with nitrogen relaxation, but still substantially less than that associated with oxygen relaxation, the dependence is again quadratic in frequency, but the coefficient is smaller, and the apparent bulk viscosity is that associated with oxygen relaxation. Then in the higher-frequency range, substantially above both relaxation frequencies, the quadratic frequency dependence is again evident, but with an even smaller coefficient, the attenuation being the same as that corresponding to classical processes, and with the intrinsic bulk viscosity associated with molecular rotation. Nevertheless, even through the coefficient of the square of the frequency drops over two intervals, the overall trend is that the attenuation constant always increases with increasing frequency.

3.7.6 Attenuation of Sound in Sea Water

The relaxation processes contributing to the attenuation of sound are associated with dissolved boric acid $B(OH)_3$ (subscript 1) and magnesium sulfate $MgSO_4$ (subscript 2). From approximate formulas derived by *Fisher* and *Simmons* [3.61] from a combination of experiment and theory one extracts the identifications

$$\frac{\delta_{\mathrm{cl}}}{c^3} = 1.42\times10^{-15} F(T_{\mathrm{C}}) G(P_{\mathrm{atm}})\,, \tag{3.266}$$

with

$$F(T_{\mathrm{C}}) = 1 - 4.24\times10^{-2} T_{\mathrm{C}} + 8.53\times10^{-4} T_{\mathrm{C}}^2 - 6.23\times10^{-6} T_{\mathrm{C}}^3\,, \tag{3.267}$$

$$G(P_{\mathrm{atm}}) = 1 - 3.84\times10^{-4} P_{\mathrm{atm}} + 7.57\times10^{-8} P_{\mathrm{atm}}^2\,, \tag{3.268}$$

$$\frac{(\Delta c)_1}{c^2} = 1.64\times10^{-9}\left(1 + 2.29\times10^{-2} T_{\mathrm{C}} - 5.07\times10^{-4} T_{\mathrm{C}}^2\right)\frac{S}{35}\,, \tag{3.269}$$

$$\frac{(\Delta c)_2}{c^2} = 8.94\times10^{-9}\,(1 + 0.0134 T_{\mathrm{C}}) \times\left(1 - 10.3\times10^{-4} P_{\mathrm{atm}} + 3.7\times10^{-7} P_{\mathrm{atm}}^2\right)\frac{S}{35}\,, \tag{3.270}$$

$$\frac{1}{2\pi\tau_1} = 1320\, T\, \mathrm{e}^{-1700/T}\,, \tag{3.271}$$

$$\frac{1}{2\pi\tau_2} = 15.5\times10^{6} T\, \mathrm{e}^{-3052/T}\,. \tag{3.272}$$

Here T_{C} is temperature in °C, T is absolute temperature, while P_{atm} is the absolute pressure in atmospheres; S is the salinity in parts per thousand (which is typically of the order of 35 for sea water). All of the quantities on the left sides of these equations are in MKS units.

Amazon EX1014 Page 77

3.8 Acoustic Intensity and Power

A complete set of linear acoustic equations, regardless of the idealization incorporated into its formulation, usually yields a corollary [3.30, 62]

$$\frac{\partial w}{\partial t} + \nabla \cdot \boldsymbol{I} = -\mathfrak{D} \,, \tag{3.273}$$

where the terms are quadratic in the acoustic field amplitudes, the quantity w contains one term that is identifiable as a kinetic energy of fluid motion per unit volume, and the quantity $\mathfrak{D}$ is either zero or positive.

3.8.1 Energy Conservation Interpretation

The relation (3.273) is interpreted as a statement of energy conservation. The quantity w is the energy density, or energy per unit volume associated with the wave disturbance, while the vector quantity $\boldsymbol{I}$ is an intensity vector or energy flux vector. Its interpretation is such that its dot product with any unit vector represents the energy flowing per unit area and time across a surface whose normal is in that designated direction. The quantity $\mathfrak{D}$ is interpreted as the energy that is dissipated per unit time and volume.

This interpretation of an equation such as (3.273) as a conservation law follows when one integrates both sides over an arbitrary fixed volume V within the fluid and reexpresses the volume integral of the divergence of $\boldsymbol{I}$ by a surface integral by means of the divergence theorem (alternately referred to as Gauss's theorem). Doing this yields

$$\frac{\partial}{\partial t} \iiint_V w \, \mathrm{d}V + \iint_S \boldsymbol{I} \cdot \boldsymbol{n} \, \mathrm{d}S = - \iiint_V \mathfrak{D} \, \mathrm{d}V \,, \tag{3.274}$$

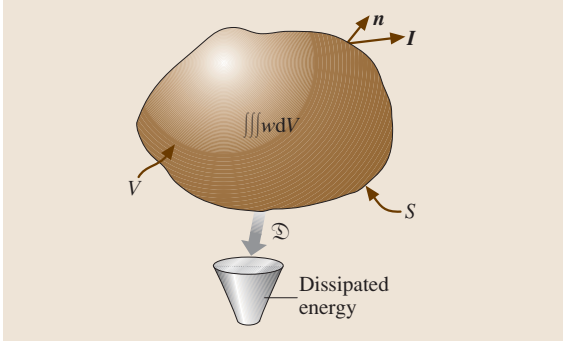


Fig. 3.16 Hypothetical volume inside a fluid, within which the acoustic energy is being dissipated and out of which acoustic energy is flowing

where $\boldsymbol{n}$ is the unit normal vector pointing out of the surface S enclosing V. This relation states that the net rate of increase of *acoustical energy* within the volume must equal the *acoustic power* flowing into the volume across its confining surface minus the energy that is being dissipated per unit time within the volume.

3.8.2 Acoustic Energy Density and Intensity

For the ideal case, when there is no ambient velocity and when viscosity and thermal conduction are neglected, the energy corollary results from (3.71) and (3.72). The derivation begins with one's taking the dot product of the fluid velocity $\boldsymbol{v}$ with (3.72), and then using vector identities and (3.71) to reexpress the right side as the sum of a divergence and a time derivative. The result yields the identification of the energy density as

$$w = \frac{1}{2}\rho v^2 + \frac{1}{2}\frac{1}{\rho c^2} p^2 \,, \tag{3.275}$$

and yields the identification of the acoustic intensity as

$$\boldsymbol{I} = p\boldsymbol{v} \,. \tag{3.276}$$

For this ideal case, there is no dissipative term on the right side. The corollary of (3.273) remains valid even if the ambient density and sound speed vary from point to point.

The first term in the expression for w is recognized as the acoustic kinetic energy per unit volume, and the second term is identified as the potential energy per unit volume due to compression of the fluid.

Intensity Carried by Plane Waves

For a plane wave, it follows from (3.186) and (3.187) that the kinetic and potential energies are the same [3.63], and that the energy density is given by

$$w = \frac{1}{\rho c^2} p^2 \,. \tag{3.277}$$

The intensity becomes

$$\boldsymbol{I} = \boldsymbol{n} \frac{p^2}{\rho c} \,. \tag{3.278}$$

For such a case, the intensity and the energy density are related by

$$\boldsymbol{I} = c\boldsymbol{n}w \,. \tag{3.279}$$

Amazon EX1014 Page 78

This yields the interpretation that the energy in a sound wave is moving in the direction of propagation with the sound speed. Consequently, the sound speed can be regarded as an energy propagation velocity. (This is in accord with the fact that sound waves in this idealization are nondispersive, so the group and phase velocities are the same.)

3.8.3 Acoustic Power

Many sound fields can be idealized as being steady, such that long-time averages are insensitive to the duration and the center time of the averaging interval. Constant-frequency sounds and continuous noises fall into this category.

In the special case of constant-frequency sounds, when complex amplitudes are used to described the acoustic field, the general theorem (3.182) for averaging over products of quantities oscillating with the same frequency applies, and one finds

$$w_{\mathrm{av}} = \frac{1}{4}\rho\hat{\boldsymbol{v}}\cdot\hat{\boldsymbol{v}}^* + \frac{1}{4}\frac{1}{\rho c^2}\left|\hat{p}\right|^2 , \tag{3.280}$$

$$\boldsymbol{I}_{\mathrm{av}} = \frac{1}{2}\mathrm{Re}\left\{\hat{p}^*\hat{\boldsymbol{v}}\right\} . \tag{3.281}$$

For steady sounds, the time derivative of the acoustic energy density will average to zero over a sufficiently long time period, so the acoustic energy corollary of (3.273), in the absence of dissipation, yields the time-averaged relation

$$\nabla\cdot\boldsymbol{I}_{\mathrm{av}} = 0 . \tag{3.282}$$

This implies that the time-averaged vector intensity field is solenoidal (zero divergence) in regions that do not contain acoustic sources. This same relation holds for any frequency component of the acoustic field or for the net contribution to the field from any given frequency band. In the following discussion, the intensity $\boldsymbol{I}_{\mathrm{av}}$ is understood to refer to such a time average for some specified frequency band.

The relation (3.282) yields the integral relation

$$\int_S \boldsymbol{I}_{\mathrm{av}}\cdot\boldsymbol{n}\ \mathrm{d}S = 0 , \tag{3.283}$$

which is interpreted as a statement that the net acoustic power flowing out of any region not containing sources must be zero when averaged over time and for any given frequency band.

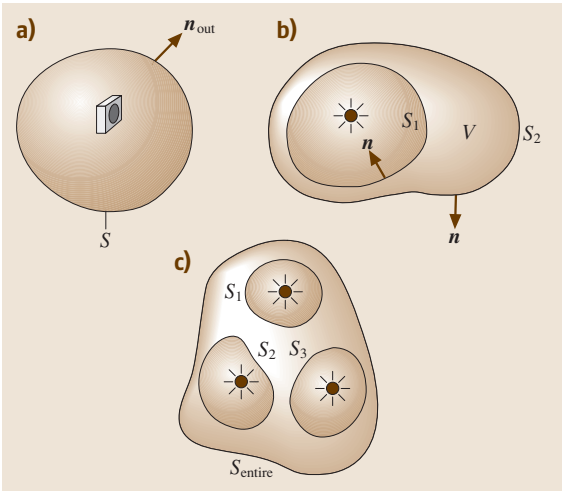


Fig. 3.17 Surfaces enclosing one or more sources. The integration of the time-averaged acoustic intensity component in the direction of the unit outward normal over any such surface yields the time average of the total power generated with the volume enclosed by the surface

For a closed surface that encloses one or more sources, such that the governing linear acoustic equations do not apply at every point within the volume, the reasoning above allows one to define the time-averaged net acoustic power of these sources as

$$\mathfrak{P}_{\mathrm{av}} = \int_S \boldsymbol{I}_{\mathrm{av}}\cdot\boldsymbol{n}\ \mathrm{d}S , \tag{3.284}$$

where the surface S encloses the sources. It follows from (3.283) that the acoustic power of a source computed in such a manner will be the same for any two choices of the surface S, provided that both surfaces enclose the same source and no other sources. The value of the integral is independent of the size and of the shape of S. This result is of fundamental importance for the measurement of source power. Instrumentation to measure the time-averaged intensity directly has become widely available in recent years and is often used in determining the principal noise sources in complicated environments.

3.8.4 Rate of Energy Dissipation

Under circumstances in which viscosity, thermal conduction, and internal relaxation are to be taken into account, the linear acoustic equations for the acoustic mode, which yield the dissipative wave equation of (3.218) and the relaxation equations described by

Amazon EX1014 Page 79

(3.219), yield [3.14] an energy corollary of the form of (3.273). To a satisfactory approximation the energy density and intensity remain as given by (3.275) and (3.276). The energy dissipation per unit volume is no longer zero, but is instead

$$\mathfrak{D}_{\mathrm{av}} = 2\frac{\delta_{\mathrm{cl}}}{\rho c^4}\left(\frac{\partial p}{\partial t}\right)^2 + 2\sum_{\nu}\frac{(\Delta c)_\nu}{\rho c^3}\tau_\nu\left(\frac{\partial p_\nu}{\partial t}\right)^2 . \tag{3.285}$$

For constant-frequency plane waves propagating in the x-direction, the time average of the time derivative of the energy density is zero, and the time averages of $\boldsymbol{I}$ and $\mathfrak{D}$ will both be quadratic in the wave amplitude $|\hat{p}|$. The identification of the attenuation coefficient α must then be such that

$$\mathfrak{D}_{\mathrm{av}} = 2\alpha I_{\mathrm{av}} . \tag{3.286}$$

The magnitude of the acoustic intensity decreases with propagation distance x as

$$I_{\mathrm{av}}(x) = I_{\mathrm{av}}(0)\,\mathrm{e}^{-2\alpha x} . \tag{3.287}$$

This identification of the attenuation coefficient is consistent with that given in (3.225).

3.8.5 Energy Corollary for Elastic Waves

An energy conservation corollary of the form of (3.273) also holds for sound in solids. The appropriate identifications for the energy density w and the components I_i of the intensity are

$$w = \frac{1}{2}\rho\sum_i\left(\frac{\partial\xi_i}{\partial t}\right)^2 + \frac{1}{2}\sum_{i,j}\epsilon_{ij}\sigma_{ij} \tag{3.288}$$

$$I_i = -\sum_j \sigma_{ij}\frac{\partial\xi_j}{\partial t} . \tag{3.289}$$

3.9 Impedance

Complex ratios of acoustic variables are often intrinsic quantities independent of the detailed nature of the acoustic disturbance.

3.9.1 Mechanical Impedance

The ratio of the complex amplitude of a sinusoidally varying force to the complex amplitude of the resulting velocity at a point on a vibrating object is called the mechanical impedance at that point. It is a complex number and usually a function of frequency. Other definitions [3.64] of impedance are also in widespread use in acoustics.

3.9.2 Specific Acoustic Impedance

The specific acoustic impedance or unit-area acoustic impedance $Z_{\mathrm{S}}(\omega)$ for a surface is defined as

$$Z_{\mathrm{S}}(\omega) = \frac{\hat{p}}{\hat{v}_{\mathrm{in}}} , \tag{3.290}$$

where $\hat{v}_{\mathrm{in}}$ is the component of the fluid velocity directed into the surface under consideration. Typically, the specific acoustic impedance, often referred to briefly as the impedance without any adjective, is used to describe the acoustic properties of materials. In many cases, surfaces of materials abutting fluids can be characterized as locally reacting, so that Z_{S} is independent of the detailed nature of the acoustic pressure field. In particular, the locally reacting hypothesis implies that the velocity of the material at the surface is unaffected by pressures other than in the immediate vicinity of the point of interest. At a nominally motionless and passively responding surface, and when the hypothesis is valid, the appropriate boundary condition on the complex amplitude $\hat{p}$ that satisfies the Helmholtz equation is given by

$$\mathrm{i}\omega\rho\hat{p} = -Z_{\mathrm{S}}\nabla\hat{p}\cdot\boldsymbol{n} , \tag{3.291}$$

where $\boldsymbol{n}$ is the unit normal vector pointing out of the material into the fluid. A surface that is perfectly rigid has $|Z_{\mathrm{S}}| = \infty$. The other extreme, where $Z_{\mathrm{S}} = 0$, corresponds to the ideal case of a pressure release surface. This is, for example, what is normally assumed for the upper surface of the ocean in underwater sound. Since a passive surface absorbs energy from the sound field, the time-averaged intensity component into the surface should be positive or zero. This observation leads to the requirement that the real part (specific acoustic resistance) of the impedance should always be nonnegative. The imaginary part (specific acoustic reactance) may be either positive or negative.

3.9.3 Characteristic Impedance

For extended substances, a related definition is that of characteristic impedance Z_{char}, defined as the ratio of $\hat{p}$ to the complex amplitude $\hat{v}$ of the fluid velocity in the

Amazon EX1014 Page 80

direction of propagation when a plane wave is propagating through the substance. As indicated by (3.187), this characteristic impedance, when the fluid is lossless, is ρc, regardless of frequency and position in the field. In the general case when the propagation is dispersive and there is a plane wave attenuation, one has

$$Z_{\text{char}} = \frac{\rho\omega}{k} , \tag{3.292}$$

where $k(\omega)$ is the complex wavenumber.

The MKS units $[(\text{kg}/\text{m}^{-3})(\text{m}/\text{s})]$ of specific acoustic impedance are referred to as MKS rayl (after Rayleigh). The characteristic impedance of air under standard conditions is approximately 400 MKS rayls, and that of water is approximately 1.5×10^6 MKS rayl.

3.9.4 Radiation Impedance

The radiation impedance Z_{rad} is defined as $\hat{p}/\hat{v}_{\text{n}}$, where $\hat{v}_{\text{n}}$ corresponds to the outward normal component of velocity at a vibrating surface. (Specific examples involving spherical waves are given in a subsequent section of this chapter.)

Given the definition of the radiation impedance, the time-averaged power flow per unit area of surface out of the surface is

$$\begin{aligned} I_{\text{rad}} &= \frac{1}{2}\text{Re}\left(\hat{p}\hat{v}_{\text{n}}^*\right) = \frac{1}{2}|\hat{v}_{\text{n}}|^2\text{Re}\left(Z_{\text{rad}}\right) \\ &= \frac{1}{2}|\hat{p}|^2\text{Re}\left(\frac{1}{Z_{\text{rad}}}\right) . \end{aligned} \tag{3.293}$$

The total power radiated is the integral of this over the surface of the body.

3.9.5 Acoustic Impedance

The term acoustic impedance Z_{A} is reserved [3.64] for the ratio of $\hat{p}$ to the volume velocity complex amplitude. Here volume velocity is the net volume of fluid flowing past a specified surface element per unit time in a specified directional sense. One may speak, for example, of the acoustic impedance of an orifice in a wall, of the acoustic impedance at the mouth of a Helmholtz resonator, and of the acoustic impedance at the end of a pipe.

3.10 Reflection and Transmission

When sound impinges on a surface, some sound is reflected and some is transmitted and possibly absorbed within or on the the other side of the surface. To understand the processes that occur, it is often an appropriate idealization to take the incident wave as a plane wave and to consider the surface as flat.

3.10.1 Reflection at a Plane Surface

When a plane wave reflects at a surface with finite specific acoustic impedance Z_{S}, a reflected wave is formed such that the angle of incidence θ_{I} equals the angle of reflection (law of mirrors). Here both angles are reckoned from the line normal to the surface and correspond to the directions of the two waves. If one takes the y-axis as pointing out of the surface and the surface as coinciding with the $y = 0$ plane, then an incident plane wave propagating obliquely in the $+x$-direction will have a complex pressure amplitude

$$\hat{p}_{\text{in}} = \hat{f}\, \text{e}^{\text{i}k_x x}\, \text{e}^{-\text{i}k_y y} , \tag{3.294}$$

where $\hat{f}$ is a constant. (For transient reflection, the quantity $\hat{f}$ can be taken as the Fourier transform of the incident pressure pulse at the origin.) The two indicated wavenumber components are $k_x = k \sin\theta_{\text{I}}$ and $k_y = k \cos\theta_{\text{I}}$.

The reflected wave has a complex pressure amplitude given by

$$\hat{p}_{\text{re}\Lambda} = \Re(\theta_{\text{I}}, \omega)\, \hat{f}\, \text{e}^{\text{i}k_x x}\, \text{e}^{\text{i}k_y y} , \tag{3.295}$$

where the quantity $\Re(\theta_{\text{I}}, \omega)$ is the pressure amplitude reflection coefficient.

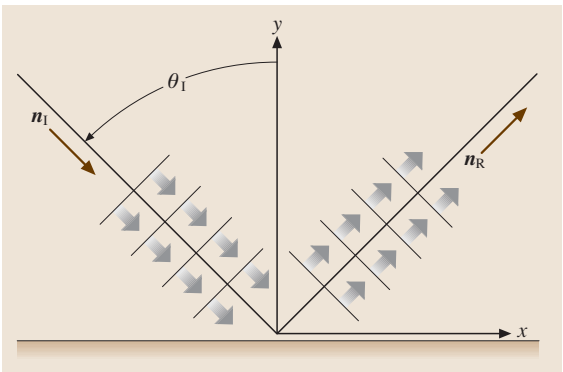


Fig. 3.18 Reflection of a plane wave at a planar surface

Analysis that makes use of the boundary condition (3.291) leads to the identification

$$\Re(\theta_\mathrm{I}, \omega) = \frac{\xi(\omega)\cos\theta_\mathrm{I} - 1}{\xi(\omega)\cos\theta_\mathrm{I} + 1} \tag{3.296}$$

for the reflection coefficient, with the abbreviation

$$\xi(\omega) = \frac{Z_\mathrm{S}}{\rho c}\,, \tag{3.297}$$

which represents the ratio of the specific acoustic impedance of the surface to the characteristic impedance of the medium.

3.10.2 Reflection at an Interface

The above relations also apply, with an appropriate identification of the quantity Z_S, to sound reflection [3.65] at an interface between two fluids with different sound speeds and densities. Translational symmetry requires that the disturbance in the second fluid have the same apparent phase velocity (ω/k_x) (trace velocity) along the x-axis as does the disturbance in the first fluid. This requirement is known as the trace velocity matching principle [3.4, 30] and leads to the observation that k_x is the same in both fluids. One distinguishes two possibilities: the trace velocity is higher than the sound speed c_2 or lower than c_2.

For the first possibility, one has the inequality

$$c_2 < \frac{c_1}{\sin\theta_\mathrm{I}}\,, \tag{3.298}$$

and a propagating plane wave (transmitted wave) is excited in the second fluid, with complex pressure amplitude

$$\hat{p}_\mathrm{trans} = \mathfrak{T}(\omega, \theta_\mathrm{I})\,\hat{f}\,\mathrm{e}^{\mathrm{i}k_x x}\,\mathrm{e}^{\mathrm{i}k_2 y\cos\theta_\mathrm{II}}\,, \tag{3.299}$$

where $k_2 = \omega/c_2$ is the wavenumber in the second fluid and θ_II (angle of refraction) is the angle at which the transmitted wave is propagating. The trace velocity matching principle leads to Snell's law,

$$\frac{\sin\theta_\mathrm{I}}{c_1} = \frac{\sin\theta_\mathrm{II}}{c_2}\,. \tag{3.300}$$

The change in propagation direction from θ_I to θ_II is the phenomenon of refraction.

The requirement that the pressure be continuous across the interface yields the relation

$$1 + \Re = \mathfrak{T}\,, \tag{3.301}$$

while the continuity of the normal component of the fluid velocity yields

$$\frac{\cos\theta_\mathrm{I}}{\rho_1 c_1}(1 - \Re) = \frac{\cos\theta_\mathrm{II}}{\rho_2 c_2}\mathfrak{T}\,. \tag{3.302}$$

From these one derives the reflection coefficient

$$\Re = \frac{Z_\mathrm{II} - Z_\mathrm{I}}{Z_\mathrm{II} + Z_\mathrm{I}}\,, \tag{3.303}$$

which involves the two impedances defined by

$$Z_\mathrm{I} = \frac{\rho_1 c_1}{\cos\theta_\mathrm{I}}\,, \tag{3.304}$$

$$Z_\mathrm{II} = \frac{\rho_2 c_2}{\cos\theta_\mathrm{II}}\,. \tag{3.305}$$

The other possibility, which is the opposite of that in (3.298), can only occur when $c_2 > c_1$ and, moreover, only if θ_I is greater than the critical angle

$$\theta_\mathrm{cr} = \arcsin(c_1/c_2)\,. \tag{3.306}$$

In this circumstance, an inhomogeneous plane wave, propagating in the x-direction, but dying out exponentially in the $+y$-direction, is excited in the second medium. Instead of (3.299), one has the transmitted pressure given by

$$\hat{p}_\mathrm{trans} = \mathfrak{T}(\omega, \theta_\mathrm{I})\,\hat{f}\,\mathrm{e}^{\mathrm{i}k_x x}\,\mathrm{e}^{-\beta k_2 y}\,, \tag{3.307}$$

with

$$\beta = [(c_2/c_1)^2 \sin^2\theta_\mathrm{I} - 1]^{1/2}\,. \tag{3.308}$$

The previously stated equations governing the reflection and transmission coefficients are still applicable, provided one replaces $\cos\theta_\mathrm{II}$ by $\mathrm{i}\beta$. This causes the magnitude of the reflection coefficient $\Re$ to become unity,

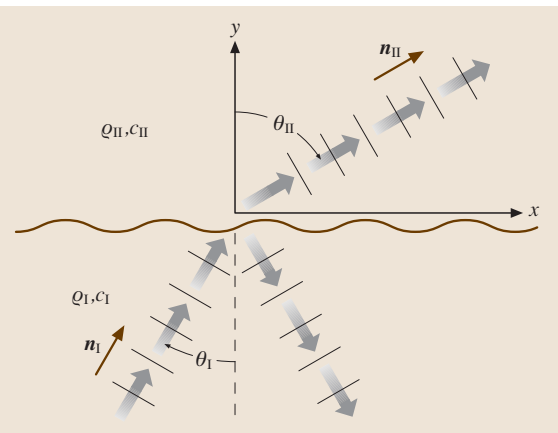


Fig. 3.19 Reflection of a plane wave at an interface between two fluids

so the time-averaged incident energy is totally reflected. Acoustic energy is present in the second fluid, but its time average over a wave period stays constant once the steady state is reached.

3.10.3 Theory of the Impedance Tube

Impedance tubes are commonly used in the measurement of specific acoustic impedances; the underlying theory [3.66, 67] is based for the most part on (3.295), (3.296), and (3.297) above. The incident and the reflected waves propagate along the axis of a cylindrical tube with the sample surface at one end. A loudspeaker at the other end creates a sinusoidal pressure disturbance that propagates down the tube. Reflections from the end covered with the test material create an incomplete standing-wave pattern inside the tube.

The wavelength of the sound emitted by the source can be adjusted, but it should be kept substantially larger than the pipe diameter, so that the plane wave assumption holds. With k_x identified as being 0, the complex amplitude that corresponds to the sum of the incident and reflected waves has an absolute magnitude given by

$$|\hat{p}| = |\hat{f}||1 + \Re e^{2iky}| \,, \tag{3.309}$$

where y is now the distance in front of the sample. The second factor varies with y and repeats at intervals of a half-wavelength, and varies from a minimum value of $1 - |\Re|$ to a maximum value of $1 + |\Re|$. Consequently,

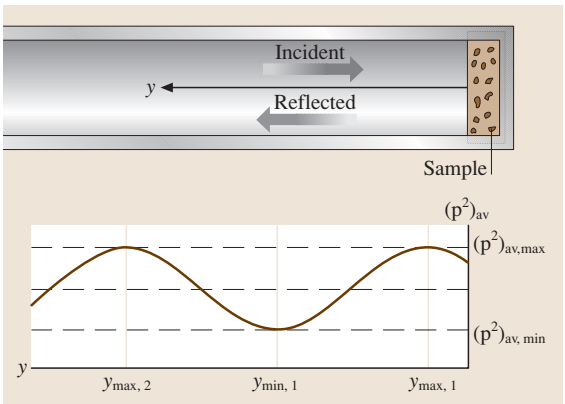


Fig. 3.20 Incident and reflected waves inside an impedance tube. The time-averaged pressure within the tube has minimum and maximum values whose ratio depends on the impedance of the sample at the end. Another measured parameter is the distance back from the sample at which the first maximum occurs

the ratio of the peak acoustic pressure amplitude $|\hat{p}|_{max}$ (which occurs at one y-position) to the minimum acoustic pressure amplitude $|\hat{p}|_{min}$ (which occurs at a position a quarter-wavelength away) determines the magnitude of the reflection coefficient via the relation

$$\frac{|\hat{p}|_{min}}{|\hat{p}|_{max}} = \frac{1 - |\Re|}{1 + |\Re|} \,. \tag{3.310}$$

The phase δ of the reflection coefficient can be determined with use of the observation that the peak amplitudes occur at y-values where $\delta + 2ky$ is an integer multiple of 2π, while the minimum amplitudes occur where it is π plus an integer multiple of 2π. Once the magnitude and phase of the reflection coefficient are determined, the specific acoustic impedance can be found from (3.296) and (3.297).

3.10.4 Transmission through Walls and Slabs

The analysis of transmission of sound through a wall or a partition [3.68] is often based on the idealization that the wall is of unlimited extent.

If the incoming plane wave has an angle of incidence θ_I and if the fluid on the opposite side of the wall has the same sound speed, then the trace velocity matching principle requires that the transmitted wave be propagating in the same direction.

A common assumption when the fluid is air is that the compression in the wall is negligible, so the wall is treated as a slab that has a uniform velocity v_{sl} throughout its thickness. The slab moves under the influence of the incident, reflected, and transmitted sound fields according to the relation (corresponding to Newton's

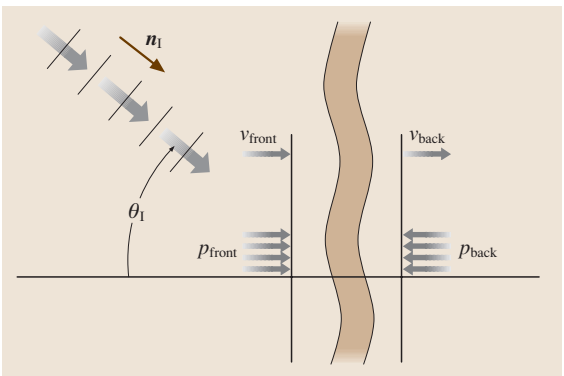


Fig. 3.21 Transmission of an incident plane wave through a thin flexible slab

second law) given by

$$m_{\mathrm{sl}}\frac{\partial v_{\mathrm{sl}}}{\partial t} = p_{\mathrm{front}} - p_{\mathrm{back}} + \text{bending term}\,, \qquad (3.311)$$

where m_{sl} is the mass per unit surface area of the slab.

The front side is here taken as the side facing the incident wave; the transmitted wave propagates away from the back side. The bending term (discussed further below) accounts for any tendency of the slab to resist bending. If the slab is regarded as nonporous then the normal component of the fluid velocity both at the front and the back is regarded the same as the slab velocity itself. If it is taken as porous [3.69, 70] then these continuity equations are replaced by the relations

$$v_{\mathrm{front}} - v_{\mathrm{sl}} = v_{\mathrm{back}} - v_{\mathrm{sl}} = \frac{1}{R_{\mathrm{f}}}(p_{\mathrm{front}} - p_{\mathrm{back}})\,, \qquad (3.312)$$

where R_{f} is the specific flow resistance. The latter can be measured in steady flow for specific materials. For a homogeneous material, it is given by the product of the slab thickness h and the flow resistivity, the latter being a commonly tabulated property of porous materials. [The law represented by (3.312) is the thin slab, or blanket, counterpart of the Darcy's law mentioned in a preceding section, where Biot's model of porous media is discussed.]

In general, when one considers the reflection at and transmission through a slab, one can define a slab specific impedance Z_{sl} such that, with regard to complex amplitudes,

$$\hat{p}_{\mathrm{front}} - \hat{p}_{\mathrm{back}} = Z_{\mathrm{sl}}\hat{v}_{\mathrm{front}} = Z_{\mathrm{sl}}\hat{v}_{\mathrm{back}}\,, \qquad (3.313)$$

where Z_{sl} depends on the angular frequency ω and the trace velocity $v_{\mathrm{tr}} = c/\sin\theta_{\mathrm{I}}$ of the incident wave over the surface of the slab. The value of the slab specific impedance can be derived using considerations such as those that correspond to (3.312) and (3.313). In terms of the slab specific impedance, the transmission coefficient $\mathfrak{T}$ is

$$\mathfrak{T} = \left(1 + \frac{1}{2}\frac{Z_{\mathrm{sl}}}{\rho c}\cos\theta_{\mathrm{I}}\right)^{-1}. \qquad (3.314)$$

The fraction τ of incident power that is transmitted is $|\mathfrak{T}|^2$.

3.10.5 Transmission through Limp Plates

If the slab can be idealized as a limp plate (no resistance to bending) and not porous, the slab specific impedance Z_{sl} is $-\mathrm{i}\omega m_{\mathrm{sl}}$ and one obtains

$$\tau = \left[1 + \left(\frac{\omega m_{\mathrm{sl}}}{2\rho c}\right)^2 \cos^2\theta_{\mathrm{I}}\right]^{-1} \approx \left(\frac{2\rho c}{\omega m_{\mathrm{sl}}\cos\theta_{\mathrm{I}}}\right)^2 \qquad (3.315)$$

for the fraction of incident power that is transmitted. The latter version, which typically holds at moderate to high audible frequencies, predicts that τ decreases by a factor of 4 when the slab mass m_{sl} per unit area is increased by a factor of 2. In the noise control literature, this behavior is sometimes referred to as the mass law.

3.10.6 Transmission through Porous Blankets

For a porous blanket that has a specific flow resistance R_{f} the specific slab impedance becomes

$$Z_{\mathrm{sl}} = \left(\frac{1}{R_{\mathrm{f}}} - \frac{1}{\mathrm{i}\omega m_{\mathrm{sl}}}\right)^{-1}, \qquad (3.316)$$

and the resulting fraction of incident power that is transmitted can be found with a substitution into (3.314), with τ equated to $|\mathfrak{T}|^2$.

3.10.7 Transmission through Elastic Plates

If the slab is idealized as a Bernoulli–Euler plate with elastic modulus E, Poisson's ratio ν, and thickness h, the bending term in (3.311) has a complex amplitude given by

$$\text{bending term} = -\frac{B_{\mathrm{pl}}k_x^4\hat{v}_{\mathrm{sl}}}{(-\mathrm{i}\omega)}\,, \qquad (3.317)$$

where

$$B_{\mathrm{pl}} = \frac{1}{12}\frac{Eh^3}{(1-\nu^2)} \qquad (3.318)$$

is the plate bending modulus. The slab specific impedance is consequently given by

$$Z_{\mathrm{sl}} = -\mathrm{i}\omega m_{\mathrm{sl}}\left[1 - \left(\frac{f}{f_{\mathrm{c}}}\right)^2 \sin^4\theta_{\mathrm{I}}\right], \qquad (3.319)$$

where

$$f_{\mathrm{c}} = \frac{c^2}{2\pi}\left(\frac{m_{\mathrm{sl}}}{B_{\mathrm{pl}}}\right)^{1/2} \qquad (3.320)$$

gives the coincidence frequency, the frequency at which the phase velocity of freely propagating bending waves in the plate equals the speed of sound in the fluid.

Although the simple result of (3.319) predicts that the fraction of incident power transmitted is unity at a frequency of $f_c/\sin^2\theta_I$, the presence of damping processes in the plate causes the fraction of incident power transmitted always to be less than unity. A simple way of taking this into account makes use of a loss factor η (assumed to be much less than unity) for the plate, which corresponds to the fraction of stored elastic energy that is dissipated through damping processes during one radian (a cycle period divided by 2π). Because twice the loss factor times the natural frequency is the time coefficient for exponential time decay of the amplitude when the system is vibrating in any natural mode, the former can be regarded as the negative of the imaginary part of a complex frequency. Then, because the natural frequency squared is always proportional to the elastic modulus, and because the loss factor is invariably small, the loss factor can be formally introduced into the mathematical model by the replacement of the real elastic modulus by the complex number $(1-i\eta)E$. When this is done, one finds

$$Z_{sl} = \omega\eta m_{pl}\left(\frac{f}{f_c}\right)^2 \sin^4\theta_I - i\omega m_{sl} \times\left[1-\left(\frac{f}{f_c}\right)^2 \sin^4\theta_I\right] \tag{3.321}$$

for the slab impedance that is to be inserted into (3.314). The extra term ordinarily has very little effect on the fraction of incident power that is transmitted except when the (normally dominant) imaginary term is close to zero. When the frequency f is $f_c/\sin^2\theta_I$, one finds the value of τ to be

$$\tau = \left(1+\frac{1}{2}\frac{\omega\eta m_{pl}}{\rho c}\cos\theta_I\right)^{-2}, \tag{3.322}$$

rather than identically unity.

3.11 Spherical Waves

In many circumstances of interest, applicable idealizations are waves that locally resemble waves spreading out radially from sources or from scatterers. The mathematical description of such waves has some similarities to plane waves, but important distinctions arise. The present section is concerned with a number of important situations where the appropriate coordinates are spherical coordinates.

3.11.1 Spherically Symmetric Outgoing Waves

For a spherically symmetric wave spreading out radially from a source in an unbounded medium, the symmetry implies that the acoustic field variables are a function of only the radial coordinate r and of time t. The Laplacian reduces then to

$$\nabla^2 p = \frac{\partial^2 p}{\partial r^2} + \frac{2}{r}\frac{\partial p}{\partial r} = \frac{1}{r}\frac{\partial^2(rp)}{\partial r^2}, \tag{3.323}$$

so the wave equation of (3.74) takes the form

$$\frac{\partial^2(rp)}{\partial r^2} - \frac{1}{c^2}\frac{\partial^2(rp)}{\partial t^2} = 0. \tag{3.324}$$

The solution of this is

$$p(r,t) = \frac{f(r-ct)}{r} + \frac{g(r+ct)}{r}. \tag{3.325}$$

Causality considerations (no sound before the source is turned on) lead to the conclusion that the second term on the right side of (3.325) is not an appropriate solution of the wave equation when the source is concentrated near the origin. The expression

$$p(r,t) = \frac{f(r-ct)}{r}, \tag{3.326}$$

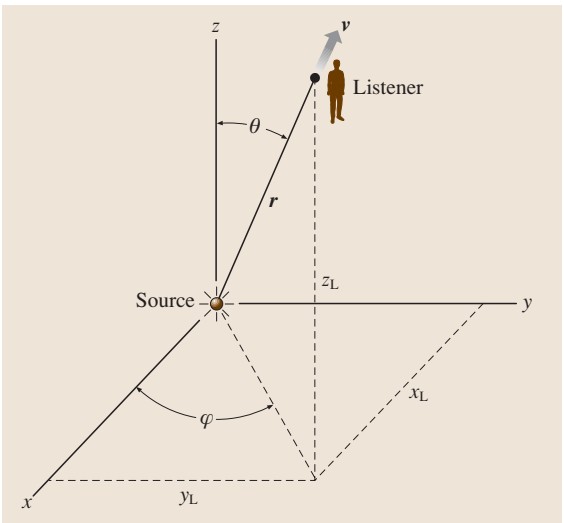


Fig. 3.22 Spherical coordinates. The common situation is when the source is at the origin and the listener (sound receiver) has coordinates (r, θ, ϕ)

which describes the acoustic pressure in an outgoing spherically symmetric wave, has the property that listeners at different radii will receive (with a time shift corresponding to the propagation time) waveforms of the same shape, but of different amplitudes. The factor of $1/r$ is characteristic of spherical spreading and implies that the peak waveform amplitudes in a spherical wave decrease with radial distance as $1/r$.

Spherical waves of constant frequency have complex amplitudes governed by the Helmholtz equation (3.176), with the Laplacian given as stated in (3.323). The complex pressure amplitude corresponding to (3.326) has the form

$$p = A\frac{\mathrm{e}^{\mathrm{i}kr}}{r} \,. \tag{3.327}$$

The fluid velocity associated with an outgoing spherical wave is purely radial and has the form

$$v_r = \frac{1}{\rho c}[-r^{-2}F(r-ct)+r^{-1}f(r-ct)] \,. \tag{3.328}$$

Here the function F is such that its derivative is the function f that appears in (3.326). Because the first term (a near-field term) decreases as the square rather than the first power of the reciprocal of the radial distance, the fluid velocity asymptotically approaches

$$v_r \to \frac{p}{\rho c} \,, \tag{3.329}$$

which is the same as the plane wave relation of (3.187).

For outgoing spherical waves of constant frequency, the complex amplitude of the fluid velocity is

$$\hat{v}_\mathrm{r} = \frac{1}{\rho c}\left(1-\frac{1}{\mathrm{i}kr}\right)\hat{p} \,. \tag{3.330}$$

In this expression, there is a term that is in phase with the pressure and another term that is 90° ($\pi/2$) out of phase with it.

The time-averaged intensity for spherical waves, in accord with (3.281), is

$$\boldsymbol{I}_\mathrm{av} = \frac{1}{2}\mathrm{Re}\left(\hat{p}\hat{v}_\mathrm{r}^*\right) \,. \tag{3.331}$$

The expression for v_r given above allows this to be simplified to

$$\boldsymbol{I}_\mathrm{av} = \frac{1}{2}\frac{1}{\rho c}|\hat{p}|^2 \,. \tag{3.332}$$

Then, with the expression (3.327) inserted for $\hat{p}$, one obtains

$$\boldsymbol{I}_\mathrm{av} = \frac{1}{2}\frac{1}{\rho c}\frac{|A|^2}{r^2} \,. \tag{3.333}$$

The result confirms that the time-averaged intensity falls off as the square of the radial distance. This behavior is what is termed spherical spreading.

The spherical spreading law also follows from energy conservation considerations. The time-averaged power flowing through a spherical surface of radius r is the area $4\pi r^2$ of the surface times the time-averaged intensity. This power should be independent of the radius r since there is no external energy input or attenuation that is included in the considered model, so the intensity must fall off as $1/r^2$.

3.11.2 Radially Oscillating Sphere

The classic example of a source that generates outgoing spherical waves is an impenetrable sphere whose radius $r_\mathrm{sp}(t)$ oscillates with time with some given velocity amplitude v_o, so that

$$r_\mathrm{sp}(t) = a + \frac{v_\mathrm{o}}{\omega}\sin(\omega t) \,. \tag{3.334}$$

Here a is the nominal radius of the sphere, and v_o/ω is the amplitude of the deviations of the actual radius from that value. For the linear acoustics idealization to be valid, it is required that this deviation be substantially less than a, so that

$$v_\mathrm{o} \ll \omega a \,. \tag{3.335}$$

The boundary condition on the fluid dynamic equations should ideally be

$$v_r = v_\mathrm{o}\cos(\omega t) \qquad \text{at} \quad r = r_\mathrm{sp}(t) \,, \tag{3.336}$$

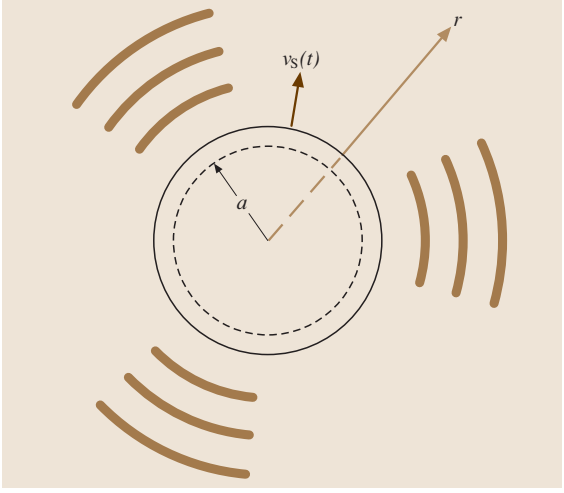


Fig. 3.23 Parameters used for the discussion of constant frequency sound radiated by a radially oscillating sphere

but, also in keeping with the linear acoustics idealization, it is replaced by

$$v_r = v_o \cos(\omega t) \qquad \text{at} \quad r = a\,. \tag{3.337}$$

The corresponding boundary condition on the complex amplitude is

$$\hat{v}_r = v_o \qquad \text{at} \quad r = a\,. \tag{3.338}$$

If the complex amplitude of the acoustic part of the pressure is taken of the general form of (3.327) then the radial fluid velocity, in accord with (3.330), has the complex amplitude

$$\hat{v}_r = \frac{1}{\rho c}\left(1 - \frac{1}{ikr}\right) A \frac{e^{ikr}}{r}\,. \tag{3.339}$$

The approximate boundary condition (3.338) consequently allows one to identify the constant A as

$$A = v_o \left(\frac{ika^2\rho c}{ika - 1}\right) e^{-ika}\,, \tag{3.340}$$

so that the acoustical part of the pressure has the complex ampitude

$$\hat{p} = v_o \left(\frac{ika\rho c}{ika - 1}\right)\left(\frac{a}{r}\right) e^{-ik[r-a]}\,. \tag{3.341}$$

Radiation Impedance

The ratio of the complex amplitude of the pressure to that of the fluid velocity in the outward direction at a point on a vibrating surface is termed the specific radiation impedance (specific here meaning per unit area), so that

$$Z_{rad} = \frac{\hat{p}}{\hat{v}_n}\,, \tag{3.342}$$

where $\hat{v}_n$ is the component of the complex amplitude of the fluid velocity in the outward normal direction. For the case of the radially oscillating sphere of nominal radius a, the analysis above yields

$$Z_{rad} = \rho c \left(\frac{ika}{ika - 1}\right)\,. \tag{3.343}$$

Usually, this is referred to simply as the radiation impedance, without the qualifying adjective *specific*.

The time-averaged power radiated by an oscillating body, in accord with (3.281), is

$$\mathfrak{P}_{av} = \frac{1}{2}\int \mathrm{Re}\left(\hat{p}^*\hat{v}_n\right) dS\,, \tag{3.344}$$

where the integral extends over the surface. Given the definition of the radiation impedance, this can be written in either of the equivalent forms

$$\begin{aligned}\mathfrak{P}_{av} &= \frac{1}{2}\int |\hat{p}|^2 \mathrm{Re}\left(\frac{1}{Z_{rad}}\right) dS \\ &= \frac{1}{2}\int |\hat{v}_n|^2 \mathrm{Re}\,(Z_{rad})\, dS\,.\end{aligned} \tag{3.345}$$

For the case of the radially oscillating sphere, the quantity $\hat{v}_n$ is v_o, and

$$\mathrm{Re}\,(Z_{rad}) = \rho c \left(\frac{k^2a^2}{1 + k^2a^2}\right)\,. \tag{3.346}$$

The latter increases monotonically from 0 to 1 as the frequency increases from 0 to ∞. The surface area of the sphere is $4\pi a^2$, so the time-averaged acoustic power is

$$\mathfrak{P}_{av} = (2\pi a^2)(\rho c) v_o^2 \left(\frac{k^2a^2}{1 + k^2a^2}\right)\,. \tag{3.347}$$

3.11.3 Transversely Oscillating Sphere

Another basic example for which the natural description is in terms of spherical coordinates is that of a rigid sphere oscillating back and forth in the z-direction about the origin.

The velocity of an arbitrary point on the surface of the sphere can be taken as $v_c \boldsymbol{e}_z \cos(\omega t)$, where v_c is the velocity amplitude of the oscillation and $\boldsymbol{e}_z$ is the unit vector in the direction of increasing z. Consistent with

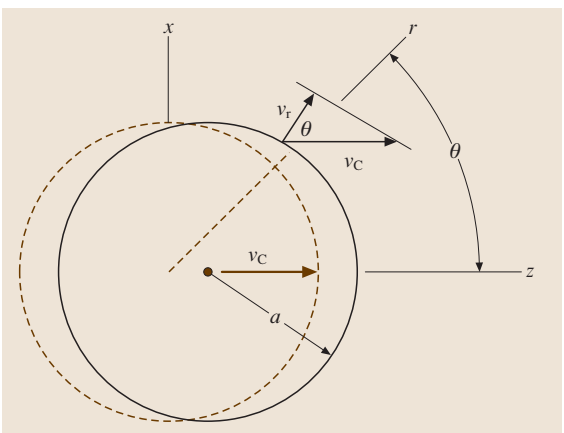


Fig. 3.24 Parameters used for the discussion of constant-frequency sound radiated by a transversely oscillating sphere

the desire to use a linear approximation, one approximates the unit normal vector for a given point on the surface of the sphere to be the same as when the sphere is centered at the origin, so that $\boldsymbol{n} \approx \boldsymbol{e}_\mathrm{r}$, where the latter is the unit vector in the radial direction. The normal component of the fluid velocity is then approximately

$$v_\mathrm{n} = v_\mathrm{c}\,(\boldsymbol{e}_z \cdot \boldsymbol{e}_\mathrm{r})\cos(\omega t)\,. \tag{3.348}$$

The dot product is $\cos\theta$, where θ is the polar angle.

One also makes the approximation that the boundary condition is to be imposed, not at the actual (moving) location of the point on the surface, but at the place in space where that point is when the sphere is centered at the origin. All these considerations lead to the linear acoustics boundary condition

$$\hat{v}_r = v_\mathrm{c}\cos\theta \qquad \text{at} \quad r = a \tag{3.349}$$

for the complex amplitude of the fluid velocity.

The feature distinguishing this boundary condition from that for the radially oscillating sphere is the factor $\cos\theta$. The plausible conjecture that both $\hat{v}_r$ and $\hat{p}$ continue to have the same θ dependence for all values of r is correct in this case, and one can look for a solution of the Helmholtz equation that has such a dependence, such as

$$\hat{p} = B\frac{\partial}{\partial z}\left(\frac{\mathrm{e}^{\mathrm{i}kr}}{r}\right) = B\cos\theta\frac{\mathrm{d}}{\mathrm{d}r}\left(\frac{\mathrm{e}^{\mathrm{i}kr}}{r}\right)\,. \tag{3.350}$$

The first part of this relation follows because a derivative of a solution with respect to any Cartesian coordinate is also a solution and because, as demonstrated in a previous part of this section, $\mathrm{e}^{\mathrm{i}kr}/r$ is a solution. The second part follows because $r^2 = z^2 + x^2 + y^2$, so $\partial r/\partial z = z/r = \cos\theta$. The quantity B is a complex numerical constant that remains to be determined.

The radial component of Euler's equation (3.175) for the constant-frequency case requires that

$$-\mathrm{i}\omega\rho\hat{v}_r = -\frac{\partial\hat{p}}{\partial r}\,, \tag{3.351}$$

where on the right side the differentiation is to be carried out at constant θ. Given the expression (3.350), the corresponding relation for the radial component of the fluid velocity is consequently

$$\hat{v}_r = \frac{B}{\mathrm{i}\omega\rho}\cos\theta\frac{\mathrm{d}^2}{\mathrm{d}r^2}\left(\frac{\mathrm{e}^{\mathrm{i}kr}}{r}\right)\,. \tag{3.352}$$

The boundary condition at $r = a$ is satisfied if one takes B to have a value such that

$$v_\mathrm{c} = \frac{B}{\mathrm{i}\omega\rho}\left[\frac{\mathrm{d}^2}{\mathrm{d}r^2}\left(\frac{\mathrm{e}^{\mathrm{i}kr}}{r}\right)\right]_{r=a}\,. \tag{3.353}$$

The indicated algebra yields

$$B = -\left(\frac{\mathrm{i}\omega\rho a^3 v_\mathrm{c}}{2 + 2\mathrm{i}ka + k^2a^2}\right)\mathrm{e}^{-\mathrm{i}ka}\,, \tag{3.354}$$

so the complex amplitude of the acoustic part of the pressure becomes

$$\hat{p} = \rho c v_\mathrm{c}\frac{k^2a^2}{2 + 2\mathrm{i}ka + k^2a^2}\left(1 - \frac{1}{\mathrm{i}kr}\right)\left(\frac{a}{r}\right) \times \mathrm{e}^{-\mathrm{i}k[r-a]}\cos\theta\,, \tag{3.355}$$

while the radial component of the fluid velocity is

$$\hat{v}_r = v_\mathrm{c}\left(\frac{2 + 2\mathrm{i}kr + k^2r^2}{2 + 2\mathrm{i}ka + k^2a^2}\right)\left(\frac{a^3}{r^3}\right)\mathrm{e}^{-\mathrm{i}k[r-a]}\cos\theta\,. \tag{3.356}$$

The radiation impedance is

$$Z_\mathrm{rad} = \rho c\left(\frac{k^2a^2 + \mathrm{i}ka}{2 + 2\mathrm{i}ka + k^2a^2}\right)\,. \tag{3.357}$$

Various simplifications result when considers limiting cases for the values of kr and ka. A case of common interest is when $ka \ll 1$ (small sphere) and $kr \gg 1$ (far field), so that

$$\hat{p} = \left(\frac{\omega^2\rho v_\mathrm{c}a^3}{c}\right)\frac{\mathrm{e}^{\mathrm{i}kr}}{r}\cos\theta\,. \tag{3.358}$$

3.11.4 Axially Symmetric Solutions

The example discussed in the previous subsection of radiation from a transversely oscillating sphere is one of a class of solutions of the linear acoustic equations where the field quantities depend on the spherical coordinates r and θ but not on the azimuthal angle ϕ. The Helmholtz equation for such circumstances has the form

$$\frac{1}{r^2}\frac{\partial}{\partial r}\left(r^2\frac{\partial\hat{p}}{\partial r}\right) + \frac{1}{r^2\sin\theta}\frac{\partial}{\partial\theta}\left(\sin\theta\frac{\partial\hat{p}}{\partial\theta}\right) + k^2\hat{p} = 0\,. \tag{3.359}$$

A common technique is to build up solutions of this equation using the principle of superposition, with the individual terms being factored solutions of the form

$$\hat{p}_\ell = P_\ell(\cos\theta)\Re_\ell(kr)\,, \tag{3.360}$$

where ℓ is an integer that distinguishes the various particular separated solutions. Insertion of this product into the Helmholtz equation leads to the conclusion that each factor must satisfy an appropriate ordinary differential

Amazon EX1014 Page 88

equation, the two differential equations being (with η replacing kr)

$$\frac{1}{\sin\theta}\frac{\mathrm{d}}{\mathrm{d}\theta}\left(\sin\theta\frac{\mathrm{d}P_\ell}{\mathrm{d}\theta}\right)+\lambda_\ell P_\ell=0\,, \tag{3.361}$$

$$\frac{\mathrm{d}}{\mathrm{d}\eta}\left(\eta^2\frac{\mathrm{d}\mathfrak{R}_\ell}{\mathrm{d}\eta}\right)-\lambda_\ell\mathfrak{R}_\ell+\eta^2\mathfrak{R}_\ell=0\,. \tag{3.362}$$

Here λ_ℓ is a constant, termed the separation constant. Equivalently, with P_ℓ regarded as a function of $\xi=\cos\theta$, the first of these two differential equations can be written

$$\frac{\mathrm{d}}{\mathrm{d}\xi}\left[\left(1-\xi^2\right)\frac{\mathrm{d}P_\ell}{\mathrm{d}\xi}\right]+\lambda_\ell P_\ell=0\,. \tag{3.363}$$

Legendre Polynomials

Usually, one desires solutions that are finite at both $\theta=0$ and $\theta=\pi$, or at $\xi=1$ and $\xi=-1$, but the solutions for the θ-dependent factor are usually singular at one of the other of these two end points. However, for special values (eigenvalues) of the separation constant λ_ℓ, there exist particular solutions (eigenfunctions) that are finite at both points. To determine these functions, one postulates a series solution of the form

$$P_\ell(\xi)=\sum_{n=0}^{\infty}a_{\ell,n}\xi^n\,, \tag{3.364}$$

and derives the recursion relation

$$n(n-1)a_{\ell,n}=[(n-1)(n-2)-\lambda_\ell]\,a_{\ell,n-2}\,. \tag{3.365}$$

The series diverges as $\xi\to\pm1$ unless it only has a finite number of terms, and such may be so if for some n the quantity in brackets on the right side is zero. The general choice of the separation constant that allows this is

$$\lambda_\ell=\ell(\ell+1)\,, \tag{3.366}$$

where ℓ is an integer, so that the recursion relation becomes

$$n(n-1)a_{\ell,n}=[(n-\ell-2)(n+\ell-1)]\,a_{\ell,n-2}\,. \tag{3.367}$$

However, $a_{\ell,0}$ and $a_{\ell,1}$ can be chosen independently and the recursion relation can only terminate one of the two possible infinite series. Consequently, one must choose

$$\begin{aligned} a_{\ell,1}&=0 \qquad \text{if } \ell \text{ even}\,;\\ a_{\ell,0}&=0 \qquad \text{if } \ell \text{ odd}\,. \end{aligned} \tag{3.368}$$

If ℓ is even the terms correspond to $n=0$, $n=2$, $n=4$, up to $n=\ell$, while if ℓ is odd the terms correspond to $n=1$, $n=3$, up to $n=\ell$. The customary normalization is that $P_\ell(1)=1$, and the polynomials that are derived are termed the Legendre polynomials. A general expression that results from examination of the recursion relation for the coefficients is

$$P_\ell(\xi)=a_{\ell,\ell}\left(\xi^\ell-\frac{\ell(\ell-1)}{2(2\ell-1)}\xi^{\ell-2}+\frac{\ell(\ell-2)(\ell-1)(\ell-3)}{(2)(4)(2\ell-1)(2\ell-3)}\xi^{\ell-4}+\dots\right)\,, \tag{3.369}$$

where the last term has ξ raised to either the power of 1 or 0, depending on whether ℓ is odd or even. Equivalently, if one sets,

$$a_{\ell,\ell}=K_\ell\frac{(2\ell)!}{2^\ell(\ell!)^2}\,, \tag{3.370}$$

where K_ℓ is to be selected, the series has the relatively simple form

$$\begin{aligned} P_\ell(\xi)&=K_\ell\sum_{m=0}^{M(\ell)}(-1)^m\frac{(2\ell-2m)!}{2^\ell m!(\ell-m)!(\ell-2m)!}\xi^{\ell-2m}\\ &=K_\ell\sum_{m=0}^{M(\ell)}b_{\ell,m}\xi^{\ell-2m}\,. \end{aligned} \tag{3.371}$$

Here $M(\ell)=\ell/2$ if ℓ is even, and $M(\ell)=(\ell-1)/2$ if ℓ is odd, so $M(0)=0$, $M(1)=0$, $M(2)=1$, $M(3)=1$, $M(4)=2$, etc.

The coefficients $b_{\ell,m}$ as defined here satisfy the relation

$$(\ell+1)b_{\ell+1,m}=(2\ell+1)b_{\ell,m}-\ell b_{\ell-1,m-1}\,, \tag{3.372}$$

as can be verified by algebraic manipulation. A consequence of this relation is

$$(\ell+1)\frac{P_{\ell+1}(\xi)}{K_{\ell+1}}=(2\ell+1)\xi\frac{P_\ell(\xi)}{K_\ell}-\ell\frac{P_{\ell-1}(\xi)}{K_{\ell-1}} \tag{3.373}$$

when $\ell\geq1$.

The customary normalization is to take $P_\ell(1)=1$. The series for $\ell=0$ and $\ell=1$ are each of only one term, and the normalization requirement leads to $K_0=1$ and $K_1=1$. The relation (3.373) indicates that the normalization requirement will result, via induction, for all successive ℓ if one takes $K_\ell=1$ for all ℓ. With this definition, the relation (3.373) yields the recursion relation among polynomials of different orders

$$(\ell+1)P_{\ell+1}(\xi)=(2\ell+1)\xi P_\ell(\xi)-\ell P_{\ell-1}(\xi)\,. \tag{3.374}$$

Amazon EX1014 Page 89

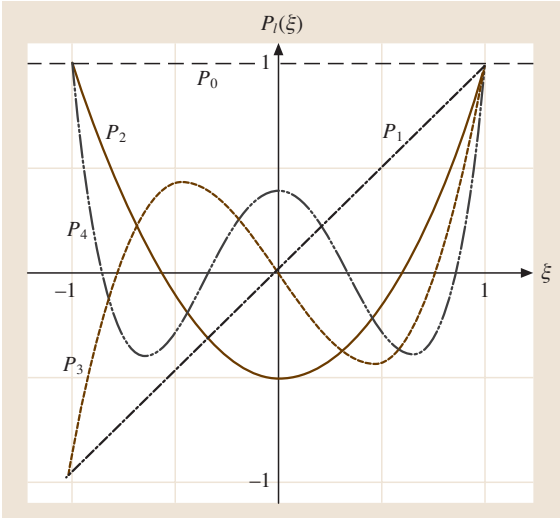


Fig. 3.25 Legendre polynomials for various orders

The latter holds for $\ell \geq 1$. With this, for example, given that $P_0(\xi) = 1$ and that $P_1(\xi) = \xi$, one derives

$$(2)P_2(\xi) = (3)\xi\xi - (1)(1)\,. \tag{3.375}$$

The first few of these polynomials are

$$P_0(\xi) = 1\,, \tag{3.376}$$

$$P_1(\xi) = \xi\,, \tag{3.377}$$

$$P_2(\xi) = \frac{1}{2}(3\xi^2 - 1)\,, \tag{3.378}$$

$$P_3(\xi) = \frac{1}{2}(5\xi^3 - 3\xi)\,, \tag{3.379}$$

$$P_4(\xi) = \frac{1}{8}(35\xi^4 - 30\xi^2 + 3)\,, \tag{3.380}$$

$$P_5(\xi) = \frac{1}{8}(63\xi^5 - 70\xi^3 + 15\xi)\,, \tag{3.381}$$

with the customary identification of $\xi = \cos\theta$.

An alternate statement for the series expression (3.371), given $K_\ell = 1$, is the Rodrigues relation,

$$P_\ell(\xi) = \frac{1}{2^\ell \ell!}\frac{\mathrm{d}^\ell}{\mathrm{d}\xi^\ell}(\xi^2 - 1)^\ell\,. \tag{3.382}$$

This can be verified by using the binomial expansion

$$(\xi^2 - 1)^\ell = (-1)^\ell \sum_{n=1}^{\ell}(-1)^n \frac{\ell!}{n!(\ell - n)!}\xi^{2n}\,, \tag{3.383}$$

so that

$$\frac{\mathrm{d}^\ell}{\mathrm{d}\xi^\ell}(\xi^2 - 1)^\ell = (-1)^\ell \sum_{n=\ell-M}^{\ell}(-1)^n \frac{\ell!}{n!(\ell - n)!} \times \frac{(2n)!}{(2n - \ell)!}\xi^{2n-\ell}\,, \tag{3.384}$$

or, with the change of summation index to $m = \ell - n$,

$$\frac{\mathrm{d}^\ell}{\mathrm{d}\xi^\ell}(\xi^2 - 1)^\ell = \sum_{m=0}^{M(\ell)}(-1)^m \frac{\ell!}{m!(\ell - m)!} \times \frac{(2\ell - 2m)!}{(\ell - 2m)!}\xi^{\ell-2m} = \ell!2^\ell P_\ell(\xi)\,. \tag{3.385}$$

Another derivable property of these functions is that they are orthogonal in the sense that

$$\int_0^\pi P_\ell(\cos\theta)P_{\ell'}(\cos\theta)\sin\theta\,\mathrm{d}\theta = 0 \qquad \text{if } \ell \neq \ell'\,. \tag{3.386}$$

This is demonstated by taking the differential equations (3.361) satisfied by P_ℓ and $P_{\ell'}$, multiplying the first by $P_{\ell'}\sin\theta$, multiplying the second by $P_\ell(\theta)\sin\theta$, then subtracting the second from the first, with a subsequent integration over θ from 0 to π. Given that $\lambda_\ell \neq \lambda_{\ell'}$ and that the two polynomials are finite at the integration limits, the conclusion is as stated above.

If the two indices are equal, the chosen normalization, whereby $P_\ell(1) = 1$, leads to

$$\int_0^\pi [P_\ell(\cos\theta)]^2 \sin\theta\,\mathrm{d}\theta = \frac{2}{2\ell + 1}\,. \tag{3.387}$$

The general derivation of this makes use of the Rodrigues relation (3.382) and of multiple integrations by parts. To carry through the derivation, one must first verify, for arbitrary nonnegative integers s and t, and with $s < t$, that

$$\frac{\mathrm{d}}{\mathrm{d}\xi^s}(\xi^2 - 1)^t = 0 \qquad \text{at } \xi = \pm 1\,, \tag{3.388}$$

which is accomplished by use of the chain rule of differential calculus. With the use of this relation and of the

Amazon EX1014 Page 90

Rodrigues relation, one has

$$\begin{aligned}
&\int_{-1}^{1} [P_\ell(\xi)]^2 \, \mathrm{d}\xi \\
&= \left(\frac{1}{2^\ell \ell!}\right)^2 (-1)^\ell \int_{-1}^{1} (\xi^2-1)^\ell \\
&\quad \times \frac{\mathrm{d}^{2\ell}}{\mathrm{d}\xi^{2\ell}} (\xi^2-1)^\ell \, \mathrm{d}\xi \qquad (3.389) \\
&= \left(\frac{1}{2^\ell \ell!}\right)^2 (2\ell)! \int_{-1}^{1} (1-\xi^2)^\ell \, \mathrm{d}\xi \\
&= \left(\frac{1}{2^\ell \ell!}\right)^2 (2\ell)! 2 \int_{0}^{\pi/2} \sin\theta^{2\ell+1} \, \mathrm{d}\theta \, . \qquad (3.390)
\end{aligned}$$

The trigonometric integral I_ℓ in the latter expression is evaluated using the trigonometric identity

$$\begin{aligned}
\frac{\mathrm{d}}{\mathrm{d}\theta}(\sin^{2\ell}\theta \cos\theta) &= -\sin^{2\ell+1}\theta \\
&\quad + 2\ell(\sin^{2\ell-2}\theta)(1-\sin^2\theta) \, , \qquad (3.391)
\end{aligned}$$

the integral of which yields the recursion relation

$$I_\ell = \frac{2\ell}{(2\ell+1)} I_{\ell-1} \, , \qquad (3.392)$$

and from this one infers

$$I_\ell = \frac{(2^\ell \ell!)^2}{(2\ell+1)!} I_0 \, . \qquad (3.393)$$

The integral for $\ell = 0$ is unity, so one has

$$\begin{aligned}
\int_{-1}^{1} [P_\ell(\xi)]^2 \, \mathrm{d}\xi &= \left(\frac{1}{2^\ell \ell!}\right)^2 (2\ell)! 2 \left(\frac{(2^\ell \ell!)^2}{(2\ell+1)!}\right) \\
&= \frac{2}{2\ell+1} \, . \qquad (3.394)
\end{aligned}$$

Spherical Bessel Functions

The ordinary differential equation (3.362) for the factor $\mathfrak{R}_\ell(\eta)$ takes the form

$$\frac{\mathrm{d}}{\mathrm{d}\eta}\left(\eta^2 \frac{\mathrm{d}\mathfrak{R}_\ell}{\mathrm{d}\eta}\right) - \ell(\ell+1)\mathfrak{R}_\ell + \eta^2 \mathfrak{R}_\ell = 0 \, , \qquad (3.395)$$

with the identification for the separation constant that results from the requirement that the θ-dependent factor be finite at $\theta = 0$ and $\theta = \pi$. For $\ell = 0$, a possible solution is

$$\mathfrak{R}_0 = A_0 \frac{\mathrm{e}^{\mathrm{i}\eta}}{\eta} \, , \qquad (3.396)$$

as can be verified by direct substitution, with A_0 being any constant. Since there is no corresponding θ dependence this is the same as the solution (3.327) for an outgoing spherical wave.

For arbitrary positive integer ℓ, a possible solution is

$$h_\ell^{(1)}(\eta) = -\mathrm{i}\eta^\ell \left(-\frac{1}{\eta}\frac{\mathrm{d}}{\mathrm{d}\eta}\right)^\ell \frac{\mathrm{e}^{\mathrm{i}\eta}}{\eta} \, , \qquad (3.397)$$

so that, in particular,

$$\begin{aligned}
h_0^{(1)}(\eta) &= -\mathrm{i}\frac{\mathrm{e}^{\mathrm{i}\eta}}{\eta} \, ; \\
h_1^{(1)}(\eta) &= \mathrm{i}\frac{\mathrm{d}}{\mathrm{d}\eta}\frac{\mathrm{e}^{\mathrm{i}\eta}}{\eta} = -\left(1+\frac{\mathrm{i}}{\eta}\right)\frac{\mathrm{e}^{\mathrm{i}\eta}}{\eta} \, . \qquad (3.398)
\end{aligned}$$

Alternately, both the real and imaginary parts should be solutions, so if one writes

$$h_\ell^{(1)}(\eta) = j_\ell(\eta) + \mathrm{i} y_\ell(\eta) \, , \qquad (3.399)$$

then

$$j_\ell(\eta) = \eta^\ell \left(-\frac{1}{\eta}\frac{\mathrm{d}}{\mathrm{d}\eta}\right)^\ell \frac{\sin\eta}{\eta} \, , \qquad (3.400)$$

$$y_\ell(\eta) = -\eta^\ell \left(-\frac{1}{\eta}\frac{\mathrm{d}}{\mathrm{d}\eta}\right)^\ell \frac{\cos\eta}{\eta} \, , \qquad (3.401)$$

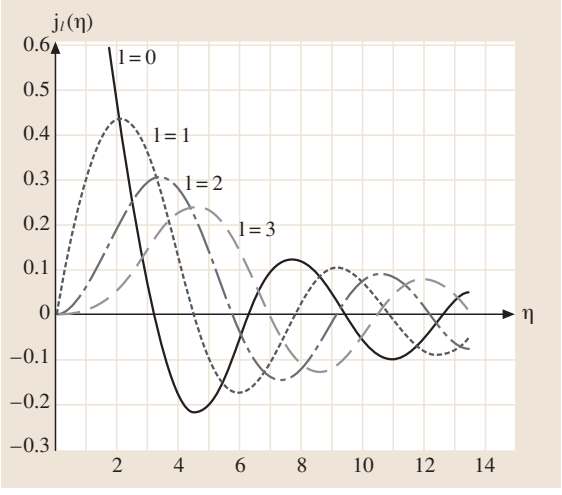


Fig. 3.26 Spherical Bessel functions for various orders

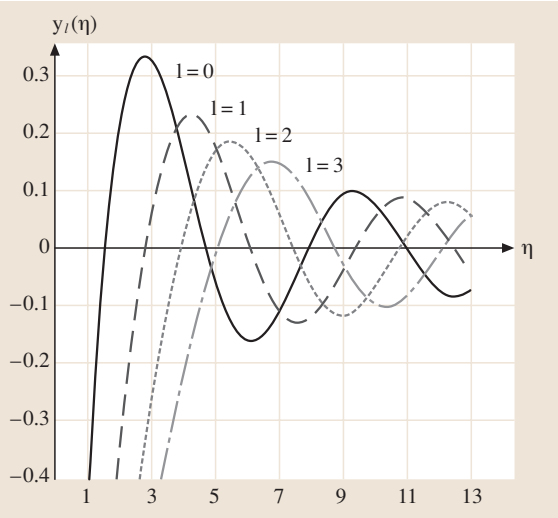


Fig. 3.27 Spherical Neumann functions for various orders

are each solutions. The function $h_\ell^{(1)}(\eta)$ is referred to as the spherical Hankel function of the ℓ-th order and first kind (the second kind has i replaced by $-$i), while $j_\ell(\eta)$ is the spherical Bessel function of the ℓ-th order, and $y_\ell(\eta)$ is the spherical Neumann function of the ℓ-th order.

A proof that $h_\ell^{(1)}(\eta)$, as defined above, satisfies the ordinary differential equation for the corresponding value of ℓ proceeds by induction. The assertion is true for $\ell = 0$ and it is easily demonstrated also to be true for $\ell = 1$, and the definition (3.397) yields the recursion relation

$$h_{\ell+1}^{(1)}(\eta) = \frac{\ell}{\eta} h_\ell^{(1)} - \frac{\mathrm{d}}{\mathrm{d}\eta} h_\ell^{(1)} \,. \tag{3.402}$$

The differential equation for $h_\ell^{(1)}$ and what results from taking the derivative of that equation gives one the relations,

$$\frac{\mathrm{d}^2}{\mathrm{d}\eta^2} h_\ell^{(1)} + \frac{2}{\eta}\frac{\mathrm{d}}{\mathrm{d}\eta} h_\ell^{(1)} + \left(1 - \frac{\ell(\ell+1)}{\eta^2}\right) h_\ell^{(1)} = 0 \,, \tag{3.403}$$

$$\frac{\mathrm{d}^2}{\mathrm{d}\eta^2}\frac{h_\ell^{(1)}}{\eta} + \frac{2}{\eta}\frac{\mathrm{d}}{\mathrm{d}\eta}\frac{h_\ell^{(1)}}{\eta} + \frac{2}{\eta^2}\frac{\mathrm{d}}{\mathrm{d}\eta} h_\ell^{(1)} + \left(1 - \frac{\ell(\ell+1)}{\eta^2}\right)\frac{h_\ell^{(1)}}{\eta} = 0 \,, \tag{3.404}$$

$$\frac{\mathrm{d}^2}{\mathrm{d}\eta^2}\frac{\mathrm{d}h_\ell^{(1)}}{\mathrm{d}\eta} + \frac{2}{\eta}\frac{\mathrm{d}}{\mathrm{d}\eta}\frac{\mathrm{d}h_\ell^{(1)}}{\mathrm{d}\eta} - \frac{2}{\eta^2}\frac{\mathrm{d}}{\mathrm{d}\eta} h_\ell^{(1)} + \frac{2}{\eta^3}\ell(\ell+1)h_\ell^{(1)} + \left(1 - \frac{\ell(\ell+1)}{\eta^2}\right)\frac{\mathrm{d}h_\ell^{(1)}}{\mathrm{d}\eta} = 0 \,. \tag{3.405}$$

Multiplication of the second of these by ℓ, then subtracting the third, subsequently making use of the recursion relation, yields

$$\frac{\mathrm{d}^2}{\mathrm{d}\eta^2} h_{\ell+1}^{(1)} + \frac{2}{\eta}\frac{\mathrm{d}}{\mathrm{d}\eta} h_{\ell+1}^{(1)} + \frac{2(\ell+1)}{\eta^2}\frac{\mathrm{d}}{\mathrm{d}\eta} h_\ell^{(1)} - \frac{2}{\eta^3}\ell(\ell+1)h_\ell^{(1)} + \left(1 - \frac{\ell(\ell+1)}{\eta^2}\right) h_{\ell+1}^{(1)} = 0 \,. \tag{3.406}$$

A further substitution that makes use of the recursion relation yields

$$\frac{\mathrm{d}^2}{\mathrm{d}\eta^2} h_{\ell+1}^{(1)} + \frac{2}{\eta}\frac{\mathrm{d}}{\mathrm{d}\eta} h_{\ell+1}^{(1)} - \frac{2(\ell+1)}{\eta^2} h_{\ell+1}^{(1)} + \left(1 - \frac{\ell(\ell+1)}{\eta^2}\right) h_{\ell+1}^{(1)} = 0 \,, \tag{3.407}$$

or, equivalently,

$$\frac{\mathrm{d}^2}{\mathrm{d}\eta^2} h_{\ell+1}^{(1)} + \frac{2}{\eta}\frac{\mathrm{d}}{\mathrm{d}\eta} h_{\ell+1}^{(1)} + \left(1 - \frac{(\ell+1)(\ell+2)}{\eta^2}\right) h_{\ell+1}^{(1)} = 0 \,, \tag{3.408}$$

which is the differential equation that one desires $h_{\ell+1}^{(1)}$ to satisfy; it is the $\ell+1$ counterpart of (3.403).

Another recursion relation derivable from (3.397) is

$$(\ell+1)h_{\ell+1}^{(1)} = -(2\ell+1)\frac{\mathrm{d}}{\mathrm{d}\eta} h_\ell^{(1)} + \ell h_{\ell-1}^{(1)} \,. \tag{3.409}$$

Limiting approximate expressions for the spherical Hankel function and the spherical Bessel function are derivable from the definition (3.397). For $\eta \ll 1$, one has

$$h_0^{(1)}(\eta) \approx -\frac{\mathrm{i}}{\eta} \,; \quad h_\ell^{(1)}(\eta) \approx -\mathrm{i}\frac{1\cdot 3\cdot 5\cdots(2\ell-1)}{\eta^{\ell+1}} \,, \tag{3.410}$$

$$j_0(\eta) \approx 1 - \frac{1}{6}\eta^2 \,; \quad j_\ell(\eta) \approx \frac{\eta^\ell}{1\cdot 3\cdot 5\cdots(2\ell+1)} \,. \tag{3.411}$$

(The second term in the expansion for j_0 is needed in the event that one desires a nonzero first approximation

Amazon EX1014 Page 92

for the derivative.) In the asymptotic limit, when $\eta \gg 1$, one has

$$h_\ell^{(1)}(\eta) \to (-\mathrm{i})^{\ell+1}\frac{\mathrm{e}^{\mathrm{i}\eta}}{\eta}\,. \tag{3.412}$$

As is evident from the $\mathrm{e}^{\mathrm{i}\eta} = \mathrm{e}^{\mathrm{i}kr}$ factor that appears here, the spherical Hankel function of the first kind corresponds to a radially outgoing wave, given that one is using the $\mathrm{e}^{-\mathrm{i}\omega t}$ time dependence. Its complex conjugate, the spherical Hankel function of the second kind, corresponds to a radially incoming wave.

Plane Wave Expansion

A mathematical identity concerning the expansion of a plane wave in terms of Legendre polynomials and spherical Bessel functions results from consideration of

$$\mathrm{e}^{\mathrm{i}kr\cos\theta} = \sum_{\ell=0}^{\infty} \mathfrak{I}_\ell(kr) P_\ell(\cos\theta)\,. \tag{3.413}$$

Because the Legendre polynomials are a complete set, such an expansion is possible and expected to converge. The coefficients $\mathfrak{I}_\ell(kr)$ are determined with the use of the orthogonality conditions, (3.386) and (3.387), to be given by

$$\begin{aligned}\mathfrak{I}_\ell(\eta) &= \frac{2\ell+1}{2}\int_0^\pi \mathrm{e}^{\mathrm{i}\eta\cos\theta} P_\ell(\cos\theta)\sin\theta\,\mathrm{d}\theta \\ &= \frac{2\ell+1}{2}\int_{-1}^{1} \mathrm{e}^{\mathrm{i}\eta\xi} P_\ell(\xi)\,\mathrm{d}\xi\,.\end{aligned} \tag{3.414}$$

The integral above evaluates, for $\ell = 0$, to

$$\mathfrak{I}_0(\eta) = \frac{1}{2}\frac{1}{\mathrm{i}\eta}(\mathrm{e}^{\mathrm{i}\eta} - \mathrm{e}^{-\mathrm{i}\eta}) = j_\ell(\eta)\,, \tag{3.415}$$

and, for $\ell = 1$, to

$$\begin{aligned}\mathfrak{I}_1(\eta) &= \frac{3}{2}\frac{\mathrm{d}}{\mathrm{d}(\mathrm{i}\eta)}\left(\frac{1}{\mathrm{i}\eta}(\mathrm{e}^{\mathrm{i}\eta} - \mathrm{e}^{-\mathrm{i}\eta})\right) \\ &= 3\mathrm{i}\left(\frac{\sin\eta}{\eta^2} - \frac{\cos\eta}{\eta}\right) = 3\mathrm{i}j_1(\eta)\,.\end{aligned} \tag{3.416}$$

To proceed to larger values of ℓ, one makes use of the recursion relations, (3.374) and (3.409), and infers the general relation

$$\mathfrak{I}_\ell(\eta) = (2\ell+1)\mathrm{i}^\ell j_\ell(\eta)\,. \tag{3.417}$$

This relation certainly holds for $\ell = 0$ and $\ell = 1$, and a general proof for arbitrary integer ℓ follows by induction. One assumes the relation is true for $\ell - 1$ and ℓ, and considers

$$\begin{aligned}&\mathfrak{I}_{\ell+1}(\eta) \\ &= \frac{2\ell+3}{2}\int_{-1}^{1} \mathrm{e}^{\mathrm{i}\eta\xi} P_{\ell+1}(\xi)\,\mathrm{d}\xi \qquad (3.418)\\ &= \frac{(2\ell+3)(2\ell+1)}{2(\ell+1)}\int_{-1}^{1} \mathrm{e}^{\mathrm{i}\eta\xi}\,\xi\, P_\ell(\xi)\,\mathrm{d}\xi \\ &\quad - \frac{(2\ell+3)\ell}{2(\ell+1)}\int_{-1}^{1} \mathrm{e}^{\mathrm{i}\eta\xi} P_{\ell-1}(\xi)\,\mathrm{d}\xi \qquad (3.419)\\ &= \frac{(2\ell+3)}{(\ell+1)}(-\mathrm{i})\frac{\mathrm{d}}{\mathrm{d}\eta}\mathfrak{I}_\ell \\ &\quad - \frac{(2\ell+3)\ell}{(\ell+1)(2\ell-1)}\mathfrak{I}_{\ell-1} \qquad (3.420)\end{aligned}$$

where the second version results from the recursion relation (3.374). Then, with the appropriate insertions from (3.417), one has

$$\begin{aligned}\mathfrak{I}_{\ell+1}(\eta) = (2\ell+3)\mathrm{i}^{\ell+1} &\times\left[-\frac{(2\ell+1)}{(\ell+1)}\frac{\mathrm{d}}{\mathrm{d}\eta}j_\ell(\eta)\right. \\ &\left. + \frac{\ell}{(\ell+1)}j_{\ell-1}(\eta)\right].\end{aligned} \tag{3.421}$$

The recursion relation (3.409) replaces the quantity in brackets by $j_{\ell+1}$, so one obtains

$$\mathfrak{I}_{\ell+1}(\eta) = (2\ell+3)\mathrm{i}^{\ell+1} j_{\ell+1}(\xi)\,, \tag{3.422}$$

which is the $\ell+1$ counterpart of (3.417). Thus the appropriate plane wave expansion is identified as

$$\mathrm{e}^{\mathrm{i}kr\cos\theta} = \sum_{\ell=0}^{\infty}(2\ell+1)\mathrm{i}^\ell j_\ell(kr)P_\ell(\cos\theta)\,. \tag{3.423}$$

3.11.5 Scattering by a Rigid Sphere

An application of the functions introduced above is the scattering of an incident plane wave by a rigid sphere (radius a). One sets the complex amplitude of the acoustic part of the pressure to

$$\hat{p} = \hat{P}_{\mathrm{inc}}\,\mathrm{e}^{\mathrm{i}kz} + \hat{p}_{\mathrm{sc}}\,. \tag{3.424}$$

The first term represents the incident wave, which has an amplitude $\hat{P}_{\mathrm{inc}}$, constant frequency ω and which is proceeding in the $+z$-direction. The second term represents

Amazon EX1014 Page 93

the scattered wave. This term is required to be made up of waves that propagate out from the sphere, which is centered at the origin. With some generality, one can use the principle of superposition and set

$$\hat{p}_{\mathrm{sc}} = \hat{P}_{\mathrm{inc}} \sum_{\ell=0} A_\ell P_\ell(\cos\theta) h_\ell^{(1)}(kr) \,, \tag{3.425}$$

with the factors in the terms in the sum representing the Legendre polynomials and spherical Hankel functions. The individual terms in the sum are sometimes referred to as partial waves. The analytical task is to determine the coefficients A_ℓ. (The expression above applies to scattering from any axisymmetric body, including spheroids and penetrable objects, where the properties might vary with r and θ. The discussion here, however, is limited to that of the rigid sphere.)

With the plane wave expansion (3.423) inserted for the direct wave, the sum of incident and scattered waves takes the form

$$\hat{p} = \hat{P}_{\mathrm{inc}} \sum_{\ell=0}^{\infty} \left[(2\ell+1)\mathrm{i}^\ell j_\ell(kr) + A_\ell h_\ell^{(1)}(kr)\right] \times P_\ell(\cos\theta) \,. \tag{3.426}$$

the boundary condition imposed by the rigidity of the sphere is that $\hat{v}_r = 0$ at $r = a$, or equivalently that $\partial\hat{p}/\partial r = 0$ at $r = a$. With the aid of the radial component of the Euler equation (3.175) and of the linear independence of the various Legendre polynomials, this yields

$$\frac{\mathrm{d}}{\mathrm{d}r}\left[(2\ell+1)\mathrm{i}^\ell j_\ell(kr) + A_\ell h_\ell^{(1)}(kr)\right] = 0 \quad \text{at} \quad r = a \,. \tag{3.427}$$

The desired coefficients are consequently

$$A_\ell = -(2\ell+1)\mathrm{i}^\ell \frac{\left[\frac{\mathrm{d}}{\mathrm{d}r} j_\ell(kr)\right]_{r=a}}{\left[\frac{\mathrm{d}}{\mathrm{d}r} h_\ell^{(1)}(kr)\right]_{r=a}} \,. \tag{3.428}$$

Far-Field Scattering

In the limit of large kr, the asymptotic expression (3.412) for the spherical Hankel function can be used, and the scattered wave takes the asymptotic form

$$\hat{p}_{\mathrm{sc}} \to \hat{P}_{\mathrm{inc}} f(\theta) \frac{\mathrm{e}^{\mathrm{i}kr}}{kr} \,, \tag{3.429}$$

where

$$f(\theta) = \sum_{\ell=0}^{\infty} (-\mathrm{i})^{\ell+1} A_\ell P_\ell(\cos\theta) \tag{3.430}$$

is a complex dimensionless function of only the angle θ.

This asymptotic form holds for scattering from any axisymmetric object of bounded extent. In the more general case when the object is not axisymmetric, one should regard the function f as being also a function of the azimuthal angle ϕ, so that

$$f(\theta) \to f(\theta, \phi) \,. \tag{3.431}$$

The prediction in all cases is that the far-field scattered wave resembles an outgoing spherical wave, but with an amplitude that depends on the direction of propagation.

The far-field intensity associated with the scattered wave is asymptotically entirely in the radial direction, and in accord with (3.281), its time average is given by

$$I_{\mathrm{sc}} = \frac{1}{2}\frac{1}{\rho c}|\hat{p}_{\mathrm{sc}}|^2 \,, \tag{3.432}$$

or,

$$I_{\mathrm{sc}} = \frac{1}{2}\frac{|\hat{P}_{\mathrm{inc}}|^2}{\rho c}|f(\theta,\phi)|^2 \frac{1}{k^2 r^2} \,. \tag{3.433}$$

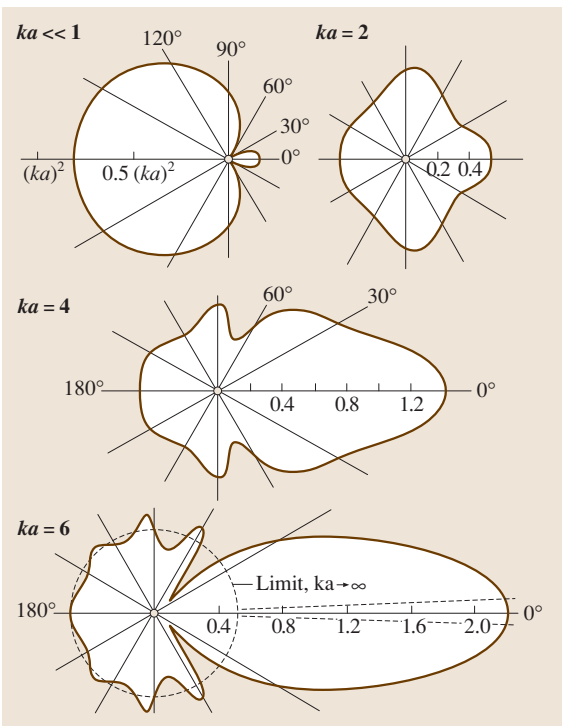


Fig. 3.28 Angular distribution of plane wave scattering by a rigid sphere of radius a. The quantity $(\mathrm{d}\sigma/\mathrm{d}\Omega)^{1/2}/a$ is plotted versus the polar angle θ

The differential scattering cross section is the power scattered per unit solid angle and per unit incident intensity, and is consequently given by

$$\frac{\mathrm{d}\sigma}{\mathrm{d}\Omega} = \frac{r^2 I_{\mathrm{sc}}}{I_{\mathrm{inc}}} = \frac{1}{k^2}|f(\theta,\phi)|^2 \,. \tag{3.434}$$

(Here the notation is such that σ corresponds to the cross-sectional area, and Ω corresponds to the solid angle in steradians, with the total solid angle in a sphere being 4π steradians.)

The total scattering cross section is the total scattered power divided by the incident intensity, so that

$$\begin{aligned}\sigma &= \frac{\mathfrak{P}_{\mathrm{sc}}}{I_{\mathrm{inc}}} = \int \frac{\mathrm{d}\sigma}{\mathrm{d}\Omega}\,\mathrm{d}\Omega = \frac{\mathfrak{P}_{\mathrm{sc}}}{I_{\mathrm{inc}}} \\ &= \int_0^{2\pi}\int_0^{\pi} \frac{1}{k^2}\,|f(\theta,\phi)|^2 \sin\theta\,\mathrm{d}\theta\,\mathrm{d}\phi \,. \end{aligned} \tag{3.435}$$

For the case of an axially symmetric scatterer, this reduces to

$$\begin{aligned}\sigma &= \frac{2\pi}{k^2}\int_0^{\pi} |f(\theta,\phi)|^2 \sin\theta\,\mathrm{d}\theta \\ &= \frac{2\pi}{k^2}\sum_{\ell}\sum_{\ell'}(-\mathrm{i})^{\ell-\ell'} A_\ell A_{\ell'} \int_0^{\pi} P_\ell P_{\ell'} \sin\theta\,\mathrm{d}\theta \,. \end{aligned} \tag{3.436}$$

The orthogonality of the Legendre polynomials reduces this to

$$\sigma = \frac{4\pi}{k^2}\sum_{\ell}\frac{1}{(2\ell+1)}\,|A_\ell|^2 \,, \tag{3.437}$$

so the powers scattered by the individual partial waves are additive, even though there may be an intricate interference pattern in the angular directionality.

Rayleigh Scattering

When the object causing the scattering is much smaller than a wavelength, considerable simplification results, and the characteristic features that result are associated with the term *Rayleigh scattering*. In the case of scattering by a rigid sphere, only the $\ell = 0$ and $\ell = 1$ terms are significant, and both have comparable influence. The small-ka approximations for the spherical Bessel function and the spherical Hankel function yield

$$A_0 \approx \mathrm{i}\frac{1}{3}(ka)^3 \,; \qquad A_1 \approx \mathrm{i}(ka)^3 \,. \tag{3.438}$$

Then with the appropriate identifications of the spherical Hankel function and the Legendre polynomial for $\ell = 0$ and $\ell = 1$, one obtains

$$\hat{p}_{\mathrm{sc}} = -\hat{P}_{\mathrm{inc}}\frac{k^2 a^3}{3}\left[1 - \frac{3}{2}\cos\theta\left(1 + \frac{\mathrm{i}}{kr}\right)\right]\frac{\mathrm{e}^{\mathrm{i}kr}}{r} \,. \tag{3.439}$$

The corresponding expressions for the differential scattering cross section and the total cross section are

$$\frac{\mathrm{d}\sigma}{\mathrm{d}\Omega} = \frac{k^4 a^6}{9}\left(1 - \frac{3}{2}\cos\theta\right)^2 \,, \tag{3.440}$$

$$\sigma = \frac{7}{9}(ka)^4 \pi a^2 \,. \tag{3.441}$$

A feature of this expression is the characteristically strong dependence on frequency. The amplitude of the scattered wave varies as the square of the frequency, and the far-field intensity and scattering cross sections vary as the fourth power of the frequency. This type of frequency dependence is invariably true for all types of small scatterers (a notable exception being when the scatterer has an internal resonance at the incident frequency) and is the distinguishing feature of Rayleigh scattering.

3.12 Cylindrical Waves

The present section is concerned with a number of important situations where the appropriate coordinates are the cylindrical coordinates (w, ϕ, z).

3.12.1 Cylindrically Symmetric Outgoing Waves

For cylindrically symmetric waves, there is no dependence on the azimuthal angle ϕ or on the axial coordinate z, so the Laplacian in cylindrical coordinates reduces to

$$\begin{aligned}\nabla^2\psi &= \frac{1}{w}\frac{\partial}{\partial w}\left(w\frac{\partial\psi}{\partial w}\right) = \frac{\partial^2\psi}{\partial w^2} + \frac{1}{w}\frac{\partial\psi}{\partial w} \\ &= \frac{1}{\sqrt{w}}\frac{\partial^2(\sqrt{w}\psi)}{\partial w^2} + \frac{\sqrt{w}\psi}{4w^{5/2}} \,, \end{aligned} \tag{3.442}$$

where w is here the radial distance from the z-axis. Consequently, the wave equation of (3.74) takes the

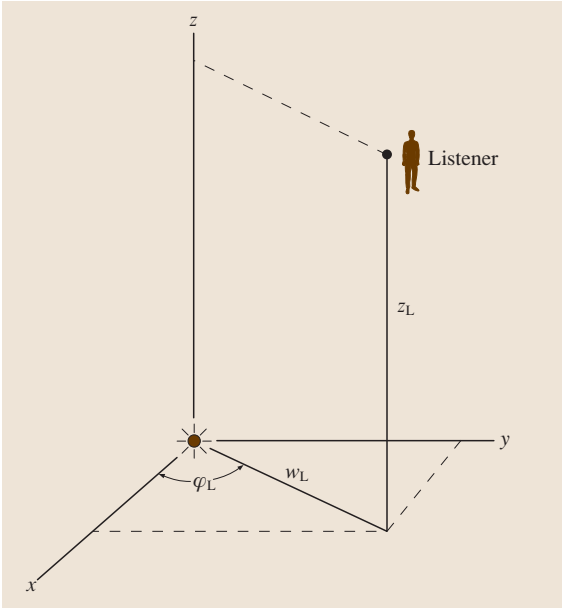


Fig. 3.29 Cylindrical coordinates. A hypothetical listener point has cylindrical coordinates w_L, ϕ_L, and z_L

form

$$\frac{\partial^2(\sqrt{w}p)}{\partial w^2} - \frac{1}{c^2}\frac{\partial^2(\sqrt{w}p)}{\partial t^2} + \frac{\sqrt{w}p}{4w^2} = 0\,, \qquad (3.443)$$

and the Helmholtz equation of (3.176) takes the form

$$\frac{\mathrm{d}^2\hat{p}}{\mathrm{d}w^2} + \frac{1}{w}\frac{\mathrm{d}\hat{p}}{\mathrm{d}w} + k^2\hat{p} = 0\,. \qquad (3.444)$$

General Transient Solution

A heuristic construction of an outgoing wave solution of (3.443) begins with an infinite line array of identical and synchronous point sources, equally spaced along the z-axis, and each giving rise to an identical spherical wave. Such waves differ, however, at any given distant point in that the radial distance R from the source depends on the z-coordinate z_0 of the source, so that

$$R = [w^2 + (z - z_0)^2]^{1/2}\,. \qquad (3.445)$$

With the taking of an appropriate limit as the source separation interval goes to zero, one finds the general solution for an outgoing cylindrical wave to be

$$p(r, t) = \int_{-\infty}^{\infty} \frac{f[t - (R/c)]}{R}\,\mathrm{d}z_0\,. \qquad (3.446)$$

Here the function $f(t)$ is arbitrary. The argument $t - (R/c)$ of this function in the integrand is the retarded time, the time at which the incremental contribution was generated. With some effort, one can show that the integral in (3.446) is independent of z, and that it satisfies the cylindrical wave equation (3.443). A consequence of the above result is that outgoing cylindrical waves must have a tail. Even if the function $f(t)$ were to be zero except within a narrow time interval, the integral will give a nonzero value for times arbitrarily later than the time when the signal is first received. This is in contrast to the case for outgoing spherical waves, where there may be no tail.

If the distance w is sufficiently great, the resulting waveform will be such that it will be frozen in shape, and will decrease in amplitude as the inverse of the square root of w. The last term in (3.443) becomes insignificant and the appropriate limiting approximation is of the form

$$p(w, t) = \frac{1}{\sqrt{w}} F\,[t - (w/c)]\,. \qquad (3.447)$$

The function $F(t)$ that appears here is related to the $f(t)$ that appears in (3.446). The relationship (derived further

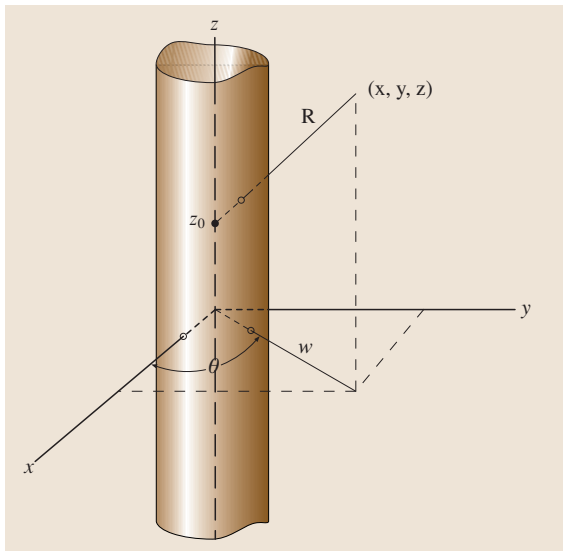


Fig. 3.30 Parameters involved in the construction of a cylindrical wave as a linear superposition of spherical waves from a continuous smear of simultaneous spherical sources spaced along a line. The quantity z_0 represents a source point along the z-axis, and R is the distance from that source point to a given listener point

Amazon EX1014 Page 96

below) is

$$F(t) = (2c)^{1/2} \int_{-\infty}^{t} \frac{f(\tau)}{(t-\tau)^{1/2}}\, \mathrm{d}\tau \,. \tag{3.448}$$

Since $f(t)$ is arbitrary, one can equally well regard $F(t)$ as arbitrary. The expression (3.447) is readily seen to be an appropriate approximate solution of (3.442), since that wave equation implies that $\sqrt{wp}$ should satisfy the equation for plane waves when w is large.

Constant-Frequency Solution

The corresponding cylindrical wave solution for the Helmholtz equation is obtained by setting

$$f(t) \to A\ \mathrm{e}^{-\mathrm{i}\omega t} \,, \tag{3.449}$$

so that

$$\hat{p}(r) = A \int_{-\infty}^{\infty} \frac{\mathrm{e}^{\mathrm{i}kR}}{R}\, \mathrm{d}z_0 \,, \tag{3.450}$$

or, equivalently,

$$\hat{p}(r) = \mathrm{i}\pi A H_0^{(1)}(kw) \,. \tag{3.451}$$

Here A is an arbitrary constant and the quantity $H_0^{(1)}(\eta)$ is the Hankel function of the first kind and zeroth order,

$$H_0^{(1)}(\eta) = \frac{1}{\mathrm{i}\pi} \int_{-\infty}^{\infty} \frac{\mathrm{e}^{\mathrm{i}[\eta^2+\zeta^2]^{1/2}}}{[\eta^2+\zeta^2]^{1/2}}\, \mathrm{d}\zeta \,. \tag{3.452}$$

3.12.2 Bessel and Hankel Functions

The Hankel function that appears above is discussed extensively in the literature, and corresponds to an outgoing wave. The differential equation that it satisfies is obtained from the Helmholtz equation for cylindrical waves by setting $kw = \eta$, so that

$$\left(\frac{\mathrm{d}^2}{\mathrm{d}\eta^2} + \frac{1}{\eta}\frac{\mathrm{d}}{\mathrm{d}\eta} + 1\right) H_0^{(1)}(\eta) = 0 \,. \tag{3.453}$$

This is a special case (with $\nu = 0$) of the second-order differential equation

$$\left[\frac{\mathrm{d}^2}{\mathrm{d}\eta^2} + \frac{1}{\eta}\frac{\mathrm{d}}{\mathrm{d}\eta} + \left(1 - \frac{\nu^2}{\eta^2}\right)\right] \mathcal{J}_\nu(\eta) = 0 \,, \tag{3.454}$$

whose general solution is

$$\mathcal{J}_\nu(\eta) = a\ J_\nu(\eta) + bY_\nu(\eta) \,. \tag{3.455}$$

Here $J_\nu(\eta)$ and $Y_\nu(\eta)$ are the Bessel function and the Neumann function. The second, frequently denoted by $N_\nu(\eta)$, is sometimes referred to as Weber's function. The Hankel functions of the first and second kinds are given by

$$\begin{aligned} H_\nu^{(1)}(\eta) &= J_\nu(\eta) + iY_\nu(\eta) \,; \\ H_\nu^{(2)}(\eta) &= J_\nu(\eta) - iY_\nu(\eta) \,. \end{aligned} \tag{3.456}$$

Both $J_\nu(\eta)$ and $Y_\nu(\eta)$ are real when ν and η are real and positive, so the two Hankel functions are a complex conjugate pair under such circumstances.

An alternate mathematical representation for the Hankel function $H_0^{(1)}$ that is more amenable to numerical computation is

$$H_0^{(1)}(\eta) = \frac{2}{\pi} \int_0^{\pi/2} \mathrm{e}^{\mathrm{i}\eta\cos\phi}\, \mathrm{d}\phi + \frac{2}{\mathrm{i}\pi} \int_0^{\infty} \mathrm{e}^{-\eta\sinh s}\, \mathrm{d}s \,, \tag{3.457}$$

and from this one identifies expressions for the Bessel and Neumann functions as

$$J_0(\eta) = \frac{2}{\pi} \int_0^{\pi/2} \cos(\eta\cos\phi)\ \mathrm{d}\phi \,, \tag{3.458}$$

$$Y_0(\eta) = \frac{2}{\pi} \int_0^{\pi/2} \sin(\eta\cos\phi)\ \mathrm{d}\phi - \frac{2}{\pi} \int_0^{\infty} \mathrm{e}^{-\eta\sinh s}\, \mathrm{d}s \,. \tag{3.459}$$

In the limit of small η, the function $H_0^{(1)}$ has a logarithmic singularity, and is approximately given by

$$H_0^{(1)}(\eta) \approx 1 - \frac{1}{4}\eta^2 - \frac{2\mathrm{i}}{\pi}[\ln(2/\eta) - \gamma] \,, \tag{3.460}$$

where

$$\gamma = \int_0^1 \frac{1-\mathrm{e}^{-s}}{s}\, \mathrm{d}s - \int_1^{\infty} \frac{\mathrm{e}^{-s}}{s}\, \mathrm{d}s = 0.5772157\cdots \tag{3.461}$$

is the Euler–Mascheroni constant. In the limit of large η, the corresponding limiting expression is

$$\lim_{\eta\to\infty} H_0^{(1)}(\eta) = \left(\frac{2}{\pi\eta}\right)^{1/2} \mathrm{e}^{-\mathrm{i}\pi/4}\, \mathrm{e}^{\mathrm{i}\eta} \,. \tag{3.462}$$

An expression valid for all positive ν and positive η is

$$H_\nu^{(1)}(\eta) = \frac{1}{\pi\mathrm{i}} \int_{-\infty}^{\infty+\mathrm{i}\pi} \mathrm{e}^{\eta\sinh\alpha - \nu\alpha}\, \mathrm{d}\alpha \tag{3.463}$$

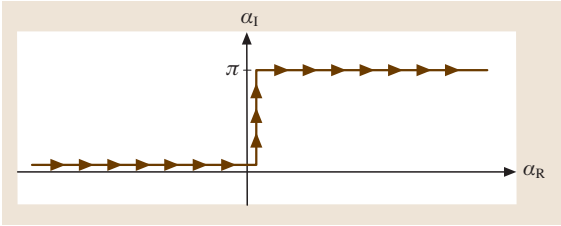


Fig. 3.31 Contour integral used for the definition of the Hankel function of the first kind

The latter is a contour integral, where a possible contour is from $-\infty$ along the negative real axis to the origin, then up the imaginary axis to $i\pi$, then parallel to the positive real axis with the imaginary part held fixed to $i\pi$ out to $\infty + i\pi$. The convergence along the latter leg is guaranteed because

$$\sinh(s + i\pi) = -\sinh(s) \,. \tag{3.464}$$

Thus, when written out explicitly for the contour just described, it becomes

$$\begin{aligned} H_\nu^{(1)}(\eta) = {} & \frac{1}{\pi i} \int_0^\infty e^{-\eta \sinh s + \nu s} \, ds \\ & + \frac{1}{\pi} \int_0^\pi e^{i\eta \sin\theta - i\nu\theta} \, d\theta \\ & + \frac{e^{-i\nu\pi}}{\pi i} \int_0^\infty e^{-\eta \sinh s - \nu s} \, ds \,. \end{aligned} \tag{3.465}$$

For $\nu = 0$, this reduces to the expression (3.457). That the above is indeed a solution of the ordinary differential equation (3.454) follows from substitution of the contour integral expression into the differential equation multiplied by η^2, followed by differentiation under the integral sign, so that one has

$$\begin{aligned} & \frac{1}{\pi i} \int_{-\infty}^{\infty + i\pi} (\eta^2 \sinh^2\alpha + \eta \sinh\alpha + \eta^2 - \nu^2) \\ & \times e^{\eta \sinh\alpha - \nu\alpha} \, d\alpha \\ & = \frac{1}{\pi i} \int_{-\infty}^{\infty + i\pi} \frac{d}{d\alpha} [(\eta \cosh\alpha + \nu) e^{\eta \sinh\alpha - \nu\alpha}] \, d\alpha = 0. \end{aligned} \tag{3.466}$$

The latter equality follows because the quantity being differentiated in the integrand vanishes at both ends of the integration contour.

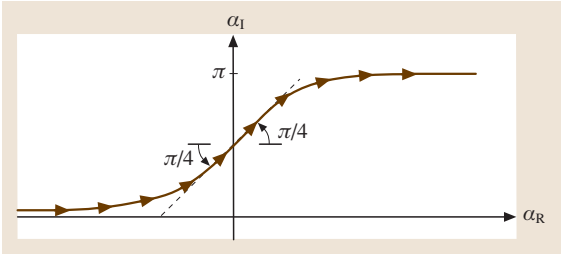


Fig. 3.32 Contour integral along the path of steepest descents, used in the derification of the asymptotic expression for the Hankel function

For arbitrary positive ν, the corresponding limiting expression at large η for the Hankel function can be derived using the method of steepest descents. The saddle point α_{sp} for the integrand in (3.463) occurs on the imaginary axis where $\cosh\alpha = \nu/\eta$, which is close to $\alpha = i\pi/2$, so that the exponent near the saddle point is approximately

$$\eta \sinh\alpha - \nu\alpha \approx i(\eta - \nu\pi/2) + i\frac{1}{2}\eta(\alpha - \alpha_{sp})^2 \,. \tag{3.467}$$

The path of steepest descent crosses the imaginary axis proceeding obliquely upwards at an angle of $\pi/4$, so the resulting asymptotic expression is

$$\lim_{\eta\to\infty} H_\nu^{(1)}(\eta) = \left(\frac{2}{\pi\eta}\right)^{1/2} e^{-i[(\nu/2)+(1/4)]\pi} e^{i\eta} \,. \tag{3.468}$$

The corresponding limiting expressions for $J_\nu(\eta)$ and $Y_\nu(\eta)$ result from taking the real and imaginary parts of this. The above reduces to (3.462) when $\nu = 0$. This asymptotic behavior, plus the requirement that the function satisfy the ordinary differential equation (3.454), is

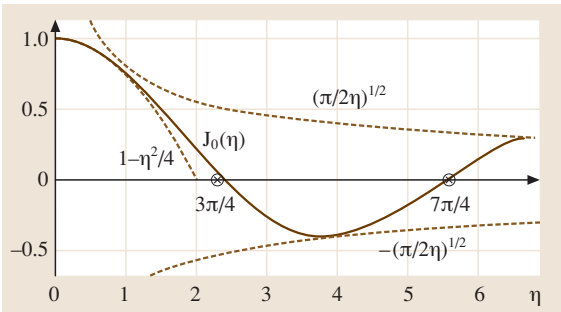


Fig. 3.33 Graph of the Bessel function of the zeroth order, shown along with common approximations used for small and large values of the argument

Amazon EX1014 Page 98

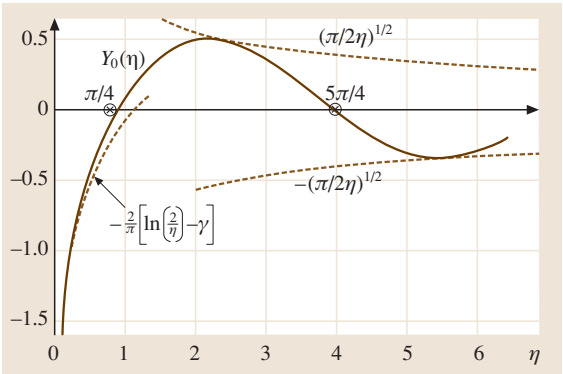


Fig. 3.34 Graph of the Neumann function of the zeroth order, shown along with common approximations used for small and large values of the argument

sufficient to define the Hankel function uniquely. The definition (3.463) is also such that it is consistent with the requirement that the real part (the Bessel function) be finite for real positive ν.

For small values of the argument η and for nonzero integer n these functions have the limiting expressions

$$J_n(\eta) \to \frac{1}{n!}\left(\frac{\eta}{2}\right)^n , \tag{3.469}$$

$$Y_n(\eta) \to -\frac{(n-1)!}{\pi}\left(\frac{2}{\eta}\right)^n . \tag{3.470}$$

These expressions also apply for noninteger positive index ν providing that one replaces $n! \to \Gamma(\nu+1)$ and $(n-1)! \to \Gamma(\nu)$, with the use of the Gamma function. The expression for the Neumann function obtained in this way is not appropriate in the limit $\nu \to 0$, as the Gamma function has a singularity when its argument is zero. Instead, one must use the logarithmic expression given by the imaginary part of (3.460).

The definition given above of the Hankel functions for arbitrary index ν yields the recursion relations

$$\frac{\mathrm{d}}{\mathrm{d}\eta} H_0^{(1)}(\eta) = -H_1^{(1)}(\eta) , \tag{3.471}$$

$$\frac{\mathrm{d}}{\mathrm{d}\eta} H_\nu^{(1)}(\eta) = H_{\nu-1}^{(1)}(\eta) - \frac{\nu}{\eta} H_\nu^{(1)}(\eta) . \tag{3.472}$$

Analogous recursion relations hold for the Bessel and Neumann functions.

Factored Solutions

One principal use of the Hankel functions and the Bessel functions of arbitrary order is in the synthesis of solutions of the Helmholtz equation in cylindrical coordinates,

$$\frac{\partial^2 \hat{p}}{\partial w^2} + \frac{1}{w}\frac{\partial \hat{p}}{\partial w} + \frac{1}{w^2}\frac{\partial^2 \hat{p}}{\partial \phi^2} + \frac{\partial^2 \hat{p}}{\partial z^2} + k^2 \hat{p} = 0 . \tag{3.473}$$

One uses factored solutions of the form

$$\hat{p} = \mathfrak{W}(w)\Phi(\phi)\mathcal{Z}(z) . \tag{3.474}$$

If one takes the latter two factors to satisfy the ordinary differential equations

$$\frac{\mathrm{d}^2}{\mathrm{d}\phi^2}\Phi + \nu^2\Phi = 0 , \tag{3.475}$$

$$\frac{\mathrm{d}^2}{\mathrm{d}z^2}\mathcal{Z} + \alpha^2\mathcal{Z} = 0 , \tag{3.476}$$

then the ordinary differential equation that results for the radial-coordinate-dependent factor is

$$\frac{\mathrm{d}^2\mathfrak{W}}{\mathrm{d}w^2} + \frac{1}{w}\frac{\mathrm{d}\mathfrak{W}}{\mathrm{d}w} - \frac{\nu^2}{w^2}\mathfrak{W} + (k^2-\alpha^2)\mathfrak{W} = 0 . \tag{3.477}$$

The latter is recognized as the ordinary differential equation satisfied by Bessel functions and Hankel functions of the ν-th order, so possible solutions are

$$\begin{aligned} \mathfrak{W} &= H_\nu^{(1)}[(k^2-\alpha^2)^{1/2}w] ; \\ &\quad J_\nu[(k^2-\alpha^2)^{1/2}w] ; \\ &\quad Y_\nu[(k^2-\alpha^2)^{1/2}w] . \end{aligned} \tag{3.478}$$

One can use combinations of such factored solutions for the synthesis of solutions of basic problems such as the scattering of a plane wave by a rigid cylinder. The solution is analogous to that discussed in a preceding section for scattering by a rigid sphere. For such problems in cylindrical coordinates, the applicable plane wave expansion theorem is

$$\mathrm{e}^{\mathrm{i}kw\cos\phi} = \sum_{n=0}^{\infty} 2\epsilon_n \cos(n\phi) J_n(kw) , \tag{3.479}$$

where

$$\epsilon_n = \left[\frac{1}{\pi}\int_0^{2\pi} \cos^2(n\phi)\,\mathrm{d}\phi\right]^{-1} \tag{3.480}$$

is $1/2$ if $n = 0$ and 1 if $n \geq 0$. This expansion formula results because of the orthogonality of the trigonometric functions and because

$$J_n(kw) = \frac{1}{2\pi}\int_0^{2\pi} \mathrm{e}^{\mathrm{i}kw\cos\phi}\cos(n\phi)\,\mathrm{d}\phi . \tag{3.481}$$

Amazon EX1014 Page 99

Cylindrical Waves at Large Distances

The asymptotic expression (3.462) indicates that, at sufficiently large w, the solution of the Helmholtz equation for outgoing cylindrical waves can be represented by

$$\hat{p} = \frac{B}{\sqrt{w}} \mathrm{e}^{\mathrm{i}kw} , \tag{3.482}$$

where B is a constant which is related to the A introduced previously through

$$B = \mathrm{i}\pi \left(\frac{2}{\pi k}\right)^{1/2} \mathrm{e}^{-\mathrm{i}\pi/4} A . \tag{3.483}$$

Consequently, the relation between the functions $F(t)$ and $f(t)$ that appear in (3.446) and (3.447) must be such that

$$F(t) = 2(2\pi c)^{1/2} \mathrm{Re} \int_0^\infty \frac{1}{\omega^{1/2}} \mathrm{e}^{\mathrm{i}\pi/4} \hat{f}(\omega) \mathrm{e}^{-\mathrm{i}\omega t} \, \mathrm{d}\omega , \tag{3.484}$$

where $\hat{f}(\omega)$ is the Fourier transform of $f(t)$. To do the requisite integration, one inserts the counterpart of (3.167) for $\hat{f}(\omega)$ and then interchanges the order of integration. The result,

$$F(t) = (2c)^{1/2} \int_{-\infty}^{t} \frac{f(\tau)}{(t-\tau)^{1/2}} \, \mathrm{d}\tau , \tag{3.485}$$

is what was previously given in (3.448).

Fluid Velocity for Cylindrical Waves

The fluid velocity induced by outgoing cylindrical waves is not as simply related to the corresponding acoustic pressure as that induced by a plane wave, although symmetry directs that the velocity must be in the appropriate radial direction when the propagation is cylindrically symmetric. For the constant-frequency case, when $\hat{p}$ is given by

$$\hat{p} = C H_0^{(1)}(kw) , \tag{3.486}$$

the radial component in cylindrical coordinates of the linearized Euler equation (3.175) requires

$$\hat{v}_w = \frac{C}{\mathrm{i}\omega\rho} \frac{\mathrm{d}}{\mathrm{d}w} H_0^{(1)}(kw) . \tag{3.487}$$

At small distances, when (3.460) applies, one has

$$\hat{v}_w \approx \frac{C}{\mathrm{i}\omega\rho} \frac{2\mathrm{i}}{\pi} \frac{1}{w} = \frac{2C}{\pi\omega\rho} \frac{1}{w} . \tag{3.488}$$

This dependence on $1/w$ is characteristic of cylindrically spreading flow from a line source. The complex amplitude, $-\mathrm{i}\omega d\hat{m}/d\ell$, of the mass efflux rate, the mass of fluid flowing out per unit axial length per unit time of the source, is $2\pi w\rho$ times the above, so that

$$-\mathrm{i}\omega \frac{\mathrm{d}\hat{m}}{\mathrm{d}\ell} = \frac{4C}{\omega} . \tag{3.489}$$

This gives one a physical interpretation of the constant C, so that $-4\mathrm{i}C$ is the complex amplitude of the second derivative with respect to time of the mass that has been expelled from a small cylinder surrounding the source per unit length of cylinder.

In the limit of large w, the asymptotic relation for the Hankel function is applicable, so that

$$\frac{\mathrm{d}}{\mathrm{d}w} H_0^{(1)} \approx \mathrm{i}k H_0^{(1)}(kw) , \tag{3.490}$$

One consequently recovers the plane wave relation

$$\hat{v}_w = \frac{1}{\rho c} \hat{p} . \tag{3.491}$$

Since this holds for Fourier transforms and since ρc is independent of frequency, it should hold for transient cylindrical waves. (Here large w implies large compared to a characteristic wavelength, or compared to c divided by a characteristic angular frequency.)

The previous discussion concerning acoustic intensity implies that the intensity of an outgoing cylindrical wave should decrease with w *as* $1/w$ so that the power flow through any cylindrical surface around the z-axis should stay constant. This has to remain so, even when one expresses the field in terms of Hankel functions, so one would expect those functions to have some mathematical property that guarantees this. To show that this is indeed the case, one expresses the intensity for the constant-frequency case as

$$\begin{aligned} I_{w,\mathrm{av}} &= [\mathrm{Re}(\hat{p}\,\mathrm{e}^{-\mathrm{i}\omega t})\mathrm{Re}(\hat{v}_w \mathrm{e}^{-\mathrm{i}\omega t})]_{\mathrm{av}} \\ &= \frac{1}{2}\mathrm{Re}(\hat{p}^* \hat{v}_w) , \end{aligned} \tag{3.492}$$

in accordance with (3.182).

Then, with the explicit substitution of the expressions involving Bessel functions one obtains

$$\begin{aligned} I_{r,\mathrm{av}} &= \frac{|C|^2}{2\rho c} \mathrm{Re}[(J_0 - \mathrm{i}Y_0)(Y_0' - \mathrm{i}J_0')] \\ &= \frac{|C|^2}{2\rho c} W(J_0, Y_0) , \end{aligned} \tag{3.493}$$

where

$$W(J_0, Y_0) = J_0 Y_0' - Y_0 J_0' \tag{3.494}$$

is the Wronskian for the Bessel and Neumann functions. Here the primes denote differentiation with respect to the argument $\eta = kw$ of the indicated function. One can derive from the differential equation (3.453) that these two functions independently satisfy the Wronskian relation

$$\eta W(J_0, Y_0) = \text{constant} , \tag{3.495}$$

and this is so regardless of the specialized definitions of the two functions. The constant can be evaluated from values and derivatives at any given point. In particular, one can use the asymptotic expressions, and the derived constant is $2/\pi$. Thus one has

$$I_{w,\text{av}} = \frac{1}{\pi}\frac{|C|^2}{\rho c w} = \frac{1}{\rho c w}\frac{1}{16\pi}\left|\omega^2 \frac{\mathrm{d}\hat{m}}{\mathrm{d}\ell}\right|^2 . \tag{3.496}$$

3.12.3 Radially Oscillating Cylinder

A classic example for the radiation of cylindrical waves is that where a cylinder has nominal radius a, and an instantaneous radius

$$w_{\text{cyl}}(t) = a + \frac{v_\text{o}}{\omega}\sin(\omega t) . \tag{3.497}$$

Here v_o/ω is the amplitude of the deviations of the actual radius from the nominal value a. For the linear acoustics idealization to be valid, it is required that this deviation be substantially less than a, so that

$$v_\text{o} \ll \omega a . \tag{3.498}$$

The boundary condition on the fluid dynamic equations should ideally be

$$v_w = v_\text{o}\cos(\omega t) \qquad \text{at} \quad w = w_{\text{cyl}}(t) , \tag{3.499}$$

but (also in keeping with the linear acoustics idealization) it is replaced by

$$v_w = v_\text{o}\cos(\omega t) \qquad \text{at} \quad w = a . \tag{3.500}$$

The corresponding boundary condition on the complex amplitude is

$$\hat{v}_w = v_\text{o} \qquad \text{at} \quad w = a . \tag{3.501}$$

If one takes the complex amplitude of the acoustic pressure to be of the form

$$\hat{p} = A\, H_0^{(1)}(kw) , \tag{3.502}$$

where A is a complex number to be determined, then the radial component of the fluid velocity is

$$\hat{v}_w = \frac{A}{\mathrm{i}\omega\rho}\frac{\mathrm{d}}{\mathrm{d}w}H_0^{(1)}(kw) . \tag{3.503}$$

The imposing of the boundary condition determines the value of A and one obtains

$$\hat{p} = \mathrm{i}\omega\rho v_\text{o}\frac{H_0^{(1)}(kw)}{\left[\frac{\mathrm{d}}{\mathrm{d}w}H_0^{(1)}(kw)\right]_{w=a}} . \tag{3.504}$$

3.12.4 Transversely Oscillating Cylinder

If the cylinder is rigid and oscillating back and forth in the x-direction, the analysis is similar to that for the transversely oscillating sphere. The complex amplitude of the acoustic part of the pressure should have the general form

$$\hat{p} = B\frac{\mathrm{d}}{\mathrm{d}x}H_0^{(1)}(kw) = B\cos\phi\frac{\mathrm{d}}{\mathrm{d}w}H_0^{(1)}(kw) , \tag{3.505}$$

where B is to be determined from the boundary condition. The latter can also be written

$$\hat{p} = -kB\cos\phi H_1^{(1)}(kw) , \tag{3.506}$$

in accord with the recursion relation (3.471). The latter version is of the standard form for a factored solution of the Helmholtz equation in cylindrical coordinates.

Euler's equation gives the radial component of the fluid velocity as

$$\hat{v}_w = \frac{1}{\mathrm{i}\omega\rho}B\cos\phi\frac{\mathrm{d}^2}{\mathrm{d}w^2}H_0^{(1)}(kw) . \tag{3.507}$$

The appropriate approximate boundary condition is that

$$\hat{v}_w = v_\text{c}\cos\phi \qquad \text{at} \quad w = a . \tag{3.508}$$

This allows one to identify

$$B = \frac{\mathrm{i}\omega\rho v_\text{c}}{\left[\frac{\mathrm{d}^2}{\mathrm{d}w^2}H_0^{(1)}(kw)\right]_{w=a}} . \tag{3.509}$$

3.13 Simple Sources of Sound

Whatever generates an acoustic wave is termed a source. In acoustical analysis, sources are incorporated into the governing equations through either boundary conditions or source terms.

3.13.1 Volume Sources

Sources that are some distance from bounding surfaces and that are small compared to a wavelength can frequently be described by source terms. The simplest such source would be one that causes a net amount of mass of fluid to flow out of or into a fixed surface that encases it. The example of a radially oscillating sphere, discussed in a preceding section, is a classic example of such a source, and the surface through which the mass is flowing can be taken as a fixed spherical surface just outside the actual moving surface of the sphere. This mass passing out per unit time divided by the ambient density ρ is a quantity $Q_S(t)$ termed the source strength function or the source volume velocity. If such a source is concentrated at a point $\boldsymbol{x}_0$, then the appropriate inhomogeneous wave equation which would replace (3.74) would be

$$\nabla^2 p - \frac{1}{c^2}\frac{\partial^2 p}{\partial t^2} = -\rho \dot{Q}_S(t)\delta(\boldsymbol{x}-\boldsymbol{x}_0)\,, \tag{3.510}$$

where $\delta(\boldsymbol{x})$ is the Dirac delta function, which has a volume integral of unity and that is concentrated at the point where its argument vanishes.

The solution of the above inhomogeneous wave equation for an isolated source at the origin ($\boldsymbol{r}_o = 0$) in an unbounded region is

$$p = \frac{\rho}{4\pi r}\dot{Q}_S[t-(r/c)] = \frac{S[t-(r/c)]}{r}\,, \tag{3.511}$$

where

$$S(t) = \frac{\rho}{4\pi}\frac{\mathrm{d}}{\mathrm{d}t}Q_S(t) \tag{3.512}$$

is called the monopole strength. The replacement of the argument by the retarded time $t-(r/c)$ accounts for the transit time lag r/c for the sound to propagate from the source to the listener.

For a radially oscillating small sphere, $Q_S(t)$ can be taken as the time derivative of the instantaneous volume within the sphere. Thus the radiated acoustic pressure is proportional to the volume acceleration, the second derivative with respect to time of the sphere's volume, so that

$$p = \frac{\rho}{4\pi r}\left(\frac{\mathrm{d}^2 V}{\mathrm{d}t^2}\right)_{t\to t-(r/c)}\,. \tag{3.513}$$

This rule holds for bodies that are not necessarily spherically shaped, provided the largest dimensions are small compared to a characteristic wavelength and provided the acoustic pressure is measured at a sufficiently large distance from the source.

3.13.2 Small Piston in a Rigid Baffle

Another example of a volume source is that of a very small (relative to a wavelength) piston mounted in an infinite rigid baffle. If the piston has area A and outward normal velocity $v_n(t)$, then symmetry (or, equivalently, the inclusion of an image source) requires that the radiated sound be the same as from an isolated source with twice the volume velocity of the piston, so one has

$$p = \frac{\rho}{2\pi r}A\dot{v}_n\,[t-(r/c)]\,. \tag{3.514}$$

3.13.3 Multiple and Distributed Sources

For assemblies of sources, each concentrated at a point, the generalization of (3.510) is to replace the right side by a sum of individual source terms; the solution to this inhomogeneous wave equation is given by

$$p = \sum_n \frac{S\,[t-(R_n/c)])}{R_n}\,, \tag{3.515}$$

where R_n is the distance of the listener from the n-th source.

When the source is continuously distributed in space, the point-source term is replaced by a smoothly varying function, so the inhomogeneous wave equation is now of the form

$$\nabla^2 p - \frac{1}{c^2}\frac{\partial^2 p}{\partial t^2} = -\rho\dot{q}_S(\boldsymbol{x},t) = -4\pi s(\boldsymbol{x},t)\,. \tag{3.516}$$

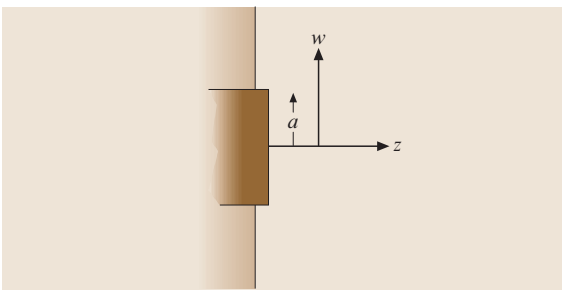


Fig. 3.35 Small piston source in a rigid baffle

The function q_S is termed the source strength density (source strength per unit volume). For an unbounded medium, the solution of this latter equation is given by the definite integral

$$p(\boldsymbol{x}, t) = \iiint \frac{1}{R} s(\boldsymbol{x}_0, t - (R/c))\, \mathrm{d}V_0 \,, \qquad (3.517)$$

where the volume integration ranges over source position $\boldsymbol{x}_0$, and where $R = |\boldsymbol{x} - \boldsymbol{x}_0|$ is the distance between the listener and source positions.

3.13.4 Piston of Finite Size in a Rigid Baffle

The concept of multiple sources and the mathematical description above allows an extension of (3.514) to the case when a finite piston is oscillating in a rigid baffle. An area element ΔA located on the $z = 0$ plane at (x_0, y_0) acts as a volume source where the time rate of change of the volume is $2v_n(x_0, y_0, t)\Delta A$. Here, as in (3.514), the factor of two results from the requirement that the contribution from this source element should give no increment of normal velocity on the surface outside of the area element. The normal velocity v_n is here the outward velocity of the piston, which is the velocity in the $+z$-direction, and is that appropriate to the surface point (x_0, y_0).

Superposition of the contribution from all the area elements subsequently yields, for the acoustic pressure

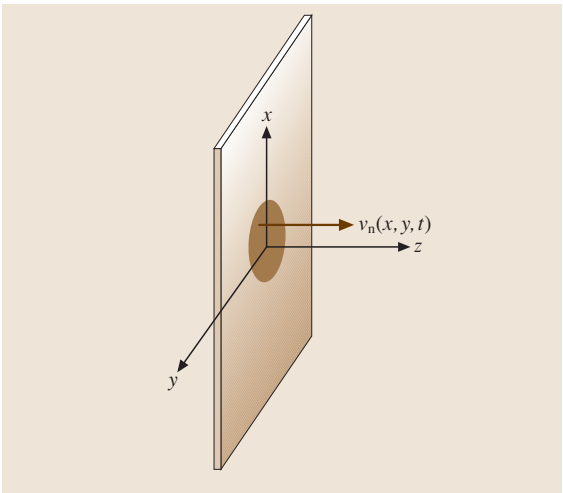


Fig. 3.36 Quantities involved in the integration to determine sound radiation from a planar surface in a state of nonuniform vibration

in the radiated wave,

$$p = \frac{\rho}{2\pi} \iint \frac{\dot{v}_n\,[x_0, y_0, t - (R/c)]}{R}\, \mathrm{d}x_0\, \mathrm{d}y_0 \,, \qquad (3.518)$$

where

$$R = \left[(x - x_0)^2 + (y - y_0)^2 + z^2\right]^{1/2} \qquad (3.519)$$

is the distance from the surface point $(x_0, y_0, 0)$ to the listener point (x, y, z). The integration extends over the portion of the surface that is moving.

If the surface is moving at a constant angular frequency ω, so that

$$v_n\,(x_0, y_0, t) = \mathrm{Re}\left[\hat{v}_n(x_0, y_0)\, \mathrm{e}^{-\mathrm{i}\omega t}\right] , \qquad (3.520)$$

then (3.518) yields the complex amplitude of the radiated pressure field as

$$\hat{p} = \frac{-\mathrm{i}\omega\rho}{2\pi} \iint \hat{v}_n(x_0, y_0) \frac{\mathrm{e}^{\mathrm{i}kR}}{R}\, \mathrm{d}x_0\, \mathrm{d}y_0 \,, \qquad (3.521)$$

with $k = \omega/c$.

Appropriate formulas for the far field when the piston is of limited extent and centered at the origin result when the quantity R in the denominator is replaced by r and when it is replaced by (with the use of the binomial expansion)

$$R \approx r - \frac{x}{r} x_0 - \frac{y}{r} y_0 \qquad (3.522)$$

in the exponent. Here r is the radial distance in spherical coordinates, and one can take

$$\frac{x}{r} = \sin\theta \cos\phi \,; \qquad \frac{y}{r} = \sin\theta \sin\phi \,, \qquad (3.523)$$

with θ as the polar angle and ϕ as the azimuthal solution. In this far-field limit, the acoustic pressure takes the form

$$\hat{p} \to F(\theta, \phi) \frac{\mathrm{e}^{\mathrm{i}kr}}{r} \,, \qquad (3.524)$$

where the directivity function is given by

$$F(\theta, \phi) = \frac{-\mathrm{i}\omega\rho}{2\pi} \iint \hat{v}_n(x_0, y_0)\, \mathrm{e}^{-\mathrm{i}kx_0 \sin\theta \cos\phi} \times \mathrm{e}^{-\mathrm{i}ky_0 \sin\theta \sin\phi}\, \mathrm{d}x_0\, \mathrm{d}y_0 \,. \qquad (3.525)$$

The integrals (3.521) and (3.525) can be evaluated in terms of standard special functions when the piston is rigid and of a simple shape.

Amazon EX1014 Page 103

Rectangular Piston

If the piston is rectangular, with dimensions a and b, and centered at the origin, the far-field pattern is given by

$$F(\theta,\phi)=\frac{-\mathrm{i}\omega\rho v_0}{2\pi}ab\frac{\sin\left[(1/2)a\sin\theta\cos\phi\right]}{(1/2)a\sin\theta\cos\phi}\times\frac{\sin\left[(1/2)b\sin\theta\sin\phi\right]}{(1/2)b\sin\theta\sin\phi}\,. \tag{3.526}$$

Circular Piston

If the piston is circular of radius a, the corresponding expression is independent of the azimuthal angle and given by

$$F(\theta)=\frac{-\mathrm{i}\omega\rho v_0}{2\pi}\int_0^a\int_0^{2\pi}\mathrm{e}^{-\mathrm{i}kw_0\sin\theta\cos\phi_0}\,\mathrm{d}\phi_0\,w_0\,\mathrm{d}w_0. \tag{3.527}$$

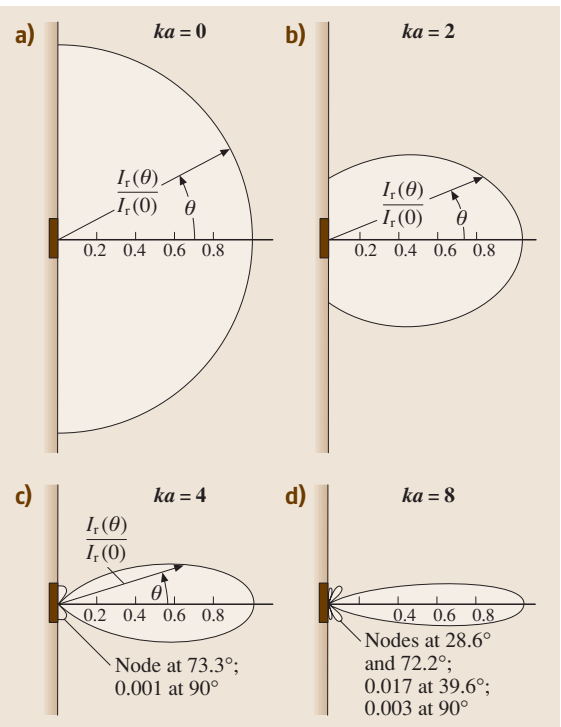


Fig. 3.37 Far-field radiation patterns of a vibrating circular piston in an otherwise rigid baffle for various values of ka. The quantity plotted is the intensity at a large radial distance r relative to that when the polar angle θ is zero, which is $[2J_1(\xi)/\xi]^2$, with $\xi=ka\sin\theta$

The integral over the azimuthal angle on the piston yields a Bessel function, so one has

$$F(\theta)=-\mathrm{i}\omega\rho v_0\int_0^a J_0(kw_0\sin\theta)w_0\,\mathrm{d}w_0\,. \tag{3.528}$$

The recursion relation (3.472) implies that

$$\frac{\mathrm{d}}{\mathrm{d}\eta}J_1(\eta)=J_0(\eta)-\frac{1}{\eta}J_1(\eta)\,, \tag{3.529}$$

so

$$\eta J_0(\eta)=\eta\frac{\mathrm{d}}{\mathrm{d}\eta}J_1(\eta)+J_1(\eta)=\frac{\mathrm{d}}{\mathrm{d}\eta}\left(\eta J_1(\eta)\right)\,. \tag{3.530}$$

Consequently the integration in (3.528) can be performed in terms of the Bessel function of the first order, with the result

$$F(\theta)=-\mathrm{i}\omega\rho v_0a^2\left(\frac{J_1(ka\sin\theta)}{ka\sin\theta}\right)\,. \tag{3.531}$$

3.13.5 Thermoacoustic Sources

The differential equation (3.516) arises when one suddenly adds heat to a fluid [3.71,72], as with a laser or by combustion, so that the entropy s per unit mass changes according to the thermodynamic relation

$$\rho T\mathrm{D}s/\mathrm{D}t=h\,, \tag{3.532}$$

so that, to first order, the equation of state (3.87) yields

$$\frac{\partial p'}{\partial t}=c^2\frac{\partial\rho'}{\partial t}+\frac{c^2\beta}{c_\mathrm{p}}h\,. \tag{3.533}$$

Here h is the heat added per unit time and unit volume, β is the volume expansion coefficient defined by (3.30), and c_p is the specific heat at constant pressure.

Equation (3.533) changes the basic linear acoustic equations (3.71) and (3.72) to

$$\frac{\partial p}{\partial t}+\rho c^2\nabla\cdot\boldsymbol{v}=\frac{c^2\beta}{c_\mathrm{p}}h\,, \tag{3.534}$$

$$\rho_0\frac{\partial\boldsymbol{v}}{\partial t}+\nabla p=0\,, \tag{3.535}$$

so the energy conservation corollary of (3.273) becomes

$$\frac{\partial w}{\partial t}+\nabla\cdot\boldsymbol{I}=\frac{\beta}{\rho c_\mathrm{p}}ph\,, \tag{3.536}$$

and the wave equation becomes

$$\nabla^2p-\frac{1}{c^2}\frac{\partial^2p}{\partial t^2}=-\frac{\beta}{c_\mathrm{p}}\frac{\partial h}{\partial t}\,. \tag{3.537}$$

Amazon EX1014 Page 104

The appropriate identification for the monopole strength density function $s(\boldsymbol{x}, t)$ in the integral expression of (3.517) is consequently given by

$$s(\boldsymbol{x}, t) = \frac{1}{4\pi}\frac{\beta}{c_\mathrm{p}}\frac{\partial h}{\partial t} . \tag{3.538}$$

3.13.6 Green's Functions

The idealization of a point source of constant frequency is of basic importance in formulating solutions to complicated acoustic radiation problems. The resulting complex pressure amplitude of the field resulting from such a single source can be expressed as a constant times a Green's function, where the Green's function is a solution of the inhomogeneous Helmholtz equation

$$(\nabla^2 + k^2)G(\boldsymbol{x}|\boldsymbol{x}_0) = -4\pi\delta(\boldsymbol{x} - \boldsymbol{x}_0) . \tag{3.539}$$

(The inclusion of the factor 4π on the right is done in much of the literature, but not universally; its objective here is that the mathematical form of the Green's function be simpler.) If the medium surrounding the source is unbounded, then the Green's function is the free-space (no external boundaries) Green's function, which can be identified from (3.511) to have the form

$$G(\boldsymbol{x}|\boldsymbol{x}_0) = \frac{1}{R}\mathrm{e}^{\mathrm{i}kR} , \tag{3.540}$$

where R is the distance between the source and observation (listener) point. When external boundary conditions are imposed on the Green's function that satisfies (3.539), then the Green's function will have a form different from that of the free-space Green's function. However, in all such cases, the Green's function will approach $1/R$ plus a bounded function when the listener position approaches the source point.

An example of a Green's function that is not the free-space Green's function is that which corresponds to a point source on one side of an infinitely-extended rigid plane. If the source point is at (x_0, y_0, z_0) where $z_0 > 0$, and if the rigid plane is the $z = 0$ plane, then

$$G(\boldsymbol{x}|\boldsymbol{x}_0) = \frac{1}{R}\mathrm{e}^{\mathrm{i}kR} + \frac{1}{R_\mathrm{i}}\mathrm{e}^{\mathrm{i}kR_\mathrm{i}} , \tag{3.541}$$

where

$$R_\mathrm{i} = [(x - x_0)^2 + (y - y_0)^2 + (z + z_0)^2]^{1/2} . \tag{3.542}$$

Because this Green's function is even in y, it automatically satisfies the boundary conditions that its normal derivative vanish at the rigid boundary.

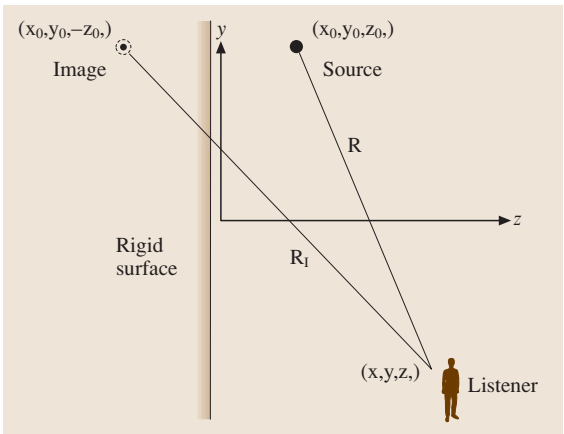


Fig. 3.38 Parameters involved in the construction of the Green's function corresponding to a point source outside a perfectly reflecting (rigid) wall. The quantity R is the direct distance from the source, and R_I is the distance from the image source

3.13.7 Multipole Series

Radiation fields from sources of limited spatial extent in unbounded environments can be described either in terms of multipoles or spherical harmonics. That such descriptions are feasible can be demonstrated with the aid of the constant-frequency version of (3.517):

$$\hat{p}(\boldsymbol{x}) = \int \hat{s}(\boldsymbol{x}_0)\frac{\mathrm{e}^{\mathrm{i}kR}}{R}\,\mathrm{d}V_0 , \tag{3.543}$$

which is the solution of the inhomogeneous Helmholtz equation with a continuous distribution of monopole sources taken into account.

The multipole series results from this when one expands $R^{-1}\mathrm{e}^{\mathrm{i}kR}$ in a power series in the coordinates of the source position $\boldsymbol{x}_0$ and then integrates term by term. Up to second order one obtains

$$\hat{p} = \hat{S}\frac{\mathrm{e}^{\mathrm{i}kr}}{r} - \sum_{\nu=1}^{3}\hat{D}_\nu\frac{\partial}{\partial x_\nu}\frac{\mathrm{e}^{\mathrm{i}kr}}{r} + \sum_{\mu,\nu=1}^{3}\hat{Q}_{\mu\nu}\frac{\partial^2}{\partial x_\mu \partial x_\nu}\frac{\mathrm{e}^{\mathrm{i}kr}}{r} , \tag{3.544}$$

Amazon EX1014 Page 105

where the coefficients are expressed by

$$\hat{S} = \int \hat{s}(\boldsymbol{x})\,\mathrm{d}V\,, \tag{3.545}$$

$$\hat{D}_\nu = -\int x_\nu \hat{s}(\boldsymbol{x})\,\mathrm{d}V\,, \tag{3.546}$$

$$\hat{Q}_{\mu\nu} = \frac{1}{2!}\int x_\mu x_\nu \hat{s}(\boldsymbol{x})\,\mathrm{d}V\,. \tag{3.547}$$

The three terms in (3.544) are said to be the monopole, dipole, and quadrupole terms, respectively. The coefficients $\hat{S}$, $\hat{D}_\nu$, and $\hat{Q}_{\mu\nu}$ are similarly labeled. The D_ν are the components of a dipole moment vector, while the $Q_{\mu\nu}$ are the components of a quadrupole moment tensor. The general validity [3.73, 74] of such a description extends beyond the manner of derivation and is not restricted to sound generated by a continuous source distribution embedded in the fluid. It applies in particular to the sound radiated by a vibrating body of arbitrary shape.

3.13.8 Acoustically Compact Sources

If the source is acoustically compact, so that its largest dimension is much shorter than a wavelength, the multipole series converges rapidly, so one typically only need retain the first nonzero term. Sources exist whose net monopole strength is zero, and sources also exist whose dipole moment vector components are all zero as well. Consequently, compact sources are frequently classed as monopole, dipole, and quadrupole sources. The prototype of a monopole source is a body of oscillating volume. One for a dipole source is a rigid solid undergoing translational oscillations; another would be a vibrating plate or shell whose thickness changes negligibly. In the former case, the detailed theory shows that in the limit of sufficiently low frequency, the dipole moment vector is given by

$$\hat{D}_\nu = \hat{F}_\nu + m_\mathrm{d}\hat{a}_{C,\nu}\,, \tag{3.548}$$

where $\hat{F}_\nu$ is associated with the force which the moving body exerts on the surrounding fluid and where $\hat{a}_{C,\nu}$ is associated with the acceleration of the geometric center of the body. The quantity m_d is the mass of fluid displaced by the body.

The simplest example of a dipole source is that of a rigid sphere transversely oscillating along the z-axis about the origin. (This is discussed in general terms in a preceding section of this chapter.) If the radius of the sphere is a and if $ka \ll 1$, then the force and acceleration have only a z-component, and the force amplitude is given by

$$\hat{F}_z = \frac{1}{2}m_\mathrm{d}\hat{a}_{C,z}\,. \tag{3.549}$$

The dipole moment when the center velocity has amplitude $\hat{v}_\mathrm{C}$ is consequently of the form

$$\hat{D}_z = -\frac{3}{2}\mathrm{i}\omega[(4/3)\rho\pi a^3]\hat{v}_\mathrm{C}\,. \tag{3.550}$$

Taking into account that the derivative of r with respect to z is $\cos\theta$, one finds the acoustic field from (3.544) to be given by

$$\hat{p} = -\hat{D}_z\cos\theta\frac{\mathrm{d}}{\mathrm{d}r}\frac{\mathrm{e}^{\mathrm{i}kr}}{r}\,. \tag{3.551}$$

When $kr \gg 1$, this approaches the limiting form

$$\hat{p} \to -\mathrm{i}kD_z\cos\theta\frac{\mathrm{e}^{\mathrm{i}kr}}{r}\,. \tag{3.552}$$

The far-field intensity, in accord with (3.276), has a time average of $|\hat{p}|^2/(2\rho c)$ and is directed in the radial direction in this asymptotic limit. The drop of intensity as $1/r^2$ with increasing radial distance is the same as for spherical spreading, but the intensity varies with direction as $\cos^2\theta$.

Vibrating bodies that radiate as quadrupole sources (and which therefore have no dipole radiation) usually do so because of symmetry. Vibrating bells [3.75] and tuning forks are typically quadrupole radiators.

A dipole source can be represented by two similar monopole sources, 180° out of phase with each other, and very close together. Since they are radiating out of phase, there is no total mass flow input into the medium. Such a dipole source will have a net acoustic power output substantially lower than that of either of the component monopoles when radiating individually. Similarly, a quadrupole can be formed by two identical but oppositely directed dipoles brought very close together. If the two dipoles have a common axis, then a longitudinal quadrupole results; when they are side by side, a lateral quadrupole results. In either case, the quadrupole radiation is much weaker than would be that from either dipole when radiating separately.

3.13.9 Spherical Harmonics

The closely related description of source radiation in terms of spherical harmonics results from (3.543) when one inserts the expansion [3.76–78]

$$\frac{\mathrm{e}^{\mathrm{i}kR}}{R} = \sum_{\ell=0}^{\infty}(2\ell+1)j_\ell(kr_0)h_\ell^{(1)}(kr)P_\ell(\cos\Theta)\,, \tag{3.553}$$

Amazon EX1014 Page 106

where j_ℓ is the spherical Bessel function and $h_\ell^{(1)}$ is the spherical Hankel function of order ℓ and of the first kind. (The expansion here assumes $r > r_0$; otherwise, one interchanges r and r_0 in the above.) The quantity $P_\ell(\cos\Theta)$ is the Legendre function of order ℓ, while Θ is the angle between the directions of $\boldsymbol{x}$ and $\boldsymbol{x}_0$. Alternately, one uses the expansion

$$P_\ell(\cos\Theta) = \sum_{m=-\ell}^{\ell} \frac{(\ell-|m|)!}{(\ell+|m|)!} Y_\ell^m(\theta,\phi) Y_\ell^{-m}(\theta_0,\phi_0), \tag{3.554}$$

where the spherical harmonics are defined by

$$Y_\ell^m(\theta,\phi) = \mathrm{e}^{\mathrm{i}m\phi} P_\ell^{|m|}(\cos\theta)\,. \tag{3.555}$$

Here the functions $P_\ell^{|m|}(\cos\theta)$ are the associated Legendre functions. [The value of $P_0(\cos\Theta)$ is identically 1.]

If such an expansion is inserted into (3.543) and if r is understood to be sufficiently large that there are no sources beyond that radius, one has the relation

$$\hat{p}(r,\theta,\phi) = a_{00} h_0^{(1)}(kr) + \sum_{\ell=1}^{\infty}\sum_{m=-\ell}^{\ell} a_{\ell m} h_\ell^{(1)}(kr) Y_\ell^m(\theta,\phi)\,, \tag{3.556}$$

with coefficients given by

$$a_{\ell m} = \mathrm{i}k(2\ell+1)\frac{(\ell-|m|)!}{(\ell+|m|)!} \times \int \hat{s}(r_0,\theta_0,\phi_0) j_\ell(kr_0) Y_\ell^{-m}(\theta_0,\phi_0)\,\mathrm{d}V_0\,. \tag{3.557}$$

These volume integrations are to be carried out in spherical coordinates. The general result of (3.557) holds for any source of limited extent; any such wave field in an unbounded medium must have such an expansion in terms of spherical Hankel functions and spherical harmonics.

The spherical Hankel functions have the asymptotic (large-r) form

$$h_\ell^{(1)}(kr) \to (-\mathrm{i})^{(\ell+1)} \frac{\mathrm{e}^{\mathrm{i}kr}}{kr}\,, \tag{3.558}$$

so the acoustic radiation field must asymptotically approach

$$\hat{p} \to \hat{F}(\theta,\phi)\frac{\mathrm{e}^{\mathrm{i}kr}}{r}\,, \tag{3.559}$$

where the function $\hat{F}(\theta,\phi)$ is a function of θ and ϕ that has an expansion in terms of spherical harmonics. In this asymptotic limit, the acoustic intensity is in the radial direction and given by

$$I_{r,\mathrm{av}} = \frac{1}{2}\frac{|\hat{F}|^2}{\rho c r^2}\,. \tag{3.560}$$

For fixed θ and ϕ, the time-averaged intensity must asymptotically decrease as $1/r^2$. The coefficient of $1/r^2$ in the above describes the far-field radiation pattern of the source, having the units of watts per steradian.

Although the two types of expansions, multipoles and spherical harmonics, are related, the relationship is not trivial. The quadrupole term in (3.544), for example, cannot be equated to the sum of the $\ell = 2$ terms in (3.556). It is possible to have spherically symmetric quadrupole radiation, so an $\ell = 0$ term would have to be included.

3.14 Integral Equations in Acoustics

There are many common circumstances where the determination of acoustic fields and their properties is approached via the solution of integral equations rather than of partial differential equations.

3.14.1 The Helmholtz–Kirchhoff Integral

For the analysis of radiation of sound from a vibrating body of limited extent in an unbounded region, there is an applicable integral corollary of the Helmholtz equation of (3.176) which dates back to 19th century works of *Helmholtz* [3.47] and *Kirchhoff* [3.79].

One considers a closed surface S where the outward normal component of the particle velocity has complex amplitude $\hat{v}_\mathrm{n}(\boldsymbol{x}_\mathrm{S})$ and complex pressure amplitude $\hat{p}_\mathrm{S}(\boldsymbol{x}_\mathrm{S})$ at a point $\boldsymbol{x}_\mathrm{S}$ on the surface. For notational convenience, one introduces a quantity defined by

$$\hat{f}_\mathrm{S} = -\mathrm{i}\omega\rho\hat{v}_\mathrm{n}\,, \tag{3.561}$$

where $\hat{v}_\mathrm{n}(\boldsymbol{x}_\mathrm{S})$ is the normal component $\boldsymbol{n}(\boldsymbol{x}_\mathrm{S})\cdot\hat{\boldsymbol{v}}(\boldsymbol{x}_\mathrm{S})$ of the complex fluid velocity vector amplitude $\hat{\boldsymbol{v}}(\boldsymbol{x})$ at the surface. One can regard $\hat{f}_\mathrm{S}$ as a convenient grouping of symbols, either as a constant multiplied by the normal velocity, or as a constant multiplied by the normal ac-

Amazon EX1014 Page 107

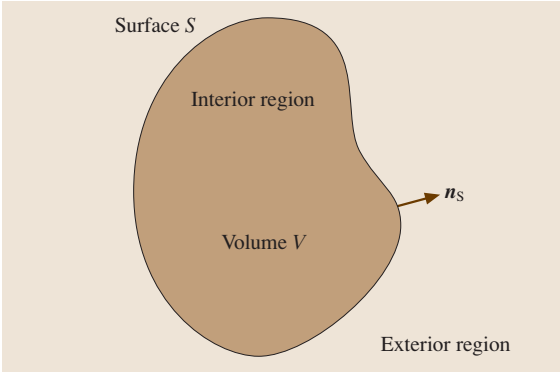


Fig. 3.39 Arbitrary surface in an arbitrary state of vibration at constant frequency, with unit normal $\boldsymbol{n}_S$

celeration, or as the normal component of the apparent body force, per unit volume, exerted on the fluid at the surface point $\boldsymbol{x}_S$. Because of the latter identification, the use of the symbol f is appropriate. The subscript S is used to denote values appropriate to the surface.

Then, given that there are no sources outside the surface, a mathematical derivation, involving the differential equation of (3.539) for the free-space Green's function of (3.540), involving the Helmholtz equation, and involving the divergence theorem, yields

$$\hat{p}(\boldsymbol{x}) = \mathfrak{M}(\boldsymbol{x}, \hat{p}_S, \hat{f}_S) \tag{3.562}$$

for the complex pressure amplitude $\hat{p}$ at a point $\boldsymbol{x}$ outside the surface. Here the right side is given by the expression

$$\mathfrak{M} = \frac{1}{4\pi} \int \left\{ \hat{f}_S(\boldsymbol{x}'_S) G(\boldsymbol{x}|\boldsymbol{x}'_S) + \hat{p}_S(\boldsymbol{x}'_S) \boldsymbol{n}(\boldsymbol{x}'_S) \cdot [\nabla' G(\boldsymbol{x}|\boldsymbol{x}')]_{\boldsymbol{x}'=\boldsymbol{x}'_S} \right\} \mathrm{d}S' \,. \tag{3.563}$$

In the integrand of this expression, the point $\boldsymbol{x}'_S$ (after the evaluation of any requisite normal derivatives) is understood to range over the surface S, with the point $\boldsymbol{x}$ held fixed during the integration. The unit outward normal vector $\boldsymbol{n}(\boldsymbol{x}'_S)$ points out of the enclosed volume V at the surface point $\boldsymbol{x}'_S$.

In (3.563), the integral $\mathfrak{M}$ is a function of the point $\boldsymbol{x}$, but a functional (function of a function) of the function arguments $\hat{p}_S$ and $\hat{f}_S$.

3.14.2 Integral Equations for Surface Fields

The functions $\hat{p}_S$ and $\hat{f}_S$ cannot be independently prescribed on the surface S. Specifying either one is a sufficient inner boundary condition on the Helmholtz

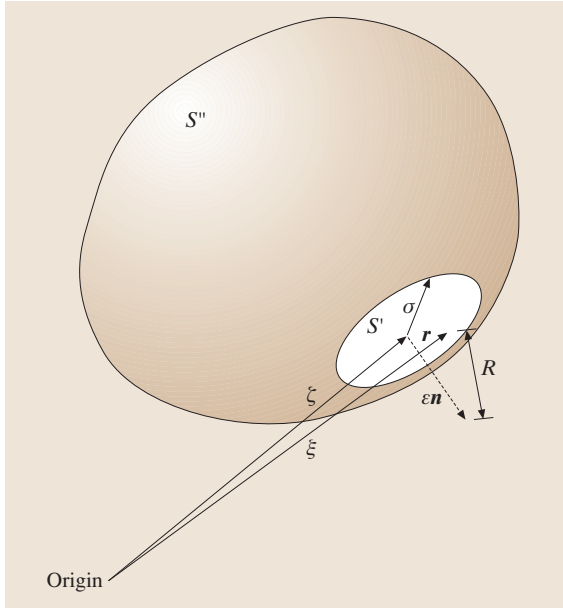


Fig. 3.40 Sketch illustrating the methodology for the derivation of an integral equation from the Helmholtz–Kelvin relation. The exterior point at $\boldsymbol{\xi} = \boldsymbol{\zeta} + \boldsymbol{n}\epsilon$ is gradually allowed to approach an arbitrary point $\boldsymbol{\zeta}$ on the surface, and the integration is represented as a sum of integrals over S' and S''. One considers the parameters ϵ and σ as small, but with $\sigma \gg \epsilon$, first takes the limit as $\epsilon \to 0$, then takes the limit as $\sigma \to 0$

equation. The corollary of (3.562) applies only if both functions correspond to a physically realizable radiation field outside the surface S. If this is so and if the point $\boldsymbol{x}$ is formally set to a point inside the enclosed volume, then analogous mathematics involving the properties of the Green's function leads to the deduction [3.80, 81]

$$\mathfrak{M}(\boldsymbol{x}_{\text{inside}}, \hat{p}_S, \hat{f}_S) = 0 \,, \tag{3.564}$$

which is a general relation between the surface value functions $\hat{p}_S$ and $\hat{f}_S$, holding for any choice of the point $\boldsymbol{x}$ inside the enclosed volume.

Equation (3.562) allows one to derive two additional relations (distinguished by the subscripts I and II) between the surface values of $\hat{p}_S$ and $\hat{f}_S$. One results when the off-surface point $\boldsymbol{x}$ is allowed to approach an arbitrary but fixed surface point $\boldsymbol{x}_S$. For one of the terms in the integral defining the quantity $\mathfrak{M}$, the limit as $\boldsymbol{x}$ approaches $\boldsymbol{x}_S$ of the integral is not the same as the integral over the limit of the integrand as $\boldsymbol{x}$ approaches $\boldsymbol{x}_S$. With

Amazon EX1014 Page 108

this subtlety taken into account, one obtains

$$\hat{p}_S(\boldsymbol{x}_S) - \mathfrak{L}_I(\boldsymbol{x}_S, \hat{p}_S) = \mathfrak{H}_I(\boldsymbol{x}_S, \hat{f}_S) \,, \tag{3.565}$$

where the two linear operators $\mathfrak{L}_I$ and $\mathfrak{H}_I$ are

$$\mathfrak{L}_I(\boldsymbol{x}_S, \hat{p}_S) = \frac{1}{2\pi} \int \hat{p}(\boldsymbol{x}'_S)\boldsymbol{n}(\boldsymbol{x}'_S)[\nabla' G(\boldsymbol{x}_S|\boldsymbol{x}')]_{\boldsymbol{x}'=\boldsymbol{x}'_S} \, \mathrm{d}S' \,, \tag{3.566}$$

$$\mathfrak{H}_I(\boldsymbol{x}_S, \hat{f}_S) = \frac{1}{2\pi} \int \hat{f}(\boldsymbol{x}'_S) G(\boldsymbol{x}'_S|\boldsymbol{x}_S) \, \mathrm{d}S' \,. \tag{3.567}$$

These linear operators operate on the surface values of $\hat{p}_S$ and $\hat{f}_S$, respectively, with the result in each case being a function of the position of the surface point $\boldsymbol{x}_S$.

The second type of surface relationship [3.82] is obtained by taking the gradient of both sides of (3.562), subsequently setting $\boldsymbol{x}$ to $\boldsymbol{x}_S + \epsilon \boldsymbol{n}(\boldsymbol{x}_S)$, where $\boldsymbol{x}_S$ is an arbitrary point on the surface, taking the dot product with $\boldsymbol{n}(\boldsymbol{x}_S)$, then taking the limit as ϵ goes to zero. The order of the processes, doing the integration and taking the limit, cannot be blindly interchanged, and some mathematical manipulations making use of the properties of the Green's function are necessary before one can obtain a relation in which all integrations are performed after all necessary limits are taken. The result is

$$-\mathfrak{L}_{II}(\boldsymbol{x}_S, \hat{p}_S) = \hat{f}_S(\boldsymbol{x}_S) + \mathfrak{H}_{II}(\boldsymbol{x}_S, \hat{f}_S) \,, \tag{3.568}$$

where the relevant operators are as given by

$$\mathfrak{L}_{II}(\boldsymbol{x}, \hat{p}_S) = [\boldsymbol{n}(\boldsymbol{x}_S) \times \nabla] \cdot \frac{1}{2\pi} \int [\boldsymbol{n}(\boldsymbol{x}'_S) \times \nabla' \hat{p}_S(\boldsymbol{x}'_S)] \times G(\boldsymbol{x}_S|\boldsymbol{x}'_S) \, \mathrm{d}S' + \frac{k^2}{2\pi} \times \int \boldsymbol{n}(\boldsymbol{x}_S) \cdot \boldsymbol{n}(\boldsymbol{x}'_S) \hat{p}_S(\boldsymbol{x}'_S) G(\boldsymbol{x}_S|\boldsymbol{x}'_S) \, \mathrm{d}S' \,, \tag{3.569}$$

$$\mathfrak{H}_{II}(\boldsymbol{x}_S, \hat{f}_S) = \frac{1}{2\pi} \int \hat{f}_S(\boldsymbol{x}'_S) \boldsymbol{n}(\boldsymbol{x}_S) \times [\nabla G(\boldsymbol{x}|\boldsymbol{x}'_S)]_{\boldsymbol{x}=\boldsymbol{x}_S} \, \mathrm{d}S' \,. \tag{3.570}$$

With regard to (3.569), one should note that the operator $\boldsymbol{n}(\boldsymbol{x}_S) \times \nabla$ involves only derivatives tangential to the surface, so that the integral on which it acts needs only be evaluated at surface points $\boldsymbol{x}_S$.

A variety of numerical techniques have been used and discussed in recent literature to solve either (3.564), (3.565), or (3.568), or some combination [3.83] of these for the surface pressure $\hat{p}_S$, given the surface force function $\hat{f}_S$. Once this is done, the radiation field at any external point $\boldsymbol{x}$ is found by numerical integration of the corollary integral relation of (3.562).

3.15 Waveguides, Ducts, and Resonators

External boundaries can channel sound propagation, and in some cases can create a buildup of acoustic energy within a confined space.

3.15.1 Guided Modes in a Duct

Pipes or ducts act as guides of acoustic waves, and the net flow of energy, other than that associated with wall dissipation, is along the direction of the duct. The general theory of guided waves applies and leads to a representation in terms of guided modes.

If the duct axis is the x-axis and the duct cross section is independent of x, the guided mode series [3.4, 84] has the form

$$\hat{p} = \sum_n X_n(x) \Psi_n(y, z) \,, \tag{3.571}$$

where the $\Psi_n(y, z)$ are eigenfunctions of the equation

$$\left(\frac{\partial^2}{\partial y^2} + \frac{\partial^2}{\partial z^2} \right) \Psi_n + \alpha_n^2 \Psi_n = 0 \,, \tag{3.572}$$

with the α_n^2 being the corresponding eigenvalues. The appropriate boundary condition, if the duct walls are idealized as being perfectly rigid, is that the normal component of the gradient of Ψ_n vanishes at the walls. Typically, the Ψ_n are required to conform to some normalization condition, such as

$$\int \Psi_n^2 \, \mathrm{d}A = A \,, \tag{3.573}$$

where A is the duct cross-sectional area.

The general theory leads to the conclusion that one can always find a complete set of Ψ_n, which with the

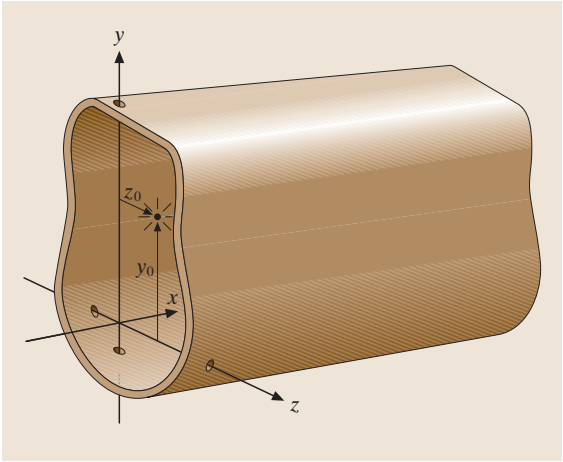


Fig. 3.41 Generic sketch of a duct that carries guided sound waves

rigid wall boundary condition imposed, are such that the cross-sectional eigenfunctions are orthogonal, so that

$$\int \Psi_{\mathrm{n}} \Psi_m \, \mathrm{d}A = 0 \tag{3.574}$$

if n and m correspond to different guided modes. The eigenvalues α_{n}^2, moreover, are all real and nonnegative. However, for cross sections that have some type of symmetry, it may be that more than one linearly independent eigenfunction Ψ_{n} (modes characterized by different values of the index n) correspond to the same numerical value of α_{n}^2. In such cases the eigenvalue is said to be degenerate.

The variation of guided mode amplitudes with source excitation is ordinarily incorporated into the axial wave functions $X_{\mathrm{n}}(x)$, which satisfy the one-dimensional Helmholtz equation

$$\frac{\mathrm{d}^2 X_{\mathrm{n}}}{\mathrm{d}x^2} + (k^2 - \alpha^2) X_{\mathrm{n}} = 0 \, . \tag{3.575}$$

Here $k = \omega/s$ is the free-space wavenumber. The form of the solution depends on whether α_{n}^2 is greater or less than k^2. If $\alpha_{\mathrm{n}}^2 < k^2$, the mode is said to be a propagating mode and the solution for X_{n} is given by

$$X_{\mathrm{n}} = A_{\mathrm{n}} \mathrm{e}^{\mathrm{i}k_{\mathrm{n}}x} + B_{\mathrm{n}} \mathrm{e}^{-\mathrm{i}k_{\mathrm{n}}x} \, , \tag{3.576}$$

where the k_{n}, defined by

$$k_{\mathrm{n}} = (k^2 - \alpha_{\mathrm{n}}^2)^{1/2} \, , \tag{3.577}$$

are the modal wavenumbers. However, if the value of α_{n}^2 is greater than k^2, the mode is evanescent (not propagating), and one has

$$X_{\mathrm{n}} = A_{\mathrm{n}} \mathrm{e}^{-\beta_{\mathrm{n}}x} + B_{\mathrm{n}} \mathrm{e}^{\beta_{\mathrm{n}}x} \, , \tag{3.578}$$

where β_{n} is given by

$$\beta_{\mathrm{n}} = (\alpha_{\mathrm{n}}^2 - k^2)^{1/2} \, . \tag{3.579}$$

Unless the termination of the duct is relatively close to the source, waves that grow exponentially with distance from the source are not meaningful, so only the term that corresponds to exponentially dying waves is ordinarily kept in the description of sound fields in ducts.

3.15.2 Cylindrical Ducts

For a duct with circular cross section and radius a, the index n is replaced by an index set (q, m, s), and the eigenfunctions Ψ_{n} are described by

$$\Psi_{\mathrm{n}} = K_{qm} J_m \left(\frac{\eta_{qm} w}{a} \right) \left\{ \begin{matrix} \cos m\phi \\ \sin m\phi \end{matrix} \right\} \, . \tag{3.580}$$

Here either the cosine ($s = 1$) or the sine ($s = -1$) corresponds to an eigenfunction. The quantities K_{qm} are normalization constants, and the J_m are Bessel functions of order m. The corresponding eigenvalues are given by

$$\alpha_{\mathrm{n}} = \eta_{qm}/a \, , \tag{3.581}$$

where the η_{qm} are the zeros of $\eta J_m'(\eta)$, arranged in ascending order with the index q ranging upwards from 1. The smaller roots [3.85] for the axisymmetric modes are $\eta_{1,0} = 0.00$, $\eta_{2,0} = 3.83171$, and $\eta_{3,0} = 7.01559$, while those corresponding to $m = 1$ are $\eta_{1,1} = 1.84118$, $\eta_{2,1} = 5.33144$, and $\eta_{3,1} = 8.53632$.

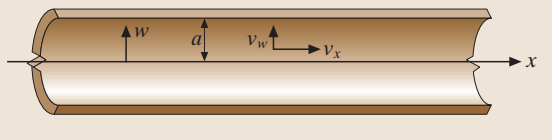


Fig. 3.42 Cylindrical duct

3.15.3 Low-Frequency Model for Ducts

In many situations of interest, the frequency of the acoustic disturbance is so low that only one guided mode can propagate, and all other modes are evanescent. Given that the walls can be idealized as rigid, there is always one mode that can propagate, this being the plane wave

Amazon EX1014 Page 110

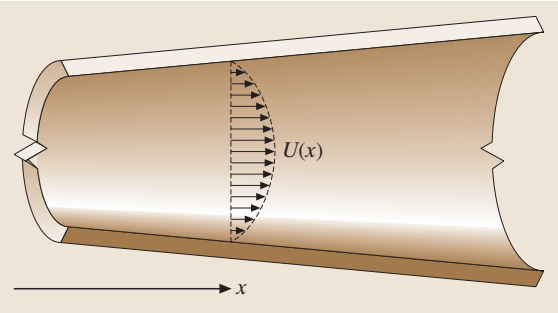


Fig. 3.43 Volume velocity in a duct

mode for which the eigenvalue α_0 is identically zero. The other modes will all be evanescent if the value of k is less than the corresponding α_n for each such mode. This would be so if the frequency is less than the lowest cutoff frequency for any of the nonplanar modes. For the circular duct case discussed above, for example, this would require that the inequality,

$$f < \frac{1.84118}{2\pi}\frac{c}{a}\,, \tag{3.582}$$

be satisfied.

When the single-guided-mode assumption is valid, and even if the duct cross-sectional area should vary with distance along the duct, the acoustic field equations can be replaced to a good approximation by the acoustic transmission-line equations,

$$\frac{\partial p}{\partial t} + \frac{\rho c^2}{A}\frac{\partial U}{\partial x} = 0\,, \tag{3.583}$$

$$\rho\frac{\partial U}{\partial t} = -A\frac{\partial p}{\partial x}\,. \tag{3.584}$$

Here U, equal to Av_x, is the volume velocity, the volume of fluid passing through the duct per unit time.

One of the implications of the low-frequency model described by (3.583) and (3.584) is that the volume velocity and the pressure are both continuous, even when the duct has a sudden change in cross-sectional area. The pressure continuity assumption is not necessarily a good approximation, but becomes better with decreasing frequency. An improved model (continuous volume-velocity two-port) takes the volume velocities on both sides of the junction as being equal, and sets the difference of the complex amplitudes of the upstream and downstream pressures just ahead and after the junction to

$$\hat{p}_{\text{ahead}} - \hat{p}_{\text{after}} = Z_J\hat{U}_{\text{junction}}\,, \tag{3.585}$$

where the junction's acoustic impedance Z_J is taken in the simplest approximation as $-\mathrm{i}\omega M_{A,J}$, and where

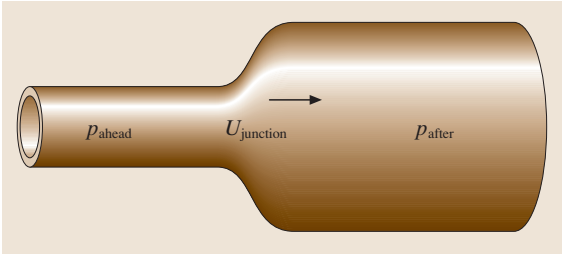


Fig. 3.44 Two dissimilar ducts with a junction modeled as a continuous volume velocity two-port. The difference in pressures is related to the volume velocity by the junction impedance

$M_{A,J}$ is a real number independent of frequency that is called the acoustic inertance of the junction. Approximate expressions for this acoustic inertance can be found in the literature [3.78, 86–88]; a simple rule is that it is ordinarily less than $8\rho/3A_{\min}$, where $A_{\min}$ is the smaller of the two cross-sectional areas. One may note, moreover, that Z_J goes to zero when the frequency goes to zero.

When an incident wave is incident at a junction, reflected and transmitted waves are created in the two ducts. The pressure amplitude reflection and transmission coefficients are given by

$$\mathfrak{R} = \frac{Z_J + \rho c/A_2 - \rho c/A_1}{Z_J + \rho c/A_2 + \rho c/A_1}\,, \tag{3.586}$$

$$\mathfrak{T} = \frac{2\rho c/A_2}{Z_J + \rho c/A_2 + \rho c/A_1}\,. \tag{3.587}$$

At sufficiently low frequencies, these are further approximated by replacing Z_J by zero.

3.15.4 Sound Attenuation in Ducts

The presence of the duct walls affects the attenuation of sound and usually causes the attenuation coefficient to be much higher than for plane waves in open space.

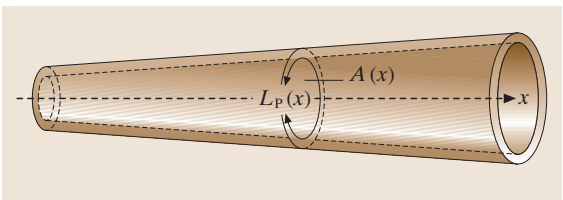


Fig. 3.45 Geometrical parameters pertaining to acoustic attenuation in a duct. The total length L_P around the perimeter gives the transverse extent of the dissipative boundary layer at the duct wall

Amazon EX1014 Page 111

A simple theory for predicting this attenuation uses the concepts of acoustic, entropy, and vorticity modes, as is indicated by the decomposition of (3.89) in a previous section of this chapter. The entropy and vorticity mode fields exist in an acoustic boundary layer near the duct walls and are such that they combine with the acoustic mode field to satisfy the appropriate boundary conditions at the walls.

With viscosity and thermal conduction thus taken into account in the acoustic boundary layer, and with the assumption that the duct walls are much better heat conductors than the fluid itself, the approximate attenuation coefficient for the plane wave guided mode is given by [3.89]

$$\alpha = \alpha_{\text{walls}} = \left(\frac{\omega}{8\rho c^2}\right)^{1/2} \left[\mu^{1/2} + (\gamma - 1)(\kappa/c_p)^{1/2}\right] \frac{L_P}{A} , \tag{3.588}$$

where L_P is the length of the perimeter of the duct cross section.

A related effect [3.90] is that sound travels slightly slower in ducts than in an open environment. The complex wavenumber corresponding to propagation down the axis of the tube is approximately

$$k \approx \frac{\omega}{c} + (1 + \mathrm{i})\alpha_{\text{walls}} , \tag{3.589}$$

and the phase velocity is consequently approximately

$$v_{\text{ph}} = \frac{\omega}{k_R} \approx c - \frac{c^2 \alpha_{\text{walls}}}{\omega} . \tag{3.590}$$

For a weakly attenuated and weakly dispersive wave, the group velocity [3.74], the speed at which energy travels, is approximately

$$v_{\text{gr}} \approx \left(\frac{\mathrm{d}k_R}{\mathrm{d}\omega}\right)^{-1} , \tag{3.591}$$

so, for the present situation,

$$v_{\text{gr}} \approx c - \frac{c^2 \alpha_{\text{walls}}}{2\omega} . \tag{3.592}$$

Thus both the phase velocity and the group velocity are less than the nominal speed of sound.

3.15.5 Mufflers and Acoustic Filters

The analysis of mufflers [3.91, 92] is often based on the idealization that their acoustic transmission characteristics are independent of sound amplitudes, so they act as linear devices. The muffler is regarded as an insertion into a duct, which reflects waves back toward the source and which alters the transmission of sound beyond the muffler. The properties of the muffler vary with frequency, so the theory analyzes the muffler's effects on individual frequency components. The frequency is assumed to be sufficiently low that only the plane wave mode propagates in the inlet and outlet ducts. Because of the assumed linear behavior of the muffler, and the single-mode assumption, the muffler conforms to the model of a linear two-port, the ports being the inlet and outlet. The model leads to the prediction that one may characterize the muffler at any given frequency by a matrix, such that

$$\begin{pmatrix} \hat{p}_{\text{in}} \\ \hat{p}_{\text{out}} \end{pmatrix} = \begin{pmatrix} K_{11} & K_{12} \\ K_{21} & K_{22} \end{pmatrix} \begin{pmatrix} \hat{U}_{\text{in}} \\ \hat{U}_{\text{out}} \end{pmatrix} , \tag{3.593}$$

where the coefficients K_{ij} represent the acoustical properties of the muffler. Reciprocity [3.30] requires that the determinant of the matrix be unity. Also, for a symmetric muffler, K_{12} and K_{21} must be identical.

It is ordinarily a good approximation that the waves reflected at the entrance of the muffler back to the source are significantly attenuated, so that they have negligible amplitude when they return to the muffler. Similarly, the assumption that the waves transmitted beyond the muffler do not return to the muffler (anechoic termination)

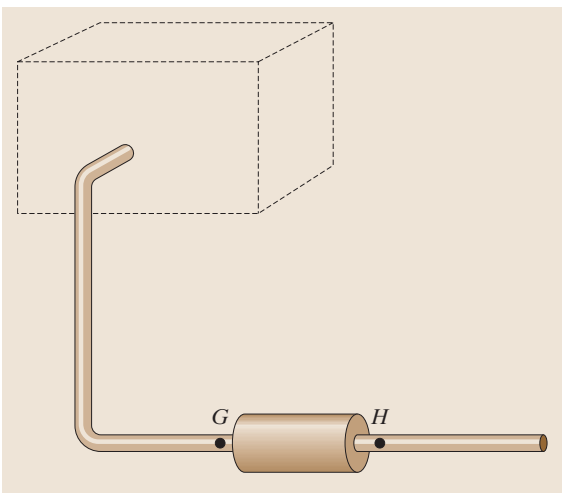


Fig. 3.46 Sketch of a prototype muffler configuration. Point G is a point on the input side of the muffler, and point H is on the output side. The noise source is upstream on the input side, and the tailpipe is downstream on the output side

is ordinarily valid. With these assumptions, the insertion of the muffler causes the mean squared pressure downstream of the muffler to drop by a factor

$$\tau = \left(\frac{1}{4}|K_{11} + K_{22} + \frac{\rho c}{A}K_{21} + \frac{A}{\rho c}K_{12}|^2\right)^{-1}, \quad (3.594)$$

where A is the cross section of the duct ahead of and behind the muffler.

Acoustic mufflers can be divided into two broad categories: reactive mufflers and dissipative mufflers. In a reactive muffler, the basic property of the muffler is that it reflects a substantial fraction of the incident acoustic energy back toward the source. The dissipation of energy within the muffler itself plays a minor role; the reflection is caused primarily by the geometrical characteristics of the muffler. In a dissipative muffler, however, a low transmission of sound is achieved by internal dissipation of acoustic energy within the muffler. Absorbing material along the walls is ordinarily used to achieve this dissipation.

3.15.6 Non-Reflecting Dissipative Mufflers

When a segment of pipe of cross section A and length L is covered with a duct lining material that attenuates the amplitude of traveling plane waves by a factor of $e^{-\alpha L}$,

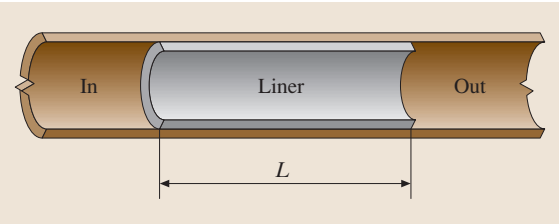


Fig. 3.47 Sketch of a nonreflective dissipative muffler

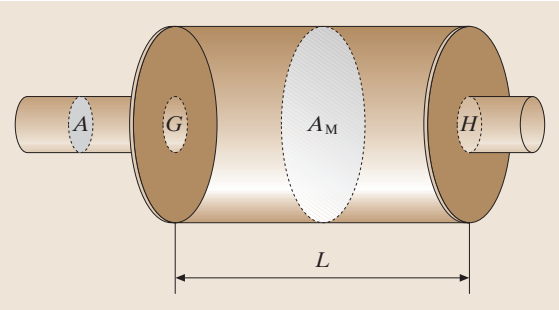


Fig. 3.48 Sketch of an expansion chamber muffler

the muffler's K-matrix is given by

$$K = \begin{pmatrix} \cos(kL + i\alpha L) & -i\frac{\rho c}{A}\sin(kL + i\alpha L) \\ -i\frac{A}{\rho c}\sin(kL + i\alpha L) & \cos(kL + i\alpha L) \end{pmatrix}, \quad (3.595)$$

so the fractional drop in mean squared pressure reduces to

$$\tau = e^{-2\alpha L}. \quad (3.596)$$

3.15.7 Expansion Chamber Muffler

The simplest reactive muffler is the expansion chamber, which consists of a duct of length L and cross section A_M connected at both ends to a pipe of smaller cross section A_P.

The K-matrix for such a muffler is found directly from (3.595) by setting α to zero (no dissipation in the chamber), but replacing A by A_M. The corresponding result for the fractional drop in mean squared pressure is

$$\tau = \left[\cos^2 kL + \frac{1}{4}(m + m^{-1})^2 \sin^2 kl\right]^{-1}, \quad (3.597)$$

where m is the expansion ratio A_M/A_P. The relative reduction in mean square pressure is thus periodic with frequency. A maximum reduction occurs when the length L is an odd multiple of quarter-wavelengths. The greatest reduction in mean squared pressure is when τ has its minimum value, which is that given by

$$\tau = \frac{4}{(m + m^{-1})^2}. \quad (3.598)$$

3.15.8 Helmholtz Resonators

An idealized acoustical system [3.47, 93] that is the prototype of commonly encountered resonance phenomena

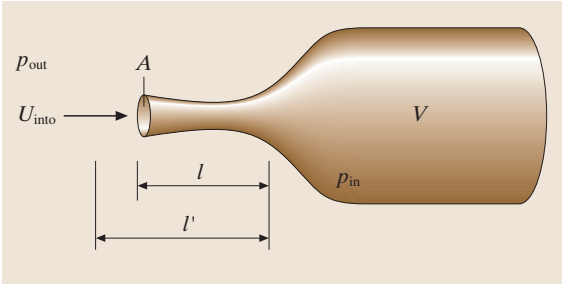


Fig. 3.49 Sketch of a Helmholtz resonator, showing the characteristic parameters involved in the analysis

consists of a cavity of volume V with a neck of length ℓ and cross-sectional area A.

In the limit where the acoustic frequency is sufficiently low that the wavelength is much larger than any dimension of the resonator, the compressible fluid in the resonator acts as a spring with spring constant

$$k_{\mathrm{sp}} = \frac{\rho c^2 A^2}{V} , \tag{3.599}$$

and the fluid in the neck behaves as a lumped mass of magnitude

$$m = \rho A \ell' . \tag{3.600}$$

Here ℓ' is ℓ plus the end corrections for the two ends of the neck. If ℓ is somewhat larger than the neck radius a, and if both ends are terminated by a flange, then the two end corrections are each $0.82a$. (The determination of end corrections has an extensive history; a discussion can be found in the text by the author [3.30].) The resonance frequency ω_{r}, in radians per second, of the resonator is given by

$$\omega_{\mathrm{r}} = 2\pi f_{\mathrm{r}} = (k_{\mathrm{sp}}/m)^{1/2} = (M_{\mathrm{A}} C_{\mathrm{A}})^{-1/2} , \tag{3.601}$$

where

$$M_{\mathrm{A}} = \rho \ell' / S \tag{3.602}$$

gives the acoustic inertance of the neck and

$$C_{\mathrm{A}} = V/\rho c^2 \tag{3.603}$$

gives the acoustic compliance of the cavity. The ratio of the complex pressure amplitude just outside the mouth of the neck to the complex volume velocity amplitude of flow into the neck is the acoustic impedance Z_{HR} of the Helmholtz resonator and given, with the neglect of damping, by

$$Z_{\mathrm{HR}} = -\mathrm{i}\omega M_{\mathrm{A}} + \frac{1}{-\mathrm{i}\omega C_{\mathrm{A}}} , \tag{3.604}$$

which vanishes at the resonance frequency.

If a Helmholtz resonator is inserted as a side branch into the wall of a duct, it acts as a reactive muffler that has a high insertion loss near the resonance frequency of the resonator. The analysis assumes that the acoustic pressures in the duct just before and just after the resonator are the same as the pressure at the mouth of the resonator. Also, the acoustical analog of Kirchhoff's circuit law for currents applies, so that the volume velocity flowing in the duct ahead of the resonator equals the sum of the volume velocities flowing into the resonator and through the duct just after the resonator. These relations, with (3.604), allow one to work out expressions for the amplitude reflection and transmission coefficients at the resonator, the latter being given by

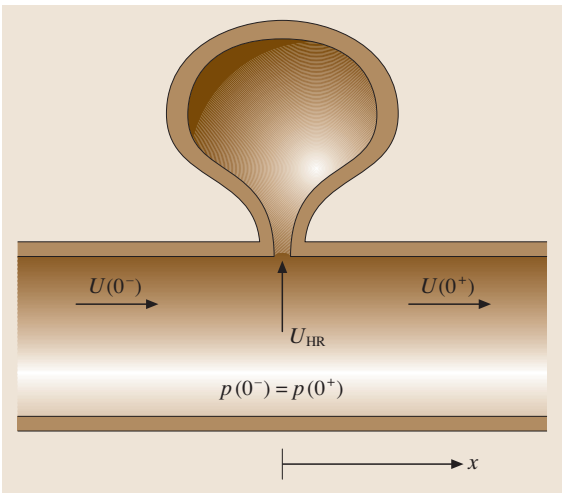


Fig. 3.50 Helmholtz resonator as a side-branch in a duct

$$\mathfrak{T} = \frac{2Z_{\mathrm{HR}}}{2Z_{\mathrm{HR}} + \rho c/A_{\mathrm{D}}} . \tag{3.605}$$

The fraction of incident power that is transmitted is consequently given by

$$\tau = \left(1 + \frac{1}{4\beta^2 (f/f_{\mathrm{r}} - f_{\mathrm{r}}/f)^2}\right)^{-1} , \tag{3.606}$$

where β is determined by

$$\beta^2 = (M_{\mathrm{A}}/C_{\mathrm{A}})(A_{\mathrm{D}}/\rho c)^3 . \tag{3.607}$$

The fraction transmitted is formally zero at the resonance frequency, but if β is large compared with unity, the bandwidth over which the drop in transmitted power is small is narrow compared with f_{r}.

3.16 Ray Acoustics

When the medium is slowly varying over distances comparable to a wavelength and if the propagation distances are substantially greater than a wavelength, it is often convenient to regard acoustic fields as being carried

along rays. These can be regarded as lines or paths in space.

3.16.1 Wavefront Propagation

A wavefront is a hypothetical surface in space over which distinct waveform features are simultaneously received. The theory of plane wave propagation predicts that wavefronts move locally with speed c when viewed in a coordinate system in which the ambient medium appears at rest. If the ambient medium is moving with velocity $\boldsymbol{v}$, the wave velocity $c\boldsymbol{n}$ seen by someone moving with the fluid becomes $\boldsymbol{v}+c\boldsymbol{n}$ in a coordinate system at rest. Here $\boldsymbol{n}$ is the unit vector normal to the wavefront; it coincides with the direction of propagation if the coordinate system is moving with the local ambient fluid velocity $\boldsymbol{v}$. A ray can be defined [3.94] as the time trajectory of a point that is always on the same wavefront, and for which the velocity is

$$\boldsymbol{v}_{\text{ray}} = \boldsymbol{v} + \boldsymbol{n}c \,. \tag{3.608}$$

To determine ray paths without explicit knowledge of wavefronts, it is appropriate to consider a function $\tau(\boldsymbol{x})$, which gives the time at which the wavefront of interest passes the point $\boldsymbol{x}$. Its gradient $\boldsymbol{s}$ is termed the wave slowness vector and is related to the local wavefront

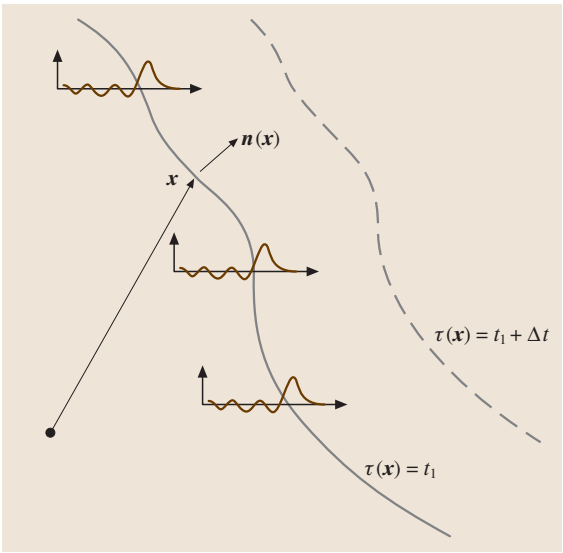


Fig. 3.51 Sketch illustrating the concept of a wavefront as a surface along which characteristic waveform features are simultaneously received. The time a given waveform passes a point $\boldsymbol{x}$ is $\tau(\boldsymbol{x})$ and the unit normal in the direction of propagation is $\boldsymbol{n}(\boldsymbol{x})$

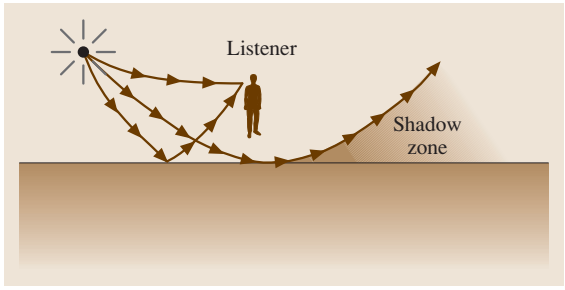


Fig. 3.52 Multipaths and shadow zones. The situation depicted is when the sound speed decreases with distance above the ground so that rays are refracted upward

normal by the equations

$$\boldsymbol{s} = \frac{\boldsymbol{n}}{c + \boldsymbol{v}\cdot\boldsymbol{n}} \,, \tag{3.609}$$

$$\boldsymbol{n} = \frac{c\boldsymbol{s}}{\Omega} \,, \tag{3.610}$$

where the quantity Ω is defined by

$$\Omega = 1 - \boldsymbol{v}\cdot\boldsymbol{s} \,. \tag{3.611}$$

Given the concepts of ray position and the slowness vector, a purely kinematical derivation leads to the ray-tracing equations

$$\frac{\mathrm{d}\boldsymbol{x}}{\mathrm{d}t} = \frac{c^2\boldsymbol{s}}{\Omega} + \boldsymbol{v} \,, \tag{3.612}$$

$$\frac{\mathrm{d}\boldsymbol{s}}{\mathrm{d}t} = -\frac{\Omega}{c}\nabla c - (\boldsymbol{s}\cdot\nabla)\boldsymbol{v} - \boldsymbol{s}\times(\nabla\times\boldsymbol{v}) \,. \tag{3.613}$$

Simpler versions result when there is no ambient flow, or when the ambient variables vary with only one coordinate. If the ambient variables are independent of position, then the ray paths are straight lines.

The above equations are often used for analysis of propagation through inhomogeneous media (moving or nonmoving) when the ambient variables do not vary significantly over distances of the order of a wavelength, even though they may do so over the total propagation distance. The rays that connect the source and listener locations are termed the eigenrays for that situation. If there is more than one eigenray, one has multipath reception. If there is no eigenray, then the listener is in a shadow zone.

3.16.2 Reflected and Diffracted Rays

This theory is readily extended to take into account solid boundaries and interfaces. When an incident ray strikes a solid boundary, a reflected ray is generated whose

direction is determined by the trace velocity matching principle, such that angle of incidence equals angle of reflection. At an interface a transmitted ray is also generated, whose direction is predicted by Snell's law.

An extension of the theory known as the geometrical theory of diffraction and due primarily to *Keller* [3.95] allows for the possibility that diffracting edges can be a source of diffracted rays which have a multiplicity of directions. The allowable diffracted rays must have the same trace velocity along the diffracting edge as does the incident ray.

The ray paths connecting the source and listener satisfy *Fermat*'s principle [3.96], that the travel time along an actual eigenray is stationary relative to other geometrically admissible paths. *Keller*'s geometrical theory of diffraction [3.95] extends this principle to include paths which have discontinuous directions and which may have portions that lie on solid surfaces.

3.16.3 Inhomogeneous Moving Media

Determination of the amplitude variation along ray paths requires a more explicit use of the equations of linear acoustics. If there is no ambient fluid velocity then an appropriate wave equation is (3.73). When there is also an ambient flow present then an appropriate generalization [3.97, 98] for the acoustic mode is

$$\frac{1}{\rho}\nabla\cdot(\rho\nabla\Phi) - \mathrm{D_t}\left(\frac{1}{c^2}\mathrm{D_t}\Phi\right) = 0\,. \tag{3.614}$$

Here $\mathrm{D_t}$, defined by

$$\mathrm{D_t} = \frac{\partial}{\partial t} + \boldsymbol{v}\cdot\nabla \tag{3.615}$$

is the time derivative following the ambient flow. The dependent variable Φ is related to the acoustic pressure perturbation by

$$p = -\rho\mathrm{D_t}\Phi\,. \tag{3.616}$$

This wave equation is derived from the linear acoustics equations for circumstances when the ambient variables vary slowly with position and time and neglects terms of second order in $1/\omega T$ and $c/\omega L$, where ω is a characteristic frequency of the disturbance, T is a characteristic time scale for temporal variations of the ambient quantities, and L is a characteristic length scale for spatial variations of these approximations. The nature of the entailed approximations is consistent with the notion that geometrical acoustics is a high-frequency approximation and yields results that are the same in the high-frequency limit as would be derived from the complete set of linear acoustic equations.

3.16.4 The Eikonal Approximation

The equations of geometrical acoustics follow [3.99] from (3.614), if one sets the potential function Φ equal to the expression

$$\Phi(\boldsymbol{x}, t) = \Psi(\boldsymbol{x})F(t-\tau)\,. \tag{3.617}$$

Here the function F is assumed to be a rapidly varying function of its argument. The quantities Ψ and τ vary only with position. (It is assumed here that the ambient variables do not vary with time.)

When such a substitution is made, one obtains terms that involve the second, first, and zeroth derivatives of the function F. The geometrical acoustics or eikonal approximation results when one requires that the coefficients of F'' and F' both vanish identically, and thus assumes that the terms involving undifferentiated F are of lesser importance in the high-frequency limit. The setting to zero of the coefficient of the second derivative yields

$$(1-\boldsymbol{v}\cdot\nabla\tau)^2 = c^2\,(\nabla\tau)^2\ , \tag{3.618}$$

which is termed the eikonal equation [3.100, 101]. The setting to zero of the coefficient of the first derivative yields

$$\nabla\cdot\left\{\frac{\rho\Psi^2}{c^2}[c^2\nabla\tau + (1-\boldsymbol{v}\cdot\nabla\tau)\boldsymbol{v}]\right\} = 0\,, \tag{3.619}$$

which is termed the transport equation. The convenient property of these equations is that they are independent of the nature of the waveform function F.

The eikonal equation, which is a nonlinear first-order partial differential equation for the eikonal $\tau(\boldsymbol{x})$ can be solved by Cauchy's method of characteristics, with $\boldsymbol{s} = \nabla\tau$. What results are the ray-tracing equations (3.612) and (3.613). However, the time variable t is replaced by the eikonal τ. The manner in which these equations solve the eikonal equation is such that if τ and its gradient $\boldsymbol{s}$ are known at any given point then the ray-tracing equations determine these same quantities at all other points on the ray that passes through this initial point. The initial value of $\boldsymbol{s}$ must conform to the eikonal equation itself, as is stated in (3.618). If this is so, then the ray-tracing equations insure that it conforms to the same equation, with the appropriate ambient variables, all along the ray.

Solution of the transport equation, given by (3.619), is facilitated by the concept of a ray tube. One conceives

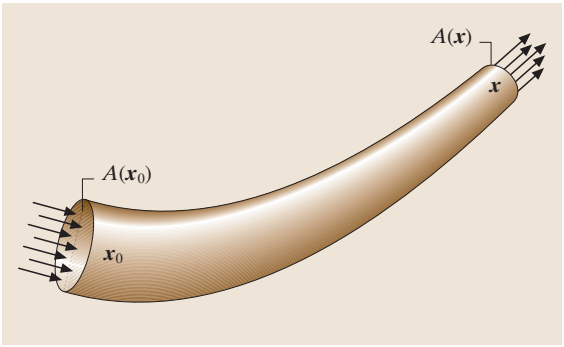


Fig. 3.53 Sketch of a ray tube. Here $\boldsymbol{x}_0$ and $\boldsymbol{x}$ are two points on the central ray

of a family of adjacent rays which comprise a narrow tube of cross-sectional area A, this area varying with distance ℓ along the path of the central ray of the tube. Then the transport equation reduces to

$$\frac{\mathrm{d}}{\mathrm{d}\ell}\left(A\frac{\rho\Psi^2}{c^2}\Omega v_{\mathrm{ray}}\right)=0\,, \tag{3.620}$$

so the quantity in brackets is constant along the ray tube.

Alternately, the relation of (3.616) implies that the acoustic pressure is locally given to an equivalent approximation by

$$p=P(\boldsymbol{x})f(t-\tau)\,, \tag{3.621}$$

where f is the derivative of F, and P is related to Ψ by

$$P=-\rho\Omega\Psi\,. \tag{3.622}$$

Then the transport equation (3.619) requires that

$$B=\frac{A\;P^2 v_{\mathrm{ray}}}{\rho c^2\Omega} \tag{3.623}$$

be constant along a ray tube, so that

$$\frac{\mathrm{d}B}{\mathrm{d}\ell}=0\,. \tag{3.624}$$

This quantity B is often referred to as the Blokhintzev invariant.

If there is no ambient flow then the constancy of B along a ray tube can be regarded as a statement that the average acoustic power flowing along the ray tube is constant, for a constant-frequency disturbance, or in general that the power appears constant along a trajectory moving with the ray velocity. The interpretation when there is an ambient flow is that the wave action is conserved [3.102].

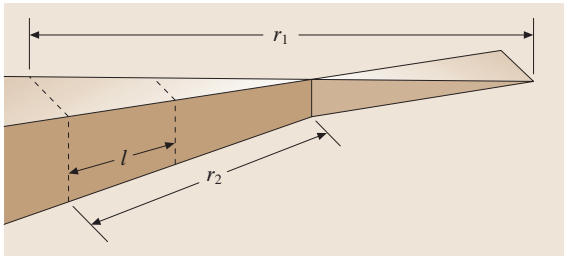


Fig. 3.54 Rectilinear propagation of sound. The wavefront at any point has two principal radii of curvature, which change with the propagation distance. In the case shown, the wavefront at the left is such that it is convex, with two different focal lengths, r_1 and r_2, these being the two radii of curvature. Over a short propagation distance ℓ, these reduce to $r_1-\ell$ and $r_2-\ell$

Geometrical acoustics (insofar as amplitude prediction is concerned) breaks down at caustics, which are surfaces along which the ray tube areas vanish. Modified versions [3.103, 104] involving Airy functions and higher transcendental functions, of the geometrical acoustics theory have been derived which overcome this limitation.

3.16.5 Rectilinear Propagation of Amplitudes

A simple but important limiting case of geometrical acoustics is for propagation in homogeneous nonmoving media. The rays are then straight lines and perpendicular to wavefronts. A given wavefront has two principal radii of curvature, R_{I} and R_{II}. With the convention that these are positive when the wavefront is concave in the corresponding direction of principal curvature, and negative when it is convex, the curvature radii increase by a distance ℓ when the wave propagates through that distance. The ray tube area is proportional to the product of the two curvature radii, so the acoustic pressure varies with distance ℓ along the ray as

$$p=\left(\frac{R_{\mathrm{I}}R_{\mathrm{II}}}{(R_{\mathrm{I}}+\ell)(R_{\mathrm{II}}+\ell)}\right)^{1/2} f[t-(\ell/c)])\,. \tag{3.625}$$

Here R_{I} and R_{II} are the two principal radii of curvature when ℓ is zero. The relations (3.326) and (3.447) for spherical and cylindrical spreading are both limiting cases of this expression.

Amazon EX1014 Page 117

3.17 Diffraction

The bending of sound around corners or around objects into shadow zones is typically referred to as diffraction. The prototype for problems of diffraction around an edge is that of a plane wave impinging on a rigid half-plane (knife edge). The problem was solved exactly by *Sommerfeld* [3.105], and the solution has subsequently been rederived by a variety of other methods. The present chapter considers a generalization of this problem where a point source is near a rigid wedge. The Sommerfeld problem emerges as a limiting case.

3.17.1 Posing of the Diffraction Problem

The geometry adopted here is such that the right surface of the wedge occupies the region where $y = 0$ and $x > 0$; the diffracting edge is the z-axis. A cylindrical coordinate system is used where w is the radial distance from the z axis and where ϕ is the polar angle measured counterclockwise from the x-axis. The other surface of the wedge is at $\phi = \beta$, where $\beta > \pi$. The region occupied by the wedge has an interior angle of $2\pi - \beta$.

One seeks solutions of the inhomogeneous wave equation

$$\nabla^2 p - \frac{1}{c^2}\frac{\partial^2 p}{\partial t^2} = -4\pi S(t)\delta(\boldsymbol{x} - \boldsymbol{x_0}) \qquad (3.626)$$

for the region

$$0 < \phi < \beta\,; \quad w \geq 0\,; \quad -\infty < z < \infty\,. \qquad (3.627)$$

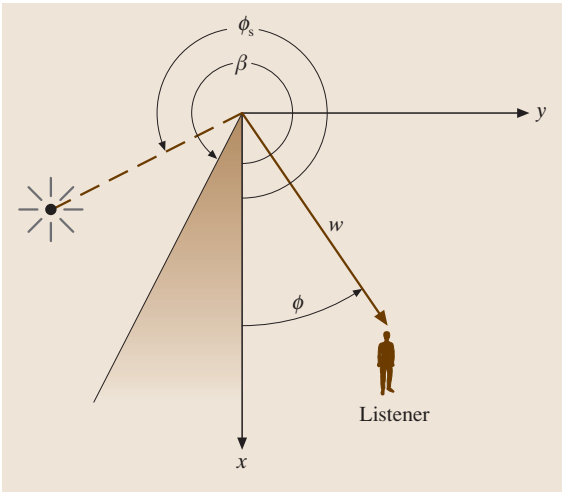


Fig. 3.55 Coordinate system and angles associated with the diffraction of sound by a wedge

The point source is located at $w = w_S$, $\phi = \phi_S$, and $z = 0$. It is assumed that the source is on the back side, so that $\phi_S > \pi$. (A person on the front face of the wedge should not be able to see the source.)

The quantity $S(t)$ is the time-dependent source strength, so that the transient acoustic pressure field near the source has a singular part given by

$$p \approx \frac{S\,[t - (R_D/c)]}{R_D}\,, \qquad (3.628)$$

where R_D is the direct distance from the source,

$$R_D = \Big[(w\cos\phi - w_S\cos\phi_S)^2 + (w\sin\phi - w_S\sin\phi_S)^2 + z^2\Big]^{1/2}\,, \qquad (3.629)$$

or

$$R_D = \left[w^2 + w_S^2 - 2ww_S\cos(\phi - \phi_S) + z^2\right]^{1/2}. \qquad (3.630)$$

Boundary conditions imposed by the rigid surfaces of the wedge are

$$\frac{\partial p}{\partial \phi} = 0 \quad \text{at} \quad \phi = 0 \quad \text{and at} \quad \phi = \beta. \qquad (3.631)$$

There is also the requirement that the field at large radial distance w should represent an outgoing wave.

3.17.2 Rays and Spatial Regions

For the problem just posed, one can distinguish three regions, one where both a direct wave and a reflected wave are possible, one where only the direct wave is

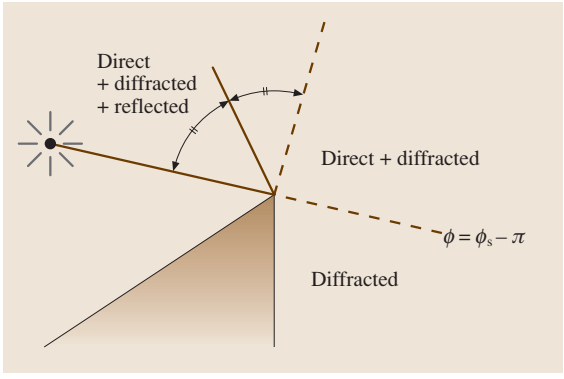


Fig. 3.56 Spatial regions associated with sound diffraction by a wedge

possible, and one where neither the direct wave nor the reflected wave is possible. The borders of these two regions are the angles ϕ_A and ϕ_B, where

$$\phi_A = \phi_S - \pi \; ; \qquad \phi_B = 2\beta - \phi_S - \pi \; . \tag{3.632}$$

Reflected Wave Possible

In this region, characterized by the largest values of the azimuthal angle ϕ, the restriction is

$$\beta > \phi > \phi_B \; . \tag{3.633}$$

For such azimuthal angles, one can have an incident ray that hits the back side ($\phi = \beta$) of the wedge, reflects according to the law of mirrors, and then passes through the listener point. This reflected wave come from the image source location at $\phi = 2\beta - \phi_S$, $w = w_S$, $z = 0$. The path distance for this reflected wave arrival is

$$R_R = \Big[w^2 + w_S^2 - 2ww_S \cos(\phi + \phi_S - 2\beta) + z^2 \Big]^{1/2} \; . \tag{3.634}$$

The requirement that defines the border of this region is that any hypothetical straight line from the image source to the listener must pass through the back side of the wedge. Equivalently stated, there must be a reflection point on the back face of the wedge itself.

In this region, the geometrical acoustics (GA) portion of the acoustic pressure field is given by

$$p_{GA} = \frac{S\,[t - (R_D/c)]}{R_D} + \frac{S\,[t - (R_R/c)]}{R_R} \; . \tag{3.635}$$

Along the plane where $\phi = \phi_B$, the reflected path distance becomes

$$R_R \to L \quad \text{as} \quad \phi \to \phi_B \; , \tag{3.636}$$

where

$$L = \big[(w + w_0)^2 + z^2 \big]^{1/2} \; . \tag{3.637}$$

The discontinuity in the geometrical acoustics portion caused by the dropping of the reflected wave is consequently

$$p_{GA}(\phi_B + \epsilon) - p_{GA}(\phi_B - \epsilon) = \frac{S\,[t - (L/c)]}{L} \; . \tag{3.638}$$

Here the dependence of interest is that on the angular coordinate ϕ; the quantity ϵ is an arbitrarily small positive number.

Direct Wave, No Reflected Wave

This is the region of intermediate values of the azimuthal angle ϕ, where

$$\phi_B > \phi > \phi_A \; , \tag{3.639}$$

and the listener can still see the source directly, but the listener cannot see the reflection of the source on the backside of the wedge. There is a direct wave, but no reflected wave.

Here the geometrical acoustics (GA) portion of the acoustic pressure field is given by

$$p_{GA} = \frac{S\,[t - (R_D/c)]}{R_D} \; . \tag{3.640}$$

At the lower angular boundary ϕ_A of this region the direct wave propagation distance becomes

$$R_D \to L \quad \text{as} \quad \phi \to \phi_A \; , \tag{3.641}$$

where L is the same length as defined above in (3.637).

The discontinuity in the geometrical acoustics portion caused by the dropping of the incident wave is consequently

$$p_{GA}(\phi_A + \epsilon) - p_{GA}(\phi_A - \epsilon) = \frac{S\,[t - (L/c)]}{L} \; , \tag{3.642}$$

which is the same expression as for the discontinuity at ϕ_B.

No Direct Wave, No Reflected Wave

In this region, where

$$\phi_A > \phi > 0 \; , \tag{3.643}$$

the listener is in the true shadow zone and there is no geometrical acoustics contribution, so

$$p_{GA} = 0 \; . \tag{3.644}$$

3.17.3 Residual Diffracted Wave

The complete solution to the problem as posed above, for a point source outside a rigid wedge, is expressed with some generality as

$$p = p_{GA} + p_{diffr} \; . \tag{3.645}$$

The geometrical acoustics portion is as defined above; in one region it is a direct wave plus a reflected wave; in a second region it is only a direct wave; in a third region (shadow region) it is identically zero. The diffracted

wave is what is needed so that the sum will be a solution of the wave equation that satisfies the appropriate boundary conditions.

Whatever the diffracted wave is, it must have a discontinuous nature at the radial planes $\phi = \phi_A$ and $\phi = \phi_B$. This is because p_{GA} is discontinuous at these two values of ϕ and because the total solution should be continuous. Thus, one must require

$$p_{diffr}(\phi_B + \epsilon) - p_{diffr}(\phi_B - \epsilon) = -\frac{S[t-(L/c)]}{L}\,, \tag{3.646}$$

$$p_{diffr}(\phi_A + \epsilon) - p_{diffr}(\phi_A - \epsilon) = -\frac{S[t-(L/c)]}{L}\,. \tag{3.647}$$

Also, except in close vicinity to these radial planes, the diffracted wave should spread out at large w as an outgoing wave. One may anticipate that, at large values of w, the amplitude decreases with w as $1/\sqrt{w}$, as in cylindrical spreading.

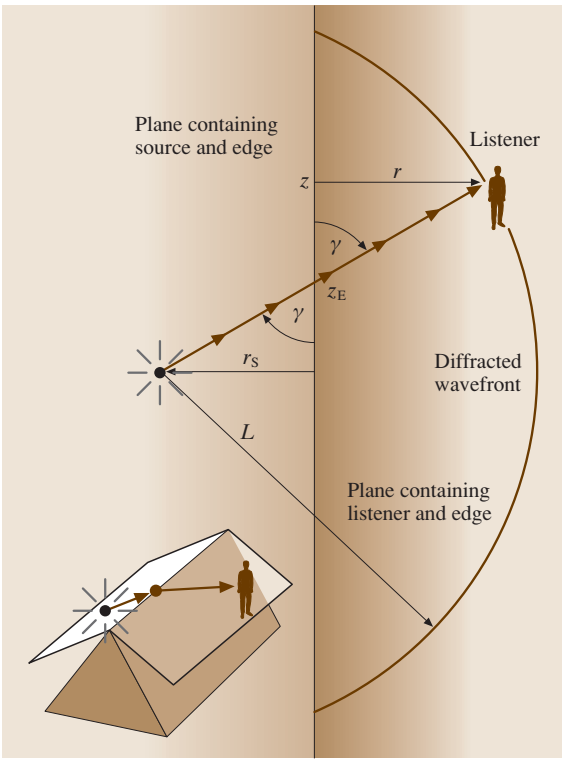


Fig. 3.57 Sketch supporting the geometrical interpretation of the parameter L as the diffracted ray length. The segment from source to edge makes the same angle γ with the edge as does the segment from edge to listener, and the sum of the two segment lengths is L

Diffracted Path Length

In the actual solution given further below for the diffracted wave, a predominant role is played by the parameter L given by (3.637). This can be interpreted as the net distance from the source to the listener along the shortest path that touches the diffracting edge. This path can alternately be called the diffracted ray.

Such a path must touch the edge at a point where each of the two segments make the same angle with the edge. This is equivalent to a statement of Keller's law of geometrical diffraction [3.95]. Here, when the listener is at $z = z_L$, the source is at $z = 0$, and the edge is the z-axis, the z-coordinate where the diffracted path leaves the edge is $[w_S/(w_S + w_L)]z_L$. Thus one has

$$L = \frac{\left[w_S^2(w_S+w_L)^2 + w_0^2 z_L^2\right]^{1/2}}{w_S + w_L} + \frac{\left[w_L^2(w_S+w_L)^2 + w_L^2 z_L^2\right]^{1/2}}{w_S + w_L}\,. \tag{3.648}$$

The first term corresponds to the segment that goes from the source to the edge, while the second corresponds to the segment that goes from the edge to the listener. All this simplifies to

$$L = \left[(w_S + w)^2 + z^2\right]^{1/2}. \tag{3.649}$$

Here the listener z-coordinate is taken simply to be z, and its radial coordinate is taken simply to be w. The time interval L/c is the shortest time that it takes for a signal to go from the source to the listener via the edge.

As is evident from the discussion above of the discontinuities in the geometrical acoustics portion of the field, this diffracted wave path is the same as the reflected wave path on the radial plane $\phi = \phi_B$ and is the same as the direct wave path on the radial plane $\phi = \phi_A$.

There is another characteristic length that enters into the solution, this being

$$Q = \left[(w_S - w)^2 + z^2\right]^{1/2}. \tag{3.650}$$

It is a shorter length than L and is the distance from the source to a hypothetical point that has the same coordinates as that of the listener, except that the ϕ coordinate is the same as that of the source. These two quantities are related, so that

$$L^2 - Q^2 = 4 w_S w\,, \tag{3.651}$$

Amazon EX1014 Page 120

which is independent of the z-coordinate separation of the source and listener.

Satisfaction of Boundary Conditions

A function that satisfies the appropriate boundary conditions (3.631) can be built up from the functions

$$\sin(\nu x_q) \quad \text{and} \quad \cos(\nu x_q); \qquad q = 1, 2, 3, 4, \tag{3.652}$$

where

$$\nu = \frac{\pi}{\beta}\,, \tag{3.653}$$

$$\begin{aligned} x_1 &= \pi + \phi + \phi_S = \phi - \phi_B + 2\beta\,, \\ x_2 &= \pi - \phi - \phi_S = -\phi - \phi_A\,, \\ x_3 &= \pi + \phi - \phi_S = \phi - \phi_A\,, \\ x_4 &= \pi - \phi + \phi_S = 2\beta - \phi_B - \phi\,. \end{aligned} \tag{3.654}$$

The trigonometric functions that appear above are not periodic with period 2π in the angles ϕ and ϕ_S, so the definition must be restricted to ranges of these quantities between 0 and β.

The satisfaction of the boundary conditions at $\phi = 0$ and $\phi = \beta$ is achieved by any function of the general form

$$\sum_{q=1}^{4} \Psi(\cos x_q, \sin x_q)\,, \tag{3.655}$$

where the function Ψ is an arbitrary function of two arguments. To demonstrate that the boundary condition at $\phi = 0$ is satisfied, it is sufficient to regard the function $\Psi(\cos x_q, \sin x_q)$ as only a function of x_q. One derives

$$\begin{aligned} &\left(\frac{\mathrm{d}}{\mathrm{d}\phi}\sum_{q=1}^{4}\Psi(x_q)\right)_{\phi=0} \\ &= \left\{\nu\Psi'[\nu(\pi+\phi_S)] - \Psi'[\nu(\pi-\phi_S)]\right. \\ &\quad \left. + \Psi'[\nu(\pi-\phi_S)] - \Psi'[\nu(\pi+\phi_S)]\right\} = 0\,. \end{aligned} \tag{3.656}$$

The first and fourth terms cancel, and the second and third terms cancel.

The boundary condition at $\phi = \beta$, however, requires explicit recognition that the postulated function Ψ depends on x_q only through the two trigonometric functions. Both are periodic in ϕ with period 2β, because $\nu\beta = \pi$. Moreover, the sum of the first and fourth terms is periodic with period β, and the same is so for the sum of the second and third terms. The entire sum has this periodicity, so if the derivative with respect to ϕ vanishes at $\phi = 0$, it also has to vanish at $\phi = \beta$.

Discontinuities in the Diffraction Term

Two of the individual x_q defined above are such that $\cos(\nu x_q)$ is unity at one or the other of the two radial planes $\phi = \phi_A$ and $\phi = \phi_B$. One notes that

$$\cos(\nu x_3) = 1 \qquad \text{at} \quad \phi = \phi_A\,, \tag{3.657}$$

$$\cos(\nu x_1) = 1 \qquad \text{at} \quad \phi = \phi_B\,. \tag{3.658}$$

Near the radial plane $\phi = \phi_A = \phi_S - \pi$, one has

$$\begin{aligned} &x_3 = \phi - \phi_A; \quad \cos(\nu x_3) \approx 1 - \frac{1}{2}(\nu^2)(\phi - \phi_A)^2\,; \\ &\sin(\nu x_3) \approx (\nu)(\phi - \phi_A)\,. \end{aligned} \tag{3.659}$$

Similarly, near the radial plane $\phi = \phi_B = 2\beta - \phi_S - \pi$,

$$\begin{aligned} &x_1 = 2\beta + \phi - \phi_B;\ \cos(\nu x_1) \approx 1 - \frac{1}{2}(\nu^2)(\phi - \phi_B)^2; \\ &\sin(\nu x_1) \approx (\nu)(\phi - \phi_B)\,. \end{aligned} \tag{3.660}$$

This behavior allows one to construct a discontinuous function of the generic form

$$U(\phi) = \sum_{q=1}^{4}\int_{\mathrm{L}}^{\infty} \frac{M(\xi)\sin(\nu x_q)}{F(\xi) - \cos(\nu x_q)}\,\mathrm{d}\xi\,, \tag{3.661}$$

where $M(\xi)$ and $F(\xi)$ are some specified functions of the dummy integration variable, such that $F \geq 1$, and $F = 1$ at only one value of ξ. This allows one to compute the discontinuity at ϕ_A, for example, as

$$\begin{aligned} &U(\phi_A + \epsilon) - U(\phi_A - \epsilon) \\ &= 2\nu\epsilon \int_{\mathrm{L}}^{\infty} \frac{M(\xi)}{F(\xi) - 1 + \frac{1}{2}\nu^2\epsilon^2}\,\mathrm{d}\xi \end{aligned} \tag{3.662}$$

where it is understood that one is to take the limit of $\epsilon \to 0$. The dominant contribution to the integration should come from the value of ξ at which $F = 1$. There are various possibilities where this limit is finite and nonzero. The one of immediate interest is where $F(L) = 1$, where the derivative is positive at $\xi = L$, and where M is singular as $1/(\xi - L)^{1/2}$ near $\xi = L$. For these circumstances the limit is

$$\begin{aligned} &\lim_{\epsilon\to 0}\left[U(\phi_A + \epsilon) - U(\phi_A - \epsilon)\right] \\ &= 4\pi\left(\frac{1}{2F'}\right)_{\mathrm{L}}^{1/2}\left[(\xi - L)^{1/2}M\right]_{\mathrm{L}} \end{aligned} \tag{3.663}$$

where the subscript L implies that the indicated quantity is to be evaluated at $\xi = L$.

Amazon EX1014 Page 121

3.17.4 Solution for Diffracted Waves

The details [3.30, 106–111] that lead to the solution vary somewhat in the literature and are invariably intricate. The procedure typically involves extensive application of the theory of the functions of a complex variable. The following takes some intermediate results from the derivation in the present author's text [3.30] and uses the results derived above to establish the plausibility of the solution.

The diffracted field at any point depends linearly on the time history of the source strength, and the shortest time for source to travel as a diffracted wave from source to listener is L/c, so the principles of causality and linearity allow one to write, with all generality, the diffracted wave as

$$p_{\text{diffr}} = -\frac{1}{\beta}\int_{\text{L}}^{\infty} S\left(t-\frac{\xi}{c}\right)K_\nu(\xi)\,\mathrm{d}\xi\,, \tag{3.664}$$

where the function $K_\nu(\xi)$ depends on the positions of the source and listener, as well as on the angular width of the wedge. The factor $-1/\beta$ in front of the integral is for mathematical convenience.

The boundary conditions at the rigid wedge are satisfied if one takes the dependence on ϕ and ϕ_{S} to be of the form of (3.655). The proper jumps will be possible if one takes the general dependence on the trigonometric functions to be as suggested in (3.661). The appropriate identification (substantiated further below) is

$$K_\nu = \frac{1}{(\xi^2-Q^2)^{1/2}}\frac{1}{(\xi^2-L^2)^{1/2}} \times\sum_{q=1}^{4}\frac{\sin(\nu x_q)}{\cosh\nu s-\cos(\nu x_q)}\,. \tag{3.665}$$

The quantity s is a function of ξ, defined as

$$s = 2\tanh^{-1}\left(\frac{\xi^2-L^2}{\xi^2-Q^2}\right)^{1/2}, \tag{3.666}$$

so that

$$\xi^2 = L^2+(L^2-Q^2)\sinh^2(s/2)\,, \tag{3.667}$$

$$\cosh\nu s = \frac{1}{2}\left[\left(\frac{(\xi^2-Q^2)^{1/2}-(\xi^2-L^2)^{1/2}}{(\xi^2-Q^2)^{1/2}+(\xi^2-L^2)^{1/2}}\right)^{\nu} + \left(\frac{(\xi^2-Q^2)^{1/2}+(\xi^2-L^2)^{1/2}}{(\xi^2-Q^2)^{1/2}-(\xi^2-L^2)^{1/2}}\right)^{\nu}\right]. \tag{3.668}$$

That this solution has the proper jump behavior at ϕ_{A} and ϕ_{B} follows because, for ξ near L,

$$-\frac{1}{\beta}\frac{1}{(\xi^2-Q^2)^{1/2}}\frac{1}{(\xi^2-L^2)^{1/2}} \to -\left(\frac{1}{\beta(L^2-Q^2)^{1/2}(2L)^{1/2}}\right)\frac{1}{(\xi-L)^{1/2}}\,, \tag{3.669}$$

$$\cosh\nu s \to 1+\frac{4\nu^2 L}{L^2-Q^2}(\xi-L)\,. \tag{3.670}$$

The result in (3.663) consequently yields

$$p_{\text{diffr}}(\phi_{\text{A}}+\epsilon)-p_{\text{diffr}}(\phi_{\text{A}}-\epsilon) = -\left(\frac{4\pi}{\beta(L^2-Q^2)^{1/2}(2L)^{1/2}}\right)\left(\frac{(L^2-Q^2)^{1/2}}{2\nu(2L)^{1/2}}\right) \times S\left[t-(L/c)\right] = -\frac{S\left[t-(L/c)\right]}{L}\,, \tag{3.671}$$

which is the same as required in (3.647).

(The solution has here been shown to satisfy the boundary conditions and the jump conditions. An explicit proof that the total solution satisfies the wave equation can be found in the text by the author [3.30].)

3.17.5 Impulse Solution

An elegant feature of the above transient solution is that no integration is required for the case when the source function is a delta function (impulse source). If

$$S(t) \to A\delta(t)\,, \tag{3.672}$$

then the integration properties of the delta function yield

$$p_{\text{diffr}} \to -\frac{Ac}{\beta}H(ct-L)\frac{1}{(c^2t^2-Q^2)^{1/2}} \times\frac{1}{(c^2t^2-L^2)^{1/2}}\sum_{q=1}^{4}\frac{\sin(\nu x_q)}{\cosh\nu s-\cos(\nu x_q)}\,, \tag{3.673}$$

where $\cosh\nu s$ is as given by (3.668), but with ξ replaced by ct. The function $H(ct-L)$ is the unit step function, equal to zero when its argument is negative and equal to unity when its argument is positive.

(In recent literature, an equivalent version of this solution is occasionally referred to as the *Biot–Tolstoy* solution [3.111], although its first derivation was by *Friedlander* [3.110]. In retrospect, it is a simple deduction from the constant-frequency solution given by *MacDonald* [3.106], *Whipple* [3.107], *Bromwich*

[3.108], and *Carslaw* [3.109]. In the modern era with digital computers, where the numerical calculation of Fourier transforms is virtually instantaneous and routine, an explicit analytical solution for the impulse response is often a good starting point for determining diffraction of waves of constant frequency.)

3.17.6 Constant-Frequency Diffraction

The transient solution (3.664) above yields the solution for when the source is of constant frequency. One makes the substitution

$$S(t) \to \hat{S}\,\mathrm{e}^{-\mathrm{i}\omega t}\,, \tag{3.674}$$

and obtains

$$\hat{p}_{\mathrm{diffr}} = -\frac{\hat{S}}{\beta}\int_L^\infty \mathrm{e}^{\mathrm{i}k\xi}\,K_\nu(\xi)\,\mathrm{d}\xi\,. \tag{3.675}$$

The integral that appears here can be reduced to standard functions in various limits. A convenient first step is to change the integration variable to the parameter s, so that

$$\xi^2 = L^2 + (L^2 - Q^2)\sinh^2(s/2)\,, \tag{3.676}$$

$$\frac{\mathrm{d}\xi}{[\xi^2 - Q^2]^{1/2}[\xi^2 - L^2]^{1/2}} = \frac{\mathrm{d}s}{2\xi}\,, \tag{3.677}$$

and so that the range of integration on s is from 0 to ∞. One notes that the integrand is even in s, so that it is convenient to extend the integration from $-\infty$ to ∞, and then divide by two. Also, one can use trigonometric identities to combine the x_1 term with the x_2 term and to combine the x_3 term with the x_4 term. All this yields the result

$$\hat{p}_{\mathrm{diffr}} = \frac{\hat{S}\sin\nu\pi}{2\beta}\sum_{+,-}\int_{-\infty}^{\infty}\frac{\mathrm{e}^{\mathrm{i}k\xi}}{\xi}\,F_\nu(s,\phi\pm\phi_{\mathrm{S}})\,\mathrm{d}s\,, \tag{3.678}$$

where

$$F_\nu(s,\phi) = \frac{U_\nu(\phi) - J(\nu s)\cos\nu\phi}{J^2(\nu s) + 2J(\nu s)V_\nu^2(\phi) + U_\nu^2(\phi)}\,, \tag{3.679}$$

with the abbreviations

$$J(\nu s) = \cosh\nu s - 1\,, \tag{3.680}$$

$$U_\nu(\phi) = \cos\nu\pi - \cos\nu\phi\,, \tag{3.681}$$

$$V_\nu(\phi) = (1 - \cos\nu\phi\cos\nu\pi)^{1/2}\,. \tag{3.682}$$

The requisite integrals exist, except when either $U_\nu(\phi+\phi_{\mathrm{S}})$ or $U_\nu(\phi-\phi_{\mathrm{S}})$ should be zero. The angles at which one or the other occurs correspond to boundaries between different regions of the diffracted field.

3.17.7 Uniform Asymptotic Solution

Although the integration in (3.678) can readily be completed numerically, considerable insight and useful formulas arise when one considers the limit when both the source and the listener are many wavelengths from the edge. One argues that the dominant contribution to the integration comes from values of s that are close to 0 (where the phase of the exponential is stationary), so one approximates

$$\xi \to L + \frac{(L^2 - Q^2)}{8L}s^2 = L + \frac{\pi}{2k}\Gamma^2 s^2\,, \tag{3.683}$$

$$\frac{\mathrm{e}^{\mathrm{i}k\xi}}{\xi} \to \frac{\mathrm{e}^{\mathrm{i}kL}}{L}\,\mathrm{e}^{\mathrm{i}(\pi/2)\Gamma^2 s^2}\,, \tag{3.684}$$

$$J(\nu s) = \cosh\nu s - 1 \to \frac{\nu^2}{2}s^2\,, \tag{3.685}$$

$$F_\nu(s,\phi) \to \frac{U_\nu(\phi)}{U_\nu^2(\phi) + \nu^2 V_\nu^2(\phi)s^2}\,, = \frac{1}{2\nu V_\nu(\phi)}\left(\frac{1}{M_\nu(\phi) + \mathrm{i}s} + \frac{1}{M_\nu(\phi) - \mathrm{i}s}\right)\,. \tag{3.686}$$

The expression (3.686) uses the abbreviation

$$M_\nu(\phi) = \frac{U_\nu(\phi)}{\nu V_\nu(\phi)} = \frac{\cos\nu\pi - \cos\nu\phi}{\nu\,(1 - \cos\nu\phi\cos\nu\pi)^{1/2}}\,, \tag{3.687}$$

while (3.684) uses the abbreviation

$$\Gamma^2 = k\frac{(L^2 - Q^2)}{4\pi L} = \frac{kww_{\mathrm{S}}}{\pi L}\,, \tag{3.688}$$

where the latter version follows from the definitions (3.649) and (3.650).

One also notes that the symmetry in the exponential factor allows one to identify

$$\int_{-\infty}^{\infty}\frac{\mathrm{e}^{\mathrm{i}(\pi/2)\Gamma^2 s^2}}{M_\nu + \mathrm{i}s}\,\mathrm{d}s = \int_{-\infty}^{\infty}\frac{\mathrm{e}^{\mathrm{i}(\pi/2)\Gamma^2 s^2}}{M_\nu - \mathrm{i}s}\,\mathrm{d}s\,, \tag{3.689}$$

so the number of required integral terms is halved. A further step is to change the the integration variable to

$$u = (\pi/2)^{1/2}\Gamma\,\mathrm{e}^{-\mathrm{i}\pi/4}s\,. \tag{3.690}$$

All this results in the uniform asymptotic expression

$$\hat{p}_{\mathrm{diffr}} = \hat{S}\frac{\mathrm{e}^{\mathrm{i}kL}}{L}\frac{\mathrm{e}^{\mathrm{i}\pi/4}}{\sqrt{2}}\sum_{+,-}\frac{\sin\nu\pi}{V_\nu(\phi\pm\phi_\mathrm{S})} \times A_\mathrm{D}\left[\Gamma M_\nu(\phi\pm\phi_\mathrm{S})\right] \tag{3.691}$$

for the diffracted wave. Here one makes use of the definition

$$A_\mathrm{D}(X) = \frac{1}{\pi 2^{1/2}}\int_{-\infty}^{\infty}\frac{\mathrm{e}^{-u^2}\,\mathrm{d}u}{(\pi/2)^{1/2}X - \mathrm{e}^{-\mathrm{i}\pi/4}\,u}\,, \tag{3.692}$$

of a complex-valued function of a single real variable. The properties of this function are discussed in detail below.

3.17.8 Special Functions for Diffraction

The diffraction integral (3.692) is a ubiquitous feature in diffraction theories. It changes sign,

$$A_\mathrm{D}(-X) = -A_\mathrm{D}(X)\,, \tag{3.693}$$

when its argument X changes sign (as can be demonstrated by changing the integration variable to $-u$ after changing the sign of X). The function is complex, so one can write in general

$$A_\mathrm{D}(X) = \mathrm{sign}(X)\left[f(|X|) - \mathrm{i}g(|X|)\right]\,, \tag{3.694}$$

where the functions f and g (referred to as the auxiliary Fresnel functions) represent the real and negative imaginary parts of $A_\mathrm{D}(|X|)$.

To relate $A_\mathrm{D}(X)$ to the often encountered Fresnel integrals, one makes use of the identity [with $\zeta = (\pi/2)^{1/2}|X|$ being positive]

$$\frac{1}{\zeta - \mathrm{e}^{-\mathrm{i}\pi/4}\,u} = \mathrm{e}^{-\mathrm{i}\pi/4}\int_0^\infty \exp[\mathrm{i}(\zeta\,\mathrm{e}^{\mathrm{i}\pi/4} - u)q]\,\mathrm{d}q\,. \tag{3.695}$$

Then, one has

$$\int_{-\infty}^{\infty}\frac{\mathrm{e}^{-u^2}\,\mathrm{d}u}{\zeta - \mathrm{e}^{-\mathrm{i}\pi/4}\,u} = \mathrm{e}^{-\mathrm{i}\pi/4}\mathrm{e}^{-\mathrm{i}\zeta^2}\int_0^\infty \mathrm{e}^{-y^2}\left(\int_{-\infty}^{\infty}\mathrm{e}^{-(u+\mathrm{i}q/2)^2}\,\mathrm{d}u\right)\mathrm{d}q\,, \tag{3.696}$$

with the abbreviation $y = q/2 + \mathrm{e}^{-\mathrm{i}\pi/4}\zeta$. The inner integral over u yields $\sqrt{\pi}$, and one sets

$$\int_0^\infty \mathrm{e}^{-y^2}\,\mathrm{d}q = 2\int_{\zeta\,\mathrm{e}^{-\mathrm{i}\pi/4}}^{\infty}\mathrm{e}^{-y^2}\,\mathrm{d}y = 2\int_{\zeta\,\mathrm{e}^{-\mathrm{i}\pi/4}}^{0}\mathrm{e}^{-y^2}\,\mathrm{d}y + 2\int_0^\infty \mathrm{e}^{-y^2}\,\mathrm{d}y\,. \tag{3.697}$$

The second term in the latter expression is $\sqrt{\pi}$, and in the first term one changes the variable of integration to $t = (2/\pi)^{1/2}y\,\mathrm{e}^{\mathrm{i}\pi/4}$, so that

$$\int_{\zeta\,\mathrm{e}^{-\mathrm{i}\pi/4}}^{0}\mathrm{e}^{-y^2}\,\mathrm{d}y = -(\pi/2)^{1/2}\,\mathrm{e}^{-\mathrm{i}\pi/4} \times \int_0^{(2/\pi)^{1/2}\zeta}\mathrm{e}^{\mathrm{i}(\pi/2)t^2}\,\mathrm{d}t\,. \tag{3.698}$$

The analytical steps outlined above lead to the result

$$A_\mathrm{D}(X) = \frac{(1-\mathrm{i})}{2}\mathrm{e}^{-\mathrm{i}[\pi/2]X^2} \times\{\mathrm{sign}(X) - (1-\mathrm{i})\left[C(X) + \mathrm{i}S(X)\right]\}\,, \tag{3.699}$$

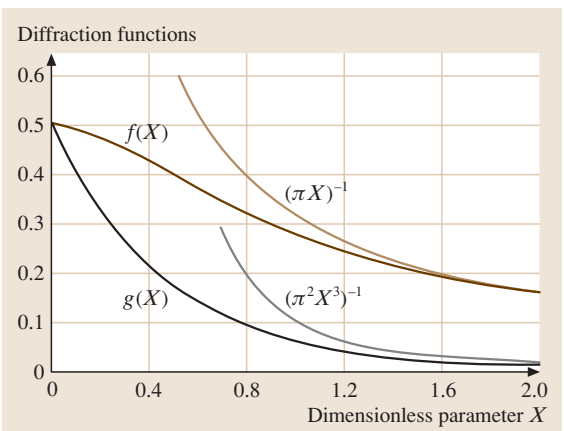


Fig. 3.58 Real and imaginary parts of the diffraction integral. Also shown are the appropriate asymptotic forms that are applicable at large arguments

Amazon EX1014 Page 124

where $C(X)$ and $S(X)$ are the Fresnel integrals

$$C(X) = \int_0^X \cos\left(\frac{\pi}{2}t^2\right) \mathrm{d}t \; ; \tag{3.700}$$

$$S(X) = \int_0^X \sin\left(\frac{\pi}{2}t^2\right) \mathrm{d}t. \tag{3.701}$$

In accordance with (3.693), the above representation of $A_\mathrm{D}(X)$ is an odd function of X, the two Fresnel integrals themselves being odd in X. The discontinuity in $A_\mathrm{D}(X)$ is readily identified from this representation as

$$A_\mathrm{D}(0+\epsilon) - A_\mathrm{D}(0-\epsilon) = 1 - \mathrm{i} \; ; \tag{3.702}$$

The behavior of the two auxiliary Fresnel functions at small to moderate values of $|X|$ can be determined by expanding the terms in (3.699) in a power series in X, so that one identifies

$$f(|X|) \approx \frac{1}{2} - \frac{\pi}{4}X^2 + \frac{\pi}{3}|X|^3 - \ldots \; , \tag{3.703}$$

$$g(|X|) \approx \frac{1}{2} - |X| + \frac{\pi}{2}X^2 - \ldots \; . \tag{3.704}$$

To determine the behavior at large values of $|X|$, it is expedient to return to the expression (3.692) and expand the integrand in powers of $1/X$ and then integrate term by term. Doing this yields

$$f(|X|) \to \frac{1}{\pi|X|} - \frac{3}{\pi^3|X|^5} + \ldots \; , \tag{3.705}$$

$$g(|X|) \to \frac{1}{\pi^2|X|^3} - \frac{15}{\pi^4|X|^7} + \ldots \; . \tag{3.706}$$

These are asymptotic series, so one should retain at most only those terms which are of decreasing value. The leading terms are a good approximation for $|X| > 2$.

3.17.9 Plane Wave Diffraction

The preceding analysis, for when the source is a point source at a finite distance from the edge, can be adapted to the case when one idealizes the incident wave as a plane wave, propagating in the direction of the unit vector

$$\boldsymbol{n}_\mathrm{inc} = n_x \boldsymbol{e}_x + n_y \boldsymbol{e}_y + n_z \boldsymbol{e}_z \; , \tag{3.707}$$

which points from a distant source (cylindrical coordinates w_S, ϕ_S, z_S) toward the coordinate origin, so that

$$n_x = \frac{-w_\mathrm{S}\cos\phi_\mathrm{S}}{\left(w_\mathrm{S}^2 + z_\mathrm{S}^2\right)^{1/2}}; \quad n_y = \frac{-w_\mathrm{S}\sin\phi_\mathrm{S}}{\left(w_\mathrm{S}^2 + z_\mathrm{S}^2\right)^{1/2}};$$
$$n_z = \frac{-z_\mathrm{S}}{\left(w_\mathrm{S}^2 + z_\mathrm{S}^2\right)^{1/2}} \; . \tag{3.708}$$

Without any loss of generality, one can consider z_S to be negative, so that n_z is positive. Then at the point on the edge where $z = 0$, the direct wave makes an angle

$$\gamma = \cos^{-1}\left(\frac{-z_\mathrm{S}}{\left(w_\mathrm{S}^2 + z_\mathrm{S}^2\right)^{1/2}}\right) \tag{3.709}$$

with the edge of the wedge, and this definition yields

$$\sin\gamma = \frac{w_\mathrm{S}}{\left(w_\mathrm{S}^2 + z_\mathrm{S}^2\right)^{1/2}}; \quad \cos\gamma = n_z \; . \tag{3.710}$$

One lets $\hat{p}_\mathrm{inc}$ be the complex amplitude of the incident wave at the origin (the point on the edge where $z = 0$), so that

$$\hat{S}\frac{1}{\left(w_\mathrm{S}^2 + z_\mathrm{S}^2\right)^{1/2}} \mathrm{e}^{\mathrm{i}\left(w_\mathrm{S}^2 + z_\mathrm{S}^2\right)^{1/2}} \to \hat{p}_\mathrm{inc} \; , \tag{3.711}$$

and one holds this quantity constant while letting $(w_\mathrm{S}^2 + z_\mathrm{S}^2)^{1/2}$ become arbitrarily large. Then, with appropriate use of Taylor series (or binomial series) expansions, one has

$$R_\mathrm{D} \to \left(w_\mathrm{S}^2 + z_\mathrm{S}^2\right)^{1/2} - w\sin\gamma\cos(\phi - \phi_\mathrm{S}) + z\cos\gamma, \tag{3.712}$$

$$R_\mathrm{R} \to \left(w_\mathrm{S}^2 + z_\mathrm{S}^2\right)^{1/2} - w\sin\gamma\cos(\phi + \phi_\mathrm{S} - 2\beta) + z\cos\gamma \; , \tag{3.713}$$

$$L \to \left(w_\mathrm{S}^2 + z_\mathrm{S}^2\right)^{1/2} + w\sin\gamma + z\cos\gamma \; , \tag{3.714}$$

$$\Gamma \to \left(\frac{kw\sin\gamma}{\pi}\right)^{1/2} \; . \tag{3.715}$$

In this limit, the geometrical acoustics portion of the solution, for waves of constant frequency, is given by one of the following three expressions. In the region $\beta > \phi > \phi_\mathrm{B}$, one has

$$\hat{p}_\mathrm{GA} = \hat{p}_\mathrm{inc}\,\mathrm{e}^{\mathrm{i}kn_z z}\left(\mathrm{e}^{\mathrm{i}kn_x x}\,\mathrm{e}^{\mathrm{i}kn_y y} + \mathrm{e}^{-\mathrm{i}kw\sin\gamma\cos(\phi+\phi_\mathrm{S}-2\beta)}\right) , \tag{3.716}$$

where the two terms correspond to the incident wave and the reflected wave. In the region $\phi_\mathrm{B} > \phi > \phi_\mathrm{A}$, one has

$$\hat{p}_\mathrm{GA} = \hat{p}_\mathrm{inc}\,\mathrm{e}^{\mathrm{i}kn_z z}\,\mathrm{e}^{\mathrm{i}kn_x x}\,\mathrm{e}^{\mathrm{i}kn_y y} \; , \tag{3.717}$$

Amazon EX1014 Page 125

which is the incident wave only. Then, in the shadow region, where $\phi_A > \phi > 0$, one has

$$\hat{p}_{GA} = 0 \,, \tag{3.718}$$

and there is neither an incident wave nor a reflected wave.

The diffracted wave, in this plane wave limit, becomes

$$\hat{p}_{diffr} = \hat{p}_{inc}\, e^{ikz\cos\gamma}\, e^{ikw\sin\gamma}\, \frac{e^{i\pi/4}}{\sqrt{2}} \times \sum_{+,-} \frac{\sin\nu\pi}{V_\nu(\phi \pm \phi_S)} A_D\left[\Gamma M_\nu(\phi \pm \phi_S)\right] \,, \tag{3.719}$$

where Γ is now understood to be given by (3.715). This result is, as before, for the case when the listener is many wavelengths from the edge, so that the parameter Γ is large compared with unity.

3.17.10 Small-Angle Diffraction

Simple approximate formulas emerge from the above general results when one limits one's attention to the diffracted field near the edge of the shadow zone boundary.

The incident wave is taken as having its direction lying in the (x, y) plane and one introduces rotated coordinates (x', y'), so that the y'-axis is in the direction of the incident sound, with the coordinate origin remaining at the edge of the wedge. One regards y' as being large compared to a wavelength. The magnitude $|x'|$ is regarded as substantially smaller than y', but not necessarily small compared to a wavelength.

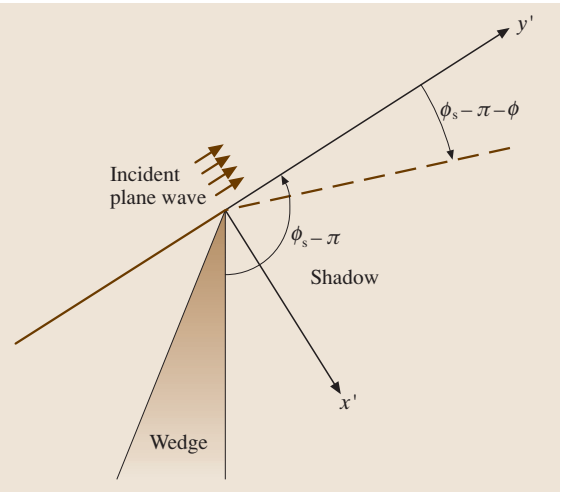


Fig. 3.59 Geometry and parameters used in discussion of small-angle diffraction of a plane wave by a rigid wedge

In the plane wave diffraction expression (3.719) the angle γ is $\pi/2$, and the only term of possible significance is that corresponding to the minus sign, so one has

$$\hat{p}_{diffr} = \hat{p}_{inc}\, e^{ikw}\, \frac{e^{i\pi/4}}{\sqrt{2}}\, \frac{\sin\nu\pi}{V_\nu(\phi - \phi_S)} \times A_D\left[\Gamma M_\nu(\phi - \phi_S)\right] \,. \tag{3.720}$$

Also, because $|x'|$ is small compared with y', one can assume that $|\phi_S - \pi - \phi|$ is small compared with unity, so that

$$\cos\nu(\phi - \phi_S) \approx \cos\nu\pi + (\nu\sin\nu\pi)\,(\phi - \phi_S + \pi) \,, \tag{3.721}$$

$$V_\nu(\phi - \phi_S) \approx \sin\nu\pi \,, \tag{3.722}$$

$$M_\nu(\phi - \phi_S) \approx \phi_S - \pi - \phi \approx \frac{x'}{y'} \,. \tag{3.723}$$

Further approximations that are consistent with this small-angle diffraction model are to set $w \to y'$ in the expression for Γ, but to set

$$w \to y' + \frac{1}{2}\frac{(x')^2}{y'} \tag{3.724}$$

in the exponent. The second term is needed if one needs to take into account any phase shift relative to that of the incident wave.

The approximations just described lead to the expression

$$\hat{p}_{diffr} = \hat{p}_{inc}\, e^{iky'}\, \frac{1+i}{2}\, e^{(\pi/2)X^2} A_D(X) \,, \tag{3.725}$$

with

$$X = \left(\frac{k}{\pi y'}\right) x' \,. \tag{3.726}$$

A remarkable feature of this result is that it is independent of the wedge angle β. It applies in the same approximate sense equally for diffraction by a thin screen and by a right-angled corner.

The total acoustic field in this region just above and just where the shadow zone begins can be found by adding the incident wave for $x' < 0$. In the shadow zone there is no incident wave, and one accounts for this by using a step function $H(-X)$. Thus the total field is approximated by

$$\hat{p}_{GA} + \hat{p}_{diffr} \to p_{inc}\, e^{iky'} \times \left[H(-X) + \frac{(1+i)}{2}\, e^{i(\pi/2)X^2} A_D(X)\right] \,. \tag{3.727}$$

Amazon EX1014 Page 126

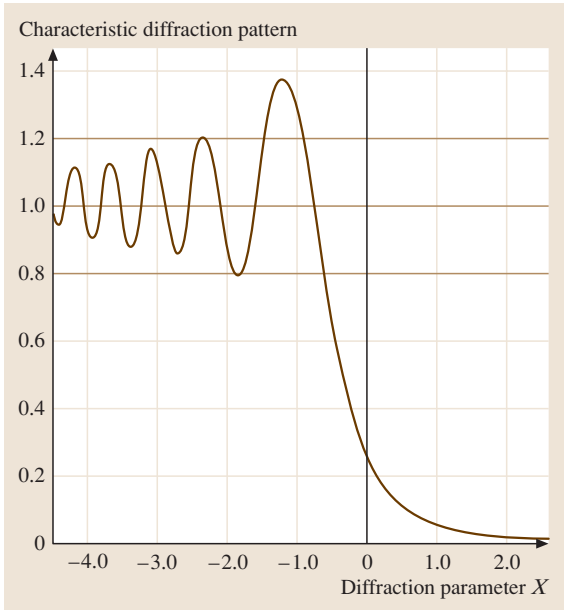


Fig. 3.60 Characteristic diffraction pattern as a function of the diffraction parameter X. The function is the absolute magnitude of the complex amplitude of the received acoustic pressure, incident plus diffracted, relative to that of the incident wave

One can now substitute into this the expression (3.699), with the result

$$\hat{p}_{\mathrm{GA}} + \hat{p}_{\mathrm{diffr}} = \hat{p}_{\mathrm{inc}}\, \mathrm{e}^{\mathrm{i}ky} \left(\frac{1-\mathrm{i}}{2}\right) \times \left\{\left[\frac{1}{2} - C(X)\right] + \mathrm{i}\left[\frac{1}{2} - S(X)\right]\right\} , \tag{3.728}$$

or, equivalently,

$$\hat{p}_{\mathrm{GA}} + \hat{p}_{\mathrm{diffr}} = \hat{p}_{\mathrm{inc}}\, \mathrm{e}^{\mathrm{i}ky} \left(\frac{1-\mathrm{i}}{2}\right) \int_X^\infty \mathrm{e}^{\mathrm{i}(\pi/2)u^2}\, \mathrm{d}u \, . \tag{3.729}$$

The definitions of the diffraction integral and of the Fresnel integrals are such that, in the latter expressions, one does not need a step function.

The expressions just given, or their equivalents, are what are most commonly used in assessments of diffraction. The plot of the magnitude squared, relative to that of the incident wave,

$$\left|\frac{\hat{p}_{\mathrm{GA}} + \hat{p}_{\mathrm{diffr}}}{\hat{p}_{\mathrm{inc}}}\right|^2 = \frac{1}{2}\left|\int_X^\infty \mathrm{e}^{\mathrm{i}(\pi/2)u^2}\, \mathrm{d}u\right|^2 , \tag{3.730}$$

shows a monotonic decay in the shadow region ($X > 0$) and a series of diminishing ripples about unity in the illuminated region ($X < 0$). The peaks are interpreted as resulting from constructive interference of the incident and diffracted waves. The valleys result from destructive interference.

3.17.11 Thin-Screen Diffraction

For the general case of plane wave diffraction, not necessarily at small angles, a relatively simple limiting case is when the wedge is a thin screen, so that $\beta = 2\pi$ and the wedge index ν is $1/2$. Additional simplicity results for the case where the incident wave's direction $\boldsymbol{n}_{\mathrm{inc}}$ is perpendicular to the edge, so that $\gamma = \pi/2$. In this limiting case, $\sin \nu\pi = 1$ and $\cos \nu\pi = 0$, so, with reference to (3.682), one finds $V_\nu(\phi \pm \phi_{\mathrm{S}}) = 1$, and with reference to (3.687), one finds

$$M_\nu(\phi \pm \phi_{\mathrm{S}}) = -2\cos\frac{1}{2}(\phi \pm \phi_{\mathrm{S}}) \, . \tag{3.731}$$

Then, with use of the fact that $A_{\mathrm{D}}(X)$ is odd in X, one obtains

$$\hat{p}_{\mathrm{diffr}} = \frac{-\hat{p}_{\mathrm{inc}}\, \mathrm{e}^{\mathrm{i}(kw+\pi/4)}}{\sqrt{2}} \times \sum_{+,-} A_{\mathrm{D}} \left[\left(\frac{4kw}{\pi}\right)^{1/2} \cos\frac{1}{2}(\phi \pm \phi_{\mathrm{S}})\right] . \tag{3.732}$$

Although derived here for the asymptotic limit when kw is large, this result is actually exact and holds for all values of w. It was derived originally by *Sommerfeld* in 1896 [3.105].

3.18 Parabolic Equation Methods

It is often useful in propagation analyses to replace the Helmholtz equation or its counterpart for inhomogeneous media by a partial differential equation that is first order, rather than second order, in the coordinate that corresponds to the primary direction of propagation. Approximations that achieve this are known generally as

Amazon EX1014 Page 127

parabolic equation approximations and stem from early work by *Fock* [3.112] and *Tappert* [3.113]. Their chief advantage is that the resulting equation is no longer elliptic, but parabolic, so it is no longer necessary to check whether a radiation condition is satisfied at large propagation distances. This is especially convenient for numerical computation, for the resulting algorithms march out systematically in propagation distance, without having to look far ahead for the determination of the field at a subsequent point.

A simple example of a parabolic equation approximation is that of two-dimensional propagation in a medium where the sound speed and density vary primarily with the coordinate y, but weakly with x. A wave of constant angular frequency ω is propagating primarily in the x-direction but is affected by the y variations of the ambient medium, and by the presence of interfaces that are nearly parallel to the x-direction. The propagation is consequently governed by the two-dimensional reduced wave equation,

$$\frac{\partial}{\partial x}\left(\frac{1}{\rho}\frac{\partial \hat{p}}{\partial x}\right)+\frac{\partial}{\partial y}\left(\frac{1}{\rho}\frac{\partial \hat{p}}{\partial y}\right)+\frac{\omega^2}{\rho c^2}\hat{p}=0 \qquad (3.733)$$

which can be obtained from (3.73) by use of the complex amplitude convention.

In the parabolic approximation, the exact solution $\hat{p}$ of (3.733), with a radiation condition imposed, is represented by

$$\hat{p}(x, y)=\mathrm{e}^{\mathrm{i}\chi(x)}F(x, y)\,, \qquad (3.734)$$

where

$$\chi(x)=\int_0^x k_0\,\mathrm{d}x\,. \qquad (3.735)$$

Here $k_0(x)$ is a judiciously chosen reference wavenumber (possibly dependent on the primary coordinate x). The crux of the method is that the function $F(x, y)$ is taken to satisfy an approximate partial differential equation [parabolic equation (PE)] that differs from what would result were (3.734) inserted into (3.733) with no discarded terms.

The underlying assumption is that the x-dependence of the complex pressure amplitude is mostly accounted for by the exponential factor, so the characteristic scale for variation of the amplitude factor F with the coordinate x is much greater than the reciprocal of k_0. Consequently second derivatives of F with respect to x can be neglected in the derived differential equation. The y derivatives of the ambient variables are also neglected. The resulting approximate equation is given by

$$\frac{\partial}{\partial x}\left(\frac{k_0}{\rho}F\right)+\frac{k_0}{\rho}\frac{\partial F}{\partial x}=\mathrm{i}\frac{\partial}{\partial y}\left(\frac{1}{\rho}\frac{\partial F}{\partial y}\right)+\mathrm{i}\frac{k_0^2}{\rho}(n^2-1)F\,, \qquad (3.736)$$

where n, the apparent index of refraction, is an abbreviation for $k_0^{-1}\omega/c$. If the reference wavenumber k_0 is selected to be independent of x, then (3.736) reduces to

$$2k_0\frac{\partial F}{\partial x}=\mathrm{i}\rho\frac{\partial}{\partial y}\left(\frac{1}{\rho}\frac{\partial F}{\partial y}\right)+\mathrm{i}k_0^2(n^2-1)F\,. \qquad (3.737)$$

Although the computational results must depend on the selection of the reference wavenumber k_0, results for various specific cases tend to indicate that the sensitivity to such a selection is not great.

References

3.1 F.V. Hunt: *Origins of Acoustics* (Yale Univ. Press, New Haven 1978)

3.2 R.B. Lindsay: *Acoustics: Historical and Philosophical Development* (Dowden, Hutchinson, Ross, Stroudsburg 1972)

3.3 C.A. Truesdell III: The theory of aerial sound, Leonhardi Euleri Opera Omnia, Ser. 2 **13**, XIX–XXII (1955)

3.4 J.W.S. Rayleigh: *The Theory of Sound*, Vol. 1 and 2 (Dover, New York 1945), The 1st ed. was published in 1878; the 2nd ed. in 1896

3.5 P.A. Thompson: *Compressible-Fluid Dynamics* (McGraw-Hill, New York 1972)

3.6 Y.C. Fung: *Foundations of Solid Mechanics* (Prentice-Hall, Englewood Cliffs 1965)

3.7 A.H. Shapiro: *The Dynamics and Thermodynamics of Compressible Fluid Flow* (Ronald, New York 1953)

3.8 G.K. Batchelor: *An Introduction to Fluid Dynamics* (Cambridge Univ. Press, Cambridge 1967)

3.9 C. Truesdell: *The Mechanical Foundations of Elasticity and Fluid Mechanics* (Gordon Breach, New York 1966)

3.10 L.D. Landau, E.M. Lifshitz: *Fluid Mechanics* (Pergamon, New York 1959)

3.11 C. Truesdell, R. Toupin: The classical field theories. In: *Principles of Classical Mechanics and Field Theory*, Handbook of Physics, Vol. 3, ed. by S. Flügge (Springer, Berlin, Heidelberg 1960) pp. 226–858

3.12 G.G. Stokes: On the theories of the internal friction of fluids in motion, and of the equilibrium and motion

Amazon EX1014 Page 128

of elastic solids, Trans. Camb. Philos. Soc. **8**, 75–102 (1845)
3.13 L.D. Landau, E.M. Lifshitz, L.P. Pitaevskii: *Statistical Physics, Part 1* (Pergamon, New York 1980)
3.14 A.D. Pierce: Aeroacoustic fluid dynamic equations and their energy corollary with O_2 and N_2 relaxation effects included, J. Sound Vibr. **58**, 189–200 (1978)
3.15 J. Fourier: *Analytical Theory of Heat* (Dover, New York 1955), The 1st ed. was published in 1822
3.16 J. Hilsenrath: *Tables of Thermodynamic and Transport Properties of Air* (Pergamon, Oxford 1960)
3.17 W. Sutherland: The viscosity of gases and molecular force, Phil. Mag. **5**(36), 507–531 (1893)
3.18 M. Greenspan: Rotational relaxation in nitrogen, oxygen, and air, J. Acoust. Soc. Am. **31**, 155–160 (1959)
3.19 R.A. Horne: *Marine Chemistry* (Wiley-Interscience, New York 1969)
3.20 J.M.M. Pinkerton: A pulse method for the measurement of ultrasonic absorption in liquids: Results for water, Nature **160**, 128–129 (1947)
3.21 W.D. Wilson: Speed of sound in distilled water as a function of temperature and pressure, J. Acoust. Soc. Am. **31**, 1067–1072 (1959)
3.22 W.D. Wilson: Speed of sound in sea water as a function of temperature, pressure, and salinity, J. Acoust. Soc. Am. **32**, 641–644 (1960)
3.23 A.B. Wood: *A Textbook of Sound*, 2nd edn. (Macmillan, New York 1941)
3.24 A. Mallock: The damping of sound by frothy liquids, Proc. Roy. Soc. Lond. A **84**, 391–395 (1910)
3.25 S.H. Crandall, N.C. Dahl, T.J. Lardner: *An Introduction to the Mechanics of Solids* (McGraw-Hill, New York 1978)
3.26 L.D. Landau, E.M. Lifshitz: *Theory of Elasticity* (Pergamon, New York 1970)
3.27 A.E.H. Love: *The Mathematical Theory of Elasticity* (Dover, New York 1944)
3.28 J.D. Achenbach: *Wave Propagation in Elastic Solids* (North-Holland, Amsterdam 1975)
3.29 M.J.P. Musgrave: *Crystal Acoustics* (Acoust. Soc. Am., Melville 2003)
3.30 A.D. Pierce: *Acoustics: An Introduction to Its Physical Principles and Applications* (Acoust. Soc. Am., Melville 1989)
3.31 P.G. Bergmann: The wave equation in a medium with a variable index of refraction, J. Acoust. Soc. Am. **17**, 329–333 (1946)
3.32 L. Cremer: Über die akustische Grenzschicht von starren Wänden, Arch. Elekt. Uebertrag. **2**, 136–139 (1948), in German
3.33 G.R. Kirchhoff: Über den Einfluß der Wärmeleitung in einem Gase auf die Schallbewegung, Ann. Phys. Chem. Ser. 5 **134**, 177–193 (1878)
3.34 L.S.G. Kovasznay: Turbulence in supersonic flow, J. Aeronaut. Sci. **20**, 657–674 (1953)
3.35 T.Y. Wu: Small perturbations in the unsteady flow of a compressible, viscous, and heat-conducting fluid, J. Math. Phys. **35**, 13–27 (1956)
3.36 R. Courant: *Differential and Integral Calculus*, Vol. 1, 2 (Wiley-Interscience, New York 1937)
3.37 H. Lamb: *Hydrodynamics* (Dover, New York 1945)
3.38 A.H. Shapiro: *Shape and Flow: The Fluid Dynamics of Drag* (Doubleday, Garden City 1961) pp. 59–63
3.39 R.F. Lambert: Wall viscosity and heat conduction losses in rigid tubes, J. Acoust. Soc. Am. **23**, 480–481 (1951)
3.40 S.H. Crandall, D.C. Karnopp, E.F. Kurtz Jr., D.C. Pridmore-Brown: *Dynamics of Mechanical and Electromechanical Systems* (McGraw-Hill, New York 1968)
3.41 A.D. Pierce: Variational principles in acoustic radiation and scattering. In: *Physical Acoustics*, Vol. 22, ed. by A.D. Pierce (Academic, San Diego 1993) pp. 205–217
3.42 M.A. Biot: Theory of propagation of elastic waves in a fluid saturated porous solid. I. Low frequency range, J. Acoust. Soc. Am. **28**, 168–178 (1956)
3.43 R.D. Stoll: *Sediment Acoustics* (Springer, Berlin, Heidelberg 1989)
3.44 J. Bear: *Dynamics of Fluids in Porous Media* (Dover, New York 1988)
3.45 H. Fletcher: Auditory patterns, Rev. Mod. Phys. **12**, 47–65 (1940)
3.46 C.J. Bouwkamp: A contribution to the theory of acoustic radiation, Phillips Res. Rep. **1**, 251–277 (1946)
3.47 H. Helmholtz: Theorie der Luftschwingunden in Röhren mit offenen Enden, J. Reine Angew. Math. **57**, 1–72 (1860)
3.48 R.T. Beyer, S.V. Letcher: *Physical Ultrasonics* (Academic, New York 1969)
3.49 J.J. Markham, R.T. Beyer, R.B. Lindsay: Absorption of sound in fluids, Rev. Mod. Phys. **23**, 353–411 (1951)
3.50 R.B. Lindsay: *Physical Acoustics* (Dowden, Hutchinson, Ross, Stroudsburg 1974)
3.51 J. Meixner: Absorption and dispersion of sound in gases with chemically reacting and excitable components, Ann. Phys. **5**(43), 470–487 (1943)
3.52 J. Meixner: Allgemeine Theorie der Schallabsorption in Gasen un Flüssigkeiten ujnter Berücksichtigung der Transporterscheinungen, Acustica **2**, 101–109 (1952)
3.53 J. Meixner: Flows of fluid media with internal transformations and bulk viscosity, Z. Phys. **131**, 456–469 (1952)
3.54 K.F. Herzfeld, F.O. Rice: Dispersion and absorption of high frequency sound waves, Phys. Rev. **31**, 691–695 (1928)
3.55 L. Hall: The origin of ultrasonic absorption in water, Phys. Rev. **73**, 775–781 (1948)
3.56 J.S. Toll: Causality and the dispersion relations: Logical foundations, Phys. Rev. **104**, 1760–1770 (1956)

Amazon EX1014 Page 129

3.57 V.L. Ginzberg: Concerning the general relationship between absorption and dispersion of sound waves, Soviet Phys. Acoust. **1**, 32–41 (1955)
3.58 C.W. Horton, Sr.: Dispersion relationships in sediments and sea water, J. Acoust. Soc. Am. **55**, 547–549 (1974)
3.59 L.B. Evans, H.E. Bass, L.C. Sutherland: Atmospheric absorption of sound: Analytical expressions, J. Acoust. Soc. Am. **51**, 1565–1575 (1972)
3.60 H.E. Bass, L.C. Sutherland, A.J. Zuckerwar: Atmospheric absorption of sound: Update, J. Acoust. Soc. Am. **87**, 2019–2021 (1990)
3.61 F.H. Fisher, V.P. Simmons: Sound absorption in sea water, J. Acoust. Soc. Am. **62**, 558–564 (1977)
3.62 G.R. Kirchhoff: *Vorlesungen über mathematische Physik: Mechanik*, 2nd edn. (Teubner, Leipzig 1877)
3.63 J.W.S. Rayleigh: On progressive waves, Proc. Lond. Math. Soc. **9**, 21 (1877)
3.64 L.L. Beranek: Acoustical definitions. In: *American Institute of Physics Handbook*, ed. by D.E. Gray (McGraw-Hill, New York 1972), Sec. 3app. 3-2 to 3-30
3.65 G. Green: On the reflexion and refraction of sound, Trans. Camb. Philos. Soc. **6**, 403–412 (1838)
3.66 E.T. Paris: On the stationary wave method of measuring sound-absorption at normal incidence, Proc. Phys. Soc. Lond. **39**, 269–295 (1927)
3.67 W.M. Hall: An acoustic transmission line for impedance measurements, J. Acoust. Soc. Am. **11**, 140–146 (1939)
3.68 L. Cremer: Theory of the sound blockage of thin walls in the case of oblique incidence, Akust. Z. **7**, 81–104 (1942)
3.69 L.L. Beranek: Acoustical properties of homogeneous, isotropic rigid tiles and flexible blanlets, J. Acoust. Soc. Am. **19**, 556–568 (1947)
3.70 L.L. Beranek: *Noise and Vibration Control* (McGraw-Hill, New York 1971)
3.71 B.T. Chu: *Pressure waves generated by addition of heat in a gaseous medium (1955), NACA Technical Note 3411* (National Advisory Committee for Aeronautics, Washington 1955)
3.72 P.J. Westervelt, R.S. Larson: Laser-excited broadside array, J. Acoust. Soc. Am. **54**, 121–122 (1973)
3.73 H. Lamb: *Dynamical Theory of Sound* (Dover, New York 1960)
3.74 M.J. Lighthill: *Waves in Fluids* (Cambridge Univ. Press, Cambridge 1978)
3.75 G.G. Stokes: On the communication of vibration from a vibrating body to a surrounding gas, Philos. Trans. R. Soc. Lond. **158**, 447–463 (1868)
3.76 P.M. Morse: *Vibration and Sound* (Acoust. Soc. Am., Melville 1976)
3.77 P.M. Morse, H. Feshbach: *Methods of Theoretical Physics*, Vol. 1, 2 (McGraw-Hill, New York 1953)
3.78 P.M. Morse, K.U. Ingard: *Theoretical Acoustics* (McGraw-Hill, New York 1968)
3.79 G.R. Kirchhoff: Zur Theorie der Lichtstrahlen, Ann. Phys. Chem. **18**, 663–695 (1883), in German
3.80 L.G. Copley: Fundamental results concerning integral representations in acoustic radiation, J. Acoust. Soc. Am. **44**, 28–32 (1968)
3.81 H.A. Schenck: Improved integral formulation for acoustic radiation problems, J. Acoust. Soc. Am. **44**, 41–58 (1968)
3.82 A.-W. Maue: Zur Formulierung eines allgemeinen Beugungsproblems durch eine Integralgleichung, Z. Phys. **126**, 601–618 (1949), in German
3.83 A.J. Burton, G.F. Miller: The application of integral equation methods to the numerical solution of some exterior boundary value problems, Proc. Roy. Soc. Lond. A **323**, 201–210 (1971)
3.84 H.E. Hartig, C.E. Swanson: Transverse acoustic waves in rigid tubes, Phys. Rev. **54**, 618–626 (1938)
3.85 M. Abramowitz, I.A. Stegun: *Handbook of Mathematical Functions* (Dover, New York 1965)
3.86 F. Karal: The analogous acoustical impedance for discontinuities and constrictions of circular cross-section, J. Acoust. Soc. Am. **25**, 327–334 (1953)
3.87 J.W. Miles: The reflection of sound due to a change of cross section of a circular tube, J. Acoust. Soc. Am. **16**, 14–19 (1944)
3.88 J.W. Miles: The analysis of plane discontinuities in cylindrical tubes, II, J. Acoust. Soc. Am. **17**, 272–284 (1946)
3.89 W.P. Mason: The propagation characteristics of sound tubes and acoustic filters, Phys. Rev. **31**, 283–295 (1928)
3.90 P.S.H. Henry: The tube effect in sound-velocity measurements, Proc. Phys. Soc. Lond. **43**, 340–361 (1931)
3.91 P.O.A.L. Davies: The design of silencers for internal combustion engines, J. Sound Vibr. **1**, 185–201 (1964)
3.92 T.F.W. Embleton: Mufflers. In: *Noise and Vibration Control*, ed. by L.L. Beranek (McGraw-Hill, New York 1971) pp. 362–405
3.93 J.W.S. Rayleigh: On the theory of resonance, Philos. Trans. R. Soc. Lond. **161**, 77–118 (1870)
3.94 E.A. Milne: Sound waves in the atmosphere, Philos. Mag. **6**(42), 96–114 (1921)
3.95 J.B. Keller: Geometrical theory of diffraction. In: *Calculus of Variations and its Applications*, ed. by L.M. Graves (McGraw-Hill, New York 1958) pp. 27–52
3.96 P. Ugincius: Ray acoustics and Fermat's principle in a moving inhomogeneous medium, J. Acoust. Soc. Am. **51**, 1759–1763 (1972)
3.97 D.I. Blokhintzev: The propagation of sound in an inhomogeneous and moving medium, J. Acoust. Soc. Am. **18**, 322–328 (1946)
3.98 A.D. Pierce: Wave equation for sound in fluids with unsteady inhomogeneous flow, J. Acoust. Soc. Am. **87**, 2292–2299 (1990)
3.99 A. Sommerfeld, J. Runge: Anwendung der Vektorrechnung geometrische Optik, Ann. Phys. **4**(35), 277–298 (1911)
3.100 G.S. Heller: Propagation of acoustic discontinuities in an inhomogeneous moving liquid medium, J. Acoust. Soc. Am. **25**, 950–951 (1953)

Amazon EX1014 Page 130

3.101 J.B. Keller: Geometrical acoustics I: The theory of weak shock waves, J. Appl. Phys. **25**, 938–947 (1954)
3.102 W.D. Hayes: Energy invariant for geometric acoustics in a moving medium, Phys. Fluids **11**, 1654–1656 (1968)
3.103 R.B. Buchal, J.B. Keller: Boundary layer problems in diffraction theory, Commun. Pure Appl. Math. **13**, 85–144 (1960)
3.104 D. Ludwig: Uniform asymptotic expansions at a caustic, Commun. Pure Appl. Math. **19**, 215–250 (1966)
3.105 A. Sommerfeld: *Mathematical Theory of Diffraction* (Springer, Berlin 2004), (R. Nagem, M. Zampolli, G. Sandri, translators)
3.106 H.M. MacDonald: A class of diffraction problems, Proc. Lond. Math. Soc. **14**, 410–427 (1915)
3.107 F.J.W. Whipple: Diffraction by a wedge and kindred problems, Proc. Lond. Math. Soc. **16**, 481–500 (1919)
3.108 T.J.A. Bromwich: Diffraction of waves by a wedge, Proc. Lond. Math. Soc. **14**, 450–463 (1915)
3.109 H.S. Carslaw: Diffraction of waves by a wedge of any angle, Proc. Lond. Math. Soc. **18**, 291–306 (1919)
3.110 F.G. Friedlander: *Sound Pulses* (Cambridge Univ. Press, Cambridge 1958)
3.111 M.A. Biot, I. Tolstoy: Formulation of wave propagation in infinite media by normal coordinates, with an application to diffraction, J. Acoust. Soc. Am. **29**, 381–391 (1957)
3.112 V.A. Fock: *Electromagnetic Diffraction and Propagation Problems* (Pergamon, London 1965)
3.113 F.D. Tappert: The parabolic propagation method, Chap. 5. In: *Wave Propagation and Underwater Acoust.*, ed. by J.B. Keller, J.S. Papadakis (Springer, Berlin, Heidelberg 1977) pp. 224–287

Amazon EX1014 Page 131

4. Sound Propagation in the Atmosphere

Propagation of sound close to the ground outdoors involves geometric spreading, air absorption, interaction with the ground, barriers, vegetation and refraction associated with wind and temperature gradients. After a brief survey of historical aspects of the study of outdoor sound and its applications, this chapter details the physical principles associated with various propagation effects, reviews data that demonstrate them and methods for predicting them. The discussion is concerned primarily with the relatively short ranges and spectra of interest when predicting and assessing community noise rather than the frequencies and long ranges of concern, for example, in infrasonic global monitoring or used for remote sensing of the atmosphere. Specific phenomena that are discussed include spreading losses, atmospheric absorption, diffraction by barriers and buildings, interaction of sound with the ground (ground waves, surface waves, ground impedance associated with porosity and roughness, and elasticity effects), propagation through shrubs and trees, wind and temperature gradient effects, shadow zones and incoherence due to atmospheric turbulence. The chapter concludes by suggesting a few areas that require further research.

4.1 **A Short History of Outdoor Acoustics** 113
4.2 **Applications of Outdoor Acoustics** 114
4.3 **Spreading Losses** 115
4.4 **Atmospheric Absorption** 116
4.5 **Diffraction and Barriers** 116
4.5.1 Single-Edge Diffraction 116
4.5.2 Effects of the Ground on Barrier Performance 118
4.5.3 Diffraction by Finite-Length Barriers and Buildings 119
4.6 **Ground Effects** 120
4.6.1 Boundary Conditions at the Ground 120
4.6.2 Attenuation of Spherical Acoustic Waves over the Ground 120
4.6.3 Surface Waves 122
4.6.4 Acoustic Impedance of Ground Surfaces 122
4.6.5 Effects of Small-Scale Roughness 123
4.6.6 Examples of Ground Attenuation under Weakly Refracting Conditions 124
4.6.7 Effects of Ground Elasticity 125
4.7 **Attenuation Through Trees and Foliage** . 129
4.8 **Wind and Temperature Gradient Effects on Outdoor Sound** 131
4.8.1 Inversions and Shadow Zones 131
4.8.2 Meteorological Classes for Outdoor Sound Propagation ... 133
4.8.3 Typical Speed of Sound Profiles ... 135
4.8.4 Atmospheric Turbulence Effects ... 138
4.9 **Concluding Remarks** 142
4.9.1 Modeling Meteorological and Topographical Effects 142
4.9.2 Effects of Trees and Tall Vegetation 142
4.9.3 Low-Frequency Interaction with the Ground 143
4.9.4 Rough-Sea Effects 143
4.9.5 Predicting Outdoor Noise 143
References 143

4.1 A Short History of Outdoor Acoustics

Early experiments on outdoor sound were concerned with the speed of sound [4.1]. Sound from explosions and the firing of large guns contains substantial low-frequency content (< 100 Hz) and is able to travel for considerable distances outdoors. The Franciscan friar, Marin Mersenne (1588–1648), suggested timing the in-

Amazon EX1014 Page 132

terval between seeing the flash and hearing the report of guns fired at a known distance. William Derham (1657–1735), the rector of a small church near London, observed and recorded the influence of wind and temperature on sound speed. Derham noted the difference in the sound of church bells at the same distance over newly fallen snow and over a hard frozen surface.

Before enough was known for the military exploitation of outdoor acoustics, there were many unwitting influences of propagation conditions on the course of battle [4.2]. In June 1666, Samuel Pepys noted that the sounds of a naval engagement between the British and Dutch fleets were heard clearly at some spots but not at others a similar distance away or closer [4.3]. During the First World War, acoustic shadow zones, similar to those observed by Pepys, were observed during the battle of Antwerp. Observers also noted that battle sounds from France only reached England during the summer months whereas they were best heard in Germany during the winter. After the war there was great interest in these observations among the scientific community. Large amounts of ammunition were detonated throughout England and the public was asked to listen for sounds of explosions. Despite the continuing interest in atmospheric acoustics after World War 1, the advent of the submarine encouraged greater efforts in underwater acoustics research during and after World War 2.

4.2 Applications of Outdoor Acoustics

Although much current interest in sound propagation in the atmosphere relates to the prediction and control of noise from land and air transport and from industrial sources, outdoor acoustics has continued to have extensive military applications in source acquisition, ranging and identification [4.4]. Acoustic disturbances in the atmosphere give rise to solid particle motion in porous ground, induced by local pressure variations as well as air-particle motion in the pores. There is a distinction between the seismic disturbances associated with direct seismic excitation of the ground and solid-particle motion in the ground induced by airborne sounds. This has enabled the design of systems that distinguish between airborne and ground-borne sources and the application of acoustical techniques to the detection of buried land mines [4.5]. The many other applications of studies of outdoor sound propagation include aspects of animal bioacoustics [4.6] and acoustic remote sounding of the atmosphere [4.7].

Atmospheric sound propagation close to the ground is sensitive to the acoustical properties of the ground surface as well as to meteorological conditions. Most natural ground surfaces are porous. The surface porosity allows sound to penetrate and hence to be absorbed and delayed through friction and thermal exchanges. There is interference between sound traveling directly between source and receiver and sound reflected from the ground. This interference, known as the ground effect [4.8, 9], is similar to the Lloyd's mirror effect in optics but is not directly analogous. Usually, the propagation of light may be described by rays. At the lower end of the audible frequency range (20–500 Hz) and near grazing incidence to the ground, the consequences of the curvature of the expanding sound waves from a finite source are significant. Consequently, ray-based modeling is not appropriate and it is necessary to use full-wave techniques. Moreover, there are few outdoor surfaces that are mirror-like to incident sound waves. Most ground surfaces cause changes in phase as well as amplitude during reflection. Apart from the relevance to outdoor noise prediction, the sensitivity of outdoor sound propagation to ground surface properties has suggested acoustical techniques for determining soil physical properties such as porosity and air permeability [4.10–12]. These are relatively noninvasive compared with other methods.

The last decade has seen considerable advances in numerical and analytical methods for outdoor sound prediction [4.13]. Details of these are beyond the scope of this work but many are described in the excellent text by *Salomons* [4.14]; a review of recent progress may be found in *Berengier* et al. [4.15]. Among the numerical methods borrowed and adapted from underwater acoustics are the fast field program (FFP) and that based on the parabolic equation (PE). The more important advances are based predominantly on the parabolic equation method since it enables predictions that allow for changes in atmospheric and ground conditions with range whereas the FFP intrinsically does not. At present methods for predicting outdoor noise are undergoing considerable assessment and change in Europe as a result of a recent European Commission (EC) directive [4.16] and the associated requirements for noise mapping. Per-

haps the most sophisticated scheme for this purpose is NORD2000 [4.17]. A European project HARMONOISE [4.18] is developing a comprehensive source-independent scheme for outdoor sound prediction. As in NORD2000 various relatively simple formulae, predicting the effect of topography for example, are being derived and tested against numerical predictions.

4.3 Spreading Losses

Distance alone will result in wavefront spreading. In the simplest case of a sound source radiating equally in all directions, the intensity I [W^{-2}] at a distance rm from the source of power P [W], is given by

$$I = \frac{P}{4\pi r^2}\,, \tag{4.1}$$

This represents the power per unit area on a spherical wavefront of radius r. In logarithmic form the relationship between sound pressure level L_p and sound power L_W, may be written

$$L_\mathrm{p} = L_\mathrm{W} - 20\log r - 11\,\mathrm{dB}\,. \tag{4.2}$$

From a point sound source, this means a reduction of $20\log 2$ dB, i. e., 6 dB, per distance doubling in all directions (a point source is omnidirectional). Most sources appear to be point sources when the receiver is at a sufficient distance from them. If the source is directional then (4.2) is modified by inclusion of the directivity index DI.

$$L_\mathrm{p} = L_\mathrm{W} + DI - 20\log r - 11\mathrm{dB}\,. \tag{4.3}$$

The directivity index is $10\log DF$dB where DF is the directivity factor, given by the ratio of the actual intensity in a given direction to the intensity of an omnidirectional source of the same power output. Such directivity is either inherent or location-induced. A simple case of location-induced directivity arises if the point source, which would usually create spherical wavefronts of sound, is placed on a perfectly reflecting flat plane. Radiation from the source is thereby restricted to a hemisphere. The directivity factor for a point source on a perfectly reflecting plane is 2 and the directivity index is 3 dB. For a point source at the junction of a vertical perfectly reflecting wall with a horizontal perfectly reflecting plane, the directivity factor is 4 and the directivity index is 6 dB. It should be noted that these adjustments ignore phase effects and assume incoherent reflection [4.19].

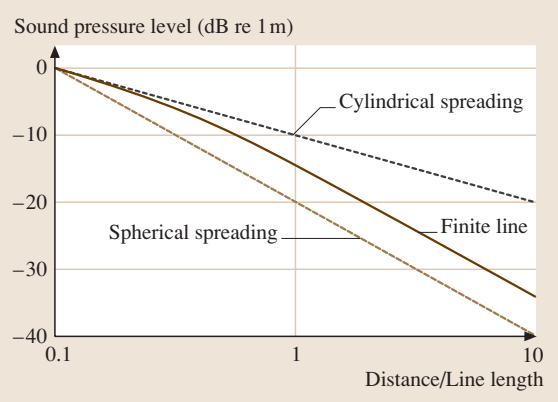


Fig. 4.1 Comparison of attenuation due to geometrical spreading from point, infinite line and finite line sources

From an infinite line source, the wavefronts are cylindrical, so wavefront spreading means a reduction of 3 dB per distance doubling. Highway traffic may be approximated by a line of incoherent point sources on an acoustically hard surface. If a line source of length l consists of contiguous omnidirectional incoherent elements of length $\mathrm{d}x$ and source strength $P\,\mathrm{d}x$, the intensity at a location halfway along the line and at a perpendicular distance d from it, so that $\mathrm{d}x = r\mathrm{d}\theta/\cos\theta$, where r is the distance from any element at angle θ from the perpendicular, is given by

$$I = \int_{-l/2}^{l/2} \frac{P}{2\pi r^2}\,\mathrm{d}x = \frac{P}{2\pi d}\left[2\tan^{-1}\left(\frac{l}{2d}\right)\right],$$

This results in

$$L_\mathrm{p} = L_\mathrm{W} - 10\log d - 8 + 10\log\left[2\tan^{-1}\left(\frac{l}{2d}\right)\right]\mathrm{dB}\,. \tag{4.4}$$

Figure 4.1 shows that the attenuation due to wavefront spreading from the finite line source behaves as that from an infinite line at distances much less than the length of the source and as that from a point source at distances greater than the length of the source.

Amazon EX1014 Page 134

4.4 Atmospheric Absorption

A proportion of sound energy is converted to heat as it travels through the air. There are heat conduction, shear viscosity and molecular relaxation losses [4.20]. The resulting air absorption becomes significant at high frequencies and at long range so air acts as a low-pass filter at long range. For a plane wave, the pressure p at distance x from a position where the pressure is p_0 is given by

$$p = p_0 \mathrm{e}^{-\alpha x/2} \tag{4.5}$$

The attenuation coefficient α for air absorption depends on frequency, humidity, temperature and pressure and may be calculated using (4.6) through (4.8) [4.21].

$$\alpha = f^2 \left[\left(\frac{1.84\times10^{-11}}{\left(\frac{T_0}{T}\right)^{\frac{1}{2}} \frac{p_s}{p_0}} \right) + \left(\frac{T_0}{T}\right)^{2.5} \left(\frac{0.106\,80\,\mathrm{e}^{-3352/T} f_{\mathrm{r,N}}}{f^2 + f_{\mathrm{r,N}}^2} + \frac{0.012\,78\,\mathrm{e}^{-2239.1/T} f_{\mathrm{r,O}}}{f^2 + f_{\mathrm{r,O}}^2} \right) \frac{\mathrm{Np}}{\mathrm{m\cdot atm}} \right], \tag{4.6}$$

where $f_{\mathrm{r,N}}$ and $f_{\mathrm{r,O}}$ are relaxation frequencies associated with the vibration of nitrogen and oxygen molecules respectively and are given by:

$$f_{\mathrm{r,N}} = \frac{p_s}{p_{s0}} \left(\frac{T_0}{T}\right)^{\frac{1}{2}} \times \left(9 + 280 He^{-4.17\left[\left(T_0/T\right)^{1/3} - 1\right]} \right), \tag{4.7}$$

$$f_{\mathrm{r,O}} = \frac{p_s}{p_{s0}} \left(24.0 + 4.04\times10^4 H \frac{0.02 + H}{0.391 + H} \right), \tag{4.8}$$

where f is the frequency. T is the absolute temperature of the atmosphere in degrees Kelvin, $T_0 = 293.15\,\mathrm{K}$ is the reference value of T (20 °C), H is the percentage molar concentration of water vapor in the atmosphere $= \rho_{\mathrm{sat}} r_{\mathrm{h}} p_0 / p_{\mathrm{s}}$, r_{h} is the relative humidity (%); p_{s} is the local atmospheric pressure and p_0 is the reference atmospheric pressure ($1\,\mathrm{atm} = 1.013\,25\times10^5\,\mathrm{Pa}$); $\rho_{\mathrm{sat}} = 10^{C_{\mathrm{sat}}}$, where $C_{\mathrm{sat}} = -6.8346(T_0/T)^{1.261} + 4.6151$. These formulae give estimates of the absorption of pure tones to an accuracy of ±10% for $0.05 < H < 5$, $253 < T < 323$, $p_0 < 200\,\mathrm{kPa}$.

Outdoor air absorption varies through the day and the year [4.22, 23].

Absolute humidity H is an important factor in the diurnal variation and usually peaks in the afternoon. Usually the diurnal variations are greatest in the summer. It should be noted that the use of (arithmetic) mean values of atmospheric absorption may lead to overestimates of attenuation when attempting to establish worst-case exposures for the purposes of environmental noise impact assessment. Investigations of local climate statistics, say hourly means over one year, should lead to more accurate estimates of the lowest absorption values.

4.5 Diffraction and Barriers

Purpose-built noise barriers have become a very common feature of the urban landscape of Europe, the Far East and America. In the USA, over 1200 miles of noise barriers were constructed in 2001 alone. The majority of barriers are installed in the vicinity of transportation and industrial noise sources to shield nearby residential properties. Noise barriers are cost effective only for the protection of large areas including several buildings and are rarely used for the protection of individual properties. Noise barriers of usual height are generally ineffective in protecting the upper levels of multi-storey dwellings. In the past two decades environmental noise barriers have become the subject of extensive studies, the results of which have been consolidated in the form of national and international standards and prediction models [4.24–26]. Extensive guides to the acoustic and visual design of noise barriers are available [4.27, 28]. Some issues remain to be resolved relating to the degradation of the noise-barrier performance in the presence of wind and temperature gradients, the influence of localized atmospheric turbulence, temporal effects from moving traffic, the influence of local vegetation, the aesthetic quality of barriers and their environmental impact.

Amazon EX1014 Page 135

4.5.1 Single-Edge Diffraction

A noise barrier works by blocking the direct path from the noise source to the receiver. The noise then reaches the receiver only via diffraction around the barrier edges. The calculation of barrier attenuation is therefore mainly dependent on the solution of the diffraction problem. Exact integral solutions of the diffraction problem were available as early as the late 19th [4.29] and early 20th century [4.30]. For practical calculations however it is necessary to use approximations to the exact solutions. Usually this involves assuming that the source and receiver are more than a wavelength from the barrier and the receiver is in the shadow zone, which is valid in almost all applications of noise barriers. The Kirchhoff–Fresnel approximation [4.31], in terms of the Fresnel numbers for thin rigid screens (4.10), and the geometrical theory of diffraction [4.32] for wedges and thick barriers have been used for deriving practical formulae for barrier calculations. For a rigid wedge barrier, the solution provided by *Hadden* and *Pierce* [4.33] is relatively easy to calculate and highly accurate. A line integral solution, based on the Kirchhoff–Fresnel approximation [4.34] describes the diffracted pressure from a distribution of sources along the barrier edge and has been extended to deal with barriers with jagged edges [4.35]. There is also a time-domain model [4.36].

As long as the transmission loss through the barrier material is sufficiently high, the performance of a barrier is dictated by the geometry (Fig. 4.2).

The total sound field in the vicinity of a semi-infinite half plane depends on the relative position of source, receiver, and the thin plane. The total sound field p_T in each of three regions shown in Fig. 4.2 is given as follows:

$$\text{In front of the barrier: } p_T = p_i + p_r + p_d\,, \tag{4.9a}$$

$$\text{Above the barrier: } p_T = p_i + p_d\,, \tag{4.9b}$$

$$\text{In the shadow zone: } p_T = p_d\,. \tag{4.9c}$$

The Fresnel numbers of the source and image source are denoted, respectively, by N_1 and N_2, and are defined as follows:

$$N_1 = \frac{R' - R_1}{\lambda/2} = \frac{k}{\pi}\left(R' - R_1\right), \tag{4.10a}$$

$$\text{and } N_2 = \frac{R' - R_2}{\lambda/2} = \frac{k}{\pi}\left(R' - R_2\right). \tag{4.10b}$$

where $R' = r_s + r_r$ is the shortest source–edge–receiver path.

The attenuation (Att) of the screen, sometimes known as the insertion loss IL, is often used to assess the acoustics performance of the barrier. It is defined as follows,

$$\text{Att} = \text{IL} = 20\lg\left(\left|\frac{p_w}{p_{w/o}}\right|\right)\text{dB}\,, \tag{4.11}$$

where p_w and $p_{w/o}$ is the total sound field with or without the presence of the barrier. Note that the barrier attenuation is equal to the insertion loss only in the absence of ground effect.

Maekawa [4.37] has provided a chart that expresses the attenuation of a thin rigid barrier based on the Fresnel number N_1 associated with the source. The chart was derived empirically from extensive laboratory experimental data but use of the Fresnel number was suggested by the Kirchhoff–Fresnel diffraction theory. Maekawa's chart extends into the illuminated zone where N_1 is taken to be negative. Maekawa's chart has been proved to be very successful and has become the de facto standard empirical method for barrier calculations. Many of the barrier calculation methods embodied in national and international standards [4.24, 38] stem from this chart. There have been many attempts to fit the chart with simple formulae. One of the simplest formulae [4.39] is

$$\text{Att} = 10\lg(3 + 20N)\text{dB}\,. \tag{4.12}$$

The *Maekawa* curve can be represented mathematically by [4.40]

$$\text{Att} = 5 + 20\lg\frac{\sqrt{2\pi N_1}}{\tanh\sqrt{2\pi N_1}}\,. \tag{4.13}$$

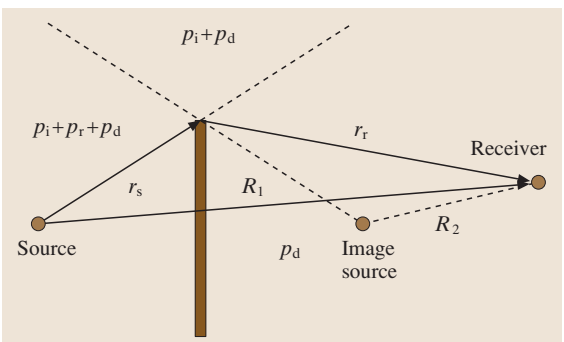


Fig. 4.2 Diffraction of sound by a thin barrier

An improved version of this result, using both Fresnel Numbers (4.10), is [4.41]

$$\mathrm{Att} = \mathrm{Att_s} + \mathrm{Att_b} + \mathrm{Att_{sb}} + \mathrm{Att_{sp}}\,, \tag{4.14a}$$

$$\text{where } \mathrm{Att_s} = 20\lg\frac{\sqrt{2\pi N_1}}{\tanh\sqrt{2\pi N_1}} - 1\,, \tag{4.14b}$$

$$\mathrm{Att_b} = 20\lg\left[1+\tanh\left(0.6\lg\frac{N_2}{N_1}\right)\right]\,, \tag{4.14c}$$

$$\mathrm{Att_{sb}} = \left(6\tanh\sqrt{N_2} - 2 - \mathrm{Att_b}\right) \times\left(1-\tanh\sqrt{10N_1}\right)\,, \tag{4.14d}$$

$$\mathrm{Att_{sp}} = -10\lg\frac{1}{\left(R'/R_1\right)^2 + \left(R'/R_1\right)}\,. \tag{4.14e}$$

The term $\mathrm{Att_s}$ is a function of N_1, which is a measure of the relative position of the receiver from the source. The second term depends on the ratio of N_2/N_1, which depends on the proximity of either the source or the receiver to the half plane. The third term is only significant when N_1 is small and depends on the proximity of the receiver to the shadow boundary. The last term, a function of the ratio R'/R_1, accounts for the diffraction effect due to spherical incident waves.

4.5.2 Effects of the Ground on Barrier Performance

Equations (4.12–4.14) only predict the amplitude of sound and do not include wave interference effects. Such interference effects result from the contributions from different diffracted wave paths in the presence of ground (see also Sect. 4.6).

Consider a source S_g located at the left side of the barrier, a receiver R_g at the right side of the barrier and E is the diffraction point on the barrier edge (see Fig. 4.3).

The sound reflected from the ground surface can be described by an image of the source S_i. On the receiver side, sound waves will also be reflected from the ground. This effect can be considered in terms of an image of the receiver R_i. The pressure at the receiver is the sum of four terms that correspond to the sound paths $S_g E R_g$, $S_i E R_g$, $S_g E R_i$ and $S_i E R_i$. If the surface is a perfectly reflecting ground, the total sound field is the sum of the diffracted fields of these four paths,

$$P_T = P_1 + P_2 + P_3 + P_4\,, \tag{4.15}$$

where

$$P_1 = P\left(S_g, R_g, E\right),$$
$$P_2 = P\left(S_i, R_g, E\right),$$
$$P_3 = P\left(S_g, R_i, E\right),$$
$$P_4 = P\left(S_i, R_i, E\right).$$

$P(S, R, E)$ is the diffracted sound field due to a thin barrier for given positions of source S, receiver R and the point of diffraction at the barrier edge E. If the ground has finite impedance (such as grass or a porous road surface) then the pressure corresponding to rays reflected from these surfaces should be multiplied by the appropriate spherical wave reflection coefficient(s) to allow for the change in phase and amplitude of the wave on reflection as follows,

$$P_T = P_1 + Q_s P_2 + Q_R P_3 + Q_s Q_R P_4\,, \tag{4.16}$$

where Q_s and Q_R are the spherical wave reflection coefficients for the source and receiver side respectively. The spherical wave reflection coefficients can be calculated for different types of ground surfaces and source/receiver geometries (Sect. 4.6).

Usually, for a given source and receiver position, the acoustic performance of the barrier on the ground is assessed by use of either the excess attenuation (EA) or the insertion loss (IL). They are defined as follows,

$$\mathrm{EA} = SPL_f - SPL_b\,, \tag{4.17}$$

$$\mathrm{IL} = SPL_g - SPL_b\,, \tag{4.18}$$

where SPL_f is the free field noise level, SPL_g is the noise level with the ground present and SPL_b is the noise level with the barrier and ground present. Note that, in the absence of a reflecting ground, the numerical value of EA (which was called Att previously) is the same as IL. If the calculation is carried out in terms of amplitude only, then the attenuation Att_n for each sound path can be directly determined from the appropriate Fresnel number F_n for that path. The excess attenuation

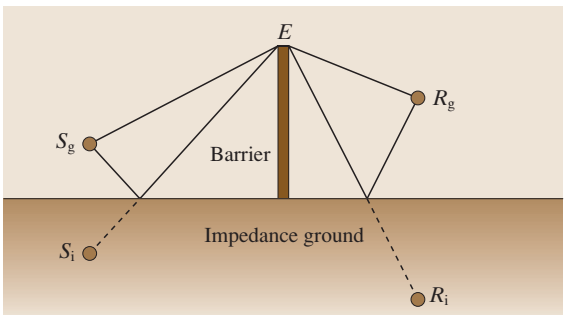


Fig. 4.3 Diffraction by a barrier on impedance ground

Amazon EX1014 Page 137

of the barrier on a rigid ground is then given by

$$A_T = 10\lg\left(10^{-\left|\frac{\mathrm{Att}_1}{10}\right|} + 10^{-\left|\frac{\mathrm{Att}_2}{10}\right|} + 10^{-\left|\frac{\mathrm{Att}_3}{10}\right|} + 10^{-\left|\frac{\mathrm{Att}_4}{10}\right|}\right). \quad (4.19)$$

The attenuation for each path can either be calculated by empirical or analytical formulae depending on the complexity of the model and the required accuracy.

A modified form of the empirical formula for the calculation of barrier attenuation is [4.24]

$$\mathrm{IL} = 10\log_{10}\left[3 + \left(C_2\frac{\delta_1}{\lambda}\right)C_3 K_{\mathrm{met}}\right], \quad (4.20)$$

where $C_2 = 20$ and includes the effect of ground reflections; $C_2 = 40$ if ground reflections are taken into account elsewhere; C_3 is a factor to take into account a double diffraction or finite barrier effect, $C_3 = 1$ for a single diffraction and $\delta_1 = (r_s + r_r) - R_1$ (Fig. 4.2). The C_3 expression for double diffraction is given later.

The term K_{met} in (4.15) is a correction factor for average downwind meteorological effects, and is given by

$$K_{\mathrm{met}} = \mathrm{e}^{-\frac{1}{2000}\sqrt{\frac{r_s r_r r_o}{2\delta_1}}}$$

for $\delta_1 > 0$ and $K_{\mathrm{met}} = 1$ for $\delta_1 \le 0$.

The formula reduces to the simple formula (4.12) when the barrier is thin, there is no ground and if meteorological effects are ignored.

There is a simple approach capable of modeling wave effects in which the phase of the wave at the receiver is calculated from the path length via the top of the screen, assuming a phase change in the diffracted wave of $\pi/4$ [4.42]. This phase change is assumed to be constant for all source–barrier–receiver geometries. The diffracted wave, for example, for the path $S_g E R_g$ would thus be given by

$$P_1 = \mathrm{Att}_1\,\mathrm{e}^{-\mathrm{i}\left[k\left(r_0 + r_r\right) + \pi/4\right]}. \quad (4.21)$$

This approach provides a reasonable approximation for the many situations of interest where source and receiver are many wavelengths from the barrier and the receiver is in the shadow zone.

For a thick barrier of width w, the International Standards Organization (ISO) standard ISO 9613-2 [4.24] provides the following form of correction factor C_3 for use in (4.20):

$$C_3 = \frac{\left[1 + \left(\frac{5\lambda}{w}\right)^2\right]}{\left[\frac{1}{3} + \left(\frac{5\lambda}{w}\right)^2\right]},$$

where for double diffraction, $\delta_1 = \left(r_s + r_r + w\right) - R_1$.

Note that this empirical method is for rigid barriers of finite thickness and does not take absorptive surfaces into account.

4.5.3 Diffraction by Finite-Length Barriers and Buildings

All noise barriers have finite length and for certain conditions sound diffracting around the vertical ends of the barrier may be significant. This will also be the case for sound diffracting around buildings. Figure 4.4 shows eight diffracted ray paths contributing to the total field behind a finite-length barrier situated on finite-impedance ground. In addition to the four normal ray paths diffracted at the top edge of the barrier (Fig. 4.3), four more diffracted ray paths result from the vertical edges – two ray paths from each one. The two rays at either side are, respectively, the direct diffracted ray and the diffracted–reflected ray. Strictly, there are two further ray paths at each side which involve two reflections at the ground as well as diffraction at the vertical edge but usually these are neglected.

The reflection angles of the two diffracted–reflected rays are independent of the barrier position. They will either reflect at the source side or on the receiver side of the barrier, which are dependent on the relative positions of the source, receiver and barrier. The total field is given by

$$P_T = P_1 + Q_s P_2 + Q_R P_3 + Q_s Q_R P_4 + P_5 + Q_R P_6 + P_7 + Q_R P_8, \quad (4.22)$$

where P_1–P_4 are those given earlier for the diffraction at the top edge of the barrier.

Although accurate diffraction formulas may be used to compute P_i $(i = 1, \ldots, 8)$, a simpler approach is to assume that each diffracted ray has a constant phase shift of $\pi/4$ regardless of the position of source, receiver and diffraction point.

To predict the attenuation due to a single building, the double diffraction calculations mentioned earlier could be used. For a source or receiver situated in a built-up area, ISO 9613-2 [4.24] proposes an empirical method for calculating the combined effects of screening

and multiple reflections. The net attenuation A_{build}dB (< 10 dB) is given by

$$A_{\text{build}} = A_{\text{build},1} + A_{\text{build},2} \tag{4.23}$$
$$A_{\text{build},1} = 0.1 B d_0 ,$$
$$A_{\text{build},2} = -10 \log \left[1 - (p/100)\right] ,$$

where B is the area density ratio of buildings (total plan area/total ground area) and d_0 is the length of the refracted path from source to receiver that passes through buildings. $A_{\text{build},2}$ is intended to be used only where there are well defined but discontinuous rows of buildings near to a road or railway and, p is the percentage of the length of facades relative to the total length of the road or railway. As with barrier attenuation, the attenuation due to buildings is to be included only when it is predicted to be greater than that due to ground effect. The ISO scheme offers also a frequency dependent attenuation coefficient (dB/m) for propagation of industrial noise through an array of buildings on an industrial site. It should be noted that there are considerable current efforts devoted to studying sound propagation through buildings and along streets but this work is not surveyed here.

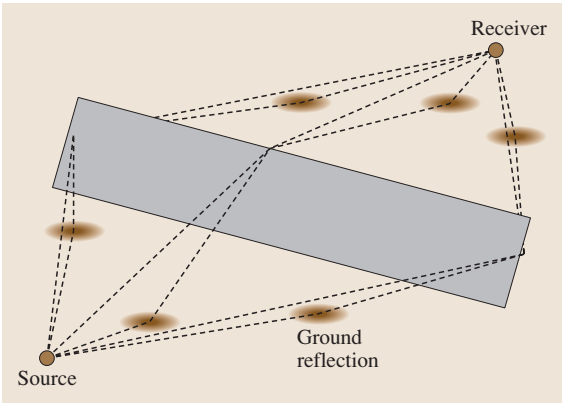


Fig. 4.4 Ray paths around a finite-length barrier or building on the ground

4.6 Ground Effects

Ground effects (for elevated source and receiver) are the result of interference between sound traveling directly from source to receiver and sound reflected from the ground when both source and receiver are close to the ground. Sometimes the phenomenon is called ground absorption but, since the interaction of outdoor sound with the ground involves interference, there can be enhancement associated with constructive interference as well as attenuation resulting from destructive interference. Close to ground such as nonporous concrete or asphalt, the sound pressure is doubled more or less over a wide range of audible frequencies. Such ground surfaces are described as *acoustically hard*. Over porous surfaces, such as soil, sand and snow, enhancement tends to occur at low frequencies since the longer the sound wave the less able it is to penetrate the pores. However, at higher frequencies, sound is able to penetrate porous ground so the surface reflection is changed in amplitude and phase. The presence of vegetation tends to make the surface layer of ground including the root zone more porous. Snow is significantly more porous than soil and sand. The layer of partly decayed matter on the floor of a forest is also highly porous. Porous ground surfaces are sometimes called *acoustically soft*.

4.6.1 Boundary Conditions at the Ground

For most environmental noise predictions porous ground may be considered to be rigid, so only one wave type, i. e., the wave penetrating the pores, need be considered. With this assumption, the speed of sound in the ground (c_1) is typically much smaller than that (c) in the air, i. e., $c \gg c_1$. The propagation of sound in the air gaps between the solid particles of which the ground is composed, is impeded by viscous friction. This in turn means that the index of refraction in the ground $n_1 = c/c_1 \gg 1$ and any incoming sound ray is refracted towards the normal as it propagates from air into the ground. This type of ground surface is called *locally reacting* because the air–ground interaction is independent of the angle of incidence of the incoming waves. The acoustical properties of locally reacting ground may be represented simply by its relative normal-incidence surface impedance (Z), or its inverse (the relative admittance β) and the ground is said to form a finite-impedance boundary. A perfectly hard ground has infinite impedance (zero admittance). A perfectly soft ground has zero impedance (infinite admittance). If the ground is not locally reacting, i. e., it is externally reacting, the impedance condition is replaced by two separate conditions governing the continuity of pres-

Amazon EX1014 Page 139

sure and the continuity of the normal component of air particle velocity.

4.6.2 Attenuation of Spherical Acoustic Waves over the Ground

The idealized case of a point (omnidirectional) source of sound at height z_s and a receiver at height z, separated by a horizontal distance r above a finite-impedance plane (admittance β) is shown in Fig. 4.5.

Between source and receiver, a direct sound path of length R_1 and a ground-reflected path of length R_2 are identified. With the restrictions of long range ($r \approx R_2$), high frequency ($kr \gg 1$, $k(z+z_s) \gg 1$, where $k = \omega/c$ and $\omega = 2\pi f$, f being frequency) and with both the source and receiver located close ($r \gg z+z_s$) to a relatively hard ground surface ($|\beta|^{big} \ll 1$), the total sound field at (x, y, z) can be determined from

$$p(x, y, z) = \frac{e^{-ikR_1}}{4\pi R_1} + \frac{e^{-ikR_2}}{4\pi R_2} + \Phi_p + \phi_s \,, \qquad (4.24)$$

where

$$\Phi_p \approx 2i\sqrt{\pi}\left(\tfrac{1}{2}kR_2\right)^{1/2} \beta e^{-w^2} \mathrm{erfc}(iw) \frac{e^{-ikR_2}}{4\pi R_2} \,. \qquad (4.25)$$

and w, sometimes called the numerical distance, is given by

$$w \approx \tfrac{1}{2}(1-i)\sqrt{kR_2}(\cos\theta + \beta) \,. \qquad (4.26)$$

ϕ_s represents a surface wave and is small compared with Φ_p under most circumstances. It is included in careful computations of the complementary error function $\mathrm{erfc}(x)$ [4.43]. In all of the above a time dependence of $e^{i\omega t}$ is understood.

After rearrangement, the sound field due to a point monopole source above a locally reacting ground becomes

$$p(x, y, z) = \frac{e^{-ikR_1}}{4\pi R_1} + \left[R_p + (1-R_p)F(w)\right] \times \frac{e^{-ikR_2}}{4\pi R_2} \,, \qquad (4.27)$$

where $F(w)$, sometimes called the boundary loss factor, is given by

$$F(w) = 1 - i\sqrt{\pi}\, w \exp(-w^2)\mathrm{erfc}(iw) \qquad (4.28)$$

and describes the interaction of a spherical wavefront with a ground of finite impedance [4.44]. The term in the square bracket of (4.27) may be interpreted as the spherical wave reflection coefficient

$$Q = R_p + (1-R_p)F(w) \,, \qquad (4.29)$$

which can be seen to involve the plane wave reflection coefficient R_p and a correction. The second term of Q allows for the fact that the wavefronts are spherical rather than plane. Its contribution to the total sound field has been called the *ground wave*, in analogy with the corresponding term in the theory of amplitude-modulated (AM) radio reception [4.45]. It represents a contribution from the vicinity of the image of the source in the ground plane. If the wavefront is plane $(R_2 \to \infty)$ then $|w| \to \infty$ and $F \to 0$. If the surface is acoustically hard, then $|\beta| \to 0$, which implies $|w| \to 0$ and $F \to 1$. If $\beta = 0$, corresponding to a perfect reflector, the sound field consists of two terms: a direct-wave contribution and a wave from the image source corresponding to specular reflection and the total sound field may be written

$$p(x, y, z) = \frac{e^{-ikR_1}}{4\pi R_1} + \frac{e^{-ikR_2}}{4\pi R_2} \,.$$

This has a first minimum corresponding to destructive interference between the direct and ground-reflected components when $k(R_2 - R_1) = \pi$, or $f = c/2(R_2 - R_1)$. Normally, for source and receiver close to the ground, this destructive interference is at too high a frequency to be of importance in outdoor sound prediction. The higher the frequency of the first minimum in the ground effect, the more likely that it will be destroyed by turbulence (Sect. 4.8).

For $|\beta| \ll 1$ but at grazing incidence ($\theta = \pi/2$), so that $R_p = -1$ and

$$p(x, y, z) = 2F(w)e^{-ikr}/r \,, \qquad (4.30)$$

the numerical distance w is given by

$$w = \tfrac{1}{2}(1-i)\beta\sqrt{kr} \,. \qquad (4.31)$$

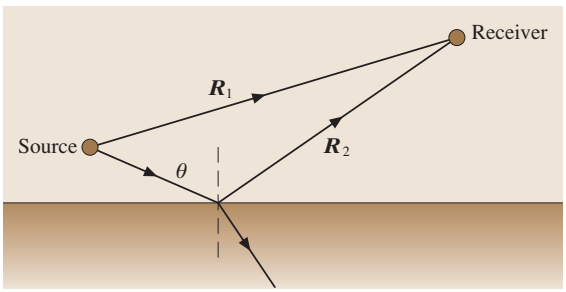


Fig. 4.5 Sound propagation from a point source to a receiver above a ground surface

If the plane wave reflection coefficient had been used instead of the spherical wave reflection coefficient for grazing incidence, it would have led to the prediction of zero sound field when both source and receiver are on the ground. Equation (4.22) is the most widely used analytical solution for predicting sound field above a locally reacting ground in a homogeneous atmosphere. There are many other accurate asymptotic and numerical solutions available but no significant numerical differences between various predictions have been revealed for practical geometries and typical outdoor ground surfaces.

4.6.3 Surface Waves

Although, numerically, it is part of the calculation of the complementary error function, physically the surface wave is a separate contribution propagating close to and parallel to the porous ground surface. It produces elliptical motion of air particles as a result of combining motion parallel to the surface with that normal to the surface in and out of the pores. The surface wave decays with the inverse square root of range rather than inversely with range as is true for other components. At grazing incidence on an impedance plane, with normalized admittance $\beta = \beta_r + \mathrm{i}\beta_x$, the condition for the existence of the surface wave is

$$\frac{1}{\beta_x^2} > \frac{1}{\beta_r^2} + 1 \,. \tag{4.32}$$

For a surface with large impedance, i. e., where $|\beta| \to 0$, the condition is simply that the imaginary part of the ground impedance (the reactance) is greater than the real part (the resistance). This type of surface impedance is possessed by cellular or lattice layers placed on smooth, hard surfaces. Surface waves due to a point source have been generated and studied extensively over such surfaces in laboratory experiments [4.46–48]. The outdoor ground type most likely to produce a measurable surface wave is a thin layer of snow over a frozen ground. By using blank pistol shots in experiments over snow, *Albert* [4.49] has confirmed the existence of the predicted type of surface wave outdoors.

There are some cases where it is not possible to model the ground surface as an impedance plane, i. e., n_1 is not sufficiently high to warrant the assumption that $n_1 \gg 1$. In this case, the refraction of the sound wave depends on the angle of incidence as sound enters the porous medium. This means that the apparent impedance depends not only on the physical properties of the ground surface but also, critically, on the angle of incidence. It is possible to define an *effective* admittance, β_e defined by:

$$\beta_\mathrm{e} = \varsigma_1 \sqrt{n_1^2 - \sin^2\theta} \,, \tag{4.33}$$

where $\varsigma_1 = \rho/\rho_1$ is the ratio of air density to the (complex) density of the rigid, porous ground.

This allows use of the same results as before but with the admittance replaced by the effective admittance for a semi-infinite non-locally reacting ground [4.50]. There are some situations where there is a highly porous surface layer above a relatively nonporous substrate. This is the case with forest floors consisting of partly decomposed litter layers above soil with a relatively high flow resistivity, with freshly fallen snow on a hard ground or with porous asphalt laid on a nonporous substrate. The minimum depth d_m for such a multiple layer ground to be treated as a semi-infinite externally reacting ground to satisfy the above condition depends on the acoustical properties of the ground and the angle of incidence. We can consider two limiting cases. If the propagation constant within the surface layer is denoted by $k_1 = k_r - \mathrm{i}k_x$, and for normal incidence, where $\theta = 0$, the required condition is simply

$$d_\mathrm{m} > 6/k_x \,. \tag{4.34}$$

For grazing incidence where $\theta = \pi/2$, the required condition is

$$d_\mathrm{m} > 6 \left(\sqrt{\frac{\left(k_r^2 - k_x^2 - 1\right)^2}{4} + k_r^2 k_x^2} - \frac{k_r^2 - k_x^2 - 1}{2} \right)^{\frac{1}{2}} . \tag{4.35}$$

It is possible to derive an expression for the effective admittance of ground with an arbitrary number of layers. However, sound waves can seldom penetrate more than a few centimeters in most outdoor ground surfaces. Lower layers contribute little to the total sound field above the ground and, normally, consideration of ground structures consisting of more than two layers is not required for predicting outdoor sound. Nevertheless, the assumption of a double-layer structure [4.50] has been found to enable improved agreement with data obtained over snow [4.51]. It has been shown rigorously that, in cases where the surface impedance depends on angle, replacing the normal surface impedance by the grazing incidence value is sufficiently accurate for predicting outdoor sound [4.52].

Amazon EX1014 Page 141

4.6.4 Acoustic Impedance of Ground Surfaces

For most applications of outdoor acoustics, porous ground may be considered to have a rigid, rather than elastic, frame. The most important characteristic of a porous ground surface that affects its acoustical character is its flow resistivity. Soil scientists tend to refer to air permeability, which is proportional to the inverse of flow resistivity. Flow resistivity is a measure of the ease with which air can move into and out of the ground. It represents the ratio of the applied pressure gradient to the induced volume flow rate per unit thickness of material and has units of $\mathrm{Pa\,s\,m^{-2}}$. If the ground surface has a high flow resistivity, it means that it is difficult for air to flow through the surface. Flow resistivity increases as porosity decreases. For example, conventional hot-rolled asphalt has a very high flow resistivity ($10\,000\,000\,\mathrm{Pa\,s\,m^{-2}}$) and negligible porosity, whereas drainage asphalt has a volume porosity of up to 0.25 and a relatively low flow resistivity ($< 30\,000\,\mathrm{Pa\,s\,m^{-2}}$). Soils have volume porosities of between 10% and 40%. A wet compacted silt may have a porosity as low as 0.1 and a rather high flow resistivity ($4\,000\,000\,\mathrm{Pa\,s\,m^{-2}}$). Newly fallen snow has a porosity of around 60% and a fairly low flow resistivity ($< 10\,000\,\mathrm{Pa\,s\,m^{-2}}$). The thickness of the surface porous layer and whether or not it has acoustically hard substrate are also important factors.

A widely used model [4.53] for the acoustical properties of outdoor surfaces involves a single parameter, the *effective* flow resistivity σ_e, to characterize the ground. According to this single-parameter model, the propagation constant k and normalized characteristic impedance Z are given by

$$\frac{k}{k_1} = \left[1 + 0.0978\left(f/\sigma_\mathrm{e}\right)^{-0.700} - \mathrm{i}0.189\left(f/\sigma_\mathrm{e}\right)^{-0.595}\right], \tag{4.36a}$$

$$Z = \frac{\rho_1 c_1}{\rho c} = 1 + 0.0571\left(f/\sigma_\mathrm{e}\right)^{-0.754} - \mathrm{i}0.087\left(f/\sigma_\mathrm{e}\right)^{-0.732}. \tag{4.36b}$$

This model may be used for a locally reacting ground as well as for an extended reaction surface. On the other hand, there is considerable evidence that (4.36a) tends to overestimate the attenuation within a porous material with high flow resistivity. On occasion better agreement with grassland data has been obtained by assuming that the ground surface is that of a hard-backed porous layer of thickness d [4.54] such that the surface impedance Z_S is given by

$$Z_\mathrm{S} = Z\coth(\mathrm{i}kd)\,. \tag{4.36c}$$

A model based on an exponential change in porosity with depth has been suggested [4.55, 56]. Although this model is suitable only for high flow resistivity, i. e., a locally reacting ground, it has enabled better agreement with measured data for the acoustical properties of many outdoor ground surfaces than equation (4.36b). The two adjustable parameters are the effective flow resistivity (σ_e) and the effective rate of change of porosity with depth (α_e). The impedance of the ground surface is predicted by

$$Z = 0.436(1-\mathrm{i})\sqrt{\frac{\sigma_\mathrm{e}}{f}} - 19.74\mathrm{i}\frac{\alpha_\mathrm{e}}{f}\,. \tag{4.37}$$

More-sophisticated theoretical models for the acoustical properties of rigid, porous materials introduce porosity, the tortuosity (or *twistiness*) of the pores and factors related to pore shape [4.57] and multiple layering. Models that introduce viscous and thermal characteristic dimensions of pores [4.58] are based on a formulation by *Johnson* et al. [4.59]. Recently, it has been shown possible to obtain explicit relationships between the characteristic dimensions and grain size by assuming a specific microstructure of identical stacked spheres [4.60]. Other developments allowing for a log-normal pore-size distribution, while assuming pores of identical shape [4.57, 61], are based on the work of *Yamamoto* and *Turgut* [4.62]. As mentioned previously, sometimes it is important to include multiple layering as well. A standard method for obtaining ground impedance is the template method based on short-range measurements of excess attenuation [4.63]. Some values of parameters deduced from data according to (4.36) and (4.37) show that there can be a wide range of parameter values for grassland.

4.6.5 Effects of Small-Scale Roughness

Some surface impedance spectra derived directly from measurements of complex excess attenuation over uncultivated grassland [4.64] indicate that the surface impedance tends to zero above 3 kHz [4.65]. The effects of incoherent scatter from a randomly rough porous surface may be used to explain these measurements. Using a boss approach, an approximate effective admittance for grazing incidence on a hard surface containing randomly distributed two-dimensional (2-D) roughness normal to

Amazon EX1014 Page 142

the roughness axes, may be written [4.66]

$$\beta \approx \left(\frac{3V^2k^3b}{2}\right)\left(1+\frac{\delta^2}{2}\right)+\mathrm{i}Vk(\delta-1)\,, \qquad (4.38)$$

where V is the roughness volume per unit area of surface (equivalent to mean roughness height), b is the mean center-to-center spacing, δ is an interaction factor depending on the roughness shape and packing density and k is the wave number. An interesting consequence of (4.38) is that a surface that would be acoustically hard if smooth has, effectively, a finite impedance at grazing incidence when rough. The real part of the admittance allows for incoherent scatter from the surface and varies with the cube of the frequency and the square of the roughness volume per unit area. The same approach can be extended to give the effective normalized surface admittance of a porous surface containing 2-D roughness [4.65, 69]. For a randomly rough porous surface near grazing incidence [4.70] it is possible to obtain the following approximation:

$$Z_r \approx Z_s - \left(\frac{\langle H\rangle R_s}{\gamma\rho_0 c_0}\right)\left(\frac{2}{\nu}-1\right)\,, \quad \left[\mathrm{Re}(Z_r)\geq 0\right], \qquad (4.39)$$

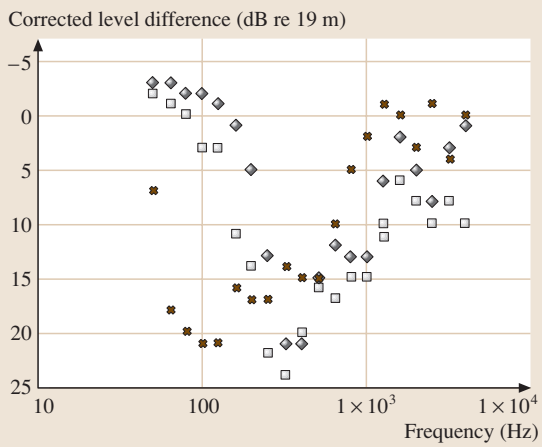


Fig. 4.6 Parkin and Scholes data for the level difference between microphones at a height of 1.5 m and at distances of 19 m and 347 m from a fixed jet engine source (nozzle-center height 1.82 m) corrected for wavefront spreading and air absorption. □ and ◇ represent data over airfields (grass covered) at Radlett and Hatfield respectively with a positive vector wind between source and receiver of 1.27 m/s (5 ft/s); × represent data obtained over approximately 0.15 m thick (6–9 inch) snow at Hatfield and a positive vector wind of 1.52 m/s (6 ft/s). (After [4.67, 68])

where $\nu = 1+\frac{2}{3}\pi\langle H\rangle$, $\langle H\rangle$ is the root mean square roughness height and Z_s is the impedance of the porous surface if it were smooth. This can be used with an impedance model or measured smooth surface impedance to predict the effect of surface roughness for long wavelengths.

Potentially, cultivation practices have important influences on ground effect since they change the surface properties. *Aylor* [4.71] noted a significant change in the excess attenuation at a range of 50 m over a soil after disking without any noticeable change in the meteorological conditions. Another cultivation practice is sub-soiling, which is intended to break up soil compaction 300 mm or more beneath the ground surface caused, for example, by the repeated passage of heavy vehicles. It is achieved by creating cracks in the compacted layer by means of a single- or double-bladed tine with sharpened leading edges. Sub-soiling only has a small effect on the surface profile of the ground. Plowing turns the soil surface over to a depth of about 0.15 m. Measurements taken over cultivated surfaces before and after sub-soiling and plowing have been shown to be consistent with the predicted effects of the resulting changes in surface roughness and flow resistivity [4.65, 72].

4.6.6 Examples of Ground Attenuation under Weakly Refracting Conditions

Pioneering studies of the combined influences of ground surface and meteorological conditions [4.67, 68] were carried out using a fixed Rolls Royce Avon jet engine as a source at two airfields. The wind speeds and temperatures were monitored at two heights and therefore it was possible to deduce something about the wind and temperature gradients during the measurements. However, perhaps because the role of turbulence was not appreciated (Sect. 4.8.3), the magnitude of turbulence was not monitored. This was the first research to note and quantify the change in ground effect with type of surface. Examples of the resulting data, quoted as the difference between sound pressure levels at 19 m (the reference location) and more distant locations corrected for the decrease expected from spherical spreading and air absorption, are shown in Fig. 4.6. During slightly downwind conditions with low wind speed ($< 2\,\mathrm{ms}^{-1}$) and small temperature gradients ($< 0.01°/\mathrm{m}$), the ground attenuation over grass-covered ground at Hatfield, although still a major propagation factor of more than 15 dB near 400 Hz, was less than that over the other grass-covered ground at Radlett and its maximum value occurred at a higher frequency. Snowfall during the pe-

Amazon EX1014 Page 143

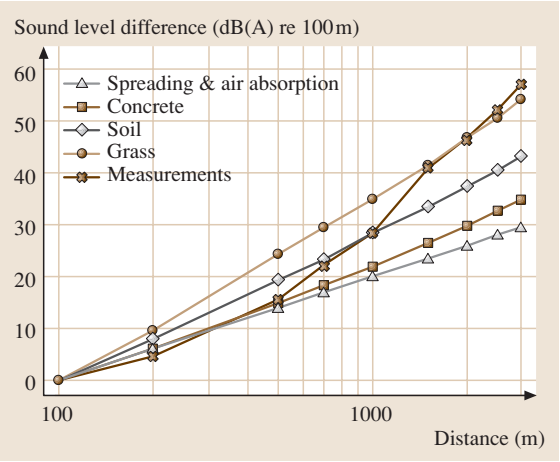


Fig. 4.7 Measured differences between the A-weighted sound level at 100 m and those measured at ranges up to 3 km during an Il-86 aircraft's engine test in the direction of maximum jet noise generation (≈ 40° from exhaust axis) and predictions for levels due to a point source at the engine center height assuming spherical spreading plus air absorption and various types of ground

riod of the measurements also enabled observation of the large change resulting from the presence of snow at low frequencies, i. e., over 20 dB attenuation in the 63 Hz and 125 Hz third-octave bands.

Noise measurements have been made to distances of 3 km during aircraft engine run-ups with the aim of defining noise contours in the vicinity of airports [4.73].

Measurements were made for a range of power settings during several summer days under weakly refracting weather conditions (wind speed < 5 m/s, temperature 20–25 °C). 7–10 measurements were made at every measurement station (in accordance with International Civil Aviation Organization (ICAO) annex 16 requirements) and the results have been averaged. Example results are shown in Fig. 4.7. It can be shown that these data are consistent with nearly acoustically neutral, i. e., zero gradient of the sound of speed, conditions. Note that at 3 km, the measured levels are more than 30 dB less than would be expected from wavefront spreading and air absorption only.

Up to distances of 500–700 m from the engine, the data suggest attenuation rates near to the concrete or spherical spreading plus air absorption predictions. Beyond 700 m the measured attenuation rate is nearer to the soil prediction or between the soil and grass predictions. These results are consistent with the fact that the run-ups took place over the concrete surface of an apron and further away (i. e., between 500–700 m in various directions) the ground surface was soil and/or grass.

4.6.7 Effects of Ground Elasticity

Noise sources such as blasts and heavy weapons shooting create low-frequency impulsive sound waves that propagate over long distances, and can create a major environmental problem for military training fields. Such impulsive sound sources tend to disturb neighbors more through the vibration and rattling induced in buildings, than by the direct audible sound itself [4.74, 75]. Human perception of whole-body vibration includes frequencies down to 1 Hz [4.76]. Moreover, the fundamental natural frequencies of buildings are in the range 1–10 Hz. Planning tools to predict and control such activities must therefore be able to handle sound propagation down to these low frequencies.

Despite their valuable role in many sound-propagation predictions, locally reacting ground impedance models have the intrinsic theoretical shortcoming that they fail to account for air-to-ground coupling through interaction between the atmospheric sound wave and elastic waves in the ground. This occurs particularly at low frequencies. Indeed air–ground coupled surface waves at low frequencies have been of considerable interest in geophysics, both because of the measured ground-roll caused by intense acoustic sources and the possible use of air sources in ground layering studies. Theoretical analyses have been carried out for spherical wave incidence on a ground consisting either of a fluid or solid layer above a fluid or solid half-space [4.77]. However, to describe the phenomenon of acoustic-to-seismic coupling accurately it has been found that the ground must be modeled as an elastic porous material [4.78, 79]. The resulting theory is relevant not only to predicting the ground vibration induced by low-frequency acoustic sources but also, as we shall see, in predicting the propagation of low-frequency sound above the ground.

The classical theory for a porous and elastic medium predicts the existence of three wave types in the porous medium: two dilatational waves and one rotational wave. In a material consisting of a dense solid frame with a low-density fluid saturating the pores, the first kind of dilatational wave has a velocity very similar to the dilatational wave (or geophysical P wave) traveling in the drained frame. The attenuation of the first dilatational wave type is however, higher than that of the P wave in the drained frame. The extra attenuation comes from the viscous forces in the pore fluid acting on the pore

Amazon EX1014 Page 144

walls. This wave has negligible dispersion and the attenuation is proportional to the square of the frequency, as is the case for the rotational wave. The viscous coupling leads to some of the energy in this propagating wave being carried into the pore fluid as the second type of dilatational wave.

In air-saturated soils, the second dilatational wave has a much lower velocity than the first and is often called the slow wave, while the dilatational wave of the first kind being called the fast wave. The attenuation of the slow wave stems from viscous forces acting on the pore walls and from thermal exchange with the pore walls. Its rigid-frame limit is very similar to the wave that travels through the fluid in the pores of a rigid, porous solid [4.80]. It should be remarked that the slow wave is the only wave type considered in the previous discussions of ground effect. When the slow wave is excited, most of the energy in this wave type is carried in the pore fluid. However, the viscous coupling at the pore walls leads to some propagation within the solid frame. At low frequencies, it has the nature of a diffusion process rather than a wave, being analogous to heat conduction. The attenuation for the slow wave is higher than that of the first in most materials and, at low frequencies, the real and imaginary parts of the propagation constant are nearly equal.

The rotational wave has a very similar velocity to the rotational wave carried in the drained frame (or the S wave of geophysics). Again there is some extra attenuation due to the viscous forces associated with differential movement between solid and pore fluid. The fluid is unable to support rotational waves, but is driven by the solid.

The propagation of each wave type is determined by many parameters relating to the elastic properties of the solid and fluid components. Considerable efforts have been made to identify these parameters and determine appropriate forms for specific materials.

In the formulation described here, only equations describing the two dilatational waves are introduced. The coupled equations governing the propagation of dilatational waves can be written as [4.81]

$$\nabla^2(He - C\xi) = \frac{\partial^2}{\partial t^2}\left(\rho e - \rho_\mathrm{f}\xi\right), \tag{4.40}$$

$$\nabla^2(Ce - M\xi) = \frac{\partial^2}{\partial t^2}\left(\rho_\mathrm{f} e - m\xi\right) - \frac{\eta}{k}\frac{\delta\xi}{\delta t}F(\lambda), \tag{4.41}$$

where $e = \nabla\cdot u$ is the dilatation or volumetric strain vector of the skeletal frame; $\xi = \Omega\nabla\cdot(u-U)$ is the relative dilatation vector between the frame and the fluid; u is the displacement of the frame, U is the displacement of the fluid, $F(\lambda)$ is the viscosity correction function, ρ is the total density of the medium, ρ_f is the fluid density, μ is the dynamic fluid viscosity and k is the permeability.

The second term on the right-hand side of (4.41), $\frac{\mu}{k}\frac{\partial\xi}{\partial t}F(\lambda)$, allows for damping through viscous drag as the fluid and matrix move relative to one another; m is a dimensionless parameter that accounts for the fact that not all the fluid moves in the direction of macroscopic pressure gradient as not all the pores run normal to the surface and is given by $m = \frac{\tau\rho_\mathrm{f}}{\Omega}$, where τ is the tortuosity and Ω is the porosity.

H, C and M are elastic constants that can be expressed in terms of the bulk moduli K_s, K_f and K_b of the grains, fluid and frame, respectively and the shear modulus μ of the frame [4.58].

Assuming that e and ξ vary as $\mathrm{e}^{\mathrm{i}\omega t}$, $\partial/\partial t$ can be replaced by $\mathrm{i}\omega$ and (4.40) can be written [4.80] as

$$\nabla^2(Ce - M\xi) = -\omega\left[\rho_f e - \rho(\omega)\xi\right], \tag{4.42}$$

where $\rho(\omega) = \frac{\tau\rho_\mathrm{f}}{\Omega} - \frac{\mathrm{i}\mu}{\omega k}F(\lambda)$ is the dynamic fluid density. The original formulation of $F(\lambda)$ [and hence of $\rho(\omega)$] was a generalization from the specific forms corresponding to slit-like and cylindrical forms but assuming pores with identical shape. Expressions are also available for triangular and rectangular pore shapes and for more arbitrary microstructures [4.57, 58, 61]. If plane waves of the form $e = A\exp\left[-\mathrm{i}(lx-\omega t)\right]$ and $\xi = B\exp\left[-\mathrm{i}(lx-\omega t)\right]$ are assumed, then the dispersion equations for the propagation constants may be derived. These are:

$$A\left(l^2H - \omega^2\rho\right) + B\left(\omega^2\rho_\mathrm{f} - l^2C\right) = 0, \tag{4.43}$$

and

$$A\left(l^2C - \omega^2\rho_\mathrm{f}\right) + B\left[m\omega^2 - l^2M - \mathrm{i}\omega F(\lambda)\eta/k\right] = 0. \tag{4.44}$$

A nontrivial solution of (4.43) and (4.44) exists only if the determinant of the coefficient vanishes, giving

$$\begin{vmatrix} l^2H - \omega^2\rho & \omega^2\rho_\mathrm{f} - l^2C \\ l^2C - \omega^2\rho_\mathrm{f} & m\omega^2 - l^2M - \mathrm{i}\omega F(\lambda)\frac{\eta}{k} \end{vmatrix} = 0. \tag{4.45}$$

There are two complex roots of this equation from which both the attenuation and phase velocities of the two dilatational waves are calculated.

At the interface between different porous elastic media there are six boundary conditions that may be

Amazon EX1014 Page 145

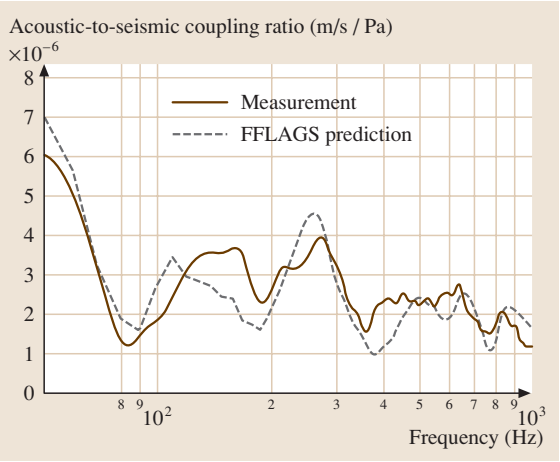


Fig. 4.8 Measured and predicted acoustic-to-seismic coupling ratio for a layered soil (range 3.0 m, source height 0.45 m)

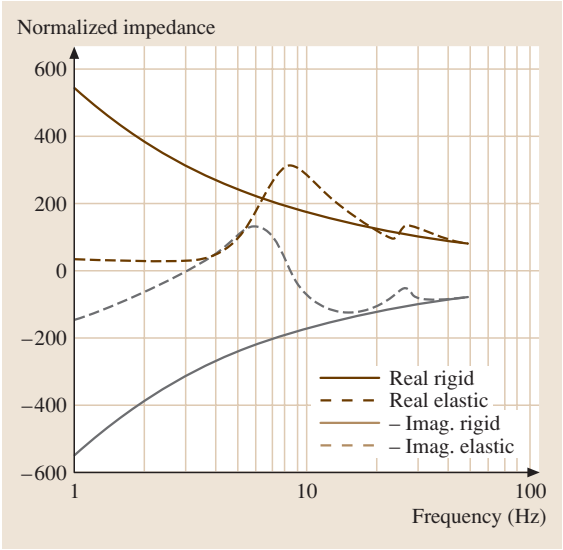


Fig. 4.9 Predicted surface impedance at a grazing angle of 0.018° for poro-elastic and rigid porous ground (four-layer system, Table 4.1)

applied. These are

1. Continuity of total normal stress
2. Continuity of normal displacement
3. Continuity of fluid pressure
4. Continuity of tangential stress
5. Continuity of normal fluid displacement
6. Continuity of tangential frame displacement

At an interface between a fluid and the poro-elastic layer (such as the surface of the ground) the first four boundary conditions apply.

The resulting equations and those for a greater number of porous and elastic layers are solved numerically [4.58].

The spectrum of the ratio between the normal component of the soil particle velocity at the surface of the ground and the incident sound pressure, the acoustic-to-seismic coupling ratio or transfer function, is strongly influenced by discontinuities in the elastic wave properties within the ground. At frequencies corresponding to peaks in the transfer function, there are local maxima in the transfer of sound energy into the soil [4.78]. These are associated with constructive interference between down- and up-going waves within each soil layer. Consequently there is a relationship between near-surface layering in soil and the peaks or *layer resonances* that appear in the measured acoustic-to-seismic transfer function spectrum: the lower the frequency of the peak in the spectrum, the deeper the associated layer. Figure 4.8 shows example measurements and predictions of the acoustic-to-seismic transfer function spectrum at the soil surface [4.12]. The measurements were made using a loudspeaker sound source and a microphone positioned close to the surface, vertically above a geophone buried just below the surface of a soil that had a loose surface layer. Seismic refraction survey measurements at the same site were used to determine the wave speeds. The predictions have been made by using a computer

Table 4.1 Ground profile and parameters used in the calculations for Figs. 4.9 and 4.10

Layer	Flow resistivity (kPa s m^{-2})	Porosity	Thickness (m)	P-wave speed (m/s)	S-wave speed (m/s)	Damping
1	1 740	0.3	0.5	560	230	0.04
2	1 740	0.3	1.0	220	98	0.02
3	1 740 000	0.01	150	1500	850	0.001
4	1 740 000	0.01	150	1500	354	0.001
5	1 740 000	0.01	Half-space	1500	450	0.001

Amazon EX1014 Page 146

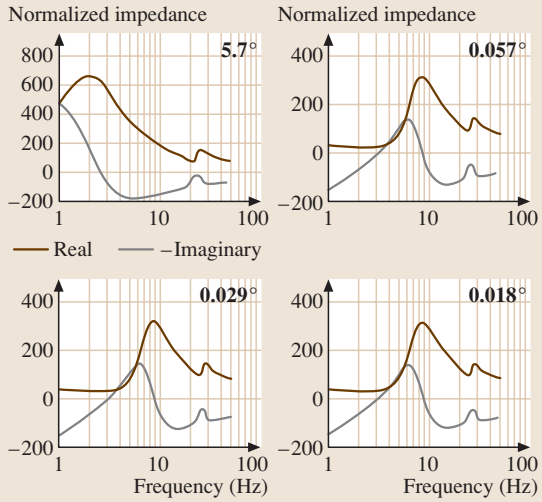


Fig. 4.10 Normalized surface impedance predicted for the four-layer structure, speed of sound in air = 329 m/s (corresponding to an air temperature of −4 °C) for grazing angles between 0.018° and 5.7°

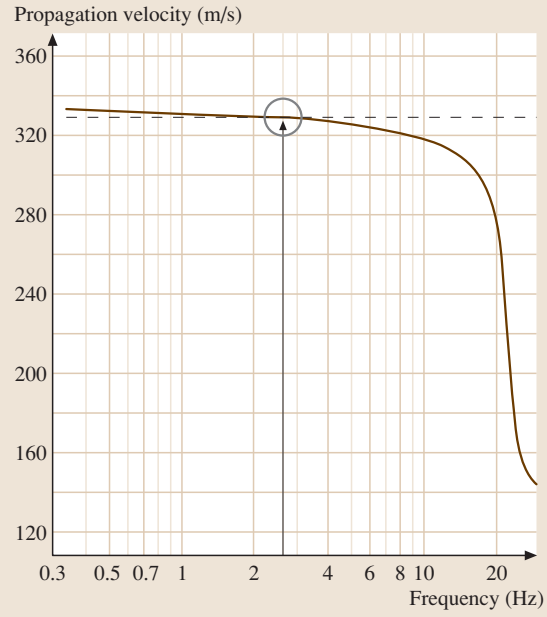


Fig. 4.11 Rayleigh-wave dispersion curve predicted for the system described by Table 4.1

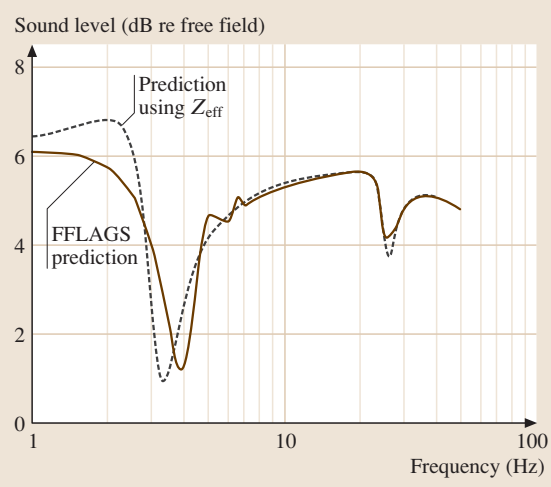


Fig. 4.12 Excess attenuation spectra predicted for source height 2 m, receiver height 0.1 m and horizontal range of 6.3 km by FFLAGS (assumed speed of sound in air of 329 m/s) and by classical theory using impedance calculated for 0.018° grazing angle

code known as the fast field program for air–ground systems (FFLAGS) that models sound propagation in a system of fluid layers and porous elastic layers [4.79].

This numerical theory (FFLAGS) may be used also to predict the ground impedance at low frequencies. In Fig. 4.9, the predictions for the surface impedance at a grazing angle of 0.018° are shown as a function of frequency for the layered porous and elastic system described by Table 4.1 and compared with those for a rigid porous ground with the same surface flow resistivity and porosity.

The influence of ground elasticity is to reduce the magnitude of the impedance considerably below 50 Hz. Potentially this is very significant for predictions of low-frequency noise, e.g., blast noise, at long range.

Figure 4.10 shows that the surface impedance of this four-layer poro-elastic system varies between grazing angles of 5.7° and 0.57° but remains more or less constant for smaller grazing angles. The predictions show two resonances. The lowest-frequency resonance is the most angle dependent. The peak in the real part changes from 2 Hz at 5.7° to 8 Hz at 0.057°. On the other hand the higher-frequency resonance peak near 25 Hz remains relatively unchanged with range.

The peak at the lower frequency may be associated with the predicted coincidence between the Rayleigh wave speed in the ground and the speed of sound in air (Fig. 4.11). Compared with the near pressure doubling predicted by classical ground impedance models, the predicted reduction of ground impedance at low frequencies above layered elastic ground can be interpreted

Amazon EX1014 Page 147

as the result of coupling of a significant fraction of the incident sound energy into ground-borne Rayleigh waves.

Numerical theory has also been used to explore the consequences of this coupling for the excess attenuation of low-frequency sound above ground [4.82].

Figure 4.12 shows the excess attenuation spectra predicted for source height 2 m, receiver height 0.1 m and horizontal range of 6.3 km over a layered ground profile corresponding to Table 4.1 (assumed a speed of sound in air of 329 m/s) and by classical theory for a point source above an impedance (locally reacting) plane (4.22) using the impedance calculated for a 0.018° grazing angle (Z_{eff}, broken lines in Fig. 4.9).

The predictions show a significant extra attenuation for 2–10 Hz. The predictions also indicate that, for an assumed speed of sound in air of 329 m/s, and, apart from an enhancement near 2 Hz, the excess attenuation spectrum might be predicted tolerably well by using modified classical theory instead of a full poro-elastic layer calculation.

It is difficult to measure the surface impedance of the ground at low frequencies [4.83, 84]. Consequently the predictions of significant ground elasticity effects have been validated only by using data for acoustic-to-seismic coupling, i. e., by measurements of the ratio of ground surface particle velocity relative to the incident sound pressure [4.82].

4.7 Attenuation Through Trees and Foliage

A mature forest or woodland may have three types of influence on sound. First is the ground effect. This is particularly significant if there is a thick litter layer of partially decomposing vegetation on the forest floor. In such a situation the ground surface consists of a thick highly porous layer with rather low flow resistivity, thus giving a primary excess attenuation maximum at lower frequencies than observed over typical grassland. This is similar to the effect, mentioned earlier, over snow. Secondly the trunks and branches scatter the sound out of the path between source and receiver. Thirdly the foliage attenuates the sound by viscous friction. To predict the total attenuation through woodland, *Price* et al. [4.85] simply added the predicted contributions to attenuation for large cylinders (representing trunks), small cylinders (representing foliage), and the ground. The predictions are in qualitative agreement with their measurements, but it is necessary to adjust several parameters to obtain quantitative agreement. Price et al. found that foliage has the greatest effect above 1 kHz and the foliage attenuation increased in approximately a linear fashion with frequency. Figure 4.13 shows a typical variation of at-

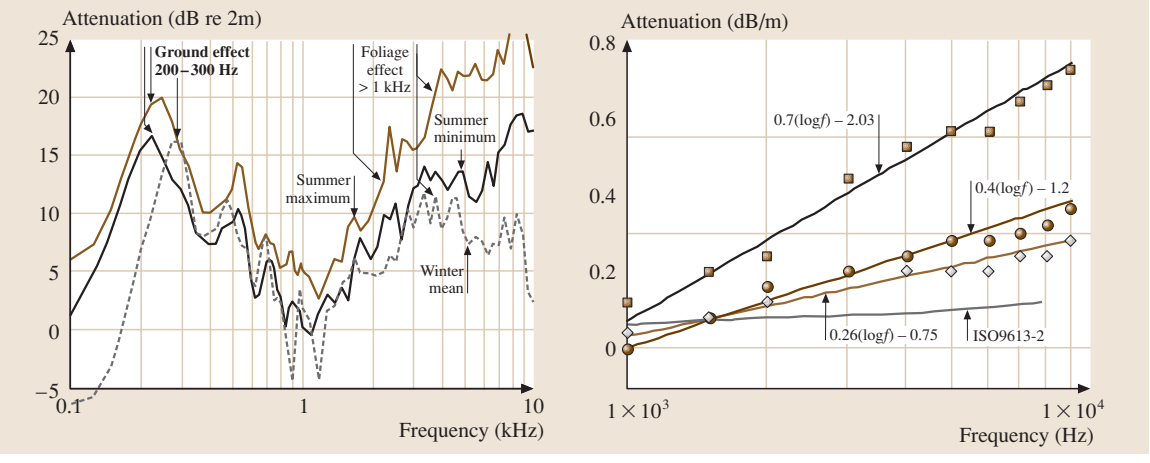


Fig. 4.13 (*Left*) Measured attenuation through alternate bands of Norway spruce and oak (planted in 1946) with hawthorn, roses and honeysuckle undergrowth; visibility less than 24 m. (*Right*) Linear fits to attenuation above 1 kHz in mixed conifers (*squares*), mixed deciduous summer (*circles*) and spruce monoculture (*diamonds*). Also shown is the foliage attenuation predicted according to ISO 9613-2. (After [4.24])

Amazon EX1014 Page 148

tenuation with frequency and linear fits to the foliage attenuation.

Often the insertion loss of tree belts alongside highways is considered relative to that over open grassland. An unfortunate consequence of the lower-frequency ground effect observed in mature tree stands is that the low-frequency destructive interference resulting from the relatively soft ground between the trees is associated with a constructive interference maximum at important frequencies (near 1 kHz) for traffic noise. Consequently many narrow tree belts alongside roads do not offer much additional attenuation of traffic noise compared with the same distances over open grassland. A Danish study found relative attenuation of 3 dB in the A-weighted L_{eq} due to traffic noise for tree belts 15–41 m wide [4.86]. Data obtained in the UK [4.87] indicates a maximum reduction of the A-weighted L_{10} level due to traffic noise of 6 dB through 30 m of dense spruce compared with the same depth of grassland. This study also found that the effectiveness of the vegetation was greatest closest to the road. A relative reduction of 5 dB in the A-weighted L_{10} level was found after 10 m of vegetation. For a narrow tree belt to be effective against traffic noise it is important that (a) the ground effect is similar to that for grassland, (b) there is substantial reduction of coherence between ground-reflected and direct sound at frequencies of 1 kHz and above, and that the attenuation through scattering is significant.

If the belt is sufficiently wide then the resulting greater extent of the ground-effect dip can compensate for its low frequency. Through 100 m of red pine forest, *Heisler* et al. [4.88] have found 8 dB reduction in the A-weighted L_{eq} due to road traffic compared with open grassland. The edge of the forest was 10 m from the edge of the highway and the trees occupied a gradual downward slope from the roadway extending about 325 m in each direction along the highway from the study site. Compared with open grassland *Huisman* [4.89] has predicted an extra 10 dB(A) attenuation of road traffic noise through 100 m of pine forest. He has remarked also that, whereas downward-refracting conditions lead to higher sound levels over grassland, the levels in woodland are comparatively unaffected. This suggests that extra attenuation obtained through the use of trees should be relatively robust to changing meteorology.

Defrance et al. [4.90] have compared results from both numerical calculations and outdoor measurements for different meteorological situations. A numerical parabolic equation code has been developed [4.91] and adapted to road traffic noise situations [4.92] where road line sources are modeled as series of equivalent point sources of height 0.5 m. The data showed a reduction in A-weighted L_{eq} due to the trees of 3 dB during downward-refracting conditions, 2 dB during homogeneous conditions and 1 dB during upward-refracting conditions. The numerical predictions suggest that in downward-refracting conditions the extra attenuation due to the forest is 2–6 dB(A) with the receiver at least 100 m away from the road. In upward-refracting conditions, the numerical model predicts that the forest may increase the received sound levels somewhat at large distances but this is of less importance since levels at larger distances tend to be relatively low anyway. In homogeneous conditions, it is predicted that sound propagation through the forest is affected only by scattering by trunks and foliage. *Defrance* et al. [4.90] have concluded that a forest strip of at least 100 m wide appears to be a useful natural acoustical barrier. Nevertheless both the data and numerical simulations were compared to sound levels without the trees present, i. e., over ground from which the trees had simply been removed. This means that the ground effect both with and without trees would have been similar. This is rarely likely to be the case.

A similar numerical model has been developed recently [4.93] including allowance for ground effect, wind speed gradient through foliage and assuming effective wave numbers deduced from multiple scattering theory for the scattering effects of trunks, branches and foliage. Again, the model predicts that the large wind speed gradient in the foliage tends to refract sound towards the ground and has an important effect particularly during upwind conditions. However, neither of the PE models [4.91, 93] include back-scatter or turbulence effects. The neglect of the back-scatter is inherent to the PE, which is a *one-way* prediction method. While this is not a serious problem for propagation over flat ground because the back-scatter is small, nor over an impermeable barrier because the back-scattered field, though strong, does not propagate through the barrier, back scatter is likely to be significant for a forest. Indeed acoustic reflections from the edges of forests are readily detectable.

Amazon EX1014 Page 149

4.8 Wind and Temperature Gradient Effects on Outdoor Sound

The atmosphere is constantly in motion as a consequence of wind shear and uneven heating of the Earth's surface (Fig. 4.14).

Any turbulent flow of a fluid across a rough solid surface generates a boundary layer. Most interest, from the point of view of community noise prediction, focuses on the lower part of the meteorological boundary layer called the surface layer. In the surface layer, turbulent fluxes vary by less than 10% of their magnitude but the wind speed and temperature gradients are largest. In typical daytime conditions the surface layer extends over 50–100 m. Usually, it is thinner at night. Turbulence may be modeled in terms of a series of moving eddies or *turbules* with a distribution of sizes.

In most meteorological conditions, the speed of sound changes with height above the ground. Usually, temperature decreases with height (the adiabatic lapse condition). In the absence of wind, this causes sound waves to bend, or refract, upwards. Wind speed adds or subtracts from sound speed. When the source is downwind of the receiver the sound has to propagate upwind. As height increases, the wind speed increases and the amount being subtracted from the speed of sound increases, leading to a negative gradient in the speed of sound. Downwind, sound refracts downwards. Wind effects tend to dominate over temperature effects when both are present. Temperature inversions, in which air temperature increases up to the inversion height, cause sound waves to be refracted downwards below that height. Under inversion conditions, or downwind, sound levels decrease less rapidly than would be expected from wavefront spreading alone.

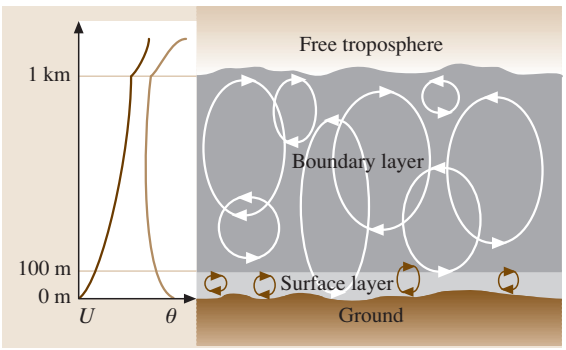


Fig. 4.14 Schematic representation of the daytime atmospheric boundary layer and turbulent eddy structures. The curve on the *left* shows the mean wind speed (U) and the potential temperature profiles ($\theta = T + \gamma_d z$, where $\gamma_d = 0.098\,^\circ\mathrm{C/km}$ is the dry adiabatic lapse rate, T is the temperature and z is the height)

In general, the relationship between the speed of sound profile $c(z)$, temperature profile $T(z)$ and wind speed profile $u(z)$ in the direction of sound propagation is given by

$$c(z) = c(0)\sqrt{\frac{T(z)+273.15}{273.15}} + u(z)\,, \qquad (4.46)$$

where T is in °C and u is in m/s.

4.8.1 Inversions and Shadow Zones

If the air temperature first increases up to some height before resuming its usual decrease with height, then there is an inversion. Sound from sources beneath the inversion height will tend to be refracted towards the ground. This is a favorable condition for sound propagation and may lead to higher levels than would be the case under acoustically neutral conditions. This will also be true for receivers downwind of a source. In terms of rays between source and receiver it is necessary to take into account any ground reflections. However, rather than use plane wave reflection coefficients to describe these ground reflections, a better approximation is to use spherical wave reflection coefficients (Sect. 4.6.2).

There are distinct advantages in assuming a linear effective speed of sound profile in ray tracing and ignoring the vector wind since this assumption leads to circular ray paths and relatively tractable analytical solutions. With this assumption, the effective speed of sound c can be written,

$$c(z) = c_0(1 + \zeta z)\,, \qquad (4.47)$$

where ζ is the normalized sound velocity gradient $[(\mathrm{d}c/\mathrm{d}z)/c_0]$ and z is the height above ground. If it also assumed that the source–receiver distance and the effective speed of sound gradient are sufficiently small that there is only a single *ray bounce*, i. e., a single ground reflection between the source and receiver, it is possible to use a simple adaptation of the formula (4.22), replacing the geometrical ray paths defining the direct and reflected path lengths by curved ones. Consequently, the sound field is approximated by

$$p = \left[\exp(-\mathrm{i}k_0\xi_1) + Q\exp(-\mathrm{i}k_0\xi_2)\right]/4\pi d\,, \qquad (4.48a)$$

where Q is the appropriate spherical wave reflection coefficient, d is the horizontal separation between the source and receiver, and ξ_1 and ξ_2 are, respectively,

Amazon EX1014 Page 150

the acoustical path lengths of the direct and reflected waves. These acoustical path lengths can be determined by [4.94, 95]

$$\xi_1 = \int_{\phi_<}^{\phi_>} \frac{\mathrm{d}\phi}{\varsigma \sin\phi} = \varsigma^{-1} \log_\mathrm{e}\left[\frac{\tan(\phi_>/2)}{\tan(\phi_</2)}\right] \qquad (4.48b)$$

and

$$\xi_2 = \int_{\theta_<}^{\theta_>} \frac{\mathrm{d}\theta}{\varsigma \sin\theta} = \varsigma^{-1} \log_\mathrm{e}\left[\tan(\theta_>/2)\tan^2(\theta_0/2)/\tan(\theta_</2)\right], \qquad (4.48c)$$

where $\phi(z)$ and $\theta(z)$ are the polar angles (measured from the positive z-axis) of the direct and reflected waves.

The subscripts $>$ and $<$ denote the corresponding parameters evaluated at $z_>$ and $z_<$ respectively, $z_> \equiv \max(z_s, z_r)$ and $z_< \equiv \min(z_s, z_r)$.

The computation of $\phi(z)$ and $\theta(z)$ requires the corresponding polar angles (ϕ_0 and θ_0) at $z = 0$ [4.96]. Once the polar angles are determined at $z = 0$, $\phi(z)$ and $\theta(z)$ at other heights can be found by using Snell's law:

$$\sin\vartheta = (1 + \varsigma z)\sin\vartheta_0\,,$$

where $\vartheta = \phi$ or θ. Substitution of these angles into (4.48b) and (4.48c) and, in turn, into (4.48a) makes it possible to calculate the sound field in the presence of a linear sound-velocity gradient.

For downward refraction, additional rays will cause a discontinuity in the predicted sound level because of the inherent approximation used in ray tracing. It is possible to determine the critical range r_c at which there are two additional ray arrivals. For $\varsigma > 0$, this critical range is given by:

$$r_\mathrm{c} = \frac{\left\{\left[\sqrt{(\varsigma z_>)^2 + 2\varsigma z_>} + \sqrt{(\varsigma z_<)^2 + 2\varsigma z_<}\right]^{2/3}\right\}^{3/2}}{\varsigma} + \frac{\left\{\left[\sqrt{(\varsigma z_>)^2 + 2\varsigma z_>} - \sqrt{(\varsigma z_<)^2 + 2\varsigma z_<}\right]^{2/3}\right\}^{3/2}}{\varsigma}. \qquad (4.49)$$

Figure 4.15 shows that, for source and receiver at 1 m height, if predictions are confined to a horizontal separation of less than 1 km and a normalized speed of sound gradient of less than 0.0001 m^{-1} (corresponding, for example, to a wind speed gradient of less than 0.1 s^{-1}) then, it is reasonable to assume a single ground bounce in ray tracing. The critical range for the single-bounce assumption increases as the source and receiver heights increase.

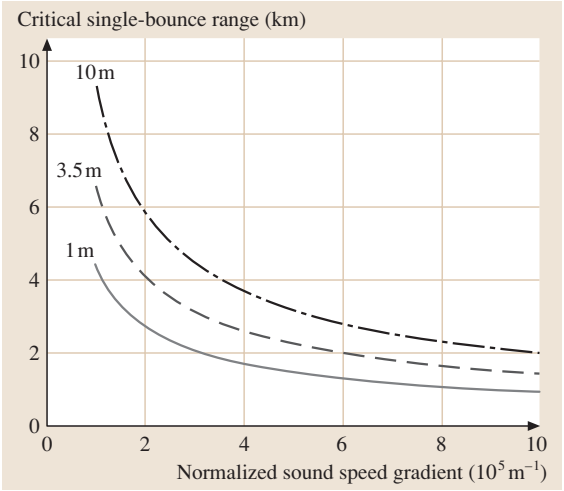


Fig. 4.15 Maximum ranges for which the single-bounce assumption is valid for a linear speed of sound gradient based on (4.35) and assuming equal source and receiver heights: 1 m (*solid line*); 3.5 m (*broken line*) and 10 m (*dot–dash line*)

A negative sound gradient means upward refraction and the creation of a sound shadow at a distance from the source that depends on the gradient. The presence of a shadow zone means that the sound level decreases faster than would be expected from distance alone. A combination of a slightly negative temperature gradient, strong upwind propagation and air absorption has been observed, in carefully monitored experiments, to reduce sound levels, 640 m from a 6 m-high source over relatively hard ground, by up to 20 dB more than expected from spherical spreading [4.97]. Since shadow zones can be areas in which there is significant excess attenuation, it is important to be able to locate their boundaries approximately.

For upward-refracting conditions, ray tracing is incorrect when the receiver is in the shadow and penumbra zones. The shadow boundary can be determined from geometrical considerations. For a given source and receiver heights, the critical range r'_c is determined as:

$$r'_\mathrm{c} = \frac{\sqrt{(\varsigma' z_>)^2 + 2\varsigma' z_>} + \sqrt{\varsigma'^2 z_< (2z_> - z_<) + 2\varsigma' z_<}}{\varsigma'}, \qquad (4.50)$$

Amazon EX1014 Page 151

where

$$\varsigma' = \frac{|\varsigma|}{1 - |\varsigma| z_>} .$$

Figure 4.16 shows that, for source and receiver heights of 1 m and a normalized speed of sound gradient of 0.0001 m^{-1}, the distance to the shadow zone boundary is about 300 m. As expected the distance to the shadow-zone boundary is predicted to increase as the source and receiver heights are increased.

A good approximation of (4.36), for the distance to the shadow zone, when the source is close to the ground and ζ is small, is

$$r_c = \left[\frac{2c_0}{-\frac{dc}{dz}} \right]^{1/2} \left(\sqrt{h_s} + \sqrt{h_r} \right) , \qquad (4.51)$$

where h_s and h_r are the heights of source and receiver respectively and dc/dz must be negative for a temperature-induced shadow zone.

Conditions of weak refraction may be said to exist where, under downward-refracting conditions, the ground-reflected ray undergoes only a single bounce and, under upward-refracting conditions, the receiver is within the illuminated zone.

When wind is present, the combined effects of temperature lapse and wind will tend to enhance the shadow zone upwind of the source, since wind speed tends to increase with height. Downwind of the source, however, the wind will counteract the effect of temperature lapse,

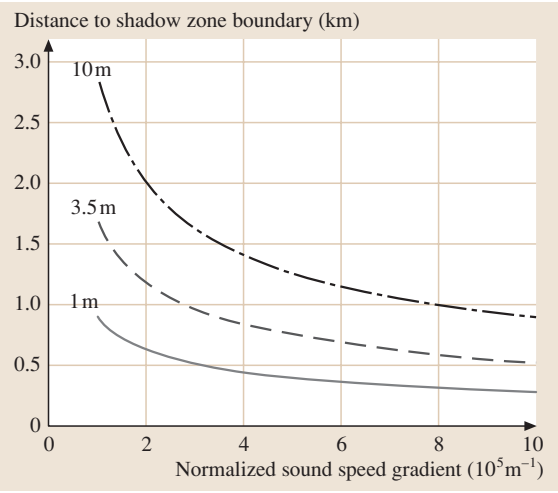


Fig. 4.16 Distances to shadow-zone boundaries for linear speed of sound gradient based on (4.36) assuming equal source and receiver heights: 1 m (*solid line*); 3.5 m (*broken line*) and 10 m (*dot–dash line*)

and the shadow zone will be destroyed. In any case, an acoustic shadow zone is never as complete as an optical one would be, as a result of diffraction and turbulence. In the presence of wind with a wind speed gradient of du/dz, the formula for the distance to the shadow-zone boundary is given by

$$r_c = \left[\frac{2c_0}{\frac{du}{dz}\cos\beta - \frac{dc}{dz}} \right]^{1/2} \left(\sqrt{h_s} + \sqrt{h_r} \right) , \qquad (4.52)$$

where β is the angle between the direction of the wind and the line between source and receiver.

Note that there will be a value of the angle β, (say β_c), given by

$$\frac{du}{dz}\cos\beta_c = \frac{dc}{dz}$$

or

$$\beta_c = \cos^{-1}\left(\frac{dc}{dz} \Big/ \frac{du}{dz} \right) \qquad (4.53)$$

at and beyond which there will not be a shadow zone. This represents the critical angle at which the effect of wind counteracts that of the temperature gradient.

4.8.2 Meteorological Classes for Outdoor Sound Propagation

There is a considerable body of knowledge about meteorological influences on air quality in general and the dispersion of plumes from stacks in particular. Plume behavior depends on vertical temperature gradients and hence on the degree of mixing in the atmosphere. Vertical temperature gradients decrease with increasing wind. The stability of the atmosphere in respect to plume dispersion is described in terms of Pasquill classes. This classification is based on incoming solar radiation, time of day and wind speed. There are six Pasquill classes (A–F) defined in Table 4.2.

Data are recorded in this form by meteorological stations and so, at first sight, it is a convenient classification system for noise prediction.

Class A represents a very unstable atmosphere with strong vertical air transport, i. e., mixing. Class F represents a very stable atmosphere with weak vertical transport. Class D represents a meteorologically neutral atmosphere. Such an atmosphere has a logarithmic wind speed profile and a temperature gradient corresponding to the normal decrease with height (adiabatic lapse rate). A meteorologically neutral atmosphere occurs for high wind speeds and large values of cloud cover. This means that a meteorologically neutral atmosphere may be far

Amazon EX1014 Page 152

Table 4.2 Pasquill (meteorological) stability categories

Wind speed[a] (m/s)	Daytime Incoming solar radiation (mW/cm^2)				1 h before sunset or after sunrise	Nighttime cloud cover (octas)		
	> 60	30–60	< 30	Overcast		0–3	4–7	8
≤ 1.5	A	A–B	B	C	D	F or G[b]	F	D
2.0–2.5	A–B	B	C	C	D	F	E	D
3.0–4.5	B	B–C	C	C	D	E	D	D
5.0–6.0	C	C–D	D	D	D	D	D	D
> 6.0	D	D	D	D	D	D	D	D

[a] measured to the nearest 0.5 m/s at 11 m height
[b] Category G is an additional category restricted to nighttime with less than 1 octa of cloud and a wind speed of less than 0.5 m/s

Table 4.3 CONCAWE meteorological classes for noise prediction

Meteorological category	Pasquill stability category and wind speed (m/s) Positive is towards receiver		
	A, B	C, D, E	F, G
1	$v < -3.0$	–	–
2	$-3.0 < v < -0.5$	$v < -3.0$	–
3	$-0.5 < v < +0.5$	$-3.0 < v < -0.5$	$v < -3.0$
4[a]	$+0.5 < v < +3.0$	$-0.5 < v < +0.5$	$-3.0 < v < -0.5$
5	$v > +3.0$	$+0.5 < v < +3.0$	$-0.5 < v < +0.5$
6	–	$v > +3.0$	$+0.5 < v < +3.0$

[a] Category with assumed zero meteorological influence

from *acoustically* neutral. Typically, the atmosphere is unstable by day and stable by night. This means that classes A–D might be appropriate classes by day and D–F by night. With practice, it is possible to estimate Pasquill stability categories in the field, for a particular time and season, from a visual estimate of the degree of cloud cover.

The Pasquill classification of meteorological conditions has been adopted as a classification system for noise-prediction schemes [4.38, 98]. However, it is clear from Table 4.2, that the meteorologically neutral category (C), while being fairly common in a temperate climate, includes a wide range of wind speeds and is therefore not very suitable as a category for noise prediction. In the CONservation of Clean Air and Water in Europe (CONCAWE) scheme [4.98], this problem is addressed by defining six noise-prediction categories based on Pasquill categories (representing the temperature gradient) and wind speed. There are 18 subcategories depending on wind speed. These are defined in Table 4.3.

CONCAWE category 4 is specified as that in which there is zero meteorological influence. So CONCAWE category 4 is equivalent to acoustically neutral conditions.

The CONCAWE scheme requires octave band analysis. Meteorological corrections in this scheme are based primarily on analysis of data from *Parkin* and *Scholes* [4.67, 68] together with measurements made at several industrial sites. The excess attenuation in each octave band for each category tends to approach asymptotic limits with increasing distance. Values at 2 km for CONCAWE categories 1 (strong wind from receiver to source, hence upward refraction) and 6 (strong downward refraction) are listed in Table 4.4.

Wind speed and temperature gradients are not independent. For example, very large temperature and

Table 4.4 Values of the meteorological corrections for CONCAWE categories 1 and 6

Octave band centre frequency (Hz)	63	125	250	500	1000	2000	4000
Category 1	8.9	6.7	4.9	10.0	12.2	7.3	8.8
Category 6	−2.3	−4.2	−6.5	−7.2	−4.9	−4.3	−7.4

Table 4.5 Estimated probability of occurrence of various combinations of wind and temperature gradient

Temperature gradient	Zero wind	Strong wind	Very strong wind
Very large negative temperature gradient	Frequent	Occasional	Rare or never
Large negative temperature gradient	Frequent	Occasional	Occasional
Zero temperature gradient	Occasional	Frequent	Frequent
Large positive temperature gradient	Frequent	Occasional	Occasional
Very large positive temperature gradient	Frequent	Occasional	Rare or never

Table 4.6 Meteorological classes for noise prediction based on qualitative descriptions

W1	Strong wind (> 3–5 m/s) from receiver to source
W2	Moderate wind (≈ 1–3 m/s) from receiver to source, or strong wind at 45°
W3	No wind, or any cross wind
W4	Moderate wind (≈ 1–3 m/s) from source to receiver, or strong wind at 45°
W5	Strong wind (> 3–5 m/s) from source to receiver
TG1	Strong negative: daytime with strong radiation (high sun, little cloud cover), dry surface and little wind
TG2	Moderate negative: as T1 but one condition missing
TG3	Near isothermal: early morning or late afternoon (e.g., one hour after sunrise or before sunset)
TG5	Moderate positive: nighttime with overcast sky or substantial wind
TG6	Strong positive: nighttime with clear sky and little or no wind

wind speed gradients cannot coexist. Strong turbulence associated with high wind speeds does not allow the development of marked thermal stratification.

Table 4.5 shows a rough estimate of the probability of occurrence of various combinations of wind and temperature gradients (TG) [4.97].

With regard to sound propagation, the component of the wind vector in the direction between source and receiver is most important. So the wind categories (W) must take this into account. Moreover, it is possible to give more detailed but qualitative descriptions of each of the meteorological categories (W and TG, see Table 4.6).

In Table 4.7, the revised categories are identified with qualitative predictions of their effects on noise levels. The classes are not symmetrical around zero meteorological influence. Typically there are more meteorological condition combinations that lead to attenuation than lead to enhancement. Moreover, the increases in noise level (say 1–5 dB) are smaller than the decreases (say 5–20 dB).

Using the values at 500 Hz as a rough guide for the likely corrections on overall A-weighted broadband levels it is noticeable that the CONCAWE meteorological corrections are not symmetrical around zero. The CONCAWE scheme suggests meteorological variations of between 10 dB less than the acoustically neutral level for strong upward refraction between source and receiver and 7 dB more than the acoustically neutral level for strong downward refraction between the source and receiver.

Table 4.7 Qualitative estimates of the impact of meteorological condition on noise levels

	W1	W2	W3	W4	W5
TG1	–	Large attenuation	Small attenuation	Small attenuation	–
TG2	Large attenuation	Small attenuation	Small attenuation	Zero meteorological influence	Small enhancement
TG3	Small attenuation	Small attenuation	Zero meteorological influence	Small enhancement	Small enhancement
TG4	Small attenuation	Zero meteorological influence	Small enhancement	Small enhancement	Large enhancement
TG5	–	Small enhancement	Small enhancement	Large enhancement	–

Amazon EX1014 Page 154

4.8.3 Typical Speed of Sound Profiles

Outdoor sound prediction requires information on wind speed, direction and temperature as a function of height near to the propagation path. These determine the speed of sound profile. Ideally, the heights at which the meteorological data are collected should reflect the application. If this information is not available, then there are alternative procedures. It is possible, for example, to generate an approximate speed of sound profile from temperature and wind speed at a given height using the Monin–Obukhov similarity theory [4.99] and to input this directly into a prediction scheme.

According to this theory, the wind speed component (m/s) in the source–receiver direction and temperature (°C) at height z are calculated from the values at ground level and other parameters as follows:

$$u(z) = \frac{u_*}{k}\left[\ln\left(\frac{z+z_M}{z_M}\right) + \psi_M\left(\frac{z}{L}\right)\right], \qquad (4.54)$$

$$T(z) = T_0 + \frac{T_*}{k}\left[\ln\left(\frac{z+z_H}{z_H}\right) + \psi_H\left(\frac{z}{L}\right)\right] + \Gamma z, \qquad (4.55)$$

where the parameters are defined in Table 4.8.

For a neutral atmosphere, $1/L = 0$ and $\psi_M = \psi_H = 0$.

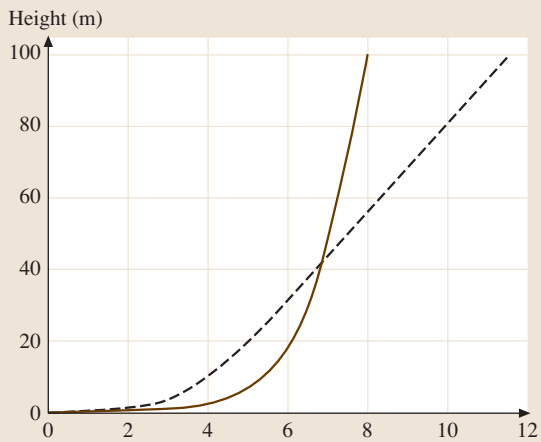


Fig. 4.17 Two downward-refracting speed of speed of sound profiles relative to the sound speed at the ground obtained from similarity theory. The *continuous curve* is approximately logarithmic corresponding to a large Obukhov length and to a cloudy, windy night. The *broken curve* corresponds to a small Obukhov length as on a calm clear night and is predominantly linear away from the ground

The associated speed of sound profile, $c(z)$, is calculated from (4.33).

Note that the resulting profiles are valid in the surface or boundary layer only but not at zero height. In fact, the profiles given by the above equations, sometimes called Businger–Dyer profiles [4.100], have been found to give good agreement with measured profiles up to 100 m. This height range is relevant to sound propagation over distances up to 10 km [4.101]. However improved profiles are available that are valid to greater heights. For example [4.102],

$$\psi_M = \psi_H = -7\ln(z/L) - 4.25/(z/L) + 0.5/(z/L)^2 - 0.852 \quad \text{for } z > 0.5L\,. \qquad (4.56)$$

Often z_M and z_H are taken to be equal. The roughness length varies, for example, between 0.0002 (still water) and 0.1 (grass). More generally, the roughness length can be estimated from the Davenport classification [4.103].

Figure 4.17 gives examples of speed of sound (difference) profiles, $[c(z) - c(0)]$, generated from (4.53) through (4.56) using

1. $z_M = z_H = 0.02$, $u_* = 0.34$, $T_* = 0.0212$, $T_{av} = 10$, $T_0 = 6$, (giving $L = 390.64$),
2. $z_M = z_H = 0.02$, $u_* = 0.15$, $T_* = 0.1371$, $T_{av} = 10$, $T_0 = 6$, (giving $L = 11.76$),

and $\Gamma = -0.01$. These parameters are intended to correspond to a cloudy windy night and a calm, clear night respectively [4.89].

Salomons et al. [4.104] have suggested a method to obtain the remaining unknown parameters, u_*, T_*, and L from the relationship

$$L = \frac{u_*^2}{kgT_*} \qquad (4.57)$$

and the Pasquill category (P).

From empirical meteorological tables, approximate relationships between the Pasquill class P the wind speed u_{10} at a reference height of 10 m and the fractional cloud cover N_c have been obtained. The latter determines the incoming solar radiation and therefore the heating of the ground. The former is a guide to the degree of mixing. The approximate relationship is

$$P(u_{10}, N_c) = 1 + 3\left[1 + \exp\left(3.5 - 0.5u_{10} - 0.5N_c\right)\right]^{-1} \quad \text{during the day}$$
$$= 6 - 2\left[1 + \exp\left(12 - 2u_{10} - 2N_c\right)\right]^{-1} \quad \text{during the night} \qquad (4.58)$$

Amazon EX1014 Page 155

Table 4.8 Definitions of parameters used in equations

$u*$	Friction velocity (m/s)	(depends on surface roughness)
z_M	Momentum roughness length	(depends on surface roughness)
z_H	Heat roughness length	(depends on surface roughness)
$T*$	Scaling temperature K	The precise value of this is not important for sound propagation. A convenient value is 283 K
k	Von Karman constant	(= 0.41)
T_0	Temperature (°C) at zero height	Again it is convenient to use 283 K
Γ	Adiabatic correction factor	$= -0.01$ °C/m for dry air. Moisture affects this value but the difference is small
L	Obukhov length (m) $> 0 \rightarrow$ stable, $< 0 \rightarrow$ unstable	$= \pm\frac{u_*^2}{kgT_*}$ $(T_{av} + 273.15)$, the thickness of the surface or boundary layer is given by $2L$m
T_{av}	Average temperature (°C)	It is convenient to use $T_{av} = 10$ so that $(T_{av} + 273.15) = \theta_0$
ψ_M	Diabatic momentum profile correction (mixing) function	$= -2\ln\left(\frac{(1+\chi_M)}{2}\right) - \ln\left(\frac{(1+\chi_M^2)}{2}\right) + 2\arctan(\chi_M) - \pi/2$ if $L < 0$ $= 5(z/L)$ if $L > 0$
ψ_H	Diabatic heat profile correction (mixing) function	$= -2\ln\left(\frac{(1+\chi_H)}{2}\right)$ if $L < 0$ $= 5(z/L)$ if $L > 0$ or for $z \le 0.5L$
χ_M	Inverse diabatic influence or function for momentum	$= \left(1 - \frac{16z}{L}\right)^{0.25}$
χ_H	Inverse diabatic influence function for momentum	$= \left(1 - \frac{16z}{L}\right)^{0.5}$

A proposed relationship between the Obukhov length L [m] as a function of P and roughness length $z_0 < 0.5$ m is:

$$\frac{1}{L(P, z_0)} = B_1(P)\log(z_0) + B_2(P)\,, \tag{4.59a}$$

where

$$B_1(P) = 0.0436 - 0.0017P - 0.0023P^2 \tag{4.59b}$$

and

$$B_2(P) = \min(0,\, 0.045P - 0.125) \text{ for } 1 \le P \le 4$$
$$\max(0,\, 0.025P - 0.125) \text{ for } 4 \le P \le 6\,. \tag{4.59c}$$

Alternatively, values of B_1 and B_2 may be obtained from Table 4.9.

Equations (4.59) give

$$L = L(u_{10}, N_c, z_0)\,. \tag{4.60}$$

Also u_{10} is given by (4.39) with $z = 10$ m, i. e.,

$$u(z) = \frac{u_*}{k}\left[\ln\left(\frac{10 + z_M}{z_M}\right) + \psi_M\left(\frac{10}{L}\right)\right]\,. \tag{4.61}$$

Equations (4.40), (4.41) and (4.61) may be solved for u_*, T_*, and L. Hence it is possible to calculate ψ_M, ψ_H, $u(z)$ and $T(z)$.

Figure 4.18 shows the results of this procedure for a ground with a roughness length of 0.1 m and two upwind and downwind daytime classes defined by the parameters listed in the caption.

As a consequence of atmospheric turbulence, instantaneous profiles of temperature and wind speed show considerable variations with both time and position. These variations are eliminated considerably by averaging over a period of the order of 10 minutes. The Monin–Obukhov or Businger–Dyer models give good descriptions of the averaged profiles over longer periods.

The Pasquill category C profiles shown in Fig. 4.18 are approximated closely by logarithmic curves of the form

$$c(z) = c(0) + b\ln\left[\frac{z}{z_0} + 1\right]\,, \tag{4.62}$$

Table 4.9 Values of the constants B1 and B2 for the six Pasquill classes

Pasquill class	A	B	C	D	E	F
B_1	0.04	0.03	0.02	0	−0.02	−0.05
B_2	−0.08	−0.035	0	0	0	0.025

Amazon EX1014 Page 156

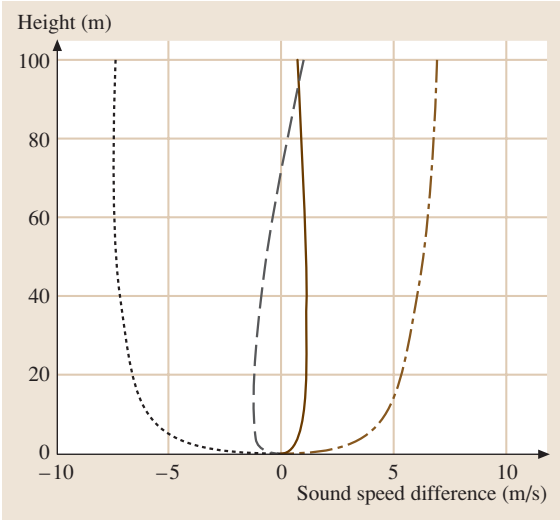


Fig. 4.18 Two daytime speed of sound profiles (upwind – *dashed* and *dotted*; downwind – *solid* and *dash-dot*) determined from the parameters listed in Table 4.9

where the parameter b (> 0 for downward refraction and < 0 for upward refraction) is a measure of the strength of the atmospheric refraction. Such logarithmic speed of sound profiles are realistic for open ground areas without obstacles particularly in the daytime.

A better fit to nighttime profiles is obtained with power laws of the form

$$c(z) = c(0) + b\left(\frac{z}{z_0}\right)^{\alpha}, \qquad (4.63)$$

where $\alpha = 0.4(P-4)^{\frac{1}{4}}$.

The temperature term in the effective speed of sound profile given by (4.33) can be approximated by truncating a Taylor expansion after the first term to give

$$c(z) = c\left[T_0\right] + \frac{1}{2}\sqrt{\frac{\kappa R}{T_0}}\left[T(z) - T_0\right] + u(z)\,. \qquad (4.64)$$

When combined with (4.39) this leads to a linear dependence on temperature and a logarithmic dependence on wind speed with height. By comparing with 12 months of meteorological data obtained at a 50 m-high meteorological tower in Germany, *Heimann* and *Salomons* [4.105] found that (4.44) is a reasonably accurate approximation to vertical profiles of effective speed of sound even in unstable conditions and in situations where Monin–Obukhov theory is not valid. By making a series of sound level predictions (using the parabolic equation method) for different meteorological conditions it was found that a minimum of 25 meteorological classes is necessary to ensure 2 dB or less deviation in the estimated annual average sound level from the reference case with 121 categories.

There are simpler, linear-segment profiles deduced from a wide range of meteorological data that may be used to represent worst-case noise conditions, i. e., best conditions for propagation. The first of these profiles may be calculated from a temperature gradient of +15 °C/km from the surface to 300 m and 8 °C/km above that, assuming a surface temperature of 20 °C. This type of profile can occur during the daytime or at night downwind due to wind shear in the atmosphere or a very high temperature inversion. If this is considered too extreme, or too rare a condition, then a second possibility is a shallow inversion, which occurs regularly at night. A typical depth is 200 m. The profile may be calculated from a temperature gradient of +20 °C/km from the surface to 200 m and −8 °C/km above that assuming a surface temperature of 20 °C.

The prediction of outdoor sound propagation also requires information about turbulence.

4.8.4 Atmospheric Turbulence Effects

Shadow zones due to atmospheric refraction are penetrated by sound scattered by turbulence and this sets a limit of the order of 20–25 dB to the reduction of sound levels within the sound shadow [4.106, 107].

Sound propagating through a turbulent atmosphere will fluctuate both in amplitude and phase as a result of fluctuations in the refractive index caused by fluctuations in temperature and wind velocity. When predicting outdoor sound, it is usual to refer to these fluctuations in wind velocity and temperature rather than the cause of the turbulence. The amplitude of fluctuations in sound level caused by turbulence initially increase with increasing distance of propagation, sound frequency and strength of turbulence but reach a limiting value fairly quickly. This means that the fluctuation in overall sound levels from distant sources (e.g., line of sight from an aircraft at a few km) may have a standard deviation of no more than about 6 dB [4.107].

There are two types of atmospheric instability responsible for the generation of turbulent kinetic energy: shear and buoyancy. Shear instabilities are associated with mechanical turbulence. High-wind conditions and a small temperature difference between the air and ground are the primary causes of mechanical turbulence. Buoyancy or convective turbulence is associated with

Amazon EX1014 Page 157

thermal instabilities. Such turbulence prevails when the ground is much warmer than the overlying air, such as, for example, on a sunny day. The irregularities in the temperature and wind fields are directly related to the scattering of sound waves in the atmosphere.

Fluid particles in turbulent flow often move in *loops* (Fig. 4.9) corresponding to swirls or eddies. Turbulence can be visualized as a continuous distribution of eddies in time and space. The largest eddies can extend to the height of the boundary layer, i. e., up to 1–2 km on a sunny afternoon. However, the outer scale of usual interest in community noise prediction is of the order of meters. In the size range of interest, sometimes called the inertial subrange, the kinetic energy in the larger eddies is transferred continuously to smaller ones. As the eddy size becomes smaller, virtually all of the energy is dissipated into heat. The length scale at which at which viscous dissipation processes begin to dominate for atmospheric turbulence is about 1.4 mm.

The size of eddies of most importance to sound propagation, for example in the shadow zone, may be estimated by considering Bragg diffraction [4.108]. For a sound with wavelength λ being scattered through angle θ, (Fig. 4.19), the important scattering structures have a spatial periodicity D satisfying

$$\lambda = 2D\sin(\theta/2)\,. \tag{4.65}$$

At a frequency of 500 Hz and a scattering angle of 10°, this predicts a size of 4 m.

When acoustic waves propagate nearly horizontally, the (overall) variance in the effective index of refraction $\langle\mu^2\rangle$ is related approximately to those in velocity and temperature by [4.109]

$$\langle\mu^2\rangle = \frac{\langle u'^2\rangle}{c_0^2}\cos^2\phi + \frac{\langle v'^2\rangle}{c_0^2}\sin^2\phi + \frac{\langle u'T\rangle}{c_0}\cos\phi + \frac{\langle T^2\rangle}{4T_0^2}\,, \tag{4.66}$$

where T, u' and v' are the fluctuations in temperature, horizontal wind speed parallel to the mean wind and horizontal wind speed perpendicular to the mean wind, respectively. ϕ is the angle between the wind and the wavefront normal. Use of similarity theory gives [4.110]

$$\langle\mu^2\rangle = \frac{5u_*^2}{c_0^2} + \frac{2.5u_*T_*}{c_0T_0}\cos\phi + \frac{T_*^2}{T_0^2}\,, \tag{4.67}$$

where u_* and T_* are the friction velocity and scaling temperature ($=-Q/u_*$, Q being the surface temperature flux), respectively.

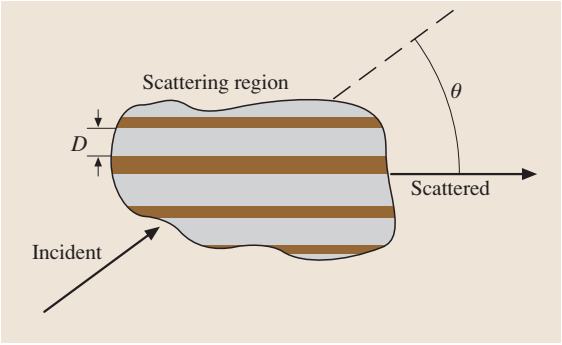


Fig. 4.19 Bragg reflection condition for acoustic scattering from turbulence

Typically, during the daytime, the velocity term in the effective index of refraction variance always dominates over the temperature term. This is true, even on sunny days, when turbulence is generated by buoyancy rather than shear. Strong buoyant instabilities produce vigorous motion of the air. Situations where temperature fluctuations have a more significant effect on acoustic scattering than velocity fluctuations occur most often during clear, still nights.

Although the second term (the covariance term) in (4.47) may be at least as important as the temperature term [4.110], it is often ignored for the purpose of predicting acoustic propagation. Estimations of the fluctuations in terms of u_* and T_* and the Monin–Obukhov length L are given by [4.111], for $L > 0$ (stable conditions, e.g., at night)

$$\sqrt{\langle u'^2\rangle} = \sigma_u = 2.4u_*\,,\ \sqrt{\langle v'^2\rangle} = \sigma_v = 1.9u_*\,,$$
$$\sqrt{\langle T^2\rangle} = \sigma_T = 1.5T_*$$

for $L < 0$ (unstable conditions, e.g., daytime)

$$\sigma_u = \left(12 - 0.5\frac{z}{L}\right)^{1/3} u_*\,,$$
$$\sigma_v = 0.8\left(12 - 0.5\frac{z}{L}\right)^{1/3} u_*\,,$$
$$\sigma_T = 2\left(1 - 18\frac{z}{L}\right)^{-1/2} T_*\,.$$

For line-of-sight propagation, the mean squared fluctuation in the phase of plane sound waves (sometimes called the strength parameter) is given by [4.112]

$$\Phi^2 = 2\langle\mu^2\rangle k_0^2 XL\,,$$

where X is the range and L is the inertial length scale of the turbulence. Alternatively, the variance in

Amazon EX1014 Page 158

the log-amplitude fluctuations in a plane sound wave propagating through turbulence is given by [4.113]

$$\langle \chi^2 \rangle = \frac{k_0^2 X}{4} \left(L_T \frac{\sigma_T^2}{T_0^2} + L_v \frac{\sigma_v^2}{c_0^2} \right) ,$$

where L_T, σ_T^2 and L_v, σ_v^2 are integral length scales and variances of temperature and velocity fluctuations respectively.

There are several models for the size distribution of turbulent eddies. In the Gaussian model of turbulence statistics, the energy spectrum $\phi_n(K)$ of the index of refraction is given by

$$\phi_n(K) = \langle \mu^2 \rangle \frac{L^2}{4\pi} \exp\left(-\frac{K^2 L^2}{4} \right) , \qquad (4.68)$$

where L is a single length scale (integral or outer length scale) proportional to the correlation length (inner length scale) ℓ_G, i. e.,

$$L = \ell_G \sqrt{\pi}/2 .$$

The Gaussian model has some utility in theoretical models of sound propagation through turbulence since it allows many results to be obtained in simple analytical form. However, as shown below, it provides a poor overall description of the spectrum of atmospheric turbulence [4.112].

In the von Karman spectrum, known to work reasonably well for turbulence with high Reynolds number, the spectrum of the variance in index of refraction is given by

$$\phi_n(K) = \langle \mu^2 \rangle \frac{L}{\pi \left(1 + K^2 \ell_K^2\right)} \qquad (4.69)$$

where $L = \ell_K \sqrt{\pi}\, \Gamma(5/6)/\Gamma(1/3)$.

Figure 4.20 compares the spectral function $[K\phi(K)/\langle \mu^2 \rangle]$ given by the von Karman spectrum for $\langle \mu^2 \rangle = 10^{-2}$ and $\ell_K = 1$ m with two spectral functions calculated assuming a Gaussian turbulence spectrum, respectively for $\langle \mu^2 \rangle = 0.818 \times 10^{-2}$ and $\ell_G = 0.93$ m and $\langle \mu^2 \rangle = 0.2 \times 10^{-2}$ and $\ell_G = 0.1$ m. The variance and inner length scale for the first Gaussian spectrum have been chosen to match the von Karman spectrum exactly for the low wave numbers (larger eddy sizes). It also offers a reasonable representation near to the spectral peak. Past the spectral peak and at high wave numbers, the first Gaussian spectrum decays far too rapidly. The second Gaussian spectrum clearly matches the von Karman spectrum over a narrow range of smaller eddy sizes. If this happens to be the wave number range of interest in scattering from turbulence, then the Gaussian spectrum may be satisfactory.

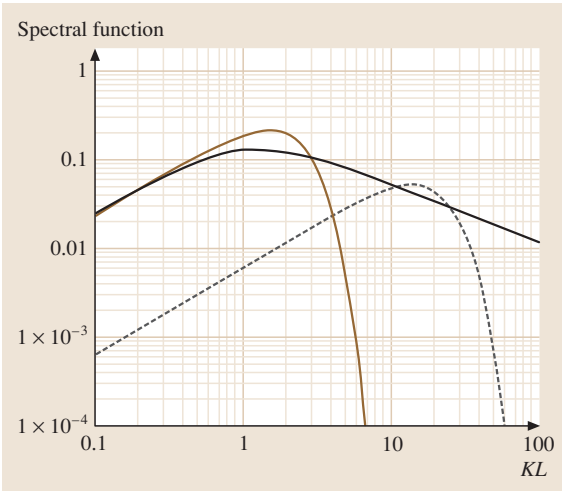


Fig. 4.20 A von Karman spectrum of turbulence and two Gaussian spectra chosen to match it at low wave numbers and over a narrow range of high wave numbers, respectively

Most recent calculations of turbulence effects on outdoor sound have relied on estimated or best-fit values rather than measured values of turbulence parameters. Under these circumstances, there is no reason to assume spectral models other than the Gaussian one.

Typically, the high-wave-number part of the spectrum is the main contributor to turbulence effects on sound propagation. This explains why the assumption of a Gaussian spectrum results in best-fit parameter values that are rather less than those that are measured.

Turbulence destroys the coherence between direct and ground-reflected sound and consequently reduces the destructive interference in the ground effect. Equation (4.22) may be modified [4.114] to obtain the mean-squared pressure at a receiver in a turbulent but *acoustically neutral* (no refraction) atmosphere

$$\langle p^2 \rangle = \frac{1}{R_1^2} + \frac{|Q|^2}{R_2^2} + \frac{2|Q|}{R_1 R_2} \cos\left[k\left(R_2 - R_1\right) + \theta \right] T , \qquad (4.70)$$

where θ is the phase of the reflection coefficient, ($Q = |Q| e^{-i\theta}$), and T is the coherence factor determined by the turbulence effect.

Hence the sound pressure level P is given by;

$$P = 10 \log_{10}\left(p^2\right) . \qquad (4.71)$$

Amazon EX1014 Page 159

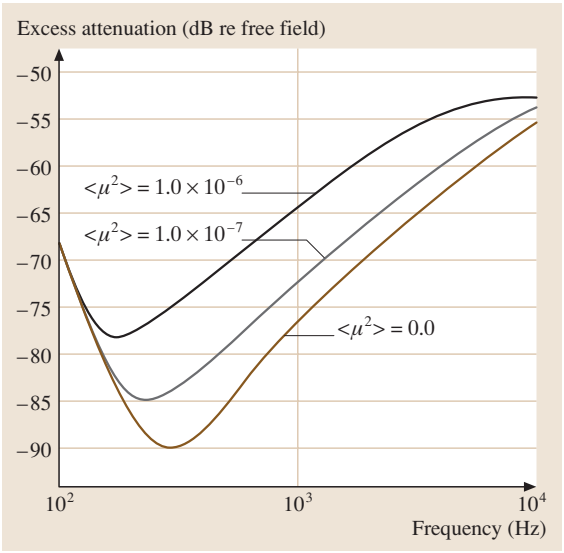


Fig. 4.21 Excess attenuation versus frequency for a source and receiver above an impedance ground in an acoustically neutral atmosphere predicted by (4.46)–(4.52) for three values of $\langle\mu^2\rangle$ between 0 and 10^{-6}. The assumed source and receiver heights are 1.8 and 1.5 m, respectively, and the assumed separation is 600 m. A two-parameter impedance model (4.31) has been used with values of 300 000 N s m^{-4} and 0.0 m^{-1}

For a Gaussian turbulence spectrum, the coherence factor T is given by [4.114]

$$T = \mathrm{e}^{-\sigma^2(1-\rho)}\,, \tag{4.72}$$

where σ^2 is the variance of the phase fluctuation along a path and ρ is the phase covariance between adjacent paths (e.g. direct and reflected)

$$\sigma^2 = A\sqrt{\pi}\langle\mu^2\rangle k^2 R L_0\,, \tag{4.73}$$

of the index of refraction, and L_0 is the outer (inertial) scale of turbulence.

The coefficient A is given by:

$$A = 0.5\,, \quad R > kL_0^2\,, \tag{4.74a}$$

$$A = 1.0\,, \quad R < kL_0^2\,. \tag{4.74b}$$

The parameters $\langle\mu^2\rangle$ and L_0 may be determined from field measurements or estimated.

The phase covariance is given by

$$\rho = \frac{\sqrt{\pi}}{2}\frac{L_0}{h}\,\mathrm{erf}\left(\frac{h}{L_0}\right)\,, \tag{4.75}$$

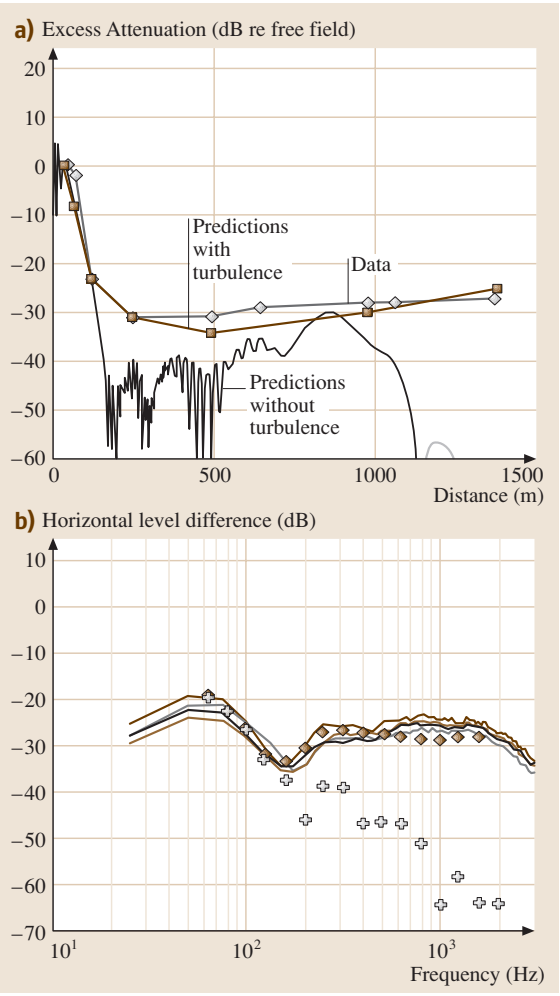


Fig. 4.22 **(a)** Data for the propagation of a 424 Hz tone as a function of range out to 1.5 km [4.115] compared to FFP predictions with and without turbulence [4.116] and **(b)** Broadband data to 2500 Hz for four 26 s averages (*lines*) of the spectra of the horizontal level differences between sound level measurements at 6.4 m high receivers, 152.4 m and 762 m from a fixed jet engine source (nozzle exit centered at 2.16 m height) compared to FFP predictions with (*diamonds*) and without (*crosses*) turbulence [4.116]

where h is the maximum transverse path separation and erf(x) is the error function defined by

$$\mathrm{erf}(x) = \frac{2}{\sqrt{\pi}}\int_0^x \mathrm{e}^{-t^2}\,\mathrm{d}t\,, \tag{4.76}$$

For a sound field consisting *only* of direct and reflected paths (which will be true at short ranges) in the absence of refraction, the parameter h is given by:

$$\frac{1}{h} = \frac{1}{2}\left(\frac{1}{h_s} + \frac{1}{h_r}\right), \tag{4.77}$$

where h_s and h_r are the source and receiver heights respectively. *Daigle* [4.117] uses half this value to obtain better agreement with data.

When $h \to 0$, then $\rho \to 1$ and $T \to 1$. This is the case near grazing incidence.

For $h \to$ large, then $T \to$ maximum. This will be the case for a greatly elevated source and/or receiver. The mean-squared refractive index may be calculated from the measured instantaneous variation of wind speed and temperature with time at the receiver. Specifically

$$\langle \mu^2 \rangle = \frac{\sigma_w^2 \cos^2 \alpha}{C_0^2} + \frac{\sigma_T^2}{4T_0^2},$$

where σ_w^2 is the variance of the wind velocity, σ_T^2 is the variance of the temperature fluctuations, α is the wind vector direction, and C_0 and T_0 are the ambient sound speed and temperature, respectively. Typical values of best-fit mean-squared refractive index are between 10^{-6} for calm conditions and 10^{-4} for strong not perfect, represents a large improvement over the results of calculations without turbulence and, in the case turbulence. A typical value of L_0 is 1 m but in general a value equal to the source height should be used.

Figure 4.21 shows example results of computations of excess attenuation spectra using (4.50) through (4.55). Note that increasing turbulence reduces the depth of the main ground-effect dip.

Figures 4.22a, b show comparisons between measured data and theoretical predictions using a full-wave numerical solution (FFP) with and without turbulence [4.116]. The data in Fig. 4.22a were obtained with a loudspeaker source [4.118] in strong upwind conditions modeled by the logarithmic speed of sound gradient [4.115]

$$c(z) = 340.0 - 2.0 \ln\left(z/6 \times 10^{-3}\right), \tag{4.78}$$

where z is the height in m.

Those in Fig. 4.22b were obtained with a fixed jet engine source during conditions with a negative temperature gradient (modeled by two linear segments) and a wind speed that was more or less constant with height at 4 ms^{-1} in the direction between receivers and source.

The agreement obtained between the predictions from the FFP including turbulence and the data, while of Fig. 4.22a, is similar to that obtained with predictions given by the parabolic equation method [4.115].

4.9 Concluding Remarks

There are several areas of outdoor acoustics in which further research is needed. This concluding section discusses current trends and lists some objectives that are yet to be fulfilled.

4.9.1 Modeling Meteorological and Topographical Effects

In Sect. 4.5 it was mentioned that the degradation of noise barrier performance in the presence of wind and temperature gradients has still to be established. Much current research is concerned with atmospheric and topographical effects and with the interaction between meteorology and topography [4.119–121]. Recent trends include combining mesoscale meteorological models with acoustic propagation models. The steady improvement in readily available computational power has encouraged the development of computationally intensive finite-difference time-domain (FDTD) models, which are based on numerical solutions of Euler's equations [4.122, 123] and models combining computational fluid dynamics (CFD) and FDTD [4.124]. Work remains to be done on the acoustical effects of barriers and hills.

4.9.2 Effects of Trees and Tall Vegetation

There is a need for more data on the effects of trees on sound propagation, if only to counteract the conventional wisdom that they have no practical part to play in reducing noise along the propagation path between source and receiver. This belief stems from the idea that there are so many holes in a belt of trees that a belt of practical width does not offer a significant barrier. Yet, as discussed in Sect. 4.7 there is increasing evidence that dense plantings with foliage to ground level can offer significant reductions. Moreover dense periodic plantings could exploit *sonic crystal* effects [4.125], whereby three dimensional (3-D) diffraction gratings produce stop bands or, after deliberate introduction of defects, can be used to direct sound away from receivers.

Amazon EX1014 Page 161

There is little data on the propagation of sound through crops and shrubs [4.126]. Indeed attenuation rates over tall crops and other vegetation remain uncertain both from the lack of measurements and from the lack of sufficiently sophisticated modeling. Improvement in multiple-scattering models of attenuation through leaves or needles might result from more sophisticated treatment of the boundary conditions. Corn and wheat plants have a large number of long ribbon-like leaves that scatter sound. Such leaves may be modeled either as elliptic cylinders or oblate spheroids, with a minor axis of length zero.

4.9.3 Low-Frequency Interaction with the Ground

Predictions of significant ground elasticity effects have been validated only by data for acoustic-to-seismic coupling, i. e., by measurements of the ratio of ground surface particle velocity relative to the incident sound pressure. Nevertheless given the significant predicted effects of layered ground elasticity on low-frequency propagation above ground it remains of interest to make further efforts to measure them.

4.9.4 Rough-Sea Effects

Coastal communities are regularly exposed to aircraft noise. To reduce the noise impact of sonic booms from civil supersonic flights, it is likely that, wherever possible, the aircraft will pass through the sound barrier over the sea. This means that prediction of aircraft noise in general, and sonic boom characteristics in particular, in coastal areas will be important and will involve propagation over the sea as well as the land. Given that the specific impedance of seawater is greater than that of air by four orders of magnitude, the sea surface may be considered to be acoustically hard. However, it is likely that sound propagation is modified during near-grazing propagation above a rough sea surface. Such propagation is likely to be of interest also when predicting sound propagation from near-ground explosions. Although the sea surface is continuously in motion associated with winds and currents, so that the scattered field is not constant, a sonic boom or blast waveform is sufficiently short compared with the period of the sea surface motion that the roughness may be considered to be static. As long as the incident acoustic wavelengths are large compared with the water wave heights and periods, the effect of the diffraction of sound waves by roughness may be modeled by an effective impedance. This is a convenient way to incorporate the acoustical properties of a rough sea surface into sonic boom and blast sound propagation models. Some modeling work has been carried out on this basis [4.127]. However it remains to be validated by data.

4.9.5 Predicting Outdoor Noise

Most current prediction schemes for outdoor sources such as transportation and industrial plant are empirical. To some extent, this is a reflection of the complexity arising from the variety of source properties, path configurations and receiver locations. On the other hand, apart from distinctions between source types and properties, the propagation factors are common. As discussed in this chapter, there has been considerable progress in modeling outdoor sound. The increasing computational power that is available for routine use makes several of the semi-analytical results and recent numerical codes of more practical value. Consequently, it can be expected that there will be a trend towards schemes that implement a common propagation package but employ differing source descriptors [4.18].

References

4.1 F.V. Hunt: *Origins in Acoustics* (Acoustical Society of America, AIP, New York 1992)

4.2 C.D. Ross: Outdoor sound propagation in the US civil war, Appl. Acoust. **59**, 101–115 (2000)

4.3 M.V. Naramoto: A concise history of acoustics in warfare, Appl. Acoust. **59**, 137–147 (2000)

4.4 G. Becker, A. Gudesen: Passive sensing with acoustics on the battlefield, Appl. Acoust. **59**, 149–178 (2000)

4.5 N. Xiang, J.M. Sabatier: Land mine detection measurements using acoustic-to-seismic coupling. In: *Detection and Remediation Technologies for Mines and Minelike Targets*, Proc. SPIE, Vol. 4038, ed. by V. Abinath, C. Dubey, J.F. Harvey (The International Society for Optical Engineering, Bellingham, WA 2000) pp. 645–655

4.6 A. Michelson: Sound reception in different environments. In: *Perspectives in Sensory Ecology*, ed. by M.A. Ali (Plenum, New York 1978) pp. 345–373

4.7 V.E. Ostashev: *Acoustics in Moving Inhomogeneous Media* (E & FN Spon, London 1999)

4.8 J.E. Piercy, T.F.W. Embleton, L.C. Sutherland: Review of noise propagation in the atmosphere, J. Acoust. Soc. Am. **61**, 1403–1418 (1977)

Amazon EX1014 Page 162

4.9 K. Attenborough: Review of ground effects on outdoor sound propagation from continuous broadband sources, Appl. Acoust. **24**, 289–319 (1988)

4.10 J.M. Sabatier, H.M. Hess, P.A. Arnott, K. Attenborough, E. Grissinger, M. Romkens: In situ measurements of soil physical properties by acoustical techniques, Soil Sci. Am. J. **54**, 658–672 (1990)

4.11 H.M. Moore, K. Attenborough: Acoustic determination of air-filled porosity and relative air permeability of soils, J. Soil Sci. **43**, 211–228 (1992)

4.12 N. D. Harrop: The exploitation of acoustic-to-seismic coupling for the determination of soil properties, Ph. D. Thesis, The Open University, 2000

4.13 K. Attenborough, H.E. Bass, X. Di, R. Raspet, G.R. Becker, A. Güdesen, A. Chrestman, G.A. Daigle, A. L'Espérance, Y. Gabillet, K.E. Gilbert, Y.L. Li, M.J. White, P. Naz, J.M. Noble, H.J.A.M. van Hoof: Benchmark cases for outdoor sound propagation models, J. Acoust. Soc. Am. **97**, 173–191 (1995)

4.14 E.M. Salomons: *Computational Atmospheric Acoustics* (Kluwer, Dordrecht 2002)

4.15 M.C. Bérengier, B. Gavreau, P. Blanc-Benon, D. Juvé: A short review of recent progress in modelling outdoor sound propagation, Acta Acustica united with Acustica **89**, 980–991 (2003)

4.16 Directive of the European parliament and of the Council relating to the assessment and management of noise 2002/EC/49: 25 June 2002, Official Journal of the European Communities **L189**, 12–25 (2002)

4.17 J. Kragh, B. Plovsing: *Nord2000. Comprehensive Outdoor Sound Propagation Model. Part I-II. DELTA Acoustics & Vibration Report, 1849-1851/00, 2000* (Danish Electronics, Light and Acoustics, Lyngby, Denmark 2001)

4.18 HARMONOISE contract funded by the European Commission IST-2000-28419, (http://www.harmonoise.org, 2000)

4.19 K.M. Li, S.H. Tang: The predicted barrier effects in the proximity of tall buildings, J. Acoust. Soc. Am. **114**, 821–832 (2003)

4.20 H.E. Bass, L.C. Sutherland, A.J. Zuckewar: Atmospheric absorption of sound: Further developments, J. Acoust. Soc. Am. **97**, 680–683 (1995)

4.21 D.T. Blackstock: *Fundamentals of Physical Acoustics, University of Texas Austin, Texas* (Wiley, New York 2000)

4.22 C. Larsson: Atmospheric Absorption Conditions for Horizontal Sound Propagation, Appl. Acoust. **50**, 231–245 (1997)

4.23 C. Larsson: Weather Effects on Outdoor Sound Propagation, Int. J. Acoust. Vibration **5**, 33–36 (2000)

4.24 ISO 9613-2: *Acoustics: Attenuation of Sound During Propagation Outdoors. Part 2: General Method of Calculation* (International Standard Organisation, Geneva, Switzerland 1996)

4.25 ISO 10847: *Acoustics – In-situ determination of insertion loss of outdoor noise barriers of all types* (International Standards Organisation, Geneva, Switzerland 1997)

4.26 ANSI S12.8: *Methods for Determination of Insertion Loss of Outdoor Noise Barriers* (American National Standard Institute, Washington, DC 1998)

4.27 G.A. Daigle: *Report by the International Institute of Noise Control Engineering Working Party on the Effectiveness of Noise Walls* (Noise/News International I-INCE, Poughkeepsie, NY 1999)

4.28 B. Kotzen, C. English: *Environmental Noise Barriers: A Guide to their Acoustic and Visual Design* (E&Fn Spon, London 1999)

4.29 A. Sommerfeld: Mathematische Theorie der Diffraction, Math. Ann. **47**, 317–374 (1896)

4.30 H.M. MacDonald: A class of diffraction problems, Proc. Lond. Math. Soc. **14**, 410–427 (1915)

4.31 S.W. Redfearn: Some acoustical source–observer problems, Philos. Mag. Ser. **7**, 223–236 (1940)

4.32 J.B. Keller: The geometrical theory of diffraction, J. Opt. Soc. **52**, 116–130 (1962)

4.33 W.J. Hadden, A.D. Pierce: Sound diffraction around screens and wedges for arbitrary point source locations, J. Acoust. Soc. Am. **69**, 1266–1276 (1981)

4.34 T.F.W. Embleton: Line integral theory of barrier attenuation in the presence of ground, J. Acoust. Soc. Am. **67**, 42–45 (1980)

4.35 P. Menounou, I.J. Busch-Vishniac, D.T. Blackstock: Directive line source model: A new model for sound diffracted by half planes and wedges, J. Acoust. Soc. Am. **107**, 2973–2986 (2000)

4.36 H. Medwin: Shadowing by finite noise barriers, J. Acoust. Soc. Am. **69**, 1060–1064 (1981)

4.37 Z. Maekawa: Noise reduction by screens, Appl. Acoust. **1**, 157–173 (1968)

4.38 K.J. Marsh: The CONCAWE Model for Calculating the Propagation of Noise from Open-Air Industrial Plants, Appl. Acoust. **15**, 411–428 (1982)

4.39 R.B. Tatge: Barrier-wall attenuation with a finite sized source, J. Acoust. Soc. Am. **53**, 1317–1319 (1973)

4.40 U.J. Kurze, G.S. Anderson: Sound attenuation by barriers, Appl. Acoust. **4**, 35–53 (1971)

4.41 P. Menounou: A correction to Maekawa's curve for the insertion loss behind barriers, J. Acoust. Soc. Am. **110**, 1828–1838 (2001)

4.42 Y.W. Lam, S.C. Roberts: A simple method for accurate prediction of finite barrier insertion loss, J. Acoust. Soc. Am. **93**, 1445–1452 (1993)

4.43 M. Abramowitz, I.A. Stegun: *Handbook of Mathematical Functions with Formulas, Graphs, and Mathematical Tables* (Dover, New York 1972)

4.44 K. Attenborough, S.I. Hayek, J.M. Lawther: Propagation of sound above a porous half-space, J. Acoust. Soc. Am. **68**, 1493–1501 (1980)

4.45 A. Banos: *Dipole radiation in the presence of conducting half-space.* (Pergamon, New York 1966), Chap. 2–4

4.46 R.J. Donato: Model experiments on surface waves, J. Acoust. Soc. Am. **63**, 700–703 (1978)

Amazon EX1014 Page 163

4.47 G.A. Daigle, M.R. Stinson, D.I. Havelock: Experiments on surface waves over a model impedance using acoustical pulses, J. Acoust. Soc. Am. **99**, 1993–2005 (1996)

4.48 Q. Wang, K.M. Li: Surface waves over a convex impedance surface, J. Acoust. Soc. Am. **106**, 2345–2357 (1999)

4.49 D.G. Albert: Observation of acoustic surface waves in outdoor sound propagation, J. Acoust. Soc. Am. **113**, 2495–2500 (2003)

4.50 K.M. Li, T. Waters-Fuller, K. Attenborough: Sound propagation from a point source over extended-reaction ground, J. Acoust. Soc. Am. **104**, 679–685 (1998)

4.51 J. Nicolas, J.L. Berry, G.A. Daigle: Propagation of sound above a finite layer of snow, J. Acoust. Soc. Am. **77**, 67–73 (1985)

4.52 J.F. Allard, G. Jansens, W. Lauriks: Reflection of spherical waves by a non-locally reacting porous medium, Wave Motion **36**, 143–155 (2002)

4.53 M.E. Delany, E.N. Bazley: Acoustical properties of fibrous absorbent materials, Appl. Acoust. **3**, 105–116 (1970)

4.54 K.B. Rasmussen: Sound propagation over grass covered ground, J. Sound Vib. **78**, 247–255 (1981)

4.55 K. Attenborough: Ground parameter information for propagation modeling, J. Acoust. Soc. Am. **92**, 418–427 (1992), see also R. Raspet, K. Attenborough: Erratum: Ground parameter information for propagation modeling. J. Acoust. Soc. Am. 92, 3007 (1992)

4.56 R. Raspet, J.M. Sabatier: The surface impedance of grounds with exponential porosity profiles, J. Acoust. Soc. Am. **99**, 147–152 (1996)

4.57 K. Attenborough: Models for the acoustical properties of air-saturated granular materials, Acta Acust. **1**, 213–226 (1993)

4.58 J.F. Allard: *Propagation of Sound in Porous Media: Modelling Sound Absorbing Material* (Elsevier, New York 1993)

4.59 D.L. Johnson, T.J. Plona, R. Dashen: Theory of dynamic permeability and tortuosity in fluid-saturated porous media, J. Fluid Mech. **176**, 379–401 (1987)

4.60 O. Umnova, K. Attenborough, K.M. Li: Cell model calculations of dynamic drag parameters in packings of spheres, J. Acoust. Soc. Am. **107**, 3113–3119 (2000)

4.61 K.V. Horoshenkov, K. Attenborough, S.N. Chandler-Wilde: Padé approximants for the acoustical properties of rigid frame porous media with pore size distribution, J. Acoust. Soc. Am. **104**, 1198–1209 (1998)

4.62 T. Yamamoto, A. Turgut: Acoustic wave propagation through porous media with arbitrary pore size distributions, J. Acoust. Soc. Am. **83**, 1744–1751 (1988)

4.63 ANSI S1.18-1999: *Template method for Ground Impedance, Standards Secretariat* (Acoustical Society of America, New York 1999)

4.64 S. Taherzadeh, K. Attenborough: Deduction of ground impedance from measurements of excess attenuation spectra, J. Acoust. Soc. Am. **105**, 2039–2042 (1999)

4.65 K. Attenborough, T. Waters-Fuller: Effective impedance of rough porous ground surfaces, J. Acoust. Soc. Am. **108**, 949–956 (2000)

4.66 P. Boulanger, K. Attenborough, S. Taherzadeh, T.F. Waters-Fuller, K.M. Li: Ground effect over hard rough surfaces, J. Acoust. Soc. Am. **104**, 1474–1482 (1998)

4.67 P.H. Parkin, W.E. Scholes: The horizontal propagation of sound from a jet close to the ground at Radlett, J. Sound Vib. **1**, 1–13 (1965)

4.68 P.H. Parkin, W.E. Scholes: The horizontal propagation of sound from a jet close to the ground at Hatfield, J. Sound Vib. **2**, 353–374 (1965)

4.69 K. Attenborough, S. Taherzadeh: Propagation from a point source over a rough finite impedance boundary, J. Acoust. Soc. Am. **98**, 1717–1722 (1995)

4.70 Airbus France SA (AM-B), Final Technical Report on Project n° GRD1-2000-25189 SOBER (2004)

4.71 D.E. Aylor: Noise reduction by vegetation and ground, J. Acoust. Soc. Am. **51**, 197–205 (1972)

4.72 K. Attenborough, T. Waters-Fuller, K.M. Li, J.A. Lines: Acoustical properties of Farmland, J. Agric. Eng. Res. **76**, 183–195 (2000)

4.73 O. Zaporozhets, V. Tokarev, K. Attenborough: Predicting Noise from Aircraft Operated on the Ground, Appl. Acoust. **64**, 941–953 (2003)

4.74 C. Madshus, N.I. Nilsen: Low frequency vibration and noise from military blast activity –prediction and evaluation of annoyance, Proc. InterNoise 2000, Nice, France (2000)

4.75 Øhrstrøm E.: (1996) Community reaction to noise and vibrations from railway traffic. Proc. Internoise 1996, Liverpool U.K.

4.76 ISO 2631-2 (1998), Mechanical vibration and shock – Evaluation of human exposure to whole body vibration – Part 2: Vibration in buildings

4.77 W.M. Ewing, W.S. Jardetzky, F. Press: *Elastic Waves in Layered Media* (McGraw-Hill, New York 1957)

4.78 J.M. Sabatier, H.E. Bass, L.M. Bolen, K. Attenborough: Acoustically induced seismic waves, J. Acoust. Soc. Am. **80**, 646–649 (1986)

4.79 S. Tooms, S. Taherzadeh, K. Attenborough: Sound propagating in a refracting fluid above a layered fluid saturated porous elastic material, J. Acoust. Soc. Am. **93**, 173–181 (1993)

4.80 K. Attenborough: On the acoustic slow wave in air filled granular media, J. Acoust. Soc. Am. **81**, 93–102 (1987)

4.81 R.D. Stoll: Theoretical aspects of sound transmission in sediments, J. Acoust. Soc. Am. **68**(5), 1341–1350 (1980)

4.82 C. Madshus, F. Lovholt, A. Kaynia, L.R. Hole, K. Attenborough, S. Taherzadeh: Air–ground interaction in long range propagation of low frequency sound

Amazon EX1014 Page 164

and vibration – field tests and model verification, Appl. Acoust. **66**, 553–578 (2005)
4.83 G.A. Daigle, M.R. Stinson: Impedance of grass covered ground at low frequencies using a phase difference technique, J. Acoust. Soc. Am. **81**, 62–68 (1987)
4.84 M.W. Sprague, R. Raspet, H.E. Bass, J.M. Sabatier: Low frequency acoustic ground impedance measurement techniques, Appl. Acoust. **39**, 307–325 (1993)
4.85 M.A. Price, K. Attenborough, N.W. Heap: Sound attenuation through trees: Measurements and Models, J. Acoust. Soc. Am. **84**, 1836–1844 (1988)
4.86 J. Kragh: Road traffic noise attenuation by belts of trees and bushes, Danish Acoustical Laboratory Report no.31 (1982)
4.87 L. R. Huddart: The use of vegetation for traffic noise screening, TRRL Research Report 238 (1990)
4.88 G. M. Heisler, O. H. McDaniel, K. K. Hodgdon, J. J. Portelli, S. B. Glesson: Highway Noise Abatement in Two Forests, Proc. NOISE-CON 87, PSU, USA (1987)
4.89 W.H.T. Huisman: *Sound propagation over vegetation-covered ground. Ph.D. Thesis* (University of Nijmegen, The Netherlands 1990)
4.90 J. Defrance, N. Barriere, E. Premat: Forest as a meteorological screen for traffic noise. Proc. 9th ICSV, Orlando (2002)
4.91 N. Barrière, Y. Gabillet: Sound propagation over a barrier with realistic wind gradients. Comparison of wind tunnel experiments with GFPE computations, Acustica-Acta Acustica **85**, 325–334 (1999)
4.92 N. Barrière: *Etude théorique et expérimentale de la propagation du bruit de trafic en forêt. Ph.D. Thesis* (Ecole Centrale de Lyon, France 1999)
4.93 M. E. Swearingen, M. White: Sound propagation through a forest: a predictive model. Proc. 11th LRSPS, Vermont (2004)
4.94 K.M. Li, K. Attenborough, N.W. Heap: Source height determination by ground effect inversion in the presence of a sound velocity gradient, J. Sound Vib. **145**, 111–128 (1991)
4.95 I. Rudnick: Propagation of sound in open air. In: *Handbook of Noise Control, Chap. 3*, ed. by C.M. Harris (McGraw-Hill, New York 1957) pp. 3:1–3:17
4.96 K.M. Li: On the validity of the heuristic ray-trace based modification to the Weyl Van der Pol formula, J. Acoust. Soc. Am. **93**, 1727–1735 (1993)
4.97 V. Zouboff, Y. Brunet, M. Berengier, E. Sechet: Proc. 6th International Symposium on Long range Sound propagation, ed. D.I.Havelock and M.Stinson, NRCC, Ottawa, 251-269 (1994)
4.98 The propagation of noise from petroleum and petrochemical complexes to neighbouring communities, CONCAWE Report no.4/81, Den Haag (1981)
4.99 A.S. Monin, A.M. Yaglom: *Statistical Fluid Mechanics: mechanics of turbulence*, Vol. 1 (MIT press, Cambridge 1979)
4.100 R.B. Stull: *An Introduction to Boundary Layer Meteorology* (Kluwer, Dordrecht 1991) pp. 347–347
4.101 E.M. Salomons: Downwind propagation of sound in an atmosphere with a realistic sound speed profile: A semi-analytical ray model, J. Acoust. Soc. Am. **95**, 2425–2436 (1994)
4.102 A.A.M. Holtslag: Estimates of diabatic wind speed profiles from near surface weather observations, Boundary-Layer Meteorol. **29**, 225–250 (1984)
4.103 A.G. Davenport: Rationale for determining design wind velocities, J. Am. Soc. Civ. Eng. **ST-86**, 39–68 (1960)
4.104 E. M. Salomons, F. H. van den Berg, H. E. A. Brackenhoff: Long-term average sound transfer through the atmosphere based on meteorological statistics and numerical computations of sound propagation. Proc. 6th International Symposium on Long range Sound propagation, ed. D.I.Havelock and M.Stinson, NRCC, Ottawa, 209-228 (1994)
4.105 D. Heimann, E. Salomons: Testing meteorological classifications for the prediction of long-term average sound levels, J. Am. Soc. Civ. Eng. **65**, 925–950 (2004)
4.106 T.F.W. Embleton: Tutorial on sound propagation outdoors, J. Acoust. Soc. Am. **100**, 31–48 (1996)
4.107 L.C. Sutherland, G.A. Daigle: Atmospheric sound propagation. In: *Encylclopedia of Acoustics*, ed. by M.J. Crocker (Wiley, New York 1998) pp. 305–329
4.108 M. R. Stinson, D. J. Havelock, G. A. Daigle: Simulation of scattering by turbulence into a shadow zone region using the GF-PE method, 283 – 307 Proc. 6th LRSPS Ottawa, NRCC, 1996
4.109 D. K. Wilson: A brief tutorial on atmospheric boundary-layer turbulence for acousticians. 111 – 122, Proc. 7th LRSPS, Ecole Centrale, Lyon, 1996
4.110 D.K. Wilson, J.G. Brasseur, K.E. Gilbert: Acoustic scattering and the spectrum of atmospheric turbulence, J. Acoust. Soc. Am. **105**, 30–34 (1999)
4.111 A. L'Esperance, G. A. Daigle, Y. Gabillet: Estimation of linear sound speed gradients associated to general meteorological conditions. Proc. 6th LRSPS Ottawa, NRCC, (1996)
4.112 D. K. Wilson: On the application of turbulence spectral/correlation models to sound propagation in the atmosphere, Proc. 8th LRSPS, Penn State (1988)
4.113 V.E. Ostashev, D.K. Wilson: Relative contributions from temperature and wind velocity fluctuations to the statistical moments of a sound field in a turbulent atmosphere, Acustica – Acta Acustica **86**, 260–268 (2000)
4.114 S.F. Clifford, R.T. Lataitis: Turbulence effects on acoustic wave propagation over a smooth surface, J. Acoust. Soc. Am. **73**, 1545–1550 (1983)
4.115 K.E. Gilbert, R. Raspet, X. Di: Calculation of turbulence effects in an upward refracting atmosphere, J. Acoust. Soc. Am. **87**(6), 2428–2437 (1990)
4.116 S. Taherzadeh, K. Attenborough: Using the Fast Field Program in a refracting, turbulent medium,

Amazon EX1014 Page 165

Report 3 for ESDU International (unpublished) (1999).
4.117 G.A. Daigle: Effects of atmospheric turbulence on the interference of sound waves above a finite impedance boundary, J. Acoust. Soc. Am. **65**, 45–49 (1979)
4.118 F.M. Weiner, D.N. Keast: Experimental study of the propagation of sound over ground, J. Acoust. Soc. Am. **31**(6), 724–733 (1959)
4.119 E.M. Salomons: Reduction of the performance of a noise screen due to screen induced wind-speed gradients. Numerical computations and wind-tunnel experiments, J. Acoust. Soc. Am. **105**, 2287–2293 (1999)
4.120 E.M. Salomons, K.B. Rasmussen: Numerical computation of sound propagation over a noise screen based on an analytic approximation of the wind speed field, Appl. Acoust. **60**, 327–341 (2000)
4.121 M. West , Y. W. Lam: Prediction of sound fields in the presence of terrain features which produce a range dependent meteorology using the generalised terrain parabolic equation (GT-PE) model. Proc. InterNoise 2000, Nice, France 2, 943 (2000)
4.122 E.M. Salomons, R. Blumrich, D. Heimann: Eulerian time-domain model for sound propagation over a finite impedance ground surface. Comparison with frequency-domain models, Acust. Acta Acust. **88**, 483–492 (2002)
4.123 R. Blumrich, D. Heimann: A linearized Eulerian sound propagation model for studies of complex meteorological effects, J. Acoust. Soc. Am. **112**, 446–455 (2002)
4.124 T. Van Renterghem, D. Botteldooren: Numerical simulation of the effect of trees on down-wind noise barrier performance, Acust. Acta Acust. **89**, 764–778 (2003)
4.125 J.V. Sanchez-Perez, C. Rubio, R. Martinez-Sala, R. Sanchez-Grandia, V. Gomez: Acoustic barriers based on periodic arrays of scatterers, Appl. Phys. Lett. **81**, 5240–5242 (2002)
4.126 D.E. Aylor: Sound transmission through vegetation in relation to leaf area density, leaf width and breadth of canopy, J. Acoust. Soc. Am. **51**, 411–414 (1972)
4.127 P. Boulanger, K. Attenborough: Effective impedance spectra for predicting rough sea effects on atmospheric impulsive sounds, J. Acoust. Soc. Am. **117**, 751–762 (2005)

Amazon EX1014 Page 166

5. Underwater Acoustics

It is well established that sound waves, compared to electromagnetic waves, propagate long distances in the ocean. Hence, in the ocean as opposed to air or a vacuum, one uses sound navigation and ranging (SONAR) instead of radar, acoustic communication instead of radio, and acoustic imaging and tomography instead of microwave or optical imaging or X-ray tomography. Underwater acoustics is the science of sound in water (most commonly in the ocean) and encompasses not only the study of sound propagation, but also the masking of sound signals by interfering phenomenon and signal processing for extracting these signals from interference. This chapter we will present the basics physics of ocean acoustics and then discuss applications.

5.1 Ocean Acoustic Environment 151
5.1.1 Ocean Environment 151
5.1.2 Basic Acoustic Propagation Paths 152
5.1.3 Geometric Spreading Loss..... 154
5.2 Physical Mechanisms..... 155
5.2.1 Transducers 155
5.2.2 Volume Attenuation 157
5.2.3 Bottom Loss..... 158
5.2.4 Scattering and Reverberation 159
5.2.5 Ambient Noise 160
5.2.6 Bubbles and Bubbly Media..... 162
5.3 SONAR and the SONAR Equation..... 165
5.3.1 Detection Threshold and Receiver Operating Characteristics Curves .. 165
5.3.2 Passive SONAR Equation 166
5.3.3 Active SONAR Equation 167
5.4 Sound Propagation Models..... 167
5.4.1 The Wave Equation and Boundary Conditions..... 168
5.4.2 Ray Theory 168
5.4.3 Wavenumber Representation or Spectral Solution 169
5.4.4 Normal-Mode Model 169
5.4.5 Parabolic Equation (PE) Model 172
5.4.6 Propagation and Transmission Loss 174
5.4.7 Fourier Synthesis of Frequency-Domain Solutions..... 175
5.5 Quantitative Description of Propagation 177
5.6 SONAR Array Processing 179
5.6.1 Linear Plane-Wave Beam-Forming and Spatio-Temporal Sampling..... 179
5.6.2 Some Beam-Former Properties ... 181
5.6.3 Adaptive Processing..... 182
5.6.4 Matched Field Processing, Phase Conjugation and Time Reversal ... 182
5.7 Active SONAR Processing 185
5.7.1 Active SONAR Signal Processing.... 185
5.7.2 Underwater Acoustic Imaging 187
5.7.3 Acoustic Telemetry..... 191
5.7.4 Travel-Time Tomography..... 192
5.8 Acoustics and Marine Animals..... 195
5.8.1 Fisheries Acoustics..... 195
5.8.2 Marine Mammal Acoustics 198
5.A Appendix: Units 201
References 201

During the two World Wars, both shallow and deep-water acoustics studies were pursued, but during the Cold War, emphasis shifted sharply to deep water. The post-World War II (WWII) history of antisubmarine warfare (ASW) actually started in 1943 with Ewing and Worzel discovering the deep sound channel (DSC) caused by a minimum in the temperature-dependent sound speed. (Brekhovskikh of the Soviet Union also discovered it independently, but later.) This minimum has been mapped (dotted line in Fig. 5.1), and typically varies from the cold surface at the poles to a depth of about 1300 m at the equator. Since sound refracts toward lower sound speeds, the DSC produces a refraction-generated waveguide (gray lines) contained within the ocean, such that sound paths oscillate about the sound speed minimum and can propagate thousands of kilometers.

Amazon EX1014 Page 167

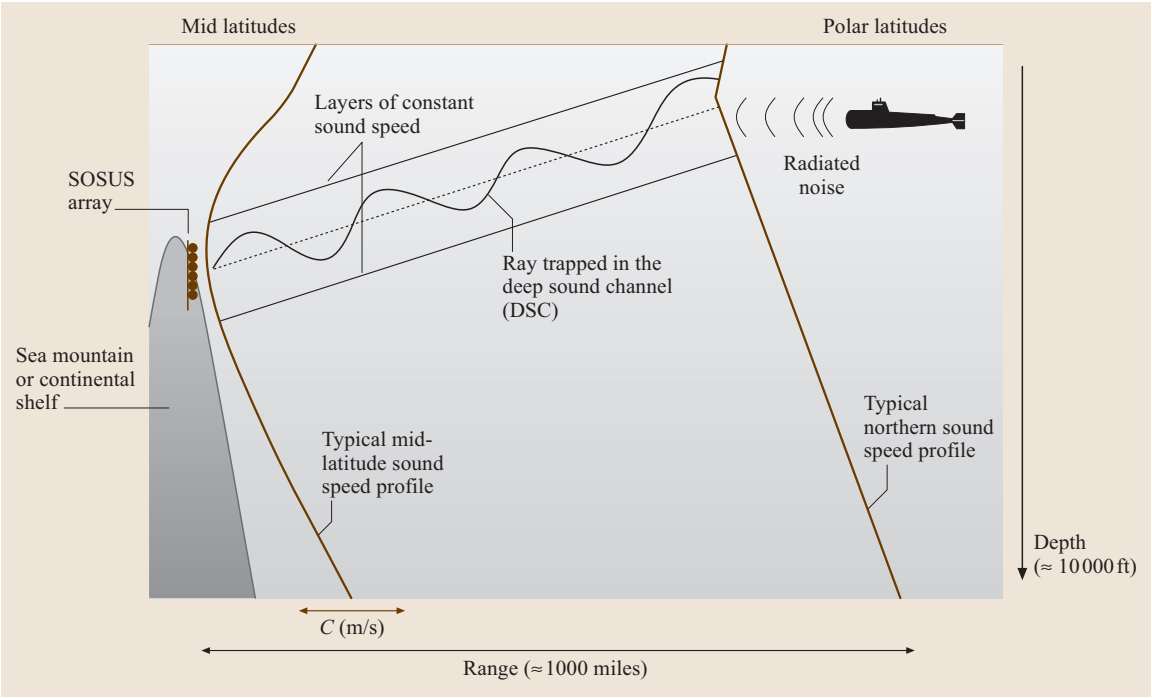


Fig. 5.1 Schematic of a long-range passive detection of a submarine in polar waters by a surveillance system in a temperate region [5.1]

Exploiting the DSC, the US Navy created the multi-billion dollar sound ocean surveillance system (SOSUS) network to monitor Soviet ballistic-missile nuclear submarines. Acoustic antennas were placed on ocean mountains or continental rises whose height extended into the DSC. These antennas were hard-wired to land stations using reliable undersea telephone cable technology. Submarines typically go down to depths of a few hundred meters. With many submarines loitering in polar waters, they were coupling into the DSC at shallower depths. Detections were made on very narrow-band radiation caused by imperfect, rotating machinery such as propellers. The advantage of detecting a set of narrow-band lines is that most of the broadband ocean noise can be filtered out. Though it was a Cold War, the multi-decade success of SOSUS was, in effect, a major Naval victory. The system was compromised by a spy episode, when the nature of the system was revealed. The result was a Soviet submarine quietening program and over the years, the Soviet fleet became quieter, reducing the long-range capability of the SOSUS system. The end of the Cold War led to an emphasis on the issue of detecting very quiet diesel–electric submarines in the noisy, shallow water that encompasses about 5% of the World's oceans on the continental shelves, roughly the region from the beach to the shelfbreak at about ≈ 200 m depth. However, there are also signs of a rekindling of interest in deep-water problems.

Parallel to these military developments, the field of ocean acoustics also grew for commercial, environmental and other purposes. Since the ocean environment has a large effect on acoustic propagation and therefore SONAR performance, acoustic methods to map and otherwise study the ocean were developed. As active SONARs were being put forward as a solution for the detection of quiet submarines, there was a growing need to study the effects of sound on marine mammals. Commercially, acoustic methods for fish finding and counting were developed as well as bottom-mapping techniques, the latter being having both commercial and military applications. All in all, ocean acoustics research and development has blossomed in the last half-century and many standard monographs and textbooks are now available (e.g. [5.2–10]).

Amazon EX1014 Page 168

5.1 Ocean Acoustic Environment

The acoustic properties of the ocean, such as the paths along which sound from a localized source travel, are mainly dependent on the ocean sound speed structure, which in turn is dependent on the oceanographic environment. The combination of water column and bottom properties leads to a set of generic sound-propagation paths descriptive of most propagation phenomena in the ocean.

5.1.1 Ocean Environment

Sound speed in the ocean water column is a function of temperature, salinity and ambient pressure. Since the ambient pressure is a function of depth, it is customary to express the sound speed (c) in m/s as an empirical function of temperature (T) in degrees centigrade, salinity (S) in parts per thousand and depth (z) in meters, for example [5.7, 11, 12]

$$c = 1449.2 + 4.6T - 0.055T^2 + 0.00029T^3 + (1.34 - 0.01T)(S - 35) + 0.016z\,. \quad (5.1)$$

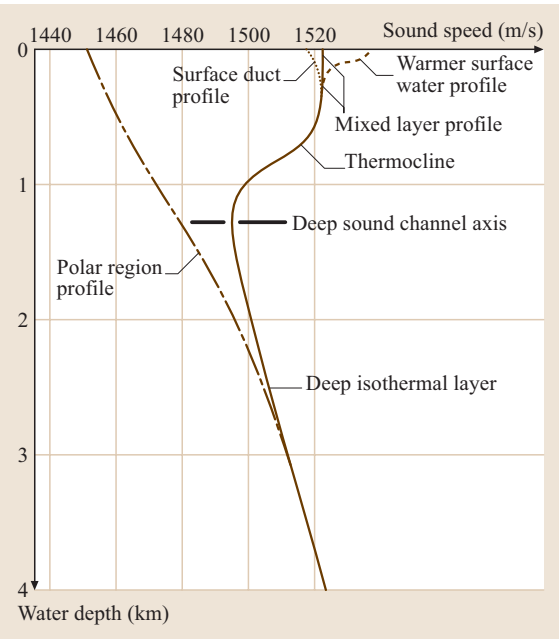


Fig. 5.2 Generic sound-speed profiles. The profiles reflect the tendencies that sound speed varies directly with temperature and hydrostatic pressure. Near-surface mixing can lead to almost isovelocity in that region. In polar waters, the coldest region is at the surface

Figure 5.2 shows a typical set of sound speed profiles indicating the greatest variability near the surface. In a warmer season (or warmer part of the day, sometimes referred to as the *afternoon effect*), the temperature increases near the surface and hence the sound speed increases toward the sea surface. In nonpolar regions where mixing near the surface due to wind and wave activity is important, a *mixed layer* of almost constant temperature is often created. In this isothermal layer the sound speed increases with depth because of the increasing ambient pressure, the last term in (5.1). This is the *surface duct* region. Below the mixed layer is the thermocline where the temperature and hence the sound speed decreases with depth. Below the thermocline, the temperature is constant and the sound speed increases because of increasing ambient pressure. Therefore, between the deep isothermal region and the mixed layer, there is a depth at minimum sound speed referred to as the axis of the *deep sound channel*. However, in polar regions, the water is coldest near the surface so that the minimum sound speed is at the surface. Figure 5.3 is a contour display of the sound speed structure of the North and South Atlantic with the deep sound channel axis indicated by the heavy dashed line. Note that the deep sound channel becomes shallower toward the poles. Aside from sound speed effects, the ocean volume is absorptive and causes attenuation that increases with acoustic frequency.

Shallower water such as that in continental shelf and slope regions is not deep enough for the depth-pressure term in (5.1) to be significant. Thus the winter profile tends to isovelocity, simply because of mixing, whereas the summer profile has a higher sound speed near the surface due to heating; both are schematically represented in Fig. 5.4.

The sound speed structure regulates the interaction of sound with the boundaries. The ocean is bounded above by air, which is a nearly perfect reflector; however, the sea surface is often rough, causing sound to scatter in directions away from the specular reflecting angle. The ocean bottom is typically a complicated, rough, layered structure supporting elastic waves. Its geoacoustic properties are summarized by density, compressional and shear speed, and attenuation profiles. The two basic interfaces, air/sea and sea/bottom, can be thought of as the boundaries of an acoustic waveguide whose internal index of refraction is determined by the fun-

Amazon EX1014 Page 169

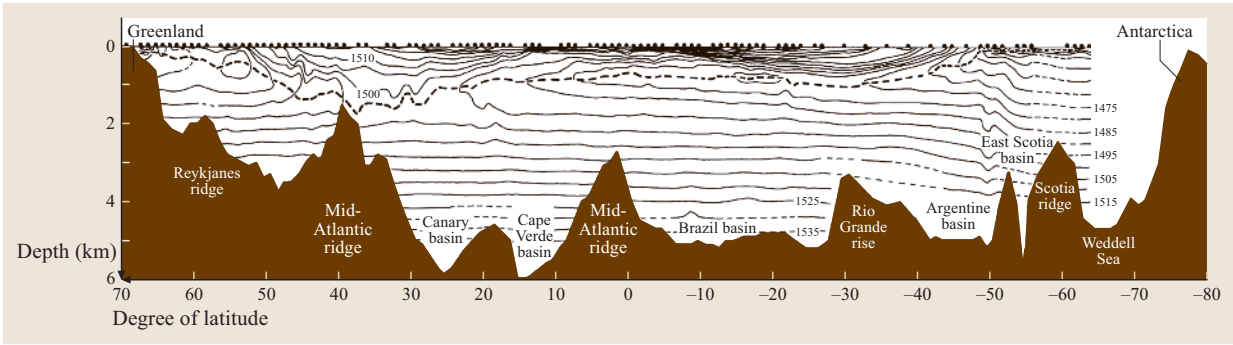


Fig. 5.3 Sound-speed contours at 5 m/s intervals taken from the North and South Atlantic along 30.50° W. The *dashed line* indicates the axis of the deep sound channel (after [5.13]). The sound channel is deepest near the equator and comes to the surface at the poles

damental oceanographic parameters represented in the sound speed equation (5.2).

Due to the density stratification of the water column, the interior of the ocean supports a variety of waves, just as the ocean surface does. One particularly important type of wave in both shallow water and deep water is the internal gravity wave (IW) [5.14]. This wave type is bounded in frequency between the inertial frequency, $f = 2\Omega \sin\theta$, where Ω is the rotation frequency of the earth and θ is the latitude, and the highest buoyancy frequency (or Brunt–Vaisala frequency) $N_{\max}(z)$, where $N^2(z) = -(g/\rho)\mathrm{d}\rho/\mathrm{d}z$, and $\rho(z)$ is the density of the fluid as a function of depth z. The inertial frequency varies from two cycles per day at the poles to zero cycles per day at the equator, and the maximum buoyancy frequency is usually on the order of 5–10 cycles per hour.

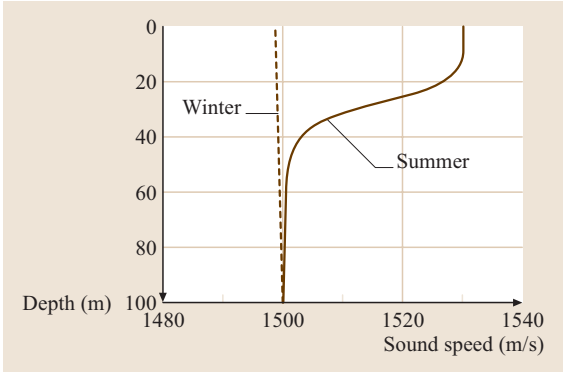


Fig. 5.4 Typical summer and winter shallow-water sound-speed profiles. Warming causes the high-speed region near the surface in the summer. Without strong heating, mixing tends to make the shallow-water region isovelocity in the winter

Two categories of IWs are found in stratified coastal waters: linear and nonlinear waves. The linear waves, found virtually everywhere, obey a standard linear wave equation for the displacement of the surfaces of constant density (*isopycnal* surfaces). The nonlinear IWs, which are generated under somewhat more specialized circumstances than the linear waves (and thus are not always present), can obey a family of nonlinear wave equations. The most useful and illustrative of them is the familiar Korteweg–deVries equation (KdV), which governs the horizontal components of the nonlinear internal waves. The vertical component of the nonlinear internal waves obeys a normal-mode equation.

5.1.2 Basic Acoustic Propagation Paths

Sound propagation in the ocean can be qualitatively broken down into three classes: very-short-range, deep-water and shallow-water propagation.

Very-Short-Range Propagation

The pressure amplitude from a point source in free space falls off with range r as r^{-1}; this geometric loss is called *spherical spreading*. Most sources of interest in the deep ocean are closer to the surface than to the bottom. Hence, the two main short-range paths are the direct path and the surface reflected path. When these two paths *interfere*, they produce a spatial distribution of sound often referred to as a Lloyd mirror pattern, as shown in insert of Fig. 5.5. Also, with reference to Fig. 5.5, note that the *transmission loss* is a decibel measure of the decay with distance of acoustic intensity from a source relative to its value at unit distance (see Appendix), the latter being proportional to the square of the acoustic amplitude.

Amazon EX1014 Page 170

Long-Range Propagation Paths

Figure 5.6 is a schematic of propagation paths in the ocean resulting from the sound-speed profiles (indicated by the dashed line) described above in Fig. 5.2. These paths can be understood from *Snell's law*,

$$\frac{\cos\theta(z)}{c(z)} = \text{constant}\,, \tag{5.2}$$

which relates the ray angle $\theta(z)$ with respect to the horizontal, to the local sound speed $c(z)$ at depth z. The equation requires that, the higher the sound speed, the smaller the angle with the horizontal, meaning that sound bends away from regions of high sound speed; or said another way, sound bends toward regions of low sound speed. Therefore, paths 1, 2, and 3 are the simplest to explain since they are paths that oscillate about the local sound speed minima. For example, path 3 depicted by a ray leaving a source near the deep sound channel axis at a small horizontal angle propagates in the deep sound channel. This path, in temperate latitudes where the sound speed minimum is far from the surface, permits propagation over distances of thousands of kilometers.

The upper turning point of this path typically interacts with the thermocline, which is a region of strong internal wave activity. Path 4, which is at slightly steeper angles and is usually excited by a near-surface source, is *convergence zone* propagation, a spatially periodic (35–65 km) refocusing phenomenon producing zones of high intensity near the surface due to the upward refracting nature of the deep sound-speed profile. Regions between these zones are referred to as shadow regions. Referring back to Fig. 5.2, there may be a depth in the deep isothermal layer at which the sound speed is the same as it is at the surface. This depth is called the *critical depth* and is the lower limit of the deep sound channel. If the critical depth is in the water column, the environment supports long-distance propagation without bottom interaction whereas if there is no critical depth in the water column, the ocean bottom is the lower boundary of the deep sound channel. The *bottom bounce* path 5 is also a periodic phenomenon but with a shorter cycle distance and shorter propagation distance because of losses when sound is reflected from the ocean bottom. Finally, note that when bottom baths are described in the general context of the spectral properties of waveguide propagation, they are described in terms of the continuous horizontal wavenumber region as explained in the discussion associated with Fig. 5.32a.

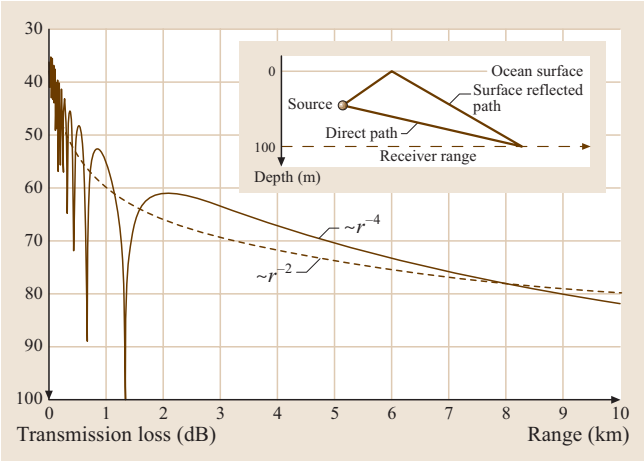


Fig. 5.5 The insert shows the geometry of the Lloyd's mirror effect. The plots show a comparison of Lloyd's mirror (*full line*) to spherical spreading (*dashed line*). Transmission losses are plotted in decibels corresponding to losses of $10\log r^2$ and $10\log r^4$, respectively, as explained in Sect. 5.1.3

Shallow Water and Waveguide Propagation

In general the ocean can be thought of as an acoustic waveguide [5.1]; this waveguide physics is particularly evident in shallow water (inshore out to the continental slope, typically to depths of a few hundred meters). Snell's law applied to the summer profile in Fig. 5.4 produces rays which bend more toward the bottom than winter profiles in which the rays tend to be straight. This implies two effects with respect to the ocean bottom: (1) for a given range, there are more bounces off

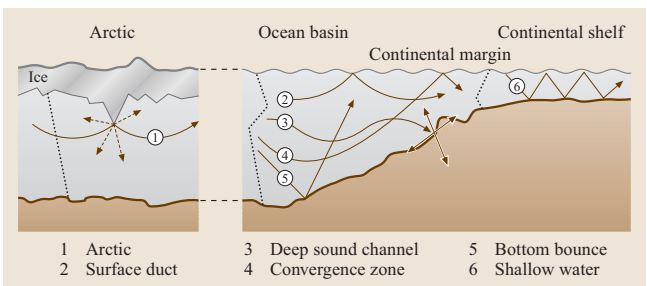


Fig. 5.6 Schematic representation of various types of sound propagation in the ocean. An intuitive guide is that Snell's law has sound turning toward lower-speed regions. That alone explains all the refractive paths: 1, 2, 3 and 4.It will also explain any curvature associated with paths 5 and 6. Thus, the summer profile would have path 6 curving downward (this curvature is not shown in the figure) while the deep sound-speed profile below the minimum curves upward (4)

Amazon EX1014 Page 171

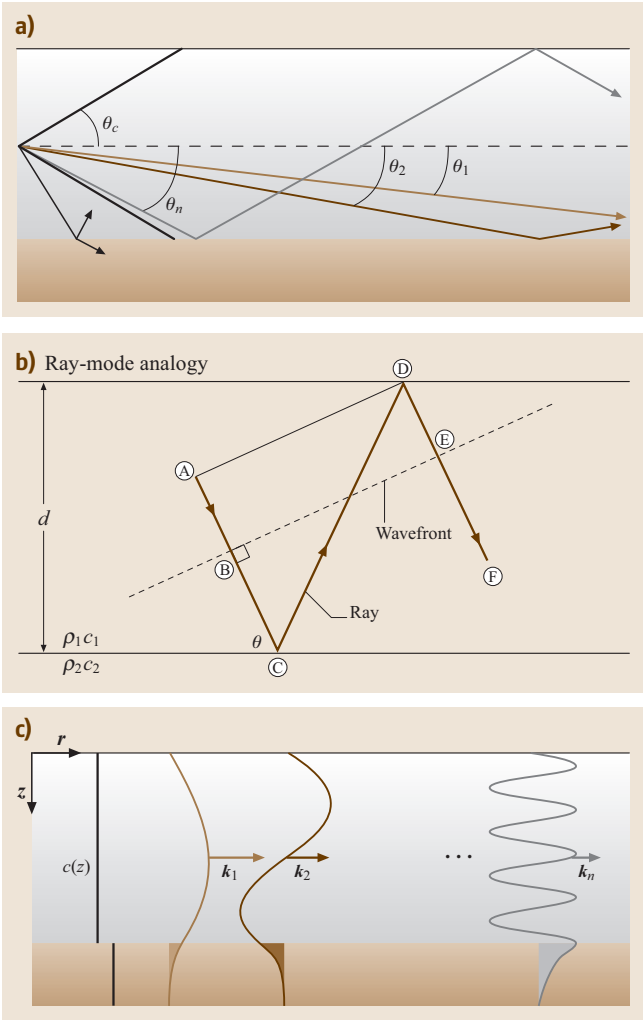


Fig. 5.7a–c Ocean waveguide propagation. **(a)** Long-distance propagation occurs within the critical angle cone of $2\theta_c$. **(b)** For the example shown, the condition for constructive interference is that the phase change along BCDE be a multiple of 2π. **(c)** The constructive interference can be interpreted as discrete modes traveling in the waveguide, each with their own horizontal wavenumber

the ocean bottom in summer than in the winter, and (2) the ray angles intercepting the bottom are steeper in the summer than in the winter. A qualitative understanding of the reflection properties of the ocean bottom should therefore be very revealing of sound propagation in summer versus winter. Basically, near-grazing incidence is much less lossy than larger, more-vertical angles of incidence. Since summer propagation paths have more bounces, each of which are at steeper angles than winter paths, summer shallow-water propagation is lossier than winter. This result is tempered by rough winter surface conditions that generate large scattering losses at the higher frequencies.

For simplicity we consider an isovelocity waveguide bounded above by the air–water interface and below by a two-fluid interface that is classically defined as a Pekeris waveguide. From Sect. 5.2.3, we have perfect reflection with a 180° phase change at the surface and for grazing angles lower than the bottom critical angle, there will also be perfect bottom reflection. Therefore, as schematically indicated in Fig. 5.7a, ray paths within a cone of $2\theta_c$ will propagate unattenuated down the waveguide. Because the up- and down-going rays have equal amplitudes, preferred angles will exist for which constructive interference occurs. These particular angles are associated with the normal modes of the waveguide, as formally derived from the wave equation in the Sect. 5.4. However, it is instructive to understand the geometric origin of the waveguide modal structure. Figure 5.7b is a schematic of a ray reflected from the bottom and then the surface of a Pekeris waveguide. Consider a ray along the path ACDF and its wavefront, which is perpendicular to the ray. The two down-going rays of equal amplitude, AC and DF, will constructively interfere if points B and E have a phase difference of a multiple of 2π (and similarly for up-going rays). The phase change at the two boundaries must be included. There is a discrete set of angles up to the critical angle for which this constructive interference takes place and, hence, for which sound propagates. This discrete set, in terms of wave physics, are called the normal modes of the waveguide, illustrated in Fig. 5.7c. They correspond to the ray schematic of Fig. 5.7a. Mode propagation is further discussed in the Sect. 5.4.4.

5.1.3 Geometric Spreading Loss

The energy per unit time emitted by a sound source is flowing through a larger area with increasing range. Intensity is the power flux through a unit area, which translates to the energy flow per unit time through a unit area. The simplest example of geometric loss is spherical spreading for a point source in free space where the area increases as r^2, where r is the range from the point source. So spherical spreading results in an intensity decay proportional to r^{-2}. Since intensity is proportional to the square of the pressure amplitude, the fluctuations in pressure induced by the sound p, decay as r^{-1}. For range-independent ducted propagation, that is, where rays are refracted or reflected back towards the horizon-

Amazon EX1014 Page 172

tal direction, there is no loss associated with the vertical dimension. In this case, the spreading surface is the area of the cylinder whose axis is in the vertical direction passing through the source $2\pi rH$, where H is the depth of the duct (waveguide), and is constant. Geometric loss in the near-field Lloyd-mirror regime requires consideration of interfering beams from direct and surface reflected paths. To summarize, the geometric spreading laws for the pressure field (recall that intensity is proportional to the square of the pressure.) are:

- Spherical spreading loss: $p \propto r^{-1}$;
- Cylindrical spreading loss: $p \propto r^{-1/2}$;
- Lloyd-mirror loss: $p \propto r^{-2}$.

5.2 Physical Mechanisms

The physical mechanisms associated with the generation, reception, attenuation and scattering of sound in the ocean are discussed in this section.

5.2.1 Transducers

A transducer converts some sort of energy to sound (source) or converts sound energy (receiver) to an electrical signal [5.15]. In underwater acoustics piezoelectric and magnetostrictive transducers are commonly used; the former connects electric polarization to mechanical strain and the latter connects the magnetization of a ferromagnetic material to mechanical strain. Piezoelectric transducers represent more than 90% of the sound sources used in the ocean. Magnetostrictive transducers are more expensive, have poor efficiency and a narrow frequency bandwidth. However, they allow large vibration amplitudes and are relevant to low-frequency high-power applications. In addition there are: electrodynamic transducers in which sound pressure oscillations move a current-carrying coil through a magnetic field causing a back emf, and electrostatic transducers in which charged electrodes moving in a sound field change the capacitance of the system. Explosives, air guns, electric discharges, and lasers are also used as wide-band sources.

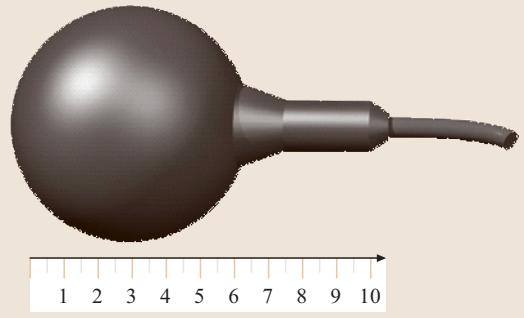
Hydrophones, underwater acoustic receivers, are commonly piezoelectric devices with good sensitivity and low internal noise levels. Hydrophones usually work on large frequency bandwidths since they do not need to be adjusted to a resonant frequency. They are associated with low-level electronics such as preamplifiers and filters.

Because the field of transducers is large by itself, we concentrate in this section on some very practical issues that are immediately necessary to either convert received voltage levels to pressure levels or transmitter excitation to pressure levels. Practical issues about transducers and hydrophones deal with the understanding of specification sheets given by the manufacturer. Among those, we will describe, based on a practical example, the definition and the use of the following quantities:

- Transmitting voltage response
- Open-circuit receiving response
- Transmitting and receiving beam patterns at specific frequencies
- Impedance and/or admittance versus frequency
- Resonant frequency, maximum voltage and maximum source level (for a transducer)

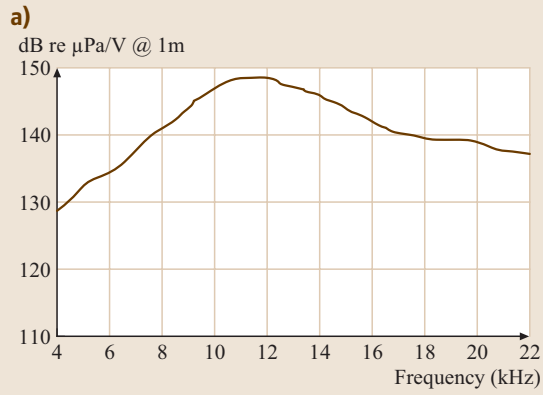
Figure 5.8 is a specification sheet provided by the ITC (Internationsal Transducer Corp.) for a deep-water omnidirectional transducer. Figure 5.8a corresponds to the transmitting sensitivity versus frequency. The units are in dB re μPa/V@1m, which means that, at the resonant frequency 11.5 kHz for example, the transducer excited with a 1 V amplitude transmits at one meter a pressure p_t such that $20\log_{10}\left(\frac{p_t}{1\times10^{-6}}\right) = 149$ dB, i. e. $p_t \approx 28.2$ Pa. Similarly, Fig. 5.8b shows the receiving sensitivity versus frequency. The units are now in dB re1V/μPa which means that, at 11.5 kHz for example, the transducer converts a 1 μPa amplitude field into a voltage V_r such that $20\log_{10}\left(\frac{V_r}{1}\right) = -186$ dB, i. e. $V_r \approx 5\times10^{-10}$ V. Figure 5.8c shows the admittance versus frequency. The complex admittance Y is the inverse of the complex impedance Z. The real part of the admittance is called the conductance G; the imaginary part is the susceptance B. Those curves directly yield the calculation of the electrical impedance of the transducer. For example, the impedance of ITC-1007 at the resonant frequency is $|Z| = 1/(\sqrt{G^2+B^2}) \approx 115\,\Omega$. When used as a source, the transducer electrical impedance has to match the output impedance of the power amplifier to allow for a good power transfer through the transducer. In the case where the impedances do not match, a customized matching box will be necessary. Knowing the electrical impedance $|Z|$ and the input power $I = 10\,000$ W, the maximum voltage can be determined as $U_{max} = \sqrt{|Z|\,I} \approx 1072$ V. According to the trans-

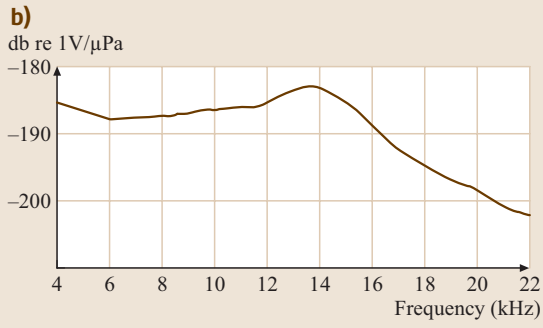
Amazon EX1014 Page 173

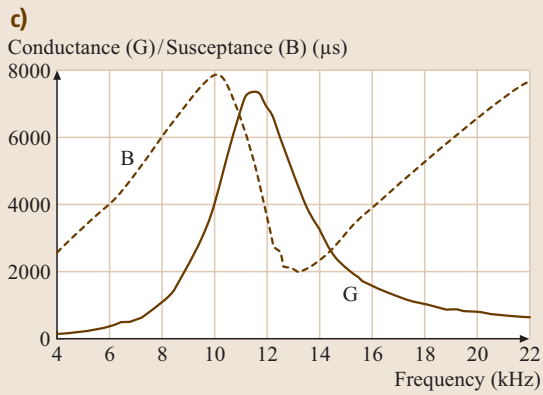


Specifications (nominal)

Type	Projector/Hydrophone
Resonance frequency f_r	11,5 kHz
Depth	1250 m
Envelope dimensions (in.)	6.5 D
TVR at f_r	149 dB/(µPa/V@1m)
Midband OCV	–188 dB/(1V/µPa)
Suggested band	0.01–20 kHz
Beam type	Spherical
Input power	10000 W







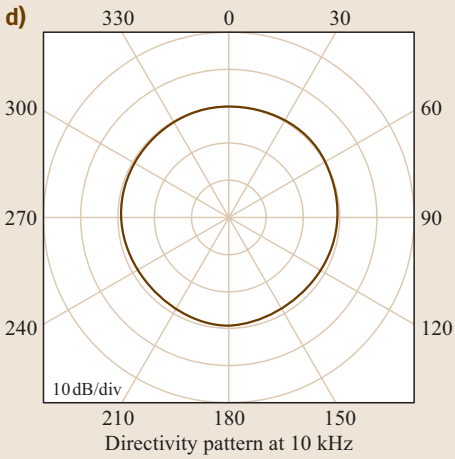


Fig. 5.8a–d Typical specification sheet of a powerful underwater acoustic transponder (*top left*). **(a)** Transmitting voltage response. **(b)** Receiving voltage response. **(c)** Real (*full line*) and imaginary part (*dashed line*) of the water admittance Y. **(d)** Directionality pattern at one frequency (Courtesy of International Transducer Corp.)

mitting voltage response, this corresponds to a source level of nearly 210 dB re µPa at the resonant frequency. Finally, Fig. 5.8d represents the directionality pattern at a given frequency. It shows that the ITC-1007 is omnidirectional at 10 kHz.

When transducers have to be coupled to a power amplifier or another electronic device, it may be useful to model the transducer as an electronic circuit (Fig. 5.9a). The frequency dependence of the conductance G and susceptance B (Fig. 5.8c) yield the components of the

Amazon EX1014 Page 174

equivalent circuit, as shown in Fig. 5.9b. Similarly, an important parameter is the quality factor Q, which measures the ratio between the mechanical energy transmitted by the transducer and the energy dissipated (Fig. 5.10). Finally, the equivalent circuit leads to the measure of the electroacoustic power efficiency k^2 that corresponds to the ratio of the output acoustic power and the input electric power.

Hydrophones are usually described with the same characteristics as transducers but they are only designed to work in reception. To this goal, hydrophones are usually connected to a preamplifier with high input impedance to avoid any loss in the signal reception. A typical hydrophone exhibits a flat receiving response on a large bandwidth far away from its resonance frequency (Fig. 5.11a). As expected, the sensitivity of a hydrophone is much higher than the sensitivity of a transducer. Low electronic noise below the ocean ambient-noise level is also an important characteristic for hydrophones (Fig. 5.11b). Finally, hydrophones are typically designed to be omnidirectional (Fig. 5.11c).

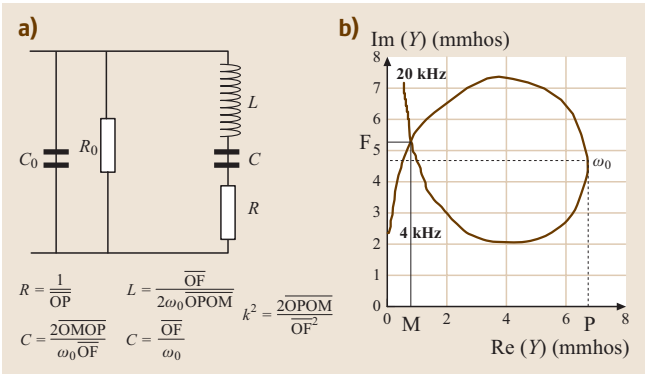


Fig. 5.9 **(a)** Representation of the transducer as an electronic circuit around the resonant frequency. The resistor R_0 corresponds to the dielectric loss in the transducer and is commonly supposed infinite. C_0 is the transducer capacity, L and C are the mass and rigidity of the material, respectively. R includes both the mechanic loss and the energy mechanically transmitted by the transducer. **(b)** The values of C_0, L, C and R are obtained from the positions of the points F, M and P in the real–imaginary admittance curve given in the specification sheet

5.2.2 Volume Attenuation

Attenuation is characterized by an exponential decay of the sound field. If A_0 is the root-mean-square (rms) amplitude of the sound field at unit distance from the source, then the attenuation of the sound field causes the amplitude to decay with distance along the path, r:

$$A = A_0 \exp(-\alpha r) , \tag{5.3}$$

where the unit of α is Nepers/distance. The attenuation coefficient can be expressed in decibels per unit distance by the conversion $\alpha' = 8.686\alpha$. Volume attenuation increases with frequency and the frequency dependence of attenuation can be roughly divided into four regimes as displayed in Fig. 5.12. In region I, leakage out of the sound channel is believed to be the main cause of attenuation. The main mechanisms associated with regions II and III are boric acid and magnesium sulfate chemical relaxation. Region IV is dominated by the shear and bulk viscosity associated with fresh water. A summary of the approximate frequency dependence (f in kHz) of attenuation (in units of dB/km) is given by

$$\alpha'(\mathrm{dB/km}) = 3.3\times10^{-3} + \frac{0.11 f^2}{1+f^2} + \frac{43 f^2}{4100+f^2} + 2.98\times10^{-4} f^2 , \tag{5.4}$$

with the terms sequentially associated with regions I–IV in Fig. 5.12.

In Fig. 5.6, the losses associated with path 3 only include volume attenuation and scattering because this path does not involve boundary interactions. The volume scattering can be biological in origin or arise from interaction with internal wave activity in the vicinity

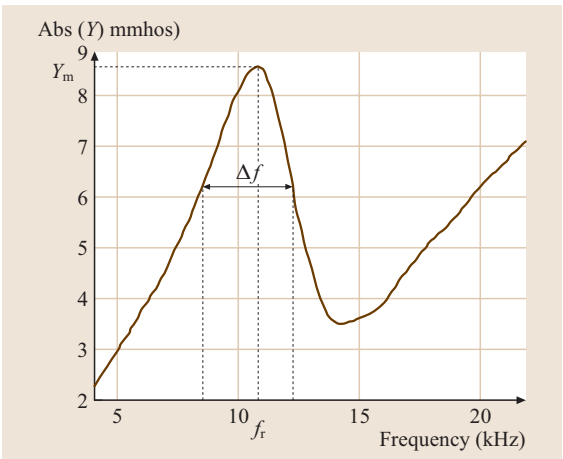


Fig. 5.10 Frequency dependence of the admittance curve that allows the calculation of the quality factor $Q = f_r/\Delta f$ of the transducer at the resonant frequency f_r. Y_m is the maximum of the admittance

Amazon EX1014 Page 175

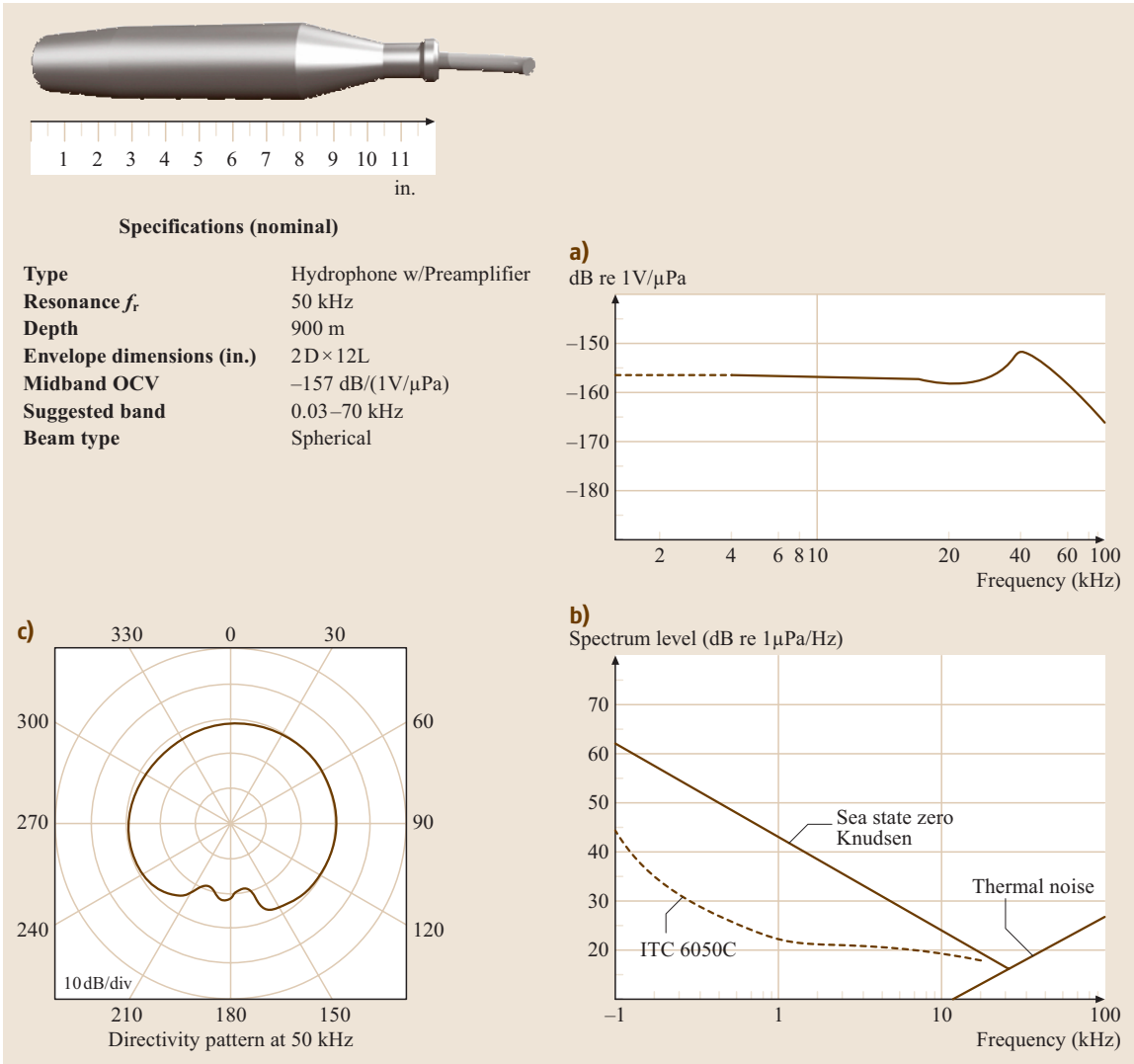


Fig. 5.11a–c Typical specification sheet of a hydrophone (top). **(a)** Receiving frequency response. **(b)** Spectral noise level of the hydrophone to be compared to the ocean ambient noise level. **(c)** Directionality pattern at one frequency (Courtesy of International Transducer Corp.)

of the upper part of the deep sound channel where paths are refracted before they interact with the surface. Both of these effects are small at low frequencies. This same internal wave region is also on the lower boundary of the surface duct, allowing scattering out of the surface duct, thereby also constituting a loss mechanism for the surface duct. This mechanism also leaks sound into the deep sound channel, a region that without scattering would be a shadow zone for a surface duct source. This type of scattering from internal waves is also a source of fluctuation of the sound field.

5.2.3 Bottom Loss

The structure of the ocean bottom affects those acoustic paths which interact with it. This bottom interaction is summarized by *bottom reflectivity*, the amplitude ratio of reflected and incident plane waves at the ocean–bottom interface as a function of grazing angle, θ (Fig. 5.13a).

Amazon EX1014 Page 176

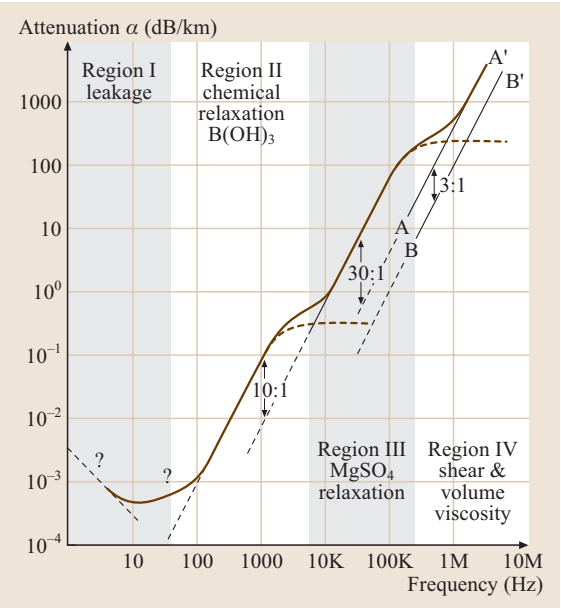


Fig. 5.12 Regions of the different dominant attenuation processes for sound propagating in seawater (after [5.16]). The attenuation is given in dB per kilometer

For a simple bottom, which can be represented by a semi-infinite half-space with constant sound speed c_2 and density ρ_2, the reflectivity is given by

$$R(\theta) = \frac{\rho_2 k_{1z} - \rho_1 k_{2z}}{\rho_2 k_{1z} + \rho_1 k_{2z}} , \tag{5.5}$$

with the subscripts 1 and 2 denoting the water and ocean bottom, respectively; the wavenumbers are given by

$$k_{iz} = (\omega/c_i)\sin\theta_i = k\ \sin\theta_i ; i = 1, 2 . \tag{5.6}$$

The incident and transmitted grazing angles are related by Snell's law,

$$c_2 \cos\theta_1 = c_1 \cos\theta_2 , \tag{5.7}$$

and the incident grazing angle θ_1 is also equal to the angle of the reflected plane wave.

For this simple water–bottom interface for which we take $c_2 > c_1$, there exists a critical grazing angle θ_c below which there is perfect reflection,

$$\cos\theta_c = \frac{c_1}{c_2} . \tag{5.8}$$

For a lossy bottom, there is no perfect reflection, as also indicated in a typical reflection curve in Fig. 5.13b. These results are approximately frequency independent.

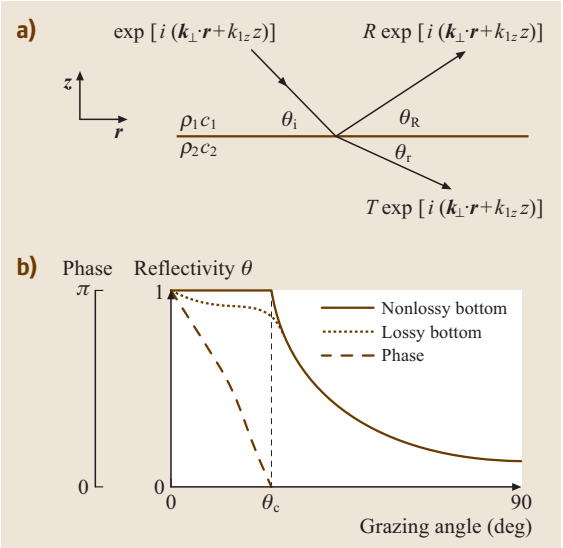


Fig. 5.13a,b The reflection and transmission process. Grazing angles are defined relative to the horizontal. **(a)** A plane wave is incident on an interface separating two media with densities and sound speeds ρ, c. $R(\theta)$ and $T(\theta)$ are reflection and transmission coefficients. Snell's law is a statement that $k_\perp$, the horizontal component of the wave vector, is the same for all three waves. **(b)** Rayleigh reflection curve $R(\theta)$ as a function of the grazing angle indicating critical angle θ_c. The dashed curve shows that, if the second medium is lossy, there is no perfect reflection below the critical angle. Note that for the non-lossy bottom, there is complete reflection below the critical angle, but with a phase change

However, for a layered bottom, the reflectivity has a complicated frequency dependence. It should be pointed out that, if the density of the second medium vanishes, the reflectivity reduces to the pressure release case of $R(\theta) = -1$.

5.2.4 Scattering and Reverberation

Scattering caused by rough boundaries or volume heterogeneities is a mechanism for loss (attenuation), reverberant interference and fluctuation. Attenuation from volume scattering is addressed in Sect. 5.2.2. In most cases, it is the mean or coherent (or specular) part of the acoustic field which is of interest for a SONAR or communications application and scattering causes part of the acoustic field to be randomized. Rough surface scattering out of the *specular direction* can be thought of as an attenuation of the mean acoustic field and typ-

Amazon EX1014 Page 177

ically increases with increasing frequency. A formula often used to describe reflectivity from a rough boundary is

$$R'(\theta) = R(\theta)\exp\left(-\frac{\Gamma^2}{2}\right), \tag{5.9}$$

where $R(\theta)$ is the reflection coefficient of the smooth interface and Γ is the Rayleigh roughness parameter defined as $\Gamma \equiv 2k\sigma\sin\theta$ where $k = 2\pi/\lambda$, λ is the acoustic wavelength, and σ is the rms roughness height [5.18–20].

The scattered field is often referred to as reverberation. Surface, bottom or volume scattering strength, $S_{S,B,V}$ is a simple parameterization of the production of reverberation and is defined as the ratio in decibels of the sound scattered by a unit surface area or volume referenced to a unit distance I_{scat} to the incident plane wave intensity I_{inc}

$$S_{\text{S,B,V}} = 10\log\frac{I_{\text{scat}}}{I_{\text{inc}}}\,. \tag{5.10}$$

The Chapman–Harris [5.21] curves predicts the ocean surface scattering strength in the 400–6400 Hz region,

$$\begin{aligned} S_{\text{S}} &= 3.3\beta\log\frac{\theta}{30} - 42.4\log\beta + 2.6\,; \\ \beta &= 107(w f^{1/3})^{-0.58}, \end{aligned} \tag{5.11}$$

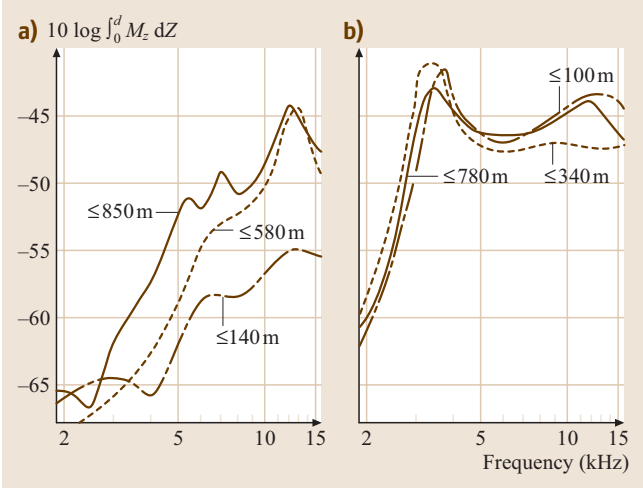


Fig. 5.14 **(a)** Day and **(b)** night scattering strength measurements using an explosive source as a function of frequency (after [5.17]). The spectra measured at various times after the explosion are labeled with the depth of the nearest scatterer that could have contributed to the reverberation. The ordinate corresponds to S_{V} in (5.13)

where θ is the grazing angle in degrees, w the wind speed in m/s and f the frequency in Hz. Ocean surface scattering is further discussed in [5.22].

The simple characterization of bottom backscattering strength utilizes Lambert's rule for diffuse scattering,

$$S_{\text{B}} = A + 10\log\sin^2\theta\,, \tag{5.12}$$

where the first term is determined empirically. Under the assumption that all incident energy is scattered into the water column with no transmission into the bottom, A is −5 dB. Typical realistic values for A [5.23] which have been measured are −17 dB for the large basalt mid-Atlantic ridge cliffs and −27 dB for sediment ponds.

The volume scattering strength is typically reduced to a surface scattering strength by taking S_{V} as an average volume scattering strength within some layer at a particular depth; then the corresponding surface scattering strength is

$$S_{\text{S}} = S_{\text{V}} + 10\log H\,, \tag{5.13}$$

where H is the layer thickness. The column or integrated scattering strength is defined as the case for which H is the total water depth.

Volume scattering usually decreases with depth (about 5 dB per 300 m) with the exception of the deep scattering layer. For frequencies less than 10 kHz, fish with air-filled swim bladders are the main scatterers. Above 20 kHz, zooplankton or smaller animals that feed upon phytoplankton and the associated biological chain are the scatterers. The deep scattering layer (DSL) is deeper in the day than in the night, changing most rapidly during sunset and sunrise. This layer produces a strong scattering increase of 5–15 dB within 100 m of the surface at night and virtually no scattering in the daytime at the surface since it migrates down to hundreds of meters. Since higher pressure compresses the fish swim bladder, the backscattering acoustic resonance (Sect. 5.2.6) tends to be at a higher frequency during the day when the DSL migrates to greater depths. Examples of day and night scattering strengths are shown in Fig. 5.14.

Finally, as explained in Sect. 5.2.6, near-surface bubbles and bubble clouds can be thought of as either volume or surface scattering mechanisms acting in concert with the rough surface. Bubbles have resonances (typically greater than 10 kHz) and at these resonances, scattering is strongly enhanced. Bubble clouds have collective properties; among these properties is that a bubbly mixture, as specified by its void fraction (total bubble gas volume divided by water volume) has a considerable lower sound speed than water.

Amazon EX1014 Page 178

5.2.5 Ambient Noise

There are essentially two types of ocean acoustic noise: manmade and natural. Generally, shipping is the most important source of manmade noise, though noise from offshore oil rigs is becoming increasingly prevalent. See also Table 5.2 in the Marine Mammal section for specific examples of manmade noise. Typically, natural noise dominates at low frequencies (below 10 Hz) and high frequencies (above a few hundred Hz). Shipping fills in the region between ten and a few hundred Hz and this component is increasing over time [5.25, 26]. A summary of the spectrum of noise is shown in Fig. 5.15. The higher-frequency noise is usually parameterized according to the sea state (also Beaufort number) and/or wind. Table 5.1 summarizes the description of the sea state.

The sound-speed profile affects the vertical and angular distribution of noise in the deep ocean. When there is a critical depth (Sect. 5.1.2), sound from surface sources travels long distances without interacting with the ocean bottom, but a receiver below this critical depth should sense less surface noise because propagation involves interaction with lossy boundaries, the surface and/or bottom. This is illustrated in Fig. 5.16a,b which shows a deep-water environment with measured ambient noise. Figure 5.16c is an example of vertical directionality of noise which also follows the propagation physics discussed above. The shallower depth is at the axis of the deep sound channel while the other is at the critical depth. The pattern is narrower at the critical depth where the sound paths tend to be horizontal since the rays are turning around at the lower boundary of the deep sound channel.

In a range-independent ocean, Snell's law predicts a horizontal noise notch at depths where the speed of sound is less than the near-surface sound speed. Returning to (5.2) and reading off the sound speeds from Fig. 5.16 at the surface ($c = 1530\,\mathrm{m/s}$) and say, 300 m

Table 5.1 Descriptor of the ocean sea surface [5.24]

Sea criteria	Beaufort scale	Wind speed range knots (m/s)	Wind speed mean knots (m/s)	12 h wind Wave height[a,b] ft (m)	Fully arisen sea Wave height[a,b] ft (m)	Fully arisen sea Duration[b,c] h	Fully arisen sea Fetch[b,c] naut. miles (km)	Sea-state scale
Mirror–like	0	< 1 (< 0.5)						0
Ripples	1	1–3 (0.5–1.7)	2 (1.1)					0.5
Small wavelets	2	4–6 (1.8–3.3)	5 (2.5)	< 1 (< 0.30)	< 1 (< 0.30)			1
Large wavelets, scattered whitecaps	3	7–10 (3.4–5.4)	8.5 (4.4)	1–2 (0.30–0.61)	1–2 (0.30–0.61)	< 2.5	< 10 (< 19)	2
Small waves, frequent whitecaps	4	11–16 (5.5–8.4)	13.5 (6.9)	2–5 (0.61–1.5)	2–6 (0.61–1.8)	2.5–6.5	10–40 (19–74)	3
Moderate waves, many whitecaps	5	17–21 (8.5–11.1)	19 (9.8)	5–8 (1.5–2.4)	6–10 (1.8–3.0)	6.5–11	40–100 (74–185)	4
Large waves, whitecapes everywhere, spray	6	22–27 (11.2–14.1)	24.5 (12.6)	8–12 (2.4–3.7)	10–17 (3.0–5.2)	11–18	100–200 (185–370)	5
Heaped–up sea, blown spray, streaks	7	28–33 (14.2–17.2)	30.5 (15.7)	12–17 (3.7–5.2)	17–26 (5.2–7.9)	18–29	200–400 (370–740)	6
Moderately high, long waves, spindrift	8	34–40 (17.3–20.8)	37 (19.0)	17–24 (5.2–7.3)	26–39 (7.9–11.9)	29–42	400–700 (740–1300)	7

Notes:
a The average height of the highest one-third of the waves (significant wave height)
b Estimated from data given in US Navy Hydrographic Office (Washington, D.C.) publications HO 604 (1951) and HO 603 (1955)
c The minimum fetch and duration of the wind needed to generate a fully arisen sea

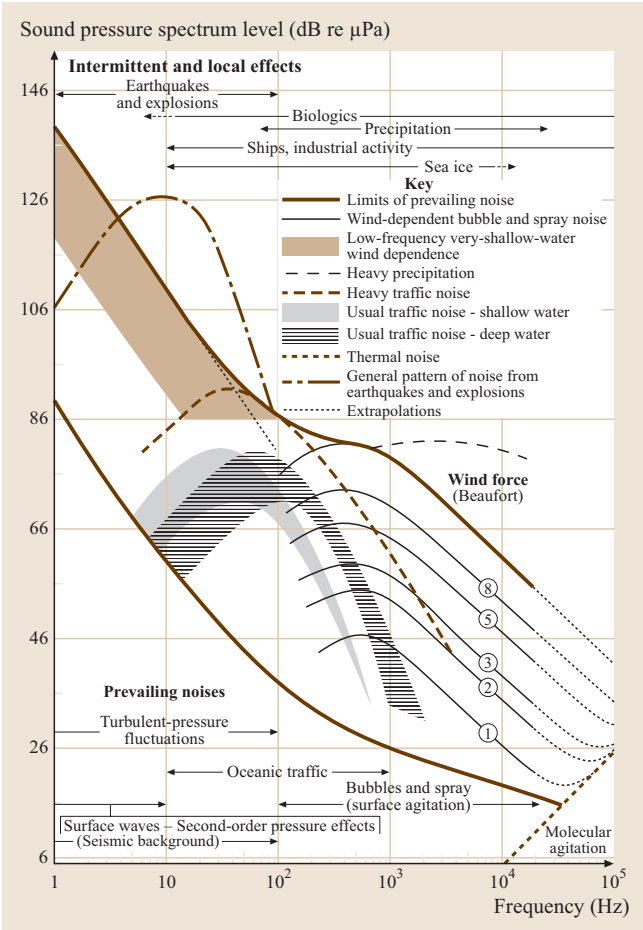


Fig. 5.15 Composite of ambient noise spectra (after [5.24])

(1500 m/s) , a horizontal ray ($\theta = 0$) launched from the ocean surface would have an angle with respect to the horizontal of about 11° at 300 m depth. All other rays would arrive with greater vertical angles. Hence we expect this horizontal notch. However, the horizontal notch is often not seen at shipping noise frequencies. That is because shipping tends to be concentrated in continental-shelf regions and propagation down a continental slope converts high-angle rays to lower angles at each bounce. There are also deep-sound-channel shoaling effects that result in the same trend in angle conversion.

The vertical directionality of noise in shallow water has a simple environmental dependence [5.27]. For example, in the summer with a downward refracting profile, the same discussion as above leads to a horizontal noise notch. However the vertical directionality of noise from the surface in the winter tends to be driven by bottom properties. Thus, if the bottom is not very lossy, surface sources exciting low-order modes can come from large distances (and hence large areas). These paths are close to the horizontal and noise will then tend to have a strong horizontal component. On the other hand, a very lossy bottom will prevent long-range propagating paths from contributing to the noise field and the noise will tend to be local and subsequently vertical.

5.2.6 Bubbles and Bubbly Media

Bubbles not only occur naturally in the ocean, but the swim bladders of fish can also be thought of as bubbles. The physics of bubbles is a large area of activity in acoustics [5.7, 28]. Here we will confine ourselves to some aspects relevant to ocean acoustics. First we discuss some properties of bubbles in terms of resonators, scatterers and then go on to some aspects of bubbly media and scattering from bubbles.

Bubble scattering follows two regimes depending on the magnitude of the bubble radius oscillations in response to the incident fluctuating pressure field [5.29]:

1. For small pressure amplitudes, the response is linear. The first step in any linear analysis is the identification of the resonance frequency of an oscillating bubble and the measurement of the bubble scattering cross section.
2. Due to nonlinear terms in the governing equations, the response of a bubble will be affected by nonlinearities as the amplitude of the pressure field is increased. In this case, the bubble may continue to oscillate stably (stable acoustic cavitation) generating (sub)harmonics in the scattered field. Under other circumstances, the change in bubble size during a single cycle of oscillation becomes so large that the bubble undergoes a cycle of explosive cavitation growth and violent collapse. Such a response is termed *transient acoustic cavitation* and is distinguished from stable acoustic cavitation by the fact that the bubble radius changes by several orders of magnitude during each cycle.

The Bubble as a Scatterer

The calculation of the natural acoustic resonance of an oscillating bubble in the linear regime requires considerable algebra combining: (1) the equation of motion, (2) mass conservation, and (3) continuity relations at the bubble surface. These developments go beyond the scope of this chapter. In the following, we simply summarize the final results, which are the expression of the

Amazon EX1014 Page 180

bubble natural acoustic resonance ω_0^2, and the expression for the scattered field from an acoustic bubble under an incident pressure field at frequency ω.

The acoustic resonance in the linear regime of a single bubble of radius a is:

$$\omega_0^2 = \left[\frac{3\gamma p_0}{\rho_w a^2} + (3\gamma - 1)\frac{2T}{\rho_w a^3}\right], \tag{5.14}$$

where p_0 is the ambient pressure outside the bubble, T is surface tension (tensile force/length in units N/m), ρ_w is the density of water and γ is the ratio of specific heats. Neglecting surface tension in (5.14) for bubble sizes larger than 1 μm and considering the acoustic expansion/compression process to be adiabatic ($c_{air}^2 = \gamma p_0/\rho_{air}$), we obtain the approximate expression

$$\omega_0 = \frac{1}{a}\sqrt{\frac{3c_{air}^2\rho_{air}}{\rho_w}}, \tag{5.15}$$

and for $c_{air} \simeq 340\,\mathrm{m/s}$, we get $f_0 \simeq \frac{3}{a}$ with a in m and f_0 in Hz.

We now consider an incident plane wave at frequency ω in the regime $ka = \omega a/c = 2\pi a/\lambda \ll 1$. The far-field expression for the spatial part of the radiated acoustic field p_r is

$$p_r(r) = -\frac{a}{r}p_i \exp\left[-\frac{i\omega}{c}(r-a)\right] \times \left[1 - \frac{\omega_0^2}{\omega^2}\left(1 - \frac{i\omega a}{c}\right)\right]^{-1}. \tag{5.16}$$

First, we note that in the high-frequency limit, we recover $p_r(r,t) = -\frac{a}{r}p_i\left(t - \frac{r-a}{c}\right)$ that was given by the boundary conditions at the bubble surface.

To understand the effect of the resonance frequency, consider two cases. The first case is $\omega \gg \omega_0$ for which we obtain:

$$p_r(r) = -\frac{a}{r}p_i\, e^{-\frac{i\omega}{c}(r-a)}, \tag{5.17}$$

whereas for the case $\omega = \omega_0$ we get:

$$p_r(r) = -\frac{ic}{\omega r}p_i\, e^{-\frac{i\omega}{c}(r-a)} = -\frac{i\lambda}{2\pi r}p_i\, e^{-\frac{i\omega}{c}(r-a)}. \tag{5.18}$$

Comparing the two equations, (5.18) appears to be the field radiating from a sphere of radius $\lambda/2\pi$ which is much larger than a. For example, neglecting surface tension, at 1 atm, $\omega_0 a \approx 20$ so that $\lambda \approx 500a$. This resonance effect is also quite apparent when considering the scattering cross section of the bubble.

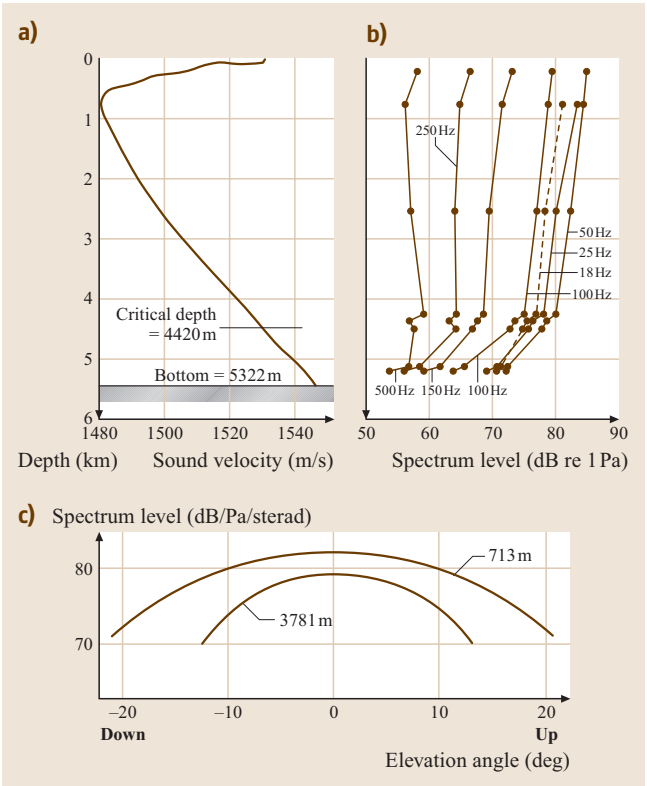


Fig. 5.16a–c Noise in the deep ocean. **(a)** Sound-speed profile and **(b)** noise level as a function of depth in the Pacific (after [5.30]). **(c)** The vertical directionality of noise at the axis of the deep sound channel and at the critical depth in the Pacific (after [5.31])

The scattering cross section σ_s is the ratio of the total scattered power (intensity × area = pressure × velocity × enclosing area) to the incident plane-wave intensity (given by $p_i^2/2\rho_w c$, with the factor of 1/2 coming from averaging over a cycle) and therefore has the units of area. We perform this calculation in the far field using (5.16) to obtain

$$\sigma_s = \frac{4\pi a^2}{\left[1 - \frac{\omega_0^2}{\omega^2}\left(1 - \frac{i\omega a}{c}\right)\right]^2} \xrightarrow{\omega=\omega_0} \frac{\lambda^2}{\pi}, \tag{5.19}$$

which is consistent with a surface area associated with the discussion below (5.18). The resonance makes the bubble appear larger in surface area than its dimension. On the other hand, for the case $\omega \ll \omega_0$, we have

$$\sigma_s = 4\pi a^2\left(\frac{\omega}{\omega_0}\right)^4, \tag{5.20}$$

Amazon EX1014 Page 181

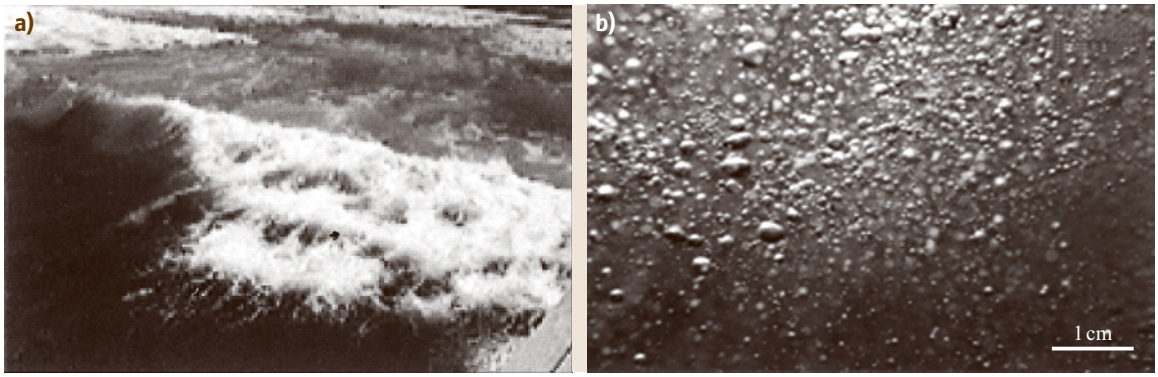


Fig. 5.17 **(a)** Wave breaking on the shore; **(b)** magnified view of individual bubbles within the plumes taken a second or so after wave breaking. The void fraction of air in these plumes is a few percent and bubbles range in size from less than 50 μm to a few mm radius. Bubble plumes found beneath breaking waves in 15–20 m/s winds in the open ocean have a similar size distribution (Courtesy of Grant Deane, Scripps Institution of Oceanography)

which is Rayleigh scattering. The analogous mechanism in electromagnetics explains why the sky is blue: blue has a higher frequency than red so it is scattered more. The above derivations only included radiation damping and we have not included lossy effects caused by thermal conductivity and shear viscosity. Looking at, for example (5.16), we can think of the radiation damping constant to be $\delta_r = ka$ or, in other words, at resonance $\sigma_s = 4\pi a^2/\delta_r^2$. Finally, we mention that the extinction cross section is the sum of the scattering cross section and the absorption cross section. The damping coefficients for thermal conductivity and shear viscosity are typically experimentally determined.

Bubbly Media

The region immediately below the surface of the ocean is a bubbly medium (Fig. 5.17). The existence of bubbles changes the effective compressibility of the water. We define a volume fraction of bubble (also called the void fraction) μ so that the density of the mixture is simply $\rho_m = \mu\rho_b + (1-\mu)\rho_w$ where the subscripts b and w refer to a bubble and water, respectively. We consider low frequencies with respect to resonance and we use the compressibility, the inverse of the bulk modulus $B = \rho(\delta p/\delta\rho)$, since it is additive and permits us to write down the compressibility of the mixture,

$$K_m = \mu K_b + (1-\mu)K_w \rightarrow \frac{1}{B_m} = \mu\frac{1}{B_b} + (1-\mu)\frac{1}{B_w} \,. \tag{5.21}$$

Using the above discussion relating sound speed and the adiabatic bulk modulus for the air bubble with $\gamma = 1.4$ (the bulk modulus of water is 2.3×10^9 Pa) we then obtain:

$$\frac{1}{\rho_m c_m^2} = \frac{\mu}{1.4p_b} + \frac{(1-\mu)}{\rho_w c_w^2} \rightarrow c_m^2 = \left(\frac{1.4p_b}{\mu\rho_w c_w^2 + 1.4p_b(1-\mu)}\right) c_w^2 \,, \tag{5.22}$$

where we have taken $\rho_m \approx \rho_w$. Substituting some typical numbers, we use atmospheric pressure, $p_b \approx 10^5$ Pa, $\rho_w \approx 10^3$ kg/m^3, $c_w = 1500$ m/s and we consider two void fractions: μ of 0.0001 and 0.001 (large). The corresponding sound speeds in the bubbly mixture are about 930 m/s and 370 m/s, respectively. A small amount a bubbles significantly changes the compressibility of the medium and therefore drastically changes the sound speeds. In reality, the speed of sound through the bubbly medium varies with frequency since compressibility is the ratio of the fractional change in volume to the incident pressure. The volume change is related to the bubble surface displacement and hence to velocity or radiated pressure as per (5.16). Therefore, the bubble compressibility is actually frequency dependent and a more rigorous treatment of propagation in bubbly media would show the dispersion of the speed through the bubbly medium.

When sound propagates through a bubbly medium, the scattering will also cause attenuation due to scattering and absorption. As stated above, the extinction cross section, σ_e, is a measure of this phenomenon. For

Amazon EX1014 Page 182

a bubbly medium (and for the simple case of single-sized bubbles), an acoustic beam will be altered by the absorption and scattering out of the beam. For an incident plane wave of intensity I_0, the power removed by each bubble is $I_0\sigma_e$ so that the rate of change of intensity as the beam travels through a bubble medium of N bubbles per unit volume is

$$\frac{dI}{dx} = -I_0\sigma_e N \rightarrow I = I_0 \exp(-\sigma_e N x) \ . \qquad (5.23)$$

Therefore, a bubbly medium changes the sound speed, absorbs sound, and is dispersive.

5.3 SONAR and the SONAR Equation

A major application of underwater acoustics is SONAR system technology. The performance of SONAR is often approximately described by the SONAR equation. The methodology of the SONAR equation is analogous to an accounting procedure involving acoustic signal, interference and system characteristics. Figure 5.18 provides a schematic of passive and active SONARs.

5.3.1 Detection Threshold and Receiver Operating Characteristics Curves

The detection threshold (DT) [5.16] is a decibel number that essentially incorporates the SONAR system's (which includes the operator) ability to decide that a detection is made or not made. The detection process includes the following probabilities:

- the probability of detection (PD): the probability that a signal is detected if it is present;
- 1-PD: the probability the signal will not be detected if it is present;
- the probability of false alarm (PFA): the probability that a signal is detected when it is not present;
- 1-PFA: the probability that the signal will not be detected when it is not present.

In practical terms, since the signal and noise are fluctuating, the detection is made (over a time interval) when the fluctuating sum of the signal and noise exceeds a threshold that is determined from empirically derived probability density functions (PDFs) of noise and signal plus noise. For example, the case that the noise alone rises above the threshold contributes to the PFA. Therefore, the process for determining a detection threshold level will depend on the PD and PFA. Typically numbers might be a PD of 0.5 and PFA of 0.0001. The probabilities will themselves be a function of the relation between the signal and noise statistics, as represented by their mean and variance. The detection index d succinctly characterizes this relation in that it indicates how easy it is to observe a signal in noise,

$$d = \frac{(M_{sn} - M_n)^2}{\sigma_n^2} \ , \qquad (5.24)$$

where M_{sn} is the mean of the signal plus noise, M_n is the noise mean and σ_n^2 is the noise variance. Figure 5.19 shows schematically the implications of the detection index where the relative proximity of the two probability density functions (PDFs) determine the detection

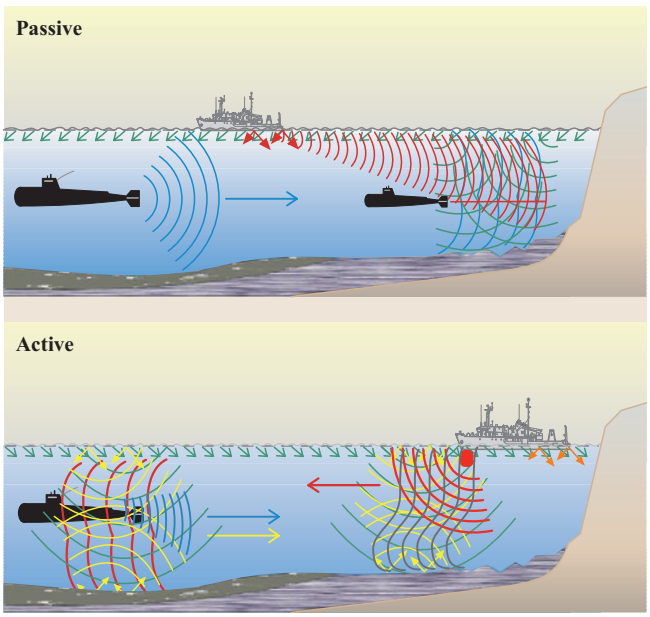


Fig. 5.18 Passive and active SONAR for submarine detection. *Passive*: the submarine on the right tries to detect sounds (blue) from the other submarine using a towed array (antenna). These sounds are distorted by the shallow-water environment and are embedded in ocean surface noise (green) and surface shipping noise (red). *Active*: the ship on the right sends out a pulse (red) and an echo (blue), distorted by the shallow-water environment, is returned to the ship SONAR which tries to distinguish it from backscattered reverberation (yellow) and ocean noise (green) [5.1]

Amazon EX1014 Page 183

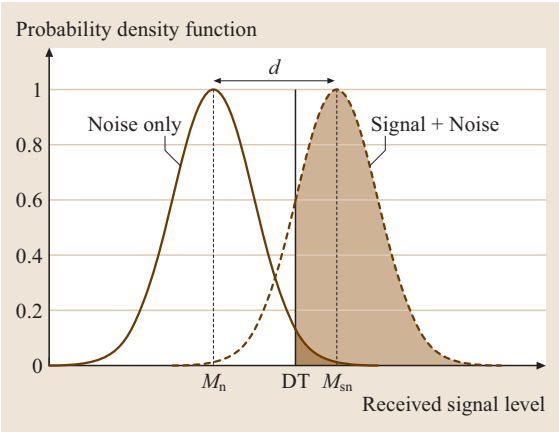


Fig. 5.19 Probability density functions (PDF) of noise and signal+noise. Various probabilities as explained in the text are related to specific regions under the curves. Thus, the probability of detection (PD) is the light-shaded area under the signal+noise PDF curve that is to the right of DT, the detection threshold (*thick vertical line*). Similarly, the probability of false alarm is the dark shaded area under the noise PDF curve that is to the right of DT

statistics. We first note that the PD is the area under the signal-plus-noise curve to the right of the DT and the PFA is the area under the noise curve to the right of the DT. Then, for example, if the mean of the signal-plus-noise PDF was further to the right [higher signal-to-noise ratio (SNR)], the detection index and PD would be larger.

We could then move the DT to the right, changing the PD, but the PFA would be smaller. Receiver operating characteristics (ROC) curves are plots of PD versus PFA parameterized by d (Fig. 5.19). Figure 5.20 gives a typical example of using this methodology and refer the reader to the SONAR literature [5.16] for a more complete treatment. A square-law detector is commonly used for a passive system dealing with unknown signal. In that case, it has been shown that the detection index for a small-SNR, narrow-band signal in Gaussian noise is given by

$$d = \omega t \left(\frac{S}{N}\right)^2 , \tag{5.25}$$

where ω, t, S and N are the bandwidth (taken to be larger than the width of the spectral line of the signal), integration time, signal power and noise power in the bandwidth, respectively. If 1 Hz is the noise bandwidth reference, the detection index is $d = \omega t\,(S/N_0)$, where N_0 is the noise in a 1 Hz band. This gives a relation between the signal-to-noise ratio at the output of an energy detector of a narrow-band signal in Gaussian noise to the detection index:

$$\mathrm{SNR} = 5 \log \left(\frac{d}{\omega t}\right) \equiv \mathrm{DT} , \tag{5.26}$$

where the equivalence symbol is for a detection criteria of a specified PD, PFA.

In reality, there are correction factors for the detection threshold related to the length of observations used to make a decision, human factors, and others that we omit from this discussion. Since the criteria are specified through the ROC curves, we can now estimate the DT for specific cases. We simply go to the the ROC curves for a selected PD versus PFA and read off the detection index, from which we can compute the detection threshold. For example, from Fig. 5.20, for a PD of 50% and a PFA of 0.01%, the detection index is $d = 16$. Using unit bandwidth and integration time, the detection threshold is DT$= 5 \log 16 = 6$ dB. This methodology is an example of the meaning of the DT term in the SONAR equation below, though the relationship between DT and d is different depending on the type of receiver and SONAR.

5.3.2 Passive SONAR Equation

A passive SONAR system uses the radiated sound from a target to detect and locate the target. A radiating object of source level (SL) (all units are in decibels) is received at a hydrophone of a SONAR system at a lower signal level S because of the transmission loss (TL) it suffers (e.g., cylindrical spreading plus attenuation or a TL computed from one of the propagation models of Sect. 5.4),

$$\mathrm{S} = \mathrm{SL} - \mathrm{TL} . \tag{5.27}$$

The noise, N at a single hydrophone is subtracted from (5.27) to obtain the signal-to-noise ratio at a single hydrophone,

$$\mathrm{SNR} = \mathrm{SL} - \mathrm{TL} - \mathrm{N} . \tag{5.28}$$

Typically a SONAR system consists of an array or antenna of hydrophones which provides signal-to-noise enhancement through a beam-forming process (Sect. 5.6). This process is quantified in decibels by the array gain (AG) (see Sect. 5.6.2) that is added to the single-hydrophone SNR to give the SNR at the output of the beam-former,

$$\mathrm{SNR_{BF}} = \mathrm{SL} - \mathrm{TL} - \mathrm{N} + \mathrm{AG} . \tag{5.29}$$

Amazon EX1014 Page 184

As discussed, because detection involves additional factors including SONAR operator ability, it is necessary to specify a detection threshold, DT level above the SNR_{BF} at which there is a 50% (by convention) probability of detection. The difference between these two quantities is called the signal excess (SE),

$$SE = SL - TL - N + AG - DT\,. \tag{5.30}$$

This decibel bookkeeping leads to an important SONAR engineering descriptor called the figure of merit (FOM) which is the transmission loss that gives a zero signal excess,

$$FOM = SL - N + AG - DT\,. \tag{5.31}$$

The FOM encompasses the various parameters a SONAR engineer must deal with: expected source level, the noise environment, array gain and the detection threshold. Conversely since the FOM is a transmission loss, one can use the output of a propagation model (or if appropriate, a simple geometric loss plus attenuation) to estimate the minimum range at which a 50% probability of detection can be expected. This range changes with oceanographic conditions and is often referred to as the range of the day in navy SONAR applications. Finally, we mention that formal detection theory involves a criterion involving the probability of detection PD versus probability of false alarm PFA. Plots of PD versus PFA as parameterized by, say SNR, are called receiver operating characteristic (ROC) curves [5.16]. Clearly, for a PFA of 1, the probability of detection goes to unity.

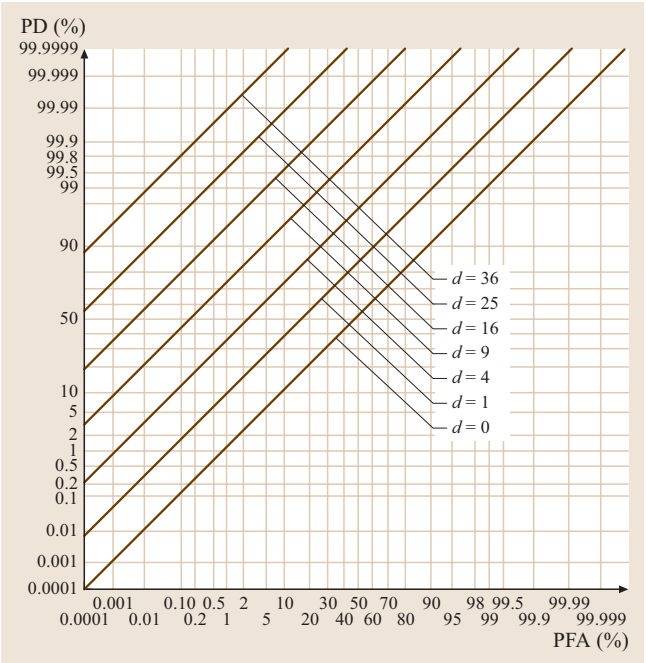


Fig. 5.20 Example of ROC curves. For a given signal plus noise, different threshold settings correspond to different PD and PFA. The ROC curves summarizes the relation between PD and PFA for different thresholds as parameterized through the detection index. (After [5.16])

5.3.3 Active SONAR Equation

A monostatic active SONAR transmits a pulse to a target and its echo is detected at a receiver co-located with the transmitter. A bistatic active SONAR has the receiver in a different location than the transmitter. The main differences between the passive and active cases are the addition of a target strength (TS) term; reverberation (reverberation level, RL) is usually the dominant source of interference, as opposed to noise; and the transmission loss is over two paths: transmitter to target and target to receiver. In the monostatic case, the transmission loss is 2TL, where TL is the one-way transmission loss, and in the bistatic case, the transmission loss is the sum (in dB) over paths from the transmitter to the target and the target to the receiver, $TL_1 + TL_2$. The concept of the detection threshold is useful for both passive and active SONARs. Hence, for signal excess, we have

$$SE = SL - TL_1 + TS - TL_2 - (RL + N) + AG - DT\,. \tag{5.32}$$

The corresponding FOM for an active system is defined for the maximum allowable two-way transmission loss with TS = 0 dB.

5.4 Sound Propagation Models

The wave equation describing sound propagation is derived from the equations of hydrodynamics and its coefficients and boundary conditions are descriptive of the ocean environment. There are essentially four types of models (computer solutions to the wave equation [5.4]) to describe sound propagation in the sea: ray theory,

the spectral method or fast field program (FFP), normal mode (NM) and parabolic equation (PE). All of these models allow for the fact that the ocean environment varies with depth. A model that also takes into account horizontal variations in the environment (i. e., sloping bottom or spatially variable oceanography) is termed range-dependent. For high frequencies (a few kilohertz or above), ray theory is the most practical. The other three model types are more applicable and useable at lower frequencies (below 1 kHz). Between these frequencies, one can choose either, noting that the wave solution is the most accurate and should probably be used in all cases where the the calculation is still feasible and/or practical. The models discussed here are essentially two-dimensional models since the index of refraction has much stronger dependence on depth than on horizontal distance. Nevertheless, bottom topography and strong ocean features can cause horizontal refraction (out of the range–depth plane). Ray models are most easily extendable to include this added complexity. Full three-dimensional wave models are extremely computationally intensive. A compromise that often works for weakly three-dimensional problems is the $N \times 2$D approximation that combines two-dimensional solutions along radials to produce a three-dimensional solution.

5.4.1 The Wave Equation and Boundary Conditions

The wave equation for the pressure p in cylindrical coordinates with the range coordinates denoted by $\boldsymbol{r} = (x, y)$ and the depth coordinate denoted by z (taken positive downward) for a source-free region is

$$\nabla^2 p(\boldsymbol{r}, z, t) - \frac{1}{c^2(\boldsymbol{r}, z)} \frac{\partial^2 p(\boldsymbol{r}, z, t)}{\partial t^2} = 0 \,, \tag{5.33}$$

where $c(\boldsymbol{r}, z)$ is the sound speed in the wave-propagating medium.

It is convenient to solve (5.33) in the frequency domain by assuming a solution with a frequency dependence of $\exp(-\mathrm{i}\omega t)$ to obtain the Helmholtz equation ($K \equiv \omega/c$),

$$\nabla^2 p(\boldsymbol{r}, z) + K^2 p(\boldsymbol{r}, z) = 0 \tag{5.34}$$

with

$$K^2(\boldsymbol{r}, z) = \frac{\omega^2}{c^2(\boldsymbol{r}, z)} \,. \tag{5.35}$$

The range-dependent environment manifests itself as the coefficient $K^2(\boldsymbol{r}, z)$ of the partial differential equation for the appropriate sound speed profile. The range-dependent bottom type and topography appears as boundary conditions. In underwater acoustics both fluid and elastic (shear-supporting sediments and bottom strata) media are of interest. For simplicity we only consider fluid media below. This is most often a good approximation to describing the bottom near the bottom interface since the material typically has a low shear speed which can be inserted into the fluid equation solution by a perturbation procedure [5.32].

The most common plane-interface boundary conditions encountered in underwater acoustics are the pressure release condition at the ocean surface,

$$p = 0 \,, \tag{5.36}$$

and at the ocean–bottom interface, continuity of pressure

$$p_1 = p_2 \,, \tag{5.37}$$

and vertical particle velocity

$$\frac{1}{\rho_1} \frac{\partial p_1}{\partial z} = \frac{1}{\rho_2} \frac{\partial p_2}{\partial z} \,, \tag{5.38}$$

where the ρ_i are the densities of the two media. These latter boundary conditions applied to the plane-wave fields in Fig. 5.13a yield the Rayleigh reflection coefficient given by (5.5).

The Helmholtz equation for an acoustic field from a point source is

$$\nabla^2 G(\boldsymbol{r}, z) + K^2(\boldsymbol{r}, z) G(\boldsymbol{r}, z) = -\delta^2(\boldsymbol{r} - \boldsymbol{r}_s)\delta(z - z_s), \tag{5.39}$$

where the subscript 's' denotes the source coordinates. The acoustic field from a point source, $G(\boldsymbol{r})$ is either obtained by solving the boundary-value problem of (5.39) (spectral method or normal modes) or by approximating (5.39) using an initial-value problem (ray theory, parabolic equation).

5.4.2 Ray Theory

Ray theory is a geometrical, high-frequency approximate solution to (5.39) of the form

$$G(\boldsymbol{R}) = A(\boldsymbol{R}) \exp[\mathrm{i}S(\boldsymbol{R})] \,, \tag{5.40}$$

where the exponential term allows for rapid variations as a function of range and $A(\boldsymbol{R})$ is a more slowly varying *envelope* that incorporates both geometrical spreading and loss mechanisms. The geometrical approximation is that the amplitude varies slowly with range (i. e.,

$(1/A)\nabla^2 A \ll K^2$) so that (5.34) yields the eikonal equation

$$(\nabla S)^2 = K^2 \,. \tag{5.41}$$

The ray trajectories are perpendicular to surfaces of constant phase (wavefronts), S, and may be expressed mathematically as follows:

$$\frac{\mathrm{d}}{\mathrm{d}l}\left(K\frac{\mathrm{d}\boldsymbol{R}}{\mathrm{d}l}\right) = \nabla K \,, \tag{5.42}$$

where l is the arc length along the direction of the ray and $\boldsymbol{R}$ is the displacement vector to a point on the ray. The direction of average flux (energy) follows that of the trajectories and the amplitude of the field at any point can be obtained from the density of rays.

The ray theory method is computationally rapid and extends to range-dependent problems. Furthermore, the ray traces give a physical picture of the acoustic paths. It is helpful in describing how sound redistributes itself when propagating long distances over paths that include shallow and deep environments and/or mid-latitude to polar regions. The disadvantage of conventional ray theory is that it does not include diffraction, including effects that describe the low-frequency dependence (degree of trapping) of ducted propagation.

5.4.3 Wavenumber Representation or Spectral Solution

The wave equation can be solved efficiently with spectral methods when the ocean environment does not vary with range. The term fast field program (FFP) had been used because the spectral methods became practical with the advent of the fast Fourier transform (FFT). Assume a solution of (5.39) of the form

$$G(\boldsymbol{r}, z) = \frac{1}{2\pi}\int\limits_{-}^{\int} \mathrm{d}^2\boldsymbol{k} g(\boldsymbol{k}, z, z_\mathrm{s}) \exp[\mathrm{i}\boldsymbol{k}\cdot(\boldsymbol{r}-\boldsymbol{r}_\mathrm{s})] \,, \tag{5.43}$$

which then leads to the equation for the depth-dependent Green's function $g(\boldsymbol{k}, z, z_\mathrm{s})$,

$$\frac{\mathrm{d}^2 g}{\mathrm{d}z^2} + \left[K^2(z) - k^2\right] g = -\frac{1}{2\pi}\delta(z - z_\mathrm{s}) \,. \tag{5.44}$$

Furthermore, we assume azimuthal symmetry, $kr > 2\pi$ and $\boldsymbol{r}_\mathrm{s} = 0$ so that (5.43) reduces to

$$G\,(r, z) = \frac{\exp\,(-\mathrm{i}\pi/4)}{(2\pi r)^{1/2}} \times \int\limits_{-\infty}^{+\infty} \mathrm{d}k k^{1/2} g(k, z, z_\mathrm{s}) \exp(\mathrm{i}kr) \,. \tag{5.45}$$

This integral is then evaluated using the fast Fourier transform algorithm. Although the method was initially labeled *fast field* it is fairly slow because of the time required to calculate the Green's functions [solve (5.44)]. However, it has advantages when one wishes to calculate the near-field region or to include shear-wave effects in elastic media; it is also often used as a benchmark for other less exact techniques. With a great deal of additional computational effort, this method is extendable to range-dependent environments.

5.4.4 Normal-Mode Model

Rather than solve (5.44) for each g for the complete set of ks (typically thousands of times), one can utilize a normal-mode expansion of the form

$$g(\boldsymbol{k}, z) = \sum a_n(\boldsymbol{k}) u_n(z) \,, \tag{5.46}$$

where the quantities u_n are eigenfunctions of the following eigenvalue problem:

$$\frac{\mathrm{d}^2 u_n}{\mathrm{d}z^2} + \left[K^2(z) - k_n^2\right] u_n(z) = 0 \,. \tag{5.47}$$

The eigenfunctions u_n are zero at $z = 0$, satisfy the local boundary conditions descriptive of the ocean bottom properties and satisfy a radiation condition for $z \to \infty$. For pressure, they form an orthonormal set in a Hilbert space with weighting function $\rho^{-1}(z)$, the local density. The range of discrete eigenvalues corresponding to the poles in the integrand of (5.45) is given by the condition

$$\min[K(z)] < k_n < \max[K(z)] \,. \tag{5.48}$$

These discrete eigenvalues correspond to discrete angles within the critical angle cone in Fig. 5.7a as discussed in Sect. 5.1.2. The eigenvalues k_n typically have a small imaginary part α_n, which serves as the modal attenuation representative of all the losses in the ocean environment. Solving (5.39) using the normal-mode expansion given by (5.46) yields (for the source at the origin).

$$G(r, z) = \frac{\mathrm{i}}{4\rho(z_\mathrm{s})}\sum_n u_n(z_\mathrm{s}) u_n(z) H_0^1(k_n r) \,. \tag{5.49}$$

The asymptotic form of the Hankel function can be used in the above equation to obtain the well-known normal-mode representation of a waveguide in cylindrical coordinates:

$$G(r, z) = \frac{\mathrm{i}}{(8\pi r)^{1/2}\rho(z_\mathrm{s})}\exp(-\mathrm{i}\pi/4) \times \sum_n \frac{u_n(z_\mathrm{s}) u_n(z)}{k_n^{1/2}} \exp(\mathrm{i}k_n r) \,. \tag{5.50}$$

Equation (5.50) is a far-field solution of the wave equation and neglects the continuous spectrum of modes [$k_n < \min[K(z)]$ of (5.48)]. For the purposes of illustrating the various portions of the acoustic field, we note that k_n is a horizontal wavenumber so that a ray angle associated with a mode with respect to the horizontal can be taken to be $\theta = \cos^{-1}[k_n/K(z)]$. For a simple waveguide the maximum sound speed is the bottom sound speed corresponding to $\min[K(z)]$. At this value of $K(z)$, we have from Snell's law $\theta = \theta_c$, the bottom critical angle. In effect, if we look at a ray picture of the modes, the continuous portion of the mode spectrum corresponds to rays with grazing angles greater than the bottom critical angle of Fig. 5.13b and therefore outside the cone of Fig. 5.7a. This portion undergoes severe loss. Hence, we note that the continuous spectrum is the near (vertical) field and the discrete spectrum is the far (more-horizontal, profile-dependent) field falling within the cone in Fig. 5.7a.

The advantages of the normal-mode procedure are that: the solution is available for all source and receiver configurations once the eigenvalue problem is solved; it is easily extended in moderately range-dependent conditions using the adiabatic approximation; it can be applied (with more effort) to extremely range-dependent environments using coupled-mode theory. However, it does not include a full representation of the near field.

Adiabatic Mode Theory

All of the range-independent normal-mode calculation method developed for environmental ocean acoustic modeling applications can be adapted to mildly range-dependent conditions using adiabatic mode theory. The underlying assumption is that individual propagating normal modes adapt to the local environment, but do not scatter or couple into each other. The coefficients of the mode expansion, a_n in (5.46), now become mild functions of range, i. e., $a_n(\boldsymbol{k}) \rightarrow a_n(\boldsymbol{k}, \boldsymbol{r})$. This modifies (5.45) as follows:

$$G(\boldsymbol{r}, z) = \frac{\mathrm{i}\rho(z_s)}{(8\pi r)^{1/2}} \exp(-\mathrm{i}\pi/4) \times \sum_n \frac{u_n(z_s) v_n(z)}{\overline{k_n^{1/2}}} \exp(\mathrm{i}\overline{k_n} r) \,, \tag{5.51}$$

where the range-averaged wavenumber (eigenvalue) is

$$\overline{k_n} = \frac{1}{r} \int_0^r k_n(r') \mathrm{d}r' \,, \tag{5.52}$$

and the $k_n(r')$ are obtained at each range segment from the eigenvalue problem (5.47) evaluated for the environment at that particular range along the path. The quantities u_n and v_n are the sets of modes at the source and the field positions, respectively.

Simply stated, the adiabatic mode theory leads to a description of sound propagation such that the acoustic field is a function of the modal structure at both the source and the receiver and some average propagation conditions between the two. Thus, for example, when sound emanates from a shallow region where only two discrete modes exist and propagates into a deeper region with the same bottom (same critical angle), the two modes from the shallow region adapt to the form of the first two modes in the deep region. However, the deep region can support many more modes; intuitively, we therefore expect the resulting two modes in the deep region will take up a smaller, more-horizontal part of the cone of Fig. 5.7a than they take up in the shallow region. This means that sound rays going from shallow to deep regions tend to become more horizontal, which is consistent with a ray picture of down-slope propagation. Finally, fully coupled mode theory for range-dependent environments has been developed but requires intensive computation.

Mode Dispersion in a Waveguide

Acoustical propagation in simple free space is nondispersive. That is, all plane waves travel with speeds independent of frequency. Further, their group and phase speeds are the same as the medium sound speed. However, geometric dispersion is a property of waveguide propagation.

We consider a shallow-water waveguide of the Pekeris type, i. e., a homogeneous water column overlying a homogeneous and denser fluid bottom. A waveguide of this type supports modal propagation, where each modes is characterized by a depth-dependent modal amplitude $u_n(z)$ and a horizontally projected propagating wavenumber k_n. Each mode is characterized by a group velocity v_{gn} and a phase velocity $v_{\varphi n}$, which are related through the formula:

$$\frac{1}{v_{gn}} = v_{\varphi n} \int_0^\infty \frac{u_n^2(z)}{\rho(z)\, c^2(z)} \mathrm{d}z \,. \tag{5.53}$$

In the case of a perfect waveguide with a constant sound speed c and no penetration in the bottom, (5.53) takes the simplest form $v_{gn} v_{pn} = c^2$. The difference in group velocities between modes results in modal dispersion in a waveguide (Fig. 5.21).

In shallow water, lower-order modes usually travel faster than higher-order modes (Figs.5.22, 23). In deep

Amazon EX1014 Page 188

water, where the deep sound channel behaves as a waveguide, the fastest modes are the higher-order modes (Fig. 5.24), a property of refraction-dominated modal propagation. Since modal wavenumbers k_n are frequency dependent, the modes can be plotted in a frequency–wavenumber space that is the Fourier transform of the time-range representation of the dispersed field in Fig. 5.25. As already seen in Fig. 5.21, Fig. 5.26 shows that modes have a cut-off frequency and that there exist a finite number of propagating modes at a given frequency.

Dispersion and The Waveguide Invariant [5.3]

There is actually a fairly robust parameter, the waveguide invariant, that describes dispersion over a (sometimes large) interval of a group of modes. The waveguide invariant β has two important interpretations; first, it is related the local change in the modal group velocity with respect to the change in phase velocity,

$$\frac{1}{\beta} = -\frac{\partial S_g}{\partial S_p}\,, \tag{5.54}$$

where S_g and S_p and group and phase slowness, where slowness is the inverse of speed.

It turns out that β often has a rather robust value for certain circumstances. For example, it is unity for many shallow-water situations that are dominated by bottom reflection; on the other hand it is negative for refraction-dominated propagation.

Figure 5.27 shows a calculation for a Pacific deep-water case. Note from the definition that β is negative up to a phase speed of about 1540; this region is one of refraction such as deep sound channel and convergence zone propagation. Beyond 1540, β is positive; this is the bottom bounce region dominated by reflections rather than refraction.

The invariant also relates the change in range in the locations of the interference peaks of a transmission loss curve to a change in frequency

$$\frac{\Delta r}{r} = \frac{1}{\beta}\frac{\Delta\omega}{\omega}\,. \tag{5.55}$$

In Fig. 5.28, we show a set of TL curves for different frequencies; the interference peaks are shifted according to the invariant formula. Another way of representing this shift is through the striations, where TL is the third dimension of a frequency–range plot as shown in Fig. 5.29, which was derived from shallow-water transmission loss data. If one represents range as the product of the velocity of the radiator and time, then, the range axis can be replaced by time and one has a frequency–time plot, often called a spectrogram. The TL curve is a slice through the spectrogram for a given frequency and time converted to the appropriate range.

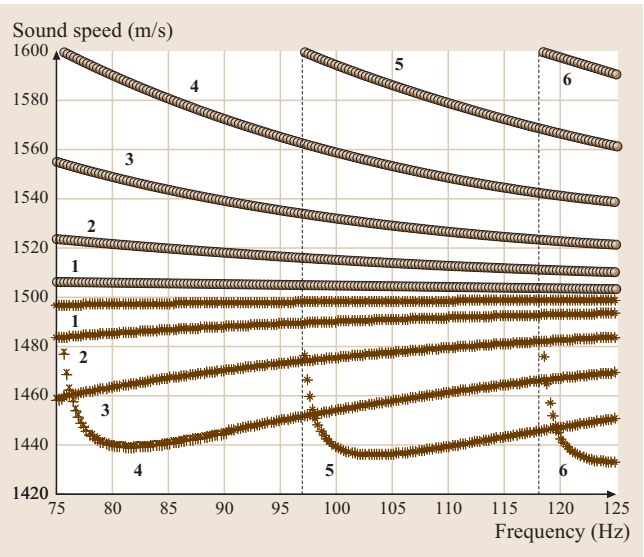


Fig. 5.21 Frequency dependence of the group speed (lower curves 1–6) and phase speed (upper curves 1–6) of modes 1–6 in a Pekeris waveguide with a 100 m water depth, a bottom sound speed c_b and density of 1600 m/s and 1800 kg/m^3. Sound speed in water c_ω is constant and equal to 1500 m/s. The bold vertical lines show the cut-off frequencies of modes 4–6, respectively

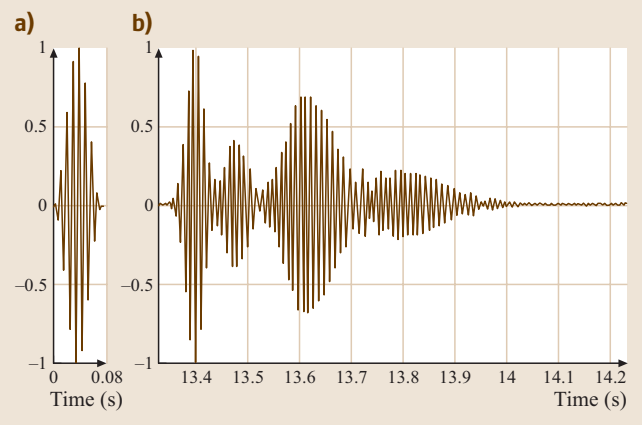


Fig. 5.22a,b Acoustic dispersion in a shallow water waveguide. The *right panel* **(a)** corresponds to the waveguide response at $R = 20$ km to the emitted signal (central frequency = 100 Hz, 50 Hz bandwidth) displayed in the *left panel*. **(b)** Source depth is at 40 m and the receiver depth at 60 m. Waveguide parameters are the same as in Fig. 5.21

Amazon EX1014 Page 189

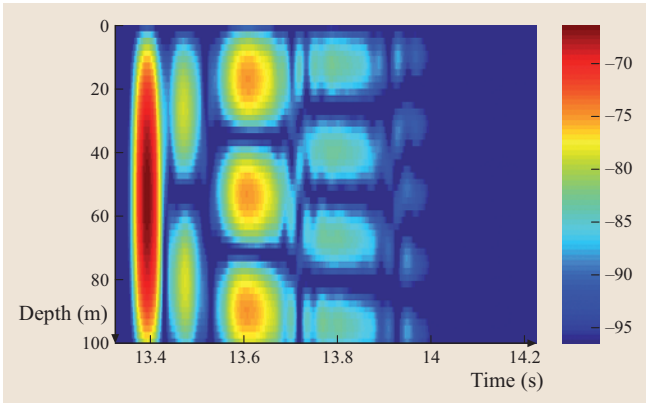


Fig. 5.23 Depth-versus-time representation of the field intensity after a $R = 20$ km propagation in a shallow-water waveguide. The waveguide characteristics are the same as in Fig. 5.21. Source depth is 40 m. The color scale is in dB with a 0 dB source level amplitude at the source

Doppler Shift in a Waveguide

The theory of Doppler shifts involving either a moving source and/or receiver is well known in acoustics, particularly in free space. However, in a waveguide, even if we limit ourselves to horizontal motion, the results are slightly more complex. The individual paths associated with modal propagation, as per Fig. 5.7a, all have finite and different angles with respect to the horizontal. Thus, each mode has a different Doppler shift. The waveguide theory for both source and/or receiver has been worked out (see [5.33], in which there is also a review of the pertinent literature). We return to (5.50) for a harmonic source of angular frequency ω, which therefore results in an additional, identical (when there is no motion) factor for each term of $e^{-i\omega t}$ in the time domain. We now consider a source with a frequency spectrum $S(\omega)$. For constant, horizontal velocities, the normal-mode field results in the *receiver reference frame* are still valid

$$\psi(\boldsymbol{r}_0 + \boldsymbol{v}_r t, z, \omega) = \frac{i}{4\rho(z_s)} \times \sum_n S(\Omega_n) u_n(z_s) u_n(z) H_0^1(k_n r), \tag{5.56}$$

but with Doppler shifted modal wavenumbers

$$k_n \to k_n \left(1 + \frac{v_r}{v_g n} \cos\theta_r\right) , \tag{5.57}$$

and Doppler-shifted frequencies (now for each modal term in the summation) of

$$\Omega_n = \omega - k_n \left(v_s \cos\theta_s - v_r \cos\theta_r\right) , \tag{5.58}$$

where v_{gn} is the group velocity of the n-th mode, $v_s \cos\theta_s$ is the radial speed of the source, and $v_r \cos\theta_r$ is the radial speed of the receiver. Here, radial refers to the projection of the velocities onto the horizontal line between the source and receiver. Note that this latter expression, when multiplied through by the wavenumber, shows that the frequency shift is proportional to the ratio of speeds to the modal phase speed, as opposed to the wavenumber shift which involves the group speed.

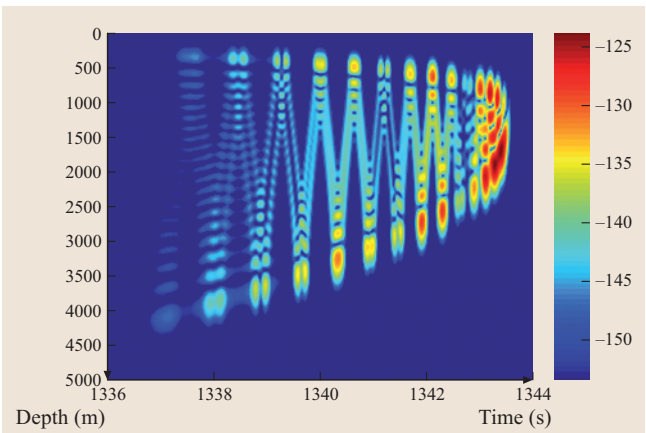


Fig. 5.24 Depth-versus-time representation of the field intensity after a $R = 2000$ km propagation in a deep-water waveguide. We used the Munk profile as a depth-dependent sound-speed profile. Source depth is 900 m, source frequency is 22.5 Hz with a 15 Hz bandwidth. The color scale is in dB with a 0 dB source level amplitude at the source

5.4.5 Parabolic Equation (PE) Model

The PE method was introduced into ocean acoustics and made viable with the development of the *Tappert split-step algorithm*, which utilized fast Fourier transforms at each range step [5.6]. Subsequent numerical developments greatly expanded the applicability and accuracy of the parabolic equation method.

Standard PE Split-Step Algorithm

The PE method is presently the most practical and all-encompassing wave-theoretic range-dependent propagation model. In its simplest form, it is a far-field narrow-angle ($\approx \pm 20°$) with respect to the horizontal – adequate for many underwater propagation problems – approximations to the wave equation. Assuming azimuthal symmetry about a source, we express the solution of (5.34) in cylindrical coordinates in a source-free

Amazon EX1014 Page 190

region in the form

$$p(r, z) = \psi(r, z)H(r)\,, \tag{5.59}$$

and we define $K^2(r, z) \equiv K_0^2 n^2$, n therefore being an *index of refraction* c_0/c, where c_0 is a reference sound speed. Substituting (5.59) into (5.34) and taking K_0^2 as the separation constant we end up with a Bessel equation for H that has a Hankel function as the outgoing solution. If we use the asymptotic form of the Hankel function, $H_0^1(K_0 r)$, and invoke the *paraxial* (narrow-angle) approximation,

$$\frac{\partial^2 \psi}{\partial \mathrm{r}^2} \ll 2K_0 \frac{\partial \psi}{\partial \mathrm{r}}\,, \tag{5.60}$$

we obtain the parabolic equation (in r),

$$\frac{\partial^2 \psi}{\partial z^2} + 2\mathrm{i}K_0 \frac{\partial \psi}{\partial r} + K_0^2(n^2 - 1)\psi = 0\,, \tag{5.61}$$

where we note that n is a function of range and depth. We use a marching solution to solve the parabolic equation. There has been an assortment of numerical solutions but the one that still remains a standard is the so-called *split-step* range-marching algorithm,

$$\psi\,(\mathrm{r} + \Delta\mathrm{r}, z) = \exp\left[\frac{\mathrm{i}K_0}{2}(n^2 - 1)\Delta\mathrm{r}\right] F^{-1} \times \left\{\left[\exp\left(-\frac{\mathrm{i}\Delta r}{2K_0}s^2\right)\right] F\,[\psi(r, z)]\right\}\,. \tag{5.62}$$

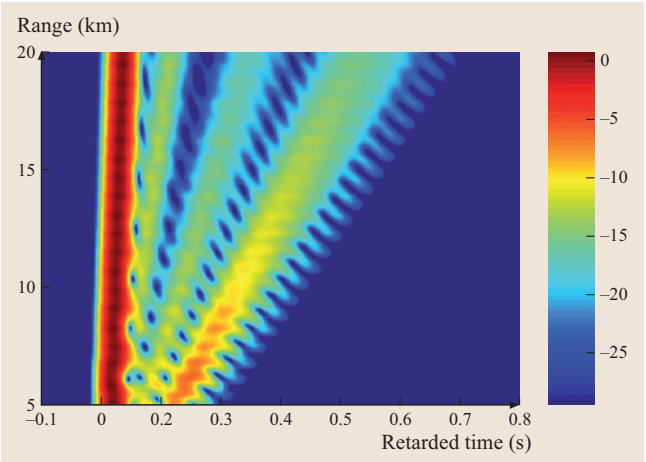


Fig. 5.25 Range-versus-time representation of the field intensity for the same waveguide and source–receiver depth as in Fig. 5.21. The figure clearly shows that modes travel at different speed. The retarded time t is $t - R/c_\omega$. The color scale is in dB with a 0 dB reference at range 5 km

The Fourier transforms F, are performed using FFTs. Equation (5.62) is the solution for n constant, but the error introduced when n (profile or bathymetry) varies with range and depth can be made arbitrarily small by increasing the transform size and decreasing the range-step size. It is possible to modify the split-step algorithm to increase its accuracy with respect to higher-angle propagation.

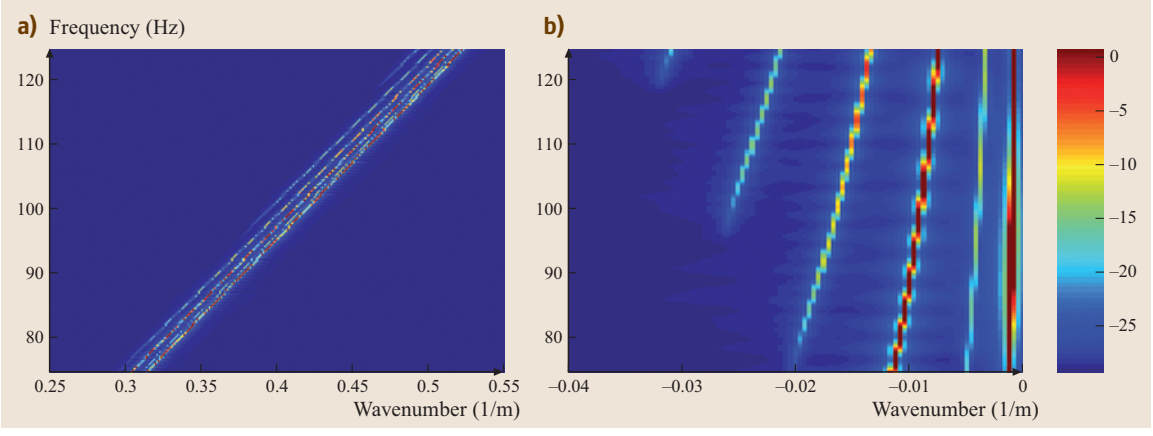
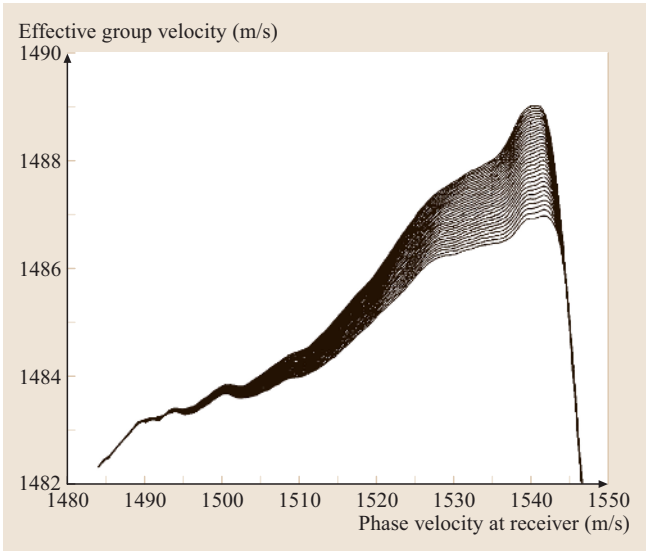


Fig. 5.26a,b Frequency–wavenumber representation of the dispersed field in the waveguide. **(a)** Obtained from a two-dimensional FFT of the range–time plot in Fig. 5.25. The wavenumbers of propagating modes are bounded by the upper and lower sound speeds in waveguide, ω/c_ω and ω/c_b. **(b)** A rotated version of **(a)**, so that the sound speed in water appears infinite. This representation is easier to see the mode separation and the mode cut-off frequency. The color scale is in dB

Amazon EX1014 Page 191



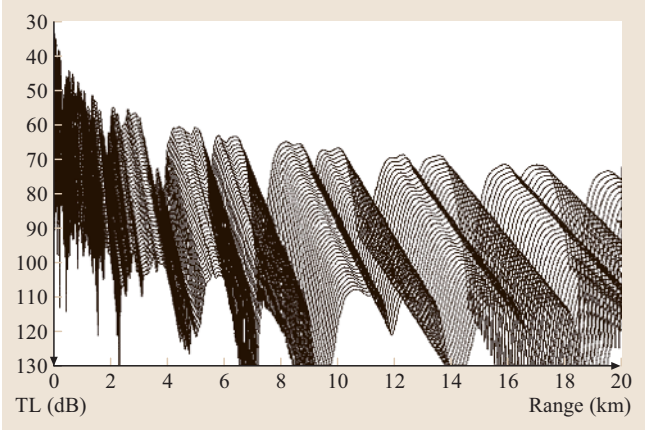


Fig. 5.28 Transmission loss versus range from 130 to 170 Hz calculated by OASES (Ocean Acoustic Seismic Exploration Synthesis) for an environment composed of a 200 m homogeneous fluid layer overlying a homogeneous, absorbing fluid half-space. The fluid layer has a 1450 m/s sound speed, whereas the bottom half-space has a sound speed of 1500 m/s and an attenuation of 10 dB/λ. The curves for increasing frequencies are progressively offset in 1 dB steps. The source and receiver depths are 20 and 100 m, respectively

Generalized or Higher-Order PE Methods

Methods of solving the parabolic equation, including extensions to higher-angle propagation, elastic media, and direct time-domain solutions including nonlinear effects have recently appeared (for example, see [5.34]). In particular, accurate high-angle solutions are important

Fig. 5.27 Group speed versus phase speed in the Pacific Deep water case. The *curves* are for different frequencies starting with the lowest frequency 60 Hz being on *top*. Low phase velocity corresponds to low mode number

when the environment supports acoustic paths that become more vertical such as when the bottom has a very high speed and hence, large critical angle with respect to the horizontal. In addition, for elastic propagation, the compressional and shear waves span a wide angle interval. Finally, Fourier synthesis for pulse modeling requires high accurate in phase and the high-angle PEs are more accurate in phase, even at low angles.

Equation (5.61) with the second-order range derivative which was neglected because of (5.60) can be written in operator notation as:

$$\left[P^2 + 2\mathrm{i}K_0 P + K_0^2(Q^2-1)\right]\psi = 0\,, \tag{5.63}$$

where

$$P \equiv \frac{\partial}{\partial \mathrm{r}},\; Q \equiv \sqrt{n^2 + \frac{1}{K_0^2}\frac{\partial^2}{\partial z^2}}\,. \tag{5.64}$$

Factoring (5.64) assuming weak range dependence and retaining only the factor associated with outgoing propagation yields a one-way equation

$$P\psi = \mathrm{i}K_0(Q-1)\psi\,, \tag{5.65}$$

which is a generalization of the parabolic equation beyond the narrow-angle approximation associated with (5.60). If we define $Q = \sqrt{1+q}$ and expand Q in a Taylor series as a function of q, the standard PE method is recovered by $Q \approx 1 + 0.5q$. The wide-angle PE to arbitrary accuracy in angle, phase, etc. can be obtained from a Padé series representation of the Q operator,

$$Q \equiv \sqrt{1+q} = 1 + \sum_{j=1}^{n} \frac{a_{j,n}q}{1+b_{j,n}q} + O(q^{2n+1})\,, \tag{5.66}$$

where n is the number of terms in the Padé expansion and

$$a_{\mathrm{j,n}} = \frac{2}{2n+1}\sin^2\left(\frac{j\pi}{2n+1}\right), b_{j,n} = \cos^2\left(\frac{j\pi}{2n+1}\right)\,. \tag{5.67}$$

The solution of (5.65) using Eqs. (5.66) and (5.67) has been implemented using finite-difference techniques for fluid and elastic media.

Amazon EX1014 Page 192

5.4.6 Propagation and Transmission Loss

Propagation loss (PL) and transmission loss (TL) are decibel (see Appendix) quantities that are either measured or derived from propagation models. They represent the loss in intensity of the acoustic field as a function of range as referenced to some location. For modeling, we typically use the intensity at one meter range from the source using the assumption of spherical spreading over that one meter. Hence, if P is the output of a propagation code, the propagation loss is

$$\mathrm{PL} = 20 \log \left| \frac{P}{p_0(r=1)} \right| \equiv -\mathrm{TL} \,, \tag{5.68}$$

where p_0 is the pressure of the source in free space. Transmission loss is a positive quantity.

Often, one sees references to coherent and incoherent propagation loss, which can be confusing. Deterministic physics has all acoustic propagation as coherent. If the medium has some randomness, than phase information is lost by some sort of averaging process. This leads to the idea of incoherent propagation. In normal-mode theory, the results is that the cross terms involving differences of modal wavenumbers do not contribute and the propagation curve is therefore smooth, without the interference pattern (Fig. 5.30c). Clearly such a calculation is easy with modes, but there is no equivalent simple way for the other wave models other than actually to introduce randomness. Figure 5.30 shows an application of this incoherent sum of modes. In shallow water an incoherent sum of modes is more or less equivalent to frequency smoothing, over, for example a third of an octave. The environment shown in Fig. 5.30a corresponds to experimental data contours of third-octave transmission loss as a function of frequency and range shown in Fig. 5.30b. Normal-mode model runs are shown in Fig. 5.30c, in which the modes are summed incoherently. Figure 5.30d is a model result of the same type of mode computations, but over the whole frequency spectrum; note the excellent agreement. This kind of analysis can be iteratively used to estimate the environment. Figures 5.30b and 5.30d are referred to an optimum frequency curves in the sense that 300–400 Hz appears to be the optimum frequency of propagation. For example, a vertical slice at 60 km indicates that the minimum loss is in that frequency interval. The curves in Fig. 5.30c are horizontal slices of the contour plot in Fig. 5.30d. The optimum frequency comes from the combination of high loss into the bottom at low frequency because of increased penetration into the lossy bottom and high losses at high frequency caused by scattering and other water volume attenuation effects that tend to have a frequency-squared dependence. Hence, the existence of an intermediate frequency at which bottom loss is small and frequency-squared dependence is not yet dominant.

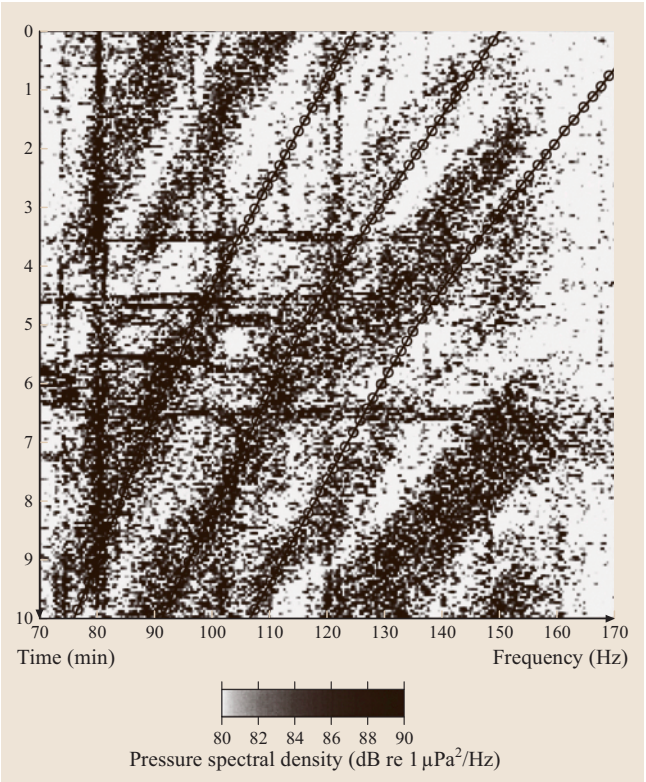


Fig. 5.29 A data example of spectrogram of a broadband moving source. The striations are the peaks in the interference pattern of the transmission loss. The time axis is converted to range if one knows the path and speed of the source [5.35]

Finally we note that there is also an incoherent sum of rays in which ray intensities and not amplitudes with phases are summed. This is not the equivalent of an incoherent sum of mode. For example, an incoherent sum of modes does not produce convergence zones while incoherent rays show convergence-zone properties.

5.4.7 Fourier Synthesis of Frequency-Domain Solutions

Using a Fourier transform, the frequency-domain solution $p(r, z, \omega)$ of the wave equation can be transformed

Amazon EX1014 Page 193

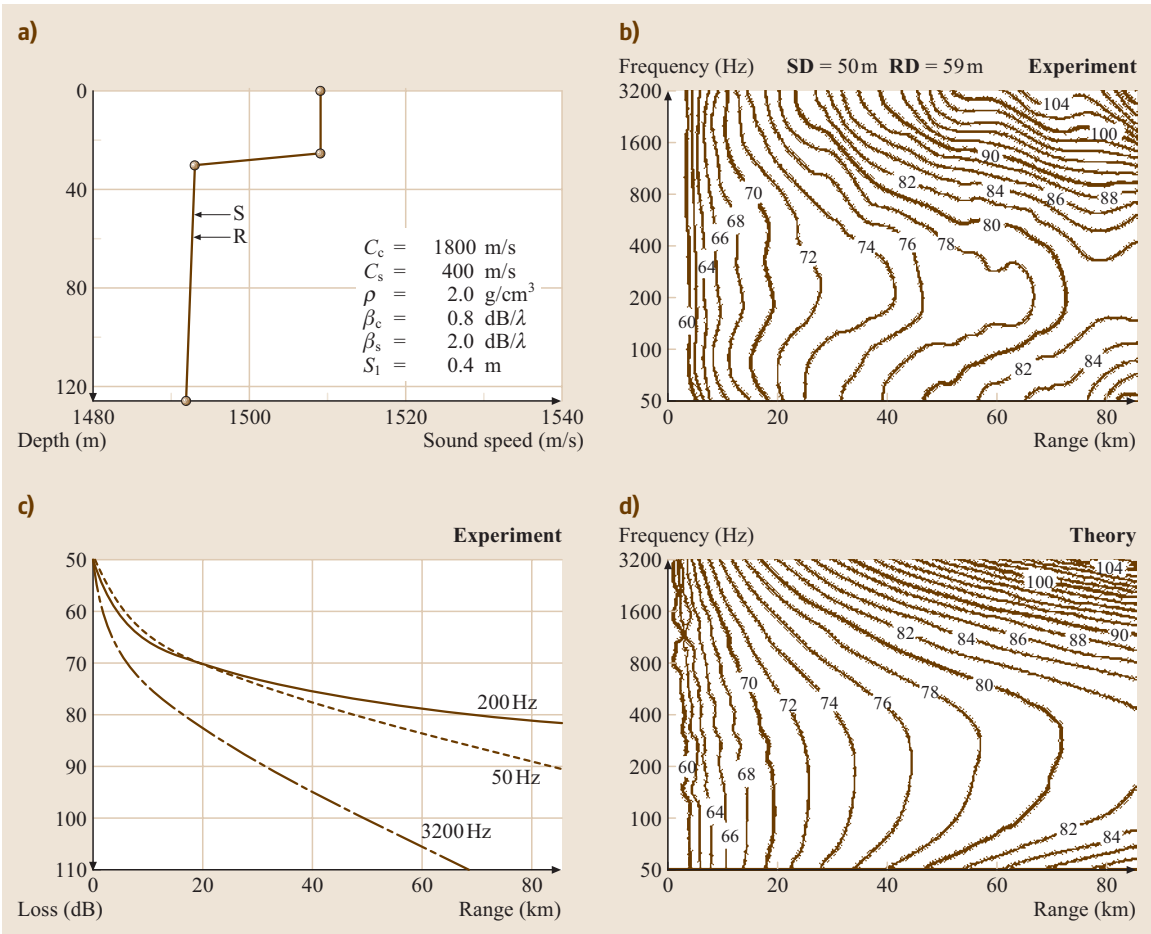


Fig. 5.30a–d Optimum frequency curves for a shallow-water environment. **(a)** The shallow-water environment. Source and receiver depths are marked by the arrows. **(b)** Contour of third-octave transmission loss data over frequency and range. **(c)** Incoherent normal-mode transmission loss. **(d)** Contour of incoherent transmission loss looking very much like the data in **(b)**

into the time-dependent solution $p(r, z, t)$. We have

$$p\,(r, z, t) = \frac{1}{2\pi} \int_{-\infty}^{+\infty} S(\omega) p\,(r, z, \omega)\, \mathrm{e}^{-\mathrm{i}\omega t}\, \mathrm{d}\omega\,. \tag{5.69}$$

S(ω) is the source spectrum defined as

$$S(\omega) = \int_{-\infty}^{+\infty} s(t) \mathrm{e}^{\mathrm{i}\omega t}\, \mathrm{d}t\,, \tag{5.70}$$

where $s(t)$ is the pulse source for which the time-domain solution $p(r, z, t)$ is investigated. Before (5.69) can be used, the transfer function $p(r, z, \omega)$ has to be determined from one of the frequency-domain [or continuous-wave (CW)] propagation models described above at a number of discrete frequencies within the frequency band of interest. This means the ocean response to a pulse $s(t)$ is obtained by combining the convenient and computationally efficient CW codes (spectral integrals, normal-mode or parabolic equations) with a Fourier synthesis approach. Even if this last step is conceptually simple, there are several numerical issues that have to be addressed like frequency and time windowing, and aliasing.

The first step in evaluating the frequency integral by means of a (fast) Fourier transform is to reduce the in-

Amazon EX1014 Page 194

tegration interval. The source pulse $s(t)$ being known, a frequency interval $[\omega_{\min}, \omega_{\max}]$ is determined, outside which the source does not emit any significant energy. Moreover, the final time-domain solution $p(r, z, t)$ being real, we know that $p(r, z, -\omega) = \overline{p(r, z, \omega)}$. This reduces the integration performed in (5.69) to the interval $[\omega_{\min}, \omega_{\max}]$

$$p(r, z, t) = \mathrm{Re}\left[\frac{1}{\pi}\int_{\omega_{\min}}^{\omega_{\max}} S(\omega) p(r, z, \omega)\, \mathrm{e}^{-\mathrm{i}\omega t}\, \mathrm{d}\omega\right]. \tag{5.71}$$

Now, the set of discrete frequencies on which the integration has to be performed on the interval $[\omega_{\min}, \omega_{\max}]$ depends on both the choice of the sampling frequency F_s of the signal and some a priori knowledge of the time spread T of the final solution $p(r, z, t)$. First, the sampling frequency F_s has to satisfy the Nyquist criterium $F_s > 2 f_{\max} = (\omega_{\max}/\pi)$. Typically, to allow for a reasonably looking graphical signal display, an appropriate value is $F_s = 8 f_{\max}$. Second, the time window T of the signal after propagation through the ocean should be taken as short as possible. However, this time window must be chosen in accordance with the waveguide physics. A conservative way to estimate the time spread is to consider that T is bounded by the slowest and fastest available speeds for the particular environment:

$$T = t_{\max} - t_{\min} \geq R\left(\frac{1}{c_{\min}} - \frac{1}{c_{\max}}\right), \tag{5.72}$$

where R is the propagation range. With the proper choice of T and F_s, we construct an N-point time vector $\boldsymbol{t} = [0 : \frac{1}{F_s} : T]$, with $N = F_s T + 1$ and a frequency vector $\frac{\boldsymbol{\omega}}{2\pi} = [0 : \frac{F_s}{N} : F_s(1 - \frac{1}{N})]$. The time vector $\boldsymbol{t}$ corresponds to the time axis on which the time-dependent solution $p(r, z, t)$ will be computed from the frequency bins of the frequency vector $\boldsymbol{\omega}$ inside the interval $[\omega_{\min}, \omega_{\max}]$. Before computing the Fourier transform, it is necessary to add a retarded time to the integral $\exp(-\mathrm{i}t_{\min}\omega)$ so that the time vector $\boldsymbol{t}$ starts at the earliest possible arrival $t = t_{\min} + [0 : \frac{1}{F_s} : T]$. From (5.80), a reasonable choice for $t_{\min}$ is $t_{\min} = (R/c_{max})$. It follows:

$$p(r, z, t) = Re\left\{\mathrm{IFFT}\left[S(\omega) p(r, z, \omega) \mathrm{e}^{-\mathrm{i}\omega t_{\min}}\right]_{\omega_{\min}}^{\omega_{\max}}\right\}, \tag{5.73}$$

where the inverse fast Fourier transform (IFFT) is performed on the frequency vector $\boldsymbol{\omega}$ in the interval $[\omega_{\min}, \omega_{\max}]$. We do not discuss here the numerous (fast) Fourier transform algorithms, which can be found in signal processing or numerical methods books. Typical results of this broadband modeling are presented in Figs. 5.22–5.25.

5.5 Quantitative Description of Propagation

All of the models described above attempt to describe reality and to solve in one way or another the Helmholtz equation. They therefore should be consistent and there is much insight to be gained from understanding this consistency. The models ultimately compute propagation loss which is taken as the decibel ratio (see Appendix) of the pressure at the field point to a reference pressure, typically one meter from the source.

Figure 5.31 shows convergence-zone-type propagation for a simplified profile. The ray trace in Fig. 5.31b shows the cyclic focusing discussed in Sect. 5.1.2. The same profile is used to calculate normal modes, shown in Fig. 5.31c which, when summed according to (5.50) referenced to 1 m, exhibits the same cyclic pattern as the ray picture. Figure 5.31d shows both the normal-mode (wave theory) and ray theory result. Ray theory exhibits sharply bounded shadow regions as expected whereas the normal-mode theory, which includes diffraction, shows that the acoustic field does exist in the shadow regions and the convergence zones have structure.

Normal-mode models sum the discrete modes that roughly correspond to angles of propagation within the cone of Fig. 5.7a. The spectral method can include the full field, discrete plus continuous, the latter corresponding to larger angles. The discussion below (5.50) defines these angles in terms of horizontal wavenumbers, and the eigenvalues of the normal-mode problem are a discrete set of horizontal wavenumbers. Hence the integrand (Green's function) of the spectral method has peaks at the eigenvalues associated with the normal modes. These peeks are shown on the right of Fig. 5.32a. The smoother portion of the spectrum is the continuous part, corresponding to the larger angles. Therefore, the consistency we expect between the normal-mode and the spectral method and the physics of Fig. 5.7 is that the continuous portion of the spectral solution decays rapidly with range so that there should be complete agreement at

Amazon EX1014 Page 195

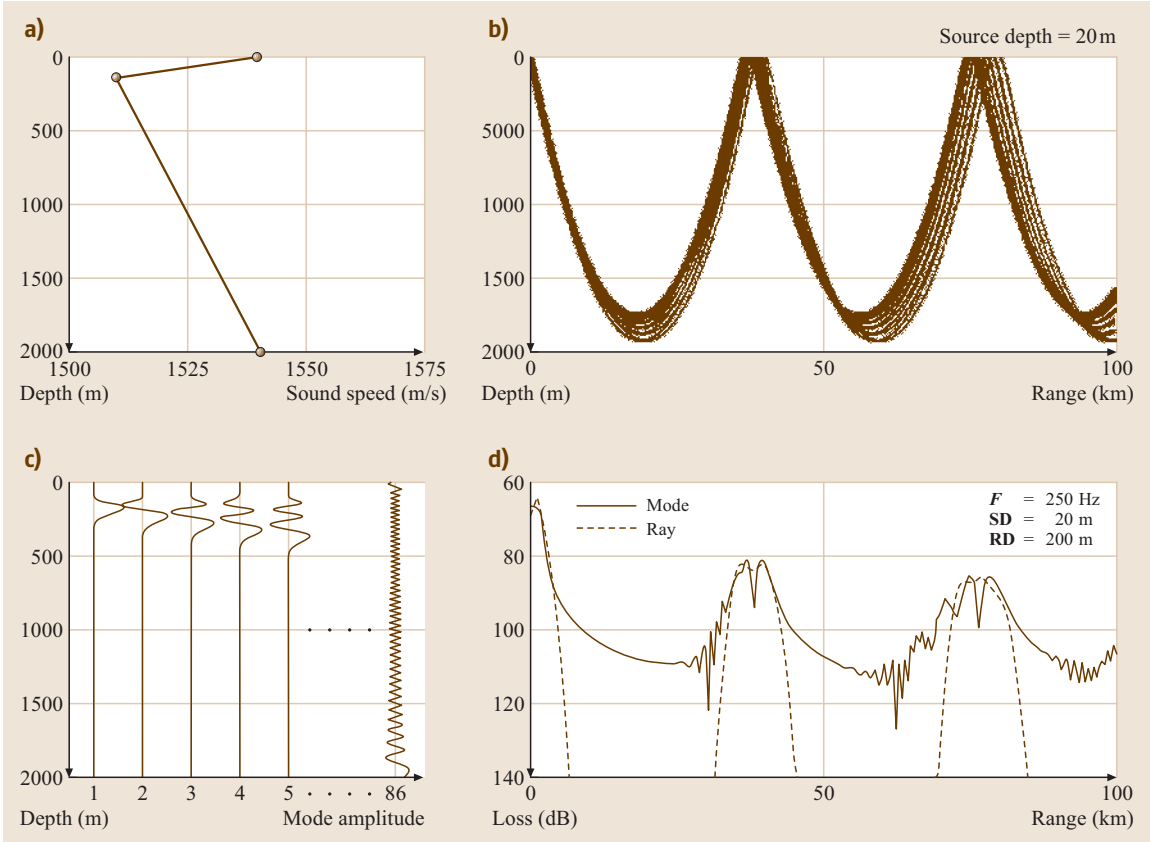


Fig. 5.31a–d Consistency between ray theory and normal mode theory. **(a)** Sound-speed profile, **(b)** ray trace, **(c)** normal modes, **(d)** propagation calculations. The shadow zones in **(d)** are much sharper for ray theory which does not include diffraction effects

long range between the normal-mode and spectral solutions. The Lloyd's mirror effect, a near-field effect, should also be exhibited in the spectral solution but not the normal-mode solution. These aspects are apparent in Fig. 5.32b. The PE solution is in good agreement with the other solutions but with some phase error associated with the average wavenumber that must be chosen in the split-step method. The PE solution, which contains part of the continuous spectrum including the Lloyd's mirror beams, is more accurate than the normal-mode solution at short range; however, the generalized PE can be made arbitrarily accurate at short range by including more expansion terms in (5.66).

Range-dependent results are shown in Fig. 5.33. A ray trace, a ray trace field result, a PE result and data are plotted together for a range-dependent sound-speed profile environment. The models agree with the data in general, with the exception that the ray results predict too sharp a leading edge for the convergence zone.

Up-slope propagation is modeled with the PE in Fig. 5.34. As the field propagates up-slope, sound is dumped into the bottom in what appears to be discrete beams. The flat region has three modes and each is cut off successively as sound propagates into the shallower water. The ray picture also has a consistent explanation for this phenomenon. The rays for each mode become steeper as they propagate up-slope. When the ray angle exceeds the critical angle the sound is significantly transmitted into the bottom.

Amazon EX1014 Page 196

5.6 SONAR Array Processing

Signal processing is common to many fields [5.36–38]. In this section we emphasize applications to underwater acoustics, mainly concentrating on spatial processing of pressure fields. We note, though, that there is also growing interest in processing vector fields such as acoustic displacement, velocity or acceleration [5.39]. Further, the array processing discussed below for passive SONARs is also applicable to active SONAR signal processing. Spatial sampling of a sound field is usually done by an array of transducers, although the synthetic aperture array, in which a sensor is moved through space to obtain measurements in both the time and space domains, is an important exception. Spatial sampling is analogous to temporal sampling with the sampling interval replaced by the sensor spacing. The Nyquist criterion requires that the sensor spacing be at least twice the spatial wavenumber of the measured sound field. Finally, we note that recently work of processing ambient noise fields have proven to yield information about the ocean environment [5.40, 41].

5.6.1 Linear Plane-Wave Beam-Forming and Spatio-Temporal Sampling

The simplest example of array processing is phase shading in the frequency domain (or time delay in the time domain) to search for the bearing of a plane-wave signal. This procedure is referred to as plane wave beam-forming, or delay and sum beam-forming in the time domain. For simplicity we consider a liner array and we take θ as the bearing angle associated with the plane-wave signal as shown in Fig. 5.35a.

Frequency-Domain Processing

A plane wave can be represented as

$$s(\theta) = \exp(\mathrm{i}\boldsymbol{k}\cdot\boldsymbol{r})\,, \tag{5.74}$$

where we have suppressed the time dependence $\exp(-\mathrm{i}\omega t)$ and $k = |\boldsymbol{k}| = (\omega/c)$. The field is summed in phase if the receiving element (hydrophone or microphone) inputs at position $\boldsymbol{d}$ is multiplied by the complex conjugate of the plane-wave phase factor,

$$\omega_i^* = \exp(-\mathrm{i}\boldsymbol{k}_\mathrm{s}\cdot\boldsymbol{d}_i) = \exp\left[-\mathrm{i}\,\mathrm{d}(k\sin\theta_\mathrm{s})\right]\,, \tag{5.75}$$

where θ_s is a scanning angle. This process will have a maximum when the scanning angle equals the incident angle of the signal.

The output of this beam-forming process is denoted $B(\theta_\mathrm{s})$, but often it is the power output of the beam-former that is of interest:

$$\begin{aligned} B(\theta_\mathrm{s}) &= \left|\sum_{i=1}^{m}\omega_i^*(\theta_\mathrm{s})\left[s_i(\theta)+n_i\right]\right|^2 \\ &= \sum_{i,j=1}^{m}\omega_i^*(\theta_\mathrm{s})\left(s_{ij}+n_{ij}\right)\omega_j(\theta_\mathrm{s})\,, \end{aligned} \tag{5.76}$$

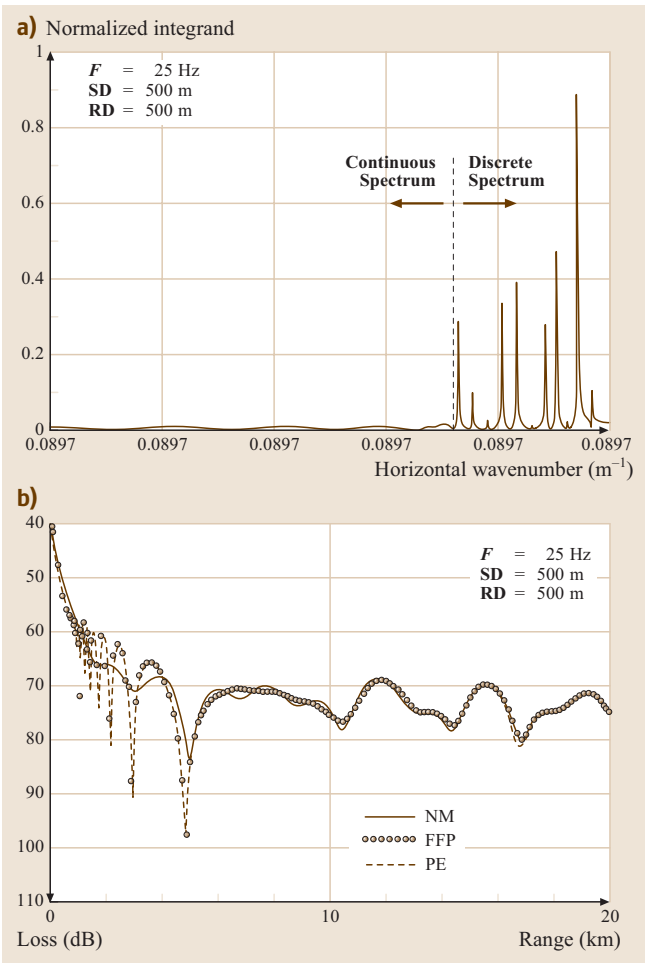


Fig. 5.32a,b Relationship between spectral (FFP), normal-mode (NM) and split-step parabolic-equation model (PE) computations. **(a)** FFP Green's function from (5.44). **(b)** Normal-mode, spectral (FFP) and PE propagation results showing some agreement in the near field and complete agreement in the far field. Higher-order PE methods will give identical results to the FFP

Amazon EX1014 Page 197

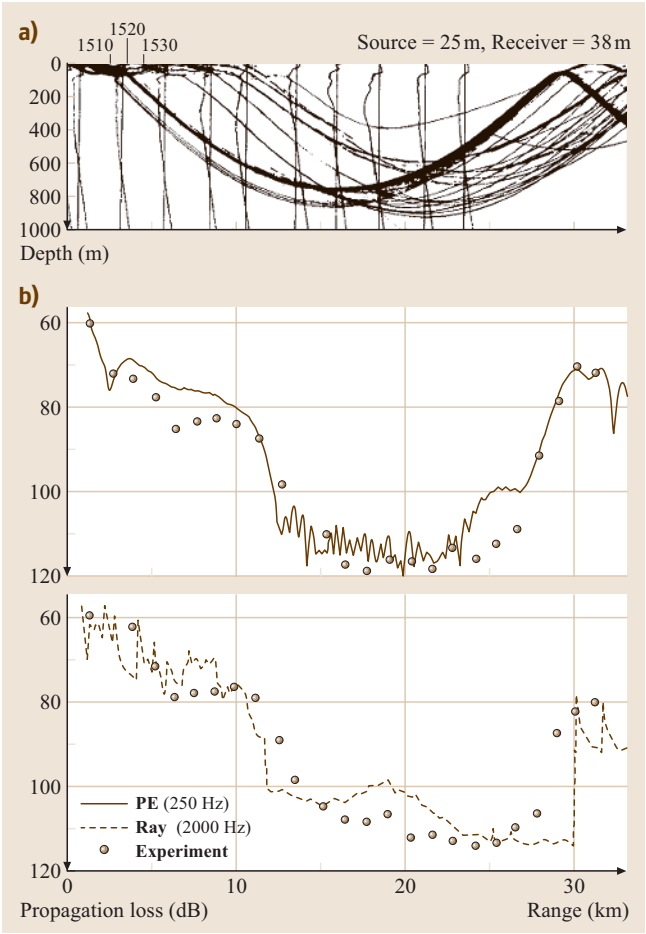


Fig. 5.33a,b Model and data comparison for a range-dependent case. **(a)** Profiles and ray trace for a case of a surface duct disappearing. **(b)** 250 Hz PE and 2 kHz ray-trace comparisons with data. Again, the diffraction-less ray theory shows more abrupt change in field

where s_i and n_i are the signal and noise at the i-th receiving element and where $s_{ij}+n_{ij}$ are elements of a cross-spectral density matrix which, when obtained from data, would involve Fourier transforms and ensemble averages as mentioned in the discussion below (5.78) augmented by Fig. 5.35b. In writing down the right-hand side of (5.76), the signal and noise fields were assumed to be mutually incoherent.

We can write the above expression in matrix notation where the boldface lower-case letters denote vectors and boldface upper-case letters denote matrices. Define a steering column vector $\boldsymbol{w}$ whose i-th element is w_i and a cross-spectral density matrix (CSDM) $\boldsymbol{K}$ of the signal and noise with elements $K_{ij}=s_{ij}+n_{ij}$ since the signal and noise are assumed to be independent. Equation (5.76) can be rewritten as

$$B(\theta_s)=\boldsymbol{w}^{\dagger}(\theta_s)\boldsymbol{K}(\theta_{\text{true}})\boldsymbol{w}(\theta_s)\equiv\boldsymbol{w}^{\dagger}\boldsymbol{K}\boldsymbol{w}\,, \tag{5.77}$$

where † denotes the complex transpose. The CSDM or the covariance of the field is composed of uncorrelated signal and noise covariances,

$$\boldsymbol{K}=\boldsymbol{K}_s+\boldsymbol{K}_n\,. \tag{5.78}$$

The data across the array as represented in the matrix $\boldsymbol{K}$ contains the information that the source is in the direction θ_{true}. Sometimes $\boldsymbol{w}(\theta_s)$ is referred to as a replica and this beam-forming process is viewed as matching the received data across the array with a replica. The type of beam-former represented by (5.77) is called a linear or Bartlett beam-former.

For the sample covariance estimation we assume we have an array with N sensors located at $\boldsymbol{d}_i$, $i=1,2,\cdots,N$ and a narrow-band model as illustrated in Fig. 5.35b. These covariances are estimated by segmenting the received data, $r_i(t)$ into *snapshots* using a sampling window, $W(t)$, that is unity in the interval $[0,T_w]$,

$$R_i^l(f)=\int_{T_l}^{T_l+T_w} r_i(t)W(t-T_l)\,\mathrm{e}^{-\mathrm{i}2\pi ft}\,\mathrm{d}t\,, \tag{5.79}$$

where here the notation uses frequency f, rather than angular frequency ω. In most beam-forming algorithms the data vectors are averaged to form the sample covariance matrix

$$\hat{K}(f)=\frac{1}{L}\sum_{l=1}^{L}R^l(f)R^l(f)^H\,, \tag{5.80}$$

where L is the number of snapshots.

Time-Domain Processing

Time delaying a signal is the time-domain analog to phase shading of the signal in the frequency domain. In general, the time domain is a viable alternative to frequency analysis when processing coherent broadband signals such as temporal impulse. Time-delay beam-forming is then the frequency equivalent of the phase beam-forming described in Sect. 5.6.1. Indeed, it can be derived formally by taking the Fourier transform of the beam-forming process with the result that the beam-

Amazon EX1014 Page 198

former output is:

$$b(\theta, t) = \int_{-\infty}^{\infty} B(\theta, \omega) \exp(\mathrm{i}\omega t)\, \mathrm{d}\omega$$
$$= \int_{-\infty}^{\infty} \sum_i R_i(\omega) \exp\left(-\mathrm{i}\frac{\omega}{c_i} d_i \sin\theta\right) \times \exp(\mathrm{i}\omega t)\, \mathrm{d}\omega$$
$$= \sum_i R_i(t - \frac{d_i}{c_i} \sin\theta)\,, \qquad (5.81)$$

where $R_i(t)$ is the time domain data, d_i the location and c_i the sound speed at the i-th phone. Physically speaking, the delay $\tau_i = (d_i/c_i)\sin\theta$ is, to a first approximation, the time delay associated with the phase shift in the frequency-domain array processing. A more rigorous approach in the case of a strong depth dependence of the sound-speed profile leads to:

$$\tau_i = \int_{d_0}^{d_i} \sqrt{\frac{1}{c^2(z)} - \frac{\cos^2(\theta)}{c^2(d_0)}}\, \mathrm{d}z\,, \qquad (5.82)$$

where d_0 is the depth of a reference hydrophone on the array. Note that, in the case of a uniform sound speed profile over the array, the above processes are plane-wave beam-forming.

Examples of the practical use of time-domain versus frequency-domain beam-forming are discussed below. Consider an incident field on a 20-element vertical array made of seven pulses arriving at different angles in a noisy waveguide environment (Fig. 5.36). The SNR ratio does not allow an accurate detection and identification of the echoes. Time-delay beam-forming results applied on these broadband signals is presented in Fig. 5.37. The SNR of the time-domain processing is a combination of array gain and frequency-coherent processing. In comparison, phase beam-forming performed on the same data and averaged incoherently over frequencies show a degraded detection of the incident echoes (Fig. 5.38).

5.6.2 Some Beam-Former Properties

Figure 5.39 shows the output results of some frequency-domain plane-wave beam-formers for the cases of one and two incident signals. To be noted are the side-lobes of the Bartlett processor and the high-resolution performance of the adaptive processors (discussed in the next section). Some of the general attributes of an array beam-former are:

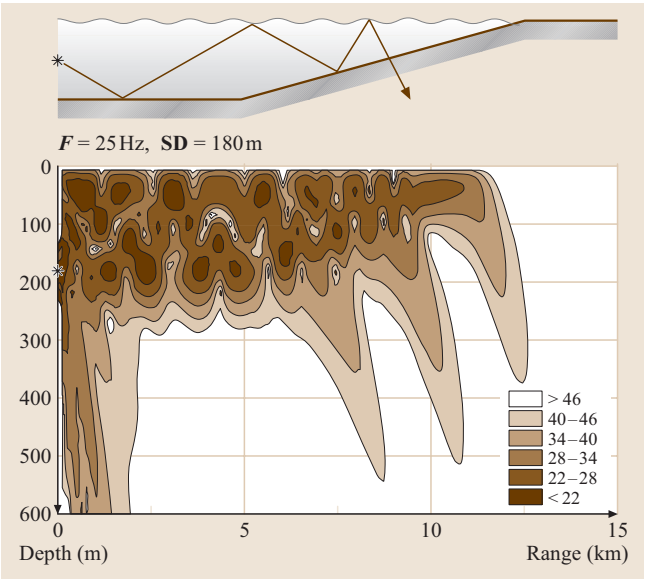


Fig. 5.34 Relation between up-slope propagation (from PE calculation) showing individual mode cut-off and energy dumping in the bottom, and a corresponding ray schematic. In this case, three modes were excited in the flat region. The ray picture shows that a ray becomes steeper as it bounces up slope and when its grazing angle exceeds the critical angle, it is partially transmitted into the bottom (and subsequently with more and more transmission with each successive, higher angle bounce)

- The main response axis (MRA): generally, one normalizes the beam pattern to have 0 dB, or unity gain in the steered direction.
- Beam width: an array with finite extent, or aperture, must have a finite beam width centered about the MRA, which is termed the *main lobe*.
- Side-lobes: angular or wavenumber regions where the array has a relatively strong response. Sometimes they can be comparable to the MRA, but in a well-designed array, they are usually −20 dB or lower, i. e., the response of the array is less than 0.1 of a signal in the direction of a side-lobe.
- Wavenumber processing: rather than scan through incident angles, one can scan through wavenumbers, $k \sin\theta_s \equiv \kappa_s$; scanning through all possible values of κ_s results in nonphysical angles that correspond to waves not propagating at the acoustic medium speed. Such waves can exist, such as those associated with array vibrations. The beams associated with these wavenumbers are sometimes referred to as virtual beams. An important aspect of these beams is that their

Amazon EX1014 Page 199

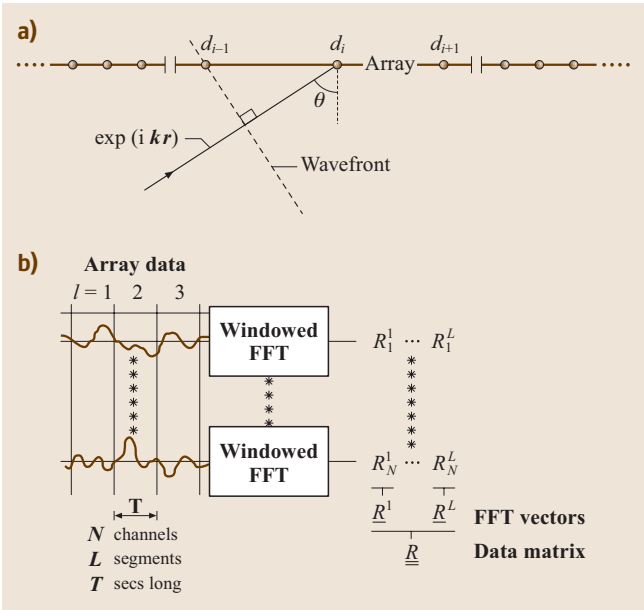


Fig. 5.35a,b Array processing. **(a)** Geometry for plane-wave beam-forming. **(b)** The data is transformed to the frequency domain in which the plane-wave processing takes place. The cross-spectral-density matrix (CSDM) is an outer product of the data vector for a given frequency

side-lobes can be in the physical angle region, thereby interfering with acoustic propagating signals.

- Array gain: defined as the decibel ratio of the signal-to-noise ratios of the array output to a single phone output. If the noise field is isotropic, the array gain is also termed the directionality index.

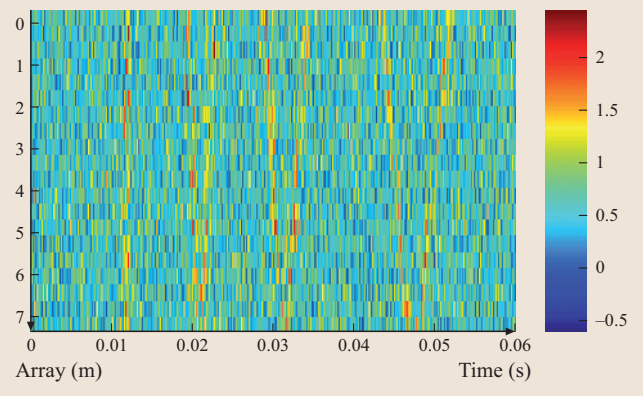


Fig. 5.36 Depth-versus-time representation of simulated broadband coherent data received on a vertical array in the presence of ambient noise. The wavefronts corresponding to different sources are nearly undistinguishable

5.6.3 Adaptive Processing

There are high-resolution methods to suppress side-lobes, usually referred to as adaptive methods since the signal processing procedure constructs weight vectors that depend on the received data itself. We briefly describe one of these procedures: the minimum-variance distortionless processor (MV), sometimes also called the maximum-likelihood method (MLM) directional spectrum-estimation procedure.

We seek a weight vector $\boldsymbol{w}_{\mathrm{MV}}$ applied to the matrix $\boldsymbol{K}$ such that its effect will be to minimize the output of the beam-former (5.77) except in the look direction, where we want the signal to pass undistorted. The weight vector is therefore chosen to minimize the functional [5.38]. From (5.72)

$$F = \boldsymbol{w}_{\mathrm{MV}} \boldsymbol{K} \boldsymbol{w}_{\mathrm{MV}} + \alpha(\boldsymbol{w}_{\mathrm{MV}} \boldsymbol{w} - 1) \,. \tag{5.83}$$

The first term is the mean-square output of the array and the second term incorporates the constraint of unity gain by means of the Lagrangian multiplier α. Following the method of Lagrange multipliers, we obtain the MV weight vector,

$$\boldsymbol{w}_{\mathrm{MV}} = \frac{\boldsymbol{K}^{-1}\boldsymbol{w}}{\boldsymbol{w}\boldsymbol{K}^{-1}\boldsymbol{w}} \,. \tag{5.84}$$

This new weight vector depends on the received data as represented by the cross-spectral density matrix; hence, the method is adaptive. Substituting back into (5.77) gives the output of our MV processor,

$$B_{\mathrm{MV}}(\theta_{\mathrm{s}}) = [\boldsymbol{w}(\theta_{\mathrm{s}})\boldsymbol{K}^{-1}(\theta_{\mathrm{true}})\boldsymbol{w}(\theta_{\mathrm{s}})]^{-1} \,. \tag{5.85}$$

The MV beam-former should have the same peak value at θ_{true} as the Bartlett beam-former, (5.77) but with side-lobes suppressed and a narrower main beam, indicating that it is a high-resolution beam-former. Examples are shown in Fig. 5.39. Of particular practical interest for this type of processor is the estimation procedure associated with Fig. 5.35b and (5.80). One must take sufficient snapshots to allow the stable inversion of the CSDM. This requirement may conflict with source motion when the source moves through multiple beams along the time interval needed to construct the CSDM.

5.6.4 Matched Field Processing, Phase Conjugation and Time Reversal

Matched field processing (MFP) [5.42] is a generalization of plane-wave beam-forming in which data

Amazon EX1014 Page 200

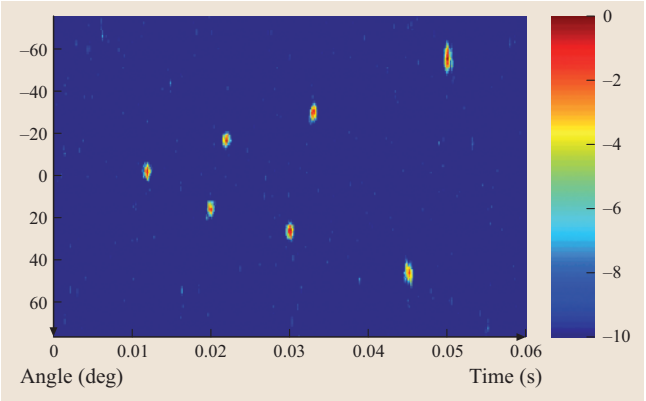


Fig. 5.37 Angle-versus-time representation of the simulated data in Fig. 5.36 after time-delay beam-forming. All sources appear clearly above the noise with their corresponding arrival angle

on an array is correlated with replicas from a (waveguide) propagation model for candidate locations $\hat{r}$, $\hat{z}$ (Fig. 5.40). Localization of a source is accomplished with a resolution consistent with the modal structure and SNR. The central difficulty with MFP is specifying the coefficients and boundary conditions of the acoustic wave equation for shallow water propagation, *i. e.*, knowing the ocean environment in order to generate the replicas. An alternative to performing this model-based processing is phase conjugation (PC), in the frequency domain or, time reversal (TR) in the time domain, in which the conjugate or time-reversed data is used as source excitations on a transmit array colocated with the receive array (Fig. 5.41a) [5.43]. The PC/TR process is equivalent to correlating the data with the *actual* transfer function from the array to the original source location. In other words, both MFP and PC are signal processing analogs to the mechanical lens adjustment feedback technique used in adaptive optics: MFP uses data together with a model (note the feedback arrow in Fig. 5.40) whereas PC/TR is an active form of adaptive optics simply retransmitting phase-conjugate/time-reversed signal through the same medium (*e.g.*, see result of Fig. 5.41). Though time reversal is thought of as as active process, it is presented in this section because of its relation to passive MFP.

Ocean Time-Reversal Acoustics

Phase conjugation, first demonstrated in nonlinear optics and its Fourier conjugate version, time reversal is a process that has recently implemented in ultrasonic laboratory acoustic experiments [5.44]. Implementation of time reversal in the ocean for single elements [5.45] and using a finite spatial aperture of sources, referred to as a *time-reversal mirror* (TRM) [5.46], is now well established.

The geometry of a time-reversal experiment is shown in Fig. 5.41. Using the well-established theory of PC and TRM in a waveguide, we just write down the result of the phase-conjugation and time-reversal process, respectively, propagating toward the focal position

$$P_{\mathrm{pc}}(r,z,\omega)=\sum_{j=1}^{J} G_{\omega}(r,z,z_j)G^{*}_{\omega}(R,z,z_{\mathrm{ps}})S^{*}(\omega) \tag{5.86}$$

and

$$P_{\mathrm{trm}}(r,z,t)=\frac{1}{(2\pi)^2}\sum_{j=1}^{J}\iint G(r,z,t'';0,z_j,t') \times G(R,z_j,t';0,z_{\mathrm{ps}},0) \times S(t''-t+T)\,\mathrm{d}t\,\mathrm{d}t'' , \tag{5.87}$$

where S is the source function, $G^{*}_{\omega}(R,z,z_{\mathrm{ps}})$ is the frequency-domain Green's function and $G(R,z_j,t';0,z_{\mathrm{ps}},0)$ is the time-domain Green's function (TDGF) from the probe source at depth z_{ps} to each element of the SRA at range R and depth z_j. Emphasizing the time-domain process, $G(r,z,t'';0,z_j,t')$ is the

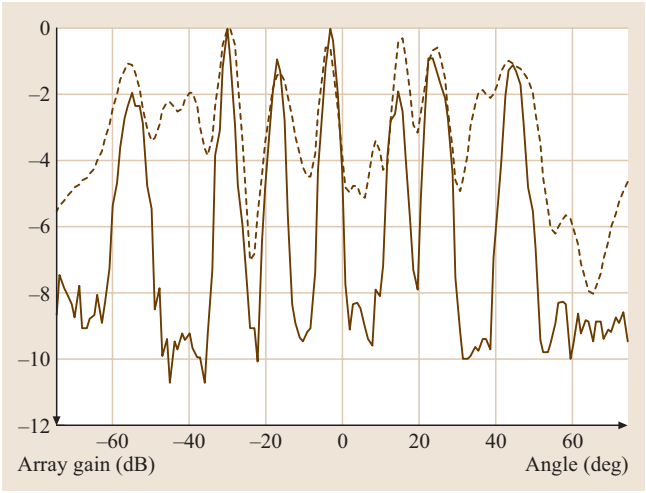


Fig. 5.38 Comparison between coherent time-delay beam-forming (*in red*) and incoherent frequency-domain beam-forming (*in blue*) for the simulated data shown in Fig. 5.35. When data come from coherent broadband sources, time-domain bema-forming show better performance than frequency analysis

Amazon EX1014 Page 201

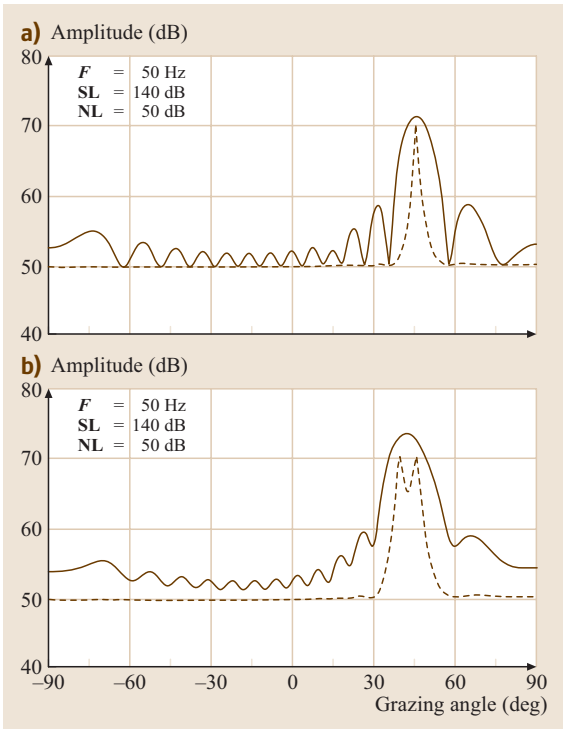


Fig. 5.39a,b Simulated beam-former outputs. **(a)** Single sources at a bearing of 45°. **(b)** Two sources with 6.3° angular separation. *Solid line*: linear processor (Bartlett). *Dashed line*: minimum variance distortion-less processor (MV) showing that the side-lobes are suppressed

TDGF from each element of the SRA back to range r and depth z. The focused field at the probe source position is $P_{\mathrm{trm}}(R, z_{\mathrm{ps}}, t)$. The summation is performed on the J elements of the TRM. The signal $S(t''-t+T)$ of duration τ is the time-reversed version of the original probe source signal and the derivation of (5.87) uses the causality requirement, $T > 2\tau$, i. e., the time reversal interval T must contain the total time of reception and transmission at the SRA, 2τ.

Figure 5.41a,b,c shows the result of a TRM experiment. The size of the focus is consistent with the spatial structure of the highest-order mode surviving the two-way propagation and can also be mathematically described by a virtual array of sources using image theory in a waveguide.

Matched Field Processing

Linear matched field processing (MFP) can be thought of as the passive signal-processing implementation of phase conjugation. Referring to the phase-conjugation process described by (5.86), rename S^*G^* as the data at each array element and call the data vector on the array $\boldsymbol{R}(\boldsymbol{a}_{\mathrm{true}})$, where $\boldsymbol{a}_{\mathrm{true}}$ represents the (unknown) location of the source (Fig. 5.35b). Now in phase conjugation, G represents an actual propagation from the source array. In MPF, we do the propagation numerically using one of the acoustic models, but rather than use the actual Green's function, we use a normalized version of it called a replica: $\omega(a) = G(a)/|G(a)|$, where $G(a)$ is a vector of Green's functions of dimension of the number of array elements that represents the propagation from a candidate source position to the array elements and is the magnitude of the vector over the array elements. Taking the square of the PC process with replica's replacing the Green's functions yields the beam-former of the matched field processor

$$B_{\mathrm{mf}}(a) = \omega^H(a) K(a_{\mathrm{true}}) \omega(a) \,, \qquad (5.88)$$

where a realization of the CSDM on the array is then $K(a_{\mathrm{true}} = R(a_{\mathrm{true}}) R^H(a_{true})$ and a sample CSDM is built up as per (5.80).

MFP works because the unique spatial structure of the field permits localization in range, depth and azimuth depending on the array geometry and complexity of the ocean environment. The process is shown schematically in Fig. 5.40. MFP is usually implemented by systematically placing a test point source at each point of a search grid, computing the acoustic field (replicas) at all the elements of the array and then correlating this modeled field with the data from the real point source, $K(a_{\mathrm{true}}) = RR^H$, whose location is unknown. When the test point source is co-located with the true point source, the correlation will be a maximum. The scalar function $B_{\mathrm{mf}}(a)$ is also referred to as the ambiguity function (or surface) of the matched field processor because it also contains ambiguous peaks which are analogous to the side-lobes of a conventional plane-wave beam-former. Side-lobe suppression can often be accomplished by using the adaptive beam-forming methods discussed in the plane-wave section.

Adaptive processors are very sensitive to the accuracy of the replica functions which, in turn, require almost impossible knowledge of the environment. Hence, much work has been done on developing robust forms of adaptive processing such as the white-noise constraint method and others [5.47, 48]. An example of matched field processing performed incoherently on eight tones between 50 Hz and 200 Hz is shown in Fig. 5.42.

Amazon EX1014 Page 202

5.7 Active SONAR Processing

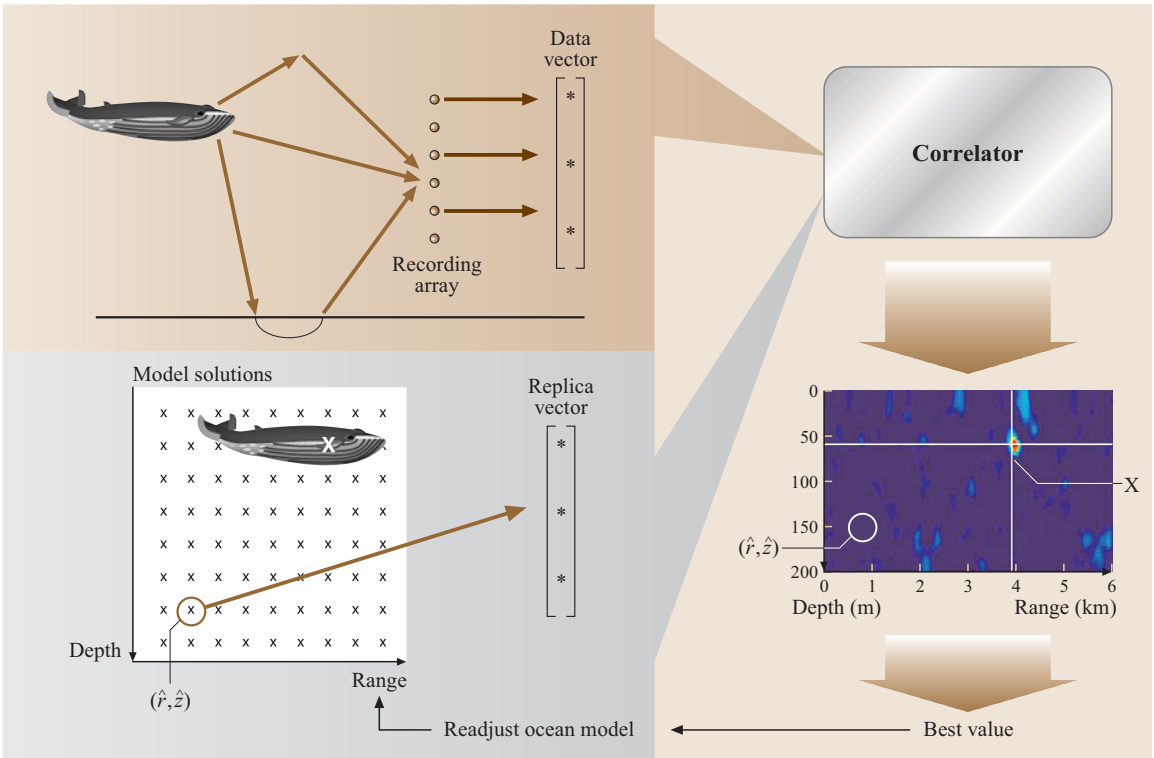


Fig. 5.40 Matched field processing (MFP). Here, the example consists in localizing a singing whale in the ocean. If your model of waveguide propagation is sufficiently accurate for this environment, then comparing the recorded sounds – the whale's data vector – one frequency at a time, for example, with replica data based on best guesses of the location $(\hat{r}, \hat{z})$ that the model provides, will eventually yield its location. The red peak in the data indicates the location of highest correlation. The small, circled × represents a bad guess, which thus does not compare well with the measured data. The feedback loop suggests a way to optimize the model: by fine-tuning the focus – the peak resolution in the plot – one can readjust the model's bases (for example, the sound-speed profile). That feedback describes a signal-processing version of adaptive optics. Matched field processing can then be used to perform acoustic tomography in the ocean [5.49]

An active SONAR system transmits a pulse and extracts information from the echo it receives as opposed to a passive SONAR system, which extracts information from signals received from radiating sources. An active SONAR system and its associated waveform is designed to detect targets and estimate their range, Doppler (speed) and bearing or to determine some properties of the medium such as ocean bottom bathymetry, ocean currents, winds, particulate concentration, etc. The spatial processing methods already discussed are applicable to the active problem so that in this section we emphasize the temporal aspects of active signal processing.

5.7.1 Active SONAR Signal Processing

The basic elements of an active SONAR are: the (waveform) transmitter, the channel through which the signal, echo and interference propagates, and the receiver [5.50]. The receiver consists of some sort of matched filter, a square-law device, and possibly a threshold device for the detector and range, Doppler and bearing scanners for the estimator.

The matched filter maximizes the ratio of the peak output signal power to the variance of the noise and is implemented by correlating the received signal with

Amazon EX1014 Page 203

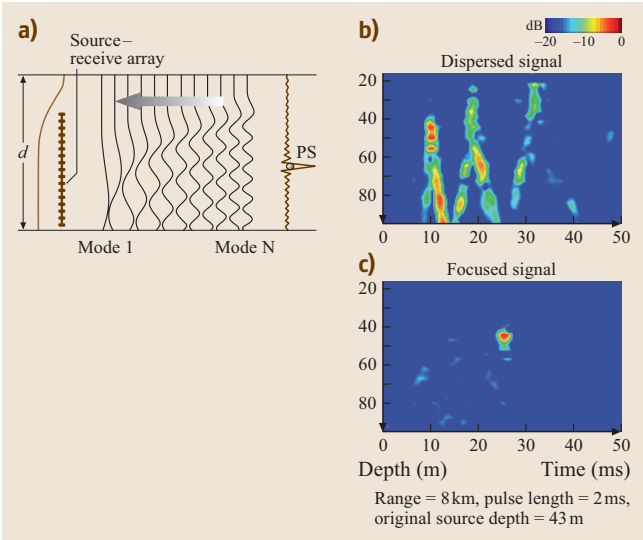


Fig. 5.41a–c Ocean acoustic time-reversal mirror **(a)** The acoustic field from a probe source (PS) is received on a source–receive array (SRA). **(b)** The signal received on the SRA with the first mode arriving first. At the SRA the signal is digitized, time-reversed and retransmitted. **(c)** The time-reversed signal received on an array at the same range as PS. The signal has been refocused at the probe source position with a resolution determined by the highest-order mode surviving the two-way process

the transmitted signal. A simple description of the received signal, $r(t)$, is that it is an attenuated, delayed, and Doppler-shifted version of the transmitted signal $s_t(t)$,

$$r(t) \to \mathrm{Re}\left[\alpha\, \mathrm{e}^{\mathrm{i}\theta\sim} s_t(t-T)\, \mathrm{e}^{2\pi \mathrm{i} f_c t}\, \mathrm{e}^{2\pi \mathrm{i} f_d t} + n(t)\right], \tag{5.89}$$

where α is the attenuation transmission loss and target cross section, θ is a random phase from the range uncertainty compared to a wavelength, T is the range delay time, f_c is the center frequency of the transmitted signal and f_d is the Doppler shift caused by the target. The correlation process will have an output related to the following process,

$$C(a) = \left| \int \tilde{r}(t)\tilde{s}(t;a)\,\mathrm{d}t \right|^2 , \tag{5.90}$$

where $\tilde{s}(t;a)$ is a replica of the transmitted signal modified by a parameter set a which include the propagation–reflection process, e.g., range delay and Doppler rate. For the detection problem, the correlation receiver is used to generate a sufficient statistic which is the basis for a threshold comparison in making a decision if a target is present. The performance of the detector is described by receiving operating characteristic (ROC) curves which plot the detection of probability versus false-alarm probability, as parameterized by a statistics of the signal and noise levels. The parameters a set the range and Doppler value in the particular resolution cell of concern. To estimate these parameters, the correlation is done as a function of a.

For a matched filter operating in a background of white noise detecting a point target in a given range–Doppler resolution cell, the detection signal-to-noise ratio depends on the average energy-to-noise ratio and not on the shape of the signal. The waveform becomes

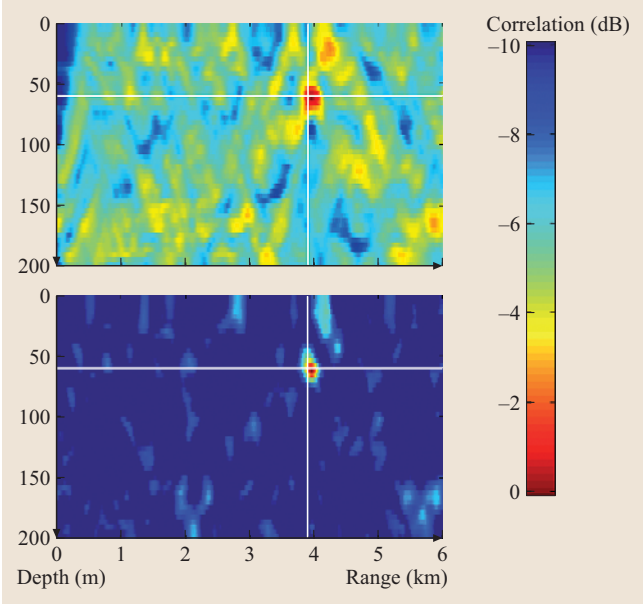


Fig. 5.42a,b Matched field processing example for a vertical array in a shallow-water environment. Specific information regarding the experiment can be found on the web at http://www.mpl.ucsd.edu/swellex96/. **(a)** Bartlett result with significant side-lobes only 3 dB down. **(b)** Adaptive processor results shows considerable side-lobe suppression. The processor is actually a *white-noise constrained* MVDP for which the diagonal of the CSDM is deliberately loaded by a specific algorithm to stabilize the processor to some uncertainty in the environment and/or array configuration. The ambiguity surfaces in **(a)** and **(b)** are an incoherent average over eight tones at 53, 85, 101, 117, 133, 149, 165, 181, and 197 Hz

Amazon EX1014 Page 204

a factor when there is a reverberant environment and when one is concerned with estimating target range and Doppler. A waveform's potential for range and Doppler resolution can be ascertained from the ambiguity function of the transmitted signal. This ambiguity function is related to the correlation process of (5.90) for a transmitted signal scanned as a function of range and Doppler,

$$\Theta(\hat{T}, T_t, \hat{f}_d, f_{d_t}) \propto \left| \int \tilde{s}(t-T)\tilde{s}_t(t-\hat{T})\, e^{2\pi i (f_{d_t}-\hat{f}_d)t}\, dt \right|^2 , \qquad (5.91)$$

where T_t and f_{d_t} are the true target range (time) and Doppler, and $\hat{T}$ and $\hat{f}_d$ are the scanning estimates of the range and Doppler. Figure 5.43 are sketches of ambiguities functions of some typical waveforms. The range resolution is determined by the reciprocal of the bandwidth and the Doppler resolution by the reciprocal of the duration. A coded or pseudo-random (PR) sequence can attain good resolution of both by appearing as long-duration noise with a wide bandwidth. Ambiguity functions can be used to design desirable waveforms for particular situations. However, one must also consider the randomizing effect of the real ocean. The *scattering function* describes how a transmitted signal statistically redistributes its energy in the reverberant ocean environment which causes multipath and Doppler spread. In particular, in a reverberation-limited environment, only increasing the transmitted power does not change the signal-to-reverberation level. Signal design should minimize the overlap of the ambiguity function of the target displaced to its range and Doppler and the scattering function.

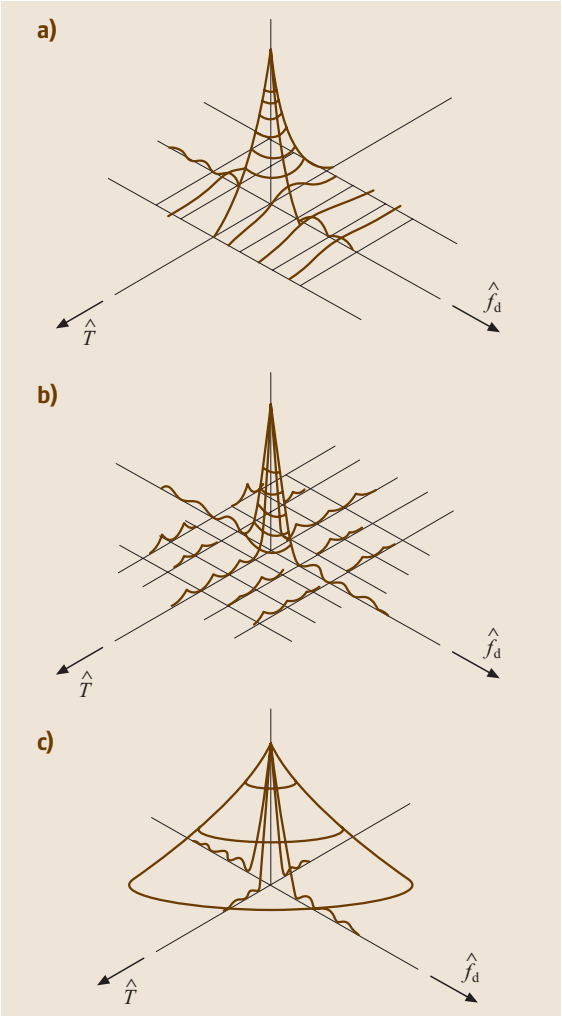


Fig. 5.43a–c Ambiguity function for several SONAR signals: **(a)** rectangular pulse; **(b)** coded pulses; **(c)** chirped FM pulse

5.7.2 Underwater Acoustic Imaging

Imaging can be divided into categories concerned with water column and bottom properties. Here we describe several applications of active SONAR to imaging the ocean.

Water Column Imaging. Backscatter from particulate objects that move along with the water motion (such as biological matter, bubbles sediments) contains velocity information because of the Doppler shift. An acoustic Doppler current profiler (ADCP) might typically consist of three or four source–receivers pointed in slightly different directions but generally up (from the bottom) or down (from a ship). The multiple directions are for resolving motion in different directions. The Doppler shift of the returning scattered field is simply $-2f(v/c)$ (as opposed to the more-complicated long-range waveguide Doppler shift discussed in Sect. 5.4.4), where f is the acoustic frequency, v is the radial velocity of the scatterer (water motion), and c is the sound speed. With three or four narrow-beam transducers, the current vector can be ascertained as a function of distance from an ADCP by gating the received signal and associating a distance with the time gated segment of the signal. Water-column motion associated with internal waves can be determined by this process also where essentially one uses a kind of ADCP points in the horizontal direction. For elab-

Amazon EX1014 Page 205

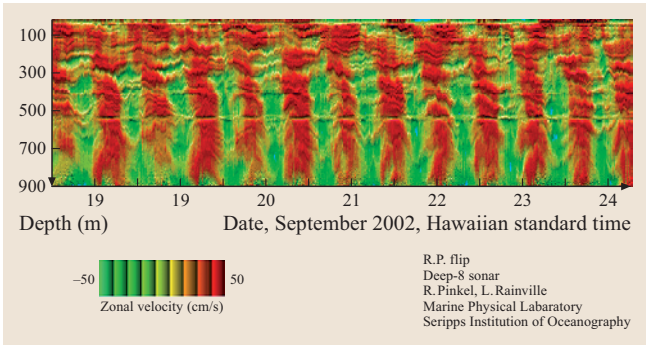


Fig. 5.44 Depth–time representation of the East–West component of water velocity over the Kaena ridge west of Oahu. The dominant signal is the 12.4 h tide, which has downward propagating crests of long vertical wavelength. The SONAR is at ≈390 m, where there is a fine scar in the record. The scar at ≈ 550 m is the echo of the sea floor at 1100 m, aliased back into the record (Courtesy Rob. Pinkel, Scripps Institution of Oceanography)

orate images of currents and the internal wave motion (Fig. 5.44), the Doppler measurements of backscattering off zooplankton are combined with array-processing techniques used in bottom mapping as discussed below.

Bottom Mapping. Because of many industrial applications, there exists a huge literature on multibeam systems for bottom mapping. Among the material available on the web, we would like to refer to two complete courses on submarine acoustic imaging methods available: (1) from the Ocean Mapping Group (University of New Brunswick, Canada) at http://www.omg.unb.ca/GGE/; (2) under a PDF format (*Multibeam Sonar: Theory of Operation*) from L3 Communication SeaBeam Instruments at http://www.mbari.org/data/mbsystem/formatdoc/. The scope of the paragraph below is to describe the basics and keywords associated with bottom mapping in underwater acoustics.

Active SONARs are devices that emit sound with specific waveforms and listen for the echoes from remote objects in the water. Among many applications, SONAR systems are used as echo-sounders for measuring water depths by transmitting acoustic pulses from the ocean surface and listening for their reflection (or echo) from the sea floor. The time between transmission of a pulse and the return of its echo is the time it takes the sound to travel to the bottom and back. Knowing this time and the speed of sound in water allows one to calculate the range to the bottom. This technique has been widely used to map much of the world's water-covered areas and has permitted ships to navigate safely through the world's oceans. The purpose of a large-scale bathymetric survey is to produce accurate depth measurements for many neighboring points on the sea floor such that an accurate picture of the geography of the bottom can be established. To do this efficiently, two things are required of the SONAR used: it must produce accurate

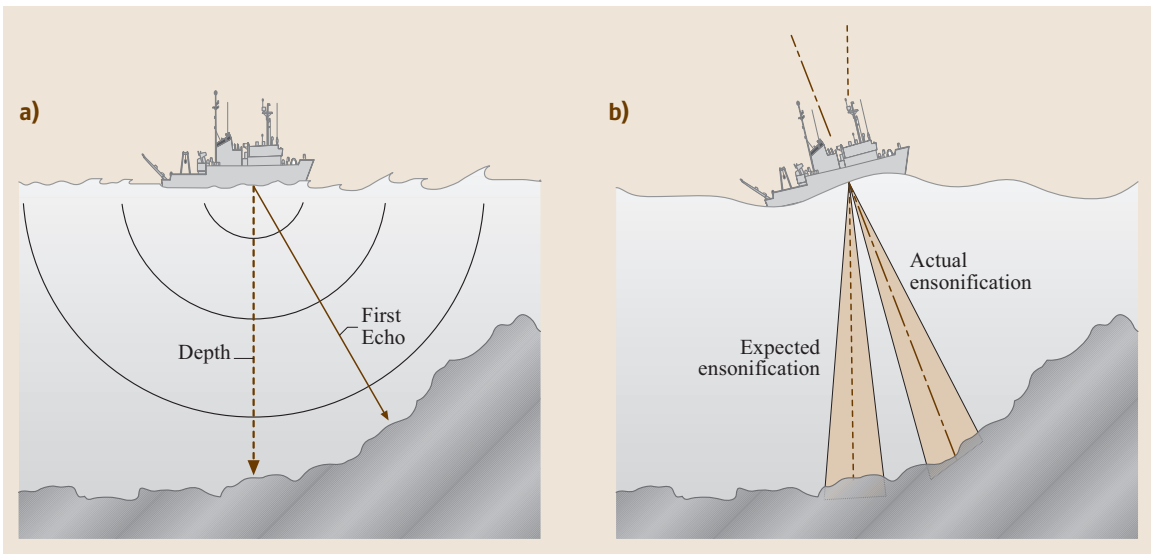


Fig. 5.45a,b Surveying an irregular sea floor **(a)** with a wide-beam SONAR and **(b)** with a narrow-beam SONAR (Courtesy L-3 Communications SeaBeam Instruments)

Amazon EX1014 Page 206

depth measurements that correspond to well-defined locations on the sea floor (that is, specific latitudes and longitudes); and it must be able to make large numbers of these measurements in a reasonable amount of time. In addition, information derived from echo sounding has aided in laying transoceanic telephone cables, exploring and drilling for offshore oil, locating important underwater mineral deposits, and improving our understanding of the Earth's geological processes.

The earliest, most basic and still most widely used echo-sounding devices are *single-beam echo sounders*. The purpose of these instruments is to make serial measurements of the ocean depth at many locations. Recorded depths can be combined with their physical locations to build a three-dimensional map of the ocean floor. In general, single-beam depth sounders are set up to make measurements from a vessel in motion. Until the early 1960s most depth sounding used single-beam echo sounders. These devices make a single depth measurement with each acoustic pulse (or ping) and include both wide- and narrow-beam systems (Fig. 5.45a,b). Relatively inexpensive wide-beam sounders detect echoes within a large solid angle under a vessel and are useful for finding potential hazards for safe navigation. However, these devices are unable to provide much detailed information about the sea bottom. On the other hand, more-expensive narrow-beam sounders are capable of providing high spatial resolution with the small solid angle encompassed by their beam, but can cover only a limited survey area with each ping. Neither system provides a method for creating detailed maps of the sea floor that minimizes ship time and is thus cost-effective.

A *multibeam SONAR* is an instrument that can map more than one location on the ocean floor with a single ping and with higher resolution than those of conventional echo sounders. Effectively, the function of a narrow single-beam echo sounder is performed at several different locations on the bottom at once. These bottom locations are arranged such that they map a contiguous area of the bottom – usually a strip of points in a direction perpendicular to the path of the survey vessel (Fig. 5.46). Clearly, this is highly advantageous. Multibeam SONARs can map complete scans of the bottom in roughly the time it takes for the echo to return from the farthest angle. Because they are far more complex, the cost of a multibeam SONAR can be many times that of a single-beam SONAR. However, this cost is more than compensated by the savings associated with reduced ship operating time. As a consequence, multibeam SONARs are the survey instrument of choice in most mapping applications, particularly in deep ocean environments where ship operating time is expensive [5.51]. Multibeam SONARs often utilize the *Mills Cross* technique which takes advantage of the high resolution obtained from two intersecting focusing regions from a perpendicular linear source and receive array.

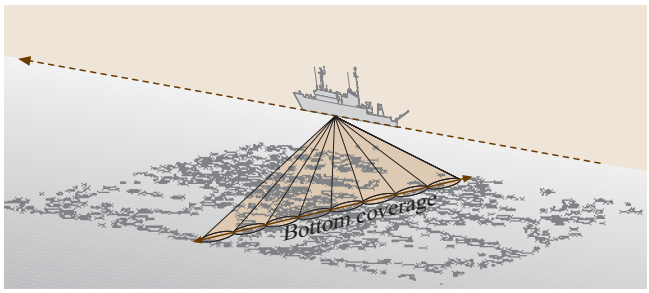


Fig. 5.46 Bottom mapping with a multibeam SONAR system (Courtesy L-3 Communications SeaBeam Instruments)

Instead of measuring the depth to the ocean bottom, a *side-scan SONAR* reveals information about the sea-floor composition by taking advantage of the different sound absorbing and reflecting characteristics of different materials. Some types of material, such as metals or recently extruded volcanic rock, are good reflectors. Clay and silt, on the other hand, do not reflect sound well. Strong reflectors create strong echoes, while weak reflectors create weaker echoes. Knowing these characteristics, you can use the strength of acoustic returns to examine the composition of the sea floor. Reporting the strength of echoes is essentially what a side-scan SONAR is designed to do. Combining bottom-composition information provided by a side-scan SONAR with the depth information from a range-finding SONRA can be a powerful tool for examining the characteristics of an ocean bottom.

The name *side scan* is used for historical reasons – because these SONARs were originally built to be sensitive to echo returns from bottom locations on either side of a survey ship, instead of directly below, as was the case for a traditional single-beam depth sounder [5.52].

Side-scan SONAR employs much of the same hardware and processes as conventional depth-sounding SONAR. Pulses are transmitted by a projector (or array of projectors), and hydrophones receive echoes of those pulses from the ocean floor and pass them to a receiver system. Where side-scan SONAR differs from a depth-sounding system is in the way it processes these returns. While a single-beam echo sounder is only concerned with the time between transmission and the earliest return echo, this first returned echo only marks when

Amazon EX1014 Page 207

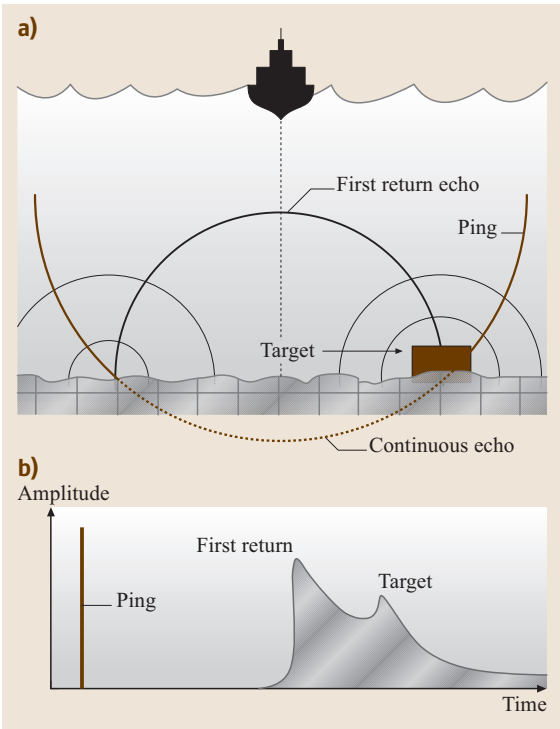


Fig. 5.47 (a) Schematic of the spherical wavefronts scattered by a detailed bottom. (b) Amplitude-versus-time representation of the backscattered signal in a side-scan SONAR system (Courtesy L-3 Communications SeaBeam Instruments)

things start to get interesting to a side-scan SONAR (Fig. 5.47a). As it continues its spherical propagation, the transmitted pulse still interacts with the bottom, thus creating at the receiver a continuous series of weakening echoes in time (Fig. 5.47b).

In the example presented in Fig. 5.47, the side-scan SONAR detects a bottom feature (the box). From the amplitude-versus-time plot, an observer can tell there is a highly reflective feature on the bottom. From the time difference between the first echo (which is presumed to be due to the bottom directly below the SONAR system) and the echo of the reflective feature, the observer can compute the range to the feature from the SONAR.

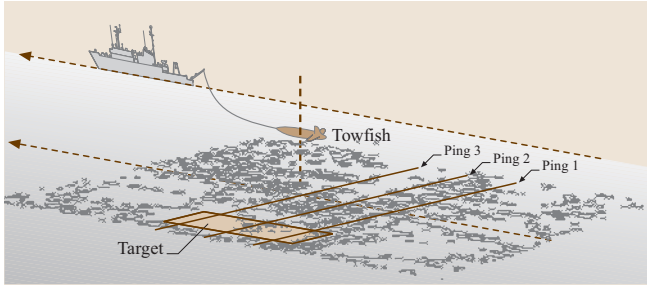


Fig. 5.48 Schematic of a side-scan SONAR imaging the ocean floor with successive pings (Courtesy L-3 Communications SeaBeam Instruments)

As a practical instrument, the simplistic side-scan SONAR described above is not very useful. While it provides the times of echoes, it does not provide their direction. Most side-scan SONARs deal with this problem by introducing some directionality into their projected pulses, and, to some degree, their receivers. This is done by using a line array of projectors to send pulses. The long axis of the line array is oriented parallel to the direction of travel of the SONAR survey vessel (often the arrays are towed behind the ship). In practice, side-scan SONARs tend to mount both the line array and hydrophones on a towfish, a device that is towed in the water below the surface behind a survey vessel (Fig. 5.48). As the survey vessel travels, the towfish transmits and listens to the echoes of a series of pulses. The echoes of each pulse are used to build up amplitude-versus-time plots for each side of the vessel. To adjust for the decline in the strength of echoes due to attenuation, a time-varying gain is applied to the amplitude values so that sea-floor features with similar reflectivities have similar amplitudes. Eventually the noise inherent in the system (which remains constant) becomes comparable to the amplitude of the echo, and the amplified trace becomes dominated by noise. Recording of each trace is usually cut off before this occurs so that the next ping can be transmitted.

Figure 5.49 shows an example of ship-wreck discovery using side-scan SONAR data performed from an automated underwater vehicle (AUV) in a 1500 m-deep ocean.

Often one is interested in sub-bottom profiling that requires high spatial and therefore temporal resolution to image closely spaced interfaces. Frequency-modulated (FM) sweeps provide such high-resolution high-intensity signals after matched filtering. Thus, for example, a matched filter output of a 1 s FM sweep from 2–12 kHz would compresses the energy of the 1 s pulse into one that has the temporal resolution of a 0.1 ms. With such high resolution, reflection coefficients from chirp SONARs can be related to sedimentary characteristics [5.53, 54]. Figure 5.50 is an example of a chirp SONAR output indicating very finely layered interfaces. Figure 5.50a shows the range dependency of the seabed

Amazon EX1014 Page 208

along the cross-shelf track taken by a chirp SONAR. Sand ridges with less acoustic penetration occupy most of the mid-shelf area with a few km spacing. In the outer-shelf area, dipping layers over the distinct *R reflector* are detected. The spikes in the water column at the mid-shelf area are schools of fish near the bottom, which were mostly seen during the surveys conducted in daylight. Figure 5.50b shows the sub-bottom profile of the along-shelf track with acoustic penetration as deep as 40 m. Along-shelf track is relatively less range-dependent. However, several scour marks (≈100 m wide, a few m deep) are detected on the sea floor. These scour marks are attributed to gouging by iceberg keels and the resultant deformations of deeper sublayers is also displayed [A. Turgut, personal communications].

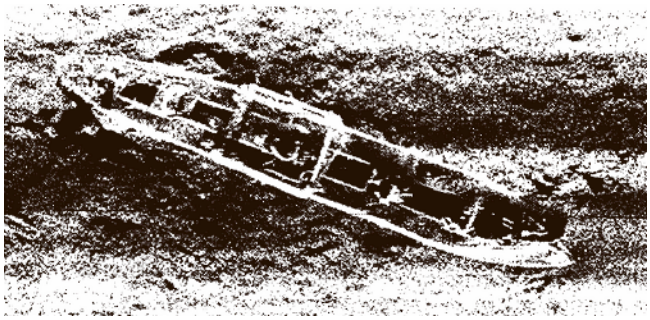


Fig. 5.49 Side-scan SONAR data obtained in 2001 from the HUGIN 3000 AUVs of a ship sunk in the Gulf of Mexico during World War II. C&C Technology Inc. (Courtesy of the National D-Day Museum, New Orleans)

5.7.3 Acoustic Telemetry

Because electromagnetic waves do not propagate in the ocean, underwater acoustic data transmission have many applications, including:

- Communication between two submarines or a submarine and a support vessel
- Communication between a ship and an automated underwater vehicle (AUV) either to get data available without recovering the instruments or to control the instruments onboard the AUV or the AUV itself
- Data transmission to an automated system

Underwater acoustic communications [5.55] are typically achieved using digital signals. We usually distinguish between coherent and incoherent transmissions. For example, incoherent transmissions might consist of transmitting the symbols "0" and "1" at different frequencies (frequency shift keying (FSK)), whereas coherent transmissions might encode using different phases of a given sinusoid (phase shift keying (PSK)) [Fig. 5.51].

Acoustic telemetry can be performed from one source to one receiver in a single-input single-output mode (SISO). To improve performance in terms of data rate and error rate, acoustic networks are now commonly used. In particular, recent works in underwater acoustic communications deal with multiple-input multiple-output (MIMO) configurations (Fig. 5.52) in shallow-water oceans [5.56].

The trend toward MIMO is justified by the fact that the amount of information – known as the information capacity, I – that can be sent between arrays of transmitters and receivers is larger than in a SISO case. Indeed, the SISO information capacity is given by Shannon's famous formula [5.57]:

$$I = \log_2\left(1+\frac{S}{N}\right) \text{ bits s}^{-1}\text{Hz}^{-1}\,, \qquad (5.92)$$

where S is the received signal power, N the noise power and the Shannon capacity I is measured in bits per second per Hertz of bandwidth available for transmission. Equation (5.92) states that the channel capacity increases with the signal-to-noise ratio. In a MIMO configuration with M_t transmitters and M_r receivers, (5.92) is changed into [5.58]:

$$I \sim M_i \log_2\left(1+\frac{SM_r/M_t}{N}\right) \text{ bits s}^{-1}\text{Hz}^{-1}\,, \qquad (5.93)$$

with $M_r \geq M_t$ to be able to decode the M_t separate transmitted signals. Sending M_t different bitstreams is advantageous since it gives a factor of M_t outside the log, linearly increasing the channel capacity I compared to a logarithmic increase when playing on the output power S.

Beside the optimized allocation of power between the M_r and M_t receivers and transmitters (the so-called water-filling approach [5.59]), other particular issues in underwater acoustic telemetry deal with Doppler tracking, channel estimation and signal-to-noise ratios. Those combined parameters often result in a tradeoff between data rate and error rate. For example, low frequencies propagate further with better signal-to-noise ratios and hence lower error rates but the data rate is poor. High frequencies provide high data rates but suffer from strong loss in the acoustic channel, potentially resulting in large error rates.

Another difficulty has to do with multipath propagation and/or reverberation in the ocean, causing intersymbol interference (ISI) and scattering, also called

Amazon EX1014 Page 209

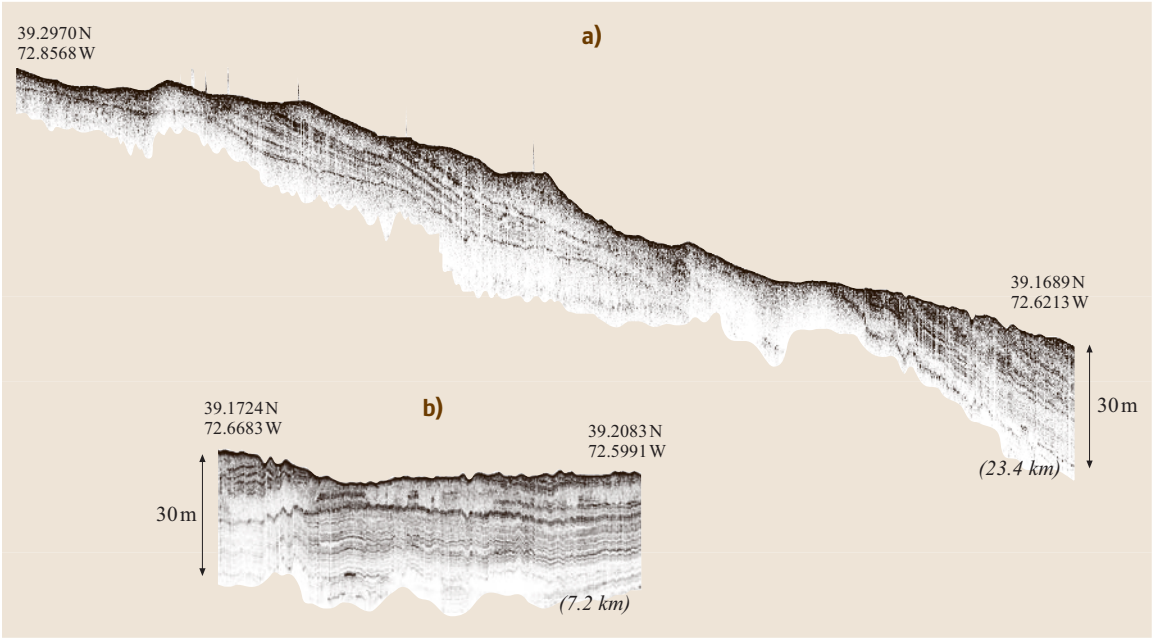


Fig. 5.50a,b Sub-bottom profiles along (a) cross-shelf and (b) along-shelf tracks on the New Jersey shelf collected by a hull-mounted chirp SONAR (2–12 kHz) during the shallow-water acoustic technology experiment (SWAT2000) (Courtesy A. Turgut, Naval Research Laboratory)

the fading effect (Fig. 5.53). As a consequence, the performance of a given system depends strongly on the acoustic environment.

Figure 5.54 shows examples of experimental channel impulse responses recorded at different frequencies in shallow-water waveguides. The difference in temporal dispersion (relative to the acoustic period) between Fig. 5.54a and Fig. 5.54c shows that high-frequency transmissions suffer from stronger ISI and shorter coherence time.

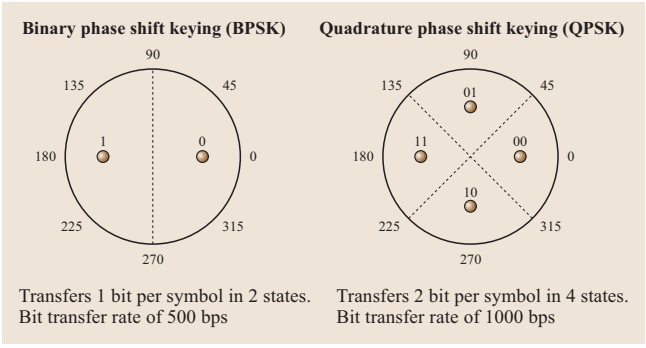


Fig. 5.51 Example of signal space diagrams for coherent communications

In the presence of ISI, Eqs. (5.92, 93) can be generalized so that the channel capacity I still depends on the signal-to-noise ratio S/N where the noise N now includes ISI [5.60]. However, there exist many ways to reduce propagation effects on the quality of the acoustic transmission. One technological solution is to use directional arrays/antenna. Another one is to further code digital signals (CDMA or turbo codes [5.61]) in order to detect and potentially correct transmission errors. But, most importantly, there are many powerful signal-processing techniques derived from telecommunications to take into account at the receiver of the channel impulse response. An efficient one is adaptive equalization that uses a time-dependent channel estimate in order to decode the next symbols from the previously decoded one [5.62]. Other methods to deal with multipath complexities use time-reversal methods, either alone or with equalization methods [5.63–65].

5.7.4 Travel-Time Tomography

Tomography [5.9, 66] generally refers to applying some form of inverse theory to observations in order to infer properties of the propagation medium. The received field from a source emitting a pulse will be spread in

time as a result of multiple paths, in which different paths have different arrival times (Fig. 5.55). Hence the arrival times are related to the acoustic sampling of the medium. In contrast, standard medical X-ray tomography utilizes the different attenuation of the paths rather than arrival time for the inversion process. Since the ocean sound speed is a function of temperature and other oceanographic parameters, the arrival structure is ultimately related to a map of these oceanographic parameters. Thus, measuring the fluctuations of the arrival times through the experiments theoretically leads to the knowledge of the spatial-temporal scale of the ocean fluctuations.

Tomographic inversion in the ocean has typically relied on these three points. First, only the arrival time (and not the amplitude) of the multipath structure is used as an observable (Table 5.2) [5.67]. Enhanced time-of-arrival resolution is typically obtained using pulse-compression techniques [5.68] as mentioned in the bottom-mapping section above. Depending on the experimental configuration, a choice of compression is to be made between M-sequences [5.69], which are strongly Doppler sensitive but have low temporal side-lobes and frequency-modulated chirps that are Doppler insensitive with higher side-lobes (Fig. 5.43). Second, the inversion is performed by comparing the experimental arrival times to those given by a model (Fig. 5.56). Last, tomographic inversion algorithm classically deals with a linearized problem. This means that the model has to match the experimental data so that the inversion only deals with small perturbations.

Thus, ocean tomography starts from a sound-speed profile $c(\boldsymbol{r})$ on which small perturbations are added $\delta c(\boldsymbol{r}, t) \ll c$. The ocean model $c(\boldsymbol{r})$ has to be accurate enough to relate without ambiguity an experimentally measured travel time T_i to a model-deduced ray path Γ_i. Typically, some baseline oceanographic information is known so that one searches for departures from this baseline information. The perturbation infers a change of travel time δT_i along the ray such that, in a first linear approximation

$$\delta T_i \approx \int_{\Gamma_i} \frac{-\delta c}{c^2} \mathrm{d}s \,, \tag{5.94}$$

where Γ_i correspond to the Fermat path of the unperturbed ray. An efficient implementation of the inversion procedure utilizes a projection of the local sound-speed fluctuations $\delta c(\boldsymbol{r}, t)$ on a set of chosen functions $\Psi_k(\boldsymbol{r})$ that constitutes a basis of the ocean structure. We have

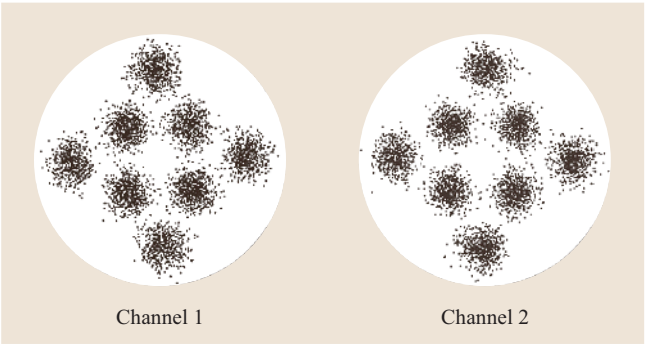


Fig. 5.52 Experimental examples of eight quadrature amplitude modulation (QAM) transmissions in a multiple-input multiple-output configuration (MIMO) at 3.5 kHz in a 9 km-long, 120 m-deep shallow-water ocean. The SNR is 30 dB on channel 1 and 2, the symbol duration is 1 ms (data rate is 8 kB/s per channel) and bit error rate (BER) is 1×10^{-4} (Courtesy H.C. Song, Scripps Institution of Oceanography)

then

$$\delta c(\boldsymbol{r}, t) = \sum_{k=1}^{N} p_k(t) \psi_k(\boldsymbol{r}) \,, \tag{5.95}$$

where $p_k(t)$ is a set of unknown parameters. In its most primitive form, the ocean can be discretized into elementary cells, each cell being characterized by an unknown sound-speed perturbation p_k. Combining the two above

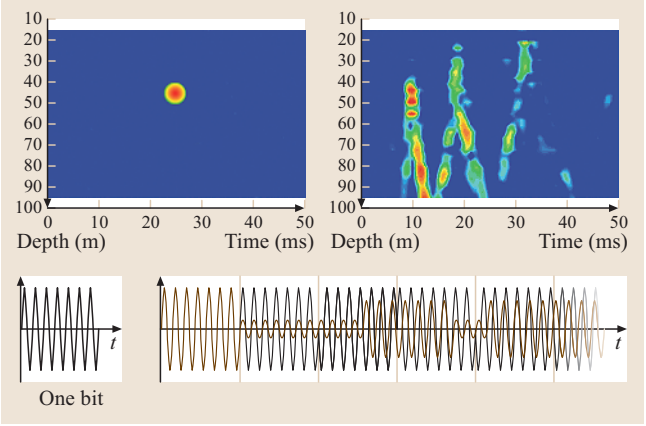


Fig. 5.53 A coherent digital communication system must deal with the intersymbol interference caused by dispersive multipath environment of the ocean waveguide (*top right*). When a sequence of phase-shifted symbols (*in black*) are sent, the resulting transmission (*in brown*) is fading out because of symbol interference

Amazon EX1014 Page 211

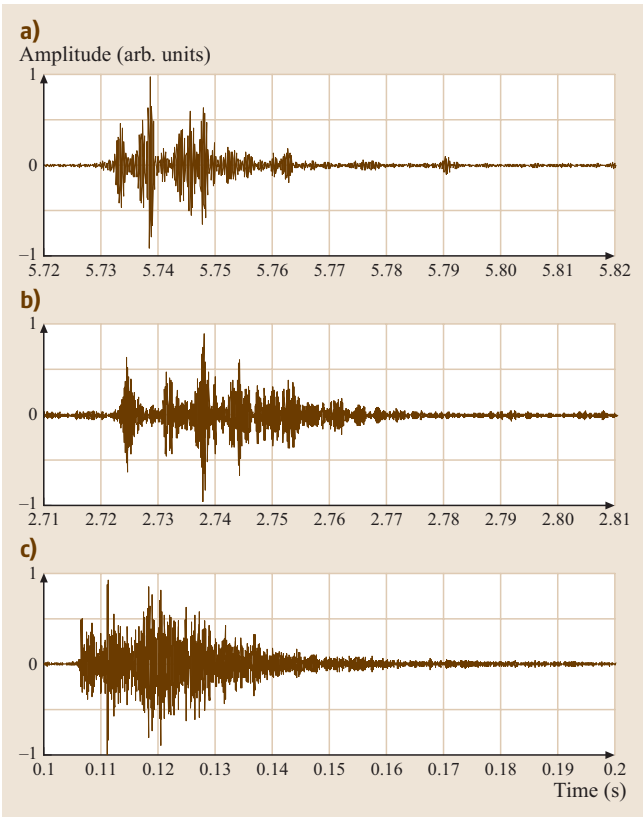


Fig. 5.54a–c Examples of transfer functions recorded at sea in different shallow-water environments at various frequencies. **(a)** Central frequency = 3.5 kHz with a 1 kHz bandwidth, 10 km range in a 120 m-deep waveguide. **(b)** Central frequency = 6.5 kHz with a 2 kHz bandwidth, 4 km range in a 50 m-deep waveguide. **(c)** Central frequency = 15 kHz with a 10 kHz bandwidth, 160 m range in a 12 m-deep waveguide

equations, it follows:

$$\delta T_i = \int_{\Gamma_i} \frac{-1}{c^2} \sum_{k=1}^{N} p_k \psi_k(\boldsymbol{r})\, \mathrm{d}s$$
$$= \sum_{k=1}^{N} p_k \int_{\Gamma_i} \frac{-\Psi_k(\boldsymbol{r})}{c^2}\, \mathrm{d}s = \sum_{k=1}^{N} p_k G_{ik} \,. \qquad (5.96)$$

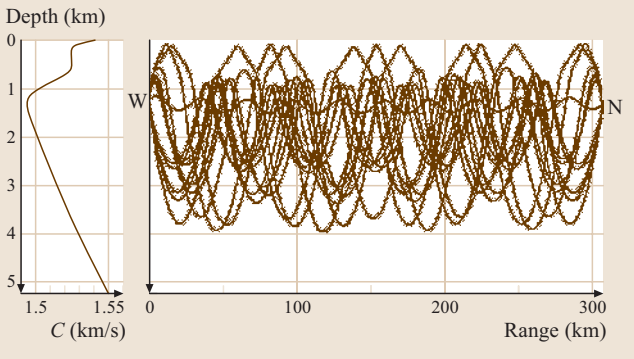


Fig. 5.55 *Left*: reference sound-speed profile $C_0(z)$. *Right*: corresponding ray traces. Table 5.2 identifies all plotted rays. Note the shallow and deep turning groups of rays as well as the axial ray (after [5.70]) (Courtesy Peter Worcester, Scripps Institution of Oceanography)

Allowing for some noise in the measurement and assuming a set of arrival times δT_i, $i \in [1, M]$, (5.94) can be rewritten in an algebraic form [5.71]:

$$\delta \boldsymbol{T} = \boldsymbol{G}\boldsymbol{p} + \boldsymbol{n} \,. \qquad (5.97)$$

There exists many algorithms to obtain an estimate of the parameters $\tilde{\boldsymbol{p}}$ of the parameters $\boldsymbol{p}$ from the data $\boldsymbol{\delta T}$ knowing the matrix $\boldsymbol{G}$. For example, when $N > M$, a least-mean-square estimator gives:

$$\tilde{\boldsymbol{p}} = G^T (G G^T)^{-1} \boldsymbol{\delta T} \,. \qquad (5.98)$$

Considerations about pertinent functions $\Psi_k(\mathbf{r})$ such as empirical orthogonal functions (EOFs) and the optimal inversion procedure can be found in the literature [5.72, 73].

Tomographic experiments have been performed to greater than megameter ranges. For example, two major experiments in the 1990s were performed by the Thetis 2 group in the western Mediterranean over a seasonal cycle [5.74] and by the North Pacific Acoustic Laboratory (NPAL, http://npal.ucsd.edu) in the North Pacific basin. The NPAL experiment was directed at using travel-time data obtained from a few acoustic sources and receivers located throughout the North Pacific Ocean to study temperature variations at large scale [5.75, 76]. The idea behind the project, known as acoustic thermometry of ocean climate (ATOC), is that sound travels slightly faster in warm water than in cold water. Thus, precisely measuring the time it takes for a sound signal to travel between two points reveals the average temperature along the path. Sound travels at about 1500 m/s in water, while typical changes in the sound speed of the ocean as a result of temperature changes are only 5–10 m/s. The tomography

Amazon EX1014 Page 212

technique is very sensitive, and experiments so far have shown that temperatures in the ocean can be measured to a precision of 0.01 °C, which is needed to detect subtle variations and trends of the ocean basin.

New trends in ocean tomography deal with full-wave inversion involving the use of both travel times and amplitudes of echoes for a better accuracy in the inversion algorithm. In this case, a full-wave kernel for acoustic propagation has to be used [5.77], which includes the sensitivity of the whole Green's functions (both travel times and amplitudes) to sound speed variations. In the case of high frequencies, the application of the travel-time-sensitivity kernel to an ocean acoustic waveguide gives a picture close to the ray-theoretic one. However, in the low-frequency case of interest in ocean acoustic tomography, there are significant deviations. Low-frequency travel times are sensitive to sound-speed changes in Fresnel-zone-scale areas surrounding the eigen-rays, but not on the eigen-rays themselves, where the sensitivity is zero. This diffraction phenomenon known as the *banana–doughnut* [5.78] debate is still actively discussed in the field of ocean and seismic tomography [5.79].

Table 5.2 Identification of rays (after [5.70]). The identifier is $\pm n(\theta_s, \theta_R, \hat{z}^+, \hat{z}^-)$, where positive (negative) rays depart upward (downward) from the source, n is the total number of upper and lower turning points, θ_s is the departure angle at the source, θ_R is the arrival angle at the receiver, and $\hat{z}^+$ and $\hat{z}^-$ are the upper and lower turning depths, respectively (Courtesy Peter Worcester, Scripps Institution of Oceanography)

	$\pm n$	θ_s (deg)	θ_R (deg)	$\hat{z}^+$ (m)	$\hat{z}^-$ (m)
1	8	11.6	11.6	126	3801
2	-8	-11.6	-11.7	125	3803
3	9	12.0	-12.0	99	3932
4	11	11.1	-11.1	617	3624
5	-11	-10.8	10.2	737	3303
6	12	9.7	9.7	776	3170
7	-12	-9.6	-9.7	780	3156
8	13	9.3	-9.3	809	3046
9	-13	-8.2	8.3	881	2746
10	14	7.9	8.0	901	2653
11	-14	-7.8	-7.9	905	2638
12	15	7.4	-7.5	925	2546
13	19	3.5	-3.8	1118	1790
	20	1.2	1.7	1221	1507

5.8 Acoustics and Marine Animals

In the context of contemporary acoustics, marine animal life is typically divided into the categories of marine mammals and non-marine mammals which include fish and others sea animals. The acoustics dealing with fish relates to either finding, counting and catching them. The acoustics concerned with marine mammals is for either studying their behavior or determining to what extent manmade sounds are harmful to them.

5.8.1 Fisheries Acoustics

An extensive introduction to fisheries acoustics is [5.80] and can be found online at http://www.fao.org/docrep/X5818E/x5818e00.htm#Contents. For more-detailed information, we recommend two special issues in [5.81, 82].

Following the development of SONAR systems, acoustic technology has had a major impact on fishing and on fisheries research. SONARs and echo sounders are now used as standard tools to search for concentrations of fish or to assess for biomass stock. With SONAR, it is possible to sample the water column much faster than trawl fishing. Moreover, SONARs have helped in our understanding of how fish are distributed in the ocean and how they behave over time. Depending on the fish density in the water column, echo-counting or echo-integration [5.83] are used to evaluate the fish biomass in the water column. Research on the signature of the echo return for a specific fish [5.84] or for a fish school [5.85, 86] is still an active area of research.

Fisheries acoustics experiments are performed with SONAR in the same way as bottom profiling [5.87–89]. The ship covers the area of interest by transect lines [5.90] while the SONAR sends and receives acoustic pulses (pings) as often as allowed by the SONAR system and the water depth (the signal from the previous ping has to die out before the next ping is transmitted). Typical SONAR frequencies are 38 kHz, 70 kHz, and 120 kHz. An echogram is a display of the instantaneous received intensity along the ship track. The echograms in Fig. 5.57a,b reveal individual fish echoes as well as fish school backscattered signals.

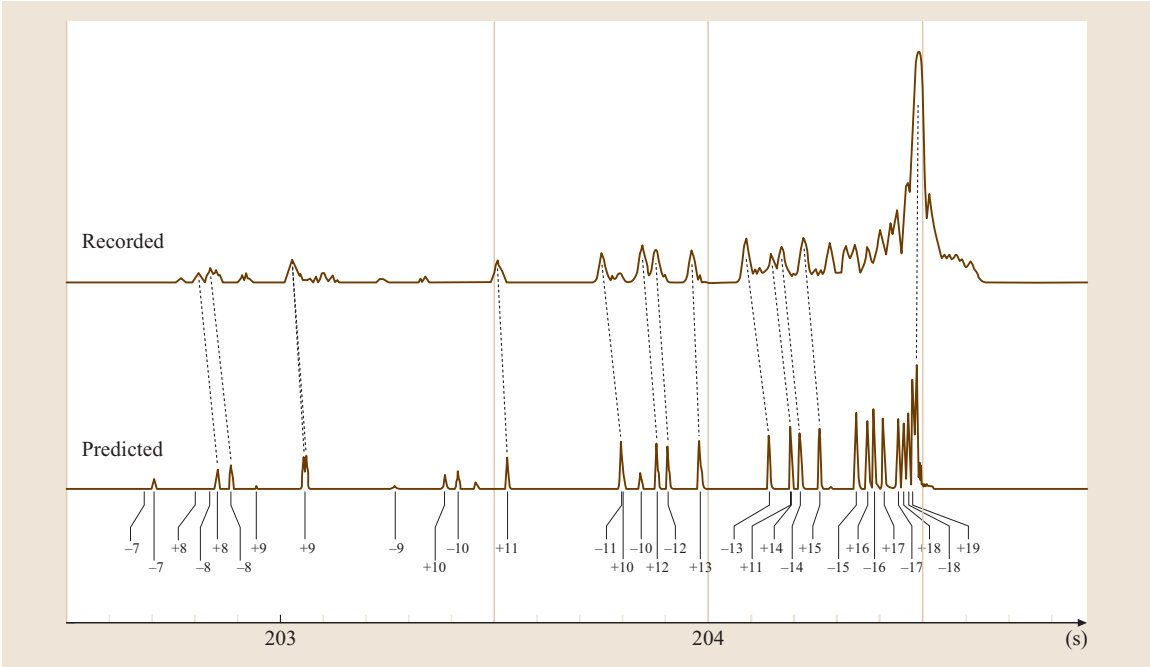


Fig. 5.56 Comparison of the predicted and measured arrival patterns (after [5.70]). The predicted arrival pattern was calculated from $C_0(z)$ as shown in Fig. 5.55. Geometric arrivals are labeled $\pm n$ as in Table 5.2. The peaks connected by *dashed lines* are the ray arrivals actually used (Courtesy Peter Worcester, Scripps Institution of Oceanography)

From a practical point of view, the relationship between an acoustic target and its received echo can be understood from the SONAR equation. With the procedure of Sect. 5.3.2 and 5.3.3, the echo level (in decibels) of a given target is

$$\mathrm{EL} = \mathrm{SL} + \mathrm{RG} + \mathrm{TS} - 2\mathrm{TL}\,, \tag{5.99}$$

where SL is the source level and TL is the geometrical spreading loss in the medium. The target strength *TS* is defined as $\mathrm{TS} = 10\log_1 0(\sigma/4\pi)$, where σ is the backscattering cross section of the target. The receiver gain RG is often set up as a time-varied gain (TVG), which compensates for the geometrical spreading loss.

In (5.99), the target is supposed to be on the acoustic axis of the transducer. In general, a single-beam SONAR cannot distinguish between a small target on the transducer axis and a big target off-axis. The two echoes may have the same amplitude because the lower *TS* for the small target will be compensated by the off-axis power loss for the big target. One way to remove this ambiguity is to use a dual-beam SONAR [5.91] (or split-beam SONAR) that provides the position of the target in the beam pattern.

Echo-integration consists of integrating in time (as changed into depth from $R = ct/2$) the received intensity coming from the fish along the ship transects [5.92]. This value is then converted to a biomass via the backscattering cross section σ. In the case of a single target (Fig. 5.57a), the intensity of the echo E_1 is

$$E_1 = \overline{\sigma}\phi^2(r)\left[\frac{\exp(-2\beta r)}{r^4}\right]\,, \tag{5.100}$$

where $\phi^2(R)$ is the depth-dependent (or time-varying) gain; the term in bracket describes the geometrical spreading $(1/r^4)$ and loss $[\exp(-2\beta r)]$ of the echo during its round trip between the source and the receiver and $\overline{\sigma}$is the scattering cross section of the target averaged over the bandwidth of the transmitted signal. In (5.100) we did not include the effect of the beam pattern and the sensitivity of the system in emission-reception. These parameters depend on the type of SONAR used and are often measured in situ from a calibration experiment [5.93,94]. In the case of a distributed targets in the water column [5.95,96] (Fig. 5.57b), the received intensity E_h is integrated over a layer h at a depth r, which

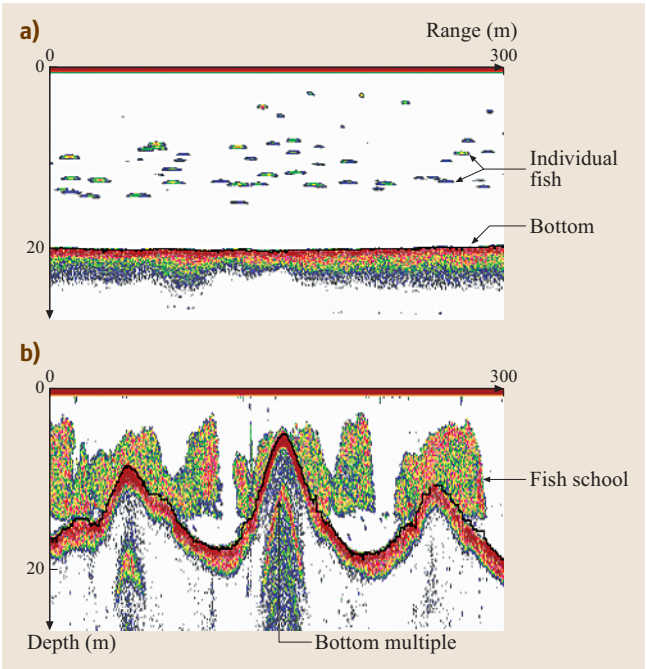


Fig. 5.57a,b Typical echogram obtained during an echo-integration campaign using a single-beam SONAR on the Gambie river. **(a)** Biomass made of individual fish. **(b)** Biomass made of fish school (Courtesy Jean Guillard, INRA)

gives:

$$E_h = h\overline{\sigma}n\phi^2(r)\left[\frac{\exp(-2\beta r)}{r^2}\right], \qquad (5.101)$$

where n corresponds to the density of fish per unit volume in the layer h. Equation (5.101) is based on the linearity principle assumption, which states that, on the average over many pings, the intensity E_h is equal to the sum of the intensity produced by each fish individually [5.97].

In the case of either a single or multiple targets, the idea is to relate directly the echo-integrated result E_1 or E_h to the fish scattering amplitudes $\overline{\sigma}$ or $n\overline{\sigma}$. To that goal, the time-varying gain $\phi^2(r)$ has to compensate appropriately for the geometric and attenuation loss. For a volume integration, $\phi^2(r) = R^2\exp(2\beta r)$, the so-called $20\log r$ gain is used while a $40\log r$ gain is applied in the case of individual echoes.

As a matter of fact, acoustic instruments, such as echo sounders and SONAR, are unique as underwater sampling tools since they detect objects at ranges of many hundreds of meters, independent of water clarity and depth. However, until recently, these instruments could only operate in two dimensions, providing observational slices through the water column. New trends in fisheries acoustics incorporate the use of multibeam SONAR – typically used in bottom mapping, see Sect. 5.7.2 – which provides detailed data describing the internal and external three-dimensional (3-D) structure of underwater objects such as fish schools [5.98] (Fig. 5.58). Multibeam SONARs are now used in a wide variety of fisheries research applications including: (1) three-dimensional descriptions of school structure and position in the water column [5.99]; knowledge of schooling is vital for understanding many aspects of fish (and fisheries) ecology [5.100]; (2) detailed internal images of fish schools, providing insights into the organization of fish within a school, for example, indicating the presence of large gaps or vacuoles and areas of higher densities or nuclei (Fig. 5.58b, d) [5.101].

In general, one tries to convert the echo-integration result into a biomass or fish density. This requires the knowledge of the target strength TS or the equivalent backscattering cross section σ of the target under

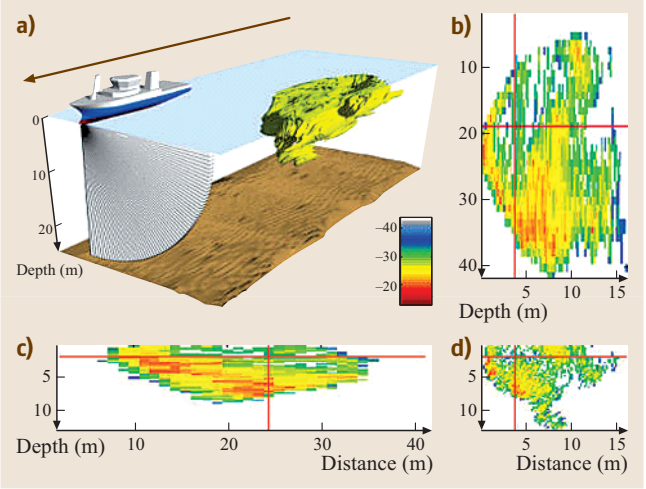


Fig. 5.58a–d Images of a fish school of *Sardinella aurita* from a multibeam SONAR. *Arrows* indicate vessel route. **(a)** 3-D reconstruction of the school. Multibeam SONAR receiving beams are shown at the front of the vessel. Remaining panels show cross sections of density in fish from: **(b)** the horizontal plane, **(c)** the vertical plane along-ships, **(d)** the vertical plane athwart ships. Red cross-hairs indicate location of the other two cross sections (Courtesy Francois Gerlotto, IRD)

Amazon EX1014 Page 215

investigation [5.102]. Several models attempt to develop equations expressing σ/λ^2 as a function of L/λ, where L is the fish length. However, physiological and behavioral differences between species make a more-empirical approach necessary, which often is of the form:

$$\mathrm{TS} = 20\log L + b\,, \tag{5.102}$$

where b depends on the acoustic frequency and the fish species. For example, we have $b = -71.3$ dB for herring and $b = -67.4$ dB for cod at 38 kHz, which makes the cod scattering cross section twice that of herring for the same fish length. In situ measurements of TS with fish at sea [5.103, 104] or in cages [5.105] have also been attempted to classify fish species acoustically.

Similar works on size distribution assessment have been performed at higher frequency (larger than 500 kHz) on small fish or zooplankton using multi-element arrays [5.106] and wide-band or multi-frequency methods [5.107, 108]. The advantage of combining the acoustic signature of fish at various frequencies is to provide an accurate target sizing. When multi-elements are used, then the position of each individual inside the acoustic beam is known. Using simultaneously multi-element arrays and broadband approaches may also be the key for the unsolved problem of species identification in fisheries acoustics.

In conclusion, SONAR systems and echo integration are now well-established techniques for the measurement of fish abundance. They provide quick results and accurate information about the pelagic fish distribution in the area covered by the ship during the survey. The recent development of multibeam SONAR has improved the reliability of the acoustic results and now provides 3-D information about fish-school size and shape. However, some important sources of error remain when performing echo-integration, among which are: (1) the discrimination between fish echoes and unwanted target echoes, (2) the difficulty of adequately sampling a large area in a limited time, (3) the problems related to the fish behavior (escaping from the transect line, for example) and (4) the physiological parameters that determine the fish target strength.

5.8.2 Marine Mammal Acoustics

In order to put into perspective both the sound levels that mammals emit and hear, we mention an assortment of sounds and noise found in the ocean. Note that the underwater acoustic decibel scale used is, as per the Appendix, relative to 1 μPa. For source levels, one is also referencing the sound level at 1 m. Lightening can be as high has 260 dB and a seafloor volcanic eruption can be as high as 255 dB. Heavy rain increases the background noise by as much as 35 dB in a band from a few hundred Hz to 20 kHz Snapping shrimp individually can have broadband source levels greater than 185 dB while fish choruses can raise ambient noise levels 20 dB in the range of 50–5000 Hz. Of course, the Wenz curves in Fig. 5.15 show a distribution of natural and manmade noise levels whereas specific examples of manmade noise are given in Table 5.3.

Table 5.3 Examples of manmade noise

Ships underway	**Broadband source level (dB re 1 μPa at 1 m)**
Tug and barge (18 km/hour)	171
Supply ship (example: Kigoriak)	181
Large tanker	186
Icebreaking	193
Seismic survey	**Broadband source level (dB re 1 μPa at 1 m)**
Air-gun array (32 guns)	259 (peak)
Military SONARS	**Broadband source level (dB re 1 μPa at 1 m)**
AN/SQS-53C (US Navy tactical mid-frequency SONAR, center frequencies 2.6 and 3.3 kHz)	235
AN/SQS-56 (US Navy tactical mid-frequency sonar, center frequencies 6.8 to 8.2 kHz)	223
Surveillance Towed Array Sensor System Low Frequency Active (SURTASS-LFA) (100–500 Hz)	215 dB per projector, with up to 18 projectors in a vertical array operating simultaneously
Ocean acoustic studies	**Broadband source level (dB re 1 μPa at 1 m)**
Heard island feasibility test (HIFT) (center frequency 57 Hz)	206 dB for a single projector, with up to 5 projectors in a vertical array operating simultaneously
Acoustic thermometry of ocean climate (ATOC)/North Pacific acoustic laboratory (NPAL) (center frequency 75 Hz)	195

Amazon EX1014 Page 216

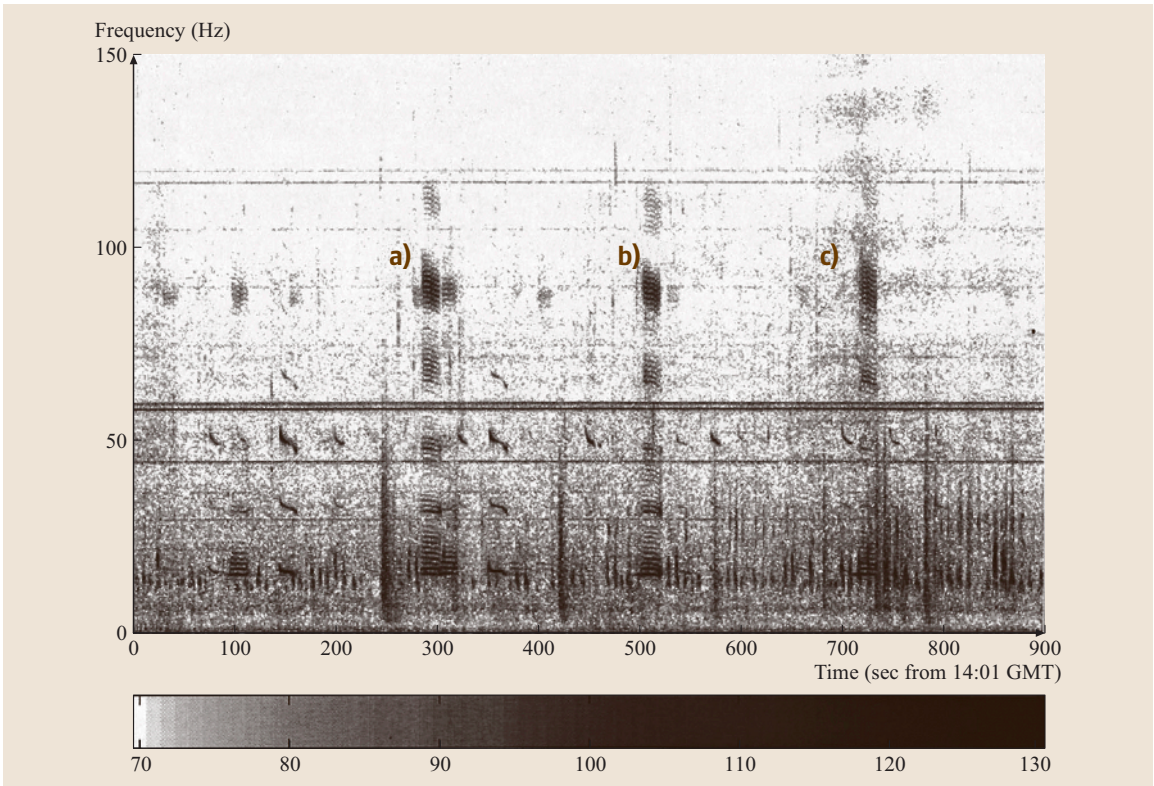


Fig. 5.59 Whale spectrogram power spectral density are in units of dB re 1 μPa^2/Hz. The blue-whale broadband signals denoted by (*a*), (*b*) and (*c*) are designated "type A calls". The FM sweeps are "type B calls". The multiple vertical energy bands between 20 and 30 Hz have the appearance of fin-whale vocalizations [5.109]

Marine mammal sounds span the spectrum from 10–200 000 kHz. Examples are: blue (see spectrogram in Fig. 5.59) and fin whales in the 20 Hz region with source levels as high as 190 dB, Wedell seals in the 1–10 kHz region producing 193 dB levels; bottlenose dolphin, 228 dB in a noisy background, sperm whale clicks are the loudest recorded levels at 232 dB. A list of typical levels is shown in Table 5.4. Most of the levels listed are substantial and strongly suggest acoustics as a modality for monitoring marine mammals. Thus, for example, Fig. 5.60 shows the acoustically derived track of a blue whale over 43 days and thousands of kilometers as determined from SOSUS arrays (see Introduction to this chapter) in the Atlantic Ocean.

The issues mostly dealt with in marine mammal acoustics are: understanding the physiology and behavior associated with the production and reception of sounds, and the effects that manmade sounds have on marine mammals from actual physical harm to causing changes in behavior. Physical harm includes actual

Table 5.4 Marine-mammal sound levels

Source	Broadband source level (dB re 1 μPa at 1 m)
Sperm whale clicks	163–223
Beluga whale echo-location click	206–225 (peak to peak)
White-beaked dolphin echo-location clicks	194–219 (peak to peak)
Spinner dolphin pulse bursts	108–115
Bottlenose dolphin whistles	125–173
Fin whale moans	155–186
Blue whate moans	155–188
Gray whale moans	142–185
Bowhead whale tonals, moans and song	128–189
Humpback whale song	144–174
Humpback whale fluke and flipper slap	183–192
Southern right whale pulsive call	172–187
Snapping shrimp	183–189 (peak to peak)

Amazon EX1014 Page 217

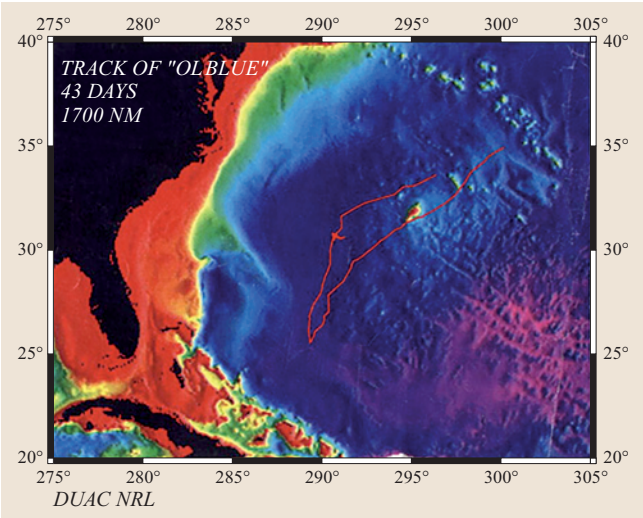


Fig. 5.60 Track of a blue whale in the Atlantic Ocean determined by US Navy personnel operating SOSUS stations. (Courtesy Clyde Nishimura, Naval Research Laboratory and Chris Clark, Cornell University)

damage (acoustic trauma) and permanent and temporary threshold shifts in hearing. A major ongoing effort is to determine the safe levels of manmade sounds. Acoustics has now become an important research tool in the marine mammal arena (e.g. [5.110–115].

Tables 5.3 and 5.4 have been taken form University of Rhode web site: http://www.dosits.org/science/ssea/2.htm with references to [5.24, 25, 116].

Advances in the bandwidth and data-storage capabilities of sea-floor autonomous acoustic recording packages (ARPs) have enabled the study of odontocete (toothed-whale) long-term acoustic behavior. Figure 5.61 illustrates one day of broadband (10 Hz–100 kHz) acoustic data collected in the Santa Barbara Channel. The passage of vocalizing dolphins is recorded by the aggregate spectra from their echolocation clicks (>20 kHz) and whistles (5–15 kHz). Varying proportions of clicks and whistles are seen for each calling

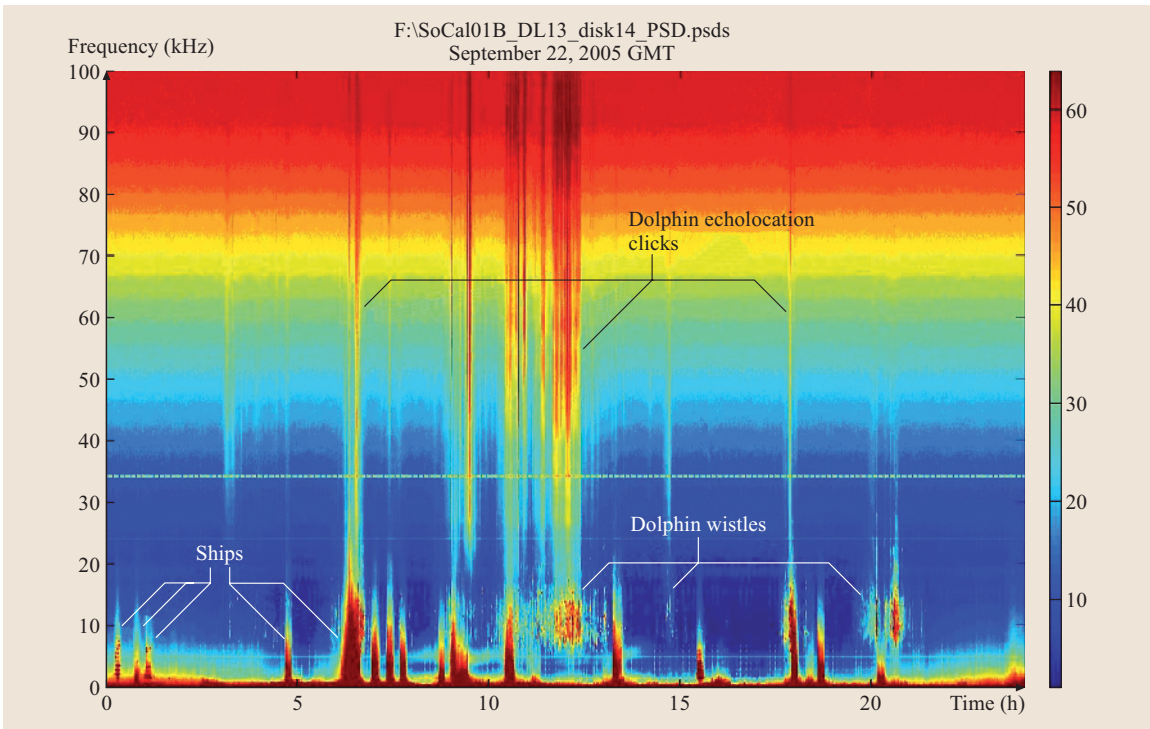


Fig. 5.61 Broadband (10 Hz–100 kHz) acoustic data collected in the Santa Barbara Channel, illustrating spectra from dolphin echolocation clicks (> 20 kHz) and whistles (5–15 kHz) as seen in a daily sonogram (Sept 22, 2005). Passages of individual commercial ships are seen at mid and low frequencies (< 15 kHz) (Courtesy John Hildebrand, Scripps Institution of Oceanography)

Amazon EX1014 Page 218

bout. These data allow for study of the acoustic behavior under varying conditions (day–night) and for the determination of the seasonal presence of calling animals.

5.A Appendix: Units

The decibel (dB) is the dominant unit in underwater acoustics and denotes a ratio of intensities (not pressures) expressed in terms of a logarithmic (base 10) scale. Two intensities, I_1 and I_2 have a ratio I_1/I_2 in decibels of $10\log I_1/I_2$ dB. Absolute intensities can therefore be expressed by using a reference intensity. The presently accepted reference intensity in underwater acoustics is based on a reference pressure of one micropascal. Therefore, taking I_2 as the intensity of a plane wave of pressure 1 μPa, a sound wave having an intensity, of, say, one million times that of a plane wave of rms pressure 1 μPa has a level of $10\log(10^6/1) \equiv 60$ dB re 1 μPa. Pressure (p) ratios are expressed in dB re 1 μPa by taking $20\log p_1/p_2$, where it is understood that the reference originates from the intensity of a plane wave of pressure equal to 1 μPa.

The average intensity, I, of a plane wave with rms pressure p in a medium of density ρ and sound speed c is $I = p^2/\rho c$. In seawater, $(\rho c)_{\text{water}}$ is 1.5×10^6 Pa sm^{-1} so that a plane wave of rms pressure 1 μ Pa has an intensity of 6.76×10^{-19} W/m^2.

For reference, we also mention the relevant units in air, where the reference pressure is related, more or less, to the minimum level of sound we can hear is. This is a pressure level 26 dB higher than the water reference. Further, since the intensity level associated with this reference is 10^{-12} W/m^2. Therefore, one should be careful when relating units between water and air, as the latter's reference intensity is higher.

References

5.1 W.A. Kuperman, J.F. Lynch: Shallow-water acoustics, Phys. Today **57**, 55–61 (2004)
5.2 L.M. Brekhovskikh: *Waves in Layered Media*, 2nd edn. (Academic, New York 1980)
5.3 L.M. Brekhovskikh, Y.P. Lysanov: *Fundamentals of Ocean Acoustics* (Springer, Berlin, Heidelberg 1991)
5.4 F.B. Jensen, W.A. Kuperman, M.B. Porter, H. Schmidt: *Computational Ocean Acoustics* (Springer, Berlin, New York 2000)
5.5 B.G. Katsnelson, V.G. Petnikov: *Shallow Water Acoustics* (Springer, Berlin, Heidelberg 2001)
5.6 J.B. Keller, J.S. Papadakis (Eds.): *Wave Propagation in Underwater Acoustics* (Springer Berlin, New York 1977)
5.7 H. Medwin, C.S. Clay: *Fundamentals of Acoustical Oceanography* (Academic, San Diego 1997)
5.8 H. Medwin: *Sounds in the Sea: From Ocean Acoustics to Acoustical Oceanography* (Cambridge Univ. Press, Cambridge 2005)
5.9 W. Munk, P. Worcester, C. Wunsch: *Ocean Acoustic Tomography* (Cambridge Univ. Press, Cambridge 1995)
5.10 D. Ross: *Mechanics of Underwater Noise* (Pergamon, New York 1976)
5.11 B.D. Dushaw, P.F. Worcester, B.D. Cornuelle, B.M. Howe: On equations for the speed of sound in seawater, J. Acoust. Soc. Am. **93**, 255–275 (1993)
5.12 J.L. Spiesberger, K. Metzger: A new algorithm for sound speed in seawater, J. Acoust. Soc. Am. **89**, 2677–2688 (1991)
5.13 J. Northrup, J.G. Colborn: Sofar channel axial sound speed and depth in the Atlantic Ocean, J. Geophys. Res. **79**, 5633–5641 (1974)
5.14 W.H. Munk: Internal waves and small scale processes. In: *Evolution of Physical Oceanography*, ed. by B. Warren, C. Wunsch (MIT, Cambridge 1981) pp. 264–291
5.15 O.B. Wilson: *An Introduction to the Theory and Design of Sonar Transducers* (Government Printing Office, Washington 1985)
5.16 R.J. Urick: *Principles of Underwater Sound*, 3rd edn. (McGraw-Hill, New York 1983)
5.17 R.P. Chapman, J.R. Marchall: Reverberation from deep scattering layers in the Western North Atlantic, J. Acoust. Soc. Am. **40**, 405–411 (1966)
5.18 J.A. Ogilvy: Wave scattering from rough surfaces, Rep. Prog. Phys. **50**, 1553–1608 (1987)
5.19 E.I. Thorsos: Acoustic scattering from a "Pierson-Moskowitz" sea surface, J. Acoust. Soc. Am. **89**, 335–349 (1990)
5.20 P.H. Dahl: On bistatic sea surface scattering: Field measurements and modeling, J. Acoust. Soc. Am. **105**, 2155–2169 (1999)
5.21 R.P. Chapman, H.H. Harris: Surface backscatterring strengths measured with explosive sound sources, J. Acoust. Soc. Am. **34**, 1592–1597 (1962)
5.22 M. Nicholas, P.M. Ogden, F.T. Erskine: Improved empirical descriptions for acoustic surface backscatter in the ocean, IEEE J. Ocean. Eng. **23**, 81–95 (1998)

Amazon EX1014 Page 219

5.23 N.C. Makris, S.C. Chia, L.T. Fialkowski: The bi-azimuthal scattering distribution of an abyssal hill, J. Acoust. Soc. Am. **106**, 2491–2512 (1999)

5.24 G.M. Wenz: Acoustics ambient noise in the ocean: spectra and sources, J. Acoust. Soc. Am **34**, 1936–1956 (1962)

5.25 R.K. Andrew, B.M. Howe, J.A. Mercer, M.A. Dzieciuch: Ocean ambient sound: Comparing the 1960s with the 1990s for a receiver off the California coast, Acoust. Res. Lett. Online **3**(2), 65–70 (2002)

5.26 M.A. McDonald, J.A. Hildebrand, S.W. Wiggins: Increases in deep ocean ambient noise in the Northeast Pacific west of San Nicolas Island, California, J. Acoust. Soc. Am. **120**, 711–718 (2006)

5.27 W.A. Kuperman, F. Ingenito: Spatial correlation of surface generated noise in a stratified ocean, J. Acoust. Soc. Am. **67**, 1988–1996 (1980)

5.28 T.G. Leighton: *The Acoustic Bubble* (Academic, London 1994)

5.29 C.E. Brennen: *Cavitation and bubble dynamics* (Oxford Univ. Press, Oxford 1995)

5.30 G.B. Morris: Depth dependence of ambient noise in the Northeastern Pacific Ocean, J. Acoust. Soc. Am. **64**, 581–590 (1978)

5.31 V.C. Anderson: Variations of the vertical directivity of noise with depth in the North Pacific, J. Acoust. Soc. Am. **66**, 1446–1452 (1979)

5.32 F. Ingenito, S.N. Wolf: Acoustic propagation in shallow water overlying a consolidated bottom, J. Acous. Soc. Am. **60**(6), 611–617 (1976)

5.33 H. Schmidt, W.A. Kuperman: Spectral and modal representation of the Doppler-shifted field in ocean waveguides, J. Acoust. Soc. Am. **96**, 386–395 (1994)

5.34 M.D. Collins, D.K. Dacol: A mapping approach for handling sloping interfaces, J. Acoust. Soc. Am. **107**, 1937–1942 (2000)

5.35 W.A. Kuperman, G.L. D'Spain (Eds.): *Ocean Acoustics Interference Phenomena and Signal Processing* (American Institution of Physics, Melville 2002)

5.36 H.L. Van Trees: *Detection Estimation and Modulation Theory* (Wiley, New York 1971)

5.37 H.L. Van Trees: *Optimum Array Processing* (Wiley, New York 2002)

5.38 D.H. Johnson, D.E. Dudgeon: *Array Signal Processing: Concepts and Techniques* (Prentice Hall, Englewood Cliffs 1993)

5.39 G.L. D'Spain, J.C. Luby, G.R. Wilson, R.A. Gramann: Vector sensors and vector line arrays: Comments on optiman array gain and detection, J. Acoust. Soc. Am. **120**, 171–185 (2006)

5.40 P. Roux, W.A. Kuperman, NPAL Group: Extracting coherent wavefronts from acoustic ambient noise in the ocean, J. Acoust. Soc. Am. **116**, 1995–2003 (2004)

5.41 M. Siderius, C.H. Harrison, M.B. Porter: A passive fathometer for determing bottom depth and imaging seaben layering using ambient noise, J. Acoust. Soc. Am. **12**, 1315–1323 (2006)

5.42 A.B. Baggeroer, W.A. Kuperman, P.N. Mikhalevsky: An Overview of matched field methods in ocean acoustics, IEEE J. Ocean. Eng. **18**(4), 401–424 (1993)

5.43 W.A. Kuperman, D.R. Jackson: Ocean acoustics, matched-field processing and phase conjugation. In: *Imaging of complex media with acoustic and seismic waves*, Topics Appl. Phys. **84**, 43–97 (2002)

5.44 M. Fink: Time Reversed Physics, Phys. Today **50**, 34–40 (1997)

5.45 A. Parvelescu, C.S. Clay: Reproducibility of signal transmissions in the ocean, Radio Electron. Eng. **29**, 223–228 (1965)

5.46 W.A. Kuperman, W.S. Hodgkiss, H.C. Song, T. Akal, C. Ferla, D. Jackson: Phase conjugation in the ocean: Experimental Demonstration of an acoustical time-reversal mirror in the ocean, J. Acoust. Soc. Am. **102**, 25–40 (1998)

5.47 H. Cox, R.M. Zeskind, M.O. Owen: Robust Adaptive Beamforming, IEEE Trans. Acoust. Speech Signal Proc. **35**, 10 (1987)

5.48 J.L. Krolik: Matched-field minimum variance beamforming in a random ocean channel, J. Acoust. Soc. Am. **92**, 1408–1419 (1992)

5.49 A. Tolstoy, O. Diachok, L.N. Frazer: Acoustic tomography via matched field processing, J. Acoust. Soc. Am. **89**, 1119–1127 (1991)

5.50 A.B. Baggeroer: *Applications of Digital Signal Processing*, ed. by A.V. Oppenheim (Prentice Hall, Englewood Cliffs 1978)

5.51 C. De Moustier: Beyond bathymetry: mapping acoustic backscattering from the deep seafloor with Sea Beam, J. Acoust. Soc. Am. **79**, 316–331 (1986)

5.52 P. Cervenka, C. De Moustier: Sidescan sonar image processing techniques, IEEE J. Ocean. Eng. **18**, 108–122 (1993)

5.53 C. De Moustier, H. Matsumoto: Seafloor acoustic remote sensing with multibeam echo-sounders and bathymetric sidescan sonar systems, Marine Geophys. Res. **15**, 27–42 (1993)

5.54 A. Turgut, M. McCord, J. Newcomb, R. Fisher: *Chirp sonar sediment characterization at the northern Gulf of Mexico Littoral Acoustic Demonstration Center experimental site, Proc. OCEANS 2002 MTS/IEEE Conf.* (IEEE, New York 2002)

5.55 D.B. Kilfoyle, A.B. Baggeroer: The state of the art in underwater acoustic telemetry, IEEE J. Ocean. Eng. **25**(1), 4–27 (2000)

5.56 D.B. Kilfoyle, J.C. Preissig, A.B. Baggeroer: Spatial modulation of partially coherent multiple-input/multiple-output channels, IEEE Trans. Signal Proc. **51**, 794–804 (2003)

5.57 C.E. Shannon: A mathematical theory of communication, Bell Syst. Tech. J. **27**, 379 (1948)

5.58 S.H. Simon, A.L. Moustakas, M. Stoychev, H. Safar: Communication in a disordered world, Phys. Today **54**(9) (2001)

Amazon EX1014 Page 220

5.59 G. Raleigh, J.M. Cioffi: Spatio-temporal coding for wireless communication, IEEE Trans. Commun. **46**, 357–366 (1998)

5.60 G.J. Foschini, M.J. Gans: On limits of wireless communications in a fading environment whe using multiple antennas, Wireless Personnal Communications **6**, 311–335 (1998)

5.61 C. Berrou, A. Glavieux: Near optimum error correcting coding and decoding: turbo-codes, IEEE Trans. Commun. **2**, 1064–1070 (1996)

5.62 J.G. Proakis: *Digital Communications* (McGraw Hill, New York 1989)

5.63 M. Stojanovich: Retrofocusing techniques for high rate acoustic communications, J. Acoust. Soc. Am. **117**, 1173–1185 (2005)

5.64 H.C. Song, W.S. Hodgkiss, W.A. Kuperman, M. Stevenson, T. Akal: Improvement of time-reversal communications using adaptive channel equalizers, IEEE J Ocean. Eng. **31**, 487–496 (2006)

5.65 T.C. Yang: Temporal resolution of time-reversal and passive-phase onjugation for underwater acoustic communications, IEEE J. Ocean. Eng. **28**, 229–245 (2003)

5.66 C. Wunsch: *The ocean circulation inverse problem* (Cambridge Univ. Press, Cambridge 1996)

5.67 E.K. Skarsoulis, B.D. Cornuelle: Travel-time sensitivity kernels in ocean acoustic tomography, J. Acoust. Soc. Am. **116**, 227 (2004)

5.68 T.G. Birdsall, K. Metzger, M.A. Dzieciuch: Signals, signal processing, and general results, J. Acoust. Soc. Am. **96**, 2343 (1994)

5.69 P.N. Mikhalevsky, A.B. Baggeroer, A. Gavrilov, M. Slavinsky: Continuous wave and M-sequence transmissions across the Arctic, J. Acoust. Soc. Am. **96**, 3235 (1994)

5.70 B.M. Howe, P.F. Worcester, R.C. Spindel: Ocean acoustic tomography: mesoscale velocity, J. Geophys. Res. **92**, 3785–3805 (1987)

5.71 R.A. Knox: Ocean acoustic tomography: A primer. In: *Ocean Circulation Models: Combining Data and Dynamics*, ed. by D.L.T. Anderson, J. Willebrand (Kluwer Academic, Dordrecht 1989)

5.72 M.I. Taroudakis: Ocean Acoustic Tomography, Lect. Notes ECUA, 77–95 (2002)

5.73 A.J.W. Duijndam, M.A. Schonewille, C.O.H. Hindriks: Reconstruction of band-limited signals, irregularly sampled along one spatial direction, Geophysics **64**(2), 524–538 (1999)

5.74 U. Send, The THETIS-2 Group: Acoustic observations of heat content across the Mediterranean Sea, Nature **38**, 615–617 (1997)

5.75 J.A. Colosi, E.K. Scheer, S.M. Flatté, B.D. Cornuelle, M.A. Dzieciuch, W.H. Munk, P.F. Worcester, B.M. Howe, J.A. Mercer, R.C. Spindel, K. Metzger, T.G. Birdsall, A.B. Baggeroer: Comparisons of measured and predicted acoustic fluctuations for a 3250 km propagation experiment in the eastern North Pacific Ocean, J. Acoust. Soc. Am. **105**, 3202–3218 (1999)

5.76 J.A. Colosi, A.B. Baggeroer, B.D. Cornuelle, M.A. Dzieciuch, W.H. Munk, P.F. Worcester, B.D. Dushaw, B.M. Howe, J.A. Mercer, R.C. Spindel, T.G. Birdsall, K. Metzger, A.M.G. Forbes: Analysis of multipath acoustic field variability and coherence in the finale of broadband basin-scale transmissions in the North Pacific Ocean, J. Acoust. Soc. Am. **117**, 1538–1564 (2005)

5.77 M. De Hoop, R. van der Hilst: On sensitivity kernels for wave equation transmission tomography, Geophys. J. Int. **160**, 621–633 (2005)

5.78 R. van der Hilst, M. de Hoop: Banana-doughnut kernels and mantle tomography, Geophys. J. Int. **163**, 956–961 (2005)

5.79 F. Dahlen, G. Nolet: Comment on the paper on sensitivity kernels for wave equation transmission tomography by de Hoop and van der Hilst, Geophys. J. Int. **163**, 949–951 (2005)

5.80 K.A. Johannesson, R.B. Mitson: *Fisheries acoustics – A practical manual for aquatic biomass estimation, FAO Fish. Tech. Paper 240* (FAO, Rome 1983)

5.81 G.L. Thomas: *Fisheries Acoustics, Special Issue, Fish. Res. 14(2/3)* (Elsevier, Amsterdam 1992)

5.82 A. Duncan: *Shallow Water Fisheries Acoustics 35(1/2)* (Elsevier, Amsterdam 1998)

5.83 B.J. Robinson: Statistics of single fish echoes observed at sea, ICES C. M. B **16**, 1–4 (1976)

5.84 D. B.Reeder, J.M. Jech, T.K. Stanton: Broadband acoustic backscatter and high-resolution morphology of fish: Measurement and modeling, J. Acoust. Soc. Am. **116**, 2489 (2004)

5.85 A. Alvarez, Z. Ye: Effects of fish school structures on acoustic scattering, ICES J. Marine Sci. **56**(3), 361–369 (1999)

5.86 D. Reid, C. Scalabrin, P. Petitgas, J. Masse, R. Aukland, P. Carrera, S. Georgakarakos: Standard protocols for the analysis of school based data from echo sounder surveys, Fish. Res. **47**(2/3), 125–136 (2000)

5.87 D.V. Holliday: Resonance Structure in Echoes from Schooled Pelagic Fish, J. Acoust. Soc. Am. **51**, 1322–1332 (1972)

5.88 D.N. MacLennan: Acoustical measurement of fish abundance, J. Acoust. Soc. Am. **87**(1), 1–15 (1990)

5.89 D.N. Mac Lennan, E.J. Simmonds: *Fisheries Acoustics* (Chapman Hall, London 1992)

5.90 P. Petitgas: A method for the identification and characterization of clusters of schools along the transect lines of fisheries-acoustic surveys, ICES J. Marine Sci. **60**(4), 872–884 (2003)

5.91 Y. Takao, M. Furusawa: Dual-beam echo integration method for precise acoustic surveys, ICES J. Marine Sci. **53**(2), 351–358 (1996)

5.92 E. Marchal, P. Petitgas: Precision of acoustic fish stock estimates: separating the number of schools

Amazon EX1014 Page 221

from the biomass in the schools, Aquat. Living Res. **6**(3), 211–219 (1993)
5.93 T.K. Stanton: Effects of transducer motion on echo-integration techniques, J. Acoust. Soc. Am. **72**, 947–949 (1982)
5.94 K.G. Foote, H.P. Knudsen, G. Vestnes, D.N. MacLennan, E.J. Simmonds: Calibration of acoustic instruments for fish density estimation: a practical guide, ICES Coop. Res. Rep. **144**, 69 (1987)
5.95 K.G. Foote: Energy in acoustic echoes from fish aggregations, Fish. Res. **1**, 129–140 (1981)
5.96 P. Petitgas, D. Reid, P. Carrera, M. Iglesias, S. Georgakarakos, B. Liorzou, J. Massé: On the relation between schools, clusters of schools, and abundance in pelagic fish stocks, ICES J. Marine Sci. **58**(6), 1150–1160 (2001)
5.97 K.G. Foote: Linearity of fisheries acoustics, with addition theorems, J. Acoust. Soc. Am. **73**(6), 1932–1940 (1983)
5.98 F. Gerlotto, M. Soria, P. Freon: From two dimensions to three: the use of multibeam sonar for a new approach in fisheries acoustics, Can. J. Fish. Aquat. Sci. **56**, 6–12 (1999)
5.99 L. Mayer, Y. Li, G. Melvin: 3D visualization for pelagic fisheries research and assessment, ICES J. Marine Sci. **59**(1), 216–225 (2002)
5.100 C. Scalabrin, N. Diner, A. Weill, A. Hillion, M.-C. Mouchot: Narrowband acoustic identification of monospecific fish shoals, ICES J. Marine Sci. **53**, 181–188 (1996)
5.101 J. Guillard, P. Brehmer, M. Colon, Y. Guennegan: 3-D characteristics of young–of–year pelagic fish schools in lake, Aqu. Liv. Res. **19**, 115–122 (2006)
5.102 K.G. Foote: Fish target strengths for use in echo integrator surveys, J. Acoust. Soc. Am. **82**, 981 (1987)
5.103 E. Josse, A. Bertrand: In situ acoustic target strength measurements of tuna associated with a fish aggregating device, ICES J. Marine Sci. **57**(4), 911–918 (2000)
5.104 B.J. Robinson: *In situ measurements of the target strengths of pelagic fishes, ICES/FAO Symp. Fish. Acoust* (FAO, Rome 2000) pp. 1–7
5.105 S. Gauthier, G.A. Rose: Target strength of encaged Atlantic redfish, ICES J. Marine Sci. **58**, 562–568 (2001)
5.106 J.S. Jaffe: Target localization for a three-dimensional multibeam sonar imaging system, J. Acoust. Soc. Am. **105**(6), 3168–3175 (1999)
5.107 D.V. Holliday, R.E. Pieper: Volume scattering strengths and zooplankton distributions at acoustic frequencies between 0.5 and 3 MHz, J. Acoust. Soc. Am. **67**, 135 (1980)
5.108 C.F. Greenlaw, D.V. Holliday, D.E. McGehee: Multistatic, multifrequency scattering from zooplankton, J. Acoust. Soc. Am. **103**, 3069 (1998)
5.109 A.M. Thode, G.L. D'Spain, W.A. Kuperman: Matched-field processing, geoacoustic inversion, and source signature recovery of blue whale vocalizations, J. Acoust. Soc. Am. **107**, 1286–1300 (2000)
5.110 M. Johnson, P. Tyack, D. Nowacek: A digital recording tag for measuring the response of marine mammals to sound, J. Acoust. Soc. Am. **108**, 2582–2583 (2000)
5.111 D.K. Mellinger, K.M. Stafford, G.C. Fox: Seasonal occurrence of sperm whale (Physeter macrocephalus) sounds in the Gulf of Alaska, 1999–2001, Marine Mammal Sci. **20**(1), 48–62 (2004)
5.112 W.J. Richardson, C.R. Greene, C.I. Malme, D.H. Thomson: *Marine Mammals and Noise* (Academic, San Diego 1995)
5.113 A. Sirovic, J.A. Hildebrand, S.M. Wiggins, M.A. McDonald, S.E. Moore, D. Thiele: Seasonality of blue and fin whale calls and the influence of sea ice in the western Antarctic penninsula, Deep Sea Res. **51**(II), 2327–2344 (2004)
5.114 A.M. Thode, D.K. Mellinger, S. Stienessen, A. Martinez, K. Mullin: Depth-dependent acoustic features of diving sperm whales (Physeter macrocephalus) in the Gulf of Mexico, J. Acoust. Soc. Am. **112**, 308–321 (2002)
5.115 P. Tyack: Acoustics communications under the sea. In: *Animal Acoustic Communication: Recent Advances*, ed. by S.L. Hopp, M.J. Owren, C.S. Evans (Springer, Berlin, Heidelberg 1988) pp. 163–220
5.116 National Research Council: *Ocean Noise and Marine Mammals* (National Academy, Washington 2003) p. 192

Amazon EX1014 Page 222

Physical a

Part B

Part B Physical and Nonlinear Acoustics

6 Physical Acoustics
Mack A. Breazeale, University, USA
Michael McPherson, University, USA

7 Thermoacoustics
Gregory W. Swift, Los Alamos, USA

8 Nonlinear Acoustics in Fluids
Werner Lauterborn, Göttingen, Germany
Thomas Kurz, Göttingen, Germany
Iskander Akhatov, Fargo, USA

Amazon EX1014 Page 223

6. Physical Acoustics

An overview of the fundamental concepts needed for an understanding of physical acoustics is provided. Basic derivations of the acoustic wave equation are presented for both fluids and solids. Fundamental wave concepts are discussed with an emphasis on the acoustic case. Discussions of different experiments and apparatus provide examples of how physical acoustics can be applied and of its diversity. Nonlinear acoustics is also described.

6.1 **Theoretical Overview** 209
6.1.1 Basic Wave Concepts 209
6.1.2 Properties of Waves 210
6.1.3 Wave Propagation in Fluids 215
6.1.4 Wave Propagation in Solids 217
6.1.5 Attenuation 218
6.2 **Applications of Physical Acoustics** 219
6.2.1 Crystalline Elastic Constants 219
6.2.2 Resonant Ultrasound Spectroscopy (RUS) 220
6.2.3 Measurement Of Attenuation (Classical Approach) 221
6.2.4 Acoustic Levitation 222
6.2.5 Sonoluminescence 222
6.2.6 Thermoacoustic Engines (Refrigerators and Prime Movers) 223
6.2.7 Acoustic Detection of Land Mines 224
6.2.8 Medical Ultrasonography 224
6.3 **Apparatus** 226
6.3.1 Examples of Apparatus 226
6.3.2 Piezoelectricity and Transduction 226
6.3.3 Schlieren Imaging 228
6.3.4 Goniometer System 230
6.3.5 Capacitive Receiver 231
6.4 **Surface Acoustic Waves** 231
6.5 **Nonlinear Acoustics** 234
6.5.1 Nonlinearity of Fluids 234
6.5.2 Nonlinearity of Solids 235
6.5.3 Comparison of Fluids and Solids .. 236
References 237

Physical acoustics involves the use of acoustic techniques in the study of physical phenomena as well as the use of other experimental techniques (optical, electronic, etc.) to study acoustic phenomena (including the study of mechanical vibration and wave propagation in solids, liquids, and gasses). The subject is so broad that a single chapter cannot cover the entire subject. For example, recently the 25th volume of a series of books entitled *Physical Acoustics* was published [6.1]. *Mason* [6.2] began the series in 1964. The intermediate volumes are not repetitious, but deal with different aspects of physical acoustics. Even though all of physical acoustics cannot be covered in this chapter, some examples will illustrate the role played by physical acoustics in the development of physics.

Since much of physics involves the use and study of waves, it is useful to begin by mentioning some different types of waves and their properties. The most basic definition of a wave is a disturbance that propagates through a medium. A simple analogy can be made with a stack of dominoes that are lined up and knocked over. As the first domino falls into the second, it is knocked over into the third, which is knocked over into the next one, and so on. In this way, the disturbance travels down the entire chain of dominoes (which we may think of as particles in a medium) even though no particular domino has moved very far. Thus, we may consider the motion of an individual domino, or the motion of the disturbance which is traveling down the entire chain of dominoes. This suggests that we define two concepts, the average particle velocity of the individual dominoes and the wave velocity (of the disturbance) down the chain of dominoes. Acoustic waves behave in a similar manner. In physical acoustics it is necessary to distinguish between particle velocity and wave (or phase) velocity.

There are two basic types of waves: longitudinal waves, and transverse waves. These waves are defined according to the direction of the particle motion in the

Amazon EX1014 Page 224

medium relative to the direction in which the wave travels. Longitudinal waves are waves in which the particle motion in the medium is in the same direction as the wave is traveling. Transverse waves are those in which the particle motion in the medium is at a right angle to the direction of wave propagation. Figure 6.1 is a depiction of longitudinal and transverse waves. Another less common type of wave, known as a torsional wave, can also propagate in a medium. Torsional waves are waves in which particles move in a circle in a plane perpendicular to the direction of the wave propagation. Figure 6.2 shows a commonly used apparatus for the demonstration of torsional waves.

There also are more-complicated types of waves that exist in acoustics. For example, surface waves (Rayleigh waves, Scholte–Stonley waves, etc.) can propagate along the boundary between two media. Another example of a more complicated type of wave propagation is that of Lamb waves, which can propagate along thin plates. A familiar example of Lamb waves are the waves that propagate along a flag blowing in a wind.

In acoustics, waves are generally described by the pressure variations that occur in the medium (solid or fluid) due to the wave. As an acoustic wave passes through the medium, it causes the pressure to vary as the acoustic energy causes the distance between the molecules or atoms of the fluid or solid to change periodically. The total pressure is given by

$$p_{\mathrm{T}}(x,t) = p_0(x,t) + p_1(x,t)\,. \tag{6.1}$$

Here p_0 represents the ambient pressure of the fluid and p_1 represents the pressure fluctuation caused by the acoustic field. Since pressure is defined as the force per unit area, it has units of newtons per square meter ($\mathrm{N/m^2}$). The official SI designation for pressure is the pascal ($1\,\mathrm{Pa} = 1\,\mathrm{N/m^2}$). Atmospheric pressure at sea level is 1 atmosphere (atm) $= 1.013 \times 10^5$ Pa. The types of sounds we encounter cause pressure fluctuations in the range from 10^{-3}–10 Pa.

One can also describe the strength of the sound wave in terms of the energy that it carries. Experimentally, one can measure the power in the acoustic wave, or the amount of energy carried by the wave per unit time. Rather than trying to measure the power at every point in space, it is usual to measure the power only at the location of the detector. So, a more convenient measurement is the power density, also referred to as the acoustic intensity I. In order to make a definition which does not depend on the geometry of the detector, one considers the power density only over an infinitesimal area of size $\mathrm{d}A$:

$$I = \frac{\mathrm{d}P}{\mathrm{d}A}\,, \tag{6.2}$$

where $\mathrm{d}P$ is the portion of the acoustic power that interacts with the area $\mathrm{d}A$ *of the detector* oriented perpendicular to the direction of the oncoming acoustic wave. The units of acoustic intensity are watts per square meter ($\mathrm{W/m^2}$).

The human ear can generally perceive sound pressures over the range from about 20 μPa up to about 200 Pa (a very large dynamic range). Because the range of typical acoustic pressures is so large, it is convenient to work with a relative measurement scale rather than an absolute measurement scale. These scales are expressed using logarithms to compress the dynamic range. In acoustics, the scale is defined so that every factor of ten increase in the amount of energy carried by the wave is represented as a change of 1 bel (named after Alexander Graham Bell). However, the bel is often too large to be useful. For this reason, one uses the decibel scale (1/10 of a bel). Therefore, one can write the sound intensity level (SIL) as the logarithm of two intensities:

$$\mathrm{SIL(dB)} = 10\log\left(\frac{I}{I_{\mathrm{ref}}}\right)\,, \tag{6.3}$$

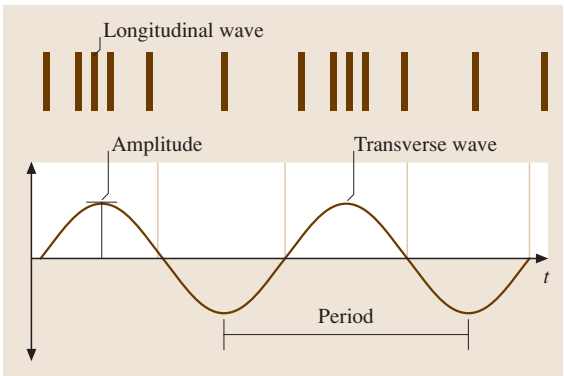


Fig. 6.1 Longitudinal and transverse waves

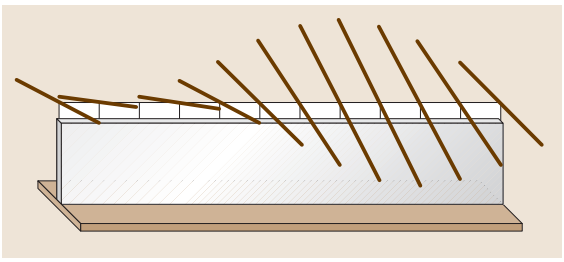


Fig. 6.2 Apparatus for the demonstration of torsional waves

where I is the intensity of the sound wave and I_{ref} is a reference intensity. (One should note that the bel, or decibel, is not a unit in the typical sense; rather, it is simply an indication of the relative sound level).

In order for scientists and engineers to communicate meaningfully, certain standard reference values have been defined. For the intensity of a sound wave in air, the reference intensity is defined to be $I_{\text{ref}} = 10^{-12}\,\text{W/m}^2$.

In addition to measuring sound intensity levels, it is also common to measure sound pressure levels (SPL). The sound pressure level is defined as

$$\text{SPL(dB)} = 20\log\left(\frac{p}{p_{\text{ref}}}\right), \tag{6.4}$$

where p is the acoustic pressure and p_{ref} is a reference pressure. (The factor of 20 comes from the fact that I is proportional to p^2.) For sound in air, the reference pressure is defined as $20\,\mu\text{Pa}$ (2×10^{-5} Pa).

For sound in water, the reference is $1\,\mu\text{Pa}$ [historically other reference pressures, for example, $20\,\mu\text{Pa}$ and 0.1 Pa, have been defined). It is important to note that sound pressure levels are meaningful only if the reference value is defined. It should also be noted that this logarithmic method of defining the sound pressure level makes it easy to compare two sound levels. It can be shown that $\text{SPL}_2 - \text{SPL}_1 = 20\log\left(\frac{p_2}{p_1}\right)$; hence, an SPL difference depends only on the two pressures and not on the choice of reference pressure used.

Since both optical and acoustic phenomena involve wave propagation, it is illustrative to contrast them. Optical waves propagate as transverse waves. Acoustic waves in a fluid are longitudinal; those in a solid can be transverse or longitudinal. Under some conditions, waves may propagate along interfaces between media; such waves are generally referred to as surface waves. Sometimes acoustic surface waves correspond with an optical analogue. However, since the acoustic wavelength is much larger than the optical wavelength, the phenomenon may be much more noticeable in physical acoustics experiments. Many physical processes produce acoustic disturbances directly. For this reason, the study of the acoustic disturbance often gives information about a physical process. The type of acoustic wave should be examined to determine whether an optical model is appropriate.

6.1 Theoretical Overview

6.1.1 Basic Wave Concepts

Although the domino analogy is useful for conveying the idea of how a disturbance can travel through a medium, real waves in physical systems are generally more complicated. Consider a spring or slinky that is stretched along its length. By rapidly compressing the end of the spring, one can send a pulse of energy down the length of the spring. This pulse would essentially be a longitudinal wave pulse traveling down the length of the spring. As the pulse traveled down the length, the material of the spring would compress or *bunch up* in the region of the pulse and *stretch out* on either side of it. The compressed regions are known as condensations and the stretched regions are known as rarefactions.

It is this compression that one could actually witness traveling down the length of the spring. No part of the spring itself would move very far (just as no domino moved very far), but the disturbance would travel down the entire length of the spring. One could also repeatedly drive the end of the spring back and forth (along its length). This would cause several pulses (each creating compressions with stretched regions around them) to propagate along the length of the spring, with the motion of the spring material being along the direction of the propagating disturbance. This would be a multipulse longitudinal wave.

Now, let us consider an example of a transverse wave, with particle motion perpendicular to the direction of propagation. Probably the simplest example is a string with one end fastened to a wall and the opposite end driven at right angles to the direction along which the string lies. This drive sends pulses down the length of the string. The motion of the particles in the string is at right angles to the motion of the disturbance, but the disturbance itself (whether one pulse or several) travels down the length of the string. Thus, one sees a transverse wave traveling down the length of the string.

Any such periodic pulsing of disturbances (whether longitudinal or transverse) can be represented mathematically as a combination of sine and/or cosine waves through a process known as Fourier decomposition. Thus, without loss of generality, one can illustrate additional wave concepts by considering a wave whose shape is described mathematically by a sine wave.

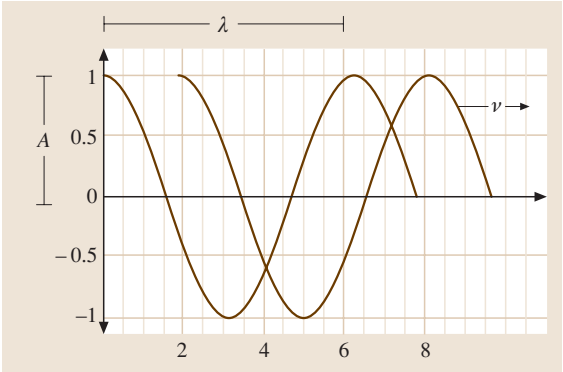


Fig. 6.3 One cycle of a sinusoidal wave traveling to the right

Figure 6.3 shows one full cycle of a sinusoidal wave which is moving to the right (as a sine-shaped wave would propagate down a string, for example). The initial wave at $t = 0$ and beginning at $x = 0$ can be described mathematically. Let the wave be traveling along the x-axis direction and let the particle displacement be occurring along the y-axis direction. In general, the profile or shape of the wave is described mathematically as

$$y(x) = A \sin(kx + \varphi) \,, \tag{6.5}$$

where A represents the maximum displacement of the string (i. e., the particle displacement) in the y-direction and k represents a scaling factor, the wave number. The argument of the sine function in (6.5) is known as the phase. For each value of x, the function $y(x)$ has a unique value, which leads to a specific y value (sometimes called a point of constant phase). The term φ is known as the phase shift because it causes a shifting of the wave profile along the x-axis (forward for a positive phase shift and backward for a negative phase shift). Such a sine function varies between $+A$ and $-A$, and one full cycle of the wave has a length of $\lambda = \frac{2\pi}{k}$. The length λ is known as the wavelength, and the maximum displacement A is known as the wave amplitude.

As this disturbance shape moves toward the right, its position moves some distance $\Delta x = x_f - x_o$ during some time interval Δt, which means the disturbance is traveling with some velocity $c = \frac{\Delta x}{\Delta t}$. Thus, the distance the wave has traveled shows this profile both before and after it has traveled the distance Δx (Fig. 6.3). The traveling wave can be expressed as a function of both position (which determines its profile) and time (which determines the distance it has traveled). The equation for a traveling wave, then, is given by

$$y(x, t) = A \sin[k(x - ct) + \varphi] \,, \tag{6.6}$$

where $t = 0$ gives the shape of the wave at $t = 0$ (which here is assumed constant), and $y(x, t)$ gives the shape and position of the wave disturbance as it travels. Again, A represents the amplitude, k represents the wave number, and φ represents the phase shift. Equation (6.6) is applicable for all types of waves (longitudinal, transverse, etc.) traveling in any type of medium (a spring, a string, a fluid, a solid, etc.).

Thus far, we have introduced several important basic wave concepts including wave profile, phase, phase shift, amplitude, wavelength, wave number, and wave velocity. There is one additional basic concept of great importance, the wave frequency. The frequency is defined as the rate at which (the number of times per second) a point of constant phase passes a point in space. The most obvious points of constant phase to consider are the maximum value (crest) or the minimum value (trough) of the wave. One can think of the concept of frequency less rigorously as the number of pulses generated per second by the source causing the wave. The velocity of the wave is the product of the wavelength and the frequency.

One can note that, rather than consisting of just one or a few pulses, (6.6) represents a continually varying wave propagating down some medium. Such waves are known as continuous waves. There is also a type of wave that is a bit between a single pulse and an infinitely continuous wave. A wave that consists of a finite number of cycles is known as a wave packet or a tone burst. When dealing with a tone burst, the concepts of phase velocity and group velocity are much more evident. Generally speaking, the center of the tone burst travels at the phase velocity – the ends travel close to the group velocity.

6.1.2 Properties of Waves

All waves can exhibit the following phenomena: reflection, refraction, interference and diffraction. (Transverse waves can also exhibit a phenomenon known as polarization, which allows oscillation in only one plane.)

Reflection

The easiest way to understand reflection is to consider the simple model of a transverse wave pulse traveling down a taut string that is affixed at the opposite end (as seen in Fig. 6.4. (A pulse is described here for purposes of clarity, but the results described apply to continu-

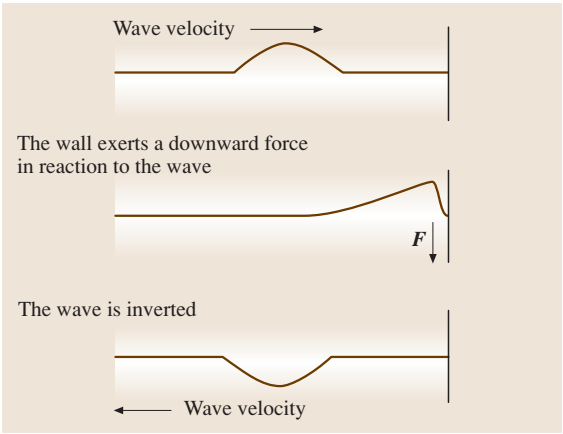


Fig. 6.4 Reflection of a wave from a fixed boundary

ous waves as well.) As the pulse reaches the end of the string, the particles start to move upward, but they cannot because the string is fastened to the pole. (This is known as a fixed or rigid boundary.) The pole exerts a force on the particles in the string, which causes the pulse to rebound and travel in the opposite direction. Since the force of the pole on the string in the y-direction must be downward (to counteract the upward motion of the particles), there is a 180° phase shift in the wave. This is seen in the figure where the reflected pulse has flipped upside down relative to the incident pulse.

Figure 6.5 shows a different type of boundary from which a wave (or pulse) can reflect; in this case the end of the string is on a massless ring that can slide freely up and down the pole. (This situation is known as a free boundary.) As the wave reaches the ring, it drives the ring upwards. As the ring moves back down, a reflected wave, which travels in a direction opposite to that of the incoming wave, is also generated. However, there is no 180° phase shift upon reflection from a free boundary.

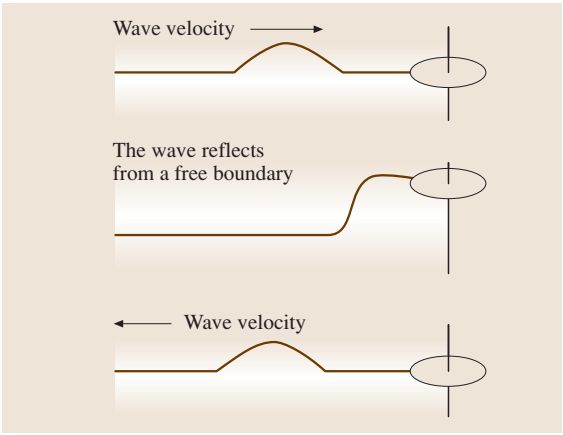


Fig. 6.5 Reflection of a wave from a free boundary

Acoustic Impedance

Another important wave concept is that of wave impedance, which is usually denoted by the variable Z. When the reflection of the wave is not total, part of the energy in the wave can be reflected and part transmitted. For this reason, it is necessary to consider acoustic waves at an interface between two media and to be able to calculate how much of the energy is reflected and how much is transmitted. The definition of media impedance facilitates this. For acoustic waves, the impedance Z is defined as the ratio of sound pressure to particle velocity. The units for impedance are the Rayl, so named in honor of Lord Rayleigh. $1\,\text{Rayl} = 1\,\text{Pa}\,\text{s/m}$.

Often one speaks of the *characteristic impedance* of a medium (a fluid or solid); in this case one is referring to the medium in the "open space" condition where there are no obstructions to the wave which would cause the wave to reflect or scatter. The characteristic impedance of a material is usually denoted by Z_0, and it can be determined by the product of the mean density of the medium ρ with the speed of sound in the medium. In air, the characteristic impedance near room temperature is about, 410 Rayl.

The acoustic impedance concept is particularly useful. Consider a sound wave that passes from an initial medium with one impedance into a second medium with a different impedance. The efficiency of the energy transfer from one medium into the next is given by the ratio of the two impedances. If the impedances (ρc) are identical, their ratio will be 1; and all of the acoustic energy will pass from the first medium into the second across the interface between them. If the impedances of the two media are different, some of the energy will be reflected back into the initial medium when the sound field interacts with the interface between the two media. Thus the impedance enables one to characterize the acoustic transmission and reflection at the boundary of the two materials. The difference in Z, which leads to some of the energy being reflected back into the initial medium, is often referred to as the impedance mismatch. When the (usual) acoustic boundary conditions apply and require that the particle velocity and pressure be continuous across the interface between the two media, one can calculate the percentage of the energy that is reflected back into the medium. This is given in fractional form by the

Amazon EX1014 Page 228

reflection coefficient given by

$$R = \left(\frac{Z_2 - Z_1}{Z_2 + Z_1}\right)^2 , \tag{6.7}$$

where Z_1 and Z_2 are the impedances of the two media. Since both values of Z must be positive, R must be less than one. The fraction of the energy transmitted into the second medium is given by $T = 1 - R$ because 100% of the energy must be divided between T and R.

Refraction

Refraction is a change of the direction of wave propagation as the wave passes from one medium into another across an interface. Bending occurs when the wave speed is different in the two media. If there is an angle between the normal to the plane of the boundary and the incident wave, there is a brief time interval when part of the wave is in the original medium (traveling at one velocity) and part of the wave is in the second medium (traveling at a different velocity). This causes the bending of the waves as they pass from the first medium to the second. (There is no bending at normal incidence.)

Reflection and refraction can occur simultaneously when a wave impinges on a boundary between two media with different wave propagation speeds. Some of the energy of the wave is reflected back into the original medium, and some of the energy is transmitted and refracted into the second medium. This means that a wave incident on a boundary can generate two waves: a reflected wave and a transmitted wave whose direction of propagation is determined by Snell's law.

All waves obey Snell's law. For optical waves the proper form of Snell's law is:

$$n_1 \sin\theta_1 = n_2 \sin\theta_2 , \tag{6.8}$$

where n_1 and n_2 are the refractive indices and θ_1 and θ_2 are propagation directions. For acoustic waves the proper form of Snell's law is:

$$\frac{\sin\theta_1}{v_1} = \frac{\sin\theta_2}{v_2} , \tag{6.9}$$

where v_1 is the wave velocity in medium 1 and v_2 is the wave velocity in medium 2. These two forms are very similar since the refractive index is $n = c/C_m$, where c is the velocity of light in a vacuum and C_m is the velocity of light in the medium under consideration.

Interference

Spatial Interference. Interference is a phenomenon that occurs when two (or more) waves add together. Consider two identical transverse waves traveling to the right (one after the other) down a string towards a boundary at the end. When the first wave encounters the boundary, it reflects and travels in the leftward direction. When it encounters the second, rightward moving wave the two waves add together linearly (in accordance with the principle of superposition). The displacement amplitude at the point in space where two waves combine is either greater than or less than the displacement amplitude of each wave. If the resultant wave has an amplitude that is smaller than that of either of the original two waves, the two waves are said to have

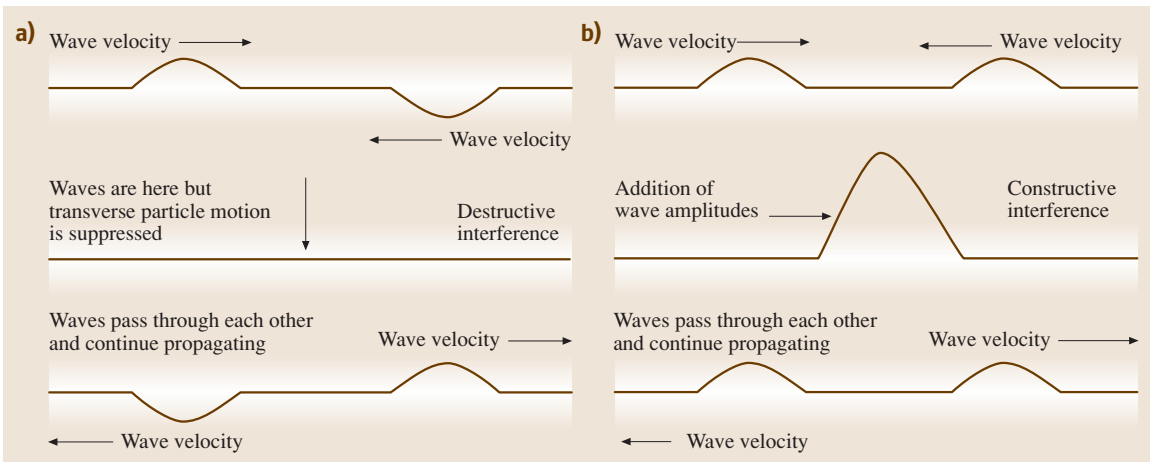


Fig. 6.6a,b Two waves passing through each other exhibiting **(a)** destructive and **(b)** constructive interference

Amazon EX1014 Page 229

destructively interfered with one another. If the combined wave has an amplitude that is greater than either of its two constituent waves, then the two waves are said to have constructively interfered with each other. The maximum possible displacement of the combination is the sum of the maximum possible displacements of the two waves (complete constructive interference); the minimum possible displacement is zero (complete destructive interference for waves of equal amplitude). It is important to note that the waves interfere only as they pass through one another. Figure 6.6 shows the two special cases of complete destructive and complete constructive interference (for clarity only a portion of the wave is drawn).

If a periodic wave is sent down the string and meets a returning periodic wave traveling in the opposite direction, the two waves interfere. This results in wave superposition, i. e., the resulting amplitude at any point and time is the sum of the amplitudes of the two waves. If the returning wave is inverted (due to a fixed boundary reflection) and if the length of the string is an integral multiple of the half-wavelength corresponding to the drive frequency, conditions for resonance are satisfied.

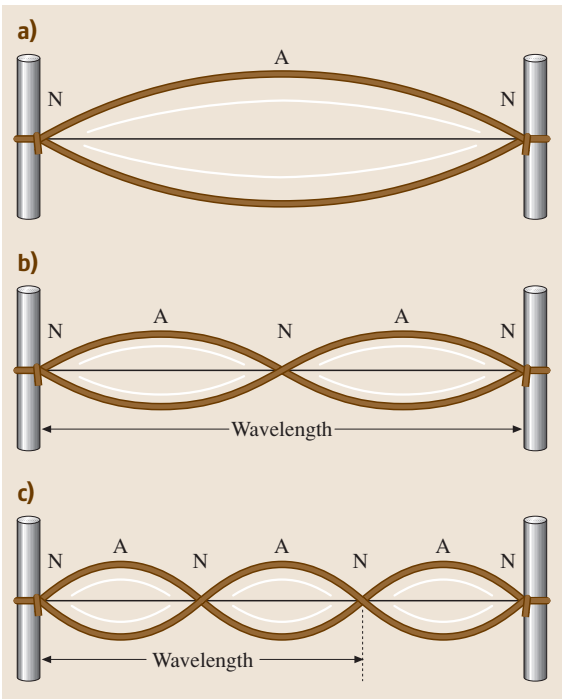


Fig. 6.7a–c Standing waves in a string with nodes and antinodes indicated. **(a)** The fundamental; **(b)** the second harmonic; **(c)** the third harmonic

This resonance produces a standing wave. An example of a standing wave is shown in Fig. 6.7. The points of maximum displacement are known as the standing-wave antinodes. The points of zero displacement are known as the standing-wave nodes.

Resonance Behavior. Every vibrating system has some characteristic frequency that allows the vibration amplitude to reach a maximum. This characteristic frequency is determined by the physical parameters (such as the geometry) of the system. The frequency that causes maximum amplitude of vibration is known as the resonant frequency, and a system driven at its resonant frequency is said to be in resonance. Standing waves are simply one type of resonance behavior.

Longitudinal acoustic waves can also exhibit resonance behavior. When the distance between a sound emitter and a reflector is an integer number of half wavelengths, the waves interfere and produce standing waves. This interference can be observed optically, acoustically or electronically. By observing a large number of standing waves one can obtain an accurate value of the wavelength, and hence an accurate value of the wave velocity.

One of the simplest techniques for observing acoustic resonances in water, or any other transparent liquid, is to illuminate the resonance chamber, then to focus a microscope on it. The microscope field of view images the nodal lines that are spaced half an acoustic wavelength apart. A screw that moves the microscope perpendicular to the lines allows one to make very accurate wavelength measurements, and hence accurate sound velocity measurements.

Temporal Interference. So far we have considered the interference of two waves that are combining in space (this is referred to as spatial interference). It is also possible for two waves to interfere because of a difference in frequency (which is referred to as temporal interference). One interesting example of this is the phenomenon of wave beating.

Consider two sinusoidal acoustic waves with slightly different frequencies that arrive at the same point in space. Without loss of generality, we can assume that these two waves have the same amplitude. The superposition principle informs us that the resultant pressure caused by the two waves is the sum of the pressure caused by each wave individually. Thus, we have for the total pressure

$$p_T(t) = A\left[\cos(\omega_1 t) + \cos(\omega_2 t)\right] . \qquad (6.10)$$

By making use of a standard trigonometric identity, this can be rewritten as

$$p_T(t) = 2A\cos\left(\frac{(\omega_1-\omega_2)}{2}t\right)\cos\left(\frac{(\omega_1+\omega_2)}{2}t\right). \quad (6.11)$$

Since the difference in frequencies is small, the two waves can be in phase, causing constructive interference and reinforcing one another. Over some period of time, the frequency difference causes the two waves to go out of phase, causing destructive interference (when $\omega_1 t$ eventually leads $\omega_2 t$ by 180°). Eventually, the waves are again in phase and, they constructively interfere again. The amplitude of the combination will rise and fall in a periodic fashion. This phenomenon is known as the beating of the two waves. This beating phenomenon can be described as a separate wave with an amplitude that is slowly varying according to

$$p(t) = A_0(t)\cos(\omega_{avg}t) \quad (6.12)$$

where

$$A_0(t) = 2A\cos\left(\frac{\omega_1-\omega_2}{2}t\right) \quad (6.13)$$

and

$$\omega_{avg} = \frac{(\omega_1+\omega_2)}{2}. \quad (6.14)$$

The cosine in the expression for $A_0(t)$ varies between positive and negative 1, giving the largest amplitude in each case. The period of oscillation of this amplitude variation is given by

$$T_b = \frac{2\pi}{\omega_1-\omega_2} = \frac{2\pi}{\omega_b} = \frac{1}{f_b}. \quad (6.15)$$

The frequency f_b of the amplitude variation is known as the beat frequency. Figure 6.8 shows the superposition of two waves that have two frequencies that are different but close together. The beat frequency corresponds to the difference between the two frequencies that are beating.

The phenomenon of beating is often exploited by musicians in tuning their instruments. By using a reference (such as a 440 Hz tuning fork that corresponds to the A above middle C) one can check the tuning of the instrument. If the A above middle C on the instrument is out of tune by 2 Hz, the sounds from the tuning fork and the note generate a 2 Hz beating sound when they are played together. The instrument is then tuned until the beating sound vanishes. Then the frequency of the instrument is the same as that of the tuning fork. Once the A is in tune, the other notes can be tuned relative to the A by counting the beats per unit time when different notes are played in various combinations.

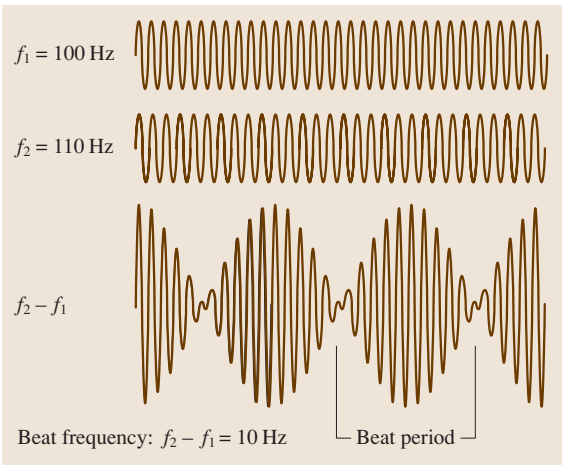


Fig. 6.8 The beating of two waves with slightly different frequencies

Multi-frequency Sound

When sound consists of many frequencies (not necessarily all close together), one needs a means of characterizing the sound level. One may use a weighted average of the sound over all the frequencies present, or one may use information about how much energy is distributed over a particular range of frequencies. A selected range of frequencies is known as a frequency band. By means of filters (either acoustic or electrical, depending on the application) one can isolate the various frequency bands across the entire frequency spectrum. One can then talk of the acoustic pressure due to a particular frequency band. The *band pressure level* is given by

$$PL_{band} = 20\log_{10}\left(\frac{p_{band}}{p_{ref}}\right) \quad (6.16)$$

where p_{band} is the room-mean-square (rms) average pressure of the sound in the frequency band range and p_{ref} is the standard reference for sound in air, 20 μPa. The average of the pressures of the frequency bands over the complete spectrum is the average acoustic signal. However, the presence of multiple frequencies complicates the situation: one does not simply add the frequency band pressures or the band pressure levels. Instead, it is the p^2 values which must be summed:

$$p_{rms}^2 = \sum p_{band}^2 \quad (6.17)$$

or:

$$\mathrm{SPL} = 10\log_{10}\left(\frac{p_{\mathrm{rms}}^2}{p_{\mathrm{ref}}^2}\right) = 10\log_{10}\sum\left(\frac{p_{\mathrm{band}}}{p_{\mathrm{ref}}}\right)^2 \tag{6.18}$$

or, simplifying further

$$\mathrm{SPL} = 10\log_{10}\sum(10)^{(\mathrm{PL}_{\mathrm{band}}/10)}\,. \tag{6.19}$$

The octave is a common choice for the width of a frequency band. With a one-octave filter, only frequencies up to twice the lowest frequency of the filter are allowed to pass. One should also note that, when an octave band filter is labeled with its center frequency, this is determined by the geometric mean (not the arithmetic mean), i. e.,

$$f_{\mathrm{center}} = \sqrt{f_{\mathrm{low}} f_{\mathrm{high}}} = \sqrt{2 f_{\mathrm{low}}^2} = \sqrt{2} f_{\mathrm{low}}\,. \tag{6.20}$$

Coherent Signals

Two signals are coherent if there is a fixed relative phase relation between them. Two loudspeakers driven by the same source would be coherent. However, two loudspeakers being driven by two compact-disc (CD) players (even if each player was playing a copy of the same CD) would not be coherent because there is no connection causing a constant phase relationship. For two incoherent sources, the total pressure is

$$p_{\mathrm{tot}}^2 = \left(p_{1(\mathrm{rms})} + p_{2(\mathrm{rms})}\right)^2 = p_{1(\mathrm{rms})}^2 + p_{2(\mathrm{rms})}^2 \tag{6.21}$$

(where the $2p_{1(\mathrm{rms})}p_{2(\mathrm{rms})}$ term has averaged out to zero). For coherent sources, however, the fixed phase relationship allows for the possibility of destructive or constructive interference. Therefore, the signal can vary in amplitude between $(p_{1(\mathrm{rms})} + p_{2(\mathrm{rms})})^2$ and $(p_{1(\mathrm{rms})} - p_{2(\mathrm{rms})})^2$.

Diffraction

In optics it is usual to begin a discussion of diffraction by pointing out grating effects. In acoustics one seldom encounters grating effects. Instead, one encounters changes in wave direction of propagation resulting from diffraction. Thus, in acoustics it is necessary to begin on a more fundamental level.

The phenomenon of diffraction is the bending of a wave around an edge. The amount of bending that occurs depends on the relative size of the wavelength compared to the size of the edge (or aperture) with which it interacts. When considering refraction or reflection it is often convenient to model the waves by drawing a single ray in the direction of the wave's propagation. However, the ray approach does not provide a means to model the bending caused by diffraction. The bending of a wave by diffraction is the result of wave interference. The more accurate approach, then, is to determine the magnitude of each wave that is contributing to the diffraction and to determine how it is interfering with other waves to cause the diffraction effect observed.

It is useful to note that diffraction effects can depend on the shape of the wavefronts that encounter the edge around which the diffraction is occurring. Near the source the waves can have a very strong curvature relative to the wavelength. Far enough from the source the curvature diminishes significantly (creating essentially plane waves). Fresnel diffraction occurs when curved wavefronts interact. Fraunhofer diffraction occurs when planar wavefronts interact. In acoustics these two regions are known as the near field (the Fresnel zone) and the far field (the Fraunhofer zone), respectively. In optics these two zones are distinguished by regions in which two different integral approximations are valid.

6.1.3 Wave Propagation in Fluids

The propagation of an acoustic wave is described mathematically by the acoustic wave equation. One can use the approach of continuum mechanics to derive equations appropriate to physical acoustics [6.3]. In the continuum approach one postulates fields of density, stress, velocity, etc., all of which must satisfy basic conservation laws. In addition, there are constitutive relations which characterize the medium. For illustration, acoustic propagation through a compressible fluid medium is considered first. As the acoustic disturbance passes through a small area of the medium, the density of the medium at that location fluctuates. As the crest of the acoustic pressure wave passes through the region, the density in that region increases; this compression is known as the acoustic condensation. Conversely, when the trough of the acoustic wave passes through the region, the density of the medium at that location decreases; this expansion is known as the acoustic rarefaction.

In a gas, the constitutive relationship needed to characterize the pressure fluctuations is the ideal gas equation of state, $PV = nRT$, where P is the pressure of the gas, V is the volume of the gas, n is the number of moles of the gas, R is the universal gas constant ($R = 8.3145\,\mathrm{J/mol\,K}$), and T is the temperature of the gas. In a given, small volume of the gas, there is a vari-

ation of the density ρ from its equilibrium value ρ_0 caused by the change in pressure $\Delta P = P - P_0$ as the disturbance passes through that volume. (Here P is the pressure at any instant in time and P_0 is the equilibrium pressure.)

In many situations, there are further constraints on the system which simplify the constitutive relationship. A gas may act as a heat reservoir. If the processes occur on a time scale that allows heat to be exchanged, the gas is maintained at a constant temperature. In this case, the constitutive relationship can be simplified and expressed as $P_0 V_0 = PV =$ a constant. Since the number of gas molecules (and hence the mass) is constant, we can express this as the isothermal condition

$$\frac{P}{P_0} = \frac{\rho}{\rho_0} , \tag{6.22}$$

which relates the instantaneous pressure to the equilibrium pressure.

Most acoustic processes occur with no exchange of heat energy between adjacent volumes of the gas. Such processes are known as adiabatic or isentropic processes. Under such conditions, the constitutive relation is modified according to the adiabatic condition. For the adiabatic compression of an ideal gas, it has been found that the relationship

$$PV^{\gamma} = P_0 V_0^{\gamma} \tag{6.23}$$

holds, where γ is the ratio of the specific heat of the gas at constant pressure to the specific heat at constant volume. This leads to an adiabatic constraint for the acoustic process given by

$$\frac{P}{P_0} = \left(\frac{\rho}{\rho_0}\right)^{\gamma} . \tag{6.24}$$

When dealing with a real gas, one can make use of a Taylor expansion of the pressure variations caused by the fluctuations in density:

$$P = P_0 + \left[\frac{\partial P}{\partial \rho}\right]_{\rho_0} (\Delta\rho) + \frac{1}{2}\left[\frac{\partial^2 P}{\partial \rho^2}\right]_{\rho_0} (\Delta\rho)^2 + \dots , \tag{6.25}$$

where

$$\Delta\rho = (\rho - \rho_0) . \tag{6.26}$$

When the fluctuations in density are small, only the first-order terms in $\Delta\rho$ are nonnegligible. In this case, one can rearrange the above equation as

$$\Delta P = P - P_0 = \left[\frac{\partial p}{\partial \rho}\right]_{\rho_0} \Delta\rho = B\frac{\Delta\rho}{\rho_0} , \tag{6.27}$$

where $B = \rho_0\left[\frac{\partial p}{\partial \rho}\right]_{\rho_0}$ is the adiabatic bulk modulus of the gas. This equation describes the relationship between the pressure of the gas and its density during an expansion or contraction. [When the fluctuations are not small one has finite-amplitude (or nonlinear) effects which are considered later.]

Let us now consider the physical motion of a fluid as the acoustic wave passes through it. We begin with an infinitesimal volume element $\mathrm{d}V$ that is fixed in space, and we consider the motion of the particles as they pass through this region. Since mass is conserved, the net flux of mass entering or leaving this fixed volume must correspond to a change in the density of the fluid contained within that volume. This is expressed through the continuity equation,

$$\frac{\partial \rho}{\partial t} = -\nabla \cdot (\rho \boldsymbol{u}) . \tag{6.28}$$

The rate of mass change in the region is

$$\frac{\partial \rho}{\partial t} \mathrm{d}V , \tag{6.29}$$

and the net influx of mass into this region is given by

$$-\nabla \cdot (\rho \boldsymbol{u})\, \mathrm{d}V . \tag{6.30}$$

Consider a volume element of fluid as it moves with the fluid. This $\mathrm{d}V$ of fluid contains some infinitesimal amount of mass, $\mathrm{d}m$. The net force acting on this small mass of fluid is given by Newton's second law, $\mathrm{d}\boldsymbol{F} = \boldsymbol{a}\,\mathrm{d}m$. It can be shown that Newton's second law leads to a relationship between the particle velocity and the acoustic pressure. This relationship, given by

$$\rho_0 \frac{\partial \boldsymbol{u}}{\partial t} = -\nabla p , \tag{6.31}$$

is known as the linear Euler equation.

By combining our adiabatic pressure condition with the continuity equation and the linear Euler equation, one can derive the acoustic wave equation. This equation takes the form

$$\nabla^2 p = \frac{1}{c^2}\frac{\partial^2 p}{\partial t^2} , \tag{6.32}$$

where c is the speed of the sound wave which is given by

$$c = \sqrt{B/\rho_0} . \tag{6.33}$$

6.1.4 Wave Propagation in Solids

Similarly, one can consider the transmission of an acoustic wave through a solid medium. As an example, consider the one-dimensional case for propagation of an acoustic wave through a long bar of length L and cross-sectional area S. In place of the pressure, we consider the stress applied to the medium, which is given by the relationship

$$\sigma = F/S \tag{6.34}$$

where σ is the stress, F is the force applied along the length (L) of the bar, and S is the cross sectional area of the bar.

A stress applied to a material causes a resultant compression or expansion of the material. This response is the strain ζ. Strain is defined by the relationship,

$$\zeta = \Delta L/L_o \,, \tag{6.35}$$

where ΔL is the change in length of the bar, and L_o is the original length of the bar.

Let us consider the actual motion of particles as an acoustic wave passes through some small length of the bar $\mathrm{d}x$. This acoustic wave causes both a stress and a strain. The Hooke's law approximation, which can be used for most materials and vibration amplitudes, provides the constitutive relationship that relates the stress applied to the material with the resulting strain. Hooke's law states that stress is proportional to strain, or

$$\sigma = -Y\zeta \,. \tag{6.36}$$

If we consider the strain over our small length $\mathrm{d}x$, we can write this as

$$\frac{F}{S} = -Y\left(\frac{\mathrm{d}L}{\mathrm{d}x}\right) \tag{6.37}$$

or

$$F = -YS\left(\frac{\mathrm{d}L}{\mathrm{d}x}\right) . \tag{6.38}$$

The net force acting on our segment $\mathrm{d}x$ is given by

$$\mathrm{d}F = -\left(\frac{\partial F}{\partial x}\right)\mathrm{d}x = YS\left(\frac{\partial^2 L}{\partial x^2}\right)\mathrm{d}x \,. \tag{6.39}$$

Again, we can make use of Newton's second law, $\boldsymbol{F} = m\boldsymbol{a}$, and express this force in terms of the mass and acceleration of our segment. The mass of the segment of length $\mathrm{d}x$ is simply the density times the volume, or $\mathrm{d}m = \rho\,\mathrm{d}V = \rho S\,\mathrm{d}x$. Thus,

$$\mathrm{d}F = \left(\frac{\partial^2 L}{\mathrm{d}t^2}\right)\mathrm{d}m = \rho S\left(\frac{\partial^2 L}{\mathrm{d}t^2}\right)\mathrm{d}x \,, \tag{6.40}$$

where $\frac{\partial^2 L}{\mathrm{d}t^2}$ is the acceleration of the particles along the length $\mathrm{d}x$ as the acoustic wave stresses it. Equating our two expressions for the net force acting on our segment, $\mathrm{d}F$,

$$\frac{\partial^2 L}{\partial x^2} = \frac{1}{c^2}\left(\frac{\partial^2 L}{\partial t^2}\right) , \tag{6.41}$$

where

$$c = \sqrt{Y/\rho} \tag{6.42}$$

is the speed at which the acoustic wave is traveling through the bar. The form of the equation for the propagation of an acoustic wave through a solid medium is very similar to that for the propagation of an acoustic wave through a fluid.

Both of the wave equations developed so far have implicitly considered longitudinal compressions; for example, the derivation of the wave equation for an acoustic wave traveling down a thin bar assumed no transverse components to the motion. However, if we consider transverse motion, the resulting wave equation is of the same form as that for longitudinal waves. For longitudinal waves, the solution to the wave equation is given by

$$L(x,t) = A\cos(\omega t \pm kx + \phi)\ \text{(longitudinal)} \,, \tag{6.43}$$

where $L(x,t)$ represents the amount of compression or rarefaction at some position x and time t. For transverse waves, the solution to the wave equation is given by

$$y(x,t) = A\cos(\omega t \pm kx + \phi)\ \text{(transverse)} \,, \tag{6.44}$$

where $y(x,t)$ represents the vibration orthogonal to the direction of wave motion as a function of x and t. In both cases, A is the vibration amplitude, $k = 2\pi/\lambda$ is the wave number, and ϕ is the phase shift (which depends on the initial conditions of the system).

One can also consider an acoustic disturbance traveling in two dimensions; let us first consider a thin,

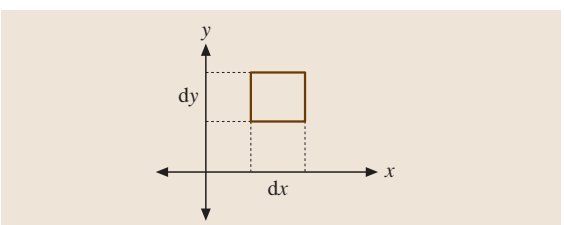


Fig. 6.9 Definitions necessary for the representation of a two-dimensional wave

Amazon EX1014 Page 234

stretched membrane as seen in Fig. 6.9. Let σ_s be the areal surface density (with units of kg/m^2), and let Γ be the tension per unit length. The transverse displacement of an infinitesimally small area of the membrane $\mathrm{d}S$ will now be a function of the spatial coordinates x and y along the two dimensions and the time t. Let us define the infinitesimal area $\mathrm{d}S = \mathrm{d}x\,\mathrm{d}y$ and the displacement of $\mathrm{d}S$ as the acoustic disturbance passes through it to be $u(x, y, t)$. Newton's second law can now be applied to our areal element $\mathrm{d}S$

$$\begin{aligned}&\left[(\Gamma\partial u/\partial x)_{x+\mathrm{d}x,y} - (\Gamma\partial u/\partial y)_{x,y}\right]\mathrm{d}y\\&\quad+\left[(\Gamma\partial u/\partial y)_{x,y+\mathrm{d}y} - (\Gamma\partial u/\partial x)_{x,y}\right]\mathrm{d}x\\&\quad=\Gamma\left(\frac{\partial^2 u}{\partial x^2}+\frac{\partial^2 u}{\partial y^2}\right)\mathrm{d}x\,\mathrm{d}y\end{aligned} \tag{6.45}$$

and

$$\Gamma\left(\frac{\partial^2 u}{\partial x^2}+\frac{\partial^2 u}{\partial y^2}\right)\mathrm{d}x\,\mathrm{d}y = \sigma_s\frac{\partial^2 u}{\partial t^2}\mathrm{d}x\,\mathrm{d}y \tag{6.46}$$

or

$$\nabla^2 u = \left(\frac{\partial^2 u}{\partial x^2}+\frac{\partial^2 u}{\partial y^2}\right) = \frac{1}{c^2}\frac{\partial^2 u}{\partial t^2}\,, \tag{6.47}$$

where $c = \sqrt{\Gamma/\sigma_s}$ is the speed of the acoustic wave in the membrane. Equation (6.47) now describes a two-dimensional wave propagating along a membrane.

The extension of this idea to three dimensions is fairly straightforward. As an acoustic wave passes through a three-dimensional medium, it can cause pressure fluctuations (leading to a volume change) in all three dimensions. The displacement u is now a function four variables $u = u(x, y, z, t)$. The volume change of a cube is given by

$$\Delta V = \Delta x\Delta y\Delta z\left(1+\frac{\partial u}{\partial x}\right)\left(1+\frac{\partial u}{\partial y}\right)\left(1+\frac{\partial u}{\partial z}\right)\,, \tag{6.48}$$

$$\Delta V \approx \Delta x\Delta y\Delta z\left(1+\frac{\partial u}{\partial x}+\frac{\partial u}{\partial y}+\frac{\partial u}{\partial z}\right)\,, \tag{6.49}$$

where the higher-order cross terms are negligibly small and have been dropped. This can be rewritten as

$$\Delta V = \Delta x\Delta y\Delta z\,(1+\nabla\cdot\boldsymbol{u})\,. \tag{6.50}$$

If the mass is held constant, and only the volume changes, the density change is given by

$$\rho_0+\rho_1 = \frac{\rho_0}{1+\nabla\cdot\boldsymbol{u}}\,. \tag{6.51}$$

But since the denominator is very close to unity, we may rewrite this using the binomial expansion. Solving for ρ_1 we have

$$\rho_1 \approx -\rho_0\nabla\cdot\boldsymbol{u}\,. \tag{6.52}$$

Again we can consider Newton's second law; without loss of generality, consider the force exerted along the x-direction from the pressure due to the acoustic wave, which is given by

$$F_x = [p(x,t)-p(x+\Delta x,t)]\,\Delta y\Delta z\,, \tag{6.53}$$

where $\Delta y\Delta z$ is the infinitesimal area upon which the pressure exerts a force. We can rewrite this as

$$F_x = -\Delta y\Delta z\left[\left(\frac{\partial p}{\partial x}\right)\Delta x\right]\,, \tag{6.54}$$

where the results for F_y and F_z are similar. Combining these, we can express the total force vector as

$$\boldsymbol{F} = -\nabla p\Delta x\Delta y\Delta z\,. \tag{6.55}$$

Using the fact that the mass can be expressed in terms of the density, we can rewrite this as

$$-\nabla p = \rho_0\frac{\partial^2\boldsymbol{u}}{\partial t^2}\,. \tag{6.56}$$

As in the case with fluids, we need a constitutive relationship to finalize the expression. For most situations in solids, the adiabatic conditions apply and the pressure fluctuation is a function of the density only. Making use of a Taylor expansion, we have

$$p \approx p(\rho_0)+(\rho-\rho_0)\frac{\mathrm{d}p}{\mathrm{d}\rho} \tag{6.57}$$

but since $p = p_0+p_1$, we can note that

$$p_1 = \rho_1\frac{\partial p}{\partial\rho}\,. \tag{6.58}$$

Using (6.52), we can eliminate ρ_1 from (6.58) to yield

$$p_1 = -\rho_0\left(\frac{\mathrm{d}p}{\mathrm{d}\rho}\right)\nabla\cdot\boldsymbol{u}\,. \tag{6.59}$$

We can eliminate the divergence of the displacement vector from this equation by taking the divergence of (6.56) and the second time derivative of (6.59). This gives two expressions that both equal $-\rho_0\partial^2(\nabla\cdot\boldsymbol{u})/\mathrm{d}t^2$ and thus are equal to each other. From this we can determine the full form of our wave equation

$$\frac{\partial^2 p_1}{\partial t^2} = c^2\nabla^2 p_1\,, \tag{6.60}$$

Amazon EX1014 Page 235

where c is again the wave speed and is given by

$$c^2 = \frac{\mathrm{d}p}{\mathrm{d}\rho} \,. \tag{6.61}$$

It should be noted that the above considerations were for an isotropic solid. In a crystalline medium, other complications can arise. These will be noted in a subsequent section.

6.1.5 Attenuation

In a real physical system, there are mechanisms by which energy is dissipated. In a gas, the dissipation comes from thermal and viscous effects. In a solid, dissipation comes from interactions with dislocations in the solid (holes, displaced atoms, interstitial atoms of other materials, etc.) and grain boundaries between adjacent parts of the solid, In practice, loss of energy over one acoustic cycle is negligible. However, as sound travels over a longer path, one expects these energy losses to cause a significant decrease in amplitude. In some situations, these dissipation effects must be accounted for in the solution of the wave equation.

The solution of the wave equation can be written in exponential form,

$$A = A_o \, \mathrm{e}^{\mathrm{i}(k'x - \omega t)} \,. \tag{6.62}$$

If one wishes to account for dissipation effects, one can assume that the wave number k' has an imaginary component, i. e.

$$k' = k + \mathrm{i}\alpha \,, \tag{6.63}$$

where k and α are both real and $\mathrm{i} = \sqrt{-1}$. Using this value of k' for the new wave number we have

$$A = A_o \, \mathrm{e}^{\mathrm{i}(k'x - \omega t)} = A_o \, \mathrm{e}^{\mathrm{i}\,[(k + \mathrm{i}\alpha)x - \omega t]} \,. \tag{6.64}$$

Simplifying, one has

$$\begin{aligned} A &= A_o \, \mathrm{e}^{\mathrm{i}(kx - \omega t) + \mathrm{i}^2 \alpha x} = A_o \, \mathrm{e}^{\mathrm{i}(kx - \omega t) - \alpha x} \\ &= A_o \, \mathrm{e}^{-\alpha x} \, \mathrm{e}^{\mathrm{i}(kx - \omega t)} \,, \end{aligned} \tag{6.65}$$

where α is known as the absorption coefficient. The resulting equation is modulated by a decreasing exponential function; i. e., an undriven acoustic wave passing through a lossy medium is damped to zero amplitude as $x \to \infty$.

6.2 Applications of Physical Acoustics

There are several interesting phenomena associated with the application of physical acoustics. The first is the wave velocity itself. Table 6.1 shows the wave velocity of sound in various fluids (both gases and liquids). Table 6.2 shows the wave velocity of sound in various solids (both metals and nonmetals). The velocity increases as one goes from gases to liquids to solids. The velocity variation from gases to liquids comes from the fact that gas molecules must travel farther before striking another gas molecule. In a liquid, molecules are closer together, which means that sound travels faster. The change from liquids to solids is associated with increase of binding strength as one goes from liquid to solid. The rigidity of a solid leads to higher sound velocity than is found in liquids.

6.2.1 Crystalline Elastic Constants

Another application of physical acoustics involves the measurement of the crystalline elastic constants in a lattice. In Sect. 6.1.2, we considered the propagation of an acoustic field along a one-dimensional solid (in which

Table 6.1 Typical values of the sound velocity in fluids (25 °C)

Gas	Velocity (m/s)	Liquid	Velocity (m/s)
Air	331	Carbon tetrachloride (CCl_4)	929
Carbon dioxide (CO_2)	259	Ethanol (C_2H_6O)	1207
Hydrogen (H_2)	1284	Ethylene glycol ($C_2H_6O_2$)	1658
Methane (CH_4)	430	Glycerol ($C_3H_8O_3$)	1904
Oxygen (O_2)	316	Mercury (Hg)	1450
Sulfur dioxide (SO_2)	213	Water (distilled)	1498
Helium (H_2)	1016	Water (sea)	1531

Amazon EX1014 Page 236

Table 6.2 Typical values of the sound velocity in solids (25 °C)

Metals	Longitudinal velocity (m/s)	Shear (transverse) velocity (m/s)
Aluminum (rolled)	6420	3040
Beryllium	12890	8880
Brass (0.70 Cu, 0.30 Zn)	4700	2110
Copper (rolled)	5010	2270
Iron	5960	3240
Tin (rolled)	3320	1670
Zinc (rolled)	4210	2440
Lead (rolled)	1960	610
Nonmetals	**Longitudinal velocity (m/s)**	**Shear (transverse) velocity (m/s)**
Fused silica	5968	3764
Glass (Pyrex)	5640	3280
Lucite	2680	1100
Rubber (gum)	1550	–
Nylon	2620	1070

the internal structure of the solid played no role in the propagation of the wave). Real solids exist in three dimensions, and the acoustic field propagation depends on the internal structure of the material. The nature of the forces between the atoms (or molecules) that make up the lattice cause the speed of sound to be different along different directions of propagation (since the elastic force constants are different along the different directions). The measurement of crystal elastic constants depends on the ability to make an accurate determination of the wave velocity in different directions in a crystalline lattice. This can be done by cutting (or lapping) crystals in such a manner that parallel faces are in the directions to be measured.

For an isotropic solid one can determine the compressional modulus and the shear modulus from a single sample since both compressional and shear waves can be excited. For cubic crystals at least two orientations are required since there are three elastic constants (and still only two waves to be excited). For other crystalline symmetries a greater number of measurements is required.

6.2.2 Resonant Ultrasound Spectroscopy (RUS)

Recently a new technique for measuring crystalline elastic constants, known as resonant ultrasound spectroscopy (RUS), has been developed [6.4]. Typically, one uses a very small sample with a shape that has known acoustic resonant modes (usually a small parallelepiped, though sometimes other geometries such as cylinders are used). The sample is placed so that the driving transducer makes a minimal contact with the surface of the sample [the boundaries of the sample must be pressure-free and (shearing) traction-free for the technique to work]. Figure 6.10 shows a photograph of a small parallelepiped sample mounted in an RUS apparatus.

After the sample is mounted, the transducer is swept through a range of frequencies (usually from a few hertz to a few kilohertz) and the response of the material is

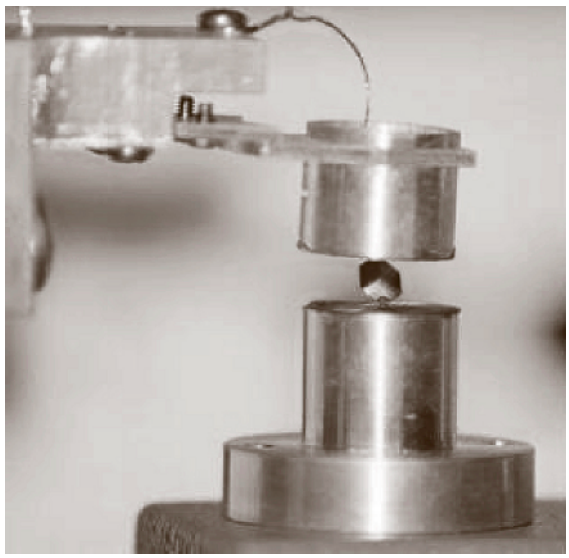


Fig. 6.10 Sample mounted for an RUS measurement. Sample dimensions are 2.0 mm × 2.5 mm × 3.0 mm

Amazon EX1014 Page 237

measured. Some resonances are caused by the geometry of the sample (just as a string of fixed length has certain resonant frequencies determined by the length of the string). In the RUS technique, some fairly sophisticated software eliminates the geometrical resonances; the remaining resonances are resonances of the internal lattice structure of the material. These resonances are determined by the elastic constants. The RUS technique, then, is used to evaluate all elastic constants from a single sample from the spectrum of resonant frequencies produced by the various internal resonances.

Measurement of Attenuation with the RUS Technique

The RUS technique is also useful for measuring the attenuation coefficients of solid materials. The resonance curves generated by the RUS experiment are plots of the response amplitude of the solid as a function of input frequency (for a constant input amplitude). Every resonance curve has a parameter known as the Q of the system. The Q value can be related to the maximum amplitude $1/e$ value, which in turn can be related to the attenuation coefficient. Thus, the resonance curves generated by the RUS experiment can be used to determine the attenuation in the material at various frequencies.

6.2.3 Measurement Of Attenuation (Classical Approach)

Measurement of attenuation at audible frequencies and below is very difficult. Attenuation is usually measured at ultrasonic frequencies since the plane-wave approximation can be satisfied. The traditional means of measuring the acoustic attenuation requires the measurement of the echo train of an acoustic tone burst as it travels through the medium. Sound travels down the length of the sample, reflects from the opposite boundary and returns to its origin. During each round trip, it travels a distance twice the length of the sample. The transducer used to emit the sound now acts as a receiver and measures the amplitude as it strikes the initial surface. The sound then continues to reflect back and forth through the sample. On each subsequent round trip, the sound amplitude is diminished.

Measured amplitude values are then fit to an exponential curve, and the value of the absorption coefficient is determined from this fit. Actually, this experimental arrangement measures the insertion loss of the system, the losses associated with the transducer and the adhesive used to bond the transducer to the sample as well as the attenuation of sound in the sample. However, the values of the insertion loss of the system and the attenuation inside the sample are usually very close to each other. If one needs the true attenuation in the sample, one can

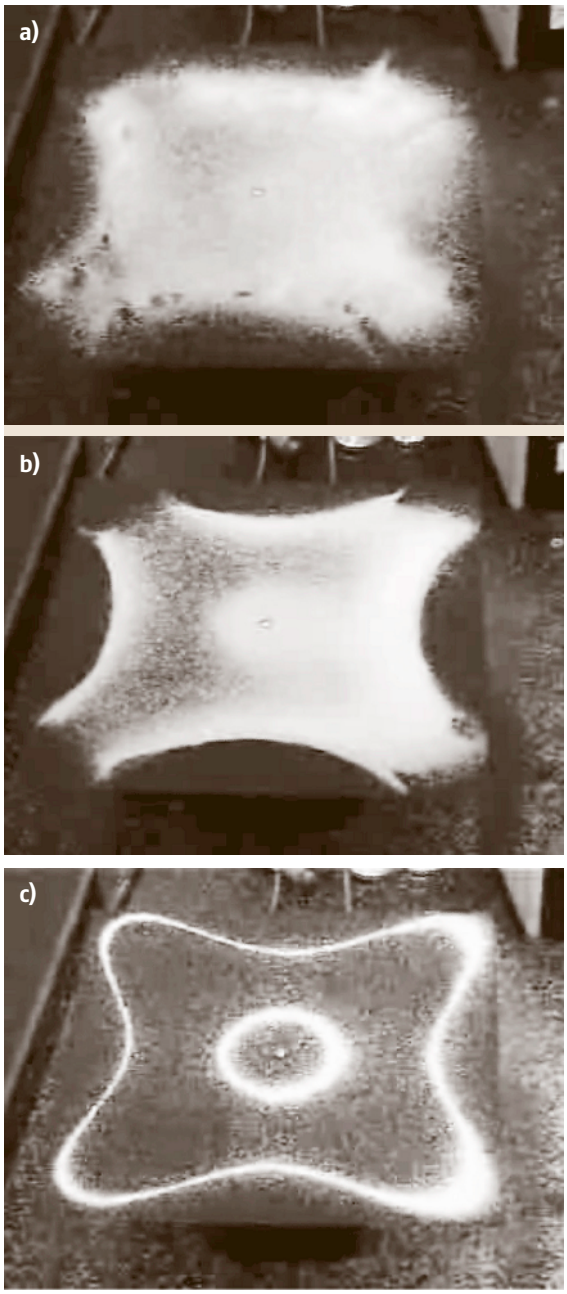


Fig. 6.11 **(a)** Fine rice on a plate; **(b)** as the plate is excited acoustically the rice begins to migrate to the nodes; **(c)** the Chladni pattern has formed

Amazon EX1014 Page 238

use various combinations of transducers to account for the other losses in the system [6.5].

Losses in a sample can come from a number of sources: viscosity, thermal conductivity, and molecular relaxation. Viscosity and thermal conductivity are usually referred to as classical losses. They can be calculated readily. Both are linearly dependent on frequency. Relaxation is a frequency-dependent phenomenon. The maximum value occurs when the sound frequency is the same as the relaxation frequency, which is determined by the characteristics of the medium. Because of this complication, determination of the attenuation to be expected can be difficult.

6.2.4 Acoustic Levitation

Acoustic levitation involves the use of acoustic vibrations to move objects from one place to the other, or to keep them fixed in space. Chladni produced an early form of acoustic levitation to locate the nodal planes in a vibrating plate. Chladni discovered that small particles on a plate were moved to the nodal planes by plate vibrations. An example of Chladni figures is shown in Fig. 6.11. Plate vibrations have caused powder to migrate toward nodal planes, making them much more obvious.

The use of radiation pressure to counterbalance gravity (or buoyancy) has recently led to a number of situations in which levitation is in evidence.

1. The force exerted on a small object by radiation pressure can be used to counterbalance the pull of gravity [6.6].
2. The radiation force exerted on a bubble in water by a stationary ultrasonic wave has been used to counteract the hydrostatic or buoyancy force on the bubble. This balance of forces makes it possible for the bubble to remain at the same point indefinitely. Single-bubble sonoluminescence studies are now possible [6.7].
3. Latex particles having a diameter of 270 μm or clusters of frog eggs can be trapped in a potential well generated by oppositely directed focused ultrasonic beams. This makes it possible to move the trapped objects at will. Such a system has been called *acoustic tweezers* by *Wu* [6.8].

6.2.5 Sonoluminescence

Sonoluminescence is the conversion of high-intensity acoustic energy into light. Sonoluminescence was first discovered in water in the early 1930s [6.9, 10]. However, interest in the phenomenon languished for several decades.

In the late seventies, a new type of sonoluminescence was found to occur in solids [6.11, 12]. This can occur when high-intensity Lamb waves are generated along a thin plate of ferroelectric material which is driven at the frequency of mechanical resonance in a partial vacuum (the phenomenon occurs at about 0.1 atm). The acoustic fields interact with dislocations and defects in the solid which leads to the generation of visible light in ferroelectric materials. Figure 6.12 shows a diagram of the experimental setup and a photograph of the light emitted during the excitation of solid-state sonoluminescence.

In the early 1990s, sonoluminescence emissions from the oscillations of a single bubble in water were discovered [6.7]. With single-bubble sonoluminescence, a single bubble is placed in a container of degassed water (often injected by a syringe). Sound is used to push the bubble to the center of the container and to set the bubble into high-amplitude oscillation. The dynamic range for the bubble radius through an oscillation can be as great

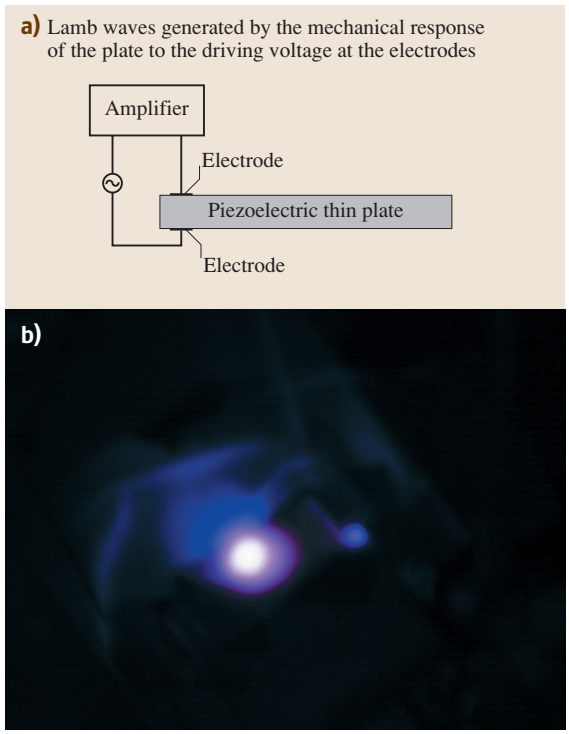


Fig. 6.12 **(a)** Block diagram of apparatus for solid-state sonoluminescence and **(b)** photograph of light emitted from a small, thin plate of $LiNbO_3$

as 50 μm to 5 μm through one oscillation [6.13–15]. The light is emitted as the bubble goes through its minimum radius. Typically, one requires high-amplitude sound corresponding to a sound pressure level in excess of 110 dB. The frequency of sound needed to drive the bubble into sonoluminescence is in excess of 30 kHz, which is just beyond the range of human hearing.

Another peculiar feature of the sonoluminescence phenomenon is the regularity of the light emissions. Rather than shining continuously, the light is emitted as a series of extremely regular periodic flashes. This was not realized in the initial sonoluminescence experiments, because the rate at which the flashes appear requires a frequency resolution available only in the best detectors. The duration of the pulses is less than 50 ps. The interval between pulses is roughly 35 μs. The time between flashes varies by less than 40 ps.

The discovery of single-bubble sonoluminescence has caused a resurgence of interest in the phenomenon. The light emitted appears to be centered in the near-ultraviolet and is apparently black body in nature (unfortunately water absorbs much of the higher-frequency light, so a complete characterization of the spectrum is difficult to achieve). Adiabatic compression of the bubble through its oscillation would suggest temperatures of about 10 000 K (with pressures of about 10 000 atm). The temperatures corresponding to the observed spectra are in excess of 70 000 K [6.13]. In fact, they may even be much higher.

Since the measured spectrum suggests that the actual temperatures and pressures within the bubble may be quite high, simple compression does not seem to be an adequate model for the phenomenon. It is possible that the collapsing bubble induces a spherically symmetric shockwave that is driven inward towards the center of the bubble. These shocks could possibly drive the temperatures and pressures in the interior of the bubble high enough to generate the light. (Indeed, some physicists have suggested that sonoluminescence might enable the ignition of fusion reactions, though as of this writing that remains speculation).

6.2.6 Thermoacoustic Engines (Refrigerators and Prime Movers)

Another interesting application of physical acoustics is that of thermoacoustics. Thermoacoustics involves the conversion of acoustic energy into thermal energy or the reverse process of converting thermal energy into sound [6.16]. Figure 6.13 shows a photograph of a thermoacoustic engine. To understand the processes

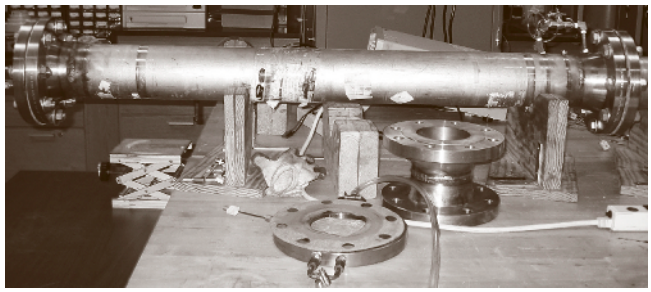


Fig. 6.13 A thermoacoustic engine

involved in thermoacoustics, let us consider a small packet of gas in a tube which has a sound wave traveling through it (thermoacoustic effects can occur with either standing or progressive waves). As the compression of the wave passes through the region containing the packet of gas, three effects occur:

1. The gas compresses adiabatically, its temperature increases in accordance with Boyle's law (due to the compression), and the packet is displaced some distance down the tube.
2. As the rarefaction phase of the wave passes through the gas, this process reverses.
3. The wall of the tube acts as a heat reservoir. As the packet of gas goes through the acoustic process, it deposits heat at the wall during the compression phase (the wall literally conducts the heat away from the compressed packet of gas).

This process is happening down the entire length of the tube; thus a temperature gradient is established down the tube.

To create a useful thermoacoustic device, one must increase the surface area of wall that the gas is in contact with so that more heat is deposited down the tube. This is accomplished by inserting a *stack* into the tube. In the inside of the tube there are several equally spaced plates which are also in contact with the exterior walls of the tube. Each plate provides additional surface area for the deposition of thermal energy and increases the overall thermoacoustic effect. (The stack must not impede the wave traveling down the tube, or the thermoacoustic effect is minimized.) Modern stacks use much more complicated geometries to improve the efficiency of the thermoacoustic device (indeed the term stack now is a misnomer, but the principle remains the same). Figure 6.14 shows a photograph of a stack used in a modern thermoacoustic engine. The stack shown in Fig. 6.14 is made of a ceramic material.

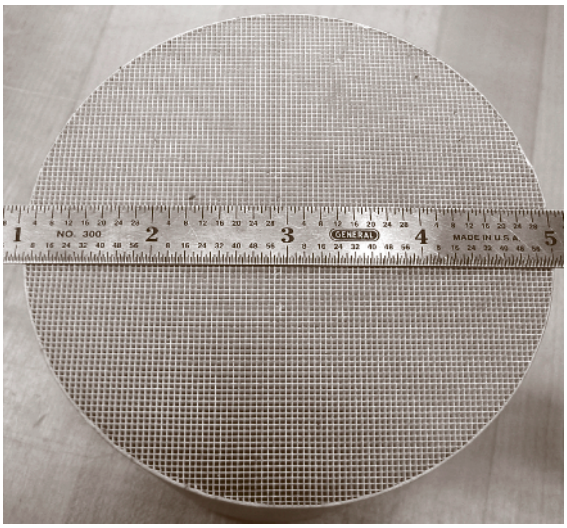


Fig. 6.14 A stack used in a thermoacoustic engine. Pores allow the gas in the tube to move under the influence of the acoustic wave while increasing the surface area for the gas to deposit heat

A thermoacoustic device used in this way is a thermoacoustic refrigerator. The sound generated down the tube (by a speaker or some other device) is literally pumping heat energy from one end of the tube to the other. Thus, one end of the tube gets hot and the other cools down (the cool end is used for refrigeration).

The reverse of this thermoacoustic refrigeration process can also occur. In this case, the tube ends are fitted with heat exchangers (one exchanger is hot, one is cold). The heat delivered to the tube by the heat exchangers does work on the system and generates sound in the tube. The frequency and amplitudes of the generated waves depend on the geometry of the tube and the stacks. When a thermoacoustic engine is driven in this way (converting heat into sound), it is known as a prime mover.

Though much research to improve the efficiency of thermoacoustic engines is ongoing, the currently obtainable efficiencies are quite low compared to standard refrigeration systems. Thermoacoustic engines, however, offer several advantages: they have no moving parts to wear out, they are inexpensive to manufacture, and they are highly reliable, which is useful if refrigeration is needed in inaccessible places.

One practical application for thermoacoustic engines is often cited: the liquefaction of natural gas for transport. This is accomplished by having two thermoacoustic engines, one working as a prime mover and the other working as a refrigerator. A small portion of the gas is ignited and burned to produce heat. The heat is applied to the prime mover to generate sound. The sound is directed into a second thermoacoustic engine that acts as a refrigerator. The sound from the prime mover pumps enough heat down the refrigerator to cool the gas enough to liquefy it for storage. The topic of thermoacoustics is discussed in greater detail in Chap. 7.

6.2.7 Acoustic Detection of Land Mines

Often, during wars and other armed conflicts, mine fields are set up and later abandoned. Even today it is not uncommon for mines originally planted during World War II to be discovered still buried and active. According to the humanitarian organization CARE, 70 people are killed each day by land mines, with the vast majority being civilians. Since most antipersonnel mines manufactured today contain no metal parts, electromagnetic-field-based metal detectors cannot locate them for removal. Acoustic detection of land mines offers a potential solution for this problem.

The approach used in acoustic land-mine detection is conceptually simple but technically challenging. Among the first efforts made at acoustic land-mine detection were those of *House* and *Pape* [6.17]. They sent sounds into the ground and examined the reflections from buried objects. *Don* and *Rogers* [6.18] and *Caulfield* [6.19] improved the technique by including a reference beam that provided information for comparison with the reflected signals. Unfortunately, this technique yielded too many false positives to be practical because one could not distinguish between a mine and some other buried object such as a rock or the root of a tree.

Newer techniques involving the coupling of an acoustic signal with a seismic vibration have been developed with much more success [6.20–24]. They make use of remote sensing and analysis by computer. Remote measurement of the acoustic field is done with a laser Doppler vibrometer (LDV), which is a an optical device used to measure velocities and displacements of vibrating bodies without physical contact. With this technique, the ground is excited acoustically with lower frequencies (usually on the order of a few hundred Hz). The LDV is used to measure the vibration of the soil as it responds to this driving force. If an object is buried under the soil in the region of excitation, it alters the resonance characteristics of the soil and introduces nonlinear effects. With appropriate digital signal processing and analysis, one can develop a system capable of recognizing different types of structures buried beneath the soil. This reduces

the number of false positives and makes the system more efficient.

6.2.8 Medical Ultrasonography

For the general public, one of the most familiar applications of physical acoustics is that of medical ultrasonography. Medical ultrasonography is a medical diagnostic technique which can use sound information to construct images for the visualization of the size, structure and lesions of internal organs and other bodily tissues. These images can be used for both diagnostic and treatment purposes (for example enabling a surgeon to visualize an area with a tumor during a biopsy). The most familiar application of this technique is obstetric ultrasonography, which uses the technique to image and monitor the fetus during a pregnancy. An ultrasonograph of a fetus is shown in Fig. 6.15.

This technique relies on the fact that in different materials the speed of sound and acoustic impedance are different. A collimated beam of high-frequency sound is projected into the body of the person being examined. The frequencies chosen will depend on the application. For example, if the tissue is deeper within the body, the sound must travel over a longer path and attenuation affects can present difficulties. Using a lower ultrasonic frequency reduces attenuation. Alternatively, if a higher resolution is needed, a higher frequency is used. In each position where the density of the tissue changes, there is an acoustic impedance mismatch. Therefore, at each interface between various types of tissues some of the sound is reflected. By measuring the time between echoes, one can determine the spatial position of the various tissues.

If a single, stationary transducer is used; one gets spatial information that lies along a straight line. Typically, the probe contains a phased array of transducers that are used to generate image information from different directions around the area of interest. The different transducers in the probe send out acoustic pulses that are reflected from the various tissues. As the acoustic signals return, the transducers receive them and convert the information into a digital, pictorial representation. One must also match the impedances between the surface of the probe and the body. The head of the probe is usually soft rubber, and the contact between the probe and the body is impedance-matched by a water-based gel.



Fig. 6.15 Ultrasonograph of a fetus

To construct the image, each transducer (which themselves are separated spatially somewhat) measures the strength of the echo. This measurement indicates how much sound has been lost due to attenuation (different tissues have different attenuation values). Additionally, each transducer measures the delay time between echoes, which indicates the distance the sound has traveled before encountering the interface causing the echo (actually since the sound has made a round trip during the echo the actual displacement between the tissues is $\frac{1}{2}$ of the total distance traveled). With this information a two-dimensional image can be created. In some versions of the technique, computers can be used to generate a three-dimensional image from the information as well.

A more esoteric form of ultrasonograpy, Doppler ultrasonography, is also used. This technique requires separate arrays of transducers, one for broadcasting a continuous-wave acoustic signal and another for receiving it. By measuring a frequency shift caused by the Doppler effect, the probe can detect structures moving towards or away from the probe. For example, as a given volume of blood passes through the heart or some other organ, its velocity and direction can be determined and visualized. More-recent versions of this technique make use of pulses rather than continuous waves and can therefore use a single probe for both broadcast and reception of the signal. This version of the technique requires more-advanced analysis to determine the frequency shift. This technique presents advantages because the timing of the pulses and their echoes can be measured to provide distance information as well.

Amazon EX1014 Page 242

6.3 Apparatus

Given the diverse nature of physical acoustics, any two laboratories conducting physical acoustics experiments might have considerably different types of equipment and apparatus (for example, experiments dealing with acoustic phenomena in water usually require tanks to hold the water). As is the case in any physics laboratory, it is highly useful to have access to a functioning machine shop and electronics shop for the design, construction, and repair of equipment needed for the physical acoustics experiment that is being conducted. Additionally, a wide range of commercial equipment is available for purchase and use in the lab setting.

6.3.1 Examples of Apparatus

Some typical equipment in an acoustic physics lab might include some of the following:

- Loudspeakers;
- Transducers (microphones/hydrophones);
- Acoustic absorbers;
- Function generators, for generating a variety of acoustic signals including single-frequency sinusoids, swept-frequency sinusoids, pulses, tone bursts, white or pink noise, etc.;
- Electronics equipment such as multimeters, impedance-matching networks, signal-gating equipment, etc.;
- Amplifiers (acoustic, broadband, Intermediate Frequency (IF), lock-in);
- Oscilloscopes. Today's digital oscilloscopes (including virtual oscilloscopes implemented on personal computers) can perform many functions that previously required several different pieces of equipment; for example, fast Fourier transform (FFT) analysis previously required a separate spectrum analyzer; waveform averaging previously required a separate boxcar integrator, etc.);
- Computers (both for control of apparatus and analysis of data).

For audible acoustic waves in air the frequency range is typically 20–20 000 Hz. This corresponds to a wavelength range of 16.5 m–16.5 mm. Since these wavelengths often present difficulties in the laboratory, and since the physical principles apply at all frequencies, the laboratory apparatus is often adapted to a higher frequency range. The propagating medium is often water since a convenient ultrasonic range of 1–100 MHz gives a convenient wavelength range of 0.014–1.4 mm. The experimental arrangements to be described below are for some specialized applications and cover this wavelength range, or somewhat lower. The results, however, are useful in the audio range as well.

6.3.2 Piezoelectricity and Transduction

In physical acoustics transducers play an important role. A transducer is a device that can convert a mechanical vibration into a current or vice versa. Transducers can be used to generate sound or to detect sound. Audible frequencies can be produced by loudspeakers and received by microphones, which often are driven electromagnetically. (For example, a magnet interacting with a current-carrying coil experiences a magnetic force that can accelerate it, or if the magnet is moved it can induce a corresponding current in the coil.) The magnet could be used to drive the cone of a loudspeaker to convert a current into an audible tone (or speech, or music, etc.). Similarly, one can use the fact that the capacitance between two parallel-plate capacitors varies as a function of the separation distance between two plates. A capacitor with one plate fixed and the other allowed to vibrate in response to some form of mechanical forcing (say the force caused by the pressure of an acoustic wave) is a transducer. With a voltage across the two plates, an electrical current is generated as the plates move with respect to one another under the force of the vibration of an acoustic wave impinging upon it. These types of transducers are described in Chap. 24.

The most common type of transducers used in the laboratory for higher-frequency work are piezoelectric-element-based transducers. In order to understand how these transducers work (and are used) we must first examine the phenomenon of piezoelectricity.

Piezoelectricity is characterized by the both direct piezoelectric effect, in which a mechanical stress applied to the material causes a potential difference across the surface of the faces to which the stress is applied, and the secondary piezoelectric effect, in which a potential difference applied across the faces of the material causes a deformation (expansion or contraction). The deformation caused by the direct piezoelectric effect is on the order of nanometers, but leads to many uses in acoustics such as the production and detection of sound, microbalance applications (where very small masses are measured by determining the change in the resonance frequency of a piezoelectric crystal when it is loaded

with the small mass), and frequency generation/control for oscillators.

Piezoelectricity arises in a crystal when the crystal's unit cell lacks a center of symmetry. In a piezoelectric crystal, the positive and negative charges are separated by distance. This causes the formation of electric dipoles, even though the crystal is electrically neutral overall. The dipoles near one another tend to orient themselves along the same direction. These small regions of aligned dipoles are known as domains because of the similarity to the magnetic analog. Usually, these domains are oriented randomly, but can be aligned by the application of a strong electric field in a process known as poling (typically the sample is poled at a high temperature and cooled while the electric field is maintained). Of the 32 different crystal classifications, 20 exhibit piezoelectric properties and 10 of those are polar (i. e. spontaneously polarized). If the dipole can be reversed by an applied external electric field, the material is additionally known as a ferroelectric (in analogy to ferromagnetism).

When a piezoelectric material undergoes a deformation induced by an external mechanical stress, the symmetry of the charge distribution in the domains is disturbed. This gives rise to a potential difference across the surfaces of the crystal. A 2 kN force ($\approx$ 500 lbs) applied across a 1 cm cube of quartz can generate up to 12 500 V of potential difference.

Several crystals are known to exhibit piezoelectric properties, including tourmaline, topaz, rochelle salt, and quartz (which is most commonly used in acoustic applications). In addition, some ceramic materials with perovskite or tungsten bronze structures, including barium titanate ($BaTiO_3$), lithium niobate ($LiNbO_3$), PZT [$Pb(ZrTi)O_3$], $Ba_2NaNb_5O_5$, and $Pb_2KNb_5O_{15}$, also exhibit piezoelectric properties. Historically, quartz was the first piezoelectric material widely used for acoustics applications. Quartz has a very sharp frequency response, and some unfavorable electrical properties such as a very high electrical impedance which requires impedance matching for the acoustic experiment. Many of the ceramic materials such as PZT or lithium niobate have a much broader frequency response and a relatively low impedance which usually does not require impedance matching. For these reasons, the use of quartz has largely been supplanted in the acoustics lab by transducers fashioned from these other materials. Although in some situations (if a very sharp frequency response is desired), quartz is still the best choice.

In addition to these materials, some polymer materials behave as electrets (materials possessing a quasi-permanent electric dipole polarization). In most piezoelectric crystals, the orientation of the polarization is limited by the symmetry of the crystal. However, in an electret this is not the case. The electret material polyvinylidene fluoride (PVDF) exhibits piezoelectricity several times that of quartz. It can also be fashioned more easily into larger shapes.

Since these materials can be used to convert a sinusoidal electrical current into a corresponding sinusoidal mechanical vibration as well as convert a mechanical vibration into a corresponding electrical current, they provide a connection between the electrical system and the acoustic system. In physical acoustics their ability to produce a single frequency is especially important. The transducers to be described here are those which are usually used to study sound propaga-

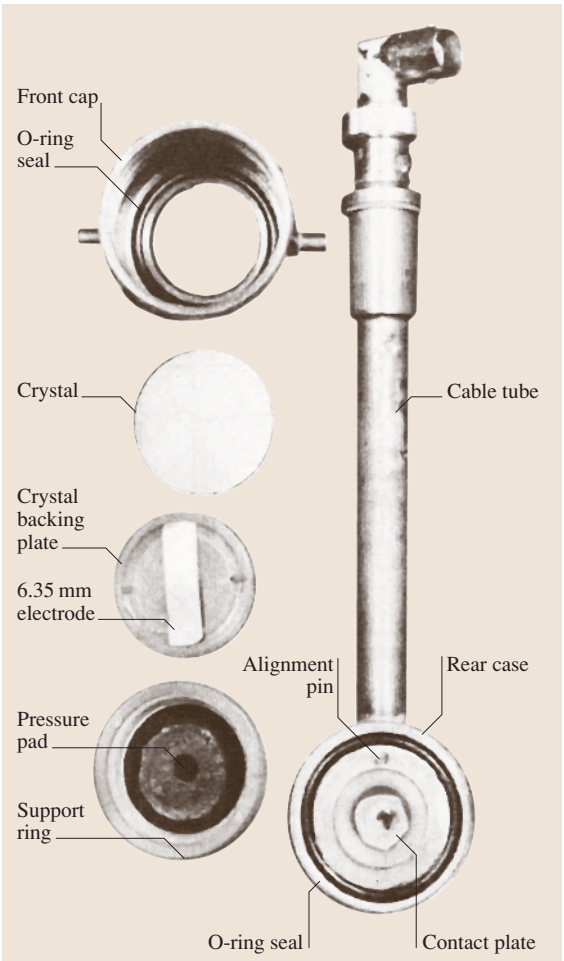


Fig. 6.16 Transducer housing

tion in liquids or in solids. The frequencies used are ultrasonic.

The first transducers were made from single crystals. Single crystals of x-cut quartz were preferred for longitudinal waves, and y-cut for transverse waves, their thickness determined by the frequency desired. Single crystals are still used for certain applications; however, the high-impedance problems were solved by introduction of polarized ceramics containing barium titanate or strontium titanate. These transducers have an electrical impedance which matches the 50 Ω impedance found on most electrical apparatus. Low-impedance transducers are currently commercially available.

Such transducers can be used to generate or receive sound. When used as a receiver in liquids such transducers are called hydrophones. For the generation of ultrasonic waves in liquids, one surface of the transducer material should be in contact with the liquid and the other surface in contact with air (or other gas). With this arrangement, most of the acoustic energy enters the liquid. In the laboratory it is preferable to have one surface at the ground potential and electrically drive the other surface, which is insulated. Commercial transducers which accomplish these objectives are available. They are designed for operation at a specific frequency. A transducer housing is shown in Fig. 6.16. The transducer crystal and the (insulated) support ring can be changed to accommodate the frequency desired. In the figure a strip back electrode is shown. For generating acoustic vibration over the entire surface, the back of the transducer can be coated with an electrode. The width which produces a Gaussian output in one dimension is described in [6.25]. The use of a circular electrode that can produce a Gaussian amplitude distribution in two dimensions is described in [6.26].

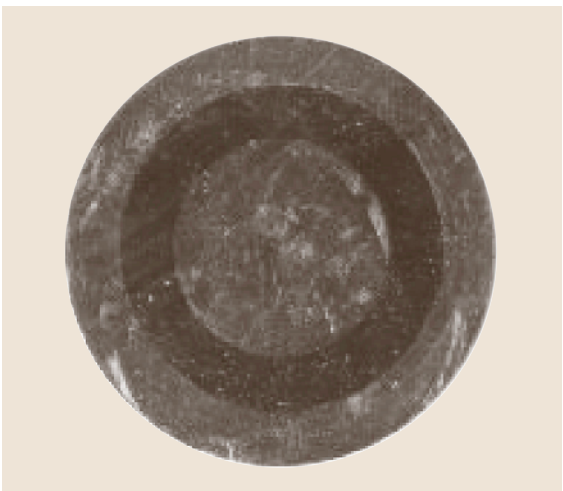


Fig. 6.17 Coaxial transducer

For experiments with solids the transducer is often bonded directly to the solid without the need for an external housing. For single-transducer pulse-echo operation the opposite end of the sample must be flat because it must reflect the sound. For two-transducer operation one transducer is the acoustic transmitter, the other the receiver.

With solids it is convenient to use coaxial transducers because both transducer surfaces must be electrically accessible. The grounded surface in a coaxial transducer can be made to wrap around the edges so it can be accessed from the top as well. An example is shown in Fig. 6.17. The center conductor is the high-voltage terminal. The outer conductor is grounded; it is in electrical contact with the conductor that covers the other side of the transducer.

6.3.3 Schlieren Imaging

Often it is useful to be able to see the existence of an acoustic field. The Schlieren arrangement shown in Fig. 6.18 facilitates the visualization of sound fields in water. Light from a laser is brought to focus on a circular aperture by lens 1. The circular aperture is located at a focus of lens 2, so that the light emerges parallel. The water tank is located in this parallel light. Lens 3 forms a real image of the contents of the water tank on the screen, which is a photographic negative for photographs. By using a wire or an ink spot on an optical flat at the focus of lens 3, one produces conditions for dark-field illumination. The image on the screen, then, is an image of the ultrasonic wave propagating through the water. The fact that the ultrasonic wave is propagating through the water means that the individual wavefronts are not seen. To see the individual wavefronts, one must add a stroboscopic light source synchronized with the ultrasonic wave. In this way the light can be on at the frequency of the sound and produce a photograph which shows the individual wavefronts.

On some occasions it may be useful to obtain color images of the sound field; for example, one can show an incident beam in one color and its reflection from an interface in a second color for clarity. The resultant photographs can be beautiful; however, to a certain extent their beauty is controlled by the operator. The merit of color Schlieren photography may be more from its aesthetic or pedagogical value, rather than its practical application. This is the reason that color Schlieren

Amazon EX1014 Page 245

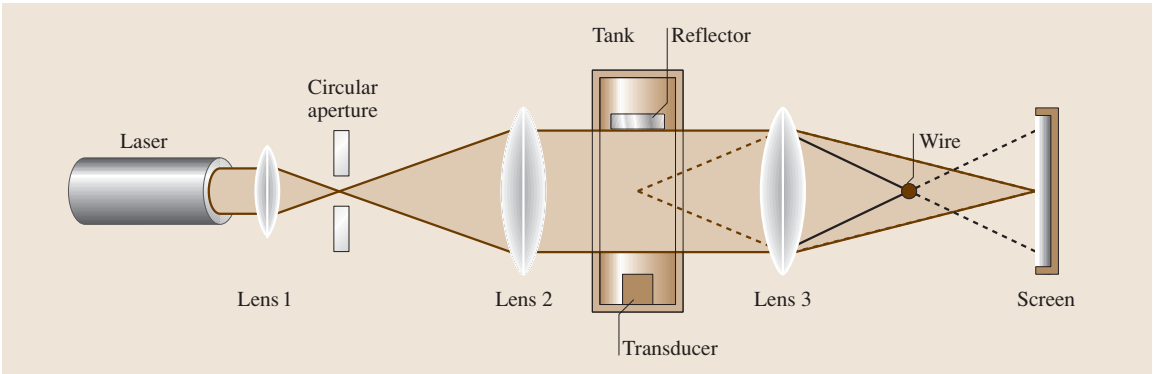


Fig. 6.18 Diagram of a Schlieren system

photographs are seldom encountered in a physical acoustic laboratory. For completeness, however, it may be worthwhile to describe the process.

The apparatus used is analogous to that given in Fig. 6.18. The difference is that a white-light source is

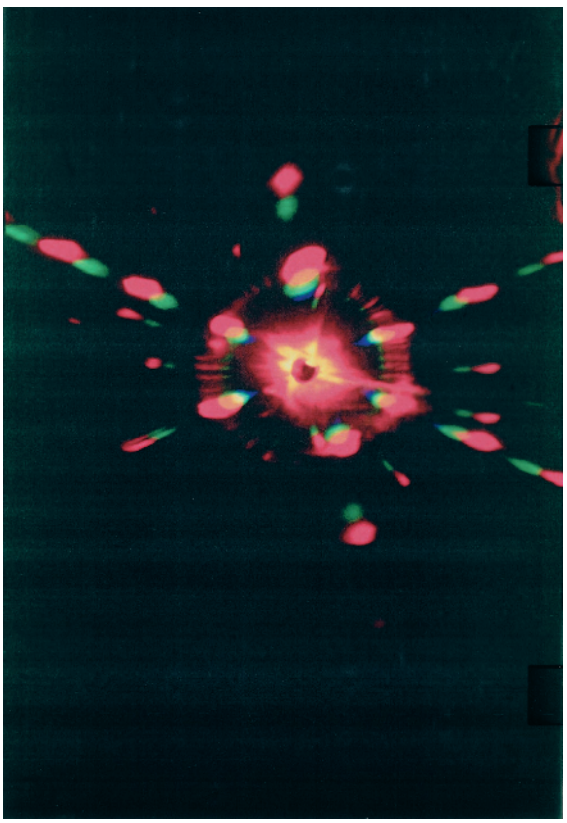


Fig. 6.19 Spectra formed by the diffraction of light through a sound field

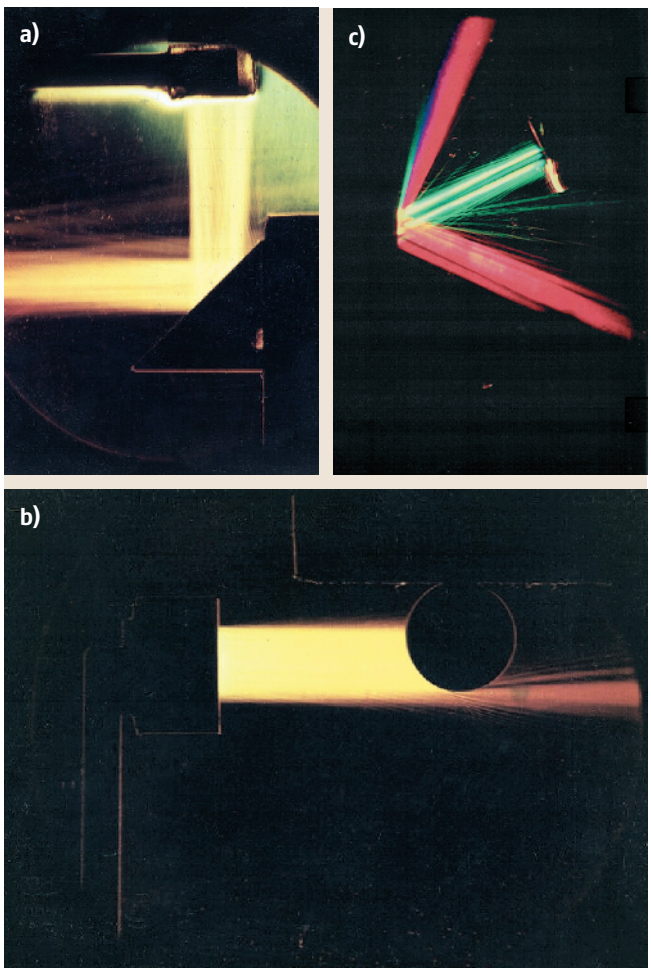


Fig. 6.20 Schlieren photographs showing reflection and diffraction of ultrasonic waves by a solid immersed in water

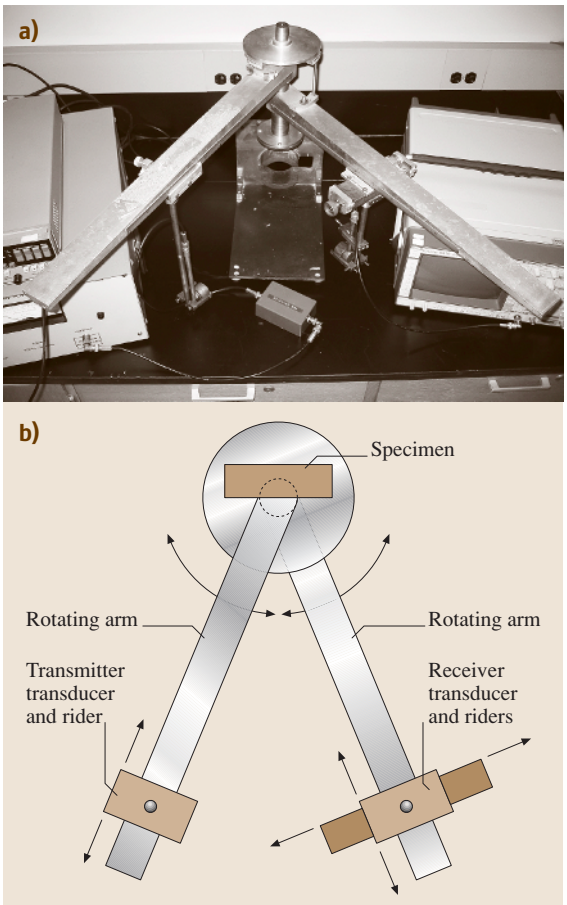


Fig. 6.21 **(a)** Photograph of a goniometer system; **(b)** diagram of a goniometer system

used in the place of the monochromatic light from the laser. As the light diffracts, the diffraction pattern formed at the focus of lens 3 is made up of complete spectra (with each color of the spectra containing a complete image of the acoustic field). A photograph showing the spectra produced is shown in Fig. 6.19. If the spectra are allowed to diverge beyond this point of focus, they will combine into a white-light image of the acoustic field. However, one can use a slit (rather than using a wire or an ink spot at this focus to produce dark-field illumination) to pass only the desired colors. The position of the slit selects the color of the light producing the image of the sound field. If one selects the blue-colored incident beam from one of the spectra, and the red-colored reflected beam from another spectrum (blocking out all the other colors), a dual-colored image results. Since each diffraction order contains enough information to produce a complete sound field image, the operator has control over its color. Spatial filtering, then, becomes a means of controlling the color of the various parts of the image. Three image examples are given in Fig. 6.20. Figure 6.20a is reflection of a sound beam from a surface. Figure 6.20b shows diffraction of sound around a cylinder. Figure 6.20c shows backward displacement at a periodic interface. The incident beam is shown in a different color from that of the reflected beam and the diffraction order.

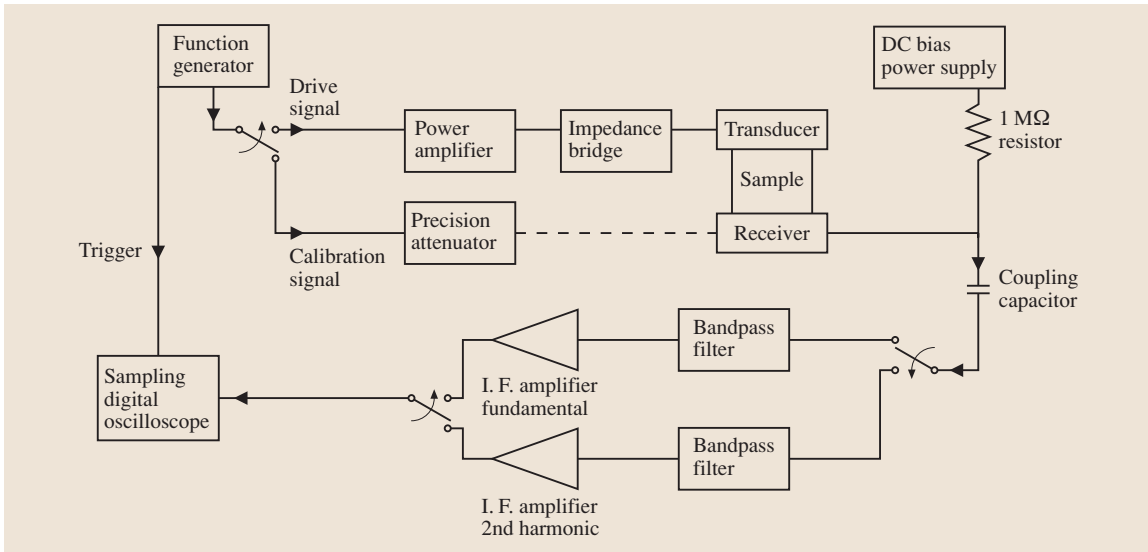


Fig. 6.22 Block Diagram of apparatus for absolute amplitude measurements

Amazon EX1014 Page 247

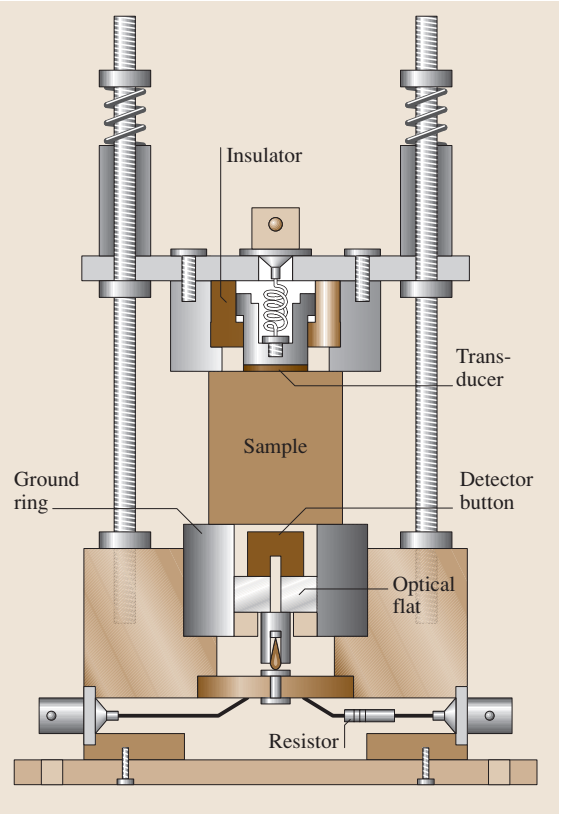


Fig. 6.23 Mounting system for room-temperature measurement of absolute amplitudes of ultrasonic waves in solids

6.3.4 Goniometer System

For studies of the propagation of an ultrasonic pulse in water one can mount the ultrasonic transducers on a goniometer such as that shown in Fig. 6.21. This is a modification of the pulse-echo system. The advantage of this system is that the arms of the goniometer allow for the adjustments indicated in Fig. 6.21b. By use of this goniometer it is possible to make detailed studies of the reflection of ultrasonic waves from a variety of water–solid interfaces. By immersing the goniometer in other liquids, the type of liquid can also be changed.

6.3.5 Capacitive Receiver

In many experiments, one measures acoustic amplitude relative to some reference amplitude, which is usually determined by the parameters of the experiment. However, in some studies it is necessary to make a measurement of the absolute amplitude of acoustic vibration. This is especially true of the measurement of the nonlinearity of solids. For the measurement of the absolute acoustic amplitude in a solid, a capacitive system can be used. If the end of the sample is coated with a conductive material, it can act as one face of a parallel-plate capacitor. A bias voltage is put across that capacitance, which enables it to work as a capacitive microphone. As the acoustic wave causes the end of the sample to vibrate, the capacitor produces an electrical signal. One can relate the measured electrical amplitude to the acoustic amplitude because all quantities relating to them can be determined.

The parallel-plate approximation, which is very well satisfied for plate diameters much larger than the plate separation, is the only approximation necessary. The electrical apparatus necessary for absolute amplitude measurements in solids is shown in the block diagram of Fig. 6.22. A calibration signal is used in such a manner that the same oscilloscope can be used for the calibration and the measurements. The mounting system for room-temperature measurements of a sample is shown in Fig. 6.23. Since stray capacitance affects the impedance of the resistor, this impedance must be measured at the frequencies used. The voltage drop in the resistor can be measured with either the calibration signal or the signal from the capacitive receiver. A comparison of the two completes the calibration. With this system acoustic amplitudes as small as 10^{-14} m (which is approximately the limit set by thermal noise) have been measured in copper single crystals [6.27].

6.4 Surface Acoustic Waves

It has been discovered that surface acoustic waves are useful in industrial situations because they are relatively slow compared with bulk waves or electromagnetic waves. Many surface acoustic wave devices are made by coating a solid with an interdigitated conducting layer. In this case, the surface acoustic wave produces the desired delay time and depends for its generation on a fringing field (or the substrate may be piezoelectric). The inverse

Amazon EX1014 Page 248

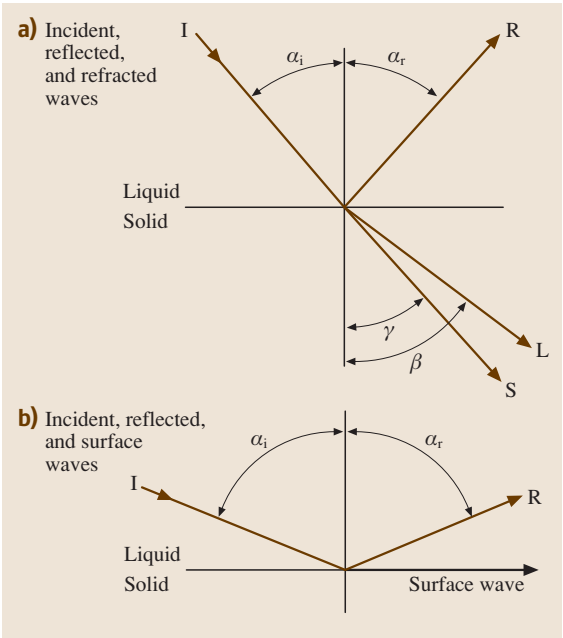


Fig. 6.24 Sound waves at a liquid–solid interface

process can be used to receive surface acoustic waves and convert them into an electrical signal, which can then be amplified.

Another type of surface wave is possibly more illustrative of the connection between surface acoustic waves and physical acoustics. This is the surface acoustic wave generated when the trace velocity of an incident wave is equal to the velocity of the surface acoustic wave. This occurs when a longitudinal wave is incident on a solid from a liquid. This is analogous to the optical case of total internal reflection [6.28], but new information comes from the acoustic investigation.

The interface between a liquid and a solid is shown in Fig. 6.24, in which the various waves and their angles are indicated. The directions in which the various waves propagate at a liquid–solid interface can be calculated from Snell's law, which for this situation can be written

$$\frac{\sin\theta_i}{v} = \frac{\sin\theta_r}{v} = \frac{\sin\theta_L}{v_L} = \frac{\sin\theta_S}{v_S} , \qquad (6.66)$$

where the velocity of the longitudinal wave in the liquid, that in the solid, and the velocity of the shear wave in the solid are, respectively, v, v_L, and v_S. The propagation directions of the various waves are indicated in Fig. 6.24.

Since much of the theory has been developed in connection with geology, the theoretical development of *Ergin* [6.29] can be used directly. Ergin has shown that the energy reflected at an interface is proportional to the square of the amplitude reflection coefficient, which can be calculated directly [6.29]. The energy reflection coefficient is given by

$$R_E = \left(\frac{\cos\beta - A\cos\alpha\,(1-B)}{\cos\beta + A\cos\alpha\,(1-B)}\right)^2 , \qquad (6.67)$$

where

$$A = \frac{\rho_1 V_L}{\rho V} \quad \text{and}$$

$$B = 2\sin\gamma\sin 2\gamma\left(\cos\gamma - \frac{v_S}{v_L}\cos\beta\right) . \qquad (6.68)$$

The relationship among the angles α, β and γ can be determined from Snell's law as given in (6.66). The book by *Brekhovskikh* [6.30] is also a good source of information on this subject.

Typical plots of the energy reflection coefficient as a function of incident angle are given in Fig. 6.25 in

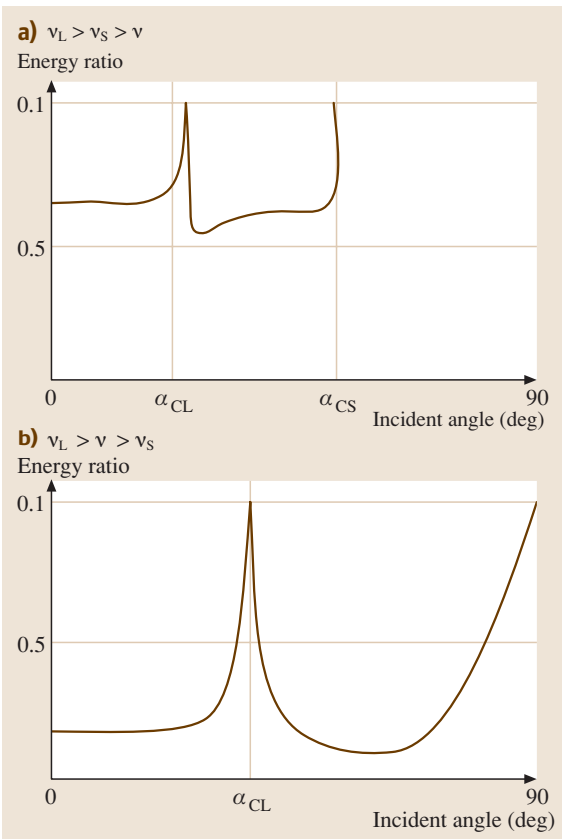


Fig. 6.25 Behavior of energy reflected at a liquid–solid interface

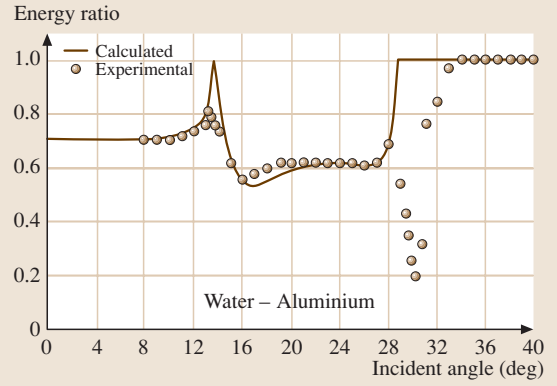


Fig. 6.26 A 2 MHz ultrasonic wave reflected at a liquid–solid interface

which the critical angles are indicated. Usually, $v_L > v_S > v$, so the curve in Fig. 6.25a is observed. It will be noticed immediately that there is a critical angle for both the longitudinal and transverse waves in the solid. In optics there is no longitudinal wave; therefore the curve has only one critical angle.

If one uses a pulse-echo system to verify the behavior of an ultrasonic pulse at an interface between a liquid and a solid, one gets results that can be graphed as shown in Fig. 6.26. At an angle somewhat greater than the critical angle for a transverse wave in the solid, one finds a dip in the data. This dip is associated with the generation of a surface wave. The surface wave is excited when the projection of the wavelength of the incident wave onto the interface matches the wavelength of the surface wave. The effect of the surface wave can be seen in the Schlieren photographs in Fig. 6.27.

Figure 6.27 shows the reflection at a water–aluminum interface at an angle less than that for excitation of a surface wave (a Rayleigh surface wave), at the angle at which a surface wave is excited, and an angle greater. When a surface wave is excited the reflected beam contains two (or more) components: the specular beam (reflected in a normal manner) and a beam displaced down the interface. Since most of the energy is contained in the displaced beam, the minimum in the data shown in Fig. 6.24 is caused by the excitation of the displaced beam by the surface wave. This has been shown to be the case by displacing the receiver to follow the displaced beam with a goniometer system, as shown in Fig. 6.21. This minimizes the dip in data shown in Fig. 6.24. *Neubauer* has shown that the ultrasonic beam excited by the surface wave is 180° out of phase with the specularly reflected

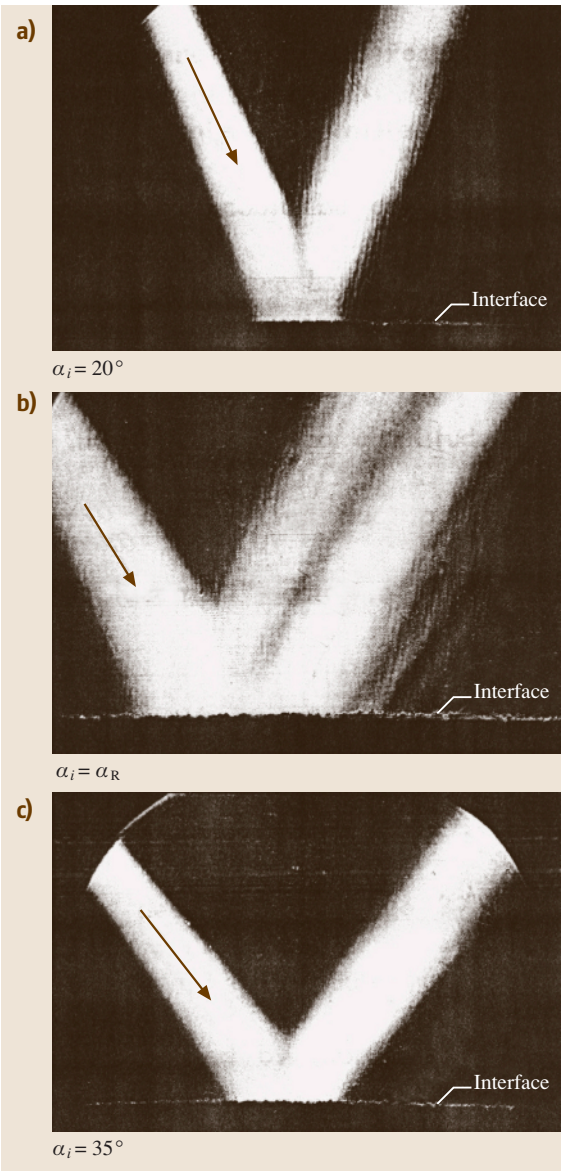


Fig. 6.27 Schlieren photographs showing the behavior of a 4 MHz ultrasonic beam reflected at a water–aluminium interface

beam [6.31]. Destructive interference resulting from phase cancelation causes these beams to be separated by a null strip. Although a water–aluminum interface has been used in these examples, the phenomenon occurs at all liquid–solid interfaces. It is less noticeable at higher ultrasonic frequencies since the wavelength is smaller.

Amazon EX1014 Page 250

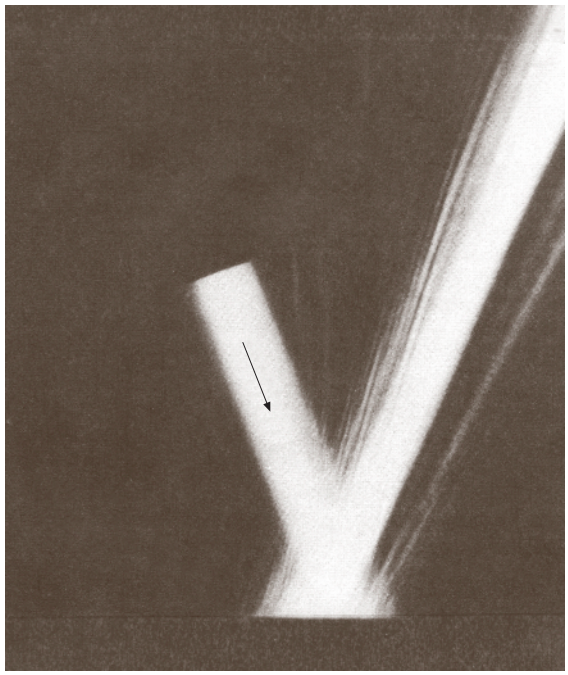


Fig. 6.28 Schlieren photograph showing backward displacement of a 6 MHz ultrasonic beam at a corrugated water–brass interface

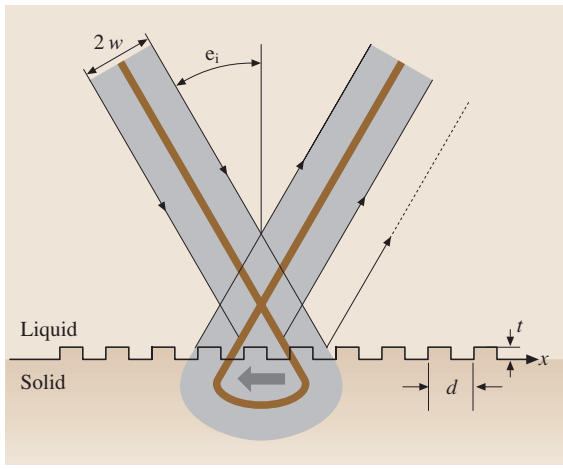


Fig. 6.29 Diagram of incident beam coupling to a backward-directed leaky wave to produce backward displacement of the reflected beam

At a corrugated interface it is possible that the incident beam couples to a negatively directed surface wave so that the reflected beam is displaced in the negative direction. This phenomenon was predicted for optical waves by *Tamir* and *Bertoni* [6.32]. They determined that the optimum angle for this to occur is given by

$$\sin\theta_\mathrm{i} = V_\mathrm{liq}\left(\frac{1}{fd} - \frac{1}{V_\mathrm{R}}\right) \tag{6.69}$$

where d is the period, f is the frequency, V_liq is the wave propagation velocity in the liquid, and V_R is the propagation velocity of the leaky surface wave. Figure 6.28 is a Schlieren photograph which shows what happens in this case [6.33]. Figure 6.29 is a diagram of the phenomenon [6.33]. The incident beam couples to a backward-directed surface wave to produce backward displacement of the reflected beam.

6.5 Nonlinear Acoustics

There are several sources of nonlinearity whether the propagating medium be a gas, liquid, or solid. They are described in more detail in Chap. 8. Even in an ideal medium in which one considers only interatomic forces, there is still a source of nonlinear behavior since compression requires a slightly different force from dilatation. With Hooke's law (strain is proportional to stress) one assumes that they are equal. This is seldom true. The subject of nonlinear acoustics has been developed to the point that it is now possible to go beyond the linear approximation with many substances.

6.5.1 Nonlinearity of Fluids

If one assumes an ideal gas and keeps the first set of nonlinear terms, *Beyer* has shown that the equation of motion in one dimension becomes [6.34]

$$\frac{\partial^2\xi}{\partial t^2} = \frac{c_o^2}{\left(1+\frac{\partial\xi}{\partial a}\right)^{\gamma+1}}\frac{\partial^2\xi}{\partial a^2}\,. \tag{6.70}$$

This form of the nondissipative wave equation in one dimension in Lagrangian coordinates includes nonlinear

terms. In this equation γ is the ratio of specific heats and

$$c_o^2 = \frac{\gamma p_o}{\rho_o} \frac{1}{\left(1+\frac{\partial \xi}{\partial a}\right)^{\gamma-1}} . \tag{6.71}$$

One can also generalize this equation in a form which applies to all fluids. By expanding the equation of state $p = p_o \left(\frac{\rho}{\rho_o}\right)^{\gamma}$ in powers of the condensation $s = \frac{\rho-\rho_o}{\rho_o}$, one obtains

$$p = p_o + As + \frac{B}{2!}s^2 + \ldots \quad \text{and}$$
$$c^2 = c_o^2 \left[1 + \left(\frac{B}{A}\right) s + \ldots\right] . \tag{6.72}$$

This makes it possible to obtain the nonlinear wave equation in the form [6.24]:

$$\frac{\partial^2 \xi}{\partial t^2} = \frac{c_o^2}{\left(1+\frac{\partial \xi}{\partial a}\right)^{2+\frac{B}{A}}} \frac{\partial^2 \xi}{\partial a^2} . \tag{6.73}$$

In this form one can recognize that the quantity $2 + B/A$ for fluids plays the same role as $\gamma + 1$ for ideal gases. Values of B/A for fluids given in Table 6.3 indicate that nonlinearity of fluids, even in the absence of bubbles of air, cannot always be ignored. The nonlinearity of fluids is discussed in greater detail in Chap. 8.

Table 6.3 Values of B/A

Substance	T (°C)	B/A
Distilled water	0	4.2
	20	5.0
	40	5.4
	60	5.7
	80	6.1
	100	6.1
Sea water (3.5%)	20	5.25
Methanol	20	9.6
Ethanol	0	10.4
	20	10.5
	40	10.6
N-propanol	20	10.7
N-butanol	20	10.7
Acetone	20	9.2
Beneze	20	9/0
Chlorobenzene	30	9.3
Liquid nitrogen	b.p.	6.6
Benzyl alcohol	30	10.2
Diethylamine	30	10.3
Ethylene glycol	30	9.7
Ethyl formate	30	9.8
Heptane	30	10.0
Hexane	30	9.9
Methyl acetate	30	9.7
Mercury	30	7.8
Sodium	110	2.7
Potassium	100	2.9
Tin	240	4.4
Monatomic gas	20	0.67
Diatomic gas	20	0.40

6.5.2 Nonlinearity of Solids

The propagation of a wave in a nonlinear solid is described by first introducing third-order elastic constants. When extending the stress–strain relationship (which essentially is a force-based approach) it becomes difficult to keep a consistent approximation among the various nonlinear terms. However, If one instead uses an energy approach, a consistent approximation is automatically maintained for all the terms of higher order.

Beginning with the elastic potential energy, one can define both the second-order constants (those determining the wave velocity in the linear approximation) and the third-order elastic constants simultaneously. The elastic potential energy is

$$\phi(\eta) = \frac{1}{2!}\sum_{ijkl} C_{ijkl}\eta_{ij}\eta_{kl} + \frac{1}{3!}\sum_{ijklmn} C_{ijklmn}\eta_{ij}\eta_{kl}\eta_{mn} + \ldots , \tag{6.74}$$

Table 6.4 K_2 and K_3 for the principal directions in a cubic crystal

Direction	K_2	K_3
[100]	C_{11}	C_{111}
[110]	$\frac{C_{11}+C_{12}+2C_{44}}{2}$	$\frac{C_{111}+3C_{112}+12C_{166}}{4}$
[111]	$\frac{C_{11}+2C_{12}+4C_{44}}{3}$	$\frac{1}{9}(C_{111}+6C_{112}+12C_{144}+24C_{166}+2C_{123}+16C_{456})$

Table 6.5 Comparison of room-temperature values of the ultrasonic nonlinearity parameters of solids. BCC = body-centered cubic; FCC = face-centered cubic

Material or structure	Bonding	β_{avg}
Zincblende	Covalent	2.2
Flourite	Ionic	3.8
FCC	Metallic	5.6
FCC (inert gas)	van der Waals	6.4
BCC	Metallic	8.2
NaCl	Ionic	14.6
Fused silica	Isotropic	−3.4
$YBa_2Cu_3O_{7-\delta}$ (ceramic)	Isotropic	14.3

where the η are the strains, C_{ijkl} are the second-order elastic constants, and C_{ijklmn} are the third-order elastic constants. For cubic crystals there are only three second-order elastic constants: C_{11}, C_{12} and C_{44}, and only six third-order elastic constants: C_{111}, C_{112}, C_{144}, C_{166}, C_{123} and C_{456}. This makes the investigation of cubic crystals relatively straightforward [6.35]. By using the appropriate form of Lagrange's equations, specializing to a specific orientation of the coordinates with respect to the ultrasonic wave propagation direction, and neglecting attenuation and higher-order terms, one can write the nonlinear wave equation for propagation in the directions that allow the propagation of purely longitudinal waves (with no excitation of transverse waves). In a cubic crystalline lattice there are three of these *pure mode* directions for longitudinal waves and the nonlinear wave equation has the form [6.35]

$$\rho_o \frac{\partial^2 u}{\partial t^2} = K_2 \frac{\partial^2 u}{\partial a^2} + (3K_2 + K_3) \frac{\partial u}{\partial a} \frac{\partial^2 u}{\partial a^2} + \dots , \tag{6.75}$$

where both K_2 and K_3 depend on the orientation considered. The quantity K_2 determines the wave velocity: $K_2 = c_o^2 \rho_o$. The quantity K_3 contains only third-order elastic constants. The quantities K_2 and K_3 are given for the three pure-mode directions in a cubic lattice in Table 6.4. The ratio of the coefficient of the nonlinear term to that of the linear term has a special significance. It is often called the *nonlinearity parameter* β and its magnitude is $\beta = 3 + \frac{K_3}{K_2}$. Since K_3 is an inherently negative quantity and is usually greater in magnitude than $3K_2$, a minus sign is often included in the definition:

$$\beta = -\left(3 + \frac{K_3}{K_2}\right) . \tag{6.76}$$

Table 6.6 Parameters entering into the description of finite-amplitude waves in gases, liquids and solids

Parameter	Ideal gas	Liquid	Solid
c_0^2	$\frac{\gamma P_0}{\rho_0}$	$\frac{A}{\rho_0}$	$\frac{K_2}{\rho_0}$
Nonlinearity parameter β	$\gamma + 1$	$\frac{B}{A} + 2$	$-\left(\frac{K_3}{K_2} + 3\right)$

The nonlinearity parameters of many cubic solids have been measured. As might be expected, there is a difference between the quantities measured in the three pure-mode directions (usually labeled as the [100], [110] and [111] directions). These differences, however, are not great. If one averages them, one gets the results shown in Table 6.5. The nonlinearity parameters cover the range 2–15. This means that for cubic crystals the coefficient of the nonlinear term in the nonlinear wave equation is 2–15 times as large as the coefficient of the linear term. This gives an impression of the approximation involved when one ignores nonlinear acoustics.

There is also a source of nonlinearity of solids that appears to come from the presence of domains in lithium niobate; this has been called *acoustic memory* [6.36].

It is possible to measure all six third-order elastic constants of cubic crystals. To do so, however, it is necessary to make additional measurements. The procedure that minimizes errors in the evaluation of third-order elastic constants from combination of nonlinearity parameters with the results of hydrostatic-pressure measurements has been considered by *Breazeale* et al. [6.37] and applied to the evaluation of the third-order elastic constants of two perovskite crystals.

6.5.3 Comparison of Fluids and Solids

To facilitate comparison between fluids and solids, it is necessary to use a binomial expansion of the denominator of (6.73)

$$\left(1 + \frac{\partial \xi}{\partial a}\right)^{-\left(\frac{B}{A}+2\right)} = 1 + \left(\frac{B}{A} + 2\right) \frac{\partial \xi}{\partial a} + \dots \tag{6.77}$$

Using this expression, (6.73) becomes

$$\frac{\partial^2 \xi}{\partial t^2} = c_o^2 \frac{\partial^2 \xi}{\partial a^2} + c_o^2 \left(\frac{B}{A} + 2\right) \frac{\partial \xi}{\partial a} \frac{\partial^2 \xi}{\partial a^2} + \dots \tag{6.78}$$

This form of the equation can be compared directly with (6.74) for solids. The ratio of the coefficient of the nonlinear term to that of the linear term can be evaluated

directly. The nonlinearity parameters of the various substances are listed in Table 6.6. Use of Table 6.6 allows one to make a comparison between the nonlinearity of fluids as listed in Table 6.3 and the nonlinearity parameters of solids listed in Table 6.5. Nominally, they are of the same order of magnitude. This means that solids exhibit intrinsic nonlinearity that is comparable to that exhibited by fluids. Thus, the approximation made by assuming that Hooke's law (strain is proportional to stress) is valid for solids is comparable to the approximation made in the derivation of the linear wave equation for fluids.

References

6.1 R.N. Thurston, A.D. Pierce (Eds.): *Physical Acoustics*, Vol. XXV (Academic, San Diego 1999)

6.2 W.P. Mason (Ed.): *Physical Acoustics*, Vol. I A,B (Academic, New York 1964)

6.3 R.N. Thurston: Wave propagation in fluids and normal solids. In: *In: Physical Acoustics*, Vol. I A, ed. by P.W. Mason (Academic, New York 1964)

6.4 A. Migliori, T.W. Darling, J.P. Baiardo, F. Freibert: Resonant ultrasound spectroscopy (RUS). In: *Handbook of Elastic Properties of Solids, Liquids, and Gases*, Vol. I, ed. by M. Levy, H. Bass, R. Stern (Academic, New York 2001) p. 10, Cha

6.5 R. Truell, C. Elbaum, B. Chick: *Ultrasonic Methods in Solid State Physics* (Academic, New York 1969)

6.6 C. Allen, I. Rudnick: A powerful high-frequency siren, J. Acoust. Soc. Am. **19**, 857–865 (1947)

6.7 D.F. Gaitan, L.A. Crum, C.C. Church, R.A. Roy: Sonoluminescence and bubble dynamics for a single, stable, cavitation bubble, J. Acoust. Soc. Am. **91**, 3166–3183 (1992)

6.8 J. Wu: Acoustical tweezers, J. Acoust. Soc. Am. **89**, 2140–2143 (1991)

6.9 N. Marinesco, J.J. Trillat: Action des ultrasons sur les plaques photographiques, C. R. Acad. Sci. Paris **196**, 858 (1933)

6.10 H. Frenzel, H. Schultes: Luminiszenz im ultraschallbeschickten Wasse, Z. Phys. Chem. **27**, 421 (1934)

6.11 I.V. Ostrovskii, P. Das: Observation of a new class of crystal sonoluminescence at piezoelectric crystal surface, Appl. Phys. Lett. **70**, 167–169 (1979)

6.12 I. Miyake, H. Futama: Sonoluminescence in X-rayed KCl crystals, J. Phys. Soc. Jpn. **51**, 3985–3989 (1982)

6.13 B.P. Barber, R. Hiller, K. Arisaka, H. Fetterman, S.J. Putterman: Resolving the picosecond characteristics of synchronous sonoluminescence, J. Acoust. Soc. Am. **91**, 3061 (1992)

6.14 J.T. Carlson, S.D. Lewia, A.A. Atchley, D.F. Gaitan, X.K. Maruyama, M.E. Lowry, M.J. Moran, D.R. Sweider: Spectra of picosecond sonoluminescence. In: *Advances in Nonlinear Acoustics*, ed. by H. Hobaek (World Scientific, Singapore 1993)

6.15 R. Hiller, S.J. Putterman, B.P. Barber: Spectrum of synchronous picosecond sonoluminescence, Phys. Rev. Lett. **69**, 1182–1184 (1992)

6.16 G.W. Swift: Thermoacoustic engines, J. Acoust. Soc. Am. **84**, 1145–1180 (1988)

6.17 L. J. House, D. B. Pape: Method and Apparatus for Acoustic Energy – Identification of Objects Buried in Soil, US Patent 5357063 (1993)

6.18 C.G. Don, A.J. Rogers: Using acoustic impulses to identify a buried non-metallic objects, J. Acoust. Soc. Am. **95**, 2837–2838 (1994)

6.19 D. D. Caulfield: Acoustic Detection Apparatus, US Patent 4922467 (1989)

6.20 D.M. Donskoy: Nonlinear vibro-acoustic technique for land mine detection, SPIE Proc. **3392**, 211–217 (1998)

6.21 D.M. Donskoy: Detection and discrimination of nonmetallic mines, SPIE Proc. **3710**, 239–246 (1999)

6.22 D.M. Donskoy, N. Sedunov, A. Ekimov, M. Tsionskiy: Optimization of seismo-acoustic land mine detection using dynamic impedances of mines and soil, SPIE Proc. **4394**, 575–582 (2001)

6.23 J.M. Sabatier, N. Xiang: Laser-doppler based acoustic-to-seismic detection of buried mines, Proc. SPIE **3710**, 215–222 (1999)

6.24 N. Xiang, J.M. Sabatier: Detection and Remediation Technologies for Mines and Minelike Targets VI, Proc. SPIE **4394**, 535–541 (2001)

6.25 F.D. Martin, M.A. Breazeale: A simple way to eliminate diffraction lobes emitted by ultrasonic transducers, J. Acoust. Soc. Am. **49**, 1668–1669 (1971)

6.26 G. Du, M.A. Breazeale: The ultrasonic field of a Gaussian transducer, J. Acoust. Soc. Am. **78**, 2083–2086 (1985)

6.27 R.D. Peters, M.A. Breazeale: Third harmonic of an initially sinusoidal ultrasonic wave in copper, Appl. Phys. Lett. **12**, 106–108 (1968)

6.28 F. Goos, H. Hänchen: Ein neuer und fundamentaler Versuch zur Totalreflexion, Ann. Phys. **1**, 333–346 (1947), 6. Folge

6.29 K. Ergin: Energy ratio of seismic waves reflected and refracted at a rock-water boundary, Bull. Seismol. Soc. Am. **42**, 349–372 (1952)

6.30 L.M. Brekhovskikh: *Waves in Layered Media* (Academic, New York 1960)

6.31 W.G. Neubauer: Ultrasonic reflection of a bounded beam at Rayleigh and critical angles for a plane liquid-solid interface, J. Appl. Phys. **44**, 48–55 (1973)

Amazon EX1014 Page 254

6.32 T. Tamir, H.L. Bertoni: Lateral displacement of optical beams at multilayered and periodic structures, J. Opt. Soc. Am. **61**, 1397–1413 (1971)
6.33 M.A. Breazeale, M.A. Torbett: Backward displacement of waves reflected from an interface having superimposed periodicity, Appl. Phys. Lett. **29**, 456–458 (1976)
6.34 R.T. Beyer: *Nonlinear Acoustics* (Naval Ships Systems Command, Washington 1974)
6.35 M.A. Breazeale: Third-order elastic constants of cubic crystals. In: *Handbook of Elastic Properties of Solids, Liquids and Gases*, Vol. I, ed. by M. Levy, H. Bass, R. Stern (Academic, New York 2001) pp. 489–510, Chap. 21
6.36 M.S. McPherson, I. Ostrovskii, M.A. Breazeale: Observation of acoustical memory in $LiNbO_3$, Phys. Rev. Lett. **89**, 115506 (2002)
6.37 M.A. Breazeale, J. Philip, A. Zarembowitch, M. Fischer, Y. Gesland: Acoustical measurement of solid state nonlinearity: Aplication to $CsCdF_3$ and $KZnF_3$, J. Sound Vib. **88**, 138–140 (1983)

Amazon EX1014 Page 255

7. Thermoacoustics

Thermodynamic and fluid-dynamic processes in sound waves in gases can convert energy from one form to another. In these *thermoacoustic* processes [7.1, 2], high-temperature heat or chemical energy can be partially converted to acoustic power, acoustic power can produce heat, acoustic power can pump heat from a low temperature or to a high temperature, and acoustic power can be partially converted to chemical potential in the separation of gas mixtures. In some cases, the thermoacoustic perspective brings new insights to decades-old technologies. Well-engineered thermoacoustic devices using extremely intense sound approach the power conversion per unit volume and the efficiency of mature energy-conversion equipment such as internal combustion engines, and the simplicity of few or no moving parts drives the development of practical applications.

This chapter surveys thermoacoustic energy conversion, so the reader can understand how thermoacoustic devices work and can estimate some relevant numbers. After a brief history, an initial section defines vocabulary and establishes preliminary concepts, and subsequent sections explain engines, dissipation, refrigeration, and mixture separation. Combustion thermoacoustics is mentioned only briefly. Transduction and measurement systems that use heat-generated surface and bulk acoustic waves in solids are not discussed.

7.1 **History** 239

7.2 **Shared Concepts** 240
7.2.1 Pressure and Velocity 240
7.2.2 Power 243

7.3 **Engines** 244
7.3.1 Standing-Wave Engines 244
7.3.2 Traveling-Wave Engines 246
7.3.3 Combustion 248

7.4 **Dissipation** 249

7.5 **Refrigeration** 250
7.5.1 Standing-Wave Refrigeration 250
7.5.2 Traveling-Wave Refrigeration 251

7.6 **Mixture Separation** 253

References 254

7.1 History

The history of thermoacoustic energy conversion has many interwoven roots, branches, and trunks. It is a complicated history because invention and technology development outside of the discipline of acoustics have sometimes preceded fundamental understanding; at other times, fundamental science has come first.

Rott [7.3, 4] developed the mathematics describing acoustic oscillations in a gas in a channel with an axial temperature gradient, with lateral channel dimensions of the order of the gas thermal penetration depth (typically ≈ 1 mm), this being much shorter than the wavelength (typically ≈ 1 m). The problem had been investigated by Rayleigh and by Kirchhoff, but without quantitative success. In Rott's time, the motivation to understand the problem arose largely from the cryogenic phenomenon known as Taconis oscillations – when a gas-filled tube is cooled from ambient temperature to a cryogenic temperature, the gas sometimes oscillates spontaneously, with large heat transport from ambient to the cryogenic environment. *Yazaki* [7.5] demonstrated convincingly that Rott's analysis of Taconis oscillations was quantitatively accurate.

A century earlier, *Rayleigh* [7.6] understood the qualitative features of such heat-driven oscillations: "If heat be given to the air at the moment of greatest condensation (i.e., greatest density) or be taken from it at the moment of greatest rarefaction, the vibration is encouraged." He had studied Sondhauss oscillations [7.7], the glassblowers' precursor to Taconis oscillations.

Amazon EX1014 Page 256

Applying Rott's mathematics to a situation where the temperature gradient along the channel was too weak to satisfy Rayleigh's criterion for spontaneous oscillations, *Hofler* [7.8] invented a standing-wave thermoacoustic refrigerator, and demonstrated [7.9] again that Rott's approach to acoustics in small channels was quantitatively accurate. In this type of refrigerator, the coupled oscillations of gas motion, temperature, and heat transfer in the sound wave are phased in time so that heat is absorbed from a load at a low temperature and waste heat is rejected to a sink at a higher temperature.

Meanwhile, completely independently, pulse-tube refrigeration was becoming the most actively investigated area of cryogenic refrigeration. This development began with *Gifford*'s [7.10] accidental discovery and subsequent investigation of the cooling associated with square-wave pulses of pressure applied to one end of a pipe that was closed at the other end. Although the relationship was not recognized at the time, this phenomenon shared much physics with Hofler's refrigerator. *Mikulin*'s [7.11] attempt at improvement in heat transfer in one part of this basic pulse-tube refrigerator led unexpectedly to a dramatic improvement of performance, and *Radebaugh* [7.12] realized that the resulting *orifice* pulse-tube refrigerator was in fact a variant of the Stirling cryocooler.

Development of Stirling engines and refrigerators started in the 19th century, the engines at first as an alternative to steam engines [7.13]. Crankshafts, multiple pistons, and other moving parts seemed at first to be essential. An important modern chapter in their development began in the 1970s with the invention of *free-piston* Stirling engines and refrigerators, in which each piston's motion is determined by interactions between the piston's dynamics and the gas's dynamics rather than by a crankshaft and connecting rod. Analysis of such complex, coupled phenomena is complicated, because the oscillating motion causes oscillating pressure differences while simultaneously the oscillating pressure differences cause oscillating motion. *Ceperley* [7.14,15] added an explicitly acoustic perspective to Stirling engines and refrigerators when he realized that the time phasing between pressure and motion oscillations in the heart of their regenerators is that of a traveling acoustic wave. Many years later, acoustic versions of such engines were demonstrated by *Yazaki* [7.16], *de-Blok* [7.17], and *Backhaus* [7.18], the last achieving a heat-to-acoustic energy efficiency comparable to that of other mature energy-conversion technologies.

7.2 Shared Concepts

7.2.1 Pressure and Velocity

For a monofrequency wave, oscillating variables can be represented with complex notation, such as

$$p(x,t) = p_\mathrm{m} + \mathrm{Re}\left[p_1(x)\mathrm{e}^{\mathrm{i}\omega t}\right] \tag{7.1}$$

for the pressure p, where p_m is the mean pressure, Re (z) indicates the real part of z, $\omega = 2\pi f$ is the angular frequency, f is the frequency, and the complex number p_1 specifies both the amplitude and the time phase of the oscillating part of the pressure. For propagation in the x direction through a cross-sectional area A in a duct, p_1 is a function of x. In the simple lossless, uniform-area situation the sinusoidal x dependence can be found from the wave equation, which can be written with $i\omega$ substituted for time derivatives as

$$\omega^2 p_1 + c^2 \frac{\mathrm{d}^2 p_1}{\mathrm{d}x^2} = 0\,, \tag{7.2}$$

where $c^2 = (\partial p/\partial\rho)_s$ is the square of the adiabatic sound speed, with ρ the density and s the entropy. In thermoacoustics, intuition is well served by thinking of (7.2) as two first-order differential equations coupling two variables, pressure p_1 and the x component of volume velocity, U_1:

$$\frac{\mathrm{d}p_1}{\mathrm{d}x} = -\frac{\mathrm{i}\omega\rho_\mathrm{m}}{A} U_1\,, \tag{7.3}$$

$$\frac{\mathrm{d}U_1}{\mathrm{d}x} = -\frac{\mathrm{i}\omega A}{\rho_\mathrm{m} c^2} p_1\,. \tag{7.4}$$

For a reasonably short length of duct Δx, these can be written approximately as

$$\Delta p_1 = -\mathrm{i}\omega L\, U_1\,, \tag{7.5}$$

$$p_1 = -\frac{1}{\mathrm{i}\omega C}\Delta U_1\,, \tag{7.6}$$

where

$$L = \frac{\rho_\mathrm{m}\Delta x}{A}\,, \tag{7.7}$$

$$C = \frac{A\Delta x}{\rho_\mathrm{m} c^2}\,. \tag{7.8}$$

Amazon EX1014 Page 257

Table 7.1 The acoustic–electric analog. The basic building blocks of thermoacoustic energy-conversion devices are inertances L, compliances C, viscous and thermal resistances R_{visc} and R_{therm}, gains (or losses) G, and power transducers

Acoustic variables	Electric variables
Pressure p_1	Voltage
Volume velocity U_1	Current
Inertance L	Series inductance
Viscous resistance R_{visc}	Series resistance
Compliance C	Capacitance to ground
Thermal-hysteresis resistance R_{therm}	Resistance to ground
Gain/loss along temperature gradient, G	Proportionally controlled current injector
Stroke-controlled transducer	Current source
Force-controlled transducer	Voltage source

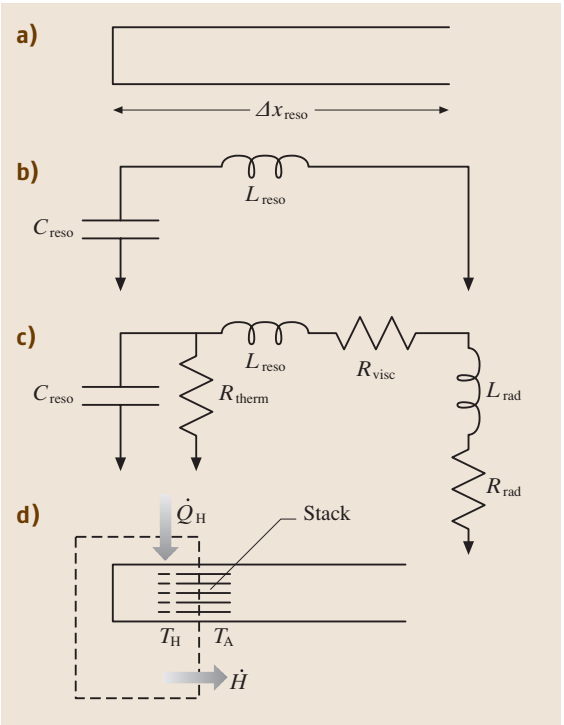


Fig. 7.1a–d Quarter-wavelength resonator. **(a)** A quarter-wavelength resonator: a tube closed at one end and open at the other. **(b)** A simple lossless lumped-element model of the resonator as a compliance C_{reso} in series with an inertance L_{reso}. **(c)** A more complicated lumped-element model, including thermal-hysteresis resistance R_{therm} in the compliance, viscous resistance R_{visc} in the inertance, and radiation impedance $R_{\mathrm{rad}} + \mathrm{i}\omega L_{\mathrm{rad}}$. **(d)** An illustration of the first law of thermodynamics for a control volume, shown enclosed by the dashed line, which intersects the stack of a well-insulated standing-wave engine. In steady state, the thermal power $\dot{Q}_{\mathrm{H}}$ that flows into the system at the hot heat exchanger must equal the total power $\dot{H}$ that flows along the stack

As introduced in Chap. 6 (Physical Acoustics) (7.3) is the acoustic Euler equation, the inviscid form of the momentum equation. It describes the force that the pressure gradient must exert to overcome the gas's inertia. In the lumped-element form (7.5), the geometrical and gas-property aspects of the inertia of the gas in the duct are represented by the duct's inertance L. Similarly introduced in Chap. 6, (7.4) and (7.6) are, respectively, the differential and lumped-element versions of the continuity equation combined with the gas's adiabatic equation of state. These describe the compressibility of the gas in response to being squeezed along the x-direction. In the lumped-element form (7.6), the geometrical and gas-property aspects of the compressibility of the gas in the duct are represented by the duct's compliance C.

Accurate calculation of the wave in a long duct or a long series of ducts requires analytical or numerical integration of differential equations [7.1], but for the purposes of this chapter we will consider lumped-element approximations, because they are satisfactorily accurate for many estimates, they allow a *circuit model* representation of devices, and they facilitate intuition based on experience with alternating-current (AC) electrical circuits. Table 7.1 shows the analogy between acoustic devices and electrical circuits.

For example, the closed–open resonator shown in Fig. 7.1a has a resonance frequency that can be calculated by setting its length Δx_{reso} equal to a quarter wavelength of sound; the result is $f_{\mathrm{reso}} = c/4\Delta x_{\mathrm{reso}}$. The simplest lumped-element approximation of the quarter-wavelength resonator is shown in Fig. 7.1b. We assign compliance C_{reso} to the left half of the resonator, because the compressibility of the gas is more important than its inertia in the left half, where $|p_1|$ is high and $|U_1|$ is low. Similarly, we assign inertance L_{reso} to the right half of the resonator, because the inertia is more important in the right half where $|U_1|$ is high. Setting $\Delta x = \Delta x_{\mathrm{reso}}/2$ in (7.7) and (7.8), and recalling that the resonance frequency of an electrical LC circuit is given by $\omega^2 = 1/LC$, we find $f_{\mathrm{reso}} = c/\pi\Delta x_{\mathrm{reso}}$, differing from the exact result only by a factor of $4/\pi$. Such accuracy will be acceptable for estimation and understanding in this chapter.

Amazon EX1014 Page 258

Circuit models can include as much detail as is necessary to convey the essential physics [7.1]. When the viscosity is included in the momentum equation, the lumped-element form becomes

$$\Delta p_1 = -\left(\mathrm{i}\omega L + R_{\mathrm{visc}}\right) U_1 \,, \tag{7.9}$$

and when the thermal conductivity and a temperature gradient in the x direction are included in the continuity equation, the lumped-element form becomes

$$\Delta U_1 = -\left(\mathrm{i}\omega C + \frac{1}{R_{\mathrm{therm}}}\right) p_1 + G U_{\mathrm{in},1} \,. \tag{7.10}$$

Figure 7.1c is a better model than Fig. 7.1b for the closed–open resonator of Fig. 7.1a, because it includes thermal-hysteresis resistance in the compliance, viscous resistance in the inertance, and the inertial and resistive radiation impedance at the open end. This model would yield reasonably accurate estimates for the free-decay time and quality factor of the resonator as well as its resonance frequency.

Ducts filled with porous media and having temperature gradients in the x-direction play a central role in thermoacoustic energy conversion [7.1]. The pore size is characterized by the hydraulic radius r_{h}, defined as the ratio of gas volume to gas–solid contact area. In a circular pore, r_{h} is half the circle's radius; in the gap between parallel plates, r_{h} is half the gap. The term *stack* is used for a porous medium whose r_{h} is comparable to the gas thermal penetration depth

$$\delta_{\mathrm{therm}} = \sqrt{2k/\omega\rho_{\mathrm{m}} c_{\mathrm{p}}} \,, \tag{7.11}$$

where k is the gas thermal conductivity and c_{p} is its isobaric heat capacity per unit mass, while a porous medium with $r_{\mathrm{h}} \ll \delta_{\mathrm{therm}}$ is known as a *regenerator*. The viscous penetration depth

$$\delta_{\mathrm{visc}} = \sqrt{2\mu/\omega\rho_{\mathrm{m}}} \,, \tag{7.12}$$

where μ is the viscosity, is typically comparable to, but smaller than, the thermal penetration depth. If the distance between a particular mass of gas and the nearest solid wall is much greater than the penetration depths, thermal and viscous interactions with the wall do not affect that gas.

In such porous media with axial temperature gradients, the gain/loss term $G U_{\mathrm{in},1}$ in (7.10) is responsible for the creation of acoustic power by engines and for the thermodynamically required consumption of acoustic power by refrigerators. This term represents cyclic thermal expansion and contraction of the gas as it moves along and experiences the temperature gradient in the solid. In regenerators, the gain G is nearly real, and ΔU_1 caused by the motion along the temperature gradient is in phase with U_1 itself, because of the excellent thermal contact between the gas in small pores and the

Table 7.2 Expressions for the lumped-element building blocks L, R_{visc}, C, R_{therm}, and GU_1, and for the total power $\dot{H}$, in the boundary-layer limit $r_{\mathrm{h}} \gg \delta$ and in the small-pore limit $r_{\mathrm{h}} \ll \delta$. The symbol "$\sim$" in the small-pore limit indicates that the numerical prefactor depends on the shape of the pore

	Boundary-layer limit	Small-pore limit
L	$\dfrac{\rho_{\mathrm{m}}\Delta x}{A}$	$\sim \dfrac{\rho_{\mathrm{m}}\Delta x}{A}$
R_{visc}	$\dfrac{\mu\Delta x}{A r_{\mathrm{h}}\delta_{\mathrm{visc}}}$	$\sim \dfrac{2\mu\Delta x}{A r_{\mathrm{h}}^2}$
C	$\dfrac{A\Delta x}{\rho_{\mathrm{m}} c^2} = \dfrac{A\Delta x}{\gamma p_{\mathrm{m}}}$	$\dfrac{\gamma A\Delta x}{\rho_{\mathrm{m}} c^2} = \dfrac{A\Delta x}{p_{\mathrm{m}}}$
R_{therm}	$\dfrac{\rho_{\mathrm{m}}^2 c_{\mathrm{p}}^2 T_{\mathrm{m}} r_{\mathrm{h}}\delta_{\mathrm{therm}}}{kA\Delta x}$	$\sim \dfrac{3kT_{\mathrm{m}}}{4\omega^2 r_{\mathrm{h}}^2 A\Delta x}$
GU_1	$\dfrac{1-\mathrm{i}}{2}\dfrac{1}{1+\sqrt{\sigma}}\dfrac{\delta_{\mathrm{therm}}}{r_{\mathrm{h}}}\dfrac{\Delta T_{\mathrm{m}}}{T_{\mathrm{m}}}U_1$	$\dfrac{\Delta T_{\mathrm{m}}}{T_{\mathrm{in,m}}}U_{\mathrm{in},1}$
$\dot{H}$	$\dfrac{\delta_{\mathrm{therm}}}{4r_{\mathrm{h}}(1+\sigma)}\mathrm{Re}\left\{\tilde{p}_1 U_1\left[\mathrm{i}\left(1+\sqrt{\sigma}\right)+\left(1-\sqrt{\sigma}\right)\right]\right\}$ $-\dfrac{\delta_{\mathrm{therm}}\rho_{\mathrm{m}} c_{\mathrm{p}}\left(1-\sigma\sqrt{\sigma}\right)\lvert U_1\rvert^2}{4r_{\mathrm{h}} A\omega\left(1-\sigma^2\right)}\dfrac{\Delta T}{\Delta x}$ $+\dot{E}-\left(Ak+A_{\mathrm{solid}}k_{\mathrm{solid}}\right)\dfrac{\Delta T}{\Delta x}$	$-A_{\mathrm{solid}}k_{\mathrm{solid}}\dfrac{\Delta T}{\Delta x}$

Amazon EX1014 Page 259

walls of the pores. (Positive G indicates gain; negative G indicates loss.) In stacks, a nonzero imaginary part of G reflects imperfect thermal contact in the pores and the resultant time delay between the gas's cyclic motion along the solid's temperature gradient and the gas's thermal expansion and contraction.

Table 7.2 gives expressions for the impedances in the boundary-layer limit, $r_h \gg \delta_{therm}$ and $r_h \gg \delta_{visc}$, which is appropriate for large ducts, and in the small-pore limit appropriate for regenerators. Boundary-layer-limit entries are usefully accurate in stacks, in which $r_h \sim \delta$. General expressions for arbitrary r_h and many common pore shapes are given in [7.1].

The lumped-element approach summarized in Table 7.1 and the limiting expressions given in Table 7.2 are sufficient for most of this overview, but quantitatively accurate thermoacoustic analysis requires slightly more sophisticated techniques and includes more phenomena [7.1]. Every differential length dx of duct has dL, dC, dR_{visc}, and $d(1/R_{therm})$, and if $dT_m/dx \neq 0$ it also has dG, so a finite-length element is more analogous to an electrical transmission line than to a few lumped impedances. In addition to smoothly varying x dependencies for all variables, important phenomena include turbulence, which increases R_{visc} above the values given in Table 7.2; pore sizes which are in neither of the limits given in Table 7.2; nonlinear terms in the momentum and continuity equations, which cause frequency doubling, tripling, etc., so that the steady-state wave is a superposition of waves of many frequencies; and streaming flows caused by the wave itself. Many of these subjects are introduced in Chap. 8 (Nonlinear Acoustics). Thermoacoustics software that includes most or all of these phenomena and has the properties of several commonly used gases is available [7.19, 20].

For estimating the behavior of thermoacoustic devices, it is useful to remember some properties of common ideal gases [7.21]. The equation of state is

$$p = \frac{\rho R_{univ} T}{M} , \tag{7.13}$$

where $R_{univ} = 8.3\,\mathrm{J/(mole\,K)}$ is the universal gas constant and M is the molar mass. The ratio of isobaric to isochoric specific heats, γ, is 5/3 for monatomic gases such as helium and 7/5 for diatomic gases such as nitrogen and air near ambient temperature, and appears in both the adiabatic sound speed

$$c = \sqrt{\frac{\gamma R_{univ} T}{M}} \tag{7.14}$$

and the isobaric heat capacity per unit mass

$$c_p = \frac{\gamma R_{univ}}{(\gamma - 1)\, M} . \tag{7.15}$$

The viscosity of many common gases (e.g., air, helium, and argon) is about

$$\mu \simeq (2 \times 10^{-5}\,\mathrm{kg/m\,s}) \left(\frac{T}{300\,\mathrm{K}} \right)^{0.7} , \tag{7.16}$$

and the thermal conductivity k can be estimated by remembering that the Prandtl number

$$\sigma = \frac{\mu c_p}{k} \tag{7.17}$$

is about 2/3 for pure gases, but somewhat lower for gas mixtures [7.22].

7.2.2 Power

In addition to ordinary acoustic power $\dot{E}$, the time-averaged thermal power $\dot{Q}$, total power $\dot{H}$, and exergy flux $\dot{X}$ are important in thermoacoustic energy conversion. These thermoacoustic powers are related to the simpler concepts of work, heat, enthalpy, and exergy that are encountered in introductory [7.21] and advanced [7.23] thermodynamics.

Just as acoustic intensity is the time-averaged product of pressure and velocity, acoustic power $\dot{E}$ is the time-averaged product of pressure and volume velocity. In complex notation,

$$\dot{E} = \frac{1}{2} \mathrm{Re}\,(\tilde{p}_1 U_1) , \tag{7.18}$$

where the tilde denotes complex conjugation. At transducers, it is apparent that acoustic power is closely related to thermodynamic work, because a moving piston working against gas in an open space with volume V transforms mechanical power to acoustic power (or vice versa) at a rate $f \oint p\, dV$, which is equal to (7.18) for sinusoidal pressure and motion. Resistances R dissipate acoustic power; the gain/loss term GU_1 in components with temperature gradients can either consume or produce acoustic power, and inertances L and compliances C neither dissipate nor produce acoustic power, but simply pass it along while changing p_1 or U_1.

Time-averaged thermal power $\dot{Q}$ (i.e., time-averaged heat per unit time) is added to or removed from the gas at heat exchangers, which are typically arrays of tubes, high-conductivity fins, or both, spanning a duct. Thermal power can be supplied to an engine by high-temperature combustion products flowing through such

Amazon EX1014 Page 260

tubes or by circulation of a high-temperature heat-transfer fluid through such tubes and a source of heat elsewhere. Thermal power is often removed from engines and refrigerators by ambient-temperature water flowing through such tubes.

Of greatest importance is the total time-averaged power

$$\dot{H} = \int \left[\frac{1}{2} \rho_m \mathrm{Re}\left(\tilde{h}_1 u_1 \right) - k \frac{\mathrm{d}T_m}{\mathrm{d}x} \right] \mathrm{d}A \,, \qquad (7.19)$$

based on the x component u of velocity and the enthalpy h per unit mass, which is the energy of most utility in fluid mechanics. Fig. 7.1d uses a simple standing-wave engine (discussed more fully below) to illustrate the centrality of $\dot{H}$ to the first law of thermodynamics in thermoacoustics. The figure shows a heat exchanger and stack in a quarter-wavelength resonator. When heat is applied to the hot heat exchanger, the resonance is driven by processes (described below) in the stack. The dashed line in Fig. 7.1d encloses a volume whose energy must be constant when the engine is running in steady state. If the side walls of the engine are well insulated and rigid within that volume, then the only energy flows per unit time into and out of the volume are $\dot{Q}_H$ and whatever power flows to the right through the stack. We define the total power flow through the stack to be $\dot{H}$, and the first law of thermodynamics ensures that $\dot{H} = \dot{Q}_H$ in this simple engine.

As shown in (7.19), the total power $\dot{H}$ is the sum of ordinary steady-state heat conduction (most importantly in the solid parts of the stack or regenerator and the surrounding duct walls) and the total power carried convectively by the gas itself. Analysis of the gas contribution requires spatial and temporal averaging of the enthalpy transport in the gas [7.4], and shows that the most important contributions are acoustic power flowing through the pores of the stack and a shuttling of energy by the gas that occurs because entropy oscillations in the gas are nonzero and have a component in phase with velocity. Remarkably, these two phenomena nearly cancel in the small pores of a regenerator.

Finally, the exergy flux $\dot{X}$ represents the rate at which thermodynamic work can be done, in principle, with unrestricted access to a thermal bath at ambient temperature [7.1,23]. Exergy flux is sometimes used in complex systems to analyze sources of inefficiency according to location or process.

7.3 Engines

Implicit in Rayleigh's criterion [7.6] for spontaneous oscillations, "If heat be given to the air at the moment of greatest (density) or be taken from it at the moment of greatest rarefaction, the vibration is encouraged," is the existence of a vibration in need of encouragement, typically a resonance with a high quality factor. Today, we would express Rayleigh's criterion in either of two ways, depending on whether we adopt a Lagrangian perspective, focusing on discrete masses of gas as they move, or an Eulerian perspective, focusing on fixed locations in space as the gas moves past them. In the Lagrangian perspective, some of the gas in a thermoacoustic engine must experience $\oint p \, \mathrm{d}V > 0$, where V is the volume of an identified mass of gas. In the Eulerian perspective, part of the device must have $\mathrm{d}\dot{E}/\mathrm{d}x > 0$, arising from $\mathrm{Re}\,(\tilde{p}_1 \, \mathrm{d}U_1/\mathrm{d}x) > 0$ and the G term in (7.10).

By *engine* we mean a prime mover, i.e., something that converts heat to work or acoustic power. We describe three varieties: standing-wave engines, traveling-wave engines, and pulse combustors.

7.3.1 Standing-Wave Engines

Continuing the quarter-wavelength example introduced in Fig. 7.1, Fig. 7.2 shows a simple standing-wave engine, of a type that is available as a classroom demonstration [7.24]. A stack and hot heat exchanger are near the left end of the resonator, and its right end is open to the air. When heat $\dot{Q}_H$ is first applied to the hot heat exchanger, the heat exchanger and the adjacent end of the stack warm up, establishing an axial temperature gradient from hot to ambient in the stack. When the gradient is steep enough (as explained below), the acoustic oscillations start spontaneously, and grow in intensity as more heat is added and a steady state is approached. In the steady state, total power $\dot{H}$ equal to $\dot{Q}_H$ (minus any heat leak to the room) flows through the stack, creating acoustic power, some of which is dissipated elsewhere in the resonator and some of which is radiated into the room. To the right of the stack, where an ambient-temperature heat exchanger would often be located, the heat is carried rightward and out of this resonator by streaming-driven

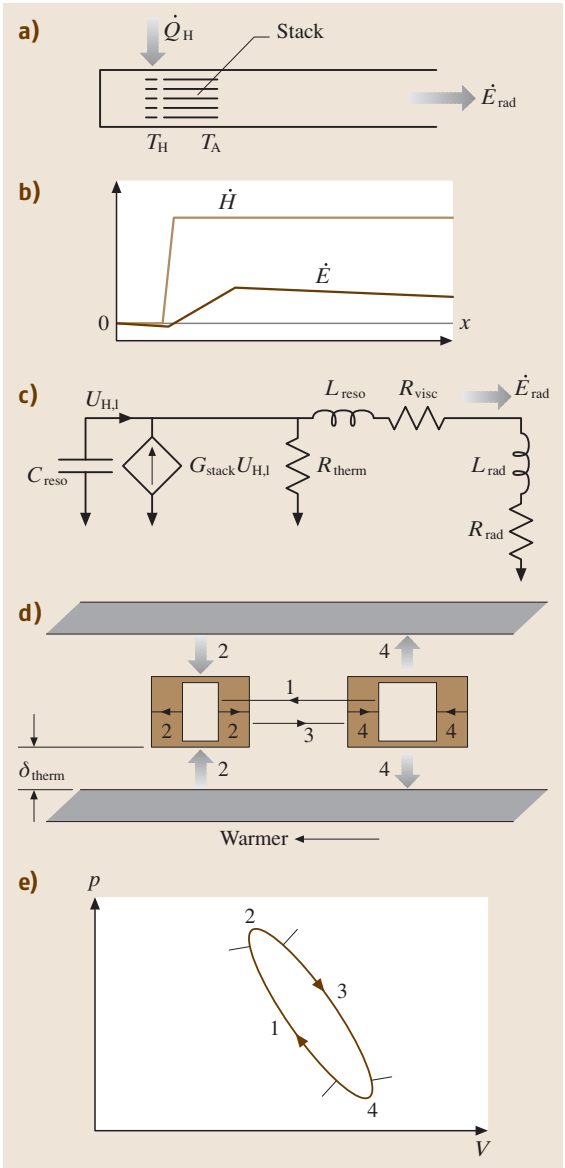


Fig. 7.2a–e A standing-wave engine. **(a)** A hot heat exchanger and a stack in a quarter-wavelength resonator. Heat $\dot{Q}_H$ is injected at the hot heat exchanger, and the device radiates acoustic power $\dot{E}_{rad}$ into the surroundings. **(b)** Total power flow $\dot{H}$ and acoustic power $\dot{E}$ as functions of position x in the device. Positive power flows in the positive-x direction. **(c)** Lumped-element model of the device. **(d)** Close-up view of part of one pore in the stack of **(a)**, showing a small mass of gas going through one full cycle, imagined as four discrete steps. *Thin arrows* represent motion, and *wide, open arrows* represent heat flow. **(e)** Plot showing how the pressure p and volume V of that small mass of gas evolve with time in a clockwise elliptical trajectory. *Tick marks* show approximate boundaries between the four numbered steps of the cycle shown in **(d)**

convection in the resonator, while fresh air at ambient temperature T_A streams inwards.

The most important process in the standing-wave engine is illustrated in Fig. 7.2d and Fig. 7.2e from a Lagrangian perspective. Figure 7.2d shows a greatly magnified view of a mass of gas inside one pore of the stack. The sinusoidal thermodynamic cycle of that mass of gas in pressure p and volume V is shown in Fig. 7.2e; the mass's temperature, entropy, density, and other properties also vary sinusoidally in time. However, for qualitative understanding of the processes, we describe the cycle as if it were a time series of four discrete steps, numbered 1–4 in Fig. 7.2d and Fig. 7.2e. In step 1, the gas is simultaneously compressed to a smaller volume and moved leftward by the wave a distance $2\,|\xi_1|$, which is much smaller than the length Δx of the stack. While the gas is moving leftwards, the pressure changes by $2\,|p_1|$ and the temperature would change by $2\,|T_1| = 2T_m(\gamma-1)\,|p_1|\,/\gamma p_m$ if the process were adiabatic. This suggests the definition of a critical temperature gradient

$$\nabla T_{crit} = |T_1| \,/\, |\xi_1| \ . \tag{7.20}$$

Thermal contact in the stack's large pores is imperfect, so step 1 is actually not too far from adiabatic. However, the temperature gradient imposed on the stack is greater than ∇T_{crit}, so the gas arrives at its new location less warm than the adjacent pore walls. Thus, in step 2, heat flows from the solid into the gas, warming the gas and causing thermal expansion of the gas to a larger volume. In step 3, the gas is simultaneously expanded to a larger volume and moved rightward by the wave. It arrives at its new location warmer than the adjacent solid, so in step 4 heat flows from the gas to the solid, cooling the gas and causing thermal contraction of the gas to a smaller volume. This brings it back to the start of the cycle, ready to repeat step 1.

Although the mass of gas under consideration returns to its starting conditions each cycle, its net effect on its surroundings is nonzero. First, its thermal expansion occurs at a higher pressure than its thermal contraction, so $\oint p\ \mathrm{d}V > 0$: the gas does work on its surroundings, satisfying Rayleigh's criterion. This work is responsible for the positive slope of $\dot{E}$ versus x in the stack in Fig. 7.2b and is represented by the gain element $G_{stack}U_{H,1}$ in

Fig. 7.2c. All masses of gas within the stack contribute to this production of acoustic power; one can think of the steady-state operation as due to all masses of gas within the stack adding energy to the oscillation every cycle, to make up for energy lost from the oscillation elsewhere, e.g., in viscous drag in the resonator and acoustic radiation to the surroundings. Second, the gas absorbs heat from the solid at the left extreme of its motion, at a relatively warm temperature, and delivers heat to the solid farther to the right at a lower temperature. In this way, all masses of gas within the stack pass heat along the solid, down the temperature gradient from left to right; within a single pore, the gas masses are like members of a bucket brigade (a line of people fighting a fire by passing buckets of water from a source of water to the fire while passing empty buckets back to the source). This transport of heat is responsible for most of $\dot{H}$ inside the stack, shown in Fig. 7.2b.

This style of engine is called *standing wave* because the time phasing between pressure and motion is close to that of a standing wave. (If it were *exactly* that of a standing wave, $\dot{E}$ would have to be exactly zero at all x.) To achieve the time phasing between pressure and volume changes that is necessary for $\oint p\ \mathrm{d}V > 0$, imperfect thermal contact between the gas and the solid in the stack is required, so that the gas can be somewhat thermally isolated from the solid during the motion in steps 1 and 3 but still exchange significant heat with the solid during steps 2 and 4. This imperfect thermal contact occurs because the distance between the gas and the nearest solid surface is of the order of δ_{therm}, and it causes R_{therm} to be significant, so standing-wave engines are inherently inefficient. Nevertheless, standing-wave engines are exceptionally simple. They include milliwatt classroom demonstrations like the illustration in Fig. 7.2, similar demonstrations with the addition of a water- or air-cooled heat exchanger at the ambient end of the stack, research engines [7.25, 26] up to several kW, and the Taconis and Sondhauss oscillations [7.5, 7]. Variants based on the same physics of intrinsically irreversible heat transfer include the *no-stack* standing-wave engine [7.27], which has two heat exchangers but no stack, and the Rijke tube [7.28], which has only a single, hot heat exchanger and uses a superposition of steady and oscillating flow of air through that heat exchanger to create $\oint p\ \mathrm{d}V > 0$.

7.3.2 Traveling-Wave Engines

One variety of what acousticians call traveling-wave engines has been known for almost two centuries as a Stirling engine [7.13, 29, 30], and is illustrated in Fig. 7.3a, Fig. 7.3b, Fig. 7.3f, and Fig. 7.3g. A regenerator bridges the gap between two heat exchangers, one at ambient temperature T_{A} and the other at hot temperature T_{H}; this assembly lies between two pistons, whose oscillations take the gas through a sinusoidal cycle that can be approximated as four discrete steps: compression, displacement rightward toward higher temperature, expansion, and displacement leftward toward lower temperature. For a small mass of gas in a single pore in the heart of the regenerator, the four steps of the cycle are illustrated in Fig. 7.3f. In step 1, the gas is compressed by rising pressure, rejecting heat to the nearby solid. In step 2, it is moved to the right, toward higher temperature, absorbing heat from the solid and experiencing thermal expansion as it moves. In step 3, the gas is expanded by falling pressure, and absorbs heat from the nearby solid. In step 4, the gas is moved leftward, toward lower temperature, rejecting heat to the solid and experiencing thermal contraction as it moves. The Stirling engine accomplishes $\oint p\ \mathrm{d}V > 0$ in Fig. 7.3g for each mass of gas in the regenerator, and this work production allows the hot piston to extract more work from the gas in each cycle than the ambient piston delivers to the gas.

The similarities and differences between this process and the standing-wave process of Fig. 7.2 are instructive. Here, the pore size is $\ll \delta_{\mathrm{therm}}$, so the thermal contact between the gas and the solid in the regenerator is excellent and the gas is always at the temperature of the part of the solid to which it is adjacent. Thus, the thermal expansion and contraction occur during the motion parts of the cycle, instead of during the stationary parts of the cycle in the standing-wave engine, and the pressure must be high during the rightward motion and low during the leftward motion to accomplish $\oint p\ \mathrm{d}V > 0$. This is the time phasing between motion and pressure that occurs in a traveling wave [7.14, 15], here traveling from left to right. The small pore size maintains thermodynamically reversible heat transfer, so R_{therm} is negligible, and traveling-wave engines have inherently higher efficiency than standing-wave engines. One remaining source of inefficiency is the viscous resistance R_{visc} in the regenerator, which can be significant because the small pores necessary for thermal efficiency cause R_{visc} to be large. To minimize the impact of R_{visc}, traveling-wave engines have $|p_1| > \rho_{\mathrm{m}} c\,|U_1|/A$, so the magnitude of the specific acoustic impedance $|z_{\mathrm{ac}}| = |p_1|\,A/|U_1|$ is greater than that of a traveling wave.

The gain G listed in Table 7.2 takes on a particularly simple form in the tight-pore limit: $G_{\mathrm{reg}} = \Delta T_{\mathrm{m}}/T_{\mathrm{in,m}}$.

Amazon EX1014 Page 263

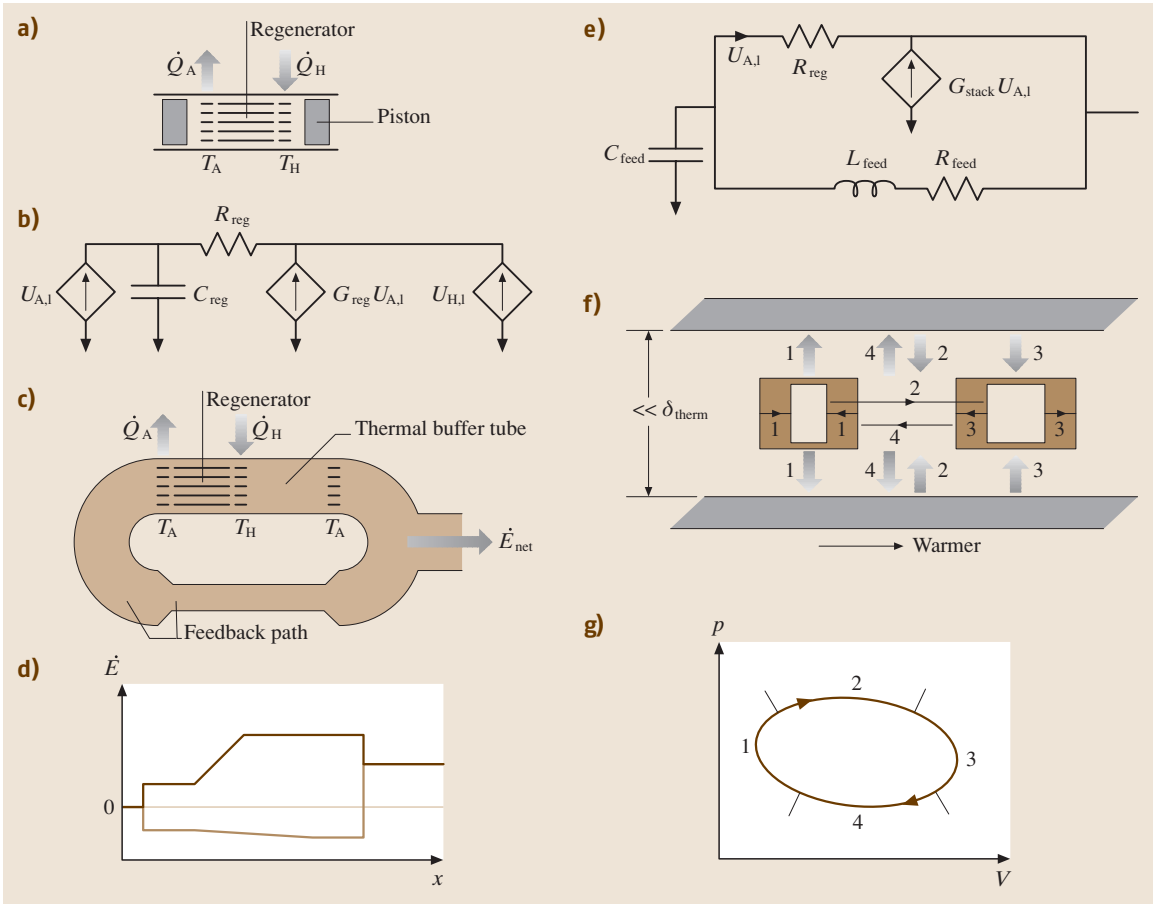


Fig. 7.3a–g Traveling-wave engines. **(a)** A Stirling engine. From *left to right*, the ambient piston, the ambient heat exchanger, the regenerator, the hot heat exchanger, and the hot piston. Time-averaged thermal power $\dot{Q}_H$ is injected into the gas at hot temperature T_H, waste thermal power $\dot{Q}_A$ is removed at ambient temperature T_A, and net mechanical power is extracted by the two pistons. **(b)** Lumped-element model of the engine in **(a)**. **(c)** Acoustic–Stirling hybrid engine, with the same processes as **(a)** in the regenerator and its two adjacent heat exchangers, but with additional acoustic components replacing the two pistons. **(d)** Acoustic power $\dot{E}$ as a function of position x in the device shown in **(c)**. Positive power flows in the positive-x direction, so the bottom branch of the curve represents power flowing leftward through the feedback path. Total power $\dot{H}$ is not shown, because it is essentially zero in the regenerator and essentially identical to $\dot{E}$ in the open parts of the device. **(e)** Lumped-element model of the engine in **(c)**. **(f)** Close-up view of part of one pore in the regenerator of **(a)** or **(c)**, showing a small mass of gas going through one full cycle, imagined as four discrete steps. **(g)** Plot showing how the pressure p and volume V of that small mass of gas evolve with time in a clockwise elliptical trajectory. *Tick marks* show approximate boundaries between the four steps of the cycle shown in **(f)**

In the engine of Fig. 7.3a, the initial temperature is T_A, and $\Delta T_m = T_H - T_A$, so the extra volume velocity that the lumped-element model injects at the right end of the regenerator is $U_{A,1}\,(T_H - T_A)\,/T_A$ and the total volume velocity at the right end of the regenerator is $U_{A,1}\,T_H/T_A$. Thus, the regenerator acts like an amplifier of volume velocity, with amplification T_H/T_A. If R_{reg} is small so that p_1 is nearly the same on both sides of the regenerator, then the regenerator amplifies $\dot{E}$ by nearly T_H/T_A.

Figure 7.3c-e illustrates a thermoacoustic–Stirling hybrid engine [7.16–18], in which the processes in the regenerator and its adjacent heat exchangers are the same

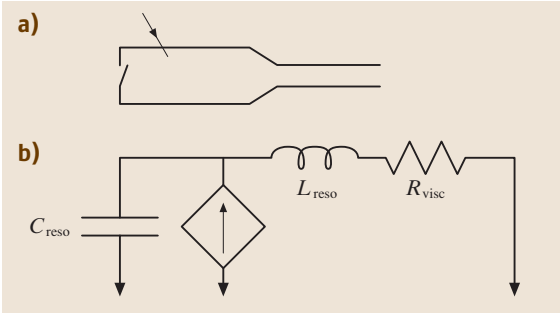


Fig. 7.4a,b Pulsed combustor. **(a)** From *left to right*, check valve for admitting fresh air, fuel injection, combustion cavity, neck. **(b)** Lumped-element model of the combustor

as in the Stirling engine and in Fig. 7.3f and Fig. 7.3g, but with acoustic elements replacing the Stirling engine's pistons. The toroidal topology of the thermoacoustic–Stirling hybrid allows some of the acoustic power that leaves the hot end of the regenerator to be fed back to the ambient end of the regenerator, eliminating the need for the Stirling engine's ambient piston. The feedback path has an inertance L_{feed} (with an unavoidable but small viscous resistance R_{feed}) and a compliance C_{feed}, with $1/L_{feed}C_{feed} \gg \omega^2$ and with ωL_{feed} significantly smaller than the regenerator viscous resistance R_{reg}. These choices let the $L_{feed}C_{feed}$ feedback path boost p_1 as acoustic power flows through it, providing the extra p_1 needed to drive U_1 into the regenerator at its ambient end.

The Stirling engine in Fig. 7.3a has a hot piston, which extracts acoustic power from the gas. From the hot piston's face, mechanical power flows from T_H to T_A along a temperature gradient in a moving part, either the piston itself or a connecting rod. In the thermoacoustic–Stirling hybrid engine of Fig. 7.3c, this thermal isolation function is accomplished by the thermal buffer tube, a thermally stratified column of moving gas. A well-designed thermal buffer tube passes acoustic power with little attenuation and has $\dot{H} \simeq \dot{E}$, so almost no thermal power flows from hot to ambient along the tube and little thermal power need be removed at the auxiliary heat exchanger at the thermal buffer tube's ambient end. Minimizing streaming and attendant heat convection in thermal buffer tubes, which otherwise causes $\dot{H} \neq \dot{E}$, is a topic of current research in thermoacoustics.

Traditional Stirling engines are used for propulsion in some submarines [7.31] and for auxiliary power in boats [7.32], and are under development for residential cogeneration of electricity and space heating [7.33], concentrated solar electricity generation, and nuclear generation of electricity for spacecraft [7.34]. In most of these applications, piston motion is converted to electricity via relative motion of wires and permanent magnets, either with a rotary alternator for crankshaft-coupled pistons or a linear alternator (reminiscent of a loudspeaker) for resonant *free-piston* configurations. Thermoacoustic-Stirling hybrid engines are under consideration for small-scale natural-gas liquefaction [7.25, 35] and for spacecraft power [7.36]. In the former case, acoustic power is fed directly from the engine to cryogenic acoustic refrigerators, without transduction to electrical power.

7.3.3 Combustion

In the standing-wave and traveling-wave engines, Rayleigh's criterion $\oint p \, dV > 0$ is met with volume changes that arise from temperature changes; those temperature changes, in turn, arise from thermal contact between the gas and nearby solid surfaces. In pulsed combustion, the volume changes needed to meet Rayleigh's criterion arise from both temperature and mole-number changes, which in turn are due to time-dependent chemical reactions whose rate is controlled by the time-dependent pressure or time-dependent velocity [7.37, 38].

Figure 7.4 illustrates one configuration in which pulsed combustion can occur. At the closed end of a closed–open resonator, a check valve periodically lets fresh air into the resonator and a fuel injector adds fuel, either steadily or periodically. If the rate of the exothermic chemical reaction increases with pressure (e.g., via the temperature's adiabatic dependence on pressure), positive dV occurs when p is high, meeting Rayleigh's criterion. A four-step diagram of the process, resembling Fig. 7.2d and Fig. 7.3f, is not included in Fig. 7.4 because the process is fundamentally not cyclic: a given mass of gas does not return to its starting conditions, but rather each mass of fresh-air–fuel mixture burns and expands only once.

Combustion instabilities can occur in rockets, jet engines, and gas turbines, with potentially devastating consequences if the pressure oscillations are high enough to cause structural damage. Much of the literature on thermoacoustic combustion is devoted to understanding such oscillations and using active or passive means to prevent them. However, some devices such as high-efficiency residential gas-fired furnaces deliberately use pulsed combustion as illustrated in Fig. 7.4 to pump fresh air in and exhaust gases out of the combus-

Amazon EX1014 Page 265

tor. This eliminates the need to leave the exhaust gases hot enough for strong chimney convection, so a larger fraction of the heat of combustion can be delivered to the home.

7.4 Dissipation

The dissipative processes represented above by R_{visc} and R_{therm} occur whenever gas-borne sound interacts with solid surfaces. Figure 7.5 illustrates this in the case of a short length dx of a large-radius duct with no axial temperature gradient. The origin of the viscous dissipation of acoustic power is viscous shear within the viscous penetration depth δ_{visc}, as shown in Fig. 7.5c. Most people find viscous dissipation intuitively plausible, imagining the frictional dissipation of mechanical energy when one surface rubs on another. More subtle is the thermal relaxation of acoustic power, illustrated in Fig. 7.5d and Fig. 7.5e. Gas is pressurized nearly adiabatically in step 1, then shrinks during thermal equilibration with the surface in step 2. It is depressurized nearly adiabatically in step 3, and then thermally expands during thermal equilibration with the surface during step 4. As shown in Fig. 7.5e, the net effect is $\oint p\ \mathrm{d}V < 0$: the gas absorbs acoustic power from the wave, because the contraction occurs at high pressure and the expansion at low pressure. To avoid a hopelessly cluttered illustration, Fig. 7.5d shows the thermal-hysteresis process superimposed on the left–right oscillating motion in steps 1 and 3, but the thermal-hysteresis process occurs even in the absence of such motion.

Differentiating (7.18) with respect to x shows that the dissipation of acoustic power in the duct in length

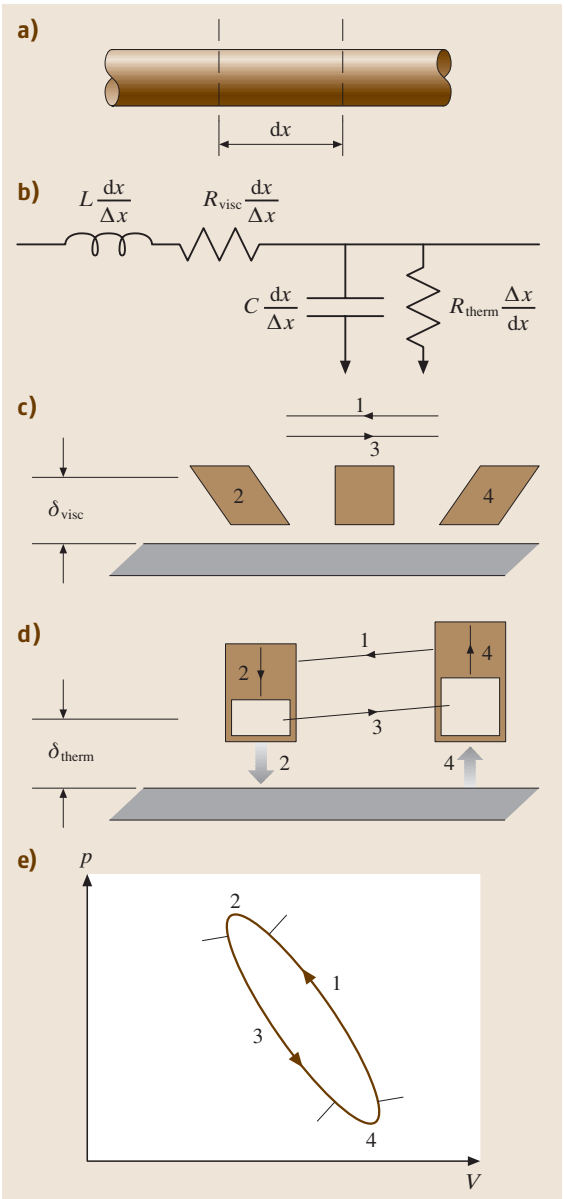


Fig. 7.5a–e Boundary dissipation in acoustic waves. **(a)** A duct with no temperature gradient, with one short length dx identified. **(b)** Each length dx has inertance, viscous resistance, compliance, and thermal hysteresis resistance. **(c)** The dissipation of acoustic power by viscous resistance is due to shear in the gas within roughly δ_{visc} of the boundary, here occurring during steps 1 and 3 of the cycle. **(d)** and **(e)** The dissipation of acoustic power by thermal relaxation hysteresis occurs within roughly δ_{therm} of the boundary. Gas is pressurized nearly adiabatically in step 1, then shrinks during thermal equilibration with the surface in step 2. It is depressurized nearly adiabatically in step 3, and then thermally expands during thermal equilibration with the surface during step 4. The net effect is that the gas absorbs acoustic power from the wave

Amazon EX1014 Page 266

$\mathrm{d}x$ is given by

$$\mathrm{d}\dot{E} = \frac{1}{2}\,\mathrm{Re}\left(\frac{\mathrm{d}\tilde{p}_1}{\mathrm{d}x}U_1 + \tilde{p}_1\frac{\mathrm{d}U_1}{\mathrm{d}x}\right)\,\mathrm{d}x\,, \tag{7.21}$$

and examination of (7.10) and (7.9) associates R_{visc} with the first term and R_{therm} with the second term. Expressions for R_{visc} and R_{therm} in the boundary-layer approximation are given in Table 7.2, and allow the expression of (7.21) in terms of the dissipation of acoustic power per unit of surface area S:

$$\mathrm{d}\dot{E} = \frac{1}{4}\rho_{\mathrm{m}}\,|u_1|^2\,\omega\delta_{\mathrm{visc}}\,\mathrm{d}S + \frac{1}{4}\,(\gamma-1)\,\frac{|p_1|^2}{\rho_{\mathrm{m}}c^2}\omega\delta_{\mathrm{therm}}\,\mathrm{d}S\,, \tag{7.22}$$

where $u_1 = U_1/A$ is the velocity outside the boundary layer, parallel to the surface. Each term in this result expresses a dissipation as the product of a stored energy per unit volume $\rho_{\mathrm{m}}\,|u_1|^2\,/4$ or $(\gamma-1)\,|p_1|^2\,/4\rho_{\mathrm{m}}c^2$, a volume $\delta_{\mathrm{visc}}\,\mathrm{d}S$ or $\delta_{\mathrm{therm}}\,\mathrm{d}S$, and a rate ω.

7.5 Refrigeration

7.5.1 Standing-Wave Refrigeration

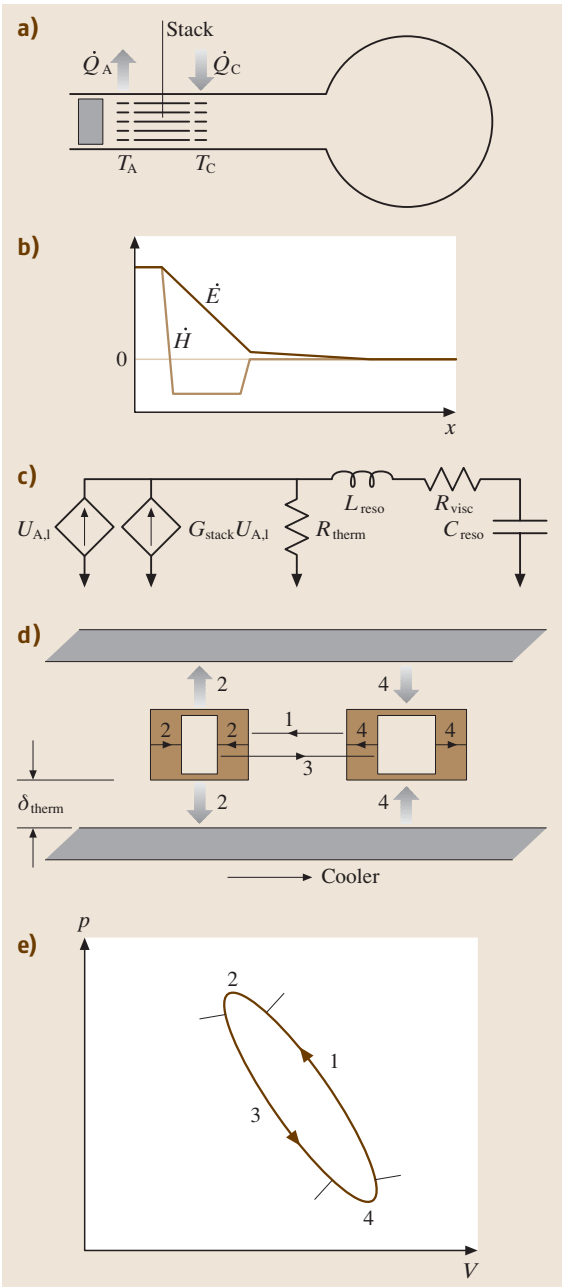
The thermal-hysteresis process described in Sect. 7.4 consumes acoustic power without doing anything thermodynamically useful. Standing-wave refrigeration consumes acoustic power via a similar process, but achieves a thermodynamic purpose: pumping heat up a temperature gradient, either to remove heat from a temperature below ambient or (less commonly) to deliver heat to a temperature above ambient. Figure 7.6a–c shows a standing-wave refrigerator of the style pioneered by *Hofler* [7.8, 9] and recently studied by *Tijani* [7.39]. At the left end, a driver such as a loudspeaker injects acoustic power $\dot{E}$, which flows rightward through the stack, causing a leftward flow of total energy $\dot{H}$.

The most important process in a standing-wave refrigerator is illustrated in Fig. 7.6d and Fig. 7.6e from a Lagrangian perspective. Fig. 7.6d shows a greatly magnified view of a small mass of gas inside one pore of the stack. The sinusoidal thermodynamic cycle of that mass of gas in pressure p and volume V is shown in Fig. 7.6e; the mass's temperature, entropy, density, and other properties also vary sinusoidally in time. However, for qualitative understanding of the processes, we describe them as if they are a time series of four discrete steps, numbered 1–4 in Fig. 7.6d and Fig. 7.6e. In step 1, the gas is simultaneously compressed to a smaller volume and moved leftward by the wave. Thermal contact is imperfect in the pores of a stack, so during step 1 the gas experiences a nearly adiabatic temperature increase due to the pressure increase that causes the compression. It arrives at its new location warmer than the adjacent solid because the temperature gradient in the solid is less than the critical temperature gradient ∇T_{crit} defined in (7.20). Thus, in step 2, heat flows from the gas into the solid, cooling the gas and causing thermal contraction of the gas to a smaller volume. In step 3, the gas is simultaneously expanded to a larger volume and moved rightward by the wave. It arrives at its new location cooler than the adjacent solid, so in step 4 heat flows from the solid to the gas, warming the gas and causing thermal expansion of the gas to a larger volume. This brings it back to the start of the cycle, ready to repeat step 1.

The mass of gas shown in Fig. 7.6d has two time-averaged effects on its surroundings. First, the gas absorbs heat from the solid at the right extreme of its motion, at a relatively cool temperature, and delivers heat to the solid farther to the left at a higher temperature. In this way, all masses of gas within the stack pass heat along the solid, up the temperature gradient from right to left—within a single pore, the gas masses are like members of a bucket brigade passing water. This provides the desired refrigeration or heat-pumping effect. If the left heat exchanger is held at ambient temperature, as shown in Fig. 7.6a, then the system is a refrigerator, absorbing thermal power $\dot{Q}_{\mathrm{C}}$ from an external load at the right heat exchanger at one end of the bucket brigade at T_{C}, as waste thermal power is rejected to an external ambient heat sink at the other end of the bucket brigade at T_{A}. (The system functions as a heat pump if the right heat exchanger is held at ambient temperature; then the left heat exchanger is above ambient temperature.) Second, the gas's thermal expansion occurs at a lower pressure than its thermal contraction, so $\oint p\,\mathrm{d}V < 0$: the gas absorbs work from its surroundings. This work is responsible for the negative slope of $\dot{E}$ versus x in the stack in Fig. 7.6b and is represented by the gain element $G_{\mathrm{stack}}U_{\mathrm{A},1}$ in Fig. 7.6c. All masses of gas within the stack contribute

to this consumption of acoustic power, which must be supplied by the driver.

As in the standing-wave engine, the time phasing between pressure and motion in the standing-wave refrigerator is close to that of a standing wave. Imperfect thermal contact between the gas and the solid in the stack is required to keep the gas rather isolated from the solid during the motion in steps 1 and 3 but still able to exchange significant heat with the solid during steps 2 and 4. This imperfect thermal contact occurs because the distance between the gas and the nearest solid surface is of the order of δ_{therm}, and it causes R_{therm} to be significant, so standing-wave refrigerators are inherently inefficient.



7.5.2 Traveling-Wave Refrigeration

Several varieties of traveling-wave refrigerator are commercially available or under development. At their core is a regenerator, in which the process shown in Fig. 7.7a,b operates. In step 1 of the process, the gas is compressed by rising pressure, rejecting heat to the nearby solid. In step 2, it is moved to the right, toward lower temperature, rejecting heat to the solid and experiencing thermal contraction as it moves. In step 3, the gas is expanded by falling pressure, and absorbs heat from the nearby solid. In step 4, the gas is moved leftward, toward higher temperature, absorbing heat from the solid and experiencing thermal expansion as it moves. The heat transfers between gas and solid in steps 2 and 4 are equal and opposite, so the net thermal effect of each mass of gas on the solid is due to steps 1 and 3, and is to move heat from right to left, up the temperature gradient. As before, the motion of any particular mass of gas is less than the length of the regenerator, so the heat is passed bucket-brigade fashion from the cold end of the regenerator to the ambient end. Each mass of gas absorbs $\oint p\, \mathrm{d}V$ of acoustic power from the wave as shown in Fig. 7.7b, because the thermal contraction in step 2 occurs at high pres-

Fig. 7.6a–e A standing-wave refrigerator. **(a)** From *left to right*, a piston, ambient heat exchanger, stack, cold heat exchanger, tube, and tank. Acoustic power is supplied to the gas by the piston to maintain the standing wave, and results in thermal power $\dot{Q}_C$ being absorbed by the gas from a load at cold temperature T_C while waste thermal power $\dot{Q}_A$ is rejected by the gas to an external heat sink at ambient temperature T_A. **(b)** Total power flow $\dot{H}$ and acoustic power $\dot{E}$ as functions of position x in the device. Positive power flows in the positive-x direction. **(c)** Lumped-element model of the device. **(d)** Close-up view of part of one pore in the stack of **(a)**, showing a small mass of gas going through one full cycle, imagined as four discrete steps. **(e)** Plot showing how the pressure p and volume V of that small mass of gas evolve with time in a counter-clockwise elliptical trajectory. *Tick marks* show approximate boundaries between the four steps of the cycle shown in **(d)**

Amazon EX1014 Page 268

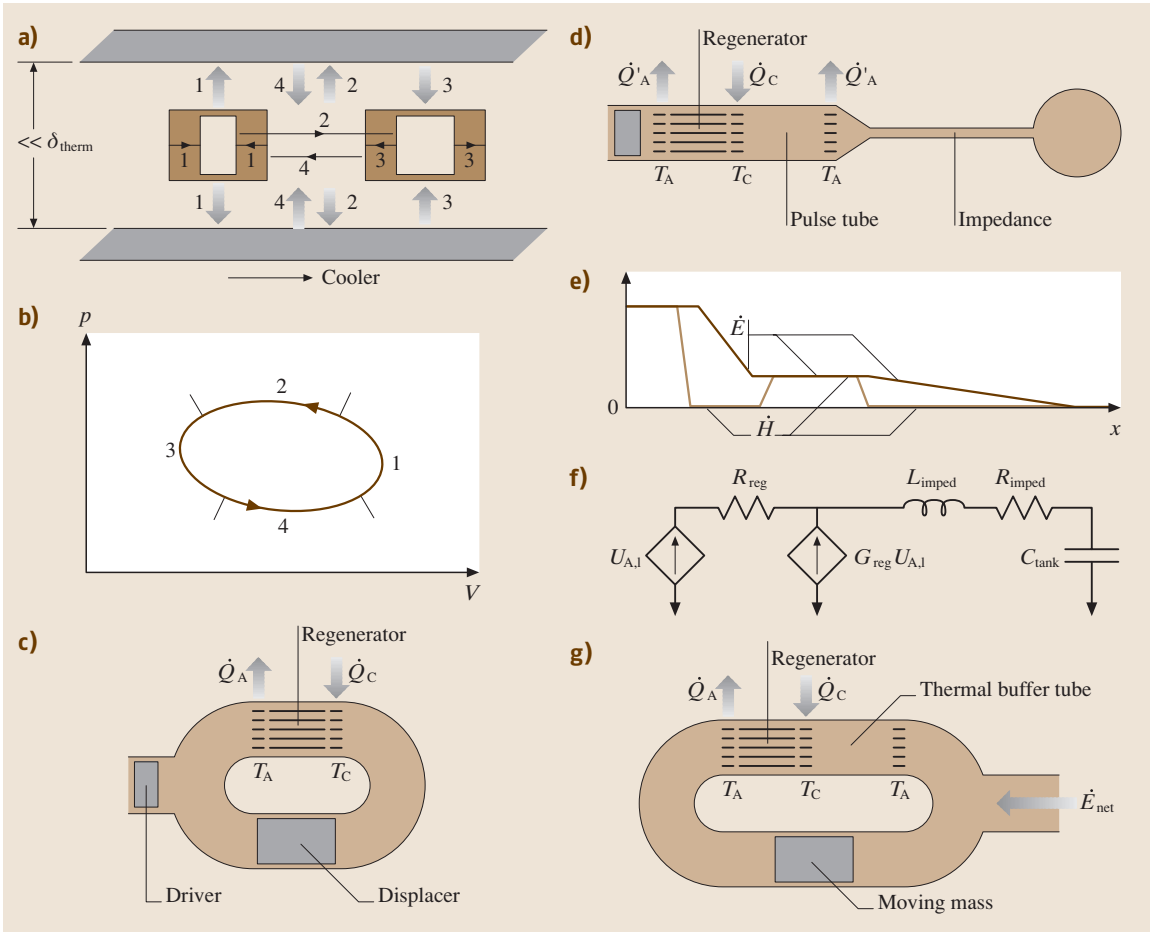


Fig. 7.7a–g Traveling-wave refrigerators. **(a)** Close-up view of part of one pore in the regenerator of a traveling-wave refrigerator, showing a small mass of gas going through one full cycle, imagined as four discrete steps. **(b)** Plot showing how the pressure p and volume V of that small mass of gas evolve with time in a counterclockwise elliptical trajectory. Tick marks show approximate boundaries between the four steps of the cycle shown in **(a)**. **(c)** A traditional Stirling refrigerator. From *left to right*, the ambient driver piston; the ambient heat exchanger, the regenerator, and the cold heat exchanger are across the top; the displacer is below. Time-averaged thermal power $\dot{Q}_C$ is removed by the gas from an external heat load at cold temperature T_C, while waste thermal power $\dot{Q}_A$ is rejected by the gas to an external heat sink at ambient temperature T_A and net acoustic power is supplied to the gas by the driver. **(d)** Pulse-tube refrigerator, with the same processes as **(c)** in the regenerator and its two adjacent heat exchangers, but with the displacer replaced by acoustic components. **(e)** Acoustic power $\dot{E}$ and total power $\dot{H}$ as functions of position x in the device shown in **(d)**. Positive power flows in the positive-x direction. **(f)** Lumped-element model of the pulse-tube refrigerator in **(d)**. **(g)** A refrigerator in which the thermal-buffer function and moving-mass function of **(c)**'s displacer are in two separate components

sure and the thermal expansion in step 4 occurs at low pressure. The small pore size, $r_h \ll \delta_{\text{therm}}$, maintains thermodynamically reversible heat transfer, so R_{therm} is negligible, and traveling-wave refrigerators have an inherently high efficiency. Acoustically, the process shown in Fig. 7.7a represents acoustic power traveling from left to right through the regenerator, and being partly consumed as it goes. Different varieties of traveling-wave refrigerator use different methods to create the necessary amplitudes and relative time phasing of motion and pressure to achieve this acoustic power flow through the regenerator.

Amazon EX1014 Page 269

The traditional Stirling refrigerator [7.40] uses two moving pistons, which can be either crankshaft-coupled in a configuration like that of the engine in Fig. 7.3a or of the *free-displacer* variety shown in Fig. 7.7c. In the free-displacer Stirling refrigerator (often called *free piston*), the solid displacer moves in response to the gas-pressure forces on it, without linkage to any external motor. Its area and mass are selected to give its motion the desired amplitude and time phase [7.29]. Acoustic power is transmitted through it, from right to left, so that the acoustic power that flows out of the right end of the regenerator is fed through the displacer to the left, added to the acoustic power supplied by the driver, and injected into the left end of the regenerator. The displacer must be a thermal insulator, because its right end is at T_C and its left end at T_A. Crankshaft-coupled Stirling refrigerators were used in the 19th century to keep beef cold on the long sea voyage from South America to Britain. Free-piston Stirling cryocoolers are in common use today for cooling infrared sensors in military night-vision goggles and surveillance satellites, and a free-piston Stirling refrigerator built into a small, portable *ice chest* is commercially available at low cost for picnics [7.41].

The pulse-tube refrigerator [7.12], illustrated in Fig. 7.7d–f, uses only one piston. The acoustic power flowing out of the right end of the regenerator is absorbed in an acoustic impedance, instead of being fed back to the left end of the regenerator. This gives the pulse-tube refrigerator a lower efficiency than the Stirling refrigerator, but for cryogenic applications the reduced efficiency is a small price to pay for the elimination of the Stirling's cold moving part. The lumped-element model of the impedance and adjacent tank shown in Fig. 7.7f correctly suggests that proper design of L_{imped}, R_{imped}, and C_{tank} can create almost any desired ratio of $|U_1|$ to $|p_1|$ and time phasing between U_1 and p_1 at the right end of the regenerator. The desired impedance is often achieved by choosing $R_{\text{visc}} \sim \omega L_{\text{imped}} \gg 1/\omega C_{\text{imped}}$. The so-called pulse tube, and the ambient heat exchanger to its right, thermally isolate the cold heat exchanger from the dissipation of acoustic power in the impedance, just as the thermal buffer tube performs that function in Fig. 7.3c. Pulse-tube refrigerators are in common use today in satellites [7.42] and are under development for many other applications such as small-scale oxygen liquefaction and cooling superconducting equipment.

Another variation of the theme is shown in Fig. 7.7g, where the thermal buffer tube and the moving mass perform the thermal-insulation and inertial functions of the free displacer of Fig. 7.7c in two separate locations [7.43,44]. This variety is under development for commercial food refrigeration [7.45]. Yet another variety [7.46] replaces the inertial moving mass of Fig. 7.7g with inertial moving gas, similar to the thermoacoustic–Stirling hybrid engine of Fig. 7.3c.

7.6 Mixture Separation

In thermoacoustic mixture separation, acoustic power causes the components of a gas mixture to separate [7.47, 48]. The process is loosely analogous to the pumping of heat through the stack in a standing-wave refrigerator. The expenditure of acoustic power results in an increase in the Gibbs free energy of the mixture's components, and the efficiency of the process is comparable to that of some other practical separation processes [7.49].

Figure 7.8 illustrates the process for a binary gas mixture of heavy and light molecules, whose motions are indicated by filled and open arrows, respectively. The motion of the molecules in steps 1 and 3 of the process is bulk motion of the gas, and the motion during steps 2 and 4 is thermal diffusion, in which light molecules diffuse toward higher temperature and heavy molecules diffuse toward lower temperature. In step 1, the gas in the center of the pore moves leftward and its pressure rises, so its temperature rises nearly adiabatically. Trapped by the viscous boundary layer near the wall of the tube is some other gas that does not move and whose thermal contact with the pore wall keeps its temperature from rising. During step 2, the temperature difference between the central gas and the peripheral gas causes light atoms to diffuse into the center and heavy atoms to diffuse out of the center, enriching the center in light atoms. Bulk motion rightward in step 3 carries this central light-enriched gas to the right. Simultaneously, the pressure drops in step 3, and hence the central temperature drops nearly adiabatically. Thus thermal diffusion in step 4 pulls heavy molecules into the center and drives light molecules out of the center, leaving the center enriched in heavy molecules so that the leftward motion during step 1 carries heavy-enriched gas leftward. The net effect of steps 1 and 3 is to move heavy molecules leftward and light molecules rightward. The process

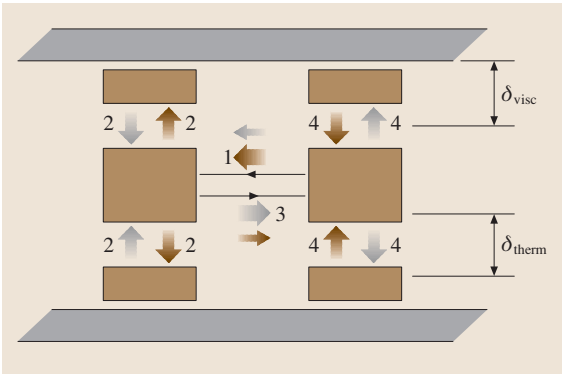


Fig. 7.8 Close-up view of part of one pore in a thermoacoustic mixture separator, showing a small body of gas in the center of the pore going through one full cycle, imagined as four discrete steps, and exchanging mass with neighboring, immobile gas. The *gray* and *brown arrows* in steps 2 and 4 signify thermally driven diffusion of light and heavy molecules between the central gas and the peripheral gas close to the wall of the pore. In steps 1 and 3, the *gray* and *brown arrows* signify bulk motion of the gas, without diffusion

takes place when the mole-fraction gradient is less than a critical gradient, analogous to the critical temperature gradient below which standing-wave refrigeration occurs.

As is evident from Fig. 7.8, the process works best for tubes with r_h somewhat larger than δ_{therm} and δ_{visc}. However, unlike the description above, the process actually works best near traveling-wave phasing, because two 45° phase shifts were ignored in that description. High separation purities require long tubes, and high mole fluxes will require many passages in parallel, perhaps in structures similar to the stacks of standing-wave engines and refrigerators.

In a 2 m-long tube, a 50–50 helium–argon mixture has been separated to yield 70% helium, 30% argon at one end and 30% helium, 70% argon at the other end; and a measurable enrichment of ^{22}Ne from natural neon has been achieved [7.50].

References

7.1 G.W. Swift: *Thermoacoustics: A Unifying Perspective for some Engines and Refrigerators* (Acoustical Society of America Publications, Sewickley PA 2002)

7.2 S.L. Garrett: Resource letter TA-1, Thermoacoustic engines and refrigerators, Am. J. Phys. **72**, 11–17 (2004)

7.3 N. Rott: Damped and thermally driven acoustic oscillations in wide and narrow tubes, Z. Angew. Math. Phys. **20**, 230–243 (1969)

7.4 N. Rott: Thermally driven acoustic oscillations, Part III: Second-order heat flux, Z. Angew. Math. Phys. **26**, 43–49 (1975)

7.5 T. Yazaki, A. Tominaga, Y. Narahara: Experiments on thermally driven acoustic oscillations of gaseous helium, J. Low Temp. Phys. **41**, 45–60 (1980)

7.6 J.W. Strutt (Baron Rayleigh): The explanation of certain acoustical phenomena, Nature **18**, 319–321 (1878)

7.7 K.T. Feldman: Review of the literature on Sondhauss thermoacoustic phenomena, J. Sound Vibrat. **7**, 71–82 (1968)

7.8 T. Hofler, J.C. Wheatley, G.W. Swift, A. Migliori: Acoustic cooling engine, US Patent No. 4,722,201. (1988)

7.9 T.J. Hofler: *Thermoacoustic refrigerator design and performance. Ph.D. thesis, Physics Department* (University of California, San Diego 1986)

7.10 W.E. Gifford, R.C. Longsworth: Pulse tube refrigeration progress, Adv. Cryogenic Eng. B **10**, 69–79 (1965)

7.11 E.L. Mikulin, A.A. Tarasov, M.P. Shkrebyonock: Low-temperature expansion pulse tubes, Adv. Cryogenic Eng. **29**, 629–637 (1984)

7.12 R. Radebaugh: *Development of the pulse tube refrigerator as an efficient and reliable cryocooler* (Proc. Inst. Refrigeration, London 2000) pp. 11–29

7.13 G. Walker: *Stirling Engines* (Clarendon, Oxford 1960)

7.14 P.H. Ceperley: A pistonless Stirling engine – The traveling wave heat engine, J. Acoust. Soc. Am. **66**, 1508–1513 (1979)

7.15 P.H. Ceperley: Gain and efficiency of a short traveling wave heat engine, J. Acoust. Soc. Am. **77**, 1239–1244 (1985)

7.16 T. Yazaki, A. Iwata, T. Maekawa, A. Tominaga: Traveling wave thermoacoustic engine in a looped tube, Phys. Rev. Lett. **81**, 3128–3131 (1998)

7.17 C.M. de Blok: Thermoacoustic system, 1998. Dutch Patent: International Application Number PCT/NL98/00515. US Patent 6,314,740, November 13 (2001)

7.18 S. Backhaus, G.W. Swift: A thermoacoustic-Stirling heat engine, Nature **399**, 335–338 (1999)

7.19 D. Gedeon: *A globally implicit Stirling cycle simulation, Proceedings of the 21st Intersociety Energy Conversion Engineering Conference* (Am. Chem. Soc.,

Amazon EX1014 Page 271

Washington 1986) pp. 550–554, Software available from Gedeon Associates, Athens, Ohio
7.20 W.C. Ward, G.W. Swift: Design environment for low amplitude thermoacoustic engines (DeltaE), J. Acoust. Soc. Am. **95**, 3671–3672 (1994), Software and user's guide available either from the Los Alamos thermoacoustics web site www.lanl.gov/thermoacoustics/ or from the Energy Science and Technology Software Center, US Department of Energy, Oak Ridge, Tennessee
7.21 R.E. Sonntag, C. Borgnakke, G.J. Van Wylen: *Fundamentals of Thermodynamics* (Wiley, New York 2003)
7.22 F.W. Giacobbe: Estimation of Prandtl numbers in binary mixtures of helium and other noble gases, J. Acoust. Soc. Am. **96**, 3568–3580 (1994)
7.23 A. Bejan: *Advanced Engineering Thermodynamics*, 2nd edn. (Wiley, New York 1997)
7.24 Acoustic Laser Kit, Graduate Program in Acoustics, P. O. Box 30, State College, PA 16804-0030 (www.acs.psu.edu/thermoacoustics/refrigeration/laserdemo.htm)
7.25 G.W. Swift, J.J. Wollan: Thermoacoustics for liquefaction of natural gas, GasTIPS **8**(4), 21–26 (2002), Also available at www.lanl.gov/thermoacoustics/Pubs/GasTIPS.pdf
7.26 D.L. Gardner, G.W. Swift: A cascade thermoacoustic engine, J. Acoust. Soc. Am. **114**, 1905–1919 (2003)
7.27 R.S. Wakeland, R.M. Keolian: Thermoacoustics with idealized heat exchangers and no stack, J. Acoust. Soc. Am. **111**, 2654–2664 (2002)
7.28 K.T. Feldman: Review of the literature on Rijke thermoacoustic phenomena, J. Sound Vibrat. **7**, 83–89 (1968)
7.29 I. Urieli, D.M. Berchowitz: *Stirling Cycle Engine Analysis* (Adam Hilger, Bristol 1984)
7.30 A.J. Organ: *Thermodynamics and Gas Dynamics of the Stirling Cycle Machine* (Cambridge Univ. Press, Cambridge 1992)
7.31 H. Nilsson, C. Bratt: Test results from a 15 kW air-independent Stirling power generator. In: *Proc. 6th International Symposium on Unmanned Untethered Submersible Technology* (IEEE, 1989) pp. 123–128
7.32 WhisperGen Limited, Christchurch, New Zealand
7.33 S. Qiu, D.L. Redinger, J.E. Augenblick: The next generation infinia free-piston Stirling engine for micro-CHP applications. In: *Proc. 12th International Stirling Engine Conference* (Durham University, 2005) pp. 156–165
7.34 M.A. White: A new paradigm for high-power Stirling applications, Proc. Space Nuclear Conference, Stirling Technology Company, Kennewick WA (2005)
7.35 B. Arman, J. Wollan, V. Kotsubo, S. Backhaus, G. Swift: Operation of thermoacoustic Stirling heat engine driven large multiple pulse tube refrigerators. In: *Cryocoolers 13*, ed. by R.G. Ross (Springer, Berlin, New York 2005) pp. 181–188
7.36 S. Backhaus, E. Tward, M. Petach: Traveling-wave thermoacoustic electric generator, Appl. Phys. Lett. **85**, 1085–1087 (2004)
7.37 B. Zinn: Pulsating combustion. In: *Advanced Combustion Methods*, ed. by F.J. Weinberg (Academic, London 1986) pp. 113–181
7.38 F.E.C. Culick: Combustion instabilities and Rayleigh's criterion. In: *Modern Research Topics in Aerospace Propulsion*, ed. by C. Casci, G. Angelino, L. DeLuca, W.A. Sirignano (Springer, Berlin, New York 1991) pp. 508–517, (in honor of Corrado Casci)
7.39 M.E.H. Tijani, J.C.H. Zeegers, A.T.A.M. deWaele: The optimal stack spacing for thermoacoustic refrigeration, J. Acoust. Soc. Am. **112**, 128–133 (2002)
7.40 G. Walker: *Cryocoolers* (Plenum, New York 1983)
7.41 N.W. Lane: Commercialization status of free-piston Stirling machines. In: *Proc. 12th International Stirling Engine Conference* (Durham University, 2005) pp. 30–37
7.42 E. Tward, C.K. Chan, C. Jaco, J. Godden, J. Chapsky, P. Clancy: Miniature space pulse tube cryocoolers, Cryogenics **39**, 717–720 (1999)
7.43 R.W.M. Smith, M.E. Poese, S.L. Garrett, R.S. Wakeland: Thermoacoustic device, US Patent No. 6,725,670.(2004)
7.44 M. E. Poese, R. W. M. Smith, R. S. Wakeland, S. L. Garrett: Bellows bounce thermoacoustic device, US Patent No. 6,792,764.(2004)
7.45 S.L. Garret: Pennsylvania State University, private communication
7.46 G.W. Swift, D.L. Gardner, S. Backhaus: Acoustic recovery of lost power in pulse tube refrigerators, J. Acoust. Soc. Am. **105**, 711–724 (1999)
7.47 D.A. Geller, G.W. Swift: Saturation of thermoacoustic mixture separation, J. Acoust. Soc. Am. **111**, 1675–1684 (2002)
7.48 P.S. Spoor, G.W. Swift: Thermoacoustic separation of a He-Ar mixture, Phys. Rev. Lett. **85**, 1646–1649 (2000)
7.49 D.A. Geller, G.W. Swift: Thermodynamic efficiency of thermoacoustic mixture separation, J. Acoust. Soc. Am. **112**, 504–510 (2002)
7.50 D.A. Geller, G.W. Swift: Thermoacoustic enrichment of the isotopes of neon, J. Acoust. Soc. Am. **115**, 2059–2070 (2004),

Amazon EX1014 Page 272

8. Nonlinear Acoustics in Fluids

At high sound intensities or long propagation distances at sufficiently low damping acoustic phenomena become nonlinear. This chapter focuses on nonlinear acoustic wave properties in gases and liquids. The origin of nonlinearity, equations of state, simple nonlinear waves, nonlinear acoustic wave equations, shock-wave formation, and interaction of waves are presented and discussed. Tables are given for the nonlinearity parameter *B/A* for water and a range of organic liquids, liquid metals and gases. Acoustic cavitation with its nonlinear bubble oscillations, pattern formation and sonoluminescence (light from sound) are modern examples of nonlinear acoustics. The language of nonlinear dynamics needed for understanding chaotic dynamics and acoustic chaotic systems is introduced.

8.1 **Origin of Nonlinearity** 258
8.2 **Equation of State** 259
8.3 **The Nonlinearity Parameter** *B/A* 260
8.4 **The Coefficient of Nonlinearity** β 262
8.5 **Simple Nonlinear Waves** 263
8.6 **Lossless Finite-Amplitude Acoustic Waves** 264
8.7 **Thermoviscous Finite-Amplitude Acoustic Waves** 268
8.8 **Shock Waves** 271
8.9 **Interaction of Nonlinear Waves** 273
8.10 **Bubbly Liquids** 275
8.10.1 Incompressible Liquids 276
8.10.2 Compressible Liquids 278
8.10.3 Low-Frequency Waves: The Korteweg–de Vries Equation 279
8.10.4 Envelopes of Wave Trains: The Nonlinear Schrödinger Equation 282
8.10.5 Interaction of Nonlinear Waves. Sound–Ultrasound Interaction 284
8.11 **Sonoluminescence** 286
8.12 **Acoustic Chaos** 289
8.12.1 Methods of Chaos Physics 289
8.12.2 Chaotic Sound Waves 291
References 293

Acoustics belongs to those areas of physics, where nonlinear phenomena were observed first [8.1–4]. All musical instruments including the human voice belong to nonlinear acoustics as they produce sound waves and these, moreover, are not simple sinusoidal waves. Generation processes are necessarily nonlinear as new phenomena appear that are not proportional to already existing ones. Propagation, on the other hand, is normally linear for propagation distances that are not too long and only starts to show nonlinear effects at high intensities. As mankind started to speak early in its history and also is supposed to have made music early on, nonlinear acoustics belongs to the oldest parts of science. Sorge in 1745 and Tartini in 1754 report that, when two tones of frequency f_1 and $f_2 > f_1$ are presented to the ear at high intensities, the difference frequency $f_2 - f_1$ is additionally heard. For a long time there was a debate of whether these tones were generated in the ear or were already present in the propagating medium. Today we know that in this case the ear generates the difference frequency. But we also know that a difference frequency can be generated in a nonlinear medium during the propagation of a sound wave [8.5]. This fact is used in the parametric acoustic array to transmit and receive highly directed low-frequency sound beams. Under suitable circumstances generally a series of combination frequencies $f_{mn} = m f_1 + n f_2$ with $m, n = 0, \pm 1, \pm 2, \ldots$ can be generated.

A special case is a single harmonic wave of frequency f propagating in a nonlinear medium. It generates the higher harmonics $f_m = m f$. This leads to a steepening of the wave and often to the formation of shock waves. Further nonlinear effects are subsumed under the heading of self-action, as changes in the medium are produced by the sound wave that act back on the wave. Examples are self-focusing and self-transparency.

Amazon EX1014 Page 273

Also forces may be transmitted to the medium setting it into motion, as exemplified by the phenomenon of acoustic streaming. Acoustic radiation forces may be used to levitate objects and keep them in traps. In other areas of science this is accomplished by electrical or electromagnetical forces (ion traps, optical tweezers). Nonlinear acoustics is the subject of many books, congress proceedings and survey articles [8.1–4, 6–19].

In liquids a special phenomenon occurs, the rupture of the medium by sound waves, called acoustic cavitation [8.20–27]. This gives rise to a plethora of special effects bringing acoustics in contact with almost any other of the natural sciences. Via the dynamics of the cavities, or the cavitation bubbles produced, dirt can be removed from surfaces (ultrasonic cleaning), light emission may occur upon bubble collapse (sonoluminescence [8.28]) and chemical reactions are initiated (sonochemistry [8.29, 30]).

Recently, the general theory of nonlinear dynamics lead to the interesting finding that nonlinear dynamical systems may not just show this simple scenario of combination tones and self-actions, but complicated dynamics resembling stochastic behavior. This is known as deterministic chaos or, in the context of acoustics, *acoustic chaos* [8.31, 32].

Nonlinear acoustics also appears in wave propagation in solids. In this case, further, entirely different, nonlinear phenomena appear, because not only longitudinal but also transverse waves are supported. A separate chapter of this Handbook is devoted to this topic.

8.1 Origin of Nonlinearity

All acoustic phenomena necessarily become nonlinear at high intensities. This can be demonstrated when looking at the propagation of a harmonic sound wave in air. In Fig. 8.1 a harmonic sound wave is represented graphically. In the upper diagram the sound pressure p is plotted versus location x. The static pressure p_{stat} serves as a reference line around which the sound pressure oscillates. This pressure p_{stat} is normally about 1 bar. In the lower diagram the density distribution is given schematically in a grey scale from black to white for the pressure range of the sound wave.

Assuming that the sound pressure amplitude is increased steadily, a point is reached where the sound pressure amplitude attains p_{stat} giving a pressure of zero in the sound pressure minimum. It is impossible to go below this point as there cannot be less than zero air molecules in the minimum. However, air can be compressed above the pressure p_{stat} just by increasing the force. Therefore, beyond a sound pressure amplitude $p = p_{\mathrm{stat}}$ no harmonic wave can exist in a gas; it must become nonlinear and contain harmonics. The obvious reason for the nonlinearity in this case (a gas)

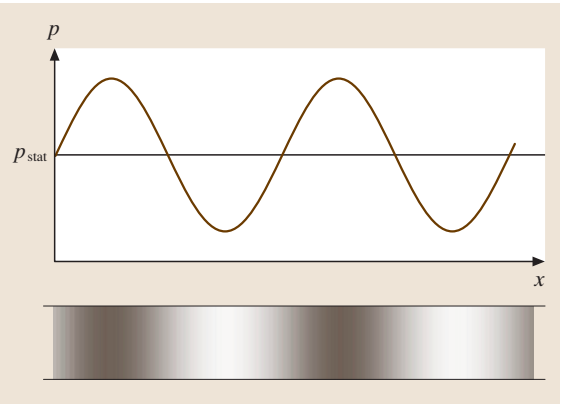


Fig. 8.1 Graphical representation of a harmonic sound wave

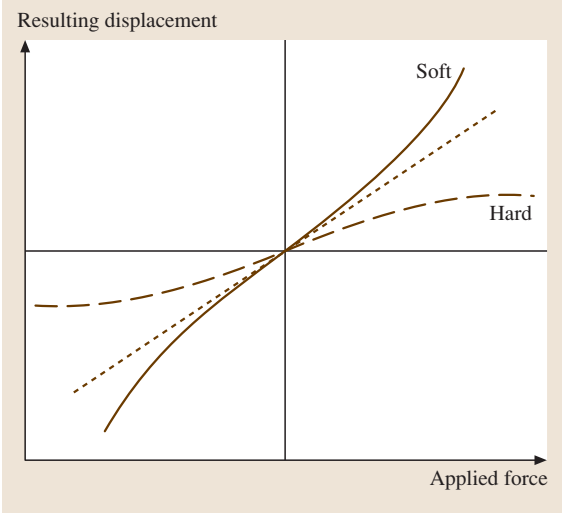


Fig. 8.2 Symmetric nonlinear expansion and compression laws compared to a linear law (*straight dotted line*) with soft spring behavior (*solid line*) and hard spring behavior (*dashed line*)

Amazon EX1014 Page 274

is the asymmetry in density between compression and expansion.

However, symmetric expansion and compression also lead to nonlinear effects when they are not proportional to an applied force or stress. Figure 8.2 shows two types of symmetric nonlinearities: hard and soft spring behavior upon expansion and compression with reference to a linear law represented by a straight (dotted) line. An example of hard spring behavior is a string on a violin, because the average string tension increases with increasing wave amplitude. It is intrinsically symmetric, as positive and negative elongation are equivalent. An example of soft spring behavior is the pendulum, also having a symmetric force–displacement law in a homogeneous gravitational field. An example of an asymmetric mixed type, but with overall soft spring behavior, is a bubble in water oscillating in a sound field. Upon compression a bubble shows hard spring behavior, upon expansion soft spring behavior in such a way that soft spring behavior dominates.

Acoustic waves also show nonlinear behavior in propagation, even without any nonlinearity of the medium. This is due to the cumulative effect of distortion of the wave profile by convection, introduced by the particle velocity that itself constitutes the sound wave. Larger particle velocities propagate faster than slower ones, leading to distortion of an acoustic wave upon propagation. This property can be considered an intrinsic self-action of the wave, leading to an intrinsic nonlinearity in acoustics. This aspect of nonlinearity is discussed below in the context of the coefficient of nonlinearity β.

8.2 Equation of State

The compression and expansion of a medium is described by the equation of state, for which an interrelation between three quantities is needed, usually the pressure p, density ϱ and specific entropy s (entropy per unit mass). Often the variation of entropy can be neglected in acoustic phenomena and the calculations can be carried out at constant entropy; the equations are then called isentropic. A basic quantity in acoustics, the velocity of sound or sound speed c of a medium, is related to these quantities:

$$c^2 = \left(\frac{\partial p}{\partial \varrho}\right)_s \,. \tag{8.1}$$

The subscript index s indicates that the entropy is to be held constant to give the isentropic velocity of sound.

Even an ideal gas is nonlinear, because it obeys the isentropic equation of state

$$p = p_0 \left(\frac{\varrho}{\varrho_0}\right)^{\gamma} \,, \tag{8.2}$$

where p_0 and ϱ_0 are the reference (ambient) pressure and density, respectively, and

$$\gamma = \frac{c_\mathrm{p}}{c_\mathrm{v}} \,, \tag{8.3}$$

where γ is the quotient of the specific heat c_p at constant pressure and c_v that at constant volume.

An empirical formula, the Tait equation, is often used for liquids, obviously constructed similarly to the equation of state of the ideal gas:

$$p = P \left(\frac{\varrho}{\varrho_0}\right)^{\gamma_\mathrm{L}} - Q \tag{8.4}$$

or

$$\frac{p+Q}{p_\infty + Q} = \left(\frac{\varrho}{\varrho_0}\right)^{\gamma_\mathrm{L}} \,. \tag{8.5}$$

The two quantities Q and γ_L have to be fitted to the experimental pressure–density curve. For water $\gamma_\mathrm{L} = 7$, $P = p_\infty + Q = 3001$ bar and $Q = 3000$ bar are used. (Note that γ_L in the Tait equation is not the quotient of the specific heats.)

There is another way of writing the equation of state where the pressure is developed as a Taylor series as a function of density and entropy [8.17]. In the isentropic case it reads [8.33–35]

$$p - p_0 = \left(\frac{\partial p}{\partial \varrho}\right)_{s,\varrho=\varrho_0} (\varrho - \varrho_0) + \frac{1}{2}\left(\frac{\partial^2 p}{\partial \varrho^2}\right)_{s,\varrho=\varrho_0} (\varrho - \varrho_0)^2 + \ldots \tag{8.6}$$

or

$$p - p_0 = A\frac{\varrho - \varrho_0}{\varrho_0} + \frac{B}{2}\left(\frac{\varrho - \varrho_0}{\varrho_0}\right)^2 + \frac{C}{6}\left(\frac{\varrho - \varrho_0}{\varrho_0}\right)^3 + \ldots \tag{8.7}$$

Amazon EX1014 Page 275

with

$$A = \varrho_0 \left(\frac{\partial p}{\partial \varrho}\right)_{s,\varrho=\varrho_0} = \varrho_0 c_0^2 \ , \tag{8.8}$$

$$B = \varrho_0^2 \left(\frac{\partial^2 p}{\partial \varrho^2}\right)_{s,\varrho=\varrho_0} \ , \tag{8.9}$$

$$C = \varrho_0^3 \left(\frac{\partial^3 p}{\partial \varrho^3}\right)_{s,\varrho=\varrho_0} \ . \tag{8.10}$$

Here, c_0 is the velocity of sound under the reference conditions. The higher-order terms of the Taylor series can normally be neglected.

8.3 The Nonlinearity Parameter *B/A*

To characterize the strength of the nonlinearity of a medium properly the relation of B to the linear coefficient A is important [8.43, 44]. Therefore A and B are combined as B/A, the *nonlinearity parameter*, a pure number.

Table 8.1 B/A values for pure water at atmospheric pressure

T(°C)	B/A	Year	Ref.
0	4.2	1974	[8.36]
20	5	1974	[8.36]
20	4.985 ± 0.063	1989	[8.37]
25	5.11 ± 0.20	1983	[8.38]
26	5.1	1989	[8.39]
30	5.31	1985	[8.40]
30	5.18 ± 0.033	1991	[8.41]
30	5.280 ± 0.021	1989	[8.37]
30	5.38 ± 0.12	2001	[8.42]
40	5.4	1974	[8.36]
40	5.54 ± 0.12	2001	[8.42]
50	5.69 ± 0.13	2001	[8.42]
60	5.7	1974	[8.36]
60	5.82 ± 0.13	2001	[8.42]
70	5.98 ± 0.13	2001	[8.42]
80	6.1	1974	[8.36]
80	6.06 ± 0.13	2001	[8.42]
100	6.1	1974	[8.36]

It is easy to show that for an ideal gas we get from (8.2) together with (8.8) and (8.9)

$$\frac{B}{A} = \gamma - 1 \ , \tag{8.11}$$

so that $B/A = 0.67$ for a monatomic gas (for example noble gases) and $B/A = 0.40$ for a diatomic gas (for example air). Moreover, it can be shown that

$$\frac{C}{A} = (\gamma - 1)(\gamma - 2) \tag{8.12}$$

for an ideal gas, leading to negative values.

When there is no analytic expression for the equation of state recourse must be made to the direct definitions of A and B and appropriate measurements. From the expressions for A (8.8) and B (8.9) a formula for the nonlinearity parameter B/A is readily found:

$$\frac{B}{A} = \frac{\varrho_0}{c_0^2} \left(\frac{\partial^2 p}{\partial \varrho^2}\right)_{s,\varrho=\varrho_0} \ . \tag{8.13}$$

To determine B/A from this formula, as well as the density and sound velocity the variation in pressure effected by an isentropic (adiabatic) variation in density has to be measured. Due to the small density variations with pressure in liquids and the error-increasing second derivative this approach is not feasible.

Fortunately, equivalent expressions for B/A have been found in terms of more easily measurable

Table 8.2 Pressure and temperature dependence of the B/A values for water [8.42]

T(K) / P(MPa)	303.15	313.15	323.15	333.15	343.15	353.15	363.15	373.15
0.1	5.38 ± 0.12	5.54 ± 0.12	5.69 ± 0.13	5.82 ± 0.13	5.98 ± 0.13	6.06 ± 0.13	–	–
5	5.46 ± 0.12	5.59 ± 0.12	5.76 ± 0.13	5.87 ± 0.13	6.04 ± 0.13	6.07 ± 0.13	6.03 ± 0.13	6.05 ± 0.13
10	5.55 ± 0.12	5.62 ± 0.12	5.78 ± 0.13	5.94 ± 0.13	6.03 ± 0.13	6.11 ± 0.13	6.06 ± 0.13	6.01 ± 0.13
15	5.57 ± 0.12	5.66 ± 0.12	5.83 ± 0.13	5.96 ± 0.13	6.07 ± 0.13	6.09 ± 0.13	6.11 ± 0.13	6.08 ± 0.13
20	5.61 ± 0.12	5.68 ± 0.13	5.81 ± 0.13	5.98 ± 0.13	6.10 ± 0.13	6.14 ± 0.14	6.12 ± 0.13	6.06 ± 0.13
30	5.63 ± 0.12	5.70 ± 0.13	5.84 ± 0.13	5.95 ± 0.13	6.07 ± 0.13	6.16 ± 0.14	6.09 ± 0.13	6.08 ± 0.13
40	5.73 ± 0.13	5.77 ± 0.13	5.86 ± 0.13	6.02 ± 0.13	6.11 ± 0.13	6.14 ± 0.14	6.16 ± 0.14	6.14 ± 0.14
50	5.82 ± 0.13	5.84 ± 0.13	5.93 ± 0.13	6.04 ± 0.13	6.13 ± 0.13	6.16 ± 0.14	6.12 ± 0.13	6.09 ± 0.13

Amazon EX1014 Page 276

Table 8.3 B/A values for organic liquids at atmospheric pressure

Substance	T(°C)	B/A	Ref.
1,2-DHCP	30	11.8	[8.36]
1-Propanol	20	9.5	[8.45]
1-Butanol	20	9.8	[8.45]
1-Pentanol	20	10	[8.45]
1-Pentanol	20	10	[8.45]
1-Hexanol	20	10.2	[8.45]
1-Heptanol	20	10.6	[8.45]
1-Octanol	20	10.7	[8.45]
1-Nonanol	20	10.8	[8.45]
1-Decanol	20	10.7	[8.45]
Acetone	20	9.23	[8.46]
	20	8.0	[8.45]
	40	9.51	[8.46]
Benzene	20	9	[8.36]
	20	8.4	[8.47]
	25	6.5	[8.48]
	40	8.5	[8.48]
Benzyl alcohol	30	10.19	[8.46]
	50	9.97	[8.46]
Carbon bisulfide	10	6.4	[8.48]
	25	6.2	[8.48]
	40	6.1	[8.48]
Carbon tetrachloride	10	8.1	[8.48]
	25	8.7	[8.48]
	25	7.85 ± 0.31	[8.38]
	40	9.3	[8.48]
Chlorobenzene	30	9.33	[8.46]
Chloroform	25	8.2	[8.48]
Cyclohexane	30	10.1	[8.36]
Diethylamine	30	10.3	[8.46]
Ethanol	0	10.42	[8.46]
	20	10.52	[8.46]
	20	9.3	[8.45]
	40	10.6	[8.46]
Ethylene glycol	25	9.88 ± 0.4	[8.38]
	26	9.6	[8.39]
	30	9.7	[8.36]
	30	9.93	[8.40]
	30	9.88 ± 0.035	[8.41]
Ethyl formate	30	9.8	[8.36]
Heptane	30	10	[8.36]
	40	10.05	[8.49]
Hexane	25	9.81 ± 0.39	[8.38]
	30	9.9	[8.36]
	40	10.39	[8.49]

Table 8.3 (cont.)

Substance	T(°C)	B/A	Ref.
Methanol	20	8.6	[8.45]
	20	9.42	[8.46]
	30	9.64	[8.46]
Methyl acetate	30	9.7	[8.36]
Methyl iodide	30	8.2	[8.36]
Nitrobenzene	30	9.9	[8.36]
n-Butanol	0	10.71	[8.46]
	20	10.69	[8.46]
	40	10.75	[8.46]
n-Propanol	0	10.47	[8.46]
	20	10.69	[8.46]
	40	10.73	[8.46]
Octane	40	9.75	[8.49]
Pentane	30	9.87	[8.49]
Toluene	20	5.6	[8.48]
	25	7.9	[8.48]
	30	8.929	[8.50]

Table 8.4 B/A values for liquid metals and gases at atmospheric pressure

Substance	T(°C)	B/A	Ref.
Liquid metals			
Bismuth	318	7.1	[8.36]
Indium	160	4.6	[8.36]
Mercury	30	7.8	[8.36]
Potassium	100	2.9	[8.36]
Sodium	110	2.7	[8.36]
Tin	240	4.4	[8.36]
Liquid gases			
Argon	-187.15	5.01	[8.51]
	-183.15	5.67	[8.51]
Helium	-271.38	4.5	[8.52]
Hydrogen	-259.15	5.59	[8.51]
	-257.15	6.87	[8.51]
	-255.15	7.64	[8.51]
	-253.15	7.79	[8.51]
Methane	-163.15	17.95	[8.51]
	-153.15	10.31	[8.51]
	-143.15	6.54	[8.51]
	-138.15	5.41	[8.51]
Nitrogen	-203.15	7.7	[8.51]
	-195.76	6.6	[8.52]
	-193.15	8.03	[8.51]
	-183.15	9.00	[8.51]
Other substances			
Sea water (3.5% NaCl)	20	5.25	[8.36]
Sulfur	121	9.5	[8.36]

Amazon EX1014 Page 277

quantities, namely the variation of sound velocity with pressure and temperature. Introducing the definition of the sound velocity the following formulation chain holds: $(\partial^2 p/\partial \varrho^2)_{s,\varrho=\varrho_0} = (\partial c^2/\partial \varrho)_{s,\varrho=\varrho_0} = 2c_0(\partial c/\partial \varrho)_{s,\varrho=\varrho_0} = 2c_0(\partial c/\partial p)_{s,p=p_0}(\partial p/\partial \varrho)_{s,\varrho=\varrho_0} = 2c_0^3(\partial c/\partial p)_{s,p=p_0}$. Insertion of this result into (8.9) yields

$$B = \varrho_0^2 \left(\frac{\partial^2 p}{\partial \varrho^2}\right)_{s,\varrho=\varrho_0} = 2\varrho_0^2 c_0^3 \left(\frac{\partial c}{\partial p}\right)_{s,p=p_0} \tag{8.14}$$

and into (8.13) results in

$$\frac{B}{A} = 2\varrho_0 c_0 \left(\frac{\partial c}{\partial p}\right)_{s,p=p_0} . \tag{8.15}$$

Here B/A is essentially given by the variation of sound velocity c with pressure p at constant entropy s. This quantity can be measured with sound waves when the pressure is varied sufficiently rapidly but still smoothly (no shocks) to maintain isentropic conditions.

Equation (8.15) can be transformed further [8.44,53] using standard thermodynamic manipulations and definitions. Starting from $c = c(p, t, s = \text{const.})$ it follows that $\mathrm{d}c = (\partial c/\partial p)_{T,p=p_0}\mathrm{d}p + (\partial c/\partial p)_{p,T=T_0}\mathrm{d}T$ or

$$\left(\frac{\partial c}{\partial p}\right)_{s,p=p_0} = \left(\frac{\partial c}{\partial p}\right)_{T,p=p_0} + \left(\frac{\partial c}{\partial T}\right)_{p,T=T_0}\left(\frac{\partial T}{\partial p}\right)_{s,p=p_0} . \tag{8.16}$$

From the general thermodynamic relation $T\mathrm{d}s = c_\mathrm{p}\mathrm{d}T - (\alpha_T/\varrho)T\mathrm{d}p = 0$ for the isentropic case the relation

$$\left(\frac{\partial T}{\partial p}\right)_{s,p=p_0} = \frac{T_0\alpha_T}{\varrho_0 c_\mathrm{p}} . \tag{8.17}$$

follows, where

$$\alpha_T = \frac{1}{V}\left(\frac{\partial V}{\partial T}\right)_{p,T=T_0} = -\frac{1}{\varrho_0}\left(\frac{\partial \varrho}{\partial T}\right)_{p,T=T_0} \tag{8.18}$$

is the isobaric volume coefficient of the thermal expansion and c_p is the specific heat at constant pressure of the liquid. Insertion of (8.17) into (8.16) together with (8.15) yields

$$\frac{B}{A} = 2\varrho_0 c_0 \left(\frac{\partial c}{\partial p}\right)_{T,p=p_0} + 2\frac{c_0 T_0 \alpha_\mathrm{T}}{\varrho_0 c_\mathrm{p}}\left(\frac{\partial c}{\partial T}\right)_{p,T=T_0} . \tag{8.19}$$

This form of B/A divides its value into an isothermal (first) and isobaric (second) part. It has been found that the isothermal part dominates.

For liquids, B/A mostly varies between 2 and 12. For water under normal conditions it is about 5. Gases (with B/A smaller than one, see before) are much less nonlinear than liquids. Water with gas bubbles, however, may have a very large value of B/A, strongly depending on the volume fraction, bubble sizes and frequency of the sound wave. Extremely high values on the order of 1000 to 10 000 have been reported [8.54, 55]. Tables with values of B/A for a large number of materials can be found in [8.43,44].

As water is the most common fluid two tables (Table 8.1, 2) of B/A for water as a function of temperature and pressure are given (see also [8.56]). Two more tables (Table 8.3, 4) list B/A values for organic liquids and for liquid metals and gases, both at atmospheric pressure.

8.4 The Coefficient of Nonlinearity β

In a sound wave the propagation velocity $\mathrm{d}x/\mathrm{d}t$ of a quantity (pressure, density) as observed by an outside stationary observer changes along the wave. As shown by *Riemann* [8.57] and *Earnshaw* [8.58], for a forward-traveling plane wave it is given by

$$\frac{\mathrm{d}x}{\mathrm{d}t} = c + u , \tag{8.20}$$

c being the sound velocity in the medium without the particle velocity u introduced by the sound wave. The sound velocity c is given by (8.1), $c^2 = (\partial p/\partial \varrho)_s$, and contains the nonlinear properties of the medium. It is customary to incorporate this nonlinearity in (8.20) in a second-order approximation as [8.59, 60]

$$\frac{\mathrm{d}x}{\mathrm{d}t} = c_0 + \beta u , \tag{8.21}$$

introducing a *coefficient of nonlinearity* β. Here c_0 is the sound velocity in the limit of vanishing sound pressure amplitude. The coefficient of nonlinearity β is related to the parameter of nonlinearity B/A as derived from the Taylor expansion of the isentropic equation of state [8.7] via

$$\beta = 1 + \frac{B}{2A} . \tag{8.22}$$

Amazon EX1014 Page 278

The number 1 in this equation comes from the u in [8.22]. For an ideal gas [8.2] $B/A = \gamma - 1$ (8.11) and thus

$$\beta = 1 + \frac{\gamma - 1}{2} = \frac{\gamma + 1}{2} \,. \tag{8.23}$$

The quantity β is made up of two terms. They can be interpreted as coming from the nonlinearity of the medium (second term) and from convection (first term). This convective part is inevitably connected with the sound wave and is an inherent (kinematic) nonlinearity that is also present when there is no nonlinearity in the medium (thermodynamic nonlinearity) [8.60].

The introduction of β besides B/A is justified because it not only incorporates the nonlinearity of the medium, as does B/A, but also the inherent nonlinearity of acoustic propagation. The deformation of a wave as it propagates is described by β.

8.5 Simple Nonlinear Waves

In the linear case the wave equation is obtained for the quantities pressure $p - p_0$, density $\varrho - \varrho_0$ and each component of the particle velocity $\boldsymbol{u} - \boldsymbol{u}_0$ (p_0 ambient pressure, ρ_0 ambient density, $\boldsymbol{u}_0$ constant (mean) velocity, often $\boldsymbol{u}_0 = 0$) from the equations for a compressible fluid. In the spatially one-dimensional case, when φ denotes one of the perturbational quantities, one gets

$$\varphi_{tt} - c_0^2 \varphi_{xx} = 0 \,, \tag{8.24}$$

where c_0 is the propagation velocity of the perturbation, given by $c_0^2 = (\partial p/\partial \varrho)_{s,\varrho=\varrho_0}$, and the subscripts t and x denote partial differentiation with respect to time and space, respectively. A simple way to incorporate the influence of nonlinearities of the medium without much mathematical effort consists in considering the propagation velocity no longer as constant. One proceeds as follows. As nonlinear waves do not superpose interaction-free, and because waves running in opposite directions (*compound waves*) would cause problems, the wave equation above is written as

$$\left(\frac{\partial}{\partial t} - c_0 \frac{\partial}{\partial x}\right)\left(\frac{\partial}{\partial t} + c_0 \frac{\partial}{\partial x}\right)\varphi = 0 \tag{8.25}$$

and only one part, i. e. a wave running in one direction only, called a *progressive* or *traveling wave*, is taken, for instance:

$$\varphi_t + c_0 \varphi_x = 0 \,, \tag{8.26}$$

a forward, i. e. in the $+x$-direction, traveling wave. The general solution of this equation is

$$\varphi(x, t) = f(x - c_0 t) \,. \tag{8.27}$$

The function f can be a quite general function of the argument $x - c_0 t$. A nonlinear extension can then be written as

$$\varphi_t + v(\varphi)\varphi_x = 0 \,, \tag{8.28}$$

whereby now the propagation velocity $v(\varphi)$ is a function of the perturbation φ. In this way the simplest propagation equation for nonlinear waves is obtained; it already leads to the problem of breaking waves and the occurrence of shock waves.

A solution to the nonlinear propagation equation (8.28) can be given in an implicit way:

$$\varphi(x, t) = f[x - v(\varphi)t] \,, \tag{8.29}$$

as can be proven immediately by insertion. This seems of little use for real calculations of the propagation of the perturbation profile. However, the equation allows for a simple physical interpretation, that is, that the quantity φ propagates with the velocity $v(\varphi)$. This leads to a simple geometric construction for the propagation of a perturbation (Fig. 8.3).

To this end the *initial-value problem* (restricted to progressive waves in one direction only and cutting out one wavelength traveling undisturbed) is considered:

$$\varphi(x, t = 0) = f(\xi) \,. \tag{8.30}$$

To each ξ value belongs a value $f(\xi)$ that propagates with the velocity $v[f(\xi)]$:

$$\left.\frac{\mathrm{d}x}{\mathrm{d}t}\right|_f = v[f(\xi)] \tag{8.31}$$

or

$$x = \xi + v[f(\xi)]t \,. \tag{8.32}$$

This is the equation of a straight line in the (x, t)-plane that crosses $x(t = 0) = \xi$ with the derivative $v(f(\xi))$. Along this straight line φ stays constant. These lines are called *characteristics* and were introduced by *Riemann* [8.57]. In this way the solution of (hyperbolic) partial differential equations can be transformed to the solution of ordinary differential equations, which is of great advantage numerically.

Amazon EX1014 Page 279

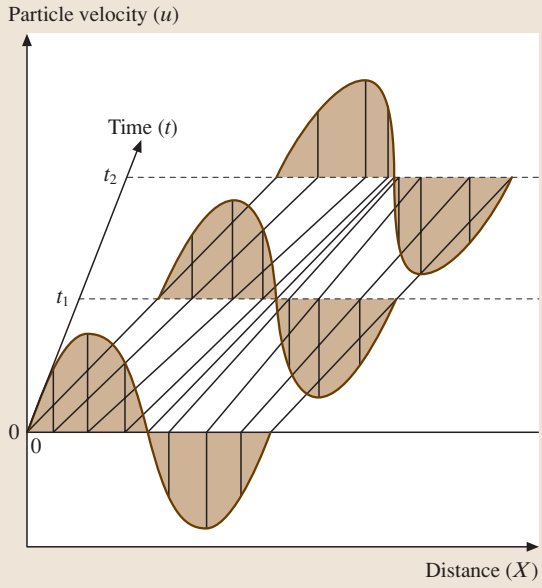


Fig. 8.3 Characteristics and the construction of the waveform for nonlinear progressive wave propagation (after Beyer [8.3])

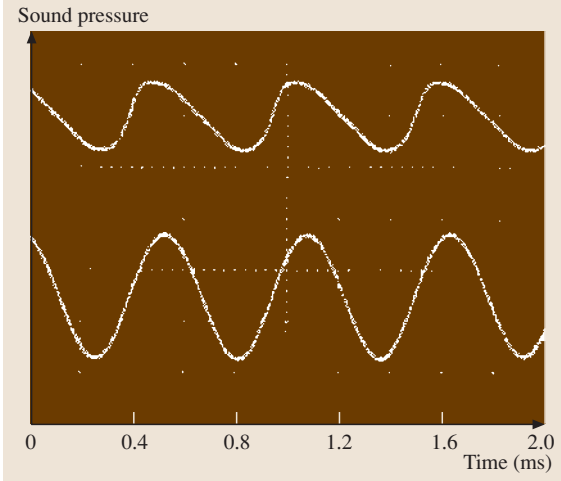


Fig. 8.4 Form of the sound wave at the launch site (lower) and after three meters of propagation (upper) in a tube filled with air. Measurement done at the Drittes Physikalisches Institut, Göttingen

The initial-value problem (8.30) is difficult to realize experimentally. Normally a sound wave is launched by a loudspeaker or transducer vibrating at some location. For one-dimensional problems a piston in a tube is a good approximation to a *boundary condition* $\varphi(x=0,t)=g(t)$, when the finite amplitude of the piston can be neglected. (The piston cannot vibrate and stay stationary at $x=0$.) Also, simple waves are produced from the outset without the complications of compound waves and their mixed flow being produced by an initial condition in which the perturbation values are given in space at a fixed time ($t=0$) [8.61].

The steepening of a wavefront has been measured this way by sending a strong sound wave through a nonlinear medium and monitoring the wave with a microphone. Figure 8.4 shows the steepening of a sound wave in air after three meters of propagation. The wave at a frequency of 2 kHz was guided inside a plastic tube. As the horizontal axis denotes time, the steepening is on the left flank, the flank of the propagation direction that passes the microphone first.

8.6 Lossless Finite-Amplitude Acoustic Waves

How elastic waves propagate through a medium is a main topic in acoustics and has been treated to various degrees of accuracy. The starting point is a set of equations from fluid mechanics. For plane acoustic waves in nondissipative fluids this set is given by three equations: the equation of continuity, the Euler equation and the equation of state:

$$\frac{\partial\varrho}{\partial t}+u\frac{\partial\varrho}{\partial x}+\varrho\frac{\partial u}{\partial x}=0\,, \tag{8.33}$$

$$\frac{\partial u}{\partial t}+u\frac{\partial u}{\partial x}+\frac{1}{\varrho}\frac{\partial p}{\partial x}=0\,, \tag{8.34}$$

$$p=p(\varrho)\,. \tag{8.35}$$

The quantities ϱ, u and p are the density of the fluid, the particle velocity and the pressure, respectively. The three equations can be condensed into two in view of the unique relation between p and ϱ. From (8.35) it follows that $\partial p/\partial x=c^2\partial\varrho/\partial x$ and with (8.34) we obtain

$$\frac{\partial u}{\partial t}+u\frac{\partial u}{\partial x}+\frac{c^2}{\varrho}\frac{\partial\varrho}{\partial x}=0\,, \tag{8.36}$$

where c is the sound velocity of the medium. The following relation between u and ϱ holds for forward-traveling

Amazon EX1014 Page 280

waves [8.57, 58] (see also [8.1]):

$$\frac{\partial u}{\partial x} = \frac{c}{\varrho}\frac{\partial \varrho}{\partial x} \tag{8.37}$$

giving the propagation equation

$$\frac{\partial u}{\partial t} + (u + c)\frac{\partial u}{\partial x} = 0 \tag{8.38}$$

for a plane progressive wave without dissipation. The propagation velocity c (here for the particle velocity we use u) due to the nonlinearity of the medium to a second-order approximation follows from $u + c = c_0 + \beta u$ (see (8.21) and (8.22)) as

$$c = c_0 + \frac{B}{2A}u \,. \tag{8.39}$$

The corresponding relation for an ideal gas,

$$c = c_0 + \frac{\gamma - 1}{2}u \,, \tag{8.40}$$

is exact.

Comparing the propagation equation (8.38) with (8.28) where a general function $v(\varphi)$ was introduced for the nonlinear propagation velocity with φ a disturbance of the medium, for instance u, the function can now be specified as

$$v(u) = u + c(u) \,. \tag{8.41}$$

This finding gives rise to the following degrees of approximation.

The linear approximation

$$v(u) = c_0 \,, \tag{8.42}$$

the kinematic approximation, where the medium is still treated as linear,

$$v(u) = u + c_0 \,, \tag{8.43}$$

the quadratic approximation

$$v(u) = u + c_0 + \frac{B}{2A}u = c_0 + \beta u \,, \tag{8.44}$$

and so forth, as further approximations are included. From these equations it follows that $v(u = 0) = c_0$ regardless of the degree of approximation. This means that the wave as a whole propagates with the linear velocity c_0; its form, however, changes. This holds true as long as the form of the wave stays continuous. Also, there is no truly linear case. Even if the medium is considered linear the kinematic approximation reveals that there is a distortion of the wave. Only in the limit of infinitely small amplitude of the particle velocity u (implying also an infinitely small amplitude of acoustic pressure $p - p_0$) does a disturbance propagate linearly. There is no finite amplitude that propagates linearly. This is different from the transverse waves that appear in solids, for instance, and in electromagnetic wave propagation. In these cases, linear waves of finite amplitude exist, because they do not experience distortion due to a kinematic term u.

A solution to the propagation equation (8.38) to a second-order approximation,

$$\frac{\partial u}{\partial t} + (c_0 + \beta u)\frac{\partial u}{\partial x} = 0 \,, \tag{8.45}$$

can be given in implicit form as for (8.28):

$$u(x, t) = f[x - (c_0 + \beta u)t] \,. \tag{8.46}$$

For the boundary condition (source or signaling problem)

$$u(x = 0, t) = u_\mathrm{a} \sin \omega t \tag{8.47}$$

the implicit solution reads with the function $f = u_\mathrm{a} \sin(\omega t - kx)$ and $k = \omega / v(u)$:

$$u(x, t) = u_\mathrm{a} \sin\left(\omega t - \frac{\omega}{c_0 + \beta u}x\right) \,, \tag{8.48}$$

or, when expanding and truncating the denominator in the argument of the sine wave:

$$u(x, t) = u_\mathrm{a} \sin\left[\omega t - \frac{\omega}{c_0}\left(1 - \beta\frac{u}{c_0}\right)x\right] \,. \tag{8.49}$$

With the wave number

$$k_0 = \frac{\omega}{c_0} \,, \tag{8.50}$$

$\omega = 2\pi f$, where f is the frequency of the sound wave, and

$$M_\mathrm{a} = \frac{u_\mathrm{a}}{c_0} \,, \tag{8.51}$$

is the initial (peak) acoustic Mach number, the solution reads:

$$\frac{u(x, t)}{u_\mathrm{a}} = \sin\left[\omega t - k_0 x\left(1 + \beta M_\mathrm{a}\frac{u(x, t)}{u_\mathrm{a}}\right)\right] \,. \tag{8.52}$$

This implicit solution can be turned into an explicit one, as shown by Fubini in 1935 [8.62] (see also [8.59, 63]), when the solution is expanded in a Fourier series ($\varphi = \omega t - k_0 x$):

$$\frac{u}{u_\mathrm{a}} = \sum_{n=1}^{\infty} B_n \sin(n\varphi) \tag{8.53}$$

Amazon EX1014 Page 281

with

$$B_n = \frac{1}{\pi}\int_0^{2\pi} \frac{u}{u_a}\sin(n\varphi)\mathrm{d}\varphi\,. \tag{8.54}$$

After insertion of (8.52) into (8.54) and some mathematical operations the Bessel functions J_n of the first kind of order n yield

$$B_n = \frac{2}{\beta M_a k_0 n x} J_n(\beta M_a k_0 n x)\,. \tag{8.55}$$

The explicit solution then reads

$$\frac{u(x,t)}{u_a} = \frac{2}{\beta M_a k_0}\sum_{n=1}^{\infty}\frac{J_n(\beta M_a k_0 n x)}{nx}\sin n(\omega t - k_0 x)\,. \tag{8.56}$$

The region of application of this solution is determined by $\beta M_a k_0$. The inverse has the dimensions of a length:

$$x_\perp = \frac{1}{\beta M_a k_0}\,, \tag{8.57}$$

and is called the *shock distance*, because at this distance the wave develops a vertical tangent, the beginning of becoming a shock wave. The solution is valid only up to this distance $x = x_\perp$.

To simplify the notation the dimensionless normalized distance σ may be introduced:

$$\sigma = \frac{x}{x_\perp}\,. \tag{8.58}$$

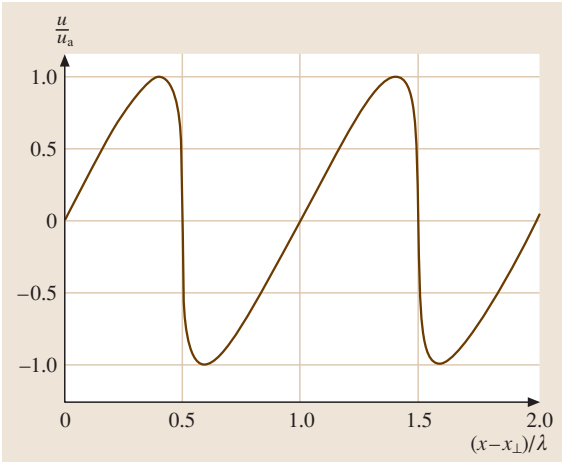


Fig. 8.5 Waveform of the Fubini solution (8.66) at the shock formation time $t_\perp$ ($\sigma_t = 1$) for the initial-value problem. λ is the wavelength of the sound wave

The Fubini solution then reads

$$\frac{u}{u_a} = 2\sum_{n=1}^{\infty}\frac{J_n(n\sigma)}{n\sigma}\sin n(\omega t - k_0 x)\,. \tag{8.59}$$

When a pure spatial sinusoidal wave is taken as the initial condition [8.64]:

$$u(x, t=0) = u_a \sin k_0 x\,, \tag{8.60}$$

the implicit solution reads

$$u(x,t) = u_a \sin k_0[x - (c_0 + \beta u)t]\,, \tag{8.61}$$

or, with the acoustic Mach number $M_a = u_a/c_0$ as before:

$$\frac{u(x,t)}{u_a} = \sin k_0\left[x - c_0 t\left(1 + \beta M_a \frac{u(x,t)}{u_a}\right)\right]\,. \tag{8.62}$$

When again doing a Fourier expansion the explicit solution emerges:

$$\frac{u(x,t)}{u_a} = \frac{2}{\beta M_a k_0 c_0}\sum_{n=1}^{\infty}(-1)^{n+1} \times \frac{J_n(\beta M_a k_0 c_0 n t)}{nt}\sin n k_0(x - c_0 t)\,. \tag{8.63}$$

The region of application is determined by $\beta M_a k_0 c_0$. The inverse has the dimension of time:

$$t_\perp = \frac{1}{\beta M_a k_0 c_0}\,. \tag{8.64}$$

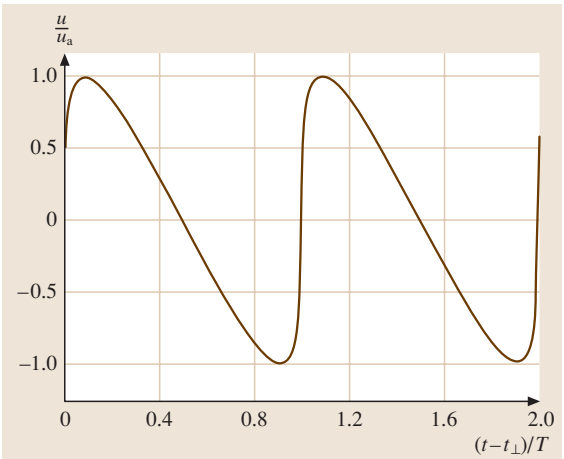


Fig. 8.6 Waveform of the Fubini solution (8.59) at the shock distance $x_\perp$ ($\sigma = 1$) for the source problem. T is the period of the sound wave. Compare the experiment in Fig. 8.4

Amazon EX1014 Page 282

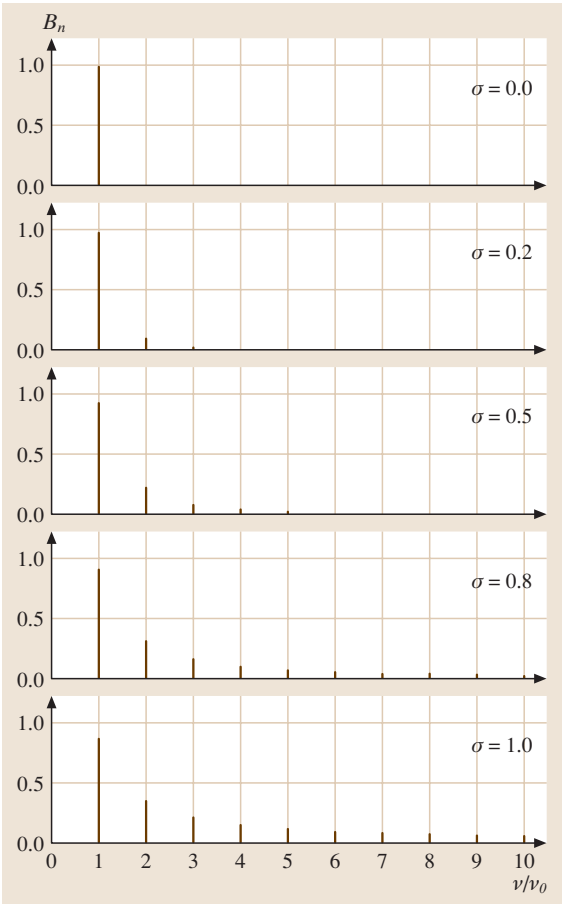


Fig. 8.7 Growth of the harmonics upon propagation for the Fubini solution (8.59) (source problem) at different normalized distances σ up to the shock distance. [8.38]

The quantity $t_\perp$ is called the *shock formation time*, because at this time the wave develops a vertical tangent. The solution is valid only up to this time $t = t_\perp$. To simplify the notation the dimensionless normalized time σ_t may be introduced

$$\sigma_t = \frac{t}{t_\perp} . \tag{8.65}$$

The Fubini solution then reads:

$$\frac{u(x,t)}{u_a} = 2\sum_{n=1}^{\infty}(-1)^{n+1}\frac{J_n(n\sigma_t)}{n\sigma_t}\sin nk_0(x - c_0 t) . \tag{8.66}$$

When comparing $t_\perp$ with $x_\perp$, the relation

$$c_0 t_\perp = x_\perp \tag{8.67}$$

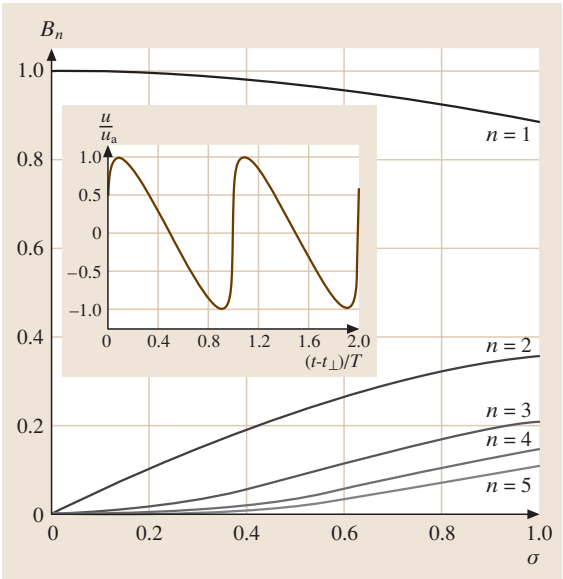


Fig. 8.8 Growth of the first five spectral components B_n of a plane wave as a function of the normalized distance σ for the Fubini solution. The *inset* gives the waveform at $\sigma = 1$ for the source problem, T being the period of the sound wave. [8.64]

is noted. This means that the shock distance is reached in the shock formation time when the wave travels at the linear sound speed c_0. This is in agreement with the earlier observation that the wave travels at the linear sound speed regardless of the nonlinearity as long as the wave stays continuous. In the case of the quadratic approximation the range in space and time for which this property holds can be quantified explicitly.

To give an impression of what the wave looks like when having propagated the shock distance $x_\perp$ in the shock formation time $t_\perp$, Fig. 8.5 shows two wavelengths at the shock formation time $t_\perp$ and Fig. 8.6 shows two periods at the shock distance $x_\perp$.

A set of spectra of the waveform for different normalized distances σ is plotted in Fig. 8.7 for the source problem, where all harmonics have positive value. The growth of the harmonics B_n (8.55) in the spectrum on the way to the shock distance is visualized. Similar plots have been given by *Fubini Ghiron* [8.65]. A plot of the first five Fourier coefficients B_n as a function of σ is given in Fig. 8.8. In the inset the waveform at the shock distance $x_\perp$ is plotted for two periods of the wave.

The solutions (8.59) and (8.66) are given for the particle velocity u. This quantity is difficult to measure. Instead, in experiments, pressure is the variable of

Amazon EX1014 Page 283

choice. When combining the equation of state for an ideal gas with the definition of sound velocity (see (8.2) and (8.1)) a relation between pressure and sound velocity is obtained:

$$\frac{p}{p_0} = \left(\frac{c}{c_0}\right)^{2\gamma/(\gamma-1)} . \tag{8.68}$$

Insertion of the expression $c = c_0 + [(\gamma-1)/2]u$ (8.40) yields:

$$p = p_0 \left(1 + \frac{\gamma-1}{2}\frac{u}{c_0}\right)^{2\gamma/(\gamma-1)} . \tag{8.69}$$

Inserting the solution for the particle velocity u into this equation will give the pressure p and the acoustic pressure $p - p_0$. This operation is easy to perform numerically but not analytically. However, the approximation scheme for moderate-strength finite-amplitude waves, $|u/c_0| \ll 1$, is only consistent when expanding (8.69) and taking only the linear part. This leads to the *linear* relation between acoustic pressure $p - p_0$ and acoustic particle velocity u (local linearity property for weak nonlinearity) [8.61, 66]:

$$p - p_0 = \varrho_0 c_0 u , \tag{8.70}$$

where the expression $\varrho_0 c_0$ is known as the impedance. When the boundary condition (8.47) is rewritten as

$$\begin{aligned}(p - p_0)(x = 0, t) &= \varrho_0 c_0 u_a \sin \omega t \\ &= (p_a - p_0) \sin \omega t\end{aligned} \tag{8.71}$$

with $p_a - p_0 = \varrho_0 c_0 u_a$, the relation

$$\frac{p - p_0}{p_a - p_0} = \frac{u}{u_a} \tag{8.72}$$

is obtained. The normalized Fubini solution then reads in terms of the acoustic pressure for the boundary-value or source problem

$$\frac{p - p_0}{p_a - p_0} = 2\sum_{n=1}^{\infty} \frac{J_n(n\sigma)}{n\sigma} \sin n(\omega t - k_0 x) , \tag{8.73}$$

and for the initial-value problem:

$$\frac{p - p_0}{p_a - p_0} = 2\sum_{n=1}^{\infty} (-1)^{n+1} \frac{J_n(n\sigma_t)}{n\sigma_t} \sin nk_0(x - c_0 t) . \tag{8.74}$$

The steepening of acoustic waves upon propagation may occur in musical wind instruments, e.g., the trombone [8.67]. It has been shown that depending on the playing level the emitted sound waves steepen when going from piano to fortissimo, even up to shock waves. Indeed, the brightness (the *metallic* sound) of loudly played brass instruments (in particular the trumpet and the trombone as opposed to the saxhorns) is attributed to the increasing harmonic content connected with wave steepening, as exemplified in Fig. 8.7.

8.7 Thermoviscous Finite-Amplitude Acoustic Waves

Because of the inherently nonlinear nature of acoustic wave propagation steep gradients of physical quantities (pressure, density, temperature, ...) inevitably appear after some time of traveling, after which losses can no longer be neglected. In the steep gradients brought about by nonlinearity, linear phenomena that could be neglected before become important [8.68]. These are losses by *diffusive* mechanisms, in particular viscosity and heat conduction, and spreading phenomena by *dispersive* mechanisms as in frequency dispersion. When losses balance nonlinearity, the characteristic waveforms of *shock waves* appear, when frequency dispersion balances nonlinearity the characteristic form of *solitons* appear. Both are given about equal space in this treatment. The inclusion of thermoviscous losses is treated in this chapter, the inclusion of frequency dispersion, small in pure air and water, but large in water with bubbles, is treated in Chap. 8.10 on liquids containing bubbles.

The extension of (8.45) when thermoviscous losses are included as a small effect leads to the Burgers equation

$$\frac{\partial u}{\partial t} + (c_0 + \beta u)\frac{\partial u}{\partial x} = \frac{1}{2}\delta \frac{\partial^2 u}{\partial x^2} . \tag{8.75}$$

Here δ, comprising the losses, has been called the diffusivity of sound by Lighthill [8.69]:

$$\begin{aligned}\delta &= \frac{1}{\rho_0}\left(\frac{4}{3}\mu + \mu_B\right) + \frac{\kappa}{\rho_0}\left(\frac{1}{c_v} - \frac{1}{c_p}\right) \\ &= \nu\left(\frac{4}{3} + \frac{\mu_B}{\mu} + \frac{\gamma-1}{Pr}\right)\end{aligned} \tag{8.76}$$

where μ is the shear viscosity, μ_B the bulk viscosity, $\nu = \mu/\varrho_0$ the kinematic viscosity, κ the thermal conductivity, c_v and c_p the specific heats at constant volume and constant pressure, respectively, and Pr being the Prandtl

Amazon EX1014 Page 284

number, $Pr = \mu c_p/\kappa$. The equation is an approximation to a more exact second-order equation that, however, does not lend itself to an exact solution as does the Burgers equation above. In the context of acoustics this relation was first derived by *Mendousse*, although for viscous losses only [8.70]. The derivations make use of a careful comparison of the order of magnitude of derivatives retaining the leading terms. The above form of the Burgers equation is best suited to initial-value problems. Source problems are best described when transforming (8.75) to new coordinates (x, τ) with the retarded time $\tau = t - x/c_0$:

$$\frac{\partial u}{\partial x} - \frac{\beta}{c_0^2} u \frac{\partial u}{\partial \tau} = \frac{\delta}{2c_0^3} \frac{\partial^2 u}{\partial \tau^2} \,. \tag{8.77}$$

The equation can be normalized to a form with only one parameter:

$$\frac{\partial W}{\partial \sigma} - W \frac{\partial W}{\partial \varphi} = \frac{1}{\Gamma} \frac{\partial^2 W}{\partial \varphi^2} \,, \tag{8.78}$$

where $W = u/u_0$, $\sigma = x/x_\perp$, $\varphi = \omega\tau = \omega t - k_0 x$, $\Gamma = \beta M_0 k_0/\alpha = 2\pi\beta M_0/\alpha\lambda$, with α being the damping constant for linear waves:

$$\alpha = \frac{\delta k_0^2}{2c_0} \,. \tag{8.79}$$

Γ is called the Gol'dberg number after *Gol'dberg* [8.71] who introduced this normalization (*Blackstock* [8.72]). It can be written as

$$\Gamma = \frac{1/x_\perp}{\alpha} \tag{8.80}$$

where $1/x_\perp = \beta M_0 k_0$ is the strength of the nonlinearity and α is the strength of the damping. The Gol'dberg number is therefore a measure of the importance of nonlinearity in relation to damping. For $\Gamma > 1$ nonlinearity takes over and for $\Gamma < 1$ damping takes over. For $\Gamma \gg 1$ nonlinearity has time to accumulate its effects, for $\Gamma \ll 1$ damping does not allow nonlinear effects to develop.

The Burgers equation is exactly integrable by the Hopf–Cole transformation [8.73, 74]:

$$W = \frac{2}{\Gamma} \frac{1}{\zeta} \frac{\partial \zeta}{\partial \varphi} = \frac{2}{\Gamma} \frac{\partial \ln \zeta}{\partial \varphi} \tag{8.81}$$

that is best done in two steps [8.10]

$$W = \frac{\partial \psi}{\partial \varphi} \,, \tag{8.82}$$

$$\psi = \frac{2}{\Gamma} \ln \zeta \,. \tag{8.83}$$

By this transformation the nonlinear Burgers equation is reduced to the linear heat conduction or diffusion equation

$$\frac{\partial \zeta}{\partial \sigma} = \frac{1}{\Gamma} \frac{\partial^2 \zeta}{\partial \varphi^2} \,. \tag{8.84}$$

For this equation a general explicit solution is available:

$$\zeta(\sigma, \varphi) = \sqrt{\frac{\Gamma}{4\pi\sigma}} \int_{-\infty}^{+\infty} \zeta(0, \varphi') \exp\left(-\Gamma \frac{(\varphi' - \varphi)^2}{4\sigma}\right) \mathrm{d}\varphi' \,. \tag{8.85}$$

For a specific solution the initial or boundary conditions must be specified. A common problem is the piston that starts to vibrate sinusoidally at time $t = 0$. This problem has been treated by *Blackstock* [8.72] whose derivation is closely followed here. The boundary condition is given by

$$\begin{aligned} u(0, t) &= 0 \qquad \text{for} \quad t \le 0 \,, \\ u(0, t) &= u_a \sin \omega t \quad \text{for} \quad t > 0 \,, \end{aligned} \tag{8.86}$$

or in terms of the variable $W(\sigma, \varphi)$

$$\begin{aligned} W(0, \varphi) &= 0 \qquad \text{for} \quad \varphi \le 0 \,, \\ W(0, \varphi) &= \sin \varphi \quad \text{for} \quad \varphi > 0 \,. \end{aligned} \tag{8.87}$$

To solve the heat conduction equation the boundary condition is needed for $\zeta(\sigma, \varphi)$. To this end the Hopf–Cole transformation (8.81) is reversed:

$$\zeta(\sigma, \varphi) = \exp\left(\frac{\Gamma}{2} \int_{-\infty}^{\varphi} W(\sigma, \varphi') \mathrm{d}\varphi'\right) . \tag{8.88}$$

Insertion of $W(0, \varphi)$ yields as the boundary condition for ζ:

$$\begin{aligned} \zeta(0, \varphi) &= 1 \qquad\qquad\quad \text{for} \quad \varphi \le 0 \\ \zeta(0, \varphi) &= \mathrm{e}^{\frac{1}{2}\Gamma(1 - \cos\varphi)} \quad \text{for} \quad \varphi > 0 \end{aligned} \tag{8.89}$$

and insertion into (8.85) yields the solution in terms of ζ. Using $\bar{\sigma} = \sqrt{4\sigma/\Gamma}$ and $q = (\varphi' - \varphi)/\bar{\sigma}$ the solution for the vibrating piston in terms of ζ reads

$$\begin{aligned} \zeta(\sigma, \varphi) = {} & \frac{1}{\sqrt{\pi}} \int_{-\infty}^{-\varphi/\bar{\sigma}} \mathrm{e}^{-q^2} \, \mathrm{d}q \\ & + \frac{1}{\sqrt{\pi}} \mathrm{e}^{\frac{1}{2}\Gamma} \int_{-\varphi/\bar{\sigma}}^{\infty} \mathrm{e}^{-\frac{1}{2}\Gamma\cos(\bar{\sigma}q + \varphi)} \, \mathrm{e}^{-q^2} \, \mathrm{d}q \,. \end{aligned} \tag{8.90}$$

Amazon EX1014 Page 285

This solution is involved and also contains the transients after starting the oscillation. When $\varphi \to \infty$ these transients decay and the steady-state solution is obtained:

$$\zeta(\sigma, \varphi \,|\, \varphi \to \infty) = \frac{1}{\sqrt{\pi}} \, \mathrm{e}^{\frac{1}{2}\Gamma} \int_{-\infty}^{\infty} \mathrm{e}^{-\frac{1}{2}\Gamma \cos(\bar{\sigma} q + \varphi)} \, \mathrm{e}^{-q^2} \, \mathrm{d}q \, . \tag{8.91}$$

With the help of the modified Bessel functions of order n, $I_n(z) = \mathrm{i}^{-n} J_n(\mathrm{i}z)$, and the relation [8.75]

$$\mathrm{e}^{z \cos\theta} = I_0(z) + 2 \sum_{n=1}^{\infty} I_n(z) \cos n\theta \tag{8.92}$$

the expression

$$\begin{aligned} &\mathrm{e}^{-\frac{1}{2}\Gamma \cos(\bar{\sigma} q + \varphi)} \\ &= I_0\left(-\tfrac{1}{2}\Gamma\right) + 2 \sum_{n=1}^{\infty} I_n\left(-\tfrac{1}{2}\Gamma\right) \cos n(\bar{\sigma} q + \varphi) \\ &= I_0\left(\tfrac{1}{2}\Gamma\right) + 2 \sum_{n=1}^{\infty} (-1)^n I_n\left(\tfrac{1}{2}\Gamma\right) \cos n(\bar{\sigma} q + \varphi) \end{aligned} \tag{8.93}$$

is valid. Inserting this into (8.91) and integrating yields, observing that $\int_{-\infty}^{+\infty} \exp(-q^2 x^2) \cos[p(x + \lambda)] \mathrm{d}x = (\sqrt{\pi}/q) \exp[-p^2/(4q^2)] \cos p\lambda$ [8.76]:

$$\zeta(\sigma, \varphi | \varphi \to \infty) = \mathrm{e}^{\frac{1}{2}\Gamma} \left[I_0\left(\tfrac{1}{2}\Gamma\right) + 2 \sum_{n=1}^{\infty} (-1)^n I_n\left(\tfrac{1}{2}\Gamma\right) \mathrm{e}^{-n^2 \sigma/\Gamma} \cos n\varphi \right] . \tag{8.94}$$

This is the exact steady-state solution for the oscillating piston problem given for ζ as a Fourier series. Transforming to $W(\sigma, \varphi)$ via (8.81) gives

$$W(\sigma, \varphi) = \frac{4\Gamma^{-1} \sum_{n=1}^{\infty} (-1)^{n+1} n I_n\left(\frac{1}{2}\Gamma\right) \mathrm{e}^{-n^2 \sigma/\Gamma} \sin n\varphi}{I_0\left(\frac{1}{2}\Gamma\right) + 2 \sum_{n=1}^{\infty} (-1)^n I_n\left(\frac{1}{2}\Gamma\right) \mathrm{e}^{-n^2 \sigma/\Gamma} \cos n\varphi} \, . \tag{8.95}$$

Finally, for $u(x, t)$ the solution reads

$$\frac{u(x,t)}{u_\mathrm{a}} = \frac{4\Gamma^{-1} \sum_{n=1}^{\infty} (-1)^{n+1} n I_n\left(\frac{1}{2}\Gamma\right) \mathrm{e}^{-n^2 \alpha x} \sin n(\omega t - k_0 x)}{I_0\left(\frac{1}{2}\Gamma\right) + 2 \sum_{n=1}^{\infty} (-1)^n I_n\left(\frac{1}{2}\Gamma\right) \mathrm{e}^{-n^2 \alpha x} \cos n(\omega t - k_0 x)} \, . \tag{8.96}$$

The equation for the acoustic pressure $p - p_0$ again can be obtained via the approximation (8.72) as before in the lossless case: $(p - p_0)/(p_\mathrm{a} - p_0) = u/u_\mathrm{a}$ gives the identical equation.

There are regions of the parameter Γ and the independent variables x and t where the solution is difficult to calculate numerically. However, in these cases approximations can often be formulated.

For $\Gamma \to \infty$ and $\sigma = x/x_\perp \ll 1$ the Fubini solution is recovered.

For $\sigma \gg \Gamma$, i. e. far away from the source, the first terms in the numerator and the denominator in (8.96) dominate, leading to

$$\frac{u(x,t)}{u_\mathrm{a}} = \frac{4}{\Gamma} \frac{I_1(\Gamma/2)}{I_0(\Gamma/2)} \, \mathrm{e}^{-\alpha x} \sin(\omega t - k_0 x) \, . \tag{8.97}$$

When additionally $\Gamma \gg 1$, i. e. nonlinearity dominates over attenuation, $I_0(\Gamma/2) \approx I_1(\Gamma/2)$ and therefore

$$\begin{aligned} u(x,t) &= u_\mathrm{a} \frac{4}{\Gamma} \, \mathrm{e}^{-\alpha x} \sin(\omega t - k_0 x) \\ &= 4 u_\mathrm{a} \alpha x_\perp \, \mathrm{e}^{-\alpha x} \sin(\omega t - k_0 x) \\ &= \frac{4\alpha c_0^2}{\beta\omega} \, \mathrm{e}^{-\alpha x} \sin(\omega t - k_0 x) \qquad (8.98) \\ &= \frac{2\delta\omega}{\beta c_0} \, \mathrm{e}^{-\alpha x} \sin(\omega t - k_0 x) \, . \qquad (8.99) \end{aligned}$$

This series of equations for the amplitude of the sinusoidal wave radiated from a piston in the far field lends itself to several interpretations. As it is known that for $\Gamma \gg 1$ harmonics grow fast at first, these must later decay leaving the fundamental to a first approximation. The amplitude of the fundamental in the far field is independent of the amplitude u_a of the source, as can be seen from the third row (8.98). This means that there is a saturation effect. Nonlinearity together with attenuation does not allow the amplitude in the far field to increase in proportion to u_a because of the extra damping introduced by the generation of harmonics that are damped more strongly than the fundamental. This even works asymptotically because otherwise u_a would finally appear. The damping constant is frequency dependent (8.79), leading to the last row (8.99). It is seen that the asymptotic amplitude of the fundamental grows with the frequency $f = \omega/2\pi$. This continues until other effects come into play, for instance relaxation effects in the medium. Equations (8.98) and (8.99) for u are different from the equations for the acoustic pressure, as they cannot be normalized with u_a or $p_\mathrm{a} - p_0$, respectively.

Amazon EX1014 Page 286

They are related via the impedance $\varrho_0 c_0$ (8.70):

$$(p-p_0)(x,t) = \frac{4\alpha\varrho_0 c_0^3}{\beta\omega}\,\mathrm{e}^{-\alpha x}\sin(\omega t - k_0 x) \quad (8.100)$$

$$= \frac{2\delta\varrho_0\omega}{\beta}\,\mathrm{e}^{-\alpha x}\sin(\omega t - k_0 x)\,. \quad (8.101)$$

Good approximations for $\Gamma \gg 1$ have been given by *Fay* [8.78]:

$$\frac{u(x,t)}{u_\mathrm{a}} = \sum_{n=1}^{\infty} \frac{2/\Gamma}{\sinh[n(1+x/x_\perp)/\Gamma]}\sin n(\omega t - k_0 x)\,, \quad (8.102)$$

and *Blackstock* [8.72]:

$$\frac{u(x,t)}{u_\mathrm{a}} = \frac{2}{\Gamma}\sum_{n=1}^{\infty}\frac{1-(n/\Gamma^2)\coth[n(1+x/x_\perp)/\Gamma]}{\sinh[n(1+x/x_\perp)/\Gamma]} \times \sin n(\omega t - k_0 x)\,. \quad (8.103)$$

With an error of less than 1% at $\Gamma = 50$ Fay's solution is valid for $\sigma > 3.3$ and Blackstock's solution for $\sigma > 2.8$, rapidly improving with σ. The gap in σ from about one to three between the Fubini and Fay solution has been closed by Blackstock. He connected both solutions using weak shock theory giving the Fubini–Blackstock–Fay solution ([8.77], see also [8.1]). Figure 8.9 shows the first three harmonic components of the Fubini–Blackstock–Fay solution from [8.79]. Similar curves have been given by *Cook* [8.80]. He developed a numerical scheme for calculating the harmonic content of a wave as it propagates by including the losses in small spatial steps linearly for each harmonic component. As there are occurring only harmonic waves that do not break the growth in each small step is given by the Fubini solution.

In the limit $\Gamma \to \infty$ the Fay solution reduces to

$$\frac{u(x,t)}{u_\mathrm{a}} = \sum_{n=1}^{\infty}\frac{2}{1+x/x_\perp}\sin n(\omega t - k_0 x)\,, \quad (8.104)$$

a solution that is also obtained by weak shock theory.

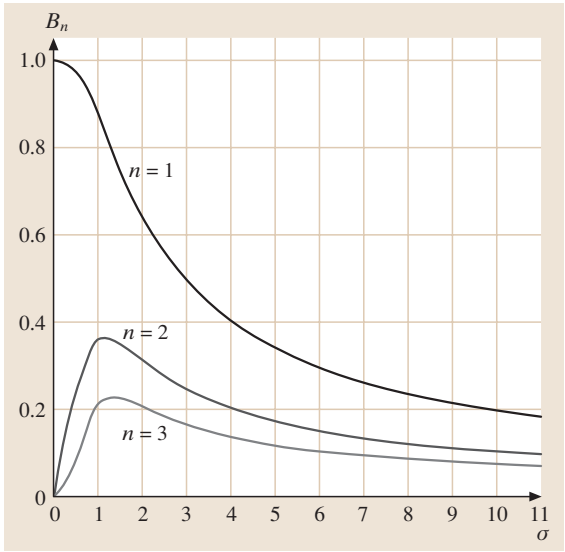


Fig. 8.9 Growth and decay of the first three harmonic components B_n of a plane wave as a function of the normalized distance σ according to the Fubini–Blackstock–Fay solution (after Blackstock [8.77])

When Fay's solution (8.102) is taken and $\sigma \gg \Gamma$ (farfield), the old-age region of the wave is reached. Then $\sinh[n(1+x/x_\perp)/\Gamma] \simeq \frac{1}{2}(\mathrm{e}^{nx/x_\perp\Gamma} - \mathrm{e}^{-nx/x_\perp\Gamma}) \simeq \frac{1}{2}\mathrm{e}^{nx/x_\perp\Gamma} = \frac{1}{2}\mathrm{e}^{n\alpha x}$ and

$$u(x,t) = \frac{4\alpha c_0^2}{\beta\omega}\,,\sum_{n=1}^{\infty}\mathrm{e}^{-n\alpha x}\sin n(\omega t - k_0 x) \quad (8.105)$$

is obtained similarly as for the fundamental (8.98). Additionally all harmonics that behave like the fundamental, i. e. that are not dependent on the initial peak particle velocity u_a, are obtained . Moreover, they do not decay (as linear waves do) proportionally to $\mathrm{e}^{-n^2\alpha x}$ but only proportionally to $\mathrm{e}^{-n\alpha x}$.

In the range $\sigma > 1$ shock waves may develop. These are discussed in the next section.

8.8 Shock Waves

The characteristics of Fig. 8.3 must cross. According to the geometrical construction the profile of the wave then becomes multivalued. This is easily envisaged with water surface waves. With pressure or density waves, however, there is only one pressure or one density at one place. The theory is therefore oversimplified and must be expanded with the help of physical arguments and the corresponding mathematical formulation. Shortly before overturning, the gradients of pressure and density become very large, and it is known that damping

Amazon EX1014 Page 287

effects brought about by viscosity and heat conduction can no longer be neglected. When these effects are taken into account, the waves no longer turn over. Instead, a thin zone is formed, a *shock wave*, in which the values of pressure, density, temperature, etc. vary rapidly. A theoretical formulation has been given in the preceding section for thermoviscous sound waves based on the Burgers equation.

It has been found that damping effects do not necessarily have to be included in the theory, but that an extended damping free theory can be developed by introducing certain shock conditions that connect the variables across a discontinuity. A description of this theory can be found in the book by *Whitham* [8.10]. The result can be described in a simple construction. In Fig. 8.10 the profile of the wave has been determined according to the methods of characteristics for a time where the characteristics have already crossed. The shock wave then has to be inserted in such a way that the areas between the shock wave and the wave profile to the left and the right are equal (the equal area rule). Moreover, it can be shown that the velocity of the shock wave is approximately given by

$$v_s = \frac{1}{2}(v_1 + v_2)\,, \tag{8.106}$$

where v_1 and v_2 are the propagation velocities of the wave before and behind the shock, respectively.

Shock waves are inherently difficult to describe by Fourier analysis as a large number of harmonics are needed to approximate a jump-like behavior. A time-domain description is often more favorable here. Such solutions have been developed for the propagation of sound waves in the shock regime. For $\Gamma > \sigma > 3$, *Khokhlov* and *Soluyan* [8.80] have given the following solution

$$\frac{u(x,t)}{u_a} = \frac{1}{1+x/x_\perp}\left(-\varphi + \pi \tanh\frac{\pi\Gamma\varphi}{2(1+x/x_\perp)}\right) \tag{8.107}$$

for $-\pi < \varphi = \omega t - k_0 x < \pi$, covering a full cycle of the wave.

Figure 8.11 shows the waveforms for $\Gamma = 10$ and $\Gamma = 100$ for different $\sigma = x/x_\perp$. When the wave is followed at fixed Γ for increasing σ (i. e. increasing x), the decay and change of the waveform upon propagation can be observed.

The solution and the waveforms are remarkable as they are exact solutions of the Burgers equation, but

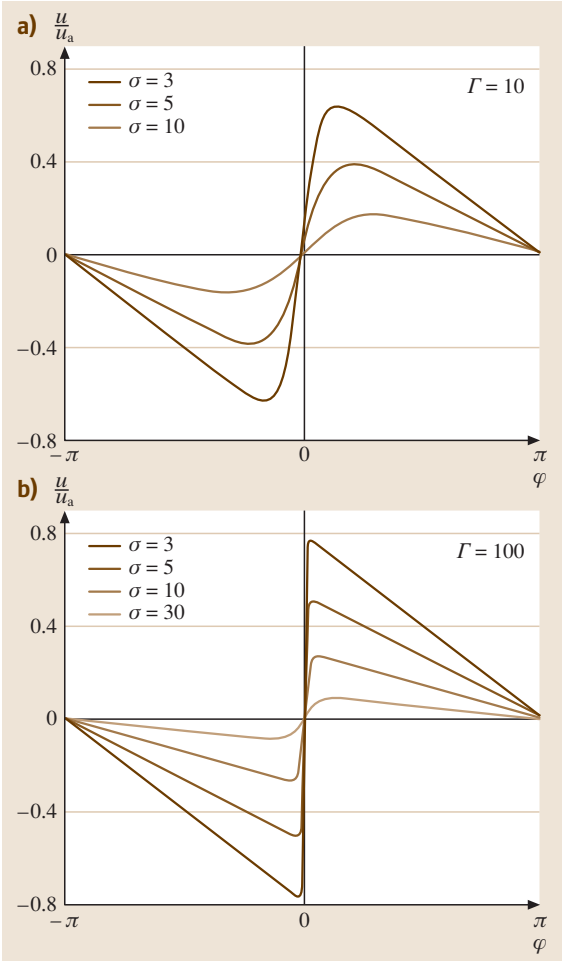


Fig. 8.11a,b Waveforms of the Khokhlov–Soluyan solution for Gol'dberg numbers $\Gamma = 10$ **(a)** and $\Gamma = 100$ **(b)** for different σ (the *age* of the wave)

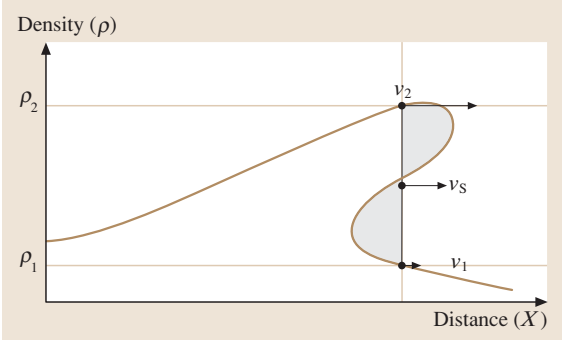


Fig. 8.10 Condition for the location of the shock wave for an overturning wave, the equal area rule

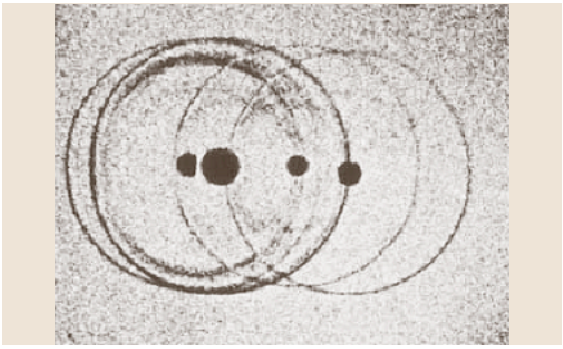


Fig. 8.12 Shock waves (*dark circles*) and bubbles (*dark spheres*) from laser-induced breakdown in water. Reconstructed image from a hologram 1.75 µs after breakdown. The size of the picture is 1.1 × 1.6 mm

approximate solutions with respect to the boundary condition.

When the wave gets very steep, i. e., in the case $\Gamma \to \infty$, it attains the shape of a sawtooth ($\sigma > 3$):

$$\frac{u(x,t)}{u_a} = \begin{cases} \dfrac{1}{1+x/x_\perp}[-\varphi+\pi] & 0 < \varphi \leq \pi \,, \\ \dfrac{1}{1+x/x_\perp}[-\varphi-\pi] & -\pi \leq \varphi < 0 \,, \end{cases} \tag{8.108}$$

where $\varphi = \omega t - k_0 x$. The amplitude of the jump is

$$\frac{u(x,t)}{u_a} = \frac{\pi}{1+x/x_\perp} \,, \tag{8.109}$$

the actual jump height from peak to peak being two times this value and falling off rapidly with x. This solution, too, is an exact solution of the Burgers equation, albeit for $1/\Gamma \equiv 0$, i. e., with the diffusion term missing in the Burgers equation.

The Fourier form solution of the sawtooth wave (8.108) is given by

$$\frac{u(x,t)}{u_a} = \frac{2}{1+x/x_\perp} \sum_{n=1}^{\infty} \frac{1}{n} \sin n(\omega t - k_0 x) \,. \tag{8.110}$$

This form can also be derived as approximation from the Fay solution (see (8.104)). This can be considered a consistency proof in the approximation approaches, one proceeding in the time domain, the other in the frequency domain.

An example of the occurrence of shock waves, albeit spherical ones, is given in Fig. 8.12. A laser pulse has been focused into water, leading to four spots of breakdown, the emission of four shock waves and the growth of four bubbles. Laser-produced bubbles are used in cavitation research to investigate bubble dynamics in liquids and their effects [8.81]. Focused shock waves are used in lithotripsy to fragment kidney stones to small enough pieces to fit through the urinary tract [8.82].

8.9 Interaction of Nonlinear Waves

Linear waves do not interact, in the sense that upon superposition they propagate independently, each according to their own parameters. This makes Fourier theory a powerful technique for linear systems. In nonlinear systems, however, the harmonic components of which an initial perturbation is composed interact and produce new components that again interact, etc. Even a single harmonic oscillation creates higher harmonics, as set out in the preceding sections.

For the description of strong nonlinear acoustic wave interaction it is very fortunate that the Burgers equation (8.78) allows for a linearizing transformation. The superposition can then be evaluated in the linear variables, giving the result of the nonlinear interaction when transforming back.

Of special interest is the interaction of two (primary) waves in the course of which the sum and, in particular, the difference frequency can be generated. A highly directional high-frequency source can be transformed into a highly directed low-frequency source (the parametric array). As the low-frequency beam generated has lower damping than the high-frequency beams it propagates to longer distances. Applications are sound navigation and ranging (SONAR) and surface and subsurface scanning of the ocean bottom.

Taking two waves with amplitudes $u_{1,2}$ and frequencies $\omega_{1,2}$, starting at $t = 0$, the boundary condition becomes

$$u(x=0,t) = \begin{cases} 0 & t < 0 \,, \\ u_1 \sin(\omega_1 t) + u_2 \sin(\omega_2 t) & t \geq 0 \,, \end{cases} \tag{8.111}$$

or with the normalized variables $W = u/u_0$, $\varphi = \omega\tau = \omega(t - x/c_0)$, $\sigma = x/x_\perp$,

Amazon EX1014 Page 289

$$W(\sigma=0,\varphi) = \begin{cases} 0 & \varphi<0\,, \\ W_1\sin(\Omega_1\varphi)+W_2\sin(\Omega_2\varphi)\,, & \varphi\geq 0\,. \end{cases} \tag{8.112}$$

Here, $\Omega_{1,2}=\omega_{1,2}/\omega$ denote the input frequencies normalized to the reference frequency ω and $W_{1,2}=u_{1,2}/u_0$ the amplitudes normalized to the reference amplitude u_0. The inverse Hopf–Cole transformation (8.88) gives the initial condition for the linearized problem in the variable ζ. For $\varphi<0$ we obtain $\zeta(\sigma=0,\varphi)=1$, while for $\varphi\geq 0$:

$$\begin{aligned}\zeta(\sigma=0,\varphi) &= \exp\left[\frac{\Gamma}{2}\int_0^{\varphi} W(\sigma=0,\varphi')\,\mathrm{d}\varphi'\right] \\ &= \exp\left\{-\frac{\Gamma}{2}\left[\frac{W_1}{\Omega_1}\cos(\Omega_1\varphi')+\frac{W_2}{\Omega_2}\cos(\Omega_2\varphi')\right]_0^{\varphi}\right\}.\end{aligned} \tag{8.113}$$

To simplify notation, introduce the Gol'dberg numbers $\Gamma_{1,2}=\Gamma W_{1,2}/\Omega_{1,2}$ which agree with the definition (8.80) applied to the two input waves, respectively. Then

$$\zeta(\sigma=0,\varphi\geq 0) = \underbrace{\exp\left(\frac{\Gamma_1}{2}+\frac{\Gamma_2}{2}\right)}_{=:C} \times\exp\left[-\frac{\Gamma_1}{2}\cos(\Omega_1\varphi)-\frac{\Gamma_2}{2}\cos(\Omega_2\varphi)\right]. \tag{8.114}$$

With this initial condition, the solution (8.85) of the diffusion equation (8.84) reads:

$$\begin{aligned}\zeta(\sigma,\varphi) &= \sqrt{\frac{\Gamma}{4\pi\sigma}}\int_{-\infty}^{0}\exp\left(-\Gamma\frac{(\varphi'-\varphi)^2}{4\sigma}\right)\mathrm{d}\varphi' \\ &\quad + C\sqrt{\frac{\Gamma}{4\pi\sigma}}\int_0^{+\infty}\exp\left[-\frac{\Gamma_1}{2}\cos(\Omega_1\varphi')\right. \\ &\quad \left.-\frac{\Gamma_2}{2}\cos(\Omega_2\varphi')-\Gamma\frac{(\varphi'-\varphi)^2}{4\sigma}\right]\mathrm{d}\varphi' \\ &= \sqrt{\frac{\Gamma}{4\pi\sigma}}\int_{-\infty}^{-\varphi}\exp\left(-\Gamma\frac{\varphi'^2}{4\sigma}\right)\mathrm{d}\varphi' \\ &\quad + C\sqrt{\frac{\Gamma}{4\pi\sigma}}\int_{-\varphi}^{+\infty}\exp\left\{-\frac{\Gamma_1}{2}\cos[\Omega_1(\varphi'+\varphi)]\right. \\ &\quad \left.-\frac{\Gamma_2}{2}\cos[\Omega_2(\varphi'+\varphi)]-\Gamma\frac{\varphi'^2}{4\sigma}\right\}\mathrm{d}\varphi'\,.\end{aligned}$$

This general solution is quite complicated as the integration limits depend on the phase φ. To dismiss the transients caused by the starting of the waves at $\varphi=0$, again the limit $\varphi\to\infty$ is considered. This means that at a certain position $x=\sigma x_\perp$ in the medium the wave is examined a long time after the passage of the initial perturbation that started at $x=0$, $t=0$. Then, the first integral of (8.115) vanishes, and the second integral can be evaluated from $-\infty$ to $+\infty$ by using the expansion (8.92), written in the following form:

$$\begin{aligned}\exp(z\cos\theta) &= I_0(z)+2\sum_{n=1}^{\infty}I_n(z)\cos(n\theta) \\ &=: \sum_{n=0}^{\infty}b_n I_n(z)\cos(n\theta)\,,\end{aligned} \tag{8.115}$$

where the numerical factors $b_0=1$, $b_n=2$ for $n>0$ have been introduced for convenient notation. Substituting this series in (8.115) and noting that I_n is an even (odd) function for even (odd) n, we get

$$\begin{aligned}\zeta(\sigma,\varphi) &= C\sqrt{\frac{\Gamma}{4\pi\sigma}}\sum_{m=0}^{\infty}\sum_{n=0}^{\infty}(-1)^{m+n}b_m b_n I_m\left(\frac{\Gamma_1}{2}\right)I_n\left(\frac{\Gamma_2}{2}\right) \\ &\quad\times\int_{-\infty}^{+\infty}\cos[m\Omega_1(\varphi'+\varphi)]\cos[n\Omega_2(\varphi'+\varphi)] \\ &\quad\times\exp\left(-\Gamma\frac{\varphi'^2}{4\sigma}\right)\mathrm{d}\varphi'\,.\end{aligned} \tag{8.116}$$

Using $\cos(\alpha)\cos(\beta)=(1/2)\,[\cos(\alpha+\beta)+\cos(\alpha-\beta)]$, and proceeding as in the derivation of (8.94) we get

$$\begin{aligned}\zeta(\sigma,\varphi) &= \frac{C}{2}\sum_{m=0}^{\infty}\sum_{n=0}^{\infty}(-1)^{m+n}b_m b_n I_m\left(\frac{\Gamma_1}{2}\right)I_n\left(\frac{\Gamma_2}{2}\right) \\ &\quad\times\left[\exp\left(-\frac{(\Omega_{mn}^{+})^2}{\Gamma}\sigma\right)\cos\left(\Omega_{mn}^{+}\varphi\right)\right. \\ &\quad\left.+\exp\left(-\frac{(\Omega_{mn}^{-})^2}{\Gamma}\sigma\right)\cos\left(\Omega_{mn}^{-}\varphi\right)\right].\end{aligned}$$

Here, a short-hand notation for the combination frequencies has been introduced: $\Omega_{mn}^{\pm}=m\Omega_1\pm n\Omega_2$. Transforming back to the original variable yields

$$W(\sigma,\varphi) = \frac{2}{\Gamma}\frac{1}{\zeta(\sigma,\varphi)}\frac{\partial\zeta(\sigma,\varphi)}{\partial\varphi} = \frac{\sum_{m=0}^{\infty}\sum_{n=0}^{\infty}(-w_{mn})\left[\Omega_{mn}^{+}\,\mathrm{e}_{mn}^{+}\sin(\Omega_{mn}^{+}\varphi)+\Omega_{mn}^{-}\,\mathrm{e}_{mn}^{-}\sin(\Omega_{mn}^{-}\varphi)\right]}{(\Gamma/2)\sum_{m=0}^{\infty}\sum_{n=0}^{\infty}w_{mn}\left[\mathrm{e}_{mn}^{+}\cos(\Omega_{mn}^{+}\varphi)+\mathrm{e}_{mn}^{-}\cos(\Omega_{mn}^{-}\varphi)\right]}\,, \tag{8.117}$$

where

$$w_{mn} = (-1)^{m+n}b_m b_n I_m\left(\frac{\Gamma_1}{2}\right)I_n\left(\frac{\Gamma_2}{2}\right)\,,$$

$$\mathrm{e}_{mn}^{+} = \exp\left(-\frac{(\Omega_{mn}^{+})^2}{\Gamma}\sigma\right)\,,$$

$$\mathrm{e}_{mn}^{-} = \exp\left(-\frac{(\Omega_{mn}^{-})^2}{\Gamma}\sigma\right)\,.$$

It is seen that for $\sigma > 0$ the solution in φ contains all combination frequencies $m\Omega_1 \pm n\Omega_2$ of the two input frequencies due to the nonlinear interaction. Note also that for $\Omega_1 = 1$, $\Gamma_1 = \Gamma$, $\Omega_2 = 0$, $\Gamma_2 = 0$ the solution (8.96) is recovered. In its full generality, the expression is rather cumbersome to analyze. However, as higher frequencies are more strongly damped for $\sigma \to \infty$ only a few frequencies remain with sufficient amplitude. In particular, if Ω_1 and $\Omega_2 < \Omega_1$ are close, the difference frequency $\Delta\Omega = \Omega_1 - \Omega_2$ $(m = n = 1)$ will be small and give a strong component with

$$W_{-}(\sigma,\varphi) = -\frac{4\Delta\Omega}{\Gamma}\frac{I_1\left(\frac{\Gamma_1}{2}\right)I_1\left(\frac{\Gamma_2}{2}\right)}{I_0\left(\frac{\Gamma_1}{2}\right)I_0\left(\frac{\Gamma_2}{2}\right)} \times\exp\left(-\frac{(\Delta\Omega)^2}{\Gamma}\sigma\right)\sin(\Delta\Omega\varphi)\,, \tag{8.118}$$

or, returning to physical coordinates and constants,

$$u_{-}(x,t) = -\frac{2\Delta\omega\,\delta}{c_0\beta}\frac{I_1\left(\frac{\Gamma_1}{2}\right)I_1\left(\frac{\Gamma_2}{2}\right)}{I_0\left(\frac{\Gamma_1}{2}\right)I_0\left(\frac{\Gamma_2}{2}\right)} \times\exp\left(-\frac{\delta(\Delta\omega)^2}{2c_0^3}x\right)\sin[\Delta\omega(t-x/c_0)] = u_{-}^{(0)}\exp\left(-\frac{\delta(\Delta\omega)^2}{2c_0^3}x\right)\sin[\Delta\omega(t-x/c_0)]\,. \tag{8.119}$$

The Gol'dberg numbers of the interacting waves determine the quantity $u_{-}^{(0)}$ of the resulting difference-frequency wave. For $\Gamma_{1,2} \ll 1$, i. e., for low-power waves, $I_0(\Gamma/2) \approx 1$ and $I_1(\Gamma/2) \approx \Gamma/4$, thus the value

$$u_{-}^{(0)} = -\frac{2\Delta\omega\,\delta}{c_0\beta}\frac{\Gamma_1\Gamma_2}{16} = -\frac{\Delta\omega\beta c_0}{2\delta}\frac{u_{01}u_{02}}{\omega_1\omega_2} \tag{8.120}$$

is proportional to the product of the amplitudes of the interacting waves. For very intense waves, $\Gamma_{1,2} \gg 1$, as $\lim_{\xi\to\infty} I_1(\xi)/I_0(\xi) = 1$, the quantity $u_{-}^{(0)}$ of the difference-frequency wave becomes independent of u_{01} and u_{02},

$$u_{-}^{(0)} = -\frac{2\Delta\omega\,\delta}{c_0\beta}\,. \tag{8.121}$$

The difference-frequency wave (8.121) has been given for the far field where the two incoming waves have essentially ceased to interact. There, the wave propagates linearly and is exponentially damped by thermoviscous dissipation.

8.10 Bubbly Liquids

Liquids with bubbles have strongly pronounced nonlinear acoustic properties mainly due to the nonlinear oscillations of the bubbles and the high compressibility of the gas inside. Within recent decades theoretical and experimental investigations have detected many kinds of nonlinear wave phenomena in bubbly fluids. To mention just a few of these: ultrasound self-focusing [8.83, 84], acoustic chaos [8.31], sound self-transparency [8.85], wavefront conjugation [8.85], the acoustic phase echo [8.86] intensification of sound waves in nonuniform bubbly fluids [8.87, 88], subharmonic wave generation [8.89], structure formation in acoustic cavitation [8.90, 91], difference-frequency sound generation [8.92, 93]. These phenomena are discussed in several books and review papers [8.2, 9, 81, 94–97].

In this section we are going to discuss some phenomena related to nonlinear acoustic wave propagation in liquids with bubbles. First, the mathematical model for pressure-wave propagation in bubbly liquids will be presented. Second, this model will be used to investigate long nonlinear pressure waves, short pressure wave trains, and some nonlinear interactions between them.

Amazon EX1014 Page 291

Let α_l and α_g be the volume fractions and ρ_l and ρ_g the densities of the liquid and the gas (vapor), respectively. Then the density of the two-phase mixture, ρ, in the bubbly liquid mixture is given by

$$\rho = \alpha_l \rho_l + \alpha_g \rho_g \,, \tag{8.122}$$

where $\alpha_l + \alpha_g = 1$. Note that the gas (vapor) volume fraction depends on the instantaneous bubble radius R,

$$\alpha_g = \frac{4}{3}\pi R^3 n \,, \tag{8.123}$$

where n is the number density of bubbles in the mixture. Equation (8.123) is true in general and applicable to the case in which bubbles oscillate in an acoustic field, as considered in the following.

8.10.1 Incompressible Liquids

First, we consider the case when the liquid can be treated as incompressible. The bubbly fluid model in this case is based on the *bubble-in-cell* technique [8.94], which divides the bubbly liquid mixture into cells, with each cell consisting of a liquid sphere of radius R_c with a bubble of radius R at its center. A similar approach has been used recently to model wet foam drop dynamics in an acoustic field [8.98] and the acoustics of bubble clusters in a spherical resonator [8.80].

It should be mentioned here that the bubble-in-cell technique may be treated as a first-order correction to a bubbly fluid dynamics model due to a small bubble volume fraction. This technique is not capable of capturing the entire bubbly fluid dynamics for high concentration of bubbles when bubbles lose their spherical shape.

According to the bubble-in-cell technique, the radius, R_c, of the liquid sphere comprising each cell and the embedded bubble, are related to the local void fraction at any instant by

$$\frac{R}{R_c} = \alpha_g^{1/3} \,. \tag{8.124}$$

We note that R_c, R, and α_g are variable in time.

The liquid conservation of mass equation and the assumed liquid incompressibility imply that the radial velocity around a single bubble depends on the radial coordinate:

$$v' = \frac{R^2 \dot{R}}{r'^2}, \quad R \le r' \le R_c \,, \tag{8.125}$$

where $R(t)$ is the instantaneous radius of the bubble, primed quantities denote local (single-cell) variables, namely, r' is the radial coordinate with origin at the bubble's center, v' is the radial velocity of the liquid at radial location r', and the dot denotes a time derivative (i. e., $R = \mathrm{d}R/\mathrm{d}t$).

The dynamics of the surrounding liquid is analyzed by writing the momentum equation for an incompressible, inviscid liquid as

$$\frac{\partial v'}{\partial t} + v' \frac{\partial v'}{\partial r'} + \frac{1}{\rho_l}\frac{\partial p'}{\partial r'} = 0 \,. \tag{8.126}$$

Integrating this equation over $r' \le R_c$ from R to some arbitrary r' and using (8.125) yields

$$p' = p_R - \rho_l \Bigg[R\ddot{R} + \frac{3}{2}\dot{R}^2 - \left(R\ddot{R} + 2\dot{R}^2\right)\frac{R}{r'} + \frac{1}{2}\dot{R}^2 \left(\frac{R}{r'}\right)^4 \Bigg] \,, \tag{8.127}$$

where p' is the liquid pressure at location r' around a bubble, and p_R is the liquid pressure at the bubble interface. Evaluating (8.127) at the outer radius of the cell, $r' = R_c$, and using (8.124), results in

$$\frac{p_R - p_c}{\rho_l} = \left(1 - \alpha_g^{1/3}\right) R\ddot{R} + \frac{3}{2}\left(1 - \frac{4}{3}\alpha_{g^{1/3}} + \frac{1}{3}\alpha_{g^{4/3}}\right)\dot{R}^2 \,. \tag{8.128}$$

This equation bears a resemblance to the well-known Rayleigh–Plesset equation that governs the motion of a single bubble in an infinite liquid. Indeed, in the limit of vanishing void fraction, $\alpha_g \to 0$, the pressure at the outer radius of the cell (p_c) becomes the liquid pressure far from the bubble ($p_c \to p_\infty$), and (8.128) reduces to the Rayleigh–Plesset equation

$$\frac{p_R - p_\infty}{\rho_l} = R\ddot{R} + \frac{3}{2}\dot{R}^2 \,. \tag{8.129}$$

Let us assume that the gas pressure inside the bubble p_g is spatially uniform. The momentum jump condition requires that the gas pressure differs from the liquid pressure at the bubble wall due to surface tension and viscous terms according to

$$p_R = p_g - \frac{2\sigma}{R} - \frac{4\mu_l \dot{R}}{R} \,, \tag{8.130}$$

where σ is the surface tension and μ_l is the liquid viscosity. Furthermore, the gas pressure may be assumed to be governed by a polytropic gas law of the form

$$p_g = \left(p_0 + \frac{2\sigma}{R_0}\right)\left(\frac{R}{R_0}\right)^{-3\kappa} \,, \tag{8.131}$$

where R_0 is the equilibrium radius of the bubble (i. e., the bubble radius at ambient pressure) and κ is a polytropic exponent. Combining (8.128)–(8.131) gives the following relationship between the liquid pressure at the edge of the cell (p_c) and the radius of the bubble (R):

$$p_c = \left(p_0 + \frac{2\sigma}{R}\right)\left(\frac{R}{R_0}\right)^{-3\kappa} - \frac{2\sigma}{R} - \frac{4\mu_l \dot{R}}{R} - \rho_l\left[\left(1-\alpha_g^{1/3}\right)R\ddot{R} + \frac{3}{2}\left(1-\frac{4}{3}\alpha_g^{1/3}+\frac{1}{3}\alpha_g^{4/3}\right)\dot{R}^2\right]. \tag{8.132}$$

Equation (8.132) can be integrated to find the bubble radius, $R(t)$, given the time-dependent pressure at $r' = R_c$ and the initial conditions.

Next, we connect the various cells at points on their outer radii and replace the configuration with an equivalent fluid whose dynamics approximate those of the bubbly liquid. We assume that the velocity of the translational motion of the bubbles in such a fluid is equal to the velocity of the bubbly fluid $\boldsymbol{v}$. The fluid is required to conserve mass, thus

$$\frac{\partial \rho}{\partial t} + \nabla\cdot(\rho \boldsymbol{v}) = 0\,, \tag{8.133}$$

where ρ is given by (8.122). The fluid also satisfies Euler's equation,

$$\rho\frac{\mathrm{d}\boldsymbol{v}}{\mathrm{d}t} + \nabla p = 0\,, \tag{8.134}$$

where $\mathrm{d}/\mathrm{d}t = \partial/\partial t + \boldsymbol{v}\cdot\nabla$ is the material derivative, and p is the mean fluid pressure, which is approximately the pressure at the outer radius of a cell, p_c.

The mass and bubble densities are related by requiring that the total mass of each cell does not change in time. The initial volume of one cell is $V_0 = 1/n_0$, so the initial mass of the cell is $M_0 = \rho_0/n_0$, where $\rho_0 = \alpha_{l0}\rho_{l0} + \alpha_{g0}\rho_{g0}$. Requiring that the mass of each cell remains constant gives

$$\frac{\rho}{n} = \frac{\rho_0}{n_0}\,. \tag{8.135}$$

This set of equations describes the nonlinear dynamics of a bubbly liquid mixture over a wide range of pressures and temperatures.

We can now linearize these equations by assuming that the time-dependent quantities only vary slightly from their equilibrium values. Specifically, we write $\rho = \rho_0 + \tilde{\rho}$, $n = n_0 + \tilde{n}$, $p = p_0 + \tilde{p}$, $\mathbf{v} = \tilde{\mathbf{v}}$, $\alpha_g = \alpha_{g0} + \tilde{\alpha_g}$, and $R = R_0 + \tilde{R}$. The perturbed quantities are assumed to be small, so that any product of the perturbations may be neglected. When these assumptions are introduced into (8.132), we arrive at the following linearized equation:

$$\tilde{p} = -\left[\left(p_0 + \frac{2\sigma}{R_0}\right)\frac{3\kappa}{R_0} - \frac{2\sigma}{R_0^2}\right]\tilde{R} - \frac{4\mu_l}{R_0}\frac{\partial \tilde{R}}{\partial t} - \rho_l\left(1-\alpha_{g0}^{1/3}\right)R_0\frac{\partial^2\tilde{R}}{\partial t^2}\,. \tag{8.136}$$

Linearizing (8.135) gives

$$\tilde{n} = \frac{n_0}{\rho_0}\tilde{\rho}\,. \tag{8.137}$$

Similarly, linearizing the density in (8.122) taking into account that $\rho_g/\rho_l \ll 1$ and using (8.137) yields

$$\tilde{\rho} = -4\pi R_0^2\rho_0 n_0 \tilde{R}, \tag{8.138}$$

where $\rho_0 \approx \rho_l\left(1-\alpha_{g0}\right)$. By combining (8.136) and (8.138) we obtain a pressure–density relationship for the bubbly fluid:

$$\tilde{p} = \frac{C_b^2}{\omega_b^2}\left(\omega_b^2\tilde{\rho} + 2\delta_b\frac{\partial\tilde{\rho}}{\partial t} + \frac{\partial^2\tilde{\rho}}{\partial t^2}\right)\,, \tag{8.139}$$

where C_b represents the low-frequency sound speed in the bubbly liquid

$$C_b^2 = \frac{3\kappa p_0 + (3\kappa-1)\dfrac{2\sigma}{R_0}}{3\alpha_{g0}(1-\alpha_{g0})\rho_l}\,, \tag{8.140}$$

and ω_b is the natural frequency of a bubble in the cell

$$\omega_b^2 = \frac{\omega_M^2}{1-\alpha_{g0}^{1/3}}\,. \tag{8.141}$$

We note that ω_M is the natural frequency of a single bubble in an infinite liquid (i. e. the so-called Minnaert frequency),

$$\omega_M^2 = \frac{3\kappa p_0 + (3\kappa-1)\dfrac{2\sigma}{R_0}}{\rho_l R_0^2}\,. \tag{8.142}$$

In (8.139) the parameter δ_b represents the dissipation coefficient due to the liquid viscosity,

$$\delta_b = \frac{2\mu_l}{\rho_l R_0^2\left(1-\alpha_{g0}^{1/3}\right)}\,. \tag{8.143}$$

Actually acoustic wave damping in bubbly liquids occurs due to several different physical mechanisms:

liquid viscosity, gas/vapor thermal diffusivity, acoustic radiation, etc. The contribution of each of these dissipation mechanisms to the total dissipation during bubble oscillations depends on frequency, bubble size, the type of gas in a bubble and liquid compressibility [8.94]. For convenience one can use an effective dissipation coefficient in the form of a viscous dissipation:

$$\delta_{\text{eff}} = \frac{2\mu_{\text{eff}}}{\rho_{\text{l}} R_0^2 \left(1-\alpha_{\text{g0}}^{1/3}\right)} , \tag{8.144}$$

where μ_{eff} denotes an effective viscosity (instead of just the liquid viscosity), which implicitly includes all the aforementioned dissipation mechanisms in a bubbly liquid. The value for μ_{eff} should be chosen to fit experimental observations and the theoretical data of amplitude versus frequency for a single bubble.

We can also linearize (8.133) and (8.134) to obtain

$$\frac{\partial \tilde{\rho}}{\partial t} + \rho_0 \nabla \cdot \mathbf{v} = 0 , \tag{8.145}$$

$$\rho_0 \frac{\partial \mathbf{v}}{\partial t} + \nabla \tilde{p} = 0 . \tag{8.146}$$

Combining the time derivative of (8.145) with the divergence of (8.146) results in

$$\frac{\partial^2 \tilde{\rho}}{\partial t^2} = \nabla^2 \tilde{p} . \tag{8.147}$$

Combining this result with (8.139) gives a wave equation for the bubbly liquid of the form

$$\frac{\partial^2 \tilde{p}}{\partial t^2} - C_{\text{b}}^2 \left(1 + \frac{2\delta_{\text{eff}}}{\omega_{\text{b}}^2}\frac{\partial}{\partial t} + \frac{1}{\omega_{\text{b}}^2}\frac{\partial^2}{\partial t^2}\right) \nabla^2 \tilde{p} = 0 . \tag{8.148}$$

Equation (8.148) describes the propagation of a linear acoustical pressure perturbations in a liquid with bubbles when the liquid can be treated as incompressible. It also accounts for the effect of a small but finite void fraction on wave propagation [8.9, 94, 95].

8.10.2 Compressible Liquids

When the pressure waves are very intense, and the void fraction is small ($\alpha_{\text{g}} \ll 1$), one should take into account liquid compressibility, which may lead to acoustic radiation by the oscillating bubbles. In this case, correction terms of $\alpha_{\text{g}}^{1/3}$, $\alpha_{\text{g}}^{4/3}$ in (8.128) may be neglected, and in order to account for acoustic radiation (8.128) should be rewritten as follows [8.99, 100]:

$$R\ddot{R} + \frac{3}{2}\dot{R}^2 = \frac{p_{\text{R}} - p}{\rho_{\text{l0}}} + \frac{R}{\rho_{\text{l0}} C_{\text{l}}}\frac{\text{d}}{\text{d}t}\left(p_{\text{R}} - p\right) , \tag{8.149}$$

where C_{l} is the speed of sound in the liquid. In (8.149) the liquid density, ρ_{l}, is taken as a constant ρ_{l0} although the equation of state of the liquid can be approximated as

$$p = p_0 + C_{\text{l}}^2 \left(\rho_{\text{l}} - \rho_{\text{l0}}\right) . \tag{8.150}$$

After linearization (8.149) becomes [compare with (8.136)]:

$$\tilde{p} = -\left[\left(p_0 + \frac{2\sigma}{R_0}\right)\frac{3\kappa}{R_0} - \frac{2\sigma}{R_0^2}\right]\tilde{R} - \frac{4\mu_{\text{l}}}{R_0}\frac{\partial \tilde{R}}{\partial t} - \rho_{\text{l0}} R_0 \left(1 + \frac{R_0}{C_{\text{l}}}\frac{\partial}{\partial t}\right)^{-1} \frac{\partial^2 \tilde{R}}{\partial t^2} . \tag{8.151}$$

In order to evaluate the last term in (8.151) and to incorporate acoustic radiation losses into an *effective* viscosity scheme we use the following approximation for the differential operator:

$$\left(1 + \frac{R_0}{C_{\text{l}}}\frac{\partial}{\partial t}\right)^{-1} \approx 1 - \frac{R_0}{C_{\text{l}}}\frac{\partial}{\partial t} . \tag{8.152}$$

Then (8.151) becomes

$$\tilde{p} \approx -\left[\left(p_0 + \frac{2\sigma}{R_0}\right)\frac{3\kappa}{R_0} - \frac{2\sigma}{R_0^2}\right]\tilde{R} - \frac{4\mu_{\text{l}}}{R_0}\frac{\partial \tilde{R}}{\partial t} - \rho_{\text{l0}} R_0 \frac{\partial^2 \tilde{R}}{\partial t^2} + \frac{\rho_{\text{l0}} R_0^2}{C_{\text{l}}}\frac{\partial^3 \tilde{R}}{\partial t^3} . \tag{8.153}$$

The third derivative in (8.153) can be estimated using the approximation of a freely oscillating bubble

$$\frac{\partial^2 \tilde{R}}{\partial t^2} \approx -\frac{\left(p_0 + \frac{2\sigma}{R_0}\right)\frac{3\kappa}{R_0} - \frac{2\sigma}{R_0^2}}{\rho_{\text{l0}} R_0}\tilde{R} . \tag{8.154}$$

Substituting (8.154) in the third-derivative term of (8.153) we get

$$\tilde{p} = -\left[\left(p_0 + \frac{2\sigma}{R_0}\right)\frac{3\kappa}{R_0} - \frac{2\sigma}{R_0^2}\right]\tilde{R} - \frac{4\mu_{\text{eff}}}{R_0}\frac{\partial \tilde{R}}{\partial t} - \rho_{\text{l0}} R_0 \frac{\partial^2 \tilde{R}}{\partial t^2} , \tag{8.155}$$

where

$$\mu_{\text{eff}} = \mu_{\text{l}} + \mu_{\text{r}}, \quad \mu_{\text{r}} = \frac{(3\kappa - 1)\sigma}{2C_{\text{l}}} + \frac{3\kappa p_0}{4C_{\text{l}}} R_0 . \tag{8.156}$$

It is easy to see from (8.156) that acoustic radiation may lead to a very large dissipation. For example, for

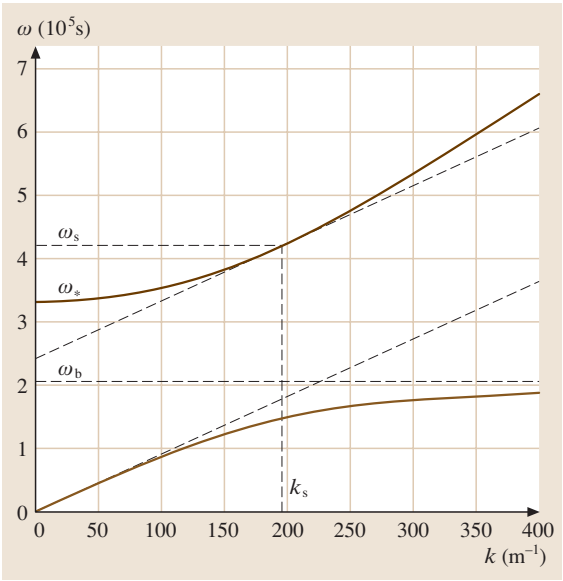


Fig. 8.13 The dispersion relation for water with air bubbles (the liquid is treated as compressible, dissipation is ignored): $C_l = 1500\,\mathrm{m/s}$, $p_0 = 10^5\,\mathrm{Pa}$, $\kappa = 1.4$, $\sigma = 0.0725\,\mathrm{N/m}$, $\rho_{l0} = 10^3\,\mathrm{kg/m}$, $\alpha_{g0} = 10^{-4}$, $R_0 = 10^{-4}\,\mathrm{m}$

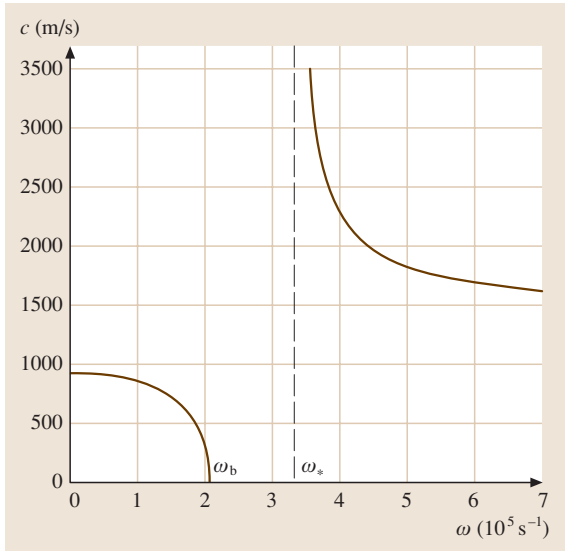


Fig. 8.14 The phase velocity for water with air bubbles (the liquid is treated as compressible, dissipation is ignored): $C_l = 1500\,\mathrm{m/s}$, $p_0 = 10^5\,\mathrm{Pa}$, $\kappa = 1.4$, $\sigma = 0.0725\,\mathrm{N/m}$, $\rho_{l0} = 10^3\,\mathrm{kg/m}$, $\alpha_{g0} = 10^{-4}$, $R_0 = 10^{-4}\,\mathrm{m}$

air bubbles of $R_0 = 10^{-4}$ m in water, effective viscosity due to acoustic radiation μ_r may be about seven times larger than the viscosity of water, μ_l.

Equation (8.135), and eventually its linearized form (8.137), are valid in the case of a compressible liquid. However, the linearized form of (8.122) changes. Now instead of (8.138) we have

$$\tilde{\rho} = \tilde{\rho}_l - 4\pi R_0^2 \rho_0 n_0 \tilde{R} \tag{8.157}$$

or, accounting for the liquid equation of state (8.150),

$$\tilde{\rho} = C_l^{-2}\tilde{p} - 4\pi R_0^2 \rho_0 n_0 \tilde{R}\,. \tag{8.158}$$

Substituting (8.158) into (8.147) we have

$$C_l^{-2}\frac{\partial^2 \tilde{p}}{\partial t^2} - \nabla^2 \tilde{p} = 4\pi R_0^2 n_0 \rho_0 \frac{\partial^2 \tilde{R}}{\partial t^2}\,. \tag{8.159}$$

Equation (8.159) together with (8.155) leads to the following wave equation for a bubbly fluid in the case of a compressible liquid:

$$\frac{\partial^2 \tilde{p}}{\partial t^2} - C_b^2\left(1 + \frac{2\delta_{\mathrm{eff}}}{\omega_b^2}\frac{\partial}{\partial t} + \frac{1}{\omega_b^2}\frac{\partial^2}{\partial t^2}\right)\times \left(\nabla^2 - C_l^{-2}\frac{\partial^2}{\partial t^2}\right)\tilde{p} = 0\,. \tag{8.160}$$

Here ω_b and δ_{eff} are calculated according to (8.141) and (8.144) in which α_{g0} is taken to be zero, and C_b is calculated according to (8.140). It is easy to see that (8.160) reduces to (8.148) in the case when $C_l \to \infty$.

The linear wave equation (8.160) admits the harmonic wave-train solution

$$\tilde{p} = p_a \exp\left[\mathrm{i}(kx - \omega t)\right]\,, \tag{8.161}$$

in which the frequency ω and wave number k are related through the following dispersion relation

$$k^2 = \omega^2\left(\frac{1}{C_l^2} + \frac{1}{C_b^2\left(1 + \mathrm{i}\dfrac{2\omega\delta_{\mathrm{eff}}}{\omega_b^2} - \dfrac{\omega^2}{\omega_b^2}\right)}\right)\,. \tag{8.162}$$

The graph of this dispersion relation is shown in Fig. 8.13. The corresponding phase velocity is given in Fig. 8.14.

8.10.3 Low-Frequency Waves: The Korteweg–de Vries Equation

In order to analyze the low-frequency nonlinear acoustics of a bubbly liquid the low-frequency limit of the

dispersion relation (8.162) is first considered:

$$\omega = Ck + \mathrm{i}\alpha_1 k^2 - \alpha_2 k^3 \,, \tag{8.163}$$

where

$$\frac{1}{C^2} = \frac{1}{C_1^2} + \frac{1}{C_\mathrm{b}^2}, \quad \alpha_1 = \frac{\delta_\mathrm{eff} C^4}{\omega_\mathrm{b}^2 C_\mathrm{b}^2}, \quad \alpha_2 = \frac{C^5}{2C_\mathrm{b}^2 \omega_\mathrm{b}^2} \,. \tag{8.164}$$

Noting that

$$\omega = -\mathrm{i}\frac{\partial}{\partial t}, \quad k = \mathrm{i}\frac{\partial}{\partial x} \,, \tag{8.165}$$

(8.163) can be treated as the Fourier-space equivalent of an operator equation which when operating on $\tilde{p}$, yields

$$\frac{\partial \tilde{p}}{\partial t} + C\frac{\partial \tilde{p}}{\partial x} - \alpha_1 \frac{\partial^2 \tilde{p}}{\partial x^2} + \alpha_2 \frac{\partial^3 \tilde{p}}{\partial x^3} = 0 \,. \tag{8.166}$$

Equation (8.166) should be corrected to account for weak nonlinearity. A systematic derivation is normally based on the *multiple-scales* technique [8.101]. Here we show how this derivation can be done less rigorously, but more simply. We assume that the nonlinearity in bubbly liquids comes only from bubble dynamics. Then (8.155) for weakly nonlinear bubble oscillations has an additional nonlinear term and becomes:

$$\tilde{p} = -B_1 \tilde{R} + B_2 \tilde{R}^2 - \frac{4\mu_\mathrm{eff}}{R_0}\frac{\partial \tilde{R}}{\partial t} - \rho_{l0} R_0 \frac{\partial^2 \tilde{R}}{\partial t^2} \,. \tag{8.167}$$

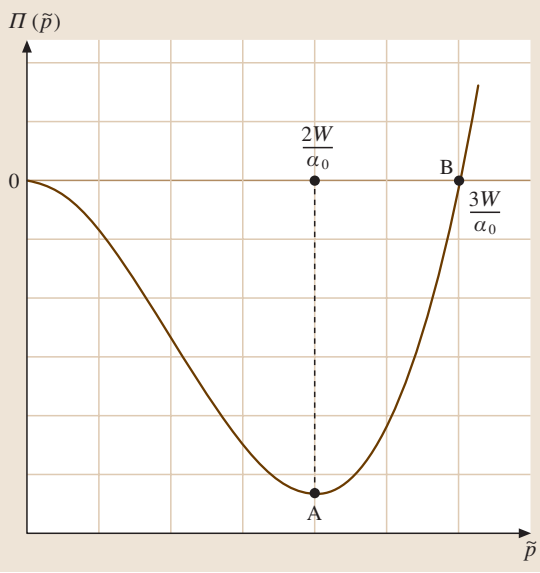


Fig. 8.15 The potential well used to illustrate the "soliton" solution for the KdV equation

$$B_1 = \left(p_0 + \frac{2\sigma}{R_0}\right)\frac{3\kappa}{R_0} - \frac{2\sigma}{R_0^2},$$
$$B_2 = \left(p_0 + \frac{2\sigma}{R_0}\right)\frac{3\kappa(3\kappa+1)}{2R_0^2} - \frac{2\sigma}{R_0^3} \,. \tag{8.168}$$

Equation (8.167) has to be combined with the linear wave equation (8.159), which in the case of plane waves can be written:

$$C_1^{-2}\frac{\partial^2 \tilde{p}}{\partial t^2} - \frac{\partial^2 \tilde{p}}{\partial x^2} = 4\pi R_0^2 n_0 \rho_0 \frac{\partial^2 \tilde{R}}{\partial t^2} \,. \tag{8.169}$$

Taking into account that all the terms except the first one on the right-hand side of (8.167) are small, i. e., of the second order of magnitude, one can derive the following nonlinear wave equation for pressure perturbations in a bubbly liquid:

$$C^{-2}\frac{\partial^2 \tilde{p}}{\partial t^2} - \frac{\partial^2 \tilde{p}}{\partial x^2} = 4\pi R_0^2 n_0 \rho_0 \times \left(\frac{B_2}{B_1^3}\frac{\partial^2 \tilde{p}^2}{\partial t^2} + \frac{4\mu_\mathrm{eff}}{R_0 B_1^2}\frac{\partial^3 \tilde{p}}{\partial t^3} + \frac{\rho_{l0} R_0}{B_1^2}\frac{\partial^4 \tilde{p}}{\partial t^4}\right) \,. \tag{8.170}$$

Equation (8.170) is derived for plane weakly nonlinear pressure waves traveling in a bubbly liquid in both directions. Namely, the left part of this equation contains a classic wave operator when applied to a pressure perturbation function describes waves traveling left to right and right to left. The right part of this equation contain terms of second order of smallness and is therefore responsible for a slight change of these waves. Thus, (8.170) may be structured as follows:

$$\left(C^{-1}\frac{\partial}{\partial t} + \frac{\partial}{\partial x}\right)\left(C^{-1}\frac{\partial}{\partial t} - \frac{\partial}{\partial x}\right)\tilde{p} = O\left(\varepsilon^2\right) \,. \tag{8.171}$$

If one considers only waves traveling left to right then

$$C^{-1}\frac{\partial}{\partial t} + \frac{\partial}{\partial x} = O\left(\varepsilon\right) \,, \tag{8.172}$$

and we can use the following derivative substitution (see [8.10])

$$\frac{\partial}{\partial t} \approx -C\frac{\partial}{\partial x} \,. \tag{8.173}$$

Then, after one time integration over space, and translation to the frame moving left to right with

Amazon EX1014 Page 296

a speed of sound C, (8.170) leads to the Burgers–Korteweg–de Vries (BKdV) equation for a pressure wave [8.94–96, 102]:

$$\frac{\partial \tilde{p}}{\partial t} + \alpha_0 \tilde{p} \frac{\partial \tilde{p}}{\partial \xi} - \alpha_1 \frac{\partial^2 \tilde{p}}{\partial \xi^2} + \alpha_2 \frac{\partial^3 \tilde{p}}{\partial \xi^3} = 0, \quad \xi = x - Ct\,, \tag{8.174}$$

where

$$\alpha_0 = \frac{C^3}{C_b^2} \cdot \frac{B_2}{B_1^2} \tag{8.175}$$

and the parameters α_1, α_2, and C are presented in (8.164).

Let us first discuss a nondissipative case, $\alpha_1 = 0$. Then (8.174) is called the Korteweg–de Vries (KdV) equation. The low-frequency dispersion relation (8.163) shows that every Fourier component of initial arbitrary pressure perturbation propagates with its own speed, and the shape of the acoustic signal changes. Since $\alpha_2 > 0$, the long-wavelength waves propagate with higher speed than lower-wavelength waves. This means that dispersion may begin to compete with nonlinearity, which stops shock-wave formation. The competition between dispersion and nonlinearity leads to the formation of a so-called *soliton*.

In order to derive the shape of soliton, here we consider a steady solution of (8.174) in the moving frame

$$\eta = \xi - Wt\,. \tag{8.176}$$

Then, assuming that there is no pressure perturbation at infinity, (8.174) can be reduced as follows:

$$\alpha_2 \frac{d^2 \tilde{p}}{d\eta^2} = -\frac{\partial \Pi}{\partial \tilde{p}}, \quad \Pi(\tilde{p}) = -\frac{W\tilde{p}^2}{2} + \frac{\alpha_0 \tilde{p}^3}{6}\,. \tag{8.177}$$

It is instructive to use the analogy that (8.177) is similar to the equation of a point-like particle in a potential well shown schematically in Fig. 8.15. The structure of the pressure *solitary* wave can be viewed as follows: initially the particle is at point O, which corresponds to the fact that far away the pressure perturbation is equal to zero; then the particle slides down to the bottom of the potential well, point A, and due to a conservation law climbs up to point B; at point B it stops and moves all the way back to point O. The solution of (8.177) represents the shape of the soliton, which in the immovable frame is

$$\tilde{p} = \frac{3W}{\alpha_0} \cosh^{-2}\left\{\sqrt{\frac{W}{4\alpha_2}}\,[x - (C + W)t]\right\}\,. \tag{8.178}$$

It was mentioned above that a soliton may be interpreted as a result of the balance between two competitors: nonlinearity and dispersion. To consider this competition in more detail the KdV equation is considered in the frame moving with the speed of sound in a bubbly liquid

$$\frac{\partial \tilde{p}}{\partial t} + \alpha_0 \tilde{p} \frac{\partial \tilde{p}}{\partial \xi} + \alpha_2 \frac{\partial^3 \tilde{p}}{\partial \xi^3} = 0, \quad \xi = x - Ct\,. \tag{8.179}$$

Then the solitary wave has the following shape:

$$\tilde{p} = \frac{3W}{\alpha_0} \cosh^{-2}\left\{\sqrt{\frac{W}{4\alpha_2}}\,(\xi - Wt)\right\} \tag{8.180}$$

with a pressure amplitude equal to $3W/\alpha_0$ and a thickness of about $\sqrt{\alpha_2/W}$.

In order to evaluate the effect of nonlinearity let us consider the simple nonlinear equation

$$\frac{\partial \tilde{p}}{\partial t} + \alpha_0 \tilde{p} \frac{\partial \tilde{p}}{\partial \xi} = 0\,. \tag{8.181}$$

The factor $\alpha_0 \tilde{p}$ stands for the velocity of transportation of pressure perturbations. Thus, part of the pressure profile which has higher pressure will be translated faster than the part which has lower pressure. According to the solitary solution (8.180) the maximum translation velocity is equal to $3W$. The time needed for the pressure peak to be translated the distance of about the thickness of the pressure wave can be estimated as $t_{nl} \sim \alpha_2^{1/2} W^{-3/2}$. This amount of time would be needed to transform the smooth solitary shape to a shock wave.

In order to evaluate the effect of dispersion let us consider the simple dispersive equation

$$\frac{\partial \tilde{p}}{\partial t} + \alpha_2 \frac{\partial^3 \tilde{p}}{\partial \xi^3} = 0\,. \tag{8.182}$$

This equation admits harmonic wave-train solutions of the form $\exp(ik\xi + i\alpha_2 k^3 t)$. The characteristic wave numbers contributing to the wave shape of thickness $\sqrt{\alpha_2/W}$ are $k \sim \sqrt{W/\alpha_2}$. Such wave numbers will gradually change the wave phase on π and thus lead to a substantial deformation of the wave shape. The time interval needed for this, t_d, is calculated as follows: $\alpha_2 \left(\sqrt{W/\alpha_2}\right)^3 t_d = \pi$, thus, $t_d \sim \alpha_2^{1/2} W^{-3/2}$, which is $\sim t_{nl}$. So, the time that is needed for nonlinearity to transform the solitary wave into a shock wave is equal to the time taken for dispersion to smooth out this wave.

One of the most important results obtained from the BKdV equation is the prediction of an oscillatory shock wave. In order to derive the shape of an oscillatory shock wave we again consider the steady-state solution

Amazon EX1014 Page 297

of (8.174) in the moving frame (8.176). Then, assuming that there is no pressure perturbation at infinity, (8.174) can be reduced to

$$\alpha_2 \frac{\mathrm{d}^2\tilde{p}}{\mathrm{d}\eta^2} - \alpha_1 \frac{\mathrm{d}\tilde{p}}{\mathrm{d}\eta} = -\frac{\partial \Pi}{\partial \tilde{p}} ,$$
$$\Pi(\tilde{p}) = -\frac{W\tilde{p}^2}{2} + \frac{\alpha_0 \tilde{p}^3}{6} . \qquad (8.183)$$

Equation (8.183) represents the equation of a point-like particle in a potential well shown schematically in Fig. 8.15 with friction. Here $\tilde{p}$ stands for the coordinate of the particle, minus ξ stands for the time (time passes from $-\infty$ to $+\infty$), α_2 is the mass of the particle, and α_1 is the friction coefficient. An oscillatory shock wave corresponds to motion of the particle from point O to the bottom of potential well (point A) with some decaying oscillations around the bottom. Thus, the amplitude of the shock wave is equal to $2W/\alpha_0$. Eventually oscillations take place only for relatively small values of the friction coefficient α_1. To derive a criterion for an oscillatory shock wave one should investigate a solution of (8.183) in close vicinity to point A. Assuming that

$$\tilde{p} = \frac{2W}{\alpha_0} + \psi(\xi) , \qquad (8.184)$$

where ψ is small, and linearizing (8.183) we get

$$\alpha_2 \frac{\mathrm{d}^2\psi}{\mathrm{d}\xi^2} - \alpha_1 \frac{\mathrm{d}\psi}{\mathrm{d}\xi} + W\psi = 0 . \qquad (8.185)$$

Equation (8.185) has a solution

$$\psi = A_1 \exp(-\lambda\xi) + A_2 \exp(\lambda\xi),$$
$$\lambda = \frac{\alpha_1}{2\alpha_2} \pm \sqrt{\frac{\alpha_1^2}{4\alpha_2^2} - \frac{W}{\alpha_1}} . \qquad (8.186)$$

It is easy to see that the shock wave has an oscillatory structure if

$$\alpha_1 < \sqrt{4\alpha_2 W} . \qquad (8.187)$$

In terms of the bubbly fluid parameters, (8.187) gives a critical effective viscosity

$$\mu_{\mathrm{eff}} < \mu_{\mathrm{crit}} = \rho_1 R_0^2 \omega_{\mathrm{b}} \frac{C_{\mathrm{b}}}{C} \sqrt{\frac{1}{2}\frac{W}{C}} . \qquad (8.188)$$

The KdV equation for describing the evolution of long-wavelength disturbances in an ideal liquid with adiabatic gas bubbles was first proposed in [8.102]. The solitons and shock waves in bubbly liquids were systematically investigated in [8.95] in the framework of the BKdV equation. Good correlation with experimental data was obtained. In [8.94] wave-propagation phenomena in bubbly liquids were analyzed using a more advanced and complete mathematical model that is valid for higher intensities of pressure waves. In [8.103] the effect of polydispersivity on long small-amplitude nonlinear waves in bubbly liquids was considered. It was shown that evolution equations of BKdV type can be applied for modeling of such waves. In particular, it was shown that for polydisperse bubbly liquids an effective monodisperse liquid model can be used with the bubble sizes found as ratios of some bubble size-distribution moments and corrections to the equation coefficients.

8.10.4 Envelopes of Wave Trains: The Nonlinear Schrödinger Equation

When the amplitude of an acoustic wave in a fluid is small enough the respective linearized system of equations will admit the harmonic wave-train solution

$$u = a \exp\{\mathrm{i}[kx - \omega(k)t]\} . \qquad (8.189)$$

If the amplitude is not small enough the nonlinearity cannot be neglected. The nonlinear terms produce higher harmonics, which react back on the original wave. Thus, the effect of nonlinearity on this sinusoidal oscillation is to cause a variation in its amplitude and phase in both space and time. This variation can be considered as small (in space) and slow (in time) for off-resonant situations. To account for a variation of amplitude and phase it is convenient to consider the amplitude as a complex function of space and time A.

Here we follow [8.104] to show what kind of equation arises as the evolution equation for a carrier-wave envelope in a general dispersive system. A linear system has a dispersion relation which is independent of the wave amplitude

$$\omega = \omega(k) . \qquad (8.190)$$

However, it is instructive to assume that the development of a harmonic wave in a weakly nonlinear system can be represented by a dispersion relation which is amplitude dependent

$$\omega = \omega(k, |A|^2) . \qquad (8.191)$$

Such a situation was initially uncovered in nonlinear optics and plasma where the refractive index or dielectric constant of a medium may be dependent on the electric field. That same situation occurs in bubbly liquids as well.

Amazon EX1014 Page 298

Let us consider a carrier wave of wave number k_0 and frequency $\omega_0 = \omega(k_0)$. A Taylor expansion of the dispersion relation (8.191) around k_0 gives

$$\Omega = \left(\frac{\partial\omega}{\partial k}\right)_0 K + \frac{1}{2}\left(\frac{\partial^2\omega}{\partial k^2}\right)_0 K^2 + \left(\frac{\partial\omega}{\partial(|A|^2)}\right)_0 |A|^2 , \tag{8.192}$$

where $\Omega = \omega - \omega_0$ and $K = k - k_0$ are the frequency and wave number of the variation of the wave-train amplitude. Equation (8.192) represents a dispersion relation for the complex amplitude modulation. Noting that

$$\Omega = -\mathrm{i}\frac{\partial}{\partial t}, \quad K = \mathrm{i}\frac{\partial}{\partial x} , \tag{8.193}$$

(8.192) can be treated as the Fourier-space equivalent of an operator equation that when operating on A yields

$$\mathrm{i}\left[\frac{\partial}{\partial t} + \left(\frac{\partial\omega}{\partial k}\right)_0 \frac{\partial}{\partial x}\right] A + \frac{1}{2}\left(\frac{\partial^2\omega}{\partial k^2}\right)_0 \frac{\partial^2 A}{\partial x^2} - \left(\frac{\partial\omega}{\partial(|A|^2)}\right)_0 |A|^2 A = 0 . \tag{8.194}$$

In the frame moving with group velocity

$$\xi = x - C_\mathrm{g} t, \quad C_\mathrm{g} = (\partial\omega/\partial k)_0 , \tag{8.195}$$

(8.194) represent the classical nonlinear Schrödinger (NLS) equation

$$\mathrm{i}\frac{\partial A}{\partial t} = \beta_\mathrm{d}\frac{\partial^2 A}{\partial\xi^2} + \gamma_\mathrm{n}|A|^2 A , \tag{8.196}$$

$$\beta_\mathrm{d} = -\frac{1}{2}\left(\frac{\partial^2\omega}{\partial k^2}\right)_0 , \quad \gamma_\mathrm{n} = \left(\frac{\partial\omega}{\partial(|A|^2)}\right)_0 , \tag{8.197}$$

which describes the evolution of wave-train envelopes.

Here A is a complex amplitude that can be represented as follows:

$$A(t,\xi) = a(t,\xi)\exp[\mathrm{i}\varphi(t,\xi)] , \tag{8.198}$$

where a and φ are the (real) amplitude and phase of the wave train. A spatially uniform solution of (8.196) corresponds to an unperturbed wave train. To analyze the stability of this uniform solution let us represent (8.196) as a set of two scalar equations:

$$-a\frac{\partial\varphi}{\partial t} = \beta_\mathrm{d}\left[\frac{\partial^2 a}{\partial\xi^2} - a\left(\frac{\partial\varphi}{\partial\xi}\right)^2\right] + \gamma_\mathrm{n} a^3 , \tag{8.199}$$

$$\frac{\partial a}{\partial t} = \beta_\mathrm{d}\left(2\frac{\partial a}{\partial\xi}\frac{\partial\varphi}{\partial\xi} + a\frac{\partial^2\varphi}{\partial\xi^2}\right) . \tag{8.200}$$

It is easy to verify that a spatially uniform solution ($\partial/\partial\xi \equiv 0$) of (8.199) and (8.200) is:

$$a = a_0, \quad \varphi = -\gamma_\mathrm{n} a_0^2 t . \tag{8.201}$$

The evolution of a small perturbation of this uniform solution

$$a = a_0 + \tilde{a}, \quad \varphi = -\gamma_\mathrm{n} a_0^2 t + \tilde{\varphi} , \tag{8.202}$$

is given by the following linearized equations:

$$a_0\frac{\partial\tilde{\varphi}}{\partial t} + \beta_\mathrm{d}\frac{\partial^2\tilde{a}}{\partial\xi^2} + 2\gamma_\mathrm{n} a_0^2\tilde{a} = 0 . \tag{8.203}$$

$$\frac{\partial\tilde{a}}{\partial t} - \beta_\mathrm{d} a_0\frac{\partial^2\tilde{\varphi}}{\partial\xi^2} = 0 . \tag{8.204}$$

Now let us consider the evolution of a periodic perturbation with wavelength $L = 2\pi/K$ that can be written as

$$\begin{pmatrix}\tilde{a}\\ \tilde{\varphi}\end{pmatrix} = \begin{pmatrix}a_1\\ \varphi_1\end{pmatrix}\exp(\sigma t + \mathrm{i}K\xi) . \tag{8.205}$$

The stability of the uniform solution depends on the sign of the real part of the growth-rate coefficient σ. To compute σ we substitute the perturbation (8.205) into the linearized equations (8.203) and (8.204) and obtain the following formula for σ

$$\sigma^2 = \beta_\mathrm{d}^2 K^2\left(\frac{2\gamma_\mathrm{n}}{\beta_\mathrm{d}} a_0^2 - K^2\right) . \tag{8.206}$$

This shows that the sign of the $\beta_\mathrm{d}\gamma_\mathrm{n}$ product is crucial for wave-train stability. If $\beta_\mathrm{d}\gamma_\mathrm{n} < 0$ then σ is always an imaginary number, and a uniform wave train is stable to small perturbations of any wavelength; if $\beta_\mathrm{d}\gamma_\mathrm{n} > 0$ then in the case that

$$K < K_\mathrm{cr} = \sqrt{\frac{2\gamma_\mathrm{n}}{\beta_\mathrm{d}}}\, a_0 \tag{8.207}$$

σ is real, and a long-wavelength instability occurs.

This heuristic derivation shows how the equation for the evolution of the wave-train envelope arises. The NLS equation has two parameters: β_d, γ_n. Eventually, the parameter β_d can be calculated from the linear dispersion relation discussed in detail earlier. However, the parameter γ_n has to be calculated from more-systematic, nonlinear arguments.

The general method of derivation is often given the name of the *method of multiple scales* [8.101]. A specific multiscale technique for weakly nonlinear oscillations of bubbles was developed in [8.105, 106]. This technique has been applied to analyze pressure-wave propagation in bubbly liquids.

In [8.107] the NLS equation describing the propagation of weakly nonlinear modulation waves in bubbly liquids was obtained for the first time. It was derived

Amazon EX1014 Page 299

using the multiple asymptotic technique from the governing continuum equations for bubbly liquids presented in detail in this chapter. The NLS equation was applied for determination of the regions of modulation stability/instability in the parametric plane for mono- and polydisperse bubbly liquids.

To understand the behavior of the coefficients of the NLS equation one can consider the simplified model of a monodisperse system presented before. For this we note that the dispersion relation for bubbly liquids with compressible carrier liquid has two branches (Fig. 8.13). The low-frequency branch is responsible for bubble compressibility, and the high-frequency branch is due to liquid compressibility.

The first (low-frequency) branch corresponds to frequencies from zero to ω_b, which is the resonance frequency for bubbles of given size, the second (high-frequency) branch corresponds to frequencies from some $\omega_\star$ to infinity. There are no solutions in the form of spatially oscillating waves for frequencies between ω_b and $\omega_\star$; in this range there are exponentially decaying solutions only. This region is known as the *window of acoustic non-transparency*.

The coefficient β_d is calculated as shown in (8.197). For bubbly liquids this quantity is always positive for the low-frequency branch and always negative for the high-frequency branch.

The coefficient γ_n (see (8.197)) represents the nonlinearity of the system and is a complicated function of frequency ω. If it is positive, then long-wavelength modulation instability occurs. An important region of instability appears near the frequency ω_s, where $C_g(\omega_s) = C_e$, with C_e being the equilibrium speed of sound ($C_e = \omega/k$ for $\omega \to 0$).

For such frequencies the coefficient γ_n has a singularity and changes sign when the frequency is changing around this point. Physically this corresponds to the Benjamin–Feir instability, and can be explained by transfer of energy from mode 0 (DC mode, or mode of zero frequency, for which perturbations propagate with velocity C_e) to the principal mode of the wave train, which moves with the group velocity C_g.

Accounting for a small dissipation in bubbly liquids leads to the Landau–Ginzburg equation, which describes how the wave amplitude should decay due to dissipation. This part includes the dissipation effect due to viscosity and due to internal bubble heat transfer. The difference between the viscous and thermal effects for bubbles is that for an oscillating bubble there is a $\pi/2$ shift in phase between the bubble volume and the heat flux, while the loss of energy due to viscous dissipation occurs in phase with bubble oscillation. This phase shift results in the effect that the pressure in the mixture has some additional shift in phase relative to the mixture density (determined mainly by the bubble volume). This, in fact, can be treated as a weak dispersive effect and included to the dispersion relation in the third-order approximation.

It is interesting to note that the system of governing equations presented can be also obtained as Euler equations for some Lagrangian [8.108, 109]. The variation formulation might be very useful for the analysis of nonlinear acoustics phenomena in bubbly liquids.

8.10.5 Interaction of Nonlinear Waves. Sound–Ultrasound Interaction

The nature of the interactions among individual wave components is quite simple and can be explained by considering the nature of dispersive waves in general.

Suppose u represents some property of the fluid motion, for example the fluid velocity. Then infinitesimal (linear) plane one-dimensional sound waves in a pure liquid are governed by the classical linear wave equation

$$\frac{\partial^2 u}{\partial t^2} - c^2 \frac{\partial^2 u}{\partial x^2} = 0 \,, \tag{8.208}$$

where c is the speed of sound. This equation has elementary solutions of the type

$$u = A \exp[\mathrm{i}(kx \pm \omega t)], \quad \omega = ck \,, \tag{8.209}$$

describing the propagation of a sinusoidal wave with a definite speed c independent of the wavelength ($\lambda = 2\pi/k$, k is the wavenumber). These waves are called nondispersive.

However, many of the waves encountered in fluids do not obey the classical wave equation, and their phase velocity may not be independent of the wavenumber. An example is wave propagation in bubbly liquids.

More generally, for an infinitesimal disturbance, the governing equation is of the type

$$\mathrm{L}(u) = 0 \,, \tag{8.210}$$

where L is a linear operator involving derivatives with respect to position and time. The form of this operator depends upon the fluid system and the particular type of wave motion considered. Again, this linear equation admits solutions of the form

$$u = A \exp[\mathrm{i}(kx \pm \omega t)] \,, \tag{8.211}$$

provided that ω and k satisfy a so-called dispersion relation

$$D(\omega, k) = 0 \tag{8.212}$$

Amazon EX1014 Page 300

that is characteristic for the fluid system and of the type of wave motion considered.

These infinitesimal wave solutions are useful since in many circumstances the nonlinear effects are weak. Thus, the infinitesimal amplitude solution in many cases represents a very useful first approximation to the motion. The interaction effects can be accounted for by considering an equation of the form

$$\mathrm{L}(u) = \epsilon \mathrm{N}(u) \,, \tag{8.213}$$

where N is some nonlinear operator whose precise nature again depends upon the particular fluid system considered, and ϵ is a small parameter characterizing the amplitude of the motion. Solutions to this equation can be built by successive approximation.

Let us consider two interacting wave trains, given to a first approximation by solutions to the linear equation (8.210):

$$\begin{aligned} u_1 &= A_1 \exp[\mathrm{i}(k_1 x - \omega_1 t)] \,, \\ u_2 &= A_2 \exp[\mathrm{i}(k_2 x - \omega_2 t)] \,, \end{aligned} \tag{8.214}$$

where the individual wave numbers and frequencies are related by the dispersion relation (8.212): $D(\omega_i, k_i) = 0$; $i = 1, 2$. These expressions are to be substituted into the small nonlinear term $\epsilon \mathrm{N}(u)$ of (8.213).

If the lowest-order nonlinearity is quadratic, this substitution leads to expressions of the type

$$\sim \exp \mathrm{i}[(k_1 \pm k_2)x - (\omega_1 \pm \omega_2)t] \,. \tag{8.215}$$

These terms act as a small-amplitude forcing function to the linear system and provide an excitation at the wave numbers ($k_3 = k_1 \pm k_2$) and frequencies ($\omega_3 = \omega_1 \pm \omega_2$). In general, the response of the linear system to this forcing is expected to be small ($\sim \epsilon$). However, if the wavelength and frequency of the forcing are related by the dispersion relation (8.212) as well: $D(\omega_3, k_3) = 0$, then we have a case which normally is referred to as nonlinear resonance wave interaction. Similarly to a well-known resonance behavior of a linear oscillator, the amplitude of the third component

$$u_3 = A_3 \exp[\mathrm{i}(k_3 x - \omega_3 t)] \tag{8.216}$$

grows linearly at the beginning. Later the energy drain from the first two components begins to reduce their amplitudes and consequently the amplitude of the forcing function.

Let us now consider a set of three wave trains undergoing resonant interactions. The solutions representing these wave trains would be expected to look like the solutions of the linear problem, although the amplitudes $A_i (i = 1, 2, 3)$ may possibly vary slowly with time:

$$\begin{aligned} u = \sum_{i=1}^{3} \big\{ & A_i(\epsilon t) \exp[\mathrm{i}(k_i x - \omega_i t)] \\ & + A_i^*(\epsilon t) \exp[-\mathrm{i}(k_i x - \omega_i t)] \big\} \,. \end{aligned} \tag{8.217}$$

Here it is used that u is necessarily real. Substitution of this set into (8.213) with subsequent averaging over a few wavelengths leads to a system of equations for the amplitudes of the interacting wave trains. This system basically describes the energy balance between these wave components.

Thus, the existence of energy transfer of this kind clearly depends upon the existence of these resonance conditions. The classic example of dispersion relations which allow for such resonance conditions are capillary gravity waves on the surface of deep water [8.110]. This example, however, is far from the scope of the present section.

In this section the nonlinear acoustics of liquids with bubbles is discussed as an example of a multiphase fluids with complicated and pronounced nonlinearity and dispersion. The dispersion encountered there may also lead to a special nonlinear wave interaction called *long-wave–short-wave resonance* in this context.

In [8.111] it was suggested a new form of triad resonance between three waves of wave numbers k_1, k_2, and k_3 and frequencies ω_1, ω_2, and ω_3, respectively, such that

$$k_1 = k_2 + k_3, \quad \omega_1 = \omega_2 + \omega_3 \,. \tag{8.218}$$

It was suggested to consider k_1 and k_2 to be very close: $k_1 = k + \varepsilon$, $k_2 = k - \varepsilon$ and $k_3 = 2\varepsilon$ ($\varepsilon \ll k$). The resonance conditions (8.218) are automatically achieved if

$$\omega(k + \varepsilon) - \omega(k - \varepsilon) = \omega_3 \tag{8.219}$$

or

$$2\varepsilon \frac{\mathrm{d}\omega}{\mathrm{d}k} = \omega_3 \,. \tag{8.220}$$

That means the group velocity of the short wave (wave number k) equals the phase velocity of the long wave (wave number 2ε). It is called the long-wave–short-wave resonance. At first sight this resonance would appear hard to achieve but it is clearly possible from Fig. 8.13.

Let us identify the lower (or low-frequency) and upper (or high-frequency) branches of the dispersion relation with subscripts "−" and "+", respectively. The

Amazon EX1014 Page 301

long-wave asymptotics of the low-frequency branch, $\omega_l(k_l) = \omega_- \,|_{k\to 0}$, and the short-wave asymptotics of the high-frequency branch, $\omega_s(k_s) = \omega_+ \,|_{k\to\infty}$, can be written as follows:

$$\omega_l = c_e k_l + O(k_l^3), \quad \omega_s = c_f k_s + O(k_s^{-1}) \,, \quad (8.221)$$

where

$$c_e = \frac{\omega_l}{k_l}\,|_{k_l\to 0}, \quad c_f = \frac{d\omega_s}{dk_s}\,|_{k_s\to\infty} \,, \quad (8.222)$$

are the *equilibrium* and the *frozen* speeds of sound in the bubbly mixture.

It is easy to see that dispersion relation (8.162) allows the existence of the long-wave–short-wave resonance. Since $c_f > c_e$, there is always some wave number k_s and frequency ω_s (Fig. 8.13) such that its group velocity is equal to the equilibrium velocity of the mixture.

It should be noted that the long-wave–short-wave resonance in bubbly liquids has nothing to do with the resonance of bubble oscillations. Suppose we consider water with air bubbles of radius $R_0 = 0.1$ mm under normal conditions ($p_0 = 0.1$ MPa, $\rho_{l0} = 10^3$ kg/m^3) and with a volume gas content $\alpha_{g0} = 2.22\times 10^{-4}$. The wavelengths of the short and long waves are then $\lambda_s \approx 0.67$ cm and $\lambda_l \approx 6.7$ m, respectively. The equilibrium speed of sound is $c_e \approx 730$ m/s. Thus, the frequency of the long wave is $f_l = c_e/\lambda_l \approx 110$ Hz (audible sound). Obviously, the short-wave frequency $f_s \geq 35.6$ kHz lies in the ultrasound region. Moreover, a decrease in the bubble radius R_0 leads to increasing the short-wave frequency f_s. Hence, the long-wave–short-wave interaction in a bubbly fluid can be considered as the interaction of ultrasound and audible sound propagating in this medium.

The long-wave–short-wave resonance interaction for pressure waves in bubbly liquids was investigated in [8.112–115] using the method of multiple scales. In particular, it was shown that in a nondissipative bubbly medium this type of resonance interaction is described by the following equations [8.116]

$$\frac{\partial L}{\partial \tau} + \frac{\alpha}{2c_e}\frac{\partial |S|^2}{\partial \xi} = 0, \quad i\frac{\partial S}{\partial \tau} + \beta\frac{\partial^2 S}{\partial \xi^2} = \delta L S, \quad (8.223)$$

where L and S are normalized amplitudes of the long- and short-wave pressure perturbations, τ is the (slow) time and ξ is the space coordinate in the frame moving with the group velocity; α and β are parameters of interaction.

It turns out that in bubbly fluids, parameters of interaction can vanish simultaneously at some specific ultrasound frequency [8.115]. The interaction between sound and ultrasound is then *degenerate*, i. e., the equations for interaction are separated. However, such a degeneracy does not mean the absence of interaction. The quasi-monochromatic ultrasonic signal will still generate sound but of much smaller intensity than in the nondegenerate case.

8.11 Sonoluminescence

Sound waves not only give rise to self-steepening and shock waves but may even become the driving agent to the emission of light, a phenomenon called sonoluminescence that is mediated by bubbles in the liquid that are driven to strong oscillations and collapse [8.20–30]. The detection of the conditions where a single bubble can be trapped in the pressure antinode of a standing sound wave [8.117] has furthered this field considerably. In Fig. 8.16 a basic arrangement for single-bubble sonoluminescence (SBSL) can be seen where a bubble is trapped in a rectangular container filled with water.

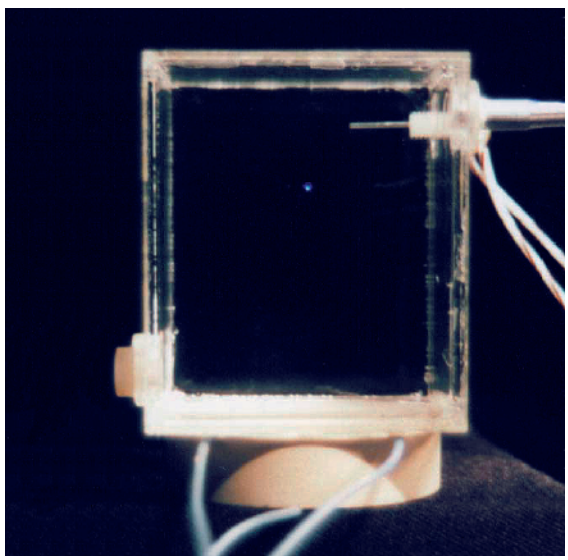


Fig. 8.16 Photograph of a rectangular container with light-emitting bubble. There is only one transducer glued to the bottom plate of the container (dimensions: 50 mm × 50 mm × 60 mm). The piezoelectric transducer (dimensions: height 12 mm, diameter 47 mm) sets up a sound field of high pressure (approx. 1.3 bar) at a frequency of approx. 21 kHz. (Courtesy of R. Geisler)

Amazon EX1014 Page 302

The sound field is produced by a circular disc of piezoelectric material glued to the bottom of the container. The bright spot in the upper part of the container is the light from the bubble. It is of blueish white color. The needle sticking out into the container in the upper left part of the figure is a platinum wire for producing a bubble via a current pulse. The bubble is then driven via acoustic radiation forces into its position where it is trapped almost forever. The bubble exerts large oscillations that can be photographed [8.118]. Figure 8.17 shows a sequence of the bubble oscillation of a light-emitting bubble. A full cycle is shown after which the oscillation repeats. Indeed, this repetition has been used to sample the series of photographs by shifting the instant of exposure by 500 ns from frame to frame with respect to the phase of the sound wave. The camera is looking directly into the illuminating light source (back illumination). The bubble then appears dark on a bright background because the light is deflected off its surface. The white spot in the middle of the bubble results from the light passing the spherical bubble undeflected.

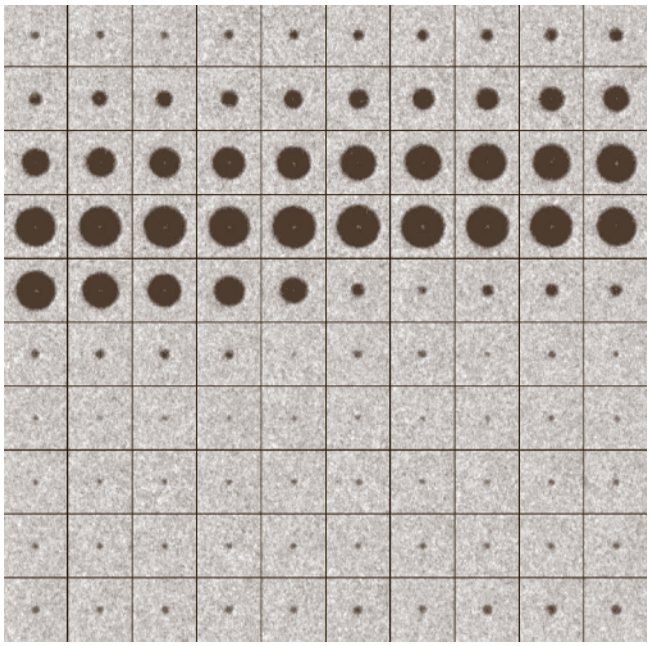


Fig. 8.17 Photographic series of a trapped, sonoluminescing bubble driven at 21.4 kHz and a pressure amplitude of 132 kPa. The interframe time is 500 ns. Picture size is 160 × 160 µm. (Courtesy of R. Geisler)

Upon the first large collapse a shock wave is radiated (Fig. 8.18). At the 30 ns interframe time the 12 frames given cover 330 ns, less than one interframe time Fig. 8.17. The shock wave becomes visible via deflection of the illuminating light. The bubble expands on a much slower time scale than the speed of the shock wave and is seen as a tiny black spot growing in the middle of the ring of the shock wave. Measurements of the shock velocity near the bubble at collapse (average from 6 to 73 µm) leads to about 2000 m/s, giving a shock pressure of about 5500 bar [8.119]. Higher-resolution measurements have increased these values to about 4000 m/s and 60 kbar [8.120].

The bubble oscillation as measured photographically can be compared with theoretical models for the motion of a bubble in a liquid. A comparison is shown in Fig. 8.19. The overall curve is reproduced well, although the steep collapse is not resolved experimentally. For details the reader is referred to [8.81].

There is the question whether shock waves are also emitted into the interior of the bubble [8.121–124]. Theoretically, shock waves occur in certain models, when the collapse is of sufficient intensity. Recently, the problem has been approached by molecular dynamics calculations [8.125–128]. As the number of molecules

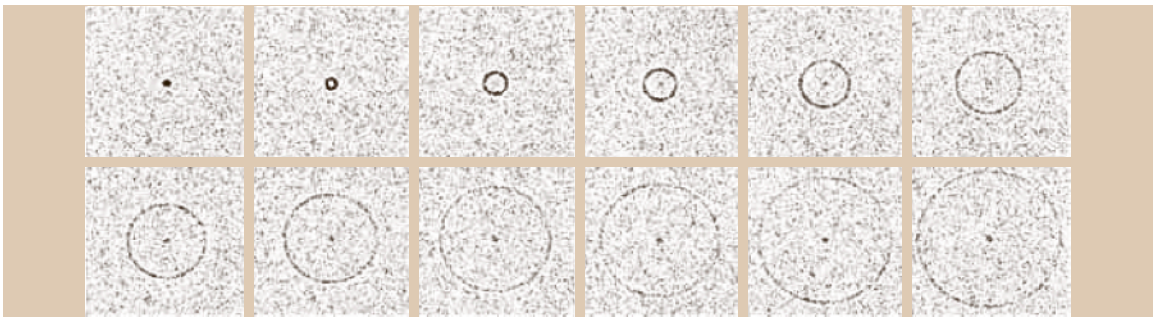


Fig. 8.18 Shock wave from a trapped, sonoluminescing bubble driven at 21.4 kHz and a pressure amplitude of 132 kPa. The interframe time is 30 ns. Picture size is 160 × 160 µm. (Courtesy of R. Geisler)

Amazon EX1014 Page 303

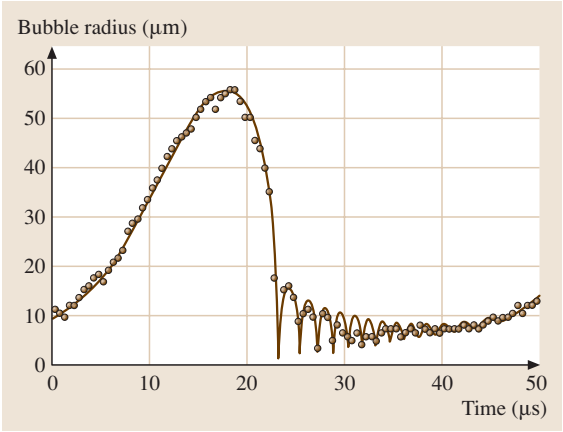


Fig. 8.19 Radius-time curve of a trapped bubble in a water-glycerine mixture derived from photographic observations. A numerically calculated curve (Gilmore model) is superimposed on the experimental data points (*open circles*). The calculation is based on the following parameters: driving frequency $f_0 = 21.4\,\text{kHz}$, ambient pressure $p_0 = 100\,\text{kPa}$, driving pressure $p_0 = 132\,\text{kPa}$, vapor pressure $p_v = 0$, equilibrium radius $R_n = 8.1\,\mu\text{m}$, density of the liquid $\rho = 1000\,\text{kg/m}^3$, viscosity $\mu = 0.0018\,\text{Ns/m}^2$ (measured) and surface tension $\sigma = 0.0725\,\text{N/m}$. The gas within the bubble is assumed to obey the adiabatic equation of state for an ideal gas with $\kappa = 1.2$. (Measured points courtesy of R. Geisler)

in a small bubble is relatively small, around 10^9 to 10^{10} molecules, this approach promises progress for the question of internal shock waves. At present molecular dynamics simulations are feasible with several million particles inside the bubble. Figure 8.20 gives a graphical view on the internal temperature distribution inside a collapsing sonoluminescence bubble with near-adiabatic conditions (reflection of the molecules at the inner boundary of the bubble) for six different times around maximum compression. The liquid

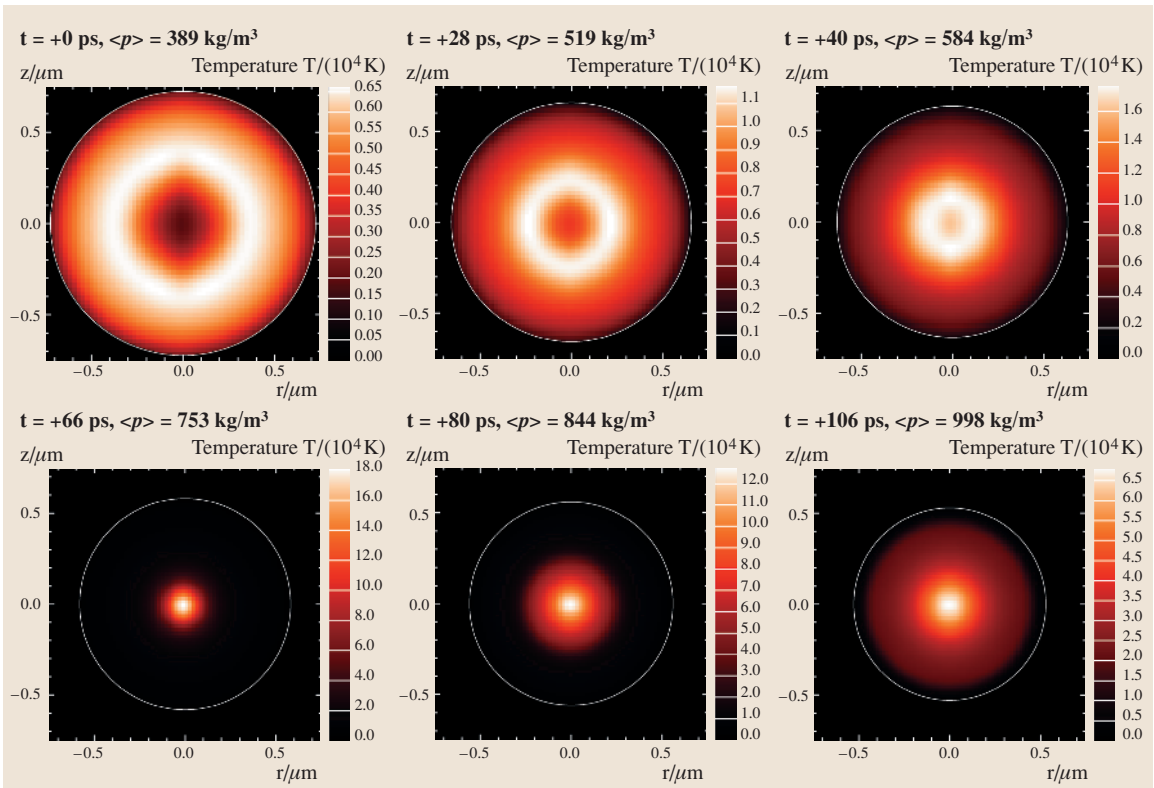


Fig. 8.20 Temperature distribution inside a collapsing sonoluminescence bubble filled with argon, one million particles, radius of the bubble at rest 4.5 μm, sound pressure amplitude 130 kPa, sound field frequency 26.5 kHz, total time covered 106 ps. (Courtesy of B. Metten [8.126])

Amazon EX1014 Page 304

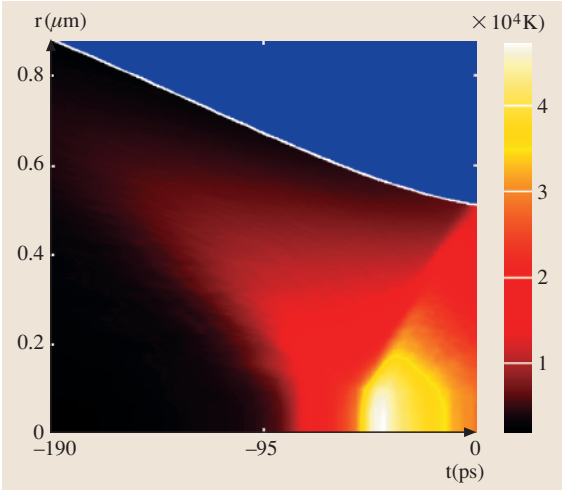


Fig. 8.21 Distribution of temperature inside an acoustically driven bubble in dependence on time. Molecular dynamics calculation with argon and water vapor including chemical reactions. (after [8.128])

motion and the inner molecular dynamics calculations are coupled via the gas pressure (at the interface), which is determined from the molecular dynamics of the 10^6 particles and inserted into the Rayleigh–Plesset equation giving the motion of the bubble wall. A strong focusing of energy inside the bubble is observed under these conditions. An inward-traveling compression wave focuses at the center and yields a core temperature of more than 10^5 K. This temperature is an overestimate as no energy-consuming effects are included.

The temperature variation inside the bubble with time can be visualized for spherical bubbles in a single picture in the following way (Fig. 8.21). The vertical axis represents the radial direction from the bubble center, the horizontal axis represents time and the color gives the temperature in Kelvin according to the color-coded scale (bar aside the figure). The upper solid line in the figure depicts the bubble wall; the blue part is water. In this case an argon bubble with water vapor is taken and chemical reactions are included. Then the temperature is lowered significantly by the endothermal processes of chemical species formation, for instance of OH^- radicals. The temperature drops to about 40 000 K in the center [8.128].

8.12 Acoustic Chaos

Nonlinearity in acoustics not only leads to shock waves and, as just demonstrated, to light emission, but to even deeper questions of nonlinear physics in general [8.4]. In his curiosity, man wants to know the future. Knowledge of the future may also be of help to master one's life by taking proper provisions. The question therefore arises: how far can we look into the future and where are the difficulties in doing so? This is the question of predictability or unpredictability. In the attempt to solve this question we find deterministic systems, stochastic systems and, nowadays, chaotic systems. The latter are special in that they combine deterministic laws that nevertheless give unpredictable output. They thus form a link between deterministic and stochastic systems.

8.12.1 Methods of Chaos Physics

A description of the methods developed to handle chaotic systems, in particular in acoustics, has been given in [8.32]. The main question in the context

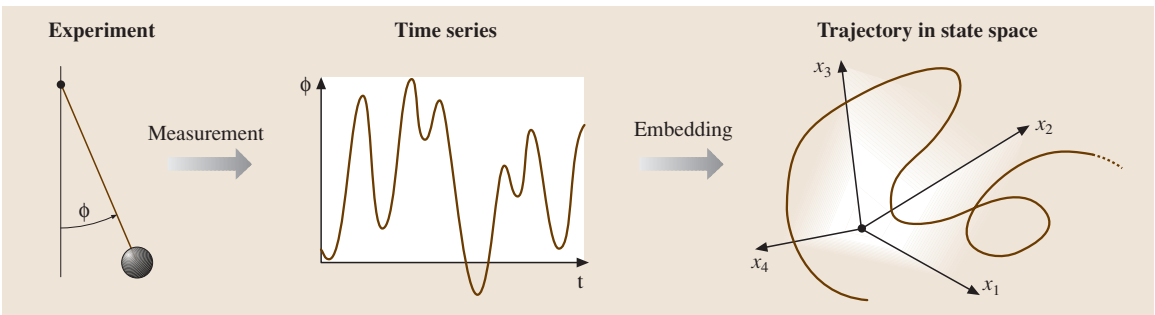


Fig. 8.22 Visualization of the embedding procedure

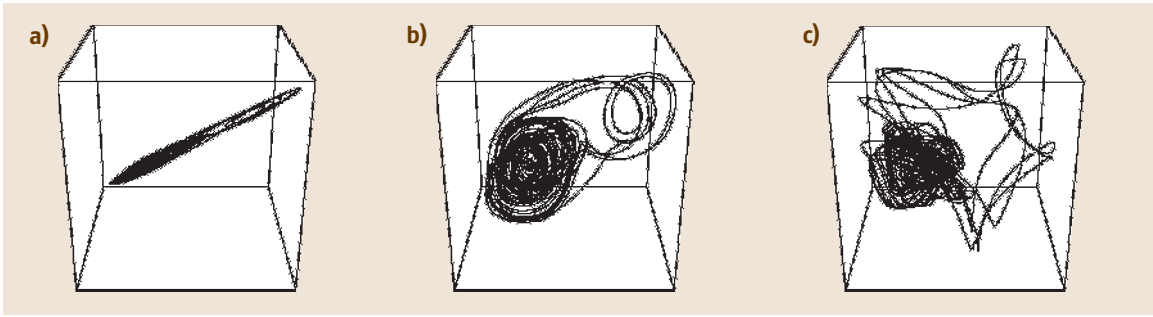


Fig. 8.23 Three embeddings with different delay times t_l for experimental data obtained from a chaotically oscillating, periodically driven pendulum. (Courtesy of U. Parlitz)

of experiments is how to connect the typically one-dimensional measurements (a time series) with the high-dimensional state space of theory (given by the number of variables describing the system). This is done by what is called *embedding* Fig. 8.22 [8.129, 130] and has led to a new field called *nonlinear time-series analysis* [8.131–133].

The embedding procedure runs as follows. Let $\{p(kt_s), k = 1, 2, \ldots, N\}$ be the measured time series, then an embedding into a n-dimensional state space is achieved by grouping n elements each of the time series to vectors $\boldsymbol{p}_k^{(n)} = [p(kt_s), p(kt_s + t_l), \ldots, p(kt_s + (n-1)t_l)]$, $k = 1, 2, \ldots, N-n$, in the n-dimensional state space. There t_s is the sampling interval at which samples of the variable p are taken. The delay time t_l is usually taken as a multiple of t_s, $t_l = lt_s$, $l = 1, 2, \ldots$, to avoid interpolation. The sampling time t_s, the delay time t_l and the embedding dimension n must all be chosen properly according to the problem under investigation. Figure 8.23 demonstrates the effect of different delay times with experimental data from a chaotically oscillating periodically driven pendulum. When the delay time t_l is too small then from one embedding vector to the next there is little difference and the embedded points all lie along the diagonal in the embedding space Fig. 8.23a. On the other hand, when the delay time t_l is too large, the reconstructed trajectory obtained by connecting successive vectors in the embedding space becomes folded and the reconstruction becomes fuzzy Fig. 8.23c. The embedding dimension n is usually not known beforehand when an unknown system is investigated for its properties. Therefore the embedding is done for increasing n until some criterion is fulfilled. The basic idea for a criterion is that a structure in the point set obtained by the embedding should appear. Then some law must be at work that generates it. The task after embedding is therefore to find and characterize the structure and to find the laws behind it. The characterization of the point set obtained can be done by determining its static structure (e.g., its dimension) and its dynamic structure (e.g., its expansion properties via the dynamics of nearby points).

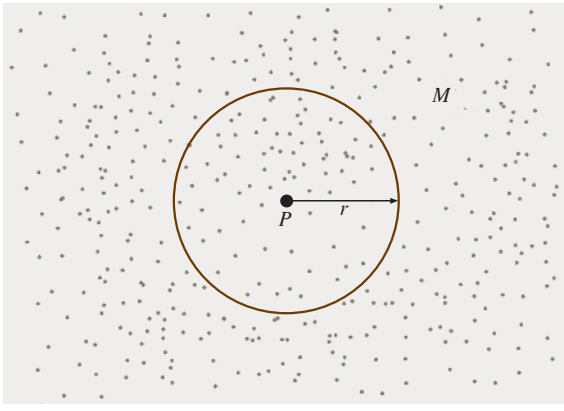


Fig. 8.24 Notations for the definition of the pointwise dimension

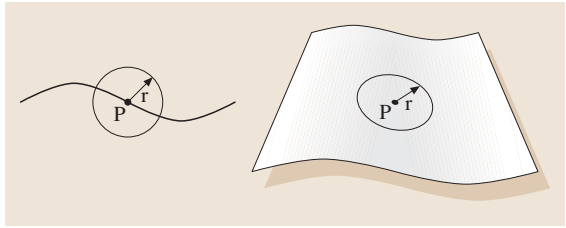


Fig. 8.25 Example of pointwise dimensions for one-dimensional (a curve) and two-dimensional (a surface) point sets

The dimension easiest to understand is the pointwise dimension. It is defined at a point P of a point set M by $N(r) \sim r^D$, $r \to 0$, where $N(r)$ is the number of



Fig. 8.26 The point set of a strange attractor of an experimental, driven pendulum. (Courtesy of M. Kaufmann)

points of the set M inside the ball of radius r around P (Fig. 8.24). Examples for a line and a surface give the right integer dimensions of one and two (Fig. 8.25), because for a line we have $N(r) \sim r^1$ for $r \to 0$ and thus $D = 1$, and for a surface we have $N(r) \sim r^2$ for $r \to 0$ and thus $D = 2$.

Chaotic or strange attractors usually give a fractal (noninteger) dimension. The pointwise dimension may not be the same in this case for each point P. The distribution of dimensions then gives a measure of the inhomogeneity of the point set. Figure 8.26 gives an example of a fractal point set. It has been obtained by sampling the angle and the angular velocity of a pendulum at a given phase of the periodic driving for parameters in a chaotic regime.

To investigate the dynamic properties of a (strange or chaotic) set the succession of the points must be retained. As chaotic dynamics is brought about by a stretching and folding mechanism and shows sensitive dependence on initial conditions (see, e.g., [8.32]) the behavior of two nearby points is of interest: do they separate or approach under the dynamics? This

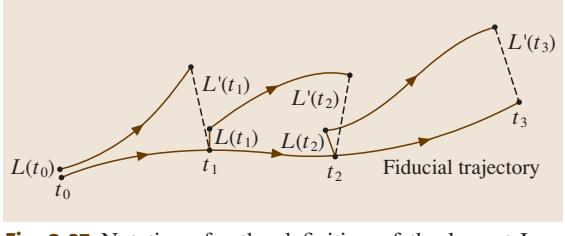


Fig. 8.27 Notations for the definition of the largest Lyapunov exponent

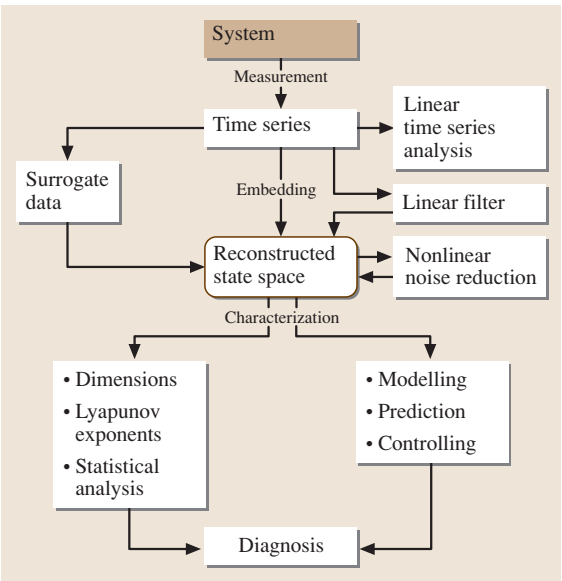


Fig. 8.28 Operations in nonlinear time-series analysis. (Courtesy of U. Parlitz)

behavior is quantified by the notion of the Lyapunov exponent. In Fig. 8.27 the calculation scheme [8.134] is depicted. It gives the maximum Lyapunov exponent via the formula

$$\lambda_{\max} = \frac{1}{t_m - t_0} \sum_{k=1}^{m} \log_2 \frac{L'(t_k)}{L(t_{k-1})} \quad \left[\frac{\text{bits}}{\text{s}}\right]. \qquad (8.224)$$

As space does not permit us to dig deeper into the operations possible with embedded data, only a graph depicting the possible operations in nonlinear time-series analysis is given in Fig. 8.28. Starting from the time series obtained by some measurement, the usual approach is to do a linear time-series analysis, for instance by calculating the Fourier transform or some correlation. The new way for chaotic systems proceeds via embedding to a reconstructed state space. There may be some filtering involved in between, but this is a dangerous operation as the results are often difficult to predict. For the surrogate data operation and nonlinear noise reduction the reader is referred to [8.131–133]. From the characterization operations we have mentioned here the dimension estimation and the largest Lyapunov exponent. Various statistical analyses can be done and the data can also be used for modeling, prediction and controlling the system. Overall, nonlinear time series analysis is a new diagnostic tool for describing (nonlinear) systems.

Amazon EX1014 Page 307

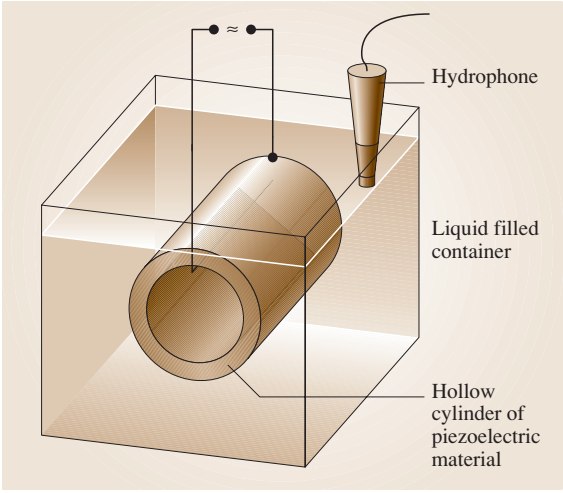


Fig. 8.29 Cylindrical transducer submerged in water for bubble oscillation, cavitation noise, and sonoluminescence studies

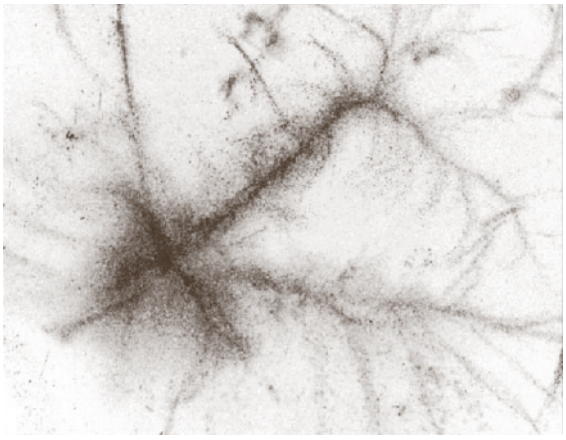
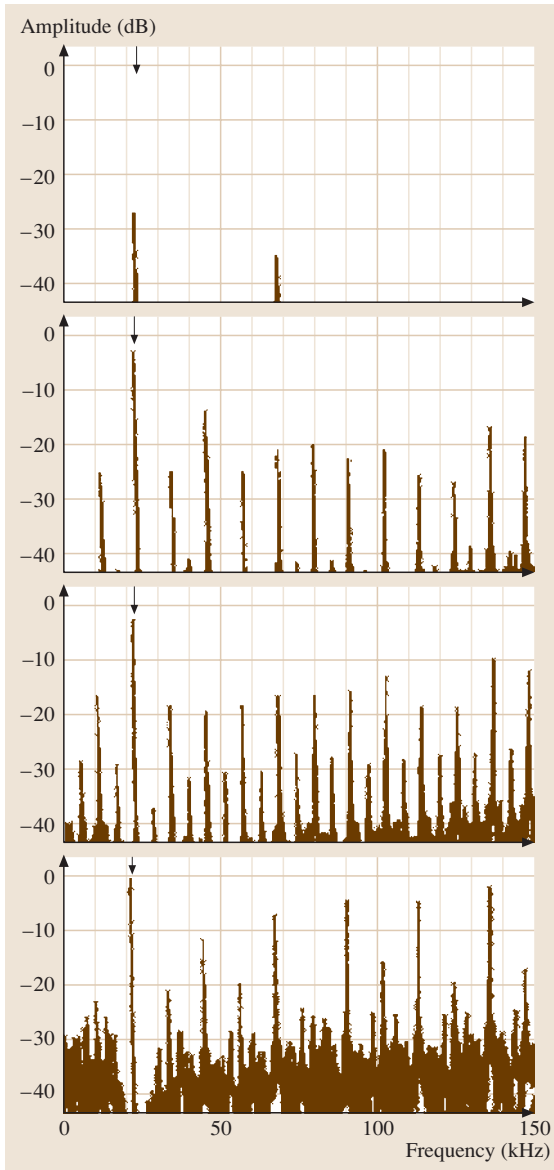


Fig. 8.30 Example of the filamentary bubble pattern (acoustic Lichtenberg figure) inside the cylinder in the projection along the axis of the transducer. (Courtesy of A. Billo)

Fig. 8.31 Power spectra of cavitation noise taken at a driving frequency of $f_0 = 23\,\text{kHz}$, marked in the figures by small triangle. The driving pressure was increased from one graph to the next, giving first a periodic, anharmonic signal (*top*), then subharmonic motion with lines at multiples of $f_0/2$ (period-2 motion, *top next*), then period-4 motion with lines at multiples of $f_0/4$ (*third plot*) and finally a broadband spectrum indicative of chaotic behavior (*bottom*)▶

8.12.2 Chaotic Sound Waves

One of the first examples of chaotic dynamics and where these methods were first applied was acoustic cavitation [8.4, 135, 136]. To investigate this phenomenon, the rupture of liquids by sound waves and the phenomena associated with it, an experimental arrangement as depicted in Fig. 8.29 was used. A cylindrical transducer of piezoelectric material is used to generate a strong sound field in water. A typical transducer was of 76 mm



Amazon EX1014 Page 308

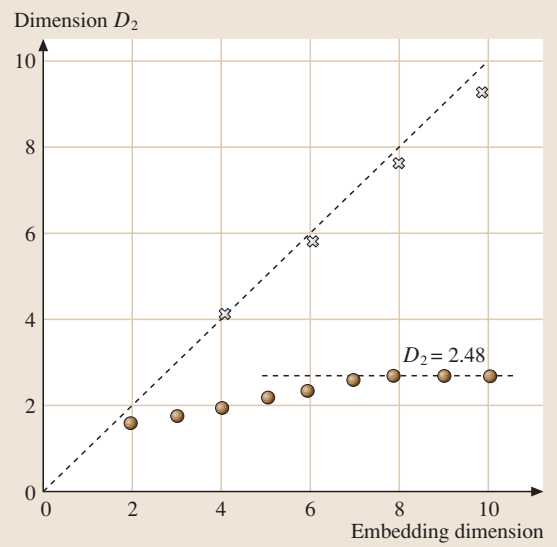


Fig. 8.32 Dimension estimation by embedding experimental acoustic cavitation sound pressure data into spaces of increasing dimension (*dots*). The *crosses* (×) are from an experiment, where noise from a noise generator has been embedded

length, 76 mm inner diameter, and 5 mm wall thickness submerged in a water-filled glass container. Cylinders of different size were available driven at different frequencies between 7 kHz and 23 kHz. A standing acoustic wave is set up inside the cylinder having its maximum pressure amplitude along the axis of the transducer. A hydrophone monitors the sound output of the liquid. Some electronics and a computer surround the experiment to drive the cylinder and to store the sampled pressure data from the hydrophone. When cavitation is fully developed, a dentritic filamentary bubble pattern is set up in the cylinder (Fig. 8.30).

When the sound field amplitude is raised the whole bubble field undergoes a period-doubling cascade to chaos [8.81, 137], a strong indication that chaotic dynamics really has been reached and that the broadband spectrum then encountered (Fig. 8.31) is not of stochastic origin. The cascade of period-doubled sound in the liquid has its origin in the cascade of period-doubled oscillations of the nonlinearly oscillating bubbles [8.81], and thus shows chaotic sound.

Embedding of the sound data into spaces of increasing dimension yields a structure with low fractal dimensions between two and three (Fig. 8.32). This is a quite surprising result in view of the thousands of oscillating bubbles of different sizes. Indeed, new results on the superposition of the sound output of a population of driven bubbles have indicated that the low dimensionality may be a result of the (weak) synchronization of their motion from the periodic driving and the scale of observation [8.138].

Chaotic sound waves also appear in other contexts [8.139]. In musical acoustics several instruments are susceptible to chaotic sound emission. Examples are the bowed string [8.140, 141], the clarinet [8.142] and gongs and cymbals [8.143].

The human speech production process is intrinsically nonlinear. To produce voice sounds the vocal cords are set into vibration through the air flow between them. The cords are a coupled system of nonlinear oscillators giving rise to bifurcations and chaos [8.144].

Sound can be generated by heat. When a gas-filled tube, closed at one end and open at the other is heated at the closed end and/or cooled at the open end, sound waves are emitted at a sufficiently high temperature difference (Sondhauss and Taconis oscillation). This phenomenon has been used to study its route to chaos [8.145]. It has been used to build a new type of refrigerator and heat pump [8.146].

References

8.1 M.F. Hamilton, D.T. Blackstock (Eds.): *Nonlinear Acoustics* (Academic, San Diego 1998)

8.2 K. Naugolnykh, L. Ostrovsky: *Nonlinear Wave Processes in Acoustics* (Cambridge Univ. Press, Cambridge 1998)

8.3 R.T. Beyer: *Nonlinear Acoustics* (Acoust. Soc. Am., Woodbury 1997)

8.4 W. Lauterborn, T. Kurz, U. Parlitz: Experimental nonlinear physics, Int. J. Bifurcation Chaos **7**, 2003–2033 (1997)

8.5 A.L. Thuras, R.T. Jenkins, H.T. O'Neil: Extraneous frequencies generated in air carrying intense sound waves, J. Acoust. Soc. Am. **6**, 173–180 (1935)

8.6 D.T. Blackstock, M.J. Crocker, D.G. Crighton, E.C. Everbach, M.A. Breazeale, A.B. Coppens, A.A. Atchley, M.F. Hamilton, W.E. Zorumski, W. Lauterborn, K.S. Suslick, L.A. Crum: Part II, Nonlinear Acoustics and Cavitation. In: *Encyclopedia of Acoustics*, Vol. 281, ed. by M.J. Crocker (Wiley, New York 1997) pp. 191–281

Amazon EX1014 Page 309

8.7 N.S. Bakhvalov, Y.M. Zhileikin, E.A. Zabolotskaya: *Nonlinear Theory of Sound Beams* (American Institute of Physics, Melville 1987)
8.8 B.K. Novikov, O.V. Rudenko, V.I. Timoshenko: *Nonlinear Underwater Acoustics* (American Institute of Physics, New York 1987)
8.9 O.V. Rudenko, S.I. Soluyan: *Theoretical Foundations of Nonlinear Acoustics* (Consultants Bureau, London 1977)
8.10 G.B. Whitham: *Linear and Nonlinear Waves* (Wiley, London 1974)
8.11 L.D. Rozenberg (Ed.): *High-Intensity Ultrasonic Fields* (Plenum, New York 1971)
8.12 M.F. Hamilton, D.T. Blackstock (Eds.): *Frontiers of Nonlinear Acoustics* (Elsevier, London 1990)
8.13 H. Hobaek (Ed.): *Advances in Nonlinear Acoustics* (World Scientific, Singapore 1993)
8.14 R.J. Wei (Ed.): *Nonlinear Acoustics in Perspective* (Nanjing Univ. Press, Nanjing 1996)
8.15 W. Lauterborn, T. Kurz (Eds.): *Nonlinear Acoustics at the Turn of the Millennium* (American Institute of Physics, Melville 2000)
8.16 O.V. Rudenko, O.A. Sapozhnikov (Eds.): *Nonlinear Acoustics at the Beginning of the 21st Century* (Faculty of Physics, Moscow State University, Moscow 2002)
8.17 S. Makarov, M. Ochmann: Nonlinear and thermoviscous phenomena in acoustics, Part I, Acustica **82**, 579–606 (1996)
8.18 S. Makarov, M. Ochmann: Nonlinear and thermoviscous phenomena in acoustics, Part II, Acustica **83**, 197–222 (1997)
8.19 S. Makarov, M. Ochmann: Nonlinear and thermoviscous phenomena in acoustics, Part III, Acustica **83**, 827–864 (1997)
8.20 C.E. Brennen: *Cavitation and Bubble Dynamics* (Oxford Univ. Press, Oxford 1995)
8.21 T.G. Leighton: *The Acoustic Bubble* (Academic, London 1994)
8.22 J.R. Blake, J.M. Boulton-Stone, N.H. Thomas (Eds.): *Bubble Dynamics and Interface Phenomena* (Kluwer, Dordrecht 1994)
8.23 F.R. Young: *Cavitation* (McGraw-Hill, London 1989)
8.24 L. van Wijngaarden (Ed.): *Mechanics and Physics of Bubbles in Liquids* (Martinus Nijhoff, The Hague 1982)
8.25 W. Lauterborn (Ed.): *Cavitation and Inhomogeneities in Underwater Acoustics* (Springer, Berlin, Heidelberg 1980)
8.26 E.A. Neppiras: Acoustic cavitation, Phys. Rep. **61**, 159–251 (1980)
8.27 H.G. Flynn: Physics of acoustic cavitation. In: *Physical Acoustics*, ed. by W.P. Mason (Academic, New York 1964) pp. 57–172
8.28 F.R. Young: *Sonoluminescence* (CRC, Boca Raton 2005)
8.29 T.J. Mason, J.P. Lorimer: *Applied Sonochemistry* (Wiley-VCH, Weinheim 2002)
8.30 K.S. Suslick (Ed.): *Ultrasound: Its Chemical, Physical and Biological Effects* (VCH, New York 1988)
8.31 W. Lauterborn: Acoustic chaos. In: *Encyclopedia of Physical Science and Technology*, 3rd edn., ed. by R.A. Meyers (Academic, San Diego 2002) pp. 117–127
8.32 W. Lauterborn, U. Parlitz: Methods of chaos physics and their application to acoustics, J. Acoust. Soc. Am. **84**, 1975–1993 (1988)
8.33 F.E. Fox, W.A. Wallace: Absorption of finite amplitude sound waves, J. Acoust. Soc. Am. **26**, 994–1006 (1954)
8.34 R.T. Beyer: Parameter of nonlinearity in fluids, J. Acoust. Soc. Am. **32**, 719–721 (1960)
8.35 A.B. Coppens, R.T. Beyer, M.B. Seiden, J. Donohue, F. Guepin, R.H. Hodson, C. Townsend: Parameter of nonlinearity. II, J. Acoust. Soc. Am. **38**, 797–804 (1965)
8.36 R.T. Beyer: *Nonlinear Acoustics* (Naval Ship Systems Command, Washington 1974), Table 3-1
8.37 E.C. Everbach: *Tissue Composition Determination via Measurement of the Acoustic Nonlinearity Parameter B/A, Ph.D. Dissertation* (Yale Univ., New Haven 1989) p. 66
8.38 Z. Zhu, M.S. Roos, W.N. Cobb, K. Jensen: Determination of the acoustic nonlinearity parameter B/A from phase measurements, J. Acoust. Soc. Am. **74**, 1518–1521 (1983)
8.39 X. Gong, Z. Zhu, T. Shi, J. Huang: Determination of the acoustic nonlinearity parameter in biological media using FAIS and ITD methods, J. Acoust. Soc. Am. **86**, 1–5 (1989)
8.40 W.K. Law, L.A. Frizell, F. Dunn: Determination of the nonlinearity parameter B/A of biological media, Ultrasound Med. Biol. **11**, 307–318 (1985)
8.41 J. Zhang, F. Dunn: A small volume thermodynamic system for B/A measurement, J. Acoust. Soc. Am. **89**, 73–79 (1991)
8.42 F. Plantier, J.L. Daridon, B. Lagourette: Measurement of the B/A nonlinearity parameter under high pressure: Application to water, J. Acoust. Soc. Am. **111**, 707–715 (2002)
8.43 E.C. Everbach: Parameters of nonlinearity of acoustic media. In: *Encyclopedia of Acoustics*, ed. by M.J. Crocker (Wiley, New York 1997) pp. 219–226
8.44 I. Rudnick: On the attenuation of finite amplitude waves in a liquid, J. Acoust. Soc. Am. **30**, 564–567 (1958)
8.45 J. Banchet, J.D.N. Cheeke: Measurements of the acoustic nonlinearity parameter B/A in solvents: Dependence on chain length and sound velocity, J. Acoust. Soc. Am. **108**, 2754–2758 (2000)
8.46 A.B. Coppens, R.T. Beyer, M.B. Seiden, J. Donohue, F. Guepin, R.H. Hodson, C. Townsend: Parameter of nonlinearity in fluids II, J. Acoust. Soc. Am. **38**, 797–804 (1965)

Amazon EX1014 Page 310

8.47 O. Nomoto: Nonlinear parameter of the 'Rao Liquid', J. Phys. Soc. Jpn. **21**, 569–571 (1966)
8.48 R.T. Beyer: Parameter of nonlinearity in fluids, J. Acoust. Soc. Am. **32**, 719–721 (1960)
8.49 K.L. Narayana, K.M. Swamy: Acoustic nonlinear parameter (B/A) in n-pentane, Acustica **49**, 336–339 (1981)
8.50 S.K. Kor, U.S. Tandon: Scattering of sound by sound from Beyers (B/A) parameters, Acustica **28**, 129–130 (1973)
8.51 K.M. Swamy, K.L. Narayana, P.S. Swamy: A study of (B/A) in liquified gases as a function of temperature and pressure from ultrasonic velocity measurements, Acustica **32**, 339–341 (1975)
8.52 H.A. Kashkooli, P.J. Dolan Jr., C.W. Smith: Measurement of the acoustic nonlinearity parameter in water, methanol, liquid nitrogen, and liquid helium-II by two different methods: A comparison, J. Acoust. Soc. Am. **82**, 2086–2089 (1987)
8.53 R.T. Beyer: The parameter B/A. In: *Nonlinear Acoustics*, ed. by M.F. Hamilton, D.T. Blackstock (Academic, San Diego 1998) pp. 25–39
8.54 L. Bjørnø: Acoustic nonlinearity of bubbly liquids, Appl. Sci. Res. **38**, 291–296 (1982)
8.55 J. Wu, Z. Zhu: Measurement of the effective nonlinearity parameter B/A of water containing trapped cylindrical bubbles, J. Acoust. Soc. Am. **89**, 2634–2639 (1991)
8.56 M.P. Hagelberg, G. Holton, S. Kao: Calculation of B/A for water from measurements of ultrasonic velocity versus temperature and pressure to 10 000 kg/cm^2, J. Acoust. Soc. Am. **41**, 564–567 (1967)
8.57 B. Riemann: Ueber die Fortpflanzung ebener Luftwellen von endlicher Schwingungsweite (On the propagation of plane waves of finite amplitude), Abhandl. Ges. Wiss. Göttingen **8**, 43–65 (1860), in German
8.58 S. Earnshaw: On the mathematical theory of sound, Philos. Trans. R. Soc. London **150**, 133–148 (1860)
8.59 D.T. Blackstock: Propagation of plane sound waves of finite amplitude in nondissipative fluids, J. Acoust. Soc. Am. **34**, 9–30 (1962)
8.60 M.F. Hamilton, D.T. Blackstock: On the coefficient of nonlinearity β in nonlinear acoustics, J. Acoust. Soc. Am. **83**, 74–77 (1988), Erratum, ibid, p. 1976
8.61 D.G. Crighton: Propagation of finite-amplitude waves in fluids. In: *Encyclopedia of Acoustics*, ed. by M.J. Crocker (Wiley, New York 1997) pp. 203–218
8.62 B.D. Cook: New procedure for computing finite-amplitude distortion, J. Acoust. Soc. Am. **34**, 941–946 (1962), see also the footnote on page 312 of 8.1
8.63 W. Keck, R.T. Beyer: Frequency spectrum of finite amplitude ultrasonic waves in liquids, Phys. Fluids **3**, 346–352 (1960)
8.64 L.E. Hargrove: Fourier series for the finite amplitude sound waveform in a dissipationless medium, J. Acoust. Soc. Am. **32**, 511–512 (1960)
8.65 E. Fubini Ghiron: Anomalie nella propagazione di onde acustiche di grande ampiezza (Anomalies in the propagation of acoustic waves of large amplitude), Alta Frequenza **4**, 530–581 (1935), in Italian
8.66 D.T. Blackstock: Nonlinear Acoustics (Theoretical). In: *American Institute of Physics Handbook*, 3rd edn., ed. by D.E. Gray (McGraw Hill, New York 1972) pp. 3/183–3/205
8.67 A. Hirschberg, J. Gilbert, R. Msallam, A.P.J. Wijnands: Shock waves in trombones, J. Acoust. Soc. Am. **99**, 1754–1758 (1996)
8.68 M.J. Lighthill: Viscosity effects in sound waves of finite amplitude. In: *Surveys in Mechanics*, ed. by G.K. Batchelor, R.M. Davies (Cambridge Univ. Press, Cambridge 1956) pp. 249–350
8.69 J. Lighthill: *Waves in Fluids* (Cambridge Univ. Press, Cambridge 1980)
8.70 J.S. Mendousse: Nonlinear dissipative distortion of progressive sound waves at moderate amplitudes, J. Acoust. Soc. Am. **25**, 51–54 (1953)
8.71 Z.A. Gol'dberg: Second approximation acoustic equations and the propagation of plane waves of finite amplitude, Sov. Phys.-Acoust. **2**, 346–350 (1956)
8.72 D.T. Blackstock: Thermoviscous attenuation of plane, periodic, finite amplitude sound waves, J. Acoust. Soc. Am. **36**, 534–542 (1964)
8.73 E. Hopf: The partial differential equation $u_t + uu_x = \mu u_{xx}$, Comm. Pure Appl. Math. **3**, 201–230 (1950)
8.74 J.D. Cole: On a quasi-linear parabolic equation occurring in aerodynamics, Quart. Appl. Math. **9**, 225–236 (1951)
8.75 M. Abramowitz, I.A. Stegun (Eds.): *Handbook of Mathematical Functions* (Dover, New York 1970)
8.76 L.S. Gradsteyn, I.M. Ryshik: *Table of Integrals, Series and Products* (Academic, Orlando 1980)
8.77 D.T. Blackstock: Connection between the Fay and Fubini solutions for plane sound waves of finite amplitude, J. Acoust. Soc. Am. **39**, 1019–1026 (1966)
8.78 R.D. Fay: Plane sound waves of finite amplitude, J. Acoust. Soc. Am. **3**, 222–241 (1931)
8.79 R.V. Khokhlov, S.I. Soluyan: Propagation of acoustic waves of moderate amplitude through dissipative and relaxing media, Acustica **14**, 241–246 (1964)
8.80 I.S. Akhatov, R.I. Nigmatulin, R.T. Lahey Jr.: The analysis of linear and nonlinear bubble cluster dynamics, Multiphase Sci. Technol. **17**, 225–256 (2005)
8.81 W. Lauterborn, T. Kurz, R. Mettin, C.D. Ohl: Experimental and theoretical bubble dynamics, Adv. Chem. Phys. **110**, 295–380 (1999)
8.82 C. Chaussy (Ed.): *Extracorporeal Shock Wave Lithotripsy* (Karger, New York 1986)
8.83 G.A. Askar'yan: Self-focusing of powerful sound during the production of bubbles, J. Exp. Theor. Phys. Lett. **13**, 283–284 (1971)
8.84 P. Ciuti, G. Jernetti, M.S. Sagoo: Optical visualization of non-linear acoustic propagation in cavitating liquids, Ultrasonics **18**, 111–114 (1980)

Amazon EX1014 Page 311

8.85 Yu.A. Kobelev, L.A. Ostrovsky: Nonlinear acoustic phenomena due to bubble drift in a gas-liquid mixture, J. Acoust. Soc. Am. **85**, 621–627 (1989)

8.86 S.L. Lopatnikov: Acoustic phase echo in liquid with gas bubbles, Sov. Tech. Phys. Lett. **6**, 270–271 (1980)

8.87 I.Sh. Akhatov, V.A. Baikov: Propagation of sound perturbations in heterogeneous gas-liquid systems, J. Eng. Phys. **9**, 276–280 (1986)

8.88 I.Sh. Akhatov, V.A. Baikov, R.A. Baikov: Propagation of nonlinear waves in gas-liquid media with a gas content variable in space, Fluid Dyn. **7**, 161–164 (1986)

8.89 E. Zabolotskaya: Nonlinear waves in liquid with gas bubbles, Trudi IOFAN (Institute of General Physics of the Academy of Sciences, Moscow) **18**, 121–155 (1989), in Russian

8.90 I.Akhatov, U. Parlitz, W. Lauterborn: Pattern formation in acoustic cavitation, J. Acoust. Soc. Am. **96**, 3627–3635 (1994)

8.91 I.Akhatov, U. Parlitz, W. Lauterborn: Towards a theory of self-organization phenomena in bubble-liquid mixtures, Phys. Rev. E **54**, 4990–5003 (1996)

8.92 O.A. Druzhinin, L.A. Ostrovsky, A. Prosperetti: Low-frequency acoustic wave generation in a resonant bubble-layer, J. Acoust. Soc. Am. **100**, 3570–3580 (1996)

8.93 L.A. Ostrovsky, A.M. Sutin, I.A. Soustova, A.I. Matveyev, A.I. Potapov: Nonlinear, low-frequency sound generation in a bubble layer: Theory and laboratory experiment, J. Acoust. Soc. Am. **104**, 722–726 (1998)

8.94 R.I. Nigmatulin: *Dynamics of Multiphase Systems* (Hemisphere, New York 1991)

8.95 V.E. Nakoryakov, V.G. Pokusaev, I.R. Shreiber: *Propagation of Waves in Gas- and Vapour-liquid Media* (Institute of Thermophysics, Novosibirsk 1983)

8.96 L. van Wijngaarden: One-dimensional flow of liquids containing small gas bubbles, Ann. Rev. Fluid Mech. **4**, 369–396 (1972)

8.97 U. Parlitz, R. Mettin, S. Luther, I. Akhatov, M. Voss, W. Lauterborn: Spatiotemporal dynamics of acoustic cavitation bubble clouds, Philos. Trans. R. Soc. London Ser. A **357**, 313–334 (1999)

8.98 J.G. McDaniel, I. Akhatov, R.G. Holt: Inviscid dynamics of a wet foam drop with monodisperse bubble size distribution, Phys. Fluids **14**, 1886–1984 (2002)

8.99 A. Prosperetti, A. Lezzi: Bubble dynamics in a compressible liquid. Part 1. First order theory, J. Fluid Mech. **168**, 457–478 (1986)

8.100 R.I. Nigmatulin, I.S. Akhatov, N.K. Vakhitova, R.T. Lahey Jr.: On the forced oscillations of a small gas bubble in a spherical liquid-filled flask, J. Fluid Mech. **414**, 47–73 (2000)

8.101 A. Jeffrey, T. Kawahara: *Asymptotic Methods in Nonlinear Wave Theory* (Pitman, London 1982)

8.102 L. van Wijngaarden: On the equations of motion for mixtures of fluid and gas bubbles, J. Fluid Mech. **33**, 465–474 (1968)

8.103 N.A. Gumerov: Propagation of long waves of finite amplitude in a liquid with polydispersed gas bubbles, J. Appl. Mech. Tech. Phys. **1**, 79–85 (1992)

8.104 A. Hasegawa: *Plasma Instabilities and Nonlinear Effects* (Springer, Berlin, Heidelberg 1975)

8.105 N.A. Gumerov: The weak non-linear fluctuations in the radius of a condensed drop in an acoustic field, J. Appl. Math. Mech. (PMM U.S.S.R.) **53**, 203–211 (1989)

8.106 N.A. Gumerov: Weakly non-linear oscillations of the radius of a vapour bubble in an acoustic field, J. Appl. Math. Mech. **55**, 205–211 (1991)

8.107 N.A. Gumerov: On quasi-monochromatic weakly nonlinear waves in a low-dissipative bubbly liquid, J. Appl. Math. Mech. **56**, 50–59 (1992)

8.108 S. Gavrilyuk: Large amplitude oscillations and their "thermodynamics" for continua with "memory", Euro. J. Mech. B/Fluids **13**, 753–764 (1994)

8.109 S.L. Gavrilyuk, V.M. Teshukov: Generalized vorticity for bubbly liquid and dispersive shallow water equations, Continuum Mech. Thermodyn. **13**, 365–382 (2001)

8.110 L.F. McGoldrick: Resonant interactions among capillary-gravity waves, J. Fluid Mech. **21**, 305–331 (1965)

8.111 D.J. Benney: A general theory for interactions between long and short waves, Studies Appl. Math. **56**, 81–94 (1977)

8.112 I.Sh. Akhatov, D.B. Khismatulin: Effect of dissipation on the interaction between long and short waves in bubbly liquids, Fluid Dyn. **35**, 573–583 (2000)

8.113 I.Sh. Akhatov, D.B. Khismatulin: Two-dimensional mechanisms of interaction between ultrasound and sound in bubbly liquids: Interaction equations, Acoust. Phys. **47**, 10–15 (2001)

8.114 I.Sh. Akhatov, D.B. Khismatulin: Mechanisms of interaction between ultrasound and sound in liquids with bubbles: Singular focusing, Acoust. Phys. **47**, 140–144 (2001)

8.115 D.B. Khismatulin, I.Sh. Akhatov: Sound – ultrasound interaction in bubbly fluids: Theory and possible applications, Phys. Fluids **13**, 3582–3598 (2001)

8.116 V.E. Zakharov: Collapse of Langmuir waves, Sov. Phys. J. Exp. Theor. Phys. **72**, 908–914 (1972)

8.117 D.F. Gaitan, L.A. Crum, C.C. Church, R.A. Roy: An experimental investigation of acoustic cavitation and sonoluminescence from a single bubble, J. Acoust. Soc. Am. **91**, 3166–3183 (1992)

8.118 Y. Tian, J.A. Ketterling, R.E. Apfel: Direct observations of microbubble oscillations, J. Acoust. Soc. Am. **100**, 3976–3978 (1996)

8.119 J. Holzfuss, M. Rüggeberg, A. Billo: Shock wave emission of a sonoluminescing bubble, Phys. Rev. Lett. **81**, 5434–5437 (1998)

8.120 R. Pecha, B. Gompf: Microimplosions: Cavitation collapse and shock wave emission on a nanosecond time scale, Phys. Rev. Lett. **84**, 1328–1330 (2000)

Amazon EX1014 Page 312

8.121 E. Heim: Über das Zustandekommen der Sonoluminеszenz (On the origin of sonoluminescence). In: *Proceedings of the Third International Congress on Acoustics, Stuttgart, 1959*, ed. by L. Cremer (Elsevier, Amsterdam 1961) pp. 343–346, in German

8.122 C.C. Wu, P.H. Roberts: A model of sonoluminescence, Proc. R. Soc. Lond. A **445**, 323–349 (1994)

8.123 W.C. Moss, D.B. Clarke, D.A. Young: Calculated pulse widths and spectra of a single sonoluminescing bubble, Science **276**, 1398–1401 (1997)

8.124 V.Q. Vuong, A.J. Szeri, D.A. Young: Shock formation within sonoluminescence bubbles, Phys. Fluids **11**, 10–17 (1999)

8.125 B. Metten, W. Lauterborn: Molecular dynamics approach to single-bubble sonoluminescence. In: *Nonlinear Acoustics at the Turn of the Millennium*, ed. by W. Lauterborn, T. Kurz (Am. Inst. Physics, Melville 2000) pp. 429–432

8.126 B. Metten: *Molekulardynamik-Simulationen zur Sonolumineszenz*, *Dissertation* (Georg-August Universität, Göttingen 2000)

8.127 S.J. Ruuth, S. Putterman, B. Merriman: Molecular dynamics simulation of the response of a gas to a spherical piston: Implication for sonoluminescence, Phys. Rev. E **66**, 1–14 (2002), 036310

8.128 W. Lauterborn, T. Kurz, B. Metten, R. Geisler, D. Schanz: Molecular dynamics approach to sonoluminescent bubbles. In: *Theoretical and Computational Acoustics 2003*, ed. by A. Tolstoy, Yu-Chiung Teng, E.C. Shang (World Scientific, New Jersey 2004) pp. 233–243

8.129 N.H. Packard, J.P. Crutchfield, J.D. Farmer, R.S. Shaw: Geometry from a time series, Phys. Rev. Lett. **45**, 712–716 (1980)

8.130 F. Takens: Detecting strange attractors in turbulence. In: *Dynamical Systems and Turbulence*, ed. by D.A. Rand, L.S. Young (Springer, Berlin, Heidelberg 1981) pp. 366–381

8.131 H.D.I. Abarbanel: *Analysis of Observed Chaotic Data* (Springer, Berlin, New York 1996)

8.132 H. Kantz, T. Schreiber: *Nonlinear Time Series Analysis* (Cambridge Univ. Press, Cambridge 1997)

8.133 U. Parlitz: Nonlinear time serie analysis. In: *Nonlinear Modeling – Advanced Black Box Techniques*, ed. by J.A.K. Suykens, J. Vandewalle (Kluwer Academic, Dordrecht 1998) pp. 209–239

8.134 A. Wolf, J.B. Swift, H.L. Swinney, J.A. Vastano: Determining Lyapunov exponents from time series, Physica D **16**, 285–317 (1985)

8.135 W. Lauterborn, E. Cramer: Subharmonic route to chaos observed in acoustics, Phys. Rev. Lett. **47**, 1445–1448 (1981)

8.136 W. Lauterborn, J. Holzfuss: Acoustic chaos, Int. J. Bifurcation Chaos **1**, 13–26 (1991)

8.137 W. Lauterborn, A. Koch: Holographic observation of period-doubled and chaotic bubble oscillations in acoustic cavitation, Phys. Rev. A **35**, 1774–1976 (1987)

8.138 S. Luther, M. Sushchik, U. Parlitz, I. Akhatov, W. Lauterborn: Is cavitation noise governed by a low-dimensional chaotic attractor?. In: *Nonlinear Acoustics at the Turn of the Millennium*, ed. by W. Lauterborn, T. Kurz (Am. Inst. Physics, Melville 2000) pp. 355–358

8.139 W. Lauterborn: Nonlinear dynamics in acoustics, Acustica acta acustica Suppl. 1 **82**, S46–S55 (1996)

8.140 M.E. McIntyre, R.T. Schumacher, J. Woodhouse: On the oscillation of musical instruments, J. Acoust. Soc. Am. **74**, 1325–1345 (1983)

8.141 N.B. Tuffilaro: Nonlinear and chaotic string vibrations, Am. J. Phys. **57**, 408–414 (1989)

8.142 C. Maganza, R. Caussé, Laloë: Bifurcations, period doublings and chaos in clarinet-like systems, Europhys. Lett. **1**, 295–302 (1986)

8.143 K.A. Legge, N.H. Fletcher: Nonlinearity, chaos, and the sound of shallow gongs, J. Acoust. Soc. Am. **86**, 2439–2443 (1989)

8.144 H. Herzel: Bifurcation and chaos in voice signals, Appl. Mech. Rev. **46**, 399–413 (1993)

8.145 T. Yazaki: Experimental observation of thermoacoustic turbulence and universal properties at the quasiperiodic transition to chaos, Phys. Rev. **E48**, 1806–1818 (1993)

8.146 G.W. Swift: Thermoacoustic engines, J. Acoust. Soc. Am. **84**, 1145–1180 (1988)

Amazon EX1014 Page 313

Part C Architect

Part C Architectural Acoustics

9 Acoustics in Halls for Speech and Music
Anders Christian Gade, Lyngby, Denmark

10 Concert Hall Acoustics Based on Subjective Preference Theory
Yoichi Ando, Makizono, Kirishima, Japan

11 Building Acoustics
James Cowan, White River Junction, USA

Amazon EX1014 Page 314

9. Acoustics in Halls for Speech and Music

This chapter deals specifically with concepts, tools, and architectural variables of importance when designing auditoria for speech and music. The focus will be on cultivating the useful components of the sound in the room rather than on avoiding noise from outside or from installations, which is dealt with in Chap. 11. The chapter starts by presenting the subjective aspects of the room acoustic experience according to consensus at the time of writing. Then follows a description of their objective counterparts, the objective room acoustic parameters, among which the classical *reverberation time* measure is only one of many, but still of fundamental value. After explanations on how these parameters can be measured and predicted during the design phase, the remainder of the chapter deals with how the acoustic properties can be controlled by the architectural design of auditoria. This is done by presenting the influence of individual design elements as well as brief descriptions of halls designed for specific purposes, such as drama, opera, and symphonic concerts. Finally, some important aspects of loudspeaker installations in auditoria are briefly touched upon.

9.1 **Room Acoustic Concepts** 302

9.2 **Subjective Room Acoustics** 303
- 9.2.1 The Impulse Response 303
- 9.2.2 Subjective Room Acoustic Experiment Techniques 303
- 9.2.3 Subjective Effects of Audible Reflections 305

9.3 **Subjective and Objective Room Acoustic Parameters** 306
- 9.3.1 Reverberation Time 306
- 9.3.2 Clarity 308
- 9.3.3 Sound Strength 308
- 9.3.4 Measures of Spaciousness 309
- 9.3.5 Parameters Relating to Timbre or Tonal Color 310
- 9.3.6 Measures of Conditions for Performers 310
- 9.3.7 Speech Intelligibility 311
- 9.3.8 Isn't One Objective Parameter Enough? 312
- 9.3.9 Recommended Values of Objective Parameters 313

9.4 **Measurement of Objective Parameters** ... 314
- 9.4.1 The Schroeder Method for the Measurement of Decay Curves 314
- 9.4.2 Frequency Range of Measurements 314
- 9.4.3 Sound Sources 315
- 9.4.4 Microphones 315
- 9.4.5 Signal Storage and Processing 315

9.5 **Prediction of Room Acoustic Parameters** 316
- 9.5.1 Prediction of Reverberation Time by Means of Classical Reverberation Theory 316
- 9.5.2 Prediction of Reverberation in Coupled Rooms 318
- 9.5.3 Absorption Data for Seats and Audiences 319
- 9.5.4 Prediction by Computer Simulations 320
- 9.5.5 Scale Model Predictions 321
- 9.5.6 Prediction from Empirical Data ... 322

9.6 **Geometric Design Considerations** 323
- 9.6.1 General Room Shape and Seating Layout 323
- 9.6.2 Seating Arrangement in Section .. 326
- 9.6.3 Balcony Design 327
- 9.6.4 Volume and Ceiling Height 328
- 9.6.5 Main Dimensions and Risks of Echoes 329
- 9.6.6 Room Shape Details Causing Risks of Focusing and Flutter 329
- 9.6.7 Cultivating Early Reflections 330
- 9.6.8 Suspended Reflectors 331
- 9.6.9 Sound-Diffusing Surfaces 333

9.7 **Room Acoustic Design of Auditoria for Specific Purposes** 334
- 9.7.1 Speech Auditoria, Drama Theaters and Lecture Halls 334

Amazon EX1014 Page 315

9.7.2 Opera Halls 335
9.7.3 Concert Halls for Classical Music .. 338
9.7.4 Multipurpose Halls 342
9.7.5 Halls for Rhythmic Music 344
9.7.6 Worship Spaces/Churches 346
9.8 **Sound Systems for Auditoria** 346
9.8.1 PA Systems 346
9.8.2 Reverberation-Enhancement Systems 348
References 349

Current knowledge about room acoustic design is based on several centuries of practical (trial-and-error) experience plus a single century of scientific research. Over the last couple of decades scientific knowledge has matured to a level where it can explain to a usable degree:

1. the subjective aspects related to how we perceive the acoustics of rooms
2. how these subjective aspects are governed by objective properties in the sound fields
3. how these objective properties of the sound field are governed by the physical variables in the architectural design

This chapter is organized in the same manner. The various subjective acoustic aspects will form the basis for our discussion and be a guide through most aspects of relevance in room acoustic design. However, some trends in current design practice based on the experience and intuition of individual acoustical designers will also be commented on. It is hoped that this approach will also have the advantage of stimulating the reader's ability to judge a room from her/his own listening experience, an ability which is important not only for designers of concert halls, but also for those responsible for creating and enjoying the sound in these halls: musicians, sound-system designers, recording engineers and concert enthusiasts.

9.1 Room Acoustic Concepts

In order to help the reader maintain a clear perspective all the way through this chapter, Fig. 9.1 illustrates the universe of architectural acoustics.

In the upper half of the figure, we have the phenomena experienced in the real world. Going from left to right, we have the auditoria, in which we can experience objective sound fields causing subjective impressions of the acoustic conditions. In all of these three domains, we find a huge number of degrees of freedom: halls can differ in a myriad of ways (from overall dimensions to detailed shaping of small details like door handles), the sound fields which we describe by the impulse response concept – as explained in a moment – contain a wealth of individual sound components (reflections), each being a function of time, level, direction and frequency. Also, every individual may have his/her own way of expressing what the room does to the sound heard.

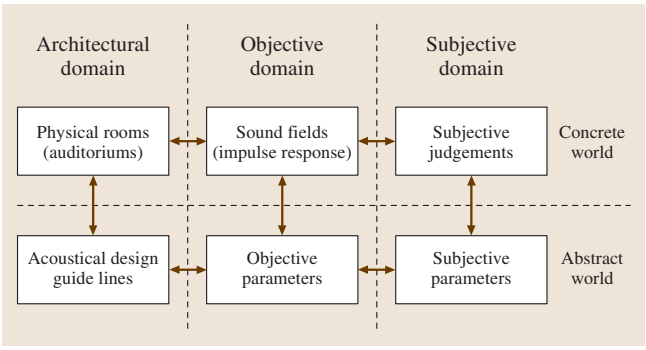


Fig. 9.1 Overview of concepts related to subjective room acoustics (after [9.1])

In other words, like in many other aspects of life, the real world is so complex that we need to simplify the problem – reduce the degrees of freedom – through definition of abstract, well-formulated and meaningful concepts and parameters in all three domains (the lower row of boxes). First, we must try to define a vocabulary to describe the subjective acoustic impression: we will isolate a set of subjective acoustic parameters that are valid to most people's listening experience (as indicated by the box in the lower-right corner), then we will try to deduce those properties from the sound fields that are responsible for our experience of each of the subjective aspects: we will define a set of objective, measurable parameters that correlate well with the subjective parameters, and finally – in order to be able to guide the architect – we must find out which aspects of the design govern the important objective and in turn the subjective

Amazon EX1014 Page 316

parameters, so we can assist in building halls meeting the specific needs of their users.

A rough historical overview: systematic search for objective acoustic parameters peaked in the 1960s and 1970s, while the relationships between the objective parameters and design variables were the topic of many research efforts in the 1980s and 1990s. However, we cannot yet claim to have the answers to all questions regarding the acoustic design of auditoria. Hopefully, there will always be room for intuition and individual judgment, not only in room acoustic design; but also as a source of inspiration for continued research efforts. Still it should be clear that room acoustic design today is based on solid research; it is not a snake-oil business.

9.2 Subjective Room Acoustics

9.2.1 The Impulse Response

The basic source of information regarding the audible properties of the sound field in a room is the impulse response signal. Actually, this signal – when recorded with a multichannel technique preserving the information about direction of incidence – can be shown to contain all information about the acoustics of a room between two specific source and receiver positions.

Consider a short sound impulse being emitted by the source on the stage, as shown in Fig. 9.2. A spherical wave propagates away from the source in all directions and the sound first heard in the listener position originates from that part of the wave that has propagated directly from the source to the receiver, called *the direct sound*. This is shown on the left in the lower part of Fig. 9.2, which shows the received signal versus time at a given position in the room.

This component is soon followed by other parts of the wave that have been reflected one or more times by the room boundaries or by objects in the room before reaching the receiver, called *the early reflections*. Besides arriving later than the direct sound, normally these reflections are also weaker because the intensity is reduced as the area of the spherical wavefront increases with time (spherical distance attenuation) and because a fraction of the energy is being absorbed each time the wave hits a more or less sound-absorbing room boundary or object in the room.

The sound wave will continue to be reflected and to pass the receiver position until all the energy has been absorbed by the boundaries/objects or by the air. The density of these later reflections increases with time (proportional to t^2), but the attenuation due to absorption at the room boundaries ensures that eventually all sound dies out. This decay is often heard as reverberation in the room, as Sabine did, when he carried out his famous experiment in the Fogg Art Museum more than 100 years ago [9.2]. This event marked the start of subjective room acoustics as a science.

9.2.2 Subjective Room Acoustic Experiment Techniques

With each of the reflections specified in time, level, spectrum and direction of incidence, the impulse response contains a huge amount of information. Now, the question is how we can reduce this to what is necessary for an explanation of why we perceive the acoustics in different rooms as being different.

Experiments trying to answer this question have mainly been carried out in the second half of the 20th century when electro-acoustic means for recording, measurement and simulation of sound fields had become available. Such experiments take place in the four rightmost boxes in Fig. 9.1: a number of impulse responses – or rather, music or speech convolved (filtered) through these responses – are presented to a number of subjects. The subjective evaluations are collected either as simple preferences between the sound fields presented in pairs or as scalings along specific subjective parameters suggested by the experimenter. The experimenter will also choose a number of different objective parameters, and calculate their values for each of the impulse responses presented. The level of correlation between these objective values and the objective scalings will then indicate which of the parameters and therefore which properties of the impulse responses are responsible for the subjective evaluations.

As can be imagined, the results of such experiments will be strongly dependent on the range of variation and degree of realism of the impulse responses presented – as well as by the sound quality of the equipment used for the presentation. Besides, the results will always be limited by the imagination of the experimenter regarding his/her:

1. suggestions of proper semantic descriptors for the subjects' evaluation (except in cases where the subjects are only asked to give preferences) and

2. suggestions of calculation of parameters from the impulse response.

In other words, before the experiments, the experimenter must have some good hypotheses regarding the contents of the lower-mid and lower-right boxes in Fig. 9.1.

Over the years, a variety of different techniques have been applied for presenting room sound fields to test subjects:

1. Collection of opinions about existing halls recalled from the memory of qualified listeners
2. Listening tests in different halls or in a hall with variable acoustics
3. Listening tests with presentation of recordings from existing halls or of *dry* speech/music convolved with impulse responses recorded in existing halls
4. Listening tests with sound fields synthesized in anechoic rooms (via multiple loudspeakers in an anechoic room) or impulse responses generated/modified by computer convolved with *dry* speech/music and presented over headphones.

It should be mentioned here that our acoustic memory is very short. Therefore, unless the subjects are highly experienced in evaluating concert hall acoustics, comparison of acoustic experiences separated by days,

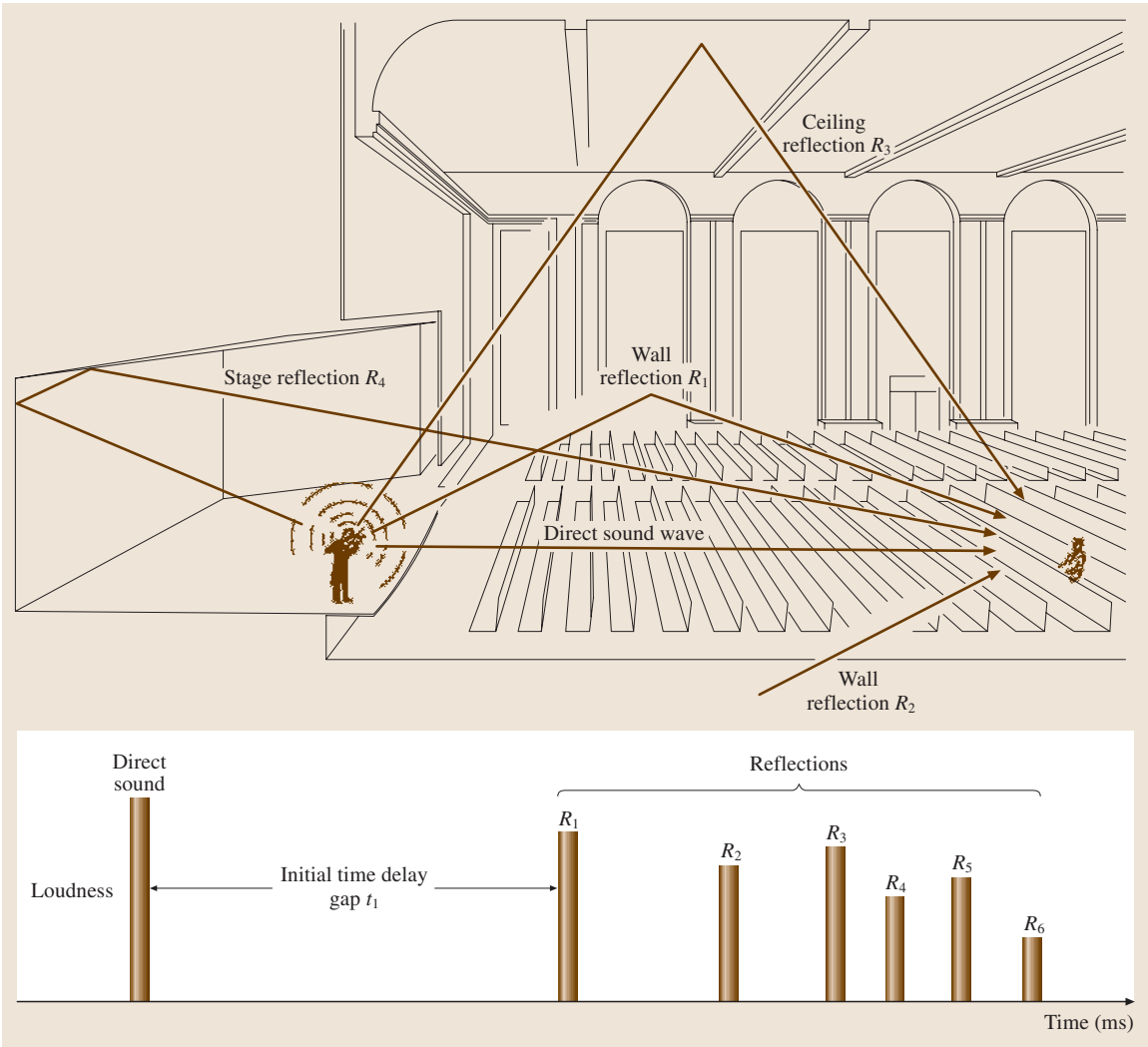


Fig. 9.2 Diagram illustrating the generation of an impulse response in a room (after [9.3])

weeks or even years is less reliable than comparison in the lab, where different recordings can be presented immediately one after the other. On the other hand, it is often difficult to get really qualified people to come to the lab to participate in scientific tests. Therefore, results from interview surveys can still be highly relevant.

These different techniques for presenting the sound fields all have different limitations. Experiments in the lab involving electro-acoustic reproduction or the generation of sound fields may lack fidelity, while listening in a real hall to a real orchestra will normally lack flexibility and control of the independent variables. Another important difference between these two methods is the absence of realistic visual cues in the lab. Enjoyment of a performance is a holistic experience, a fact which is now given increased scientific attention. In all cases elaborate statistical analysis of the results are needed in order to separate the significant facts from the error variance present in any experiment involving subjective judgements. Since the 1960s, multidimensional statistical tool such as factor analysis and multidimensional scaling have been very useful in distinguishing between the different subjective parameters which are present – consciously or not – in our evaluation. In any case, published results are more likely to be close to the truth, if they have been verified by several experiments – and experimenters – using different experimental approaches.

9.2.3 Subjective Effects of Audible Reflections

As the impulse response consists of the direct sound followed by a series of reflections, the simplest case possible would be to have only the direct sound plus a single reflection (and perhaps some late, artificial reverberation). Many experiments in simulated sound fields have been conducted using such a simple setup, and in spite of the obvious lack of realism, we can still learn a lot about the subjective effects of reflections from these experiments.

First of all, due to the psycho-acoustic phenomenon called forward masking, the reflection will be inaudible if it arrives very soon after the direct sound and/or its level is very low relative to the direct sound. Thus, there exists a level threshold of audibility depending on delay and direction of incidence relative to the direct sound. Only if the level of the reflection is above this threshold will the reflection have an audible effect, which again depends on its level, delay and direction of incidence. The possible effects are (at least):

- Increased level (energy addition)
- Increased clarity, if it arrives within 50–80 ms after the direct sound
- Increased spaciousness, if the reflection direction in the horizontal plane is different from that of the direct as this causes the signals received at the two ears to be different (If the angle between the direct and reflected sounds differs in the vertical plane only, the effect is rather a change in *timbre* or coloration of the sound.)
- Echo, typically observed for delays beyond 50 ms and at high reflection levels. If the delay is very long, say 200 ms, then the echo may even be detected at a much lower level;
- Coloration. If the delay is short, say below 30 ms, and the level is high, phase addition of the direct sound and the reflection will create a *comb filter* effect, which severely deteriorates the original frequency spectrum
- Change in localization direction, in cases where the reflection is louder than the direct sound. This may happen either due to amplification of the reflection via a concave surface or due to excess attenuation of the direct sound, for instance by an orchestra pit rail.

Audibility thresholds, echo risk and other effects also depend on spectral and temporal properties of the signal itself. Thus, with speech and fast, staccato played music (not to speak of artificial, impulsive *click* sounds), echoes are much easier to detect than when the signal

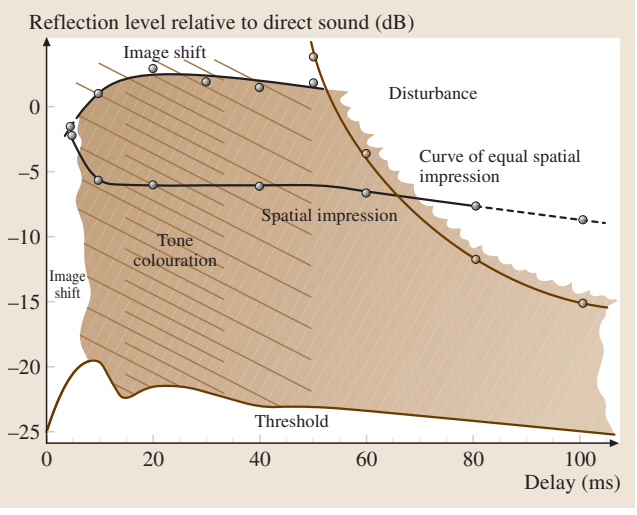


Fig. 9.3 Various audible effects of a single reflection arriving from the side. The signal used was music (after [9.4])

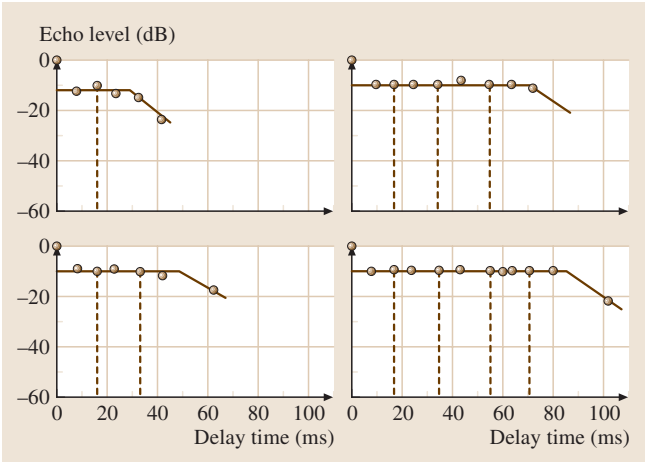


Fig. 9.4 Thresholds of perception of a new reflection (*circles* and *horizontal lines*) being added to impulse responses already containing one, two, three, or four other reflections with delay and relative levels, as indicated by the *vertical lines* (after [9.5])

is slow, legato music. On the other hand, these slower signals are more sensitive for the detection of coloration effects.

The temporal properties of sounds are sometimes described by the autocorrelation function. According to Ando (see Chap. 10 in this book) not only the thresholds of audibility but also the preferred delay of early reflections and the preferred reverberation time depend strongly on the autocorrelation of the signal. However, such a strong effect on concert hall preference – derived from listening experiments in rather simplified simulated sound fields in the lab – is not in accordance with everyday listening experiences in concert halls, in which we gladly accept listening to different music pieces of different tempo from different seats (different reflection delays) in the same hall (fixed reverberation time).

Figure 9.3 illustrates the various audible effects of a single reflection arriving from a 40° angle relative to a frontal direct sound. In this experiment music was used as the stimulus signal. Below the lower threshold (reflection level below about −20 dB and almost independent of the delay), the reflection is inaudible. In the upper-right region it causes a distinct echo, while in the shaded area we experience *spatial impression* or a broadening of the area from which the sound seem to originate. For delays lower than about 30 ms, this single reflection also causes an unpleasant change in *timbre* or *tonal color*, which is due to the combination of the direct and reflected signal forming a comb filter giving systematic changes in the spectrum. If the level of the reflection is increased to be louder than the direct sound (above 0 dB) while the delay is still below say 50 ms, we experience an *image shift* or a change in localization from the direction of the direct sound towards the direction from which the reflection is coming.

In practice, of course, the impulse response from a room contains many reflections, and we therefore need to know how the threshold of perceptibility of the incoming reflection changes in cases where the impulse response contains other reflections already. As seen from Fig. 9.4, the threshold level increases substantially in the delay range already occupied by other reflections. This phenomenon is primarily due to masking.

From this we can conclude that many of the details in a complex impulse response will be masked and only some of the dominant components or some of its overall characteristics seriously influence our perception of the acoustics. This is the reason why it is possible to create rather simple objective room acoustic parameters, as listed in the following section, which still describe the main features of the room acoustic experience. Thus, we seem to have some success describing the complex real world (the upper-middle and right boxes in Fig. 9.1) by simpler, abstract concepts. Also, it will be seen that the subjective effects caused by a single reflection remain important in the evaluation of more-realistic and complicated impulse responses.

9.3 Subjective and Objective Room Acoustic Parameters

From a consensus of numerous subjective experiments in real rooms and in simulated sound fields (representing all of the previously mentioned subjective research techniques), we now have a number of subjective parameters and corresponding objective measures available. Most of these are generally recognized as relevant descriptors of major aspects in our experience of the acoustics in rooms. This situation has promoted standardization of measurement methods and many of the objective parameters are now described in an appendix to the International Organization for Standardization (ISO) standard [9.6]. In order to maintain a clear distinction between the subjective and objective parameters in the following, the names for the subjective parameters will be printed in italics.

Amazon EX1014 Page 320

9.3.1 Reverberation Time

Reverberance is probably the best known of all subjective room acoustic aspects. When a room creates too much *reverberance*, speech loses intelligibility because important details (consonants) are masked by louder, lingering speech sounds (the vowels). For many forms of music, however, *reverberance* can add an attractive fullness to the sound by bonding adjacent notes together and blending the sounds from the different instruments/voices in an ensemble.

The reverberation time T which is the traditional objective measure of this quality, was invented 100 years ago by W. C. Sabine. T is defined as the time it takes for the sound level in the room to decrease by 60 dB after a continuous sound source has been shut off. In practice, the evaluation is limited to a smaller interval of the decay curve, from -5 dB to -35 dB (or -5 dB to -25 dB) below the start value; but still relating to a 60 dB decay (Fig. 9.5), i. e.:

$$T = 60\,\mathrm{dB}\,\frac{(t_{-35}) - (t_{-5})}{(-5\,\mathrm{dB}) - (-35\,\mathrm{dB})}. \tag{9.1}$$

In this equation, t_{-x} denotes the time when the decay has decreased to XdB below its start value, or, if we let $R(t)$ represent the squared value of the decaying sound pressure and shut off the sound source at time $t = 0$:

$$10\log_{10}\left(\frac{R(t_{-X})}{R(0)}\right) = -X\,\mathrm{dB}\,. \tag{9.2}$$

With the fluctuations always present in decay curves, T should rather be determined from the decay rate, A dB/s, as found from a least-squares regression line (determined from the relevant interval of the decay curve). Hereby we get for T:

$$T = \frac{60\,\mathrm{dB}}{A\,\frac{\mathrm{dB}}{\mathrm{s}}} = \frac{60}{A}\mathrm{s}\,. \tag{9.3}$$

Ways to obtain the decay curve from the impulse response will be further explained in the section on measurement techniques.

Due to masking, the entire decay process is only perceivable during breaks in the speech or music. Besides, the rate of decay is often different in the beginning and further down the decay curve. During running music or speech, the later, weaker part of the reverberation will be masked by the next syllable or musical note. Therefore an alternative measure, early decay time (EDT) has turned out to be better correlated with the *reverberance* perceived during running speech and music. This parameter, like T, also measures the rate of the decay; but now evaluated from the initial part, the interval between 0 and -10 dB, only. Thus,

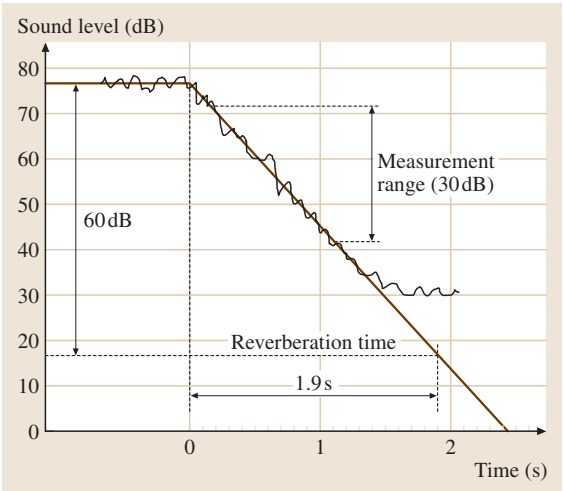


Fig. 9.5 The definition of reverberation time (after [9.4])

$$\mathrm{EDT} = 6(t_{-10}) \quad \text{or} \quad \mathrm{EDT} = \frac{60}{A_{(0\,\mathrm{dB}\to-10\,\mathrm{dB})}}\mathrm{s}\,. \tag{9.4}$$

The detailed behavior of the early part of the reverberation curve is influenced by the relative levels and distribution in time of the early reflections, which in turn vary depending on the positions of the source and receiver in the room. Likewise, the value of EDT is often found to vary throughout a hall, which is seldom the case with T.

In spite of the fact that EDT is a better descriptor of *reverberance* than T, T is still regarded the basic and most important objective parameter. This is mainly due to the general relationship between T and many of the other room acoustic parameters and because a lot of room acoustic theory relates to this concept, not least diffuse field theory, which is the basis for measurements of sound power, sound absorption, and sound insulation. T is also important by being referred to in legislation regarding room acoustic conditions in buildings.

Talking about diffuse field theory, it is often of relevance to compare the measured values of certain objective parameters with their expected values according to diffuse field theory and the measured or calculated reverberation time. As diffuse field theory predicts the decay to be purely exponential, the distribution in time of the impulse response squared should

Amazon EX1014 Page 321

follow the function:

$$h^2(t) = A \exp\left(\frac{-13.8}{T} t\right) , \tag{9.5}$$

in which the constant −13.8 is determined by the requirement that for $t = T$:

$$10 \log_{10}\left(\exp\left(\frac{-13.8}{T} t\right)\right) = 60\,\text{dB} . \tag{9.6}$$

With an exponential decay, the decay curve in dB becomes a straight line. Consequently, the expected value of EDT, EDT_{exp}, equals T.

When evaluating measurement results, it is also relevant to compare differences with the smallest change that can be detected subjectively. For EDT, this so-called subjective difference limen is about 5% [9.7].

9.3.2 Clarity

Clarity describes the degree to which every detail of the performance can be perceived as opposed to everything being blurred together by later-arriving, reverberant sound components. Thus, *clarity* is to a large extent a property complementary to *reverberance*.

When reflections are delayed by no more than 50–80 ms relative to the direct sound, the ear will integrate these contributions and the direct sound together, which means that we mainly perceive the effect as if the clear, original sound has been amplified relative to the later, reverberant energy. Thus, an objective parameter that compares the ratio between energy in the impulse response before and after 80 ms has been found to be a reasonably good descriptor of *clarity*

$$C = 10 \log_{10}\left[\int_0^{80\,\text{ms}} h^2(t)\,\text{d}t \Big/ \int_{80\,\text{ms}}^{\infty} h^2(t)\,\text{d}t\right] . \tag{9.7}$$

The higher the value of C, the more the early sound dominates, and the higher the impression of *clarity*.

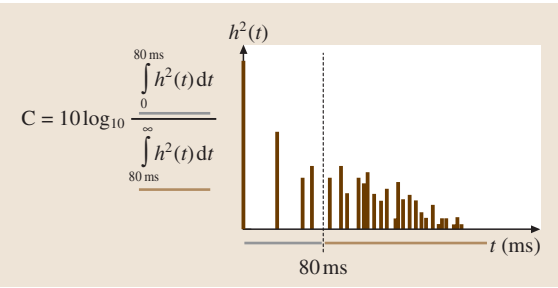


Fig. 9.6 The definition of C: the ratio between early and late energy in the impulse response

With exponential decay, the expected value of C becomes a function of T alone:

$$C_{\text{exp}} = 10 \log_{10}\left[\exp\left(\frac{1.104}{T}\right) - 1\right] \text{dB} . \tag{9.8}$$

The subjective difference limen for C (the equal best difference perceivable) is about 0.5 dB.

The definition of C is illustrated in Fig. 9.6.

Another parameter, which is also used to describe the balance between early and late sound or the balance between *clarity* and *reverberance*, is the center time t_s, which describes the center of gravity of the squared impulse response:

$$t_s = \int_0^{\infty} t h^2(t)\,\text{d}t \Big/ \int_0^{\infty} h^2(t)\,\text{d}t . \tag{9.9}$$

A low value of t_s corresponds to a clear sound, whereas higher values indicate dominance of the late, reverberant energy. The main advantage of t_s is that it does not contain a sharp time limit between early and late energy, since this sharp distinction is not justified by our knowledge about the functioning of our hearing system. The subjective difference limen for t_s is about 10 ms, and the expected diffuse field value is simply given by:

$$t_{s,\text{exp}} = \frac{T}{13.8} \tag{9.10}$$

9.3.3 Sound Strength

The influence of the room on the perceived *loudness* is another important aspect of room acoustics. A relevant measurement of this property is simply the difference in dB between the level of a continuous, calibrated sound source measured in the room and the level the same source generates at 10 m distance in anechoic surroundings. This objective measure called the (relative) strength G can also be obtained from impulse response recordings from the ratio between the total energy of the impulse response and the energy of the direct sound with the latter being recorded at a fixed distance (10 m) from the impulsive sound source:

$$G = 10 \log_{10} \frac{\int_0^{\infty} h^2(t)\,\text{d}t}{\int_0^{t_{\text{dir}}} h^2_{10\,\text{m}}(t)\,\text{d}t} . \tag{9.11}$$

Here the upper integration limit in the denominator t_{dir} should be limited to the duration of the direct sound pulse (which in practice will depend on the bandwidth

selected). A distance different from 10 m can be used, if a correction for the distance attenuation is applied as well.

The expected value of G according to diffuse field theory becomes a function of T as well as of the room volume, V:

$$G_{\mathrm{exp}} = 10\log_{10}\left(\frac{T}{V}\right) + 45\,\mathrm{dB}\,. \qquad (9.12)$$

The subjective difference limen for G is about 1.0 dB. The definition of G is illustrated in Fig. 9.7.

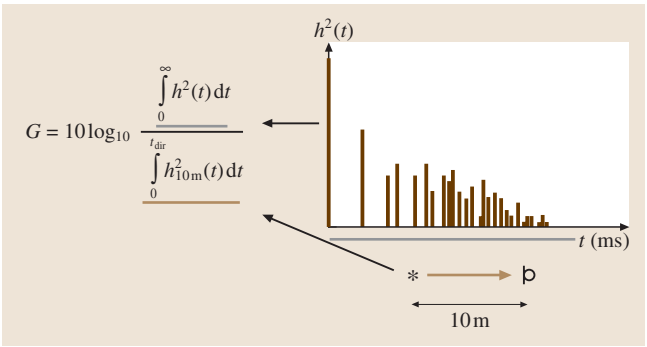


Fig. 9.7 The definition of strength G: the total energy in the impulse response measured relative to the direct sound level at 10 m distance from the source

9.3.4 Measures of Spaciousness

Spaciousness is the feeling that the sound is arriving from many different directions in contrast to a monophonic impression of all sound reaching the listener through a narrow opening. It is now clear that there are two aspects of *spaciousness*, both of which are attractive, particularly when listening to music:

- *apparent source width* (ASW): the impression that the sound image is wider than the visual, physical extent of the source(s) on stage. This should not be confused with localization errors, which of course should be avoided.

and

- *listener envelopment* (LEV): the impression of being inside and surrounded by the reverberant sound field in the room.

Both aspects have been found to be dependent on the direction of incidence of the impulse response reflections. When a larger portion of the early reflection energy (up to about 80 ms) arrives from lateral directions (from the sides) the ASW increases. When the level of the late, lateral reflections is high, strong LEV results.

The lateral components of the impulse response energy can be recorded using a figure-of-eight microphone with the sensitive axis held horizontal and perpendicular to the direction towards the sound source (so that the source lies in the deaf plane of the microphone). For measurement of the lateral energy fraction (LEF), the early part (up to 80 ms) of this lateral sound energy is compared with the energy of the direct sound plus all early reflections picked up by an ordinary omnidirectional microphone:

$$\mathrm{LEF} = \int_{t=5\,\mathrm{ms}}^{t=80\,\mathrm{ms}} h_1^2(t)\,dt \Big/ \int_{t=0\,\mathrm{ms}}^{t=80\,\mathrm{ms}} h^2(t)\,dt\,, \qquad (9.13)$$

where h_1 is the impulse response pressure recorded with a figure-of-eight microphone, whereas h is captured through the (usual) omnidirectional microphone.

It is mainly the energy at low and mid frequencies that contribute to the *spaciousness*. Consequently, LEF is normally averaged over the four octaves 125–1000 Hz. The higher the value of LEF, the wider the ASW. The literature contains many data on LEF values in different, existing concert halls.

LEF does not have an expected value related to T. In a completely diffuse field, LEF would be constant with a value of 0.33, which is higher than that normally found in real halls. The subjective difference limen for LEF is about 5%.

The definition of LEF is illustrated in Fig. 9.8.

The ASW aspect of *spaciousness* is not only dependent on the ratio between early lateral and total early

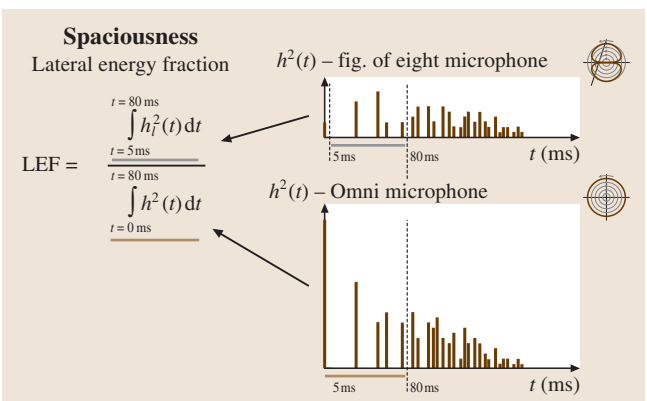


Fig. 9.8 The definition of lateral energy fraction LEF: the ratio between early reflection energy arriving from the sides and total early energy

sound; but also on the total level of the sound. The higher the G value (and the louder the sound source), the broader the acoustic image of the source. However, at the time of writing, there is no solid way of incorporating the influence of level into the objective measure.

Listener envelopment seems to be determined mainly by the spatial distribution and the level of the late reflections (arriving after 80 ms). A parameter called *late lateral strength* (LG) relating the late lateral energy to the direct sound at 10 m distance from the source has been proposed to measure this quality [9.8]:

$$\mathrm{LG} = \int_{t=80\,\mathrm{ms}}^{t=\infty} h_1^2(t)\,\mathrm{d}t \Big/ \int_{t=0\,\mathrm{ms}}^{t=t_{\mathrm{dir}}} h_{10\,\mathrm{m}}^2(t)\,\mathrm{d}t\,. \qquad (9.14)$$

LG is likely to be included in the ISO 3382 standard (from 2007); but so far LG has only been found correlating with subjective responses in laboratory experiments using synthetic sound fields. Therefore, it may be wise not to put too much emphasis on this parameter until its value has also been confirmed by experiments in real halls.

In contrast to reflections arriving in the median plane, lateral reflections will cause the instantaneous pressure at the two ears of the listener to be different. Such a dissimilarity of the signals at the two ears can also be measured by means of the interaural cross-correlation coefficient IACC:

$$\mathrm{IACC}_{t_1,t_2} = \max \left| \frac{\int_{t_1}^{t_2} h_{\mathrm{L}}(t) h_{\mathrm{R}}(t+\tau)\,\mathrm{d}t}{\sqrt{\int_{t_1}^{t_2} h_{\mathrm{L}}^2(t)\,\mathrm{d}t \int_{t_1}^{t_2} h_{\mathrm{R}}^2(t)\,\mathrm{d}t}} \right| \qquad (9.15)$$

in which t_1 and t_2 define the time interval of the impulse response within which the correlation is calculated, h_{L} and h_{R} represent the impulse response measured at the entrance of the left and right ear, respectively, and τ is the interval within which we search for the maximum of the correlation. Normally, the range of τ is chosen between -1 and $+1$ ms, covering roughly the time it takes for sound to travel the distance from one ear to the other. As the correlation is normalized by the product of the energy of h_{L} and h_{R}, the IACC will take a value between 0 and 1. Results are often reported as $1-\mathrm{IACC}$ in order to obtain a value increasing with increasing dissimilarity, corresponding to an increasing impression of *spaciousness*. If the time interval for the calculation (t_1, t_2) is (0 ms, 100 ms), then the IACC will measure the ASW, while a later interval $(t_1, t_2) = (100\,\mathrm{ms}, 1000\,\mathrm{ms})$ may be used to describe the LEV. The literature on measured values in halls mainly contain data on IACC related to the 0–100 ms time interval.

Although the LEF and IACC parameters relate to the same subjective quality, they are not highly correlated in practice. Another puzzling fact is that LEF and IACC emphasize different frequency regions being of importance. LEF is primarily measured in the four lowest octaves, 125 Hz, 250 Hz, 500 Hz and 1000 Hz while IACC should rather be measured in the octave bands above 500 Hz. IACC values would always be high in the lower octaves, because the distance between the ears (< 30 cm) is small compared to 1/4 of the wave length (≈ 70 cm at 125 Hz).

9.3.5 Parameters Relating to Timbre or Tonal Color

Timbre describes the degree to which the room influences the frequency balance between high, middle and low frequencies, i. e. whether the sound is *harsh*, *bright*, *hollow*, *warm*, or whatever other adjective one would use to describe *tonal color*. Traditionally, a graph of the frequency variation of T (per 1/1 or 1/3 octave) has been used to indicate this quality; but a convenient single-number parameter intended to measure the warmth of the hall has been suggested [9.9]: the bass ratio (BR) given by:

$$\mathrm{BR} = \frac{T_{125\,\mathrm{Hz}} + T_{250\,\mathrm{Hz}}}{T_{500\,\mathrm{Hz}} + T_{1000\,\mathrm{Hz}}}\,. \qquad (9.16)$$

Likewise, a *treble ratio* (TR) can be formed as:

$$\mathrm{TR} = \frac{T_{2000\,\mathrm{Hz}} + T_{4000\,\mathrm{Hz}}}{T_{500\,\mathrm{Hz}} + T_{1000\,\mathrm{Hz}}}\,. \qquad (9.17)$$

However, in some halls, a lack of bass sound is experienced in spite of high T values at low frequencies. Therefore EDT or perhaps G versus frequency would be a better – and intuitively more logical – parameter for measurement of *timbre*. Likewise, BR or TR could be based on G rather than T values.

Besides the subjective parameters mentioned above, a quality called *intimacy* is also regarded as being important when listening in auditoria. *Beranek* [9.9] originally suggested this quality to be related to the initial time delay gap ITDG; but this has not been experimentally verified (At the time of writing, Beranek no longer advocates this idea but mentions the observation that, if the ITDG exceeds 45 ms, the hall has no intimacy [9.10]). It is likely that *intimacy* is related to a combination of some of the other parameters already mentioned, such as a high sound level combined with a clear and envelop-

ing sound, as will naturally be experienced fairly close to the source or in small rooms.

9.3.6 Measures of Conditions for Performers

In rooms for performance of music it is also relevant to consider the acoustic conditions for the musicians, partly because it is important to ensure that the musicians are given the best working conditions possible and partly because the product as heard by the audience will also be better if the conditions are optimal for the performers.

Musicians will be concerned about *reverberance* and *timbre* as mentioned above; but also about at least two aspects which are unique for their situation: *ease of ensemble* and *support* [9.11] and [9.12].

Ease of ensemble relate to how well musicians can hear – and play together with – their colleagues. If ensemble is difficult to achieve, the result – as perceived by musicians and listeners alike – might be less precision in rhythm and intonation and a lack of balance between the various instruments. *Ease of ensemble* has been found to be related to the amount of early reflection energy being distributed on the stage. So far, the only widely recognized objective parameter suggested for objective measurement of this quality is *early support* $\mathrm{ST}_{\mathrm{early}}$.

$\mathrm{ST}_{\mathrm{early}}$ is calculated from the ratio between the early reflection energy and the direct sound in an impulse response recorded on the stage with a distance of only one meter between the source and receiver:

$$\mathrm{ST}_{\mathrm{early}} = 10\log_{10}\frac{\int_{20\,\mathrm{ms}}^{100\,\mathrm{ms}} h_{1\,\mathrm{m}}^2(t)\,\mathrm{d}t}{\int_{0\,\mathrm{ms}}^{t_{\mathrm{dir}}} h_{1\,\mathrm{m}}^2(t)\,\mathrm{d}t}\,. \tag{9.18}$$

Support relates to the degree to which the room supports the musicians' efforts to create the tone on their own instruments, whether they find it easy to play or whether they have to force their instruments to fill the room. Having to force the instrument leads to playing fatigue and inferior quality of the sound.

Support is also related to the amount of reflected energy on the stage measured using only a one meter source/microphone distance. For measurement of *support*, however, one needs to consider also the later reflections. This is because for many types of instruments, (especially strings), the early reflections will be masked by the strong direct sound from the instrument itself. Consequently, it seems relevant to define a measure

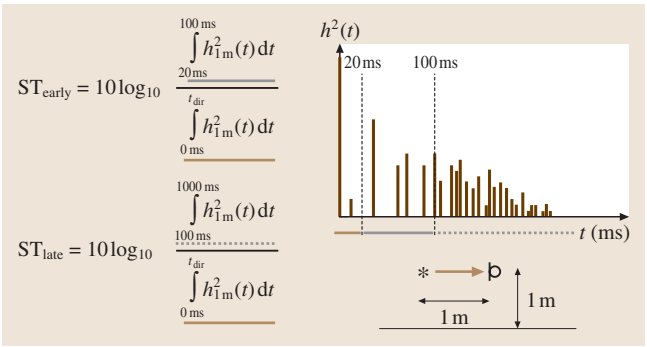


Fig. 9.9 The definition of early support $\mathrm{ST}_{\mathrm{early}}$ and late support $\mathrm{ST}_{\mathrm{late}}$, the ratio between early and late reflection energy respectively and the direct sound in the impulse response. Both are measured at 1 m distance from the source

such as *late support*, $\mathrm{ST}_{\mathrm{late}}$:

$$\mathrm{ST}_{\mathrm{late}} = 10\log_{10}\frac{\int_{100\,\mathrm{ms}}^{1000\,\mathrm{ms}} h_{1\,\mathrm{m}}^2(t)\,\mathrm{d}t}{\int_{0\,\mathrm{ms}}^{t_{\mathrm{dir}}} h_{1\,\mathrm{m}}^2(t)\,\mathrm{d}t} \tag{9.19}$$

which relates to late response (after 100 ms) from the room to the sound emitted.

$\mathrm{ST}_{\mathrm{early}}$ and $\mathrm{ST}_{\mathrm{late}}$ are typically measured in the four octaves 150 Hz, 500 Hz, 1000 Hz, 2000 Hz. The lowest octave is omitted primarily because it is not possible to isolate the direct sound from the early reflections in a narrow band measurement. The definitions of early and late support are illustrated in Fig. 9.9.

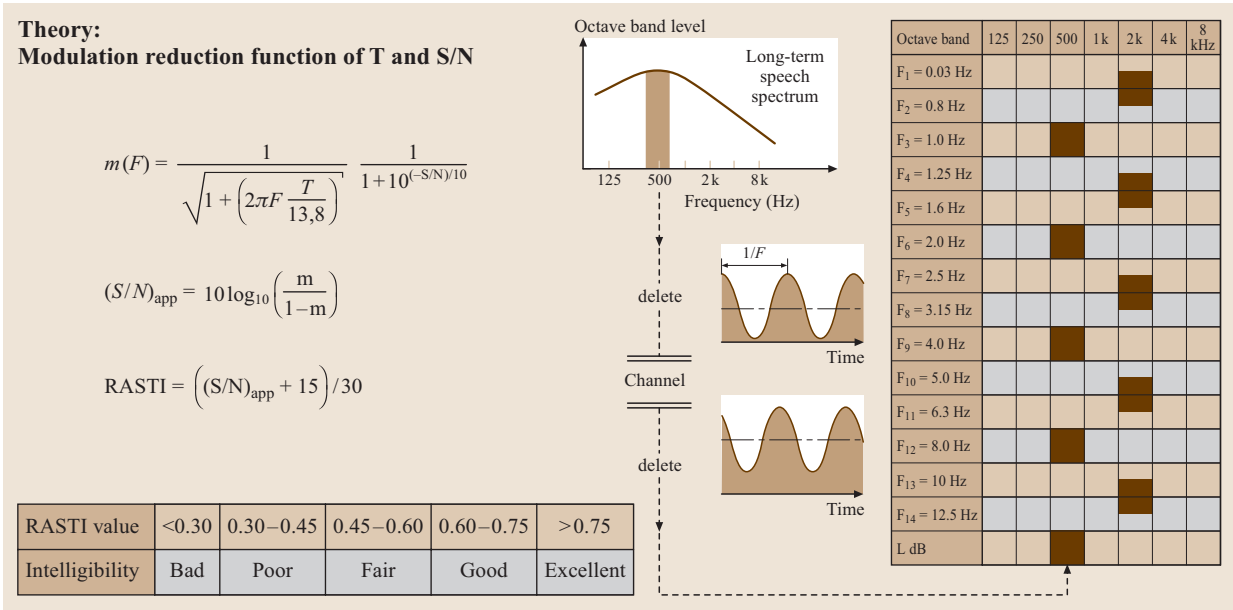
Also the support parameters are planned to be included in the ISO 3382 standard (from 2007); but like LG the experiences and amount of data available from existing halls are still rather limited.

The amount of *reverberance* on the stage may be measured by means of EDT, (with a source–receiver distance of, say, 5 m or more).

9.3.7 Speech Intelligibility

All the objective parameters mentioned above (except the basic T parameter), are mainly relevant in larger auditoria intended for performance of music. In auditoria used for speech, such as lecture halls or theaters, the influence of the acoustics on intelligibility is a major issue.

Currently, the most common way to assess objectively *speech intelligibility* in rooms is by measurement of the speech transmission index STI.



RASTI value	<0.30	0.30–0.45	0.45–0.60	0.60–0.75	>0.75
Intelligibility	Bad	Poor	Fair	Good	Excellent

Fig. 9.10 Illustration of the theory and principle in the measurement of STI or RASTI. The scale for the evaluation of RASTI values is shown at the bottom (after [9.13])

As illustrated in Fig. 9.10, this measure is based on the idea that speech can be regarded as an amplitude-modulated signal in which the degree of modulation carries the speech information. If the transmission path adds noise or reverberation to the signal, the degree of modulation in the signal will be reduced, resulting in reduced intelligibility.

The modulation transfer is tested by emitting noise in seven octave bands, each modulated with 14 different modulation frequencies as listed in the table in Fig. 9.10 and then calculating the ratio between the original and the received degree of modulation, the modulation reduction factor, in each of these 98 combinations. A weighted average of the modulation reduction factor then results in a number between 0 and 1, corresponding to very poor and excellent conditions respectively.

A faster measurement method using only two carrier bands of noises and four plus five modulation frequencies (indicated by the dark squares in Fig. 9.10) is called rapid STI (RASTI). The STI/RASTI method is described in an International Electrotechnical Commission (IEC) standard: IEC 286-16.

Although the original method of STI or RASTI measurement employs modulated noise signals, it is also possible to calculate the modulation reduction factor from the impulse response. Thus, the modulation reduction factor versus modulation frequency F, which is called the modulation transfer function (MTF), can be found as the Fourier transform of the squared impulse response normalized by the total impulse response energy.

According to *Bradley* [9.14], a simpler parameter, called the *useful-to-detrimental sound ratio* U_{80} is equally suitable for measurement of speech intelligibility. U_{80} is simply a modified version of the clarity parameter defined in Sect. 9.3.2, in which a correction is made according to the ratio between the levels of speech and background noise.

9.3.8 Isn't One Objective Parameter Enough?

It is important to notice that all the parameters mentioned above – apart from T – may show large differences between different seats within the same hall. Actually, differences within a single hall are sometimes as large (both objectively and subjectively) as the differences between two different halls.

It should also be mentioned that the objective parameters related to the three subjectively different aspects: *reverberance/clarity*, *loudness* and *spaciousness* show low mutual correlation when measured in different seats or in different halls. In other words, they behave as orthogonal factors and do not monitor the same properties

Amazon EX1014 Page 326

of the sound fields. Consequently, it is obviously necessary to apply one objective parameter for each of these subjective aspects.

It is also clear that different listeners will judge the importance of the various subjective parameters differently. While some may base their judgment primarily on *loudness* or *reverberance* others may be more concerned about *spaciousness* or *timbre*.

For these reasons, one should be very sceptical when people attempt to rank concert halls along a single, universal, one-dimensional quality scale or speak about the best hall in the world. Fortunately, the diversity of room acoustic design and the complexity of our perception does not justify such simplifications.

9.3.9 Recommended Values of Objective Parameters

In view of the remarks above, it may be regarded risky to recommend values for the various objective acoustic parameters. On the other hand, there is a long tradition of suggesting optimal values for reverberation time T as a function of hall volume and type of performance. Besides, most of the other parameters will seldom deviate drastically from the expected value determined by T. As we shall see later, this deviation is primarily influenced by how we shape the room to control early reflections. Designing for strong early reflections can increase *clarity*, *sound strength* and *spaciousness*. Current taste regarding concert hall acoustics for classical music seems to be in favor of high values for these factors in addition to strong *reverberance*. This could lead to suggested ranges for the various parameters in small and large halls, as shown in Table 9.1. These values relate to empty halls with well-upholstered seating, assuming that, when fully occupied with musicians and audience, the T values will drop by no more than say 0.2 s. The reason for relating the values to the unoccupied condition is that it is seldom possible to make acoustic measurements in the occupied state and almost all reference data existing regarding parameters other than T are from unoccupied halls. On the other hand, suggesting well-upholstered seats is a sound recommendation in most cases, which will ensure only small changes depending on the degree of occupancy. This will also justify extrapolation of the unoccupied values of the other parameters to the occupied condition, as mentioned later in this section.

The values listed in the table were arrived at by first choosing values for T ensuring high *reverberance*, while the correlative values for EDT, G and C stem from the diffuse field expected values; but these have been slightly changed to promote high *clarity* and high *levels*. As this is particularly important in larger halls, it has been suggested to use an EDT value 0.1 s lower than T ($=\mathrm{EDT}_{\mathrm{exp}}$) and C values 1 dB higher than C_{exp} in a 2500 m^3 hall, but 0.2 s less than T and 2 dB higher than C_{exp}, respectively, in the 25 000 m^2 hall. Likewise, it is suggested to use G values 2 dB less than G_{exp} in the small halls; but only 1 dB less than or even equal to G_{exp} in large halls. For halls of size between the 2500 and 25 000 m^3 listed in the table, one may of course interpolate to taste. Please note that, in general, G is found to be 2–3 dB lower that G_{exp} (Sect. 9.5.6) so the G values suggested here are actually 1–2 dB higher than those found in "normal" halls.

In the occupied condition, one may expect EDT, C and G to be reduced by amounts equal to the difference between the expected values calculated using T for the empty and occupied conditions respectively. In any case,

Table 9.1 Suggested position-averaged values of objective room acoustic parameters in unoccupied concert halls for classical music. It is assumed that the seats are highly absorptive, so that T will be reduced by no more than 0.2 s when the hall is fully occupied. 2.4 s should be regarded as an upper limit mainly suitable for terraced arena or DRS halls with large volumes per seat (Sect. 9.7.3), whereas 2.0 s will be more suitable for shoe-box-shaped halls, which are often found to be equally reverberant with lower T values and lower volumes per seat

Parameter	Symbol	Chamber music	Symphony
Hall size	V/N	2500 m^3/300 seats	25 000 m^3/2000 seats
Reverberation time	T	1.5 s	2.0–2.4 s
Early decay time	EDT	1.4 s	2.2 s
Strength	G	10 dB	3 dB
Clarity	C	3 dB	−1 dB
Lateral energy fraction	LEF	0.15–0.20	0.20–0.25
Interaural cross correlation	1 − IACC	0.6	0.7
Early support	$\mathrm{ST}_{\mathrm{early}}$	−10 dB	−14 dB

if the empty–occupied difference in T is limited to 0.2 s, as suggested here, then the difference in these parameters will be fairly limited, with changes in both C and G being less than one dB - given that the audience does not introduce additional grazing incidence attenuation of direct sound and early reflections (Sect. 9.6.2).

For opera, one may aim towards the same relationships between the diffuse field expected and the desired values of EDT, C and G, as mentioned above for symphonic halls; but the goal for the reverberation time will normally be set somewhat lower, 1.4–1.8 s in order to obtain a certain intelligibility of the libretto and perhaps to make breaks in the music sound more dramatic (Sect. 9.7.2).

For rhythmic music, T values of 0.8–1.5 s, depending on room size, are appropriate, and certainly the value should not increase towards low frequencies in this case. In very large rock venues such as sports arenas, it may actually be very difficult to get T below 3–5 s; but even then the conditions can be satisfactory with a properly designed sound system. The reason is that in such large room volumes the level of the reverberant sound can often be controlled, if highly directive loudspeakers are being used. In these spaces, the biggest challenge is often to avoid highly delayed echoes, which are very annoying. For amplified music, only recommendations for T are relevant, because the acoustic aspects related to the other parameters will be determined primarily by the sound system (Sect. 9.7.5).

In order to ensure adequate speech intelligibility in lecture halls and theaters, values for STI/RASTI should be at least 0.6. In reverberant houses of worship values higher than 0.55 are hard to achieve even with a well-designed loudspeaker system.

9.4 Measurement of Objective Parameters

Whenever the acoustic specifications of a building are of importance we need to be able to predict the acoustic conditions during the design process as well as document the conditions after completion. Therefore, in this and the following sections, techniques for measurement and prediction of room acoustic conditions will be presented.

In Sect. 9.2.1 it was claimed that the impulse response contains all relevant information about the acoustic conditions in a room. If this is correct, it must also be true that all relevant acoustic parameters can be derived from impulse response measurements. Fortunately, this has also turned out to be the truth.

9.4.1 The Schroeder Method for the Measurement of Decay Curves

Originally, reverberation decays were recorded from the decay of the sound level following the termination of a stationary sound source. However, *Schroeder* [9.15] has shown that the reverberation curve can be measured with increased precision by *backwards* integration of the impulse response, $h(t)$, as follows:

$$R(t) = \int_t^\infty h^2(t)\,\mathrm{d}t = \int_0^\infty h^2(t)\,\mathrm{d}t - \int_0^t h^2(t)\,\mathrm{d}t \quad (9.20)$$

in which $R(t)$ is equivalent to the decay of the squared pressure decay. The method is called backwards integration because the fixed upper integration limit, *infinite time*, is not known when we start the recording. Therefore, in the days of magnetic tape recorders, the integration was done by playing the tape backwards. In this context *infinite time* means the duration of the recording, which should be comparable with the reverberation time. Traditional noise decays contain substantial, random fluctuations because of interference by the different eigenmodes present within the frequency range of the measurement (normally 1/3 or 1/1 octaves). These fluctuations will be different each time the measurement is carried out because the modes will be excited with random phase by the random noise (and the random time of the noise interruption). When, instead, the room is exited by a repeatable impulse, the response will be repeatable as well without such random fluctuations. In fact, Schroeder showed that the ensemble average of interrupted noise decays (recorded in the same source and receiver positions) will converge towards $R(t)$ as the number of averages goes towards infinity.

In (9.20), the right-hand side indicates that the impulse response decay can be derived by subtracting the running integration (from time zero to t) from the total energy. Contrary to the registration of noise decays, this means that the entire impulse response must be stored before the decay function is calculated. However, with modern digital measurement equipment, this is not a problem. From the $R(t)$ data, T is calculated by linear regression as explained in Sect. 9.3.1. As the EDT is evaluated from a smaller interval of the decay curve than T, the EDT is more sensitive to random decay fluctuations than is T. Therefore, EDT should never

be derived from interrupted noise decays – only from integrated impulse responses.

9.4.2 Frequency Range of Measurements

T may be measured per 1/3 octave; but regarding the other objective parameters mentioned in this chapter, it makes no sense to use a frequency resolution higher than 1/1 octave. The reason is that the combination of narrow frequency intervals and narrow time windows in the other parameters will lead to extreme fluctuations with position of the measured values due to the acoustic relation of uncertainty. Such fluctuations have no parallel in our subjective experience. *Bradley* [9.16] has shown that, with 1/1 octave resolution, a change in microphone position of only 30 cm can already cause fluctuations in the clarity C and strength G of about 0.5–1 dB, which is equal to the subjective difference limen. Higher fluctuations would not make sense, as normally we do not experience an audible change when moving our head 30 cm in a concert hall.

The frequency range in which room acoustic measurements are made is normally the six octaves from 125 to 4000 Hz, but it may be extended to 63–8000 Hz when possible. Particularly for reverberation measurements in halls for amplified music, the 63 Hz octave is important.

9.4.3 Sound Sources

With the possibility of deriving all of the objective parameters described above from impulse response measurements, techniques for creating impulses are described briefly in the following.

Basically, the measurements require an omnidirectional sound source emitting short sound pulses (or other signals that can be processed to become impulses) covering the frequency interval of interest, an omnidirectional microphone and a medium for the storage of the electrical signal generated by the microphone.

Impulsive sources such as pistols firing blank cartridges, bursting balloons, or paper bags and electrical spark sources may be used; but these sources are primarily used for noncritical measurements, as their directivity and acoustic power are not easy to control.

For measurements requiring higher precision and repeatability, omnidirectional loudspeakers are preferable, as the power and directivity characteristics of loudspeakers are more stable and well defined. Omnidirectional loudspeakers are often built as six units placed into the sides of a cube, 12 units placed into a dodecahedron or 20 units in an icosahedron, see Fig. 9.11. The requirements regarding omnidirectivity of the source are described in the ISO 3382 standard.

Loudspeakers, however, cannot always emit sufficient acoustic power if an impulsive signal is applied directly. Therefore, special signals of longer duration such as maximum-length sequences or tone sweeps have been developed, which have the interesting property that their autocorrelation functions are band-limited delta pulses. This means that the loudspeaker can emit a large amount of energy without challenging its limited peak-power capability while impulse responses with high time resolution can still be obtained afterwards through post-processing (a correlation/convolution process) of the recorded noise or sweep responses.

In certain cases, other source directivity patterns than omnidirectional can be of interest. For example, a directivity like that of a human talker may be relevant if the measurement is related to the intelligibility of speech or to measurements on the stage in an opera house. A suitable talker/singer directivity can be obtained by using a small loudspeaker unit (membrane diameter about three to four inches) mounted in a closed box of size comparable to that of the human head. Using only one of the loudspeakers in a cube or dodecahedron speaker of limited size is another possibility.

9.4.4 Microphones

For most of the parameters mentioned, the microphone should be omnidirectional, while omni plus figure-of-eight directivity and dummy heads are used when the impulse responses are to be used for the calculation of LEF and IACC.

Three-dimensional intensity probes, sound field microphones or microphone arrays have also been suggested in attempts to obtain more-complete information about the amplitude and direction of incidence of individual reflections [9.17] or for wave field analysis [9.18]. However, such measurements are mainly for research or diagnostic purposes. As such, they do not fulfill the goal set up in Sect. 9.1 of reducing the information to what is known to be subjectively relevant. A selection of relevant microphones are shown in Fig. 9.12.

9.4.5 Signal Storage and Processing

For the storage of the impulse responses the following choices appear.

- The hard disk on a personal computer (PC) equipped with a sound card or special analog-to-digital (A/D) converter card